

0830-N-10  
319  
MAY 30 1980

NASA 155-3061  
NASA Conference Publication 3061

# Carbon in the Galaxy: Studies From Earth and Space

*Invited papers from a meeting held at  
Ames Research Center  
Moffett Field, California  
November 5-6, 1987*

**NASA**

*NASA Conference Publication 3061*

# **Carbon in the Galaxy: Studies From Earth and Space**

*Edited by*  
Jill C. Tarter  
*SETI Institute*  
*Mountain View, California*

Sherwood Chang  
*Ames Research Center*  
*Moffett Field, California*

Doug J. DeFrees  
*Molecular Research Institute*  
*Palo Alto, California*

Invited papers from a meeting sponsored by the  
Life Science Division, National Aeronautics and  
Space Administration, Washington, D.C., and held at  
Ames Research Center  
Moffett Field, California  
November 5-6, 1987



National Aeronautics and  
Space Administration  
Office of Management  
Scientific and Technical  
Information Division

1990

*I*

## TABLE OF CONTENTS

	Page
PROLOGUE .....	vii
ACKNOWLEDGMENTS .....	xiii
MEETING PARTICIPANTS .....	xv
STUDIES OF CARBON IN PRIMITIVE BODIES	
Carbon in Primitive Meteorites .....	3
<i>John F. Kerridge</i>	
Carbon in Comet Dust .....	21
<i>D. E. Brownlee</i>	
Carbon-rich Particles in Comet Halley .....	27
<i>Benton C. Clark</i>	
STUDIES OF CARBON IN INTERSTELLAR SPACE	
Astronomical Observations of Solid Phase Carbon .....	39
<i>M. Jura</i>	
Survival of Carbon Grains in Shocks .....	47
<i>C. Gregory Seab</i>	
Carbon Stardust: From Soot to Diamonds .....	59
<i>A. G. G. M. Tielens</i>	
Interstellar Grain Chemistry and Organic Molecules .....	113
<i>L. J. Allamandola and S. A. Sandford</i>	
Carbon Chemistry of Circumstellar Envelopes .....	147
<i>John H. Bieging</i>	
Carbon Chemistry in Dense Molecular Clouds: Theory and Observational Constraints .....	159
<i>Geoffrey A. Blake</i>	
CI, CII, and CO as Tracers of Gas Phase Carbon .....	181
<i>Jocelyn Keene</i>	

## LABORATORY STUDIES OF CARBON

Down-to-Earth Studies of Carbon Clusters .....	199
<i>R. E. Smalley</i>	
Electronic and Molecular Structure of Carbon Grains .....	245
<i>Jan Almlöf and Hans-Peter Lüthi</i>	
A Unifying Picture of Gas-Phase Formation and Growth of PAH, Soot, Diamond and Graphite .....	259
<i>Michael Frenklach</i>	
The Formation and Structure of Circumstellar and Interstellar Dust .....	275
<i>H. W. Kroto</i>	

## STUDIES OF CARBON FROM SPACE

SIRTF: Probing the Dark Corners of the Galaxy .....	287
<i>Michael W. Werner and Dora S. Willoughby</i>	
Research Opportunities on the Space Station .....	303
<i>Guy Fogleman</i>	

## SUMMARY AND CONCLUDING REMARKS

What Have We Learned; Where Do We Go From Here? .....	311
<i>J. Mayo Greenberg</i>	

## ABSTRACTS FROM CONTRIBUTED POSTER PAPERS

The Possible Presence of Interstellar PAHs in Meteorites and Interplanetary Dust Particles .....	319
<i>L. J. Allamandola, S. A. Sandford, and B. Wopenka</i>	
Laboratory Simulation of Interstellar Grain Chemistry and the Production of Complex Organic Molecules .....	321
<i>L. J. Allamandola, S. A. Sandford, and G. J. Valero</i>	
Nature and Origin of Interstellar Diamond from the Allende CV3 Meteorite .....	323
<i>David Blake, Friedemann Freund, Ted Bunch, Kannan Krishnan, Alexander Tielens, Mitch Stampfer, and Sherwood Chang</i>	
An Ionic Mechanism of Carbon Formation in Flames .....	325
<i>H. F. Calcote</i>	

On Planetary Nebulae as Sources of Carbon Dust: Infrared Emission from Planetary Nebulae of the Galactic Halo .....	327
<i>Harriet L. Dinerstein and Daniel F. Lester</i>	
Impact Fracture Experiments Simulating Interstellar Grain-Grain Collisions .....	328
<i>Friedemann Freund, Sherwood Chang, and J. Thomas Dickinson</i>	
Diamonds in Detonation Soot .....	330
<i>N. Roy Greiner, Dave Phillips, J. D. Johnson, and Fred Volk</i>	
Probing the Possibility of a $^{12}\text{C}/^{13}\text{C}$ Galactic Abundance Gradient .....	331
<i>Isabel Hawkins</i>	
New Observations of Interstellar Organic Molecules .....	333
<i>W. M. Irvine, P. Friberg, H. E. Matthews, Y. C. Minh, and L. M. Ziurys</i>	
Search for Interstellar Methane .....	335
<i>R. F. Knacke, Y. H. Kim, K. S. Noll, and T. R. Geballe</i>	
Raman Spectroscopic Studies of Carbon in Extra-Terrestrial Materials .....	336
<i>John Macklin, Donald Brownlee, Sherwood Chang, and Ted Bunch</i>	
Can the Chirality of the ISM Be Measured? .....	337
<i>Y. Pendleton, S. Sandford, M. Werner, J. Lauer, and S. Chang</i>	
On Diamond, Graphitic and Amorphous Carbons in Primitive Extraterrestrial Solar System Materials .....	339
<i>Frans J. M. Rietmeijer</i>	
FT-IR Spectroscopic Studies of Polycyclic Aromatic Hydrocarbons .....	341
<i>D. W. Salisbury, J. E. Allen, Jr., B. Donn, W. J. Moore, and R. K. Khanna</i>	
Carbon in the Outer Solar System .....	342
<i>D. P. Simonelli, J. B. Pollack, and C. P. McKay</i>	

# Carbon in the Galaxy: Studies from Earth and Space



## PROLOGUE

On November 5 and 6, 1987, the Planetary Biology Branch at Ames Research Center, with support from the Exobiology Program of the Life Sciences Division at NASA Headquarters, conducted a meeting on "Carbon in the Galaxy: Studies from Earth and Space." The meeting brought together over 50 scientists from diverse disciplines who had in common a keen interest in the various forms of carbon that are found throughout the galaxy and on Earth. The papers and abstracts of posters presented at that meeting (as reproduced in this Conference Publication) give some of the flavor of the exciting interchange that took place when the scientists began to consider areas of carbon research that had previously seemed unrelated to their own work.

Carbon is one of the chemical elements characteristic of life on the Earth. Indeed, the chemistry of carbon is predominantly organic chemistry - the chemistry of material usually associated with living organisms. The purpose of the Exobiology Program is to determine the origin and distribution of life and life-related molecules throughout the universe. Thus, the recent discoveries of carbon in its various forms and in various cosmic environments has been the cause of much interest and excitement for exobiologists.

The Ames meeting was designed to bring scientists from various disciplines together and focus on aspects of the study of carbon that are related to the origins of life and of life-related compounds in the galaxy. Many forms of carbon were available on the nascent Earth and some must have played an important role in the processes leading to the evolution of life. Likewise, these forms of carbon are available on other bodies in the Solar System and in other planetary systems that may have formed throughout the galaxy. By bringing these scientists together, the sponsors of the meeting hoped to identify the major open questions about the nature, origin and distribution of carbon in the galaxy, as well as the most fruitful observational, theoretical and/or experimental approaches to answering those questions with ground- and space-based activities. This meeting provided a new perspective on the status of research into the nature and origin of the various forms of carbon and its potential relationship to the origin of life. As expected, the interactions among the scientists attending the meeting led to new suggestions of observations and experiments; new ways of trying to answer old questions. Overall, the conference had the desired result of providing an overview and establishing a sound basis for continued ground-and space-based research on carbon in the galaxy.

The papers presented at the meeting divide naturally into four subject areas: 1) studies of carbon in primitive bodies, 2) studies of carbon in interstellar space, 3) laboratory studies of carbon, and 4) studies of carbon from space. As a general rule, speakers on any one topic were familiar with the research of other speakers on that topic and the real educational opportunities came from listening to researchers speaking on one of the other topics. Professor Mayo Greenberg made an outstanding attempt to summarize the lessons learned from this scientific cross-fertilization, but some of the most important results may not be appreciated for a long time to come.

### **Studies of Carbon in Primitive Bodies:**

The most direct source of information about the nature and history of carbon in the galaxy are the primitive bodies of the solar system which have not been subjected to severe processing by planet formation. The three papers of the section on Studies of Carbon in Primitive Bodies summarize aspects of our current knowledge.

Laboratory measurements show that carbon grains in carbonaceous meteorites exhibit anomalous ratios in the stable isotopes of C, N and H which signify origins in stellar and interstellar environments predating our solar system. Amino acids, carboxylic acids, and high molecular weight organic matter contain D/H ratios approaching those found in interstellar molecules and suggest a common ion-molecule synthesis mechanism. In addition to very small amounts of silicon carbide and minute diamond grains, there are more abundant grains of high molecular weight organic matter, as well as other trace carbon components, which are poorly characterized, but attributed with nova or supernova origins by virtue of their contents of nucleosynthetically derived noble gases. In some interplanetary dust particles thought to have originated from comets, organic matter has been found with unusually high D/H ratios like those in organic compounds and grains of carbonaceous meteorites. The bulk of the carbon in carbonaceous meteorites and IDPs appears to be in the form of amorphous to highly disordered graphitic carbon, typically in the micron to much smaller size range. Lonsdaleite, a hexagonal form of diamond, and FeNi carbide have also been found in IDP, but their origin is not well understood.

The elemental compositions of IDPs are consistent with the range measured for dust grains in comet Halley by the particle analyzer experiments on the Giotto spacecraft. The sizes of the Halley grains are in the micron to sub-micron range. Surprisingly, the Giotto experiments revealed a population of particles in which the elements C, H, O, and N were predominant with particles containing the combinations (C,H,O,N), (H,C,N), (H,C,O) and (HC). The structure of these grains is unknown, but the apparent complexity in the carbon chemistry of comet dust belies the relative simplicity of the gas phase species observed in coma and tail.

The available data indicate a variety of presolar as well as solar system sources for the carbon in primitive bodies, but many uncertainties exist with respect to the production mechanisms and subsequent histories of these materials. Tantalizing relationships are emerging connecting the carbon components of primitive bodies and dusty materials observed around carbon stars and in various interstellar cloud environments. Further studies are needed, however, particularly of IDPs and samples returned from the nucleus of a comet. Additional isotopic measurements of C, H, O, N and S in the compounds and grains of primitive samples may reveal isotopic patterns that can be related to common synthesis mechanisms and source regions.

### **Studies of Interstellar Carbon:**

Astrophysical observations at mm, IR, and UV wavelengths are beginning to provide an understanding of the life cycle of carbon and carbon compounds in the interstellar medium. We can now inventory the production mechanisms for gas phase and solid carbon compounds, make extremely sophisticated chemical models for ion-molecule and surface chemistry to track the modification of carbon close to its source of origin and throughout the dense and diffuse components of the interstellar medium and we can estimate the efficiency with which carbon grains are

formed in outflows and in clouds and then destroyed by shocks. All the pieces are in place, although not necessarily self-consistent. An inventory of interstellar carbon and an understanding of its evolutionary sequences seems close at hand. The seven papers presented on this topic focussed on specific production or destruction or alteration mechanisms for gas and solid phase carbon compounds, relating observations to theoretical calculations and laboratory experiments. Mayo Greenberg's summary highlights some of the discrepancies and provides one interpretation of the evolutionary history of carbon.

Between 1/3 to 1/2 of the carbon inventory in the ISM exists in the gas phase. In the diffuse ISM this is almost entirely in the form of singly ionized carbon CII, whereas, in the dense interstellar clouds, gas phase carbon occurs predominantly as CO, CII and neutral carbon, CI, in the ratio 7:3:1. Carbon is injected into the ISM from a large variety of evolved stellar sources at a cumulative rate of  $2 \times 10^{-5} M_{\odot}/\text{yr}/\text{kpc}^2$  with 10 - 50% of it coming from the carbon-rich envelopes of red giant stars. Of this carbon, only 20% is in the form of carbon stardust. This stardust survives on average for only  $10^9$  years in the ISM, encountering about 10 high velocity shocks from supernovae that destroy it. This fast destruction rate coupled with the low estimate for the injection rate of carbon stardust and the observed interstellar gas phase carbon depletion argue strongly for an interstellar production mechanism of solid phase carbon. Laboratory experiments have begun to confirm in detail the suggestion that UV photolysis of carbon molecules incorporated in and on icy grain mantles can efficiently manufacture refractory carbon mantles that remain intact when the initial ice sublimates at temperatures in excess of 200K.

A number of the papers provided compelling evidence for the existence of a form of refractory carbon on the border between a large molecule and a small particle, having extraordinary survival characteristics against UV photodissociation and destructive shocks. Whether this material is the polycyclic aromatic hydrocarbon (PAH) beloved of infrared spectroscopists or related to the extraordinarily stable  $C_{60}$  "Bucky Balls" that have been studied in the laboratory, or something else entirely, remains one of the most intriguing questions. If, as seems most likely, this material formed in the circumstellar envelopes of carbon-rich giant stars, what role does it play in the formation of the observed carbon stardust? Traditional gas-phase ion-molecule chemistry seems adequate to explain the abundance and production sites for the smaller carbon containing molecules in dense molecular clouds and in the circumstellar envelopes of giant carbon stars, but it "fails spectacularly" with respect to the larger molecules and is unable to explain the observed presence of HCN in the envelopes of oxygen-rich stars. Better chemical rate coefficients and the inclusion of grain surface chemistry are needed to make progress.

Observations at mm wavelengths are now obtaining sufficient spatial resolution to study simple gas phase carbon chemistry as a function of distance into the envelope around giant carbon stars such as IRC+10216. Indeed, the observations are becoming so precise that many of the simplifying assumptions included in the standard radiative transfer calculations must now be abandoned in favor of detailed models in order to make proper interpretations of the data. Observational techniques are also outstripping the capabilities of theoretical prediction as sub-mm and far-IR facilities offer the possibility of detecting the bending modes of much larger molecules than the current 13 atoms detected by mm observations. Laboratory measurements are urgently needed to define the sub-mm and far-IR rotational-vibrational spectra of these very large molecules if we are to make progress in understanding the growth mechanisms that transform gas phase carbon into some sort of soot and finally into carbon stardust.

Two papers discussed one area where theory appears to be well on the way to explaining the recent, startling, discovery of small diamonds in the Allende meteorite. Although the theoretically predicted yield is still a bit low, high velocity collisions between grains containing amorphous carbon behind rapid shocks ( $V > 100$  km/sec) in the ISM appear to be capable of producing just the type of small diamonds that have been observed.

The entire field of interstellar chemistry began only 20 years ago with the detection of OH. It has grown incredibly rapidly and today the study of interstellar carbon compounds and organic chemistry offers both spectacular successes and tantalizing inconsistencies, problems on the verge of solution, and others that may require technological break-throughs or results from seemingly unrelated laboratory studies before progress can be made.

### **Laboratory Studies of Carbon:**

While sample analysts, astronomers and astrophysicists have been studying carbonaceous materials in meteorites, comets, cosmic dust, circumstellar shells and the interstellar medium, chemists independently have been developing new techniques to study the formation and properties of carbon clusters and grains.

Using laser-vaporization sources of clusters in supersonic beam experiments, research on carbon clusters has yielded new insight into the processes and products of carbon condensation. Apparently, with increasing size of clusters, the stable forms occur as linear species ( $C_2$ - $C_9$ ), then monocyclic rings ( $C_{10}$ - $C_{29}$ ), and finally as even-numbered closed spheroidal shells or odd-numbered nearly-closed spheroidal shells ( $C_{32}$ - $C_{100+}$ ). The reactions are thought to proceed by way of spiraling graphitic sheets. Under certain conditions a remarkably stable  $C_{60}$  structure (thought to be the truncated icosahedron, buckminsterfullerene) forms as the predominant product.

Theoretical calculations show that, energetically, the  $C_{60}$  structure compares favorably with sheets of graphitic carbon. Calculations also show that with increasing cluster size, polycyclic aromatic hydrocarbons (PAHs) will have central domains which mimic graphite surfaces, while the edges of these molecules may have quite different properties. Similar calculations on the energetics and bonding characteristics of spiraling graphitic sheets and spheroidal structures would be desirable for comparison of experimental properties with those predicted theoretically.

In other experiments involving sooting flames, pyrolysis of acetylene in shock tubes, and plasma-assisted vapor deposition of carbon, PAHs and carbon grains are also commonly produced. Moreover, the  $C_{60}$  species has also been reported in sooting flames, while diamond has been formed by vapor deposition. Mechanistic studies of these processes suggest that carbon growth in all these systems may depend on temperature: carbon clustering predominating at high temperatures; hydrogen abstractions and acetylene additions at low temperatures.

All the molecular species described above may occur in astrophysical environments which are conducive to carbon cluster formation, for example, the atmospheres of carbon stars or interstellar clouds. They may be a major source for the observed interstellar linear carbon chain species, as well as for the PAHs thought to be responsible for interstellar spectroscopic features such as the Diffuse Interstellar

Features, the 2170Å UV Absorption and the Unidentified Infrared Bands. The stability of closed spheroidal products against chemical or photophysical attack suggests that they may be surviving entities in harsh environments where primary product distributions have been altered by subsequent astrophysical/chemical processing.

Further advances in laboratory studies, including studies of carbon grains in primitive materials, and astronomical spectroscopy hold promise of verifying the role of carbon clusters, PAHs, spiralling graphitic shells and spheroidal closed shell species, particularly  $C_{60}$ , in the interstellar medium.

### **Studies of Carbon from Space:**

Near infrared observations from ground-based telescopes must be made through the small semi-transparent windows of our atmosphere. Airborne observations have broadened these windows and opened new ones in the far infrared. Yet the successful observations of the IRAS satellite provided a four-wavelength look at the infrared universe that startled the scientific community and posed more questions than it answered. SIRTf (Space Infrared Telescope Facility) has been designed to try and answer these new questions, many of them involving the chemistry of carbon. This satellite will be cryogenically cooled to achieve extremely good sensitivity from 2 - 700  $\mu\text{m}$  and it will have a long lifetime on orbit. Thus, SIRTf will provide an excellent research platform for guest investigators studying gas and solid phase carbon in the vicinity of evolved stars and newly formed stars, in the interstellar medium and the surface layer of some of the cold dark bodies of our own solar system. While awaiting the sensitivity that can only be achieved by SIRTf, observers may take advantage of the infrared capabilities provided by ESA's ISO (Infrared Satellite Observatory) and a second generation set of near-infrared instruments now being developed for the Hubble Space Telescope. Facilities proposed for Space Station Freedom will offer researchers the opportunity to enhance what is learned from remote observations by conducting experiments on manufactured carbon bearing samples and by collecting cosmic dust grains. The Gas-Grain Simulation Facility will take advantage of the microgravity environment of the space station in order to extend the particle settling time and permit studies of solid phase carbon grain formation, growth, nucleation, collisions and other processes regulating the creation and destruction of carbon rich particles under conditions simulating stellar, interstellar and protostellar environments. The Cosmic Dust Collection Facility is proposed for attachment to the space station early in the initial operating configuration. This passive collector should provide for intact capture of grains with enough information concerning their trajectories to permit a determination of the likely astrophysical source. Even when the structure of the grain cannot be preserved, elemental and isotopic composition is retained. Space will soon become another laboratory for all those interested in the study of carbon.

## ACKNOWLEDGMENTS

Many individuals helped to make this a smooth running and extremely rewarding meeting. Of particular note are the meeting organizers, the scientific staff within the Planetary Biology Branch at Ames Research Center and volunteers from the SETI Institute. The meeting would not have been possible without the financial support furnished by the Exobiology Program Office at NASA Headquarters and the encouragement of the Exobiology Program Scientist, Dr. John Rummel.

## MEETING PARTICIPANTS

Carbon in the Galaxy:  
Studies from Earth and Space  
November 5 and 6, 1987

Dr. Lou Allamandola  
Mail Stop 245-6  
NASA Ames Research Center  
Moffett Field, CA 94035

Dr. John E. Allen, Jr.  
Code 691  
NASA Goddard Space Flt. Ctr.  
Greenbelt, MD 20771

Dr. Jan Almlof  
Department of Chemistry  
University of Minnesota  
Minneapolis, MN 55455

Dr. Sheldon Aronowitz  
875 Lily Avenue  
Cupertino, CA 95014

Dr. John H. Bieging  
Radio Astronomy Laboratory  
University of California  
601 Campbell Hall  
Berkeley, CA 94720

Dr. David C. Black  
NASA Ames Research Center  
Mail Stop 200-7  
Moffett Field, CA 94035

Dr. David Blake  
Mail Stop 239-4  
Moffett Field, CA 94035

Dr. Geoffrey A. Blake  
Chemistry Department  
University of California  
Berkeley, CA 94720

Dr. Jesse Bregman  
Mail Stop 245-6  
NASA Ames Research Center  
Moffett Field, CA 94035

Dr. D. E. Brownlee  
Dept. of Astronomy  
University of Washington  
Seattle, WA 98195

Dr. H. F. Calcote  
AeroChem Research  
Laboratories  
P.O. Box 12  
Princeton, NJ 08540

Dr. Larry Caroff  
Mail Stop 245-6  
NASA Ames Research Center  
Moffett Field, CA 94035

Dr. Pat Cassen  
NASA Ames Research Center  
Mail Stop 245-3  
Moffett Field, CA 94035

Dr. Sherwood Chang  
Mail Stop 239-4  
NASA Ames Research Center  
Moffett Field, CA 94035

Dr. Benton C. Clark  
Martin Marietta Aerospace  
Planetary Sciences Lab (0560)  
P.O. Box 179  
Denver, CO 80201

Dr. Alan Covington  
NASA Ames Research Center  
Mail Stop 234-1  
Moffett Field, CA 94035

Dr. Dale P. Cruikshank  
Institute for Astronomy  
2680 Woodlawn Drive  
Honolulu, HI 96822

Ms. Wanda L. Davis  
SETI Institute  
NASA Ames Research Center  
Mail Stop 239-4  
Moffett Field, CA 94035

Dr. David W. Deamer  
Department of Zoology  
University of California  
Davis, CA 95616

Dr. Doug DeFrees  
Molecular Research Institute  
701 Welch Road, Ste. 213  
Palo Alto, CA 94304

Dr. Harriet Dinerstein  
Astron. Dept.  
University of Texas at Austin  
Austin, TX 78712

Dr. Guy Fogelman  
Mail Stop 239-12  
NASA Ames Research Center  
Moffett Field, CA 94035

Dr. Michael Frenklach  
202 Academic Projects Bldg.  
Penn State University  
University Park, PA 16802

Dr. Friedemann Freund  
Mail Stop 239-4  
NASA Ames Research Center  
Moffett Field, Ca 94035

Dr. J. Mayo Greenberg  
Lab Astrophysics  
Niels Bohrweg 2, Postbus 9504  
2300 RA Leiden,  
THE NETHERLANDS

Dr. N. Roy Greiner  
Los Alamos National Lab  
Los Alamos, NM 87545

Dr. Isabel Hawkins  
Lawrence Livermore  
National Laboratory  
P.O. Box 808  
Livermore, CA 94550

Prof. William M. Irvine  
Dept. of Physics and  
Astronomy  
University of Massachusetts  
Amherst, MA 01003

Dr. Michael Jura  
Department of Astronomy  
Mathematics and Science Bldg.  
University of California  
Los Angeles, CA 90024

Dr. Andrew Kaldor  
Corporate Research Lab  
Exxon Research & Eng. Co.  
Annandale, NJ 08801

Dr. Jocelyn Keene  
Mail Stop 248-1  
NASA Ames Research Center  
Moffett Field, CA 94035

Dr. John F. Kerridge  
Institute of Geophysics  
& Planetary Physics  
University of California  
Los Angeles, CA 90024

Dr. Harry W. Kroto  
Department of Chemistry  
Folmer, Brighton BN19QH  
ENGLAND

Dr. Roy S. Lewis  
Enrico Fermi Institute  
5640 S. Ellis Avenue  
Chicago, IL 60637

Dr. Ken Lincoln  
NASA Ames Research Center  
Mail Stop 239-1  
Moffett Field, CA 94035

Dr. Ian D. Mackinnon  
Department of Geology  
University of New Mexico  
Albuquerque, NM 87131

Dr. John Macklin  
University of Washington  
Seattle, WA 98185

Dr. Christopher P. McKay  
NASA Ames Research Center  
Mail Stop 239-12  
Moffett Field, CA 94035

Dr. Keith Noll  
Lunar & Planetary  
University of Arizona  
Tucson, AZ 85721

Dr. Yvonne Pendleton  
Mail Stop 245-6  
NASA Ames Research Center  
Moffett Field, CA 94035

Dr. Frans J. Rietmeijer  
Johnson Space Center  
SN4  
Houston, TX 77058

Dr. Eric Rohlifing  
Division 8353  
SANDIA National Lab  
Livermore, CA 94550

Dr. David S. Ross  
SRI International  
333 Ravenswood Avenue  
PS 269  
Menlo Park, CA 94025

Dr. David W. Salisbury  
Department of Chemistry  
Box 312  
University of Maryland  
College Park, MD 20742

Dr. Scott Sandford  
Mail Stop 245-6  
NASA Ames Research Center  
Moffett Field, CA 94035

Dr. Roberta Saxon  
SRI International PN093  
333 Ravenswood Avenue  
Menlo Park, CA 94025

Prof. Rich Saykally  
Department of Chemistry  
University of California  
Berkeley, CA 94720

Dr. Tom Scattergood  
NASA Ames Research Center  
Mail Stop 239-4  
Moffett Field, CA 94035

Dr. Greg Seab  
Virginia Inst. for Theoretical Astronomy  
University of Virginia  
Department of Astronomy  
P.O. Box 3818 University Station  
Charlottesville, VA 22903

Dr. David Simonelli  
Mail Stop 245-3  
NASA Ames Research Center  
Moffett Field, CA 94035

Dr. Rick E. Smalley  
Department of Chemistry  
Rice University  
Houston, TX 77001

Dr. Carol Stoker  
NASA Ames Research Center  
Mail Stop 245-3  
Moffett Field, CA 94035

Dr. Jill C. Tarter  
UC Berkeley and  
SETI Institute  
Mail Stop 229-8  
Moffett Field, CA 94035

Dr. Alexander G. Tielens  
Astronomy Department  
University of California  
Berkeley, CA 94720

Dr. Peter Tsou  
Jet Propulsion Laboratory  
4800 Oak Grove Drive  
Mail Stop 233-301  
Pasadena, CA 91109

Dr. Gale Ulrich  
Department of Chemical  
Engineering  
University of New Hampshire  
Durham, NH 03824

Dr. Nyle G. Utterback  
718 Willowglen Road  
Santa Barbara, CA 93105

Dr. G. J. Valero  
NASA Ames Research Center  
Mail Stop 245-6  
Moffett Field, CA 94035

Dr. John F. Wacker  
Battelle Pacific Northwest Lab  
300 Area/ Bldg 320  
P.O. Box 999  
Richland, WA 99352

Prof. Robert M. Walker  
McDonnell Center for the  
Space Sciences  
Washington University Box 1105  
St. Louis, MO 63130

**Dr. William Watson  
Dept. of Physics  
University of Illinois  
Urbana, IL 61801**

**Dr. Mike Werner  
Mail Stop 245-6  
NASA Ames Research Center  
Moffett Field, CA 94035**

**Dr. Ted Wydeven  
NASA Ames Research Center  
Mail Stop 239-4  
Moffett Field, CA 94035**

**STUDIES OF CARBON IN PRIMITIVE BODIES**

## CARBON IN PRIMITIVE METEORITES

John F. Kerridge  
University of California at Los Angeles

### INTRODUCTION

No meteorites are truly primitive, in the sense of being pristine collections of interstellar grains or solar-nebular condensates. Nonetheless, some chondritic meteorites have been so little altered by secondary processing that they are commonly termed "primitive" and it is almost a definition of such chondrites that they contain significant quantities of carbon. Most of that carbon is of apparently local, i.e., solar-system, origin but a proportion that ranges from trace, in some cases, to minor, in others, is believed to be exotic, i.e., of circumstellar or interstellar origin, and it is upon such material that we focus here. However, before delving into the observational record, we must discuss briefly the nature of the meteoritic samples and the techniques used to analyse them.

Essentially all the studies performed so far have involved those meteorites known as carbonaceous chondrites. The abundant, and therefore conspicuous, carbon that gives them their name is mainly combined with hydrogen, oxygen and nitrogen to form a variety of organic compounds, discussed in more detail later. Separating the exotic carbon from the much more abundant organic matter, as well as from the lithic constituents of the meteorites, has been difficult task. The experimental approach may be briefly described as follows.

A sample of the meteorite is first demineralised using a combination of hydrofluoric and hydrochloric acids, and then oxidised, typically with dichromate and perchloric acid, to remove the organic matter. A variety of grain-size and density fractions are then prepared, which may in turn be treated with certain reagents to remove specific minerals, e.g., phosphoric acid to dissolve spinel. The residue from such treatments consists predominantly of inorganic carbides and various forms of elemental carbon. It is commonly necessary to separate such carbonaceous species further from each other, usually by means of further oxidation, including use of oxygen plasma.

Further separation is possible during subsequent analysis. An exotic origin for a carbon fraction is inferred if either the carbon itself or an element associated with it is characterised by an anomalous isotopic composition. The first step in a conventional isotopic analysis involves either pyrolysing or combusting the carbon in a gas-extraction system. Such an extraction can be performed in steps, so that, in some cases, species can be separated from each other on the basis of their susceptibility to either pyrolysis or further oxidation. It is found, for example, that turbostratic carbon combusts at a lower temperature than diamond and fine-grained material before

coarse-grained. At each step, the gases evolved are collected and analysed in a mass spectrometer. Carbon itself is collected and analysed as carbon dioxide. Other gases collected and analysed are nitrogen and the noble gases, i.e., helium, neon, argon, krypton and xenon. In a few cases, hydrogen is evolved as water and is analysed isotopically after reduction to molecular hydrogen.

Recently, conventional mass spectrometry has been augmented in these studies by use of the ion microprobe. This permits isotopic, and elemental, analysis of much smaller particles than can be accommodated by conventional mass spectrometry, though at a cost of a modest reduction in precision. An ion-microprobe analysis can in principle be carried out on a particle while still embedded in a meteorite section, but in practice it is more convenient to concentrate the sample by prior demineralisation.

An anomalous isotopic composition, taken as diagnostic of an exotic origin, can be recognised in either of two ways. For elements with three or more isotopes, i.e., neon, argon, krypton and xenon, the test of anomalous behavior is whether or not the observed composition, after correction for the effects of radionuclide decay and cosmic-ray spallation, can be derived from the common terrestrial composition by mass-dependent fractionation. On a three-isotope plot, such as figure 1, mass-dependent fractionation follows a unique trajectory: deviation from that trajectory is the signature of anomalous behavior. For an element, such as carbon, nitrogen, hydrogen or helium, with only two stable isotopes, such a test is not possible. In such a case, the criterion for anomalous behavior is based on the magnitude of the observed departure from normal composition: if the deviation exceeds what can be attributed to plausible fractionation processes, the composition is regarded, at least tentatively, as anomalous.

Having determined that a carbonaceous component is isotopically anomalous and therefore probably exotic, it is obviously desirable to learn as much about its physical and chemical properties as possible. The ultimate objective of such a study is to characterise the astrophysical source of the component as fully as possible. Because the exotic components identified so far have in common a very fine grain size, the techniques available for characterisation are severely limited. Elemental analyses are restricted to the ion microprobe and various electron optical techniques, such as the electron microprobe, electron energy loss spectroscopy, analytical electron microscopy and energy-dispersive X-ray analysis using the scanning electron microscope. The same electron microscope techniques can be used to image the carbonaceous particles, and high-resolution transmission electron microscopy can also yield crystallographic information. Further crystal-structural data can be obtained by means of electron diffraction and laser Raman microprobe analysis. Because these different analyses are invariably performed on different splits of the same sample, it is not always possible to establish a rigorous one-to-one correspondence between, say, the particle imaged in the electron microscope and the noble-gas component measured in the mass spectrometer. Many of the associations described below are therefore inferential.

Before discussing the anomalies observed so far, it is desirable to expand somewhat on what we mean by normal. As noted above, this is largely based on terrestrial values but in some cases this choice of standard warrants elaboration.

#### WHAT IS NORMAL?

Because we are interested in identifying material that originated outside the solar system, we first need to establish the average solar system composition. Many tabulations of such "cosmic" abundances have been published, and for the great majority of the elements there is good evidence that those abundances are very reliable guides to the composition of the early solar system (e.g., ref. 1). However, for the five elements of most concern to us here, i.e., hydrogen, carbon, nitrogen, neon and xenon, a variety of factors make it desirable to discuss briefly their isotopic compositions in the early solar system.

##### Hydrogen

The terrestrial value of D/H is  $1.55 \times 10^{-4}$ . However, this value undoubtedly reflects substantial mass-dependent fractionation during accretion and early evolution of the earth. Because D is destroyed by nuclear reactions in the Sun, we cannot be guided by solar spectroscopy or solar-wind analysis. Our best estimates for the protosolar value come from observations of the present interstellar medium (ref. 2), spectroscopy of the atmospheres of the giant planets (ref. 3) and reconstructions based on the present ratio of  $^3\text{He}$  to  $^4\text{He}$  in the sun, much of the  $^3\text{He}$  having been derived from primordial D (ref. 4). These approaches all converge on a value for D/H of about  $2 \times 10^{-5}$  for the hydrogen from which the solar system was made (ref. 5), though there is good evidence that the H isotopes were inhomogeneously distributed in the solar nebula, so that a unique solar-system ratio may have no physical significance (ref. 3).

##### Carbon

The terrestrial value for  $^{12}\text{C}/^{13}\text{C}$  is about 89, and a closely similar value is also observed in the solar wind (ref. 6) so that we are probably justified in taking it as characteristic of the solar system as a whole. Considerable variability in this ratio is observed for the interstellar medium but the data are believed to be consistent with a value around 90 at 4.5 Gyr ago (ref. 7).

##### Nitrogen

A value of 276.8 characterises the  $^{14}\text{N}/^{15}\text{N}$  ratio in the terrestrial atmosphere. The solar ratio is not uniquely determined, values ranging from 247 to 360 having been inferred for the solar wind at different epochs (ref. 8). Bulk meteorite values range from 140 to

over 300, but because nitrogen is grossly depleted in most meteorites relative to its cosmic abundance, even bulk values could be significantly affected either by isotopic fractionation prior to, during or after agglomeration of the meteorite or by the presence of anomalous components. The composition of the interstellar medium is not helpful in this regard, and values for the giant planets are imprecise at this time, though the Galileo mission to Jupiter will greatly improve that situation. Nonetheless, as for hydrogen, it is quite plausible that there was no unique, solar-system-wide value for  $^{14}\text{N}/^{15}\text{N}$ , i.e., that primordial solar-system nitrogen consisted of more than one isotopic component, presumably of nucleogenetic origin (ref. 9).

## Neon

The isotopic composition of neon in the solar wind is precisely constrained by measurements made on the lunar surface (ref. 10). On a three-isotope plot, figure 2, all local, i.e., solar-system, values fall within the triangle bounded by "solar wind", "spallation" (resulting from cosmic-ray interactions) and a common meteoritic value, termed neon-A, of uncertain origin. Curiously, a composition equivalent to that of neon-A has been observed in solar flares (ref. 11). Because of the uncertain relationship between solar-wind neon and neon-A, it is not clear whether the solar nebula was homogeneous with respect to the neon isotopes. However, as will be seen, the magnitude of the observed anomaly vastly outweighs that uncertainty.

## Xenon

Defining a unique proto-solar-system value for the xenon isotopes, if in fact such a value existed, is not straightforward (ref. 12), but fortunately the plethora of xenon isotopes and the variety of astrophysical sites in which they are made have made anomalous xenon components fairly easy to recognise.

## ROSTER OF ANOMALOUS CARBON COMPONENTS

The exotic carbon components that have been recognised so far in meteorites, based on the anomalous isotopic composition of one or more elements, are listed in table 1, together with a summary of their properties. The reader is reminded that the association of such properties with specific phases is in some cases inferential and may therefore be subject to change in light of future results. In what follows, we discuss each component in some detail. The study of some of these components has had a long and contentious history, but here we shall focus mainly on the results of the most recent studies. For convenience, we shall employ the nomenclature advanced by Anders and his colleagues (e.g., ref. 13), as in table 1. Although the distribution of these components among different types of meteorites has not been fully mapped out, it seems likely that all of those listed in table 1 occur to a greater or less extent in all carbonaceous chond-

Name	Ca	C $\beta$	C $\delta$	Q	C $\epsilon$	Organic
Mineralogy		SiC	Diamond	Diamond?	SiC	
Anomaly	Ne-E(L)	Xe-S	Xe-III	Planetary	Ne-E(H)	Hydrogen
Enrichment	$^{22}\text{Ne}$	$^{130}\text{Xe}$	$^{124},^{136}\text{Xe}$	Heavy	$^{22}\text{Ne}$	D
Pyrolysis T $^{\circ}\text{C}$	700	1400	1000	variable	1200	300-1300
Combustion T $^{\circ}\text{C}$	600	1090	500	500	1000	250-450
$^{12}\text{C}/^{13}\text{C}$	66.5	36-56	92.5	92.5?	<12.7	85.3-90.8
$^{14}\text{N}/^{15}\text{N}$	<221	395-462	413	?	<358	252-278
D/H $\times 10^{-5}$			~20.3	?		?-62.4
Abundance ( $\mu\text{g/g}$ )	5	2	400	(as C $\delta$ ?)	7	2-3wt%
Grain size ( $\mu\text{m}$ )	1-10	0.03-0.2	0.0026	(as C $\delta$ ?)	0.03-1	
Probable source	nova	red giant	C: red giant (as C $\delta$ ?) Xe: supernova		nova?	molecular cloud(s) nebula? asteroid?

TABLE 1. Summary of the apparently exotic carbonaceous components identified so far in primitive meteorites. Based largely on ref. 13.

rites. Most studies have focused on Orgueil (type CI), Murchison (CM2) and Allende (CV3).

### Carbon Alpha

This component was recognised by the isotopically anomalous neon that it contains. This neon, termed neon-E, is essentially pure  $^{22}\text{Ne}$  (ref. 14), as can be seen in figure 2. Careful scrutiny of that figure will also reveal that neon-E is released in two distinct temperature ranges: one around 700 $^{\circ}\text{C}$  and one around 1000 $^{\circ}\text{C}$ . The neon released in these ranges is termed neon-E(L) and neon-E(H), respectively. Carbon alpha is the host phase of the neon-E(L). Both neon-E components are believed to have been produced by decay of  $^{22}\text{Na}$ , which has a half life of 2.6yr. Because of the shortness of that half life, decay must have taken place in the atmosphere of the star in which the  $^{22}\text{Na}$  was synthesised. Enrichment of carbon alpha in both  $^{13}\text{C}$  and  $^{15}\text{N}$  points towards that star having been a nova (ref. 13). Selective filtration indicates that carbon alpha has a grain size between 1 and 10 micrometers (ref. 13), thereby supplying a provisional measure of the grain growth achieved in nova outflows. Carbon alpha has not been well characterised but its low density, below 2.4g/cm $^3$ , hints at a form of elemental carbon.

### Carbon Beta

The signature of carbon beta is a xenon component that matches with remarkable accuracy the composition predicted to be produced by the s-process (nucleosynthesis that proceeds by the capture of neutrons on a time scale that is long compared with the half lives of the species being produced). This match between theory and observation is illustrated in figure 3 (ref. 15). Physically, carbon beta has been identified as silicon carbide with a grain size in the range 0.03 to

0.2 micrometers (ref. 16). The silicon and the carbon are both substantially enriched in the heavy isotopes: the  $^{30}\text{Si}/^{28}\text{Si}$  ratio, not given in table 1, is up to 5% higher than the terrestrial value (ref. 17). Nitrogen, whose physical state in carbon beta is unknown, is heavily depleted in  $^{15}\text{N}$  ( $^{14}\text{N}/^{15}\text{N}$  as high as 462). An origin for carbon beta in a red giant star has been proposed (ref. 13).

#### Carbon Delta

The presence of this component is also recognised by anomalous xenon, as shown in figure 4. The host phase of this xenon appears to be diamond with a grain size of only 10s of angstroms (ref. 18). Perhaps because of this fine grain size with the consequent large proportion of surficial carbon, as much as 25% of carbon delta appears to behave as amorphous material (ref. 19). At least in the acid-resistant residues studied so far, the tiny crystallites occur as aggregates measuring up to about 0.5 micrometers in diameter, figure 5 (ref. 21). As can be seen in figure 4, the anomalous xenon consists of two components, one enriched in the heavy isotopes (H), the other in light (L) (ref. 13). These components are closely coupled and it has not proved possible to separate them experimentally. The nitrogen that accompanies xenon-HL is highly enriched in  $^{14}\text{N}$ , table 1, but its  $^{12}\text{C}/^{13}\text{C}$  ratio is 92.5, remarkably close to the "local" value (ref. 13). One model to explain the properties of carbon delta postulates condensation of the diamond in the atmosphere of a red giant, at which time freshly synthesised nitrogen was also incorporated into the diamond structure by substitution for carbon. The red giant subsequently developed into a supernova, creating xenon-L in neutron-poor regions and xenon-H in neutron-rich zones. The resulting mixture was explosively ejected from the supernova, overtook the relatively slowly moving diamond grains, and became implanted in them (ref. 13 and 20). An alternative model (ref. 19) invokes melting of interstellar carbonaceous grains by supernova shock waves followed by nucleation of diamonds from the transiently high-pressure liquid.

#### Q

In a strict sense, the component termed Q is not anomalous; it is characterised by the presence of a noble-gas population that seems to be prevalent on planetary objects in the solar system, figure 6. However, these noble gases are closely associated in nature with xenon-HL, though readily separated from it in the laboratory, so that a common host phase seems possible. In fact, it has been suggested (ref. 21) that Q-gas is trapped in pores at the surfaces of carbon delta grains. This trapping is postulated to have taken place in the solar nebula and to have been accompanied by substantial fractionation, resulting in the observed systematic compositional difference between Q-gas and solar gas (ref. 21 and 22).

#### Carbon Epsilon

As noted earlier, neon-E has a bimodal release as a function of temperature. The host of the higher-temperature fraction is another silicon carbide component, termed carbon epsilon, figure 7. In many

respects, it resembles carbon beta but possesses enough distinguishing features to identify it as a separate phase. Thus, although both are enriched in the heavy isotopes of silicon and carbon and the light isotope of nitrogen, carbon epsilon is characterised by much greater enrichments than carbon beta (ref. 17). In addition, the silicon-isotopic data for carbon epsilon require a minimum of three nucleogenetically distinct components (ref. 17). Although the origins of those silicon components are not yet clear, the other isotopic properties of carbon epsilon indicate a nova origin, as for carbon beta.

### Organic Matter

The components discussed so far have been present, even in the most primitive chondrites, at only trace levels. By contrast, organic carbon is a major component in both CI and CM chondrites, amounting to about 3wt% and 2wt%, respectively (ref. 23). At the molecular level, this organic matter consists of a complex mixture of a wide variety of organic compounds (ref. 24). The origin of this material is disputed: it seems likely that more than one process contributed to the melange currently present in the meteorites. Isotopically, the organic carbon is mundane, in fact it is not inconceivable that it represented the major source of carbon for the terrestrial planets. Similarly, the organically combined nitrogen, although it exhibits significant isotopic variability, does not fall outside the range of plausible fractionation by possible solar-system processes, though the uncertainty about the protosolar  $^{14}\text{N}/^{15}\text{N}$  ratio reduces the force of this argument.

Where the organic matter manifests its exotic character is in the isotopic composition of its hydrogen. The detailed distribution of the hydrogen isotopes among the different organic constituents is complex and not fully understood at this time. However, existing data are consistent with all meteoritic organic molecules being enormously enriched in deuterium with respect to protosolar hydrogen (e.g., ref. 25 and 26). These enrichments exceed the fractionating capacity of any known solar-nebular or planetesimal processes, so that they are commonly attributed to the isotopic fractionations associated with ion-molecule reactions taking place at very low translational temperatures (ref. 5, 27 and 28). Such reactions are believed to be responsible for the extremely large deuterium enrichments observed in gas-phase molecules of dense interstellar molecular clouds (ref. 29), leading to the conclusion that some fraction of the organic hydrogen in meteorites originated in such interstellar clouds (ref. 30). Exactly in what form this anomalous hydrogen traversed interstellar space and how it entered the solar nebula and became combined with apparently local carbon to form organic molecules represent problems that are not fully understood. Preservation of the interstellar deuterium signature in the face of abundant low-deuterium hydrogen in the solar nebula constitutes a serious constraint on models that attribute the production of meteoritic organic matter to catalysed gas-phase reactions in the nebula (e.g., ref. 24).

## CONCLUSIONS

The components discussed above by no means exhaust the list of carbonaceous phases present in meteorites but include all those for which an extrasolar signature has been reliably observed. Two other, probably local, carbonaceous components of meteorites deserve mention, however. Inorganic carbonates are common constituents of CI and CM carbonaceous chondrites and it has been suggested that these might also be of interstellar origin (ref. 31). However, their compositions, morphology and petrology show clearly that they were formed by aqueous activity on asteroidal parent bodies (ref. 32).

In addition, poorly graphitised (or turbostratic) carbon (PGC) occurs in many ordinary and carbonaceous chondrites together, in most cases, with amorphous carbon. In ordinary chondrites, such material is also commonly associated with fine-grained metallic iron (ref. 33). Well-ordered graphite appears to be very rare in these primitive meteorites. Textural relations suggest that many, if not all, chondritic occurrences of PGC resulted from dehydrogenation of kerogen-like organic matter (ref. 33 and 34). Such kerogen-like material is the dominant constituent of the organic matter in carbonaceous chondrites (ref. 24).

Nuth (ref. 35) has pointed out that the extreme scarcity of graphite in primitive meteorites that contain measurable amounts of interstellar carbon in other, less refractory forms, suggests strongly that graphite is similarly rare in the interstellar medium and that spectral features that have commonly been attributed to graphite are probably due to other species. He also inferred that grain lifetimes in the interstellar medium are considerably longer than the  $10^8$  yr of most generally accepted models.

Clearly, the study of exotic carbon preserved in meteorites has been informative about sites of nucleosynthesis, processes of nucleation and growth of grains in stellar outflows, grain survival in the interstellar medium, and many other topics of astrophysical significance. Much more work, particularly of an interdisciplinary nature remains to be done, however.

## REFERENCES

1. Anders, E.; and Ebihara, M.: Solar-system abundances of the elements. *Geochim. Cosmochim. Acta*, vol. 46, 1970, pp. 2363-2380.
2. Vidal-Madjar, A.; and Gry, C.: Deuterium, helium, and the Big-Bang nucleosynthesis. *Astron. Astrophys.*, vol. 138, 1984, pp. 285-289.
3. Owen, T.; Lutz, B. L.; and de Bergh, C.: Deuterium in the outer Solar System: evidence for two distinct reservoirs. *Nature*, vol. 320, 1986, pp. 244-246.

4. Geiss, J.; and Reeves, H.: Cosmic and solar system abundances of D and  $^3\text{He}$ . *Astron. Astrophys.*, vol.18, 1972, pp.126-132.
5. Geiss, J.; and Reeves, H.: Deuterium in the solar system. *Astron. Astrophys.*, vol.93, 1981, pp.189-199.
6. Kerridge, J.F.; and Kaplan, I.R.: Sputtering: its relationship to isotopic fractionation on the lunar surface. In: *Proc. Lunar Planet Sci. Conf. 9th.*, Pergamon Press, 1978, pp.1687-1709.
7. Wannier, P.G.: Nuclear abundances and evolution of the interstellar medium. *Ann. Rev. Astron. Astrophys.*, vol.18, 1980, pp.399-437.
8. Kerridge, J.F.: Secular variations in composition of the solar wind: evidence and causes. In: *Proc. Conf. Ancient Sun*, Pergamon Press, 1980, pp.475-489.
9. Geiss, J.; and Bochsler, P.: Nitrogen isotopes in the solar system. *Geochim. Cosmochim. Acta*, vol.46, 1982, pp.529-548.
10. Geiss, J.; Buehler, F.; et al.: Solar wind composition experiment. In: *Apollo 16 Prelim. Sci. Rep.*, NASA SP-315, 1972, section 14, pp.1-10.
11. Mewaldt, R.A.; Spalding, J.D.; and Stone, E.C.: A high-resolution study of the isotopes of solar flare nuclei. *Astrophys. J.*, vol. 280, 1984, pp.892-901.
12. Pepin, R.O.; and Phinney, D.: Components of xenon in the solar system. Preprint, 1978, 186pp.
13. Anders, E.: Circumstellar material in meteorites: noble gases, carbon and nitrogen. In: *Meteorites and the Early Solar System*, Univ. Arizona Press, 1988, in press.
14. Eberhardt, P.; Jungck, M.H.A.; Meier, F.O.; and Niederer, F.: A neon-E rich phase in Orgueil: results obtained on density separates. *Geochim. Cosmochim. Acta*, vol.45, 1981, pp.1515-1528.
15. Srinivasan, B.; and Anders, E.: Noble gases in the Murchison meteorite: possible relics of s-process nucleosynthesis. *Science*, vol. 201, 1978, pp.51-56.
16. Bernatowicz, T.; Fraundorf, G.; et al.: Evidence for interstellar SiC in the Murray carbonaceous meteorite. *Nature*, vol.330, 1987, pp.728-730.
17. Zinner, E.; Tang, M.; and Anders, E.: Large isotopic anomalies of Si, C, N and noble gases in interstellar silicon carbide from the Murray meteorite. *Nature*, vol.330, 1987, pp.730-732.
18. Lewis, R.S.; Tang, M.; et al.: Interstellar diamonds in meteorites. *Nature*, vol.326, 1987, pp.160-162.

19. Blake, D.; Freund, F.; et al.: The nature and origin of interstellar diamond. *Nature*, 1988, in press.
20. Clayton, D.D.: Some key issues in isotopic anomalies: Astrophysical history and aggregation. In: *Proc. Lunar Planet. Sci. Conf. 12th.*, Pergamon Press, 1981, pp.1781-1802.
21. Zadnick, M.G.; Wacker, J.F.; and Lewis, R.S.: Laboratory simulation of meteoritic noble gases. II. Sorption of xenon on carbon: Etching and heating experiments. *Geochim. Cosmochim. Acta*, vol.49, 1985, pp.1049-1059.
22. Swindle, T.D.: Trapped noble gases in meteorites. In: *Meteorites and the Early Solar System*, Univ. Arizona Press, 1988, in press.
23. Kerridge, J.F.: Carbon, hydrogen and nitrogen in carbonaceous chondrites: abundances and isotopic compositions in bulk samples. *Geochim. Cosmochim. Acta*, vol.49, 1985, pp.1707-1714.
24. Hayatsu, R.; and Anders, E.: Organic compounds in meteorites and their origins. *Topics Curr. Chem.*, vol.99, 1981, pp.1-37.
25. Epstein, S.; Krishnamurthy, R.V.; et al.: Unusual stable isotope ratios in amino acid and carboxylic acid extracts from the Murchison meteorite. *Nature*, vol.326, 1987, pp.477-479.
26. Kerridge, J.F.; Chang, S.; and Shipp, R.: Isotopic characterisation of kerogen-like material in the Murchison carbonaceous chondrite. *Geochim. Cosmochim. Acta*, vol.51, 1987, pp.2527-2540.
27. Robert, F.; and Epstein, S.: The concentration and isotopic composition of hydrogen, carbon and nitrogen in carbonaceous meteorites. *Geochim. Cosmochim. Acta*, vol.46, 1982, pp.81-95.
28. Kerridge, J.F.: Isotopic composition of carbonaceous-chondrite kerogen: evidence for an interstellar origin of organic matter in meteorites. *Earth Planet. Sci. Lett.*, vol.64, 1983, pp.186-200.
29. Smith, D.; Adams, N.G.; and Alge, E.: Some H/D exchange reactions involved in the deuteration of interstellar molecules. *Astrophys. J.*, vol.263, 1982, pp.123-129.
30. Kolodny, Y.; Kerridge, J.F.; and Kaplan, I.R.: Deuterium in carbonaceous chondrites. *Earth Planet. Sci. Lett.*, vol.46, 1980, pp.149-158.
31. Tomeoka, K.; and Buseck, P.R.: A carbonate-rich, hydrated, interplanetary dust particle: possible residue from protostellar clouds. *Science*, vol.231, 1986, pp.1544-1546.
32. Fredriksson, K.; and Kerridge, J.F.: Carbonates and sulfates in CI chondrites: formation by aqueous activity on the parent body. *Meteoritics*, vol.23, 1988, pp.35-44.

33. Brearley, A.J.; Scott, E.R.D.; and Keil, K.: Carbon-rich aggregates in ordinary chondrites: transmission electron microscope observations of Sharps (H3) and Plainview (H, regolith breccia). *Meteoritics*, vol.22, 1987, pp.338-339.
34. Rietmeijer, F.J.M.; and Mackinnon, I.D.R.: Poorly graphitized carbon as a new cosmo thermometer for primitive extraterrestrial materials. *Nature*, vol.315, 1985, pp.733-736.
35. Nuth, J.A.: Meteoritic evidence that graphite is rare in the interstellar medium. *Nature*, vol.318, 1985, pp.166-168.
36. Hunten, D.M.; Pepin, R.O.; and Owen, T.C.: Planetary atmospheres. In: *Meteorites and the Early Solar System*, Univ. Arizona Press, 1988, in press.

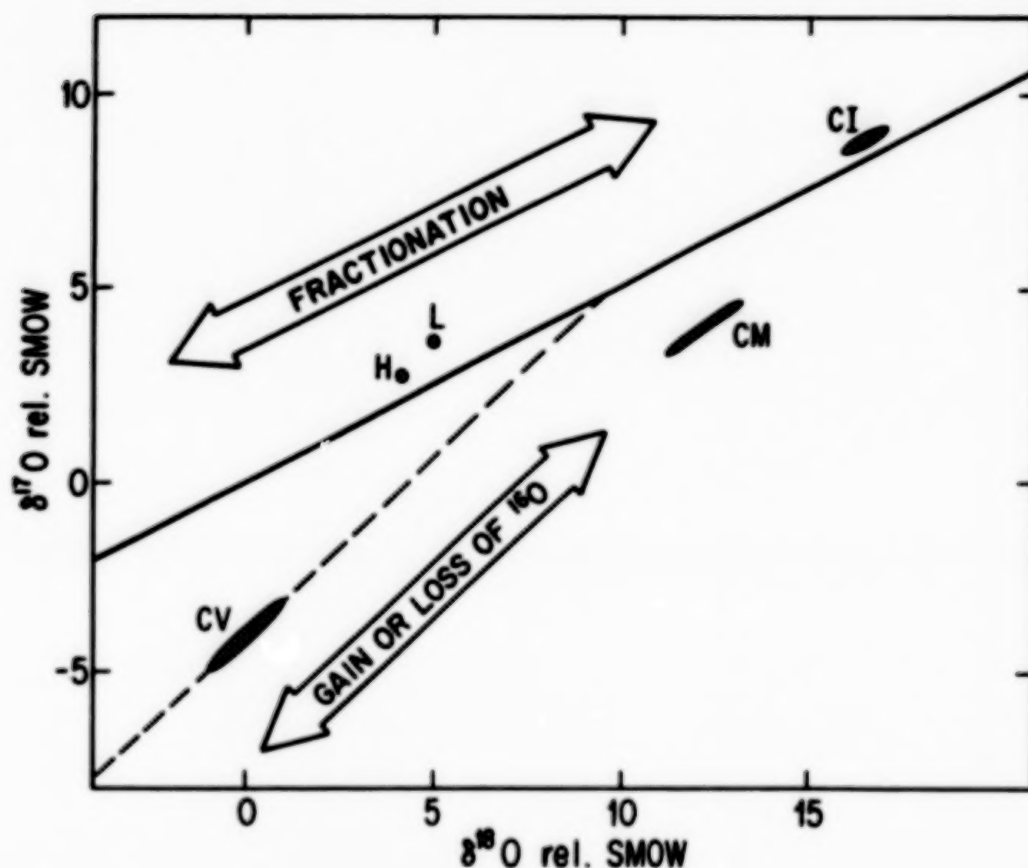


Figure 1.— Three-isotope plot for the oxygen isotopic system. The ratio  $^{17}\text{O}/^{16}\text{O}$  is plotted against  $^{18}\text{O}/^{16}\text{O}$  for several groups of chondrites. Ratios are expressed as deviations (delta units) in parts per  $10^3$  relative to the ratios for Standard Mean Ocean Water. On such a plot, mass-dependent fractionation defines a line with a slope close to 0.5, as shown by the solid line, which is the locus of all data for terrestrial samples. Deviations from that line, as exhibited by the chondritic data, cannot be explained by such fractionation but apparently require addition or subtraction of one or more anomalous components, such as the hypothetical pure  $^{16}\text{O}$  one illustrated. Data from the laboratory of R. N. Clayton.

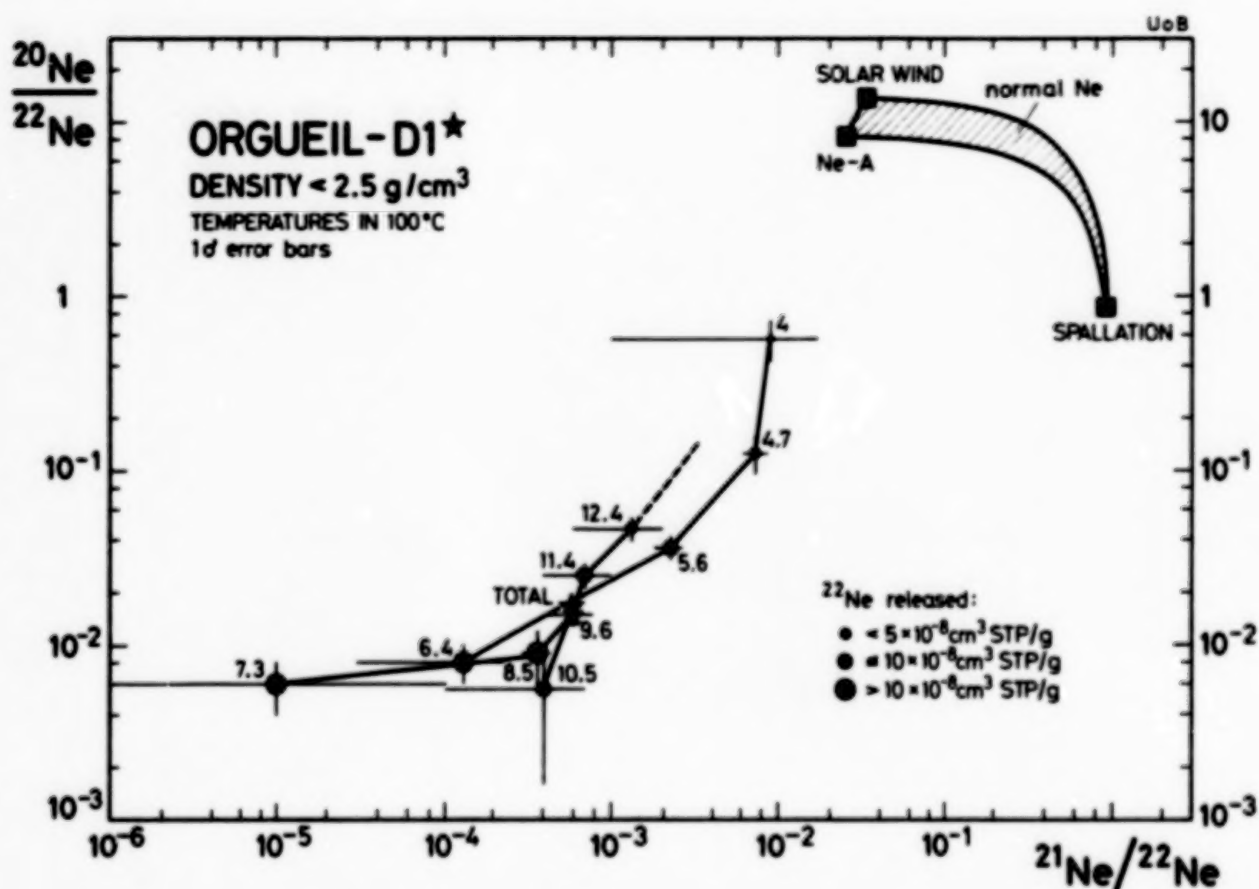


Figure 2.— Three-isotope plot for Ne extracted from a low-density fraction separated from the Orgueil carbonaceous chondrite. Note the logarithmic scale and the enormous enrichment of the D1 fraction in  $^{22}\text{Ne}$ , which amounts to more than 98% of the Ne released. Data from the laboratory of P. Eberhardt. Figure from Anders (1988).

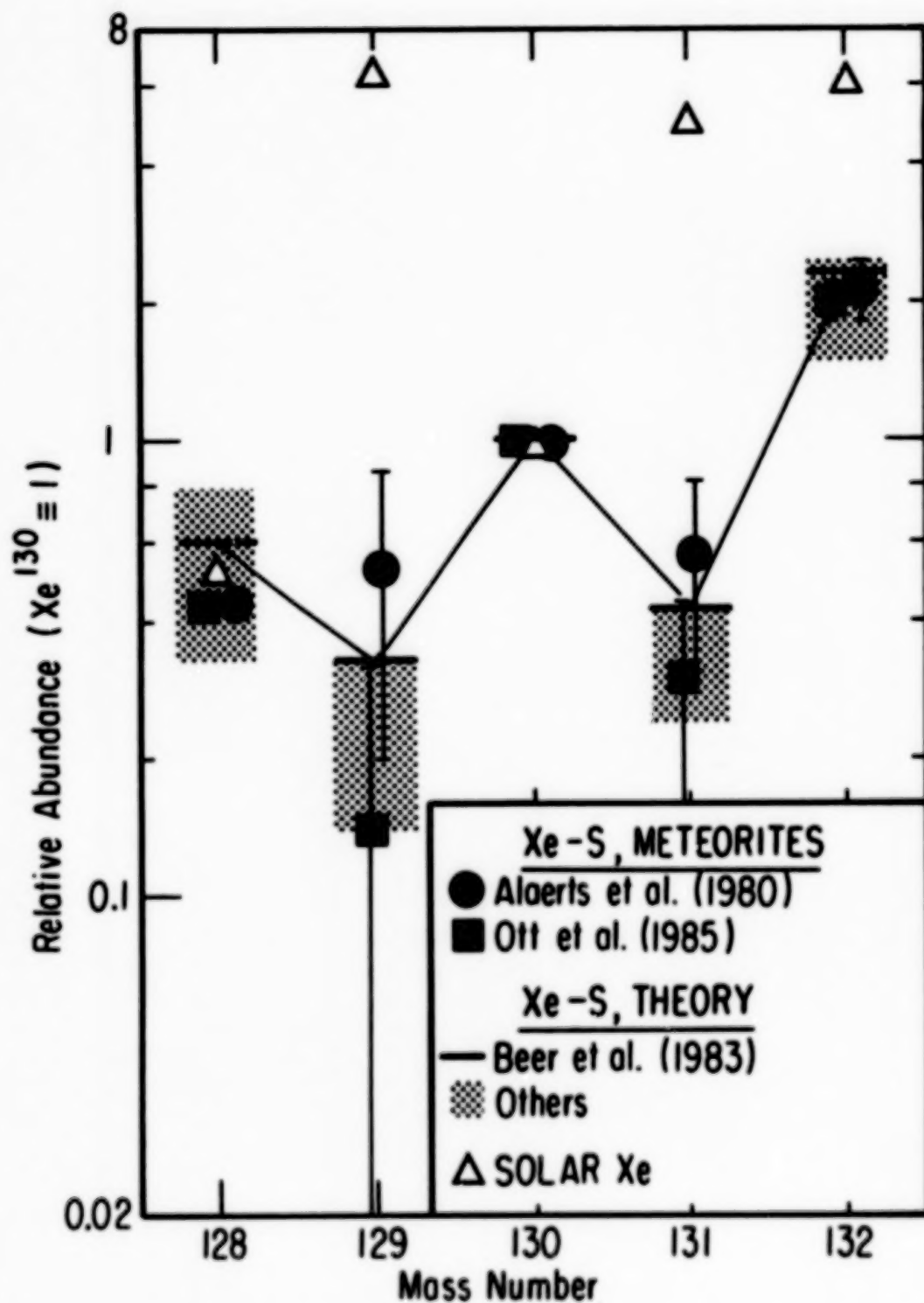


Figure 3.— The isotopic composition of the meteoritic Xe-S component, compared with the theoretical yield of s-process nucleosynthesis and with solar Xe. The match with s-process theory is excellent. Figure from Anders (1988).

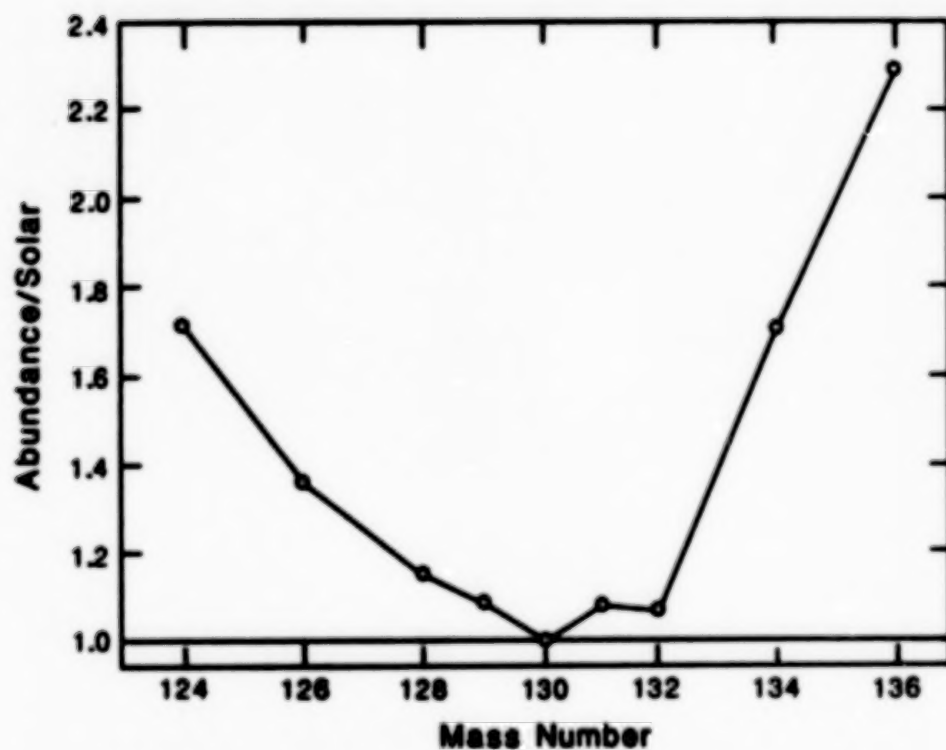


Figure 4.— The isotopic composition of a meteoritic Xe component enriched in both heavy and light isotopes and therefore known as Xe-HL.



Figure 5.— Bright-field (upper) and dark-field (lower) images of diamond in a C delta residue from the Allende meteorite. Inset diffraction pattern can be indexed as diamond. Dark-field image obtained using a portion of the (111) powder ring indicated in the diffraction pattern. Bright irregular regions in dark-field micrograph correspond to 5-70Å crystallites of diamond which are in proper orientation for diffraction. Courtesy of David Blake.

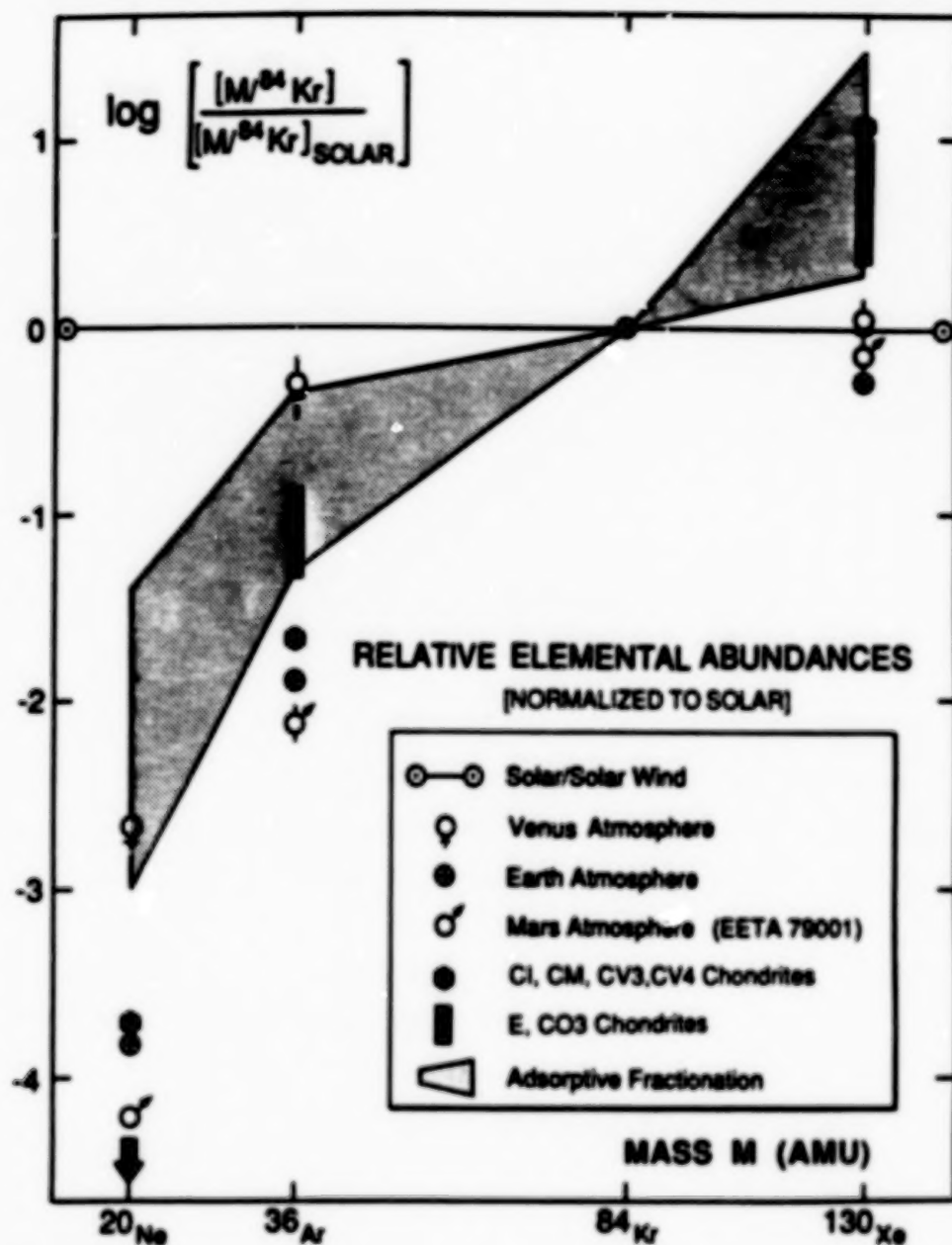


Figure 6.— Noble-gas abundance ratios (normalized to Kr) in atmospheres of terrestrial planets and in volatile-rich meteorites. Despite differences in detail, those inventories, loosely categorized as "planetary gas," have in common an enrichment in the heavy gases relative to solar composition. In primitive chondrites, planetary gas is sometimes termed "Q gas." Figure from Hunten, Pepin and Owen (ref. 36).



Figure 7.— Transmission electron micrograph of a SiC particle, identified as Carbon Epsilon, from the Murray carbonaceous chondrite. The scale bar measures 2000Å. Attached to the SiC are some fine-grained diamonds and round blobs of a Si-oxide phase. Micrograph courtesy of Thomas Bernatowicz and Ernst Zinner.

## CARBON IN COMET DUST

D.E. Brownlee

University of Washington

Comets are small, cold bodies that are likely to contain chemical, mineralogical and isotopic records of conditions and processes that existed in the outer regions of the solar nebula as well as interstellar and circumstellar environments that predate the planetary system. Carbon and carbon compounds in comet dust are of particular importance because of the rather broad and interesting range of processes that can form and alter solid carbonaceous matter. Many of the compounds may have formed by nonequilibrium processes such as catalysis and radiation processing. Carbon in cometary "solids" could range from refractory phases like elemental carbon and silicon carbide to comparatively volatile polymers. Detailed knowledge of the abundance, distribution and chemical forms of carbon in comet dust is fundamental to an understanding of the origin and evolution of comets.

The only direct measurements of carbon in comet dust came from the three particle impact mass spectrometers flown to Halley by the Giotto and Vega spacecraft [1,2]. These instruments measured thousands of mass spectra from individual micron and submicron particles. The detected particles fall into three major groups; pure silicate, mixtures of C, O, Mg, Si and Fe, and pure low atomic weight elements (the CHON particles [3]). The nature of carbon in Halley dust and its association with other elements are discussed in this volume by Ben Clark. The present paper will concentrate on the association of Halley particle results with data from existing meteoritic materials that can be analyzed in the laboratory. Comet samples must exist in present collections of meteoritic materials and the Halley results provide clues for identifying them. Although it is not presently possible to positively identify cometary meteorites or cometary interplanetary dust (IDP) samples, it is possible to determine which materials are similar to Halley dust and which ones are distinctly unlike Halley. The properties of these existing "Halley-compatible" samples provide insight into the possible properties of cometary material. Positive identification of meteoritic comet samples or direct samples returned from a comet nucleus would of course revolutionize our ability to study carbonaceous matter in comets. Modern analytical techniques are very powerful and it is possible to perform elemental, chemical, mineralogical and even limited isotopic analysis on micron-size particles.

The bulk composition of Halley dust appears to be chondritic [4,5] for the majority of elements but uncertainties in conversion of experiment data to element ratios does not allow association of the bulk heavy element composition with any particular chondrite class. Jessberger *et al.* [4] estimate that the abundances of Na, Mg, Al, Si, S, Ca, and Mn in Halley are within a factor of two of their relative abundances in CI chondrites. The carbon and nitrogen abundances in the Halley material appear to be much higher than in any of the chondrites. Jessberger *et al.* estimate that the C/Mg and N/Mg in Halley dust are enhanced relative to CI by factors of 6 to 12 and 6 to 8 respectively. These numbers are uncertain because ion production in the mass spectrometers is not well understood, but it is reasonably certain that the carbon and nitrogen abundances in Halley dust are much higher than in any chondrite. The clearest indication of this is the finding that roughly a third of the particles are dominated by C, H, O and N [5]. This result is rather insensitive to uncertainties in ion production. If the carbon and nitrogen in Halley dust are in stable forms capable of surviving storage in the interplanetary medium and meteorite parent bodies, then the high abundance of these elements implies that Halley dust is different from all chondritic meteorites. Carbon and nitrogen are strongly fractionated among the chondrite groups, varying by a factor of 100 between the CI and ordinary chondrites but in most cases they are minor elements [6]. The atomic abundance of carbon in CI's approaches that of silicon but this is still significantly smaller than found in Halley. Chondrites do not have high carbon abundances and their lack of appreciable porosity rules out the possibility that they could

have contained transient carbon that was lost solely by gentle sublimation. Production of rocks from Halley dust that would even crudely approximate the elemental composition and structure of chondrites would require loss of carbon and nitrogen followed by compaction to solid, nonporous matter.

Carbon and nitrogen are more abundant in Halley dust than in chondrites but it is not presently known if they are more abundant than in interplanetary dust. There are experimental difficulties with carbon analysis of small particles and the first carbon determinations are just being published. Early measurements indicate that at least some of the collected particles have high carbon abundances that are intermediate between CI and the estimated abundance in Halley [7,8].

In addition to bulk elemental composition, the compositional variability seen in the Halley data provides a means of investigating similarities between Halley and meteoritic material. The Halley data shows considerable variation among the elemental composition of submicron particles. If Halley dust is dominated by mineral grains then the observed variability suggests that the fundamental grain size is in the submicron to micron range. Even with uncertainties in instrument calibration, the observed compositional variations provide a powerful method for comparing Halley with meteoritic materials. The distribution of Fe, Mg, and Si in the Halley material is distinctly different from that seen in any of the carbonaceous chondrites or in matrix of the unequilibrated ordinary chondrites at the micron and submicron size scale [9]. A straight forward distinction is that Halley contains abundant submicron grains of pure Mg silicates and Fe rich material while the meteorites do not. The meteorites are more homogeneous at the submicron scale than Halley. In a way this is evidence that Halley is more "primitive" than the chondrites. The term primitive is used here in the sense that Halley solids could be modified by alteration processes to produce the chondrites, which are coarser grained and more homogeneous, but it is unlikely that chondrites could be modified by simple processing to form Halley dust, a more complex and heterogeneous material.

The dispersion of abundances in Halley dust is also distinct from some of the hydrated types of interplanetary dust samples collected in the stratosphere. Interplanetary particles can be grouped into two major mineralogical classes, those dominated by hydrated silicates and those that are composed entirely of anhydrous phases [10,11,12]. A subclass of the hydrated IDP's, predominately composed of serpentine, is very similar to the carbonaceous chondrites. Like the C chondrites their fine scale compositional variability is much less than is seen in the Halley data. For example less than 1% of the micron grains in the serpentine particles are Mg silicates, a factor of ten lower frequency than seen in Halley. A second subclass of hydrated particles contain smectite minerals. These particles are more heterogeneous than the serpentine IDP's and the C chondrites but are not the best "match" to Halley. The compositional dispersion of the major elements in Halley best resembles that seen in the anhydrous interplanetary particles. This particle type is also the most porous meteoritic material and for this reason it has previously been speculated that the anhydrous porous particles might be cometary [13]. The anhydrous IDP's are open aggregates of rather equidimensional submicron grains of silicates, sulfides and carbonaceous matter. Like Halley dust the major submicron components are pure silicate, mixed silicate and carbonaceous matter and pure carbonaceous matter.

The tentative best "match" between Halley dust and the anhydrous class of interplanetary dust, gives special importance to laboratory studies of carbon that have been performed on particles in this group. Transmission electron microscope (TEM) studies of microtome thin sections of these particles show that carbon exists as grains of pure low atomic weight material, "tar balls" (mixtures of  $<1000\text{\AA}$  silicates, metal, sulfides and carbon) and grain coatings [10,13]. The chemical forms and quantitative distribution of carbon in these particles are poorly known but they are subjects of intense investigation at the present time. A question of major interest is whether or not the submicron lumps of organic matter in these particles resemble the CHON particles seen at Halley. This will be partly answered when C, N and O measurements are made on submicron grains in the laboratory samples. As viewed in the electron microscope, most of the low atomic weight grains appear to be amorphous and it is evident that the bulk

of the total carbon in typical particle types is either amorphous or highly disordered. Although 3.4Å fringes from graphite are seen, they are rare and an important result from examination of typical interplanetary particles is the observation that well crystallized graphite is only a trace constituent. Rare IDP's do contain abundant well ordered elemental carbon. TEM observations on two hydrated particles revealed that carbon-2H (lonsdaleite) was an important constituent [14]. Lonsdaleite is metastable and its existence places constraints of the thermal processing of the particles. Reitmeijer and Mackinnon [14] suggest that the carbon-2H detected in the particles was produced by hydrous pyrolysis below 350°C. The abundant elemental and polymeric carbon in anhydrous particles has been studied by laser Raman spectroscopy of individual particles. The shape of the carbon Raman bands agree with the TEM studies showing that well ordered graphite is not a significant phase [15]. The shape of the first order Raman lines provides information on the sizes of aromatic domains. Many of the particles have domain sizes smaller than 25Å showing that they are less ordered than commercial "glassy" amorphous carbon. The Raman bands are similar in position and strength to interstellar IR features that have been attributed to molecular-size polycyclic aromatic hydrocarbons (PAH's) [15]. The Raman studies have also detected luminescence that is similar to excess red emission in some astronomical sources that has been attributed to PAH's or hydrogenated amorphous carbon.

The IDP's contain a several carbon compounds other than polymers. A minor but unique constituent IDP's is epsilon FeNi carbide, a mineral not found elsewhere in nature [16,17]. The carbide is seen as micron and smaller grains occurring in association with with amorphous carbon, metal and magnetite. The existence and distribution of this carbide is evidence for formation by heterogeneous catalysis from CO on grain surfaces. The amorphous carbon adjacent to the carbide may be a product of Fischer-Tropsch-like surface catalysis reactions also evolving CO. Fegley [18] has estimated that F-T reactions could have occurred on submicron nebular grains at temperatures as low as 440K. Another minor carbon bearing phase in IDP's is Mg, Ca carbonate [19], a phase also seen in carbonaceous chondrites. A 6.8µm absorption feature seen in the IR spectra of hydrated particles has been demonstrated, by electron microscopy and chemical etching, to be carbonate [20]. The IDP absorption may be related to the 6.8µm feature seen in young stellar objects.

One of the most important findings in IDP studies has been the discovery of small regions within particles that have very large D/H excesses [21]. The highest observed enhancement is 10,000 per mil excess D/H, a value that exceeds the highest D/H seen in chondrites and approaches the level of fractionation observed in molecular clouds. The high degree of fractionation seen in molecular clouds is widely believed to be the result of ion-molecule reactions [22]. The deuterium rich material in IDP's is contained in micron or smaller "nuggets" giving the particles a highly heterogeneous and unequilibrated distribution of D/H. Although there is a general positive correlation of D with C/O it is not a precise correlation and it has not been proven that the high D anomaly is carried by carbon rich matter [21]. The lack of correlation of excess D with OH is however strongly suggestive that enhanced deuterium is associated with carbonaceous matter [23].

The observed properties of interplanetary dust provide insight, but perhaps features that are not observed provide some of most important constraints on the nature of carbon in cometary dust. Hundreds of IDP's have been studied in the laboratory and surely the most common types of cometary grains have been seen. The previously discussed abundance of amorphous carbon and scarcity of well ordered graphite strongly implies that graphite is not an important phase in comets. The complex distribution of carbon implies that carbon in comets is not a simple interstitial filling material as one might expect if it had been extensively mobilized on the parent body. Carbon also does not form thick mantles on silicate grains similar to those proposed by Greenberg [24] for interstellar and cometary grains. Grains do have carbonaceous coatings but typical coatings are thin, in the 100Å thickness range or less. With pure carbonaceous grains, "tar balls" and grain coatings the distribution of carbon is more complex than predicted by the model. While the collected samples do not match a literal interpretation of the Greenberg model there are possible grounds for reconciliation. One possibility is that comet dust does have a

core-mantle structure in the comet but the collected samples are modified either in the comet, in the interplanetary medium or during entry into the atmosphere. Another possibility is that instead of a simple core mantle structure, comet grains actually are mixtures of many smaller silicate cores imbedded in a carbonaceous matrix. This type of plum-pudding structure would better match the "tar balls" seen in anhydrous IDP's.

Taking into account the interplanetary dust data and the Halley results it is interesting to speculate on the true nature of carbon in Halley-like comets. The author's best conjecture is that the Halley dust is very similar to many of the anhydrous IDP's. A comet made from this material would be an ice-dust conglomerate with ice filling many of the voids between the largely submicron silicate grains. The material would be very fine grained, heterogenous at the submicron scale but rather homogenous for scales greater than 10 $\mu$ m. Like the IDP's the ice-dust material would be black even for pieces as small as 3 $\mu$ m. Some carbon would be in volatile constituents of ice phases but a substantial fraction would be less volatile and remain as a component of the dust. Elemental carbon, carbides, and some polymeric material would permanently remain with the silicates but intermediate volatility compounds would sublime on time scales of days to millennia. Evidence for the presence of intermediate material comes from the observed CN jets [25] and grain fragmentation [26]. Carbonates and hydrated silicate minerals would be rare and the IR spectral features of these minerals should be absent or at least minor. The silicates would be anhydrous phases that include well preserved high temperature minerals such as pure magnesium pyroxene and olivine. The silicates have not interacted with water in the parent body or via gas phase reactions in the nebula and is likely that carbon compounds would also not be affected by such processes. Like carbonaceous chondrites the cometary solids would contain minor amounts of diamond, silicon carbide and other carbon bearing phases that preserve large isotopic effects that predate the formation of the solar system.

There is an important synergism between the laboratory studies of collected samples and astronomical data from comets and interstellar grains. However to fully interpret results however there must be convincing methods for associating a particular class or classes of meteoritic material with comets. Ultimately this will be done by direct comet sample return such as the Rosetta mission under development by ESA. At the present time the only "links" that can be made involve comparison with sample properties and measurable properties of comets. Unfortunately there is at present no known unique property of cometary dust that allows its absolute identification in the laboratory. The results from Halley encounters and observations do however provide much new information on cometary grains. The Halley grain compositions, density, size distribution and scattering properties all provide a basis for future investigations. Other Halley properties such as the presence of polyoxymethylene [27] and the 3.4 $\mu$ m emission feature [28] could play key roles for making convincing links in the future.

#### References

1. Kissel, J. *et al.* Composition of comet Halley dust particles from Giotto observations, *Nature* **321**, pp 280-282 (1986).
2. Kissel, J. *et al.* Composition of comet Halley dust particles from Vega observations, *Nature* **321**, pp 336-337 (1986).
3. Clark, B., Mason, L. W., and Kissel, J., Systematics of the "CHON" and other light-element particles populations in comet Halley, ESA SP-250, pp 353-358 (1986).
4. Jessberger, E. K., Christoforidis, A., and Kissel, J., Aspects of the major element composition of Halley dust, *Nature* **332**, pp 691-695 (1988).
5. Langevin, J., Kissel, J., Bertaux, J-L, and Chassefiere, E., First statistical analysis of 5000 mass spectra of cometary grains obtained by PUMA1 (VEGA 1) and PIA (GIOTTO) impact ionization mass spectrometers in the compressed modes, *Astron. Astrophys.* **187**, pp 761-766 (1987).
6. Mason, B., Data of Geochemistry, Chapter B. Cosmochemistry, Geological Survey Professional Paper 440-B-1, US Gov. printing office (1979).

7. Blanford, G. E., Thomas, K. L., and McKay, D. S., Microbeam analysis of chondritic interplanetary dust particles for carbon, oxygen and major elements, *Lunar and Planet. Sci.* **19**, pp102-103 (1988)
8. Schramm, L. S., Brownlee, D. E., and Wheelock, M. W. The elemental composition of interplanetary dust, *Lunar and Planet. Sci.* **19**, pp 1033-1034 (1988).
9. Brownlee, D. E., Wheelock M. W., Temple, S., Bradley, J. P., and Kissel, J., A quantitative comparison of comet Halley and; carbonaceous chondrites at the submicron level, *Lunar and Planet. Sci.* **18**, pp133-134 (1987).
10. Bradley, J. B., Analysis of chondritic interplanetary dust thin-sections, *Geochim. Cosmochim. Acta* **52**, pp 889-900 (1988).
11. Sandford, S. A. The collection and analysis of extraterrestrial dust particles, *Fundamentals of Cosmic Physics* **12**, pp 1-73 (1987).
12. Mackinnon, I. D. R., and Reitmeijer, F. J. M., Mineralogy of chondritic interplanetary dust particles, *Reviews of Geophys.* **25**, pp 1527-1553 (1987).
13. Bradley, J. B., and Brownlee, D. E., Cometary particles: thin sectioning and electron beam analysis, *Science* **231**, pp 133-134 (1986).
14. Reitmeijer, F. J. M., and Mackinnon, I. D. R., Metastable carbon in two chondritic interplanetary dust particles, *Nature* **326**, pp 1162-1165 (1987).
15. Allamandola, L. J., Sandford, S. A., and Wopenka, B., Interstellar polycyclic aromatic hydrocarbons and carbon in interplanetary dust particles and meteorites, *Science* **237**, pp 56-59 (1987).
16. Christofferson, R., and Buseck, P. R., Epsilon carbide: a low temperature component of interplanetary dust particles. *Science* **222**, pp 1327-1328 (1983).
17. Bradley, J. P., and Brownlee, D. E., Carbon compounds in interplanetary dust: evidence for heterogenous catalysis, *Science* **223**, pp 56-58 (1984).
18. Fegley, B., Cosmochemical trends of volatile elements in the solar system, in Workshop of the origins of the solar system, *Lunar and Planet. Instit. Tech. Rept.* No. 88-04, pp 51-60 (1988).
19. Tomeoka, K., and Buseck, P. R., A carbonate-rich, hydrated, interplanetary dust particle: possible residue from protostellar clouds, *Science* **231**, pp 1544-1546 (1986).
20. Sandford, S. A., Acid dissolution experiments: carbonates and the 6.8-micrometer bands in interplanetary dust particles, *Science* **231**, pp 1540-1541 (1986).
21. McKeegan, K. D., Swan, P., Walker, R. M., Wopenka, B., and Zinner, E., Hydrogen isotopic variations in interplanetary dust, *Lunar Planet. Sci.* **18**, pp 627-628, (1987).
22. Yang, J., and Epstein, S., Interstellar organic matter in meteorites, *Geochim. Cosmochim. Acta* **47**, pp 2199-2216 (1984).
23. McKeegan, K. D., Ion microprobe measurements of H, C, O, Mg and Si isotopic abundances in individual interplanetary dust particles, Ph.D. thesis, Washington Univ. (1987).
24. Greenberg, M., What are comets made of? A model based on interstellar dust, in Comets, Ed. L.L. Wilkening, U. Arizona press, pp 131-163 (1982).
25. A'Hearn, M. F., Hoban, S., Birch, P. V., Bowers, C., Martin, R., and Llingesmith, D. A., Cynaogen jets in comet Halley, *Nature* **324**, pp 649-650 (1986).
26. Simpson, J. A., Rabinowits, D., Ksanformality, L. V. and Sagdeev, R.Z., Halley's comet coma dust particle mass spectra, flux distributions and jet structures derived from measurements on the VEGA-1 and VEGA-2 spacecraft, *Astron. and Astrophys.* **187**, pp 742-752 (1987).
27. Huebner, W. F., First polymer identified in comet Halley, *Science* **237**, pp 628-630 (1987).
28. Greenberg, J. M. and Nansheng, Z., The 3.4um and 10um emissions from comet Halley: a blizzard of fluffy aggregates of interstellar dust, *Nature*, in press (1988).

# Carbon-rich Particles in Comet Halley\*

Benton C. Clark  
Martin Marietta Astronautics

## INTRODUCTION

The majority of particles detected in the coma of Comet Halley contain carbon atoms; many of these grains appear to consist preponderately or only of light elements. These light-element particles may be composed of organic compounds. Of the possible combinations of the elements hydrogen, carbon, nitrogen, and oxygen, numerous examples are found of particles containing the combinations (H,C,O,N), (H,C,N), (H,C,O), and (H,C). These results may bear on the recent detection of polyoxymethylene fragments, the observation of cyanojets (CN patterns consistent with release from solid particles), the possible presence of cyanopolyacetylenes or HCN polymer, and the make-up of the CHON particles. If cometary matter could reach the surface of the earth without complete disruption, these diverse organic and mixed particles could create unique microenvironments, possibly with significant or even pivotal prebiotic chemical activity.

This report provides a speculative insight into possible relationships between carbon in comets and carbon in life, as well as providing a brief overview of on-going analysis of data from the highly successful Particle Impact Analyzer (PIA) experiment flown on the Giotto spacecraft for the flyby of Comet Halley (development and implementation of PIA was under the direction of J. Kissel of the Max Planck Institute for Kernphysik, Heidelberg). PIA is a time-of-flight analyzer which obtains mass spectra of ions from individual particles impacting on a Pt-Ag foil target within the instrument. It is a pleasure to acknowledge the collaboration of L. W. Mason, who has accomplished invaluable work on data manipulation and scanning algorithms for implementing automatic classification of the empirically-deduced particle types.

## RESULTS

### Particle Types

At the relative speed of 70 km/s, particle kinetic energy is much higher than the average molecular binding energies of the constituents, resulting in a spectrum which to first order is of the singly-charged ions of these atoms. Several thousand instrument triggers occurred, due to impacts and trigger noise, with at least 2,000 spectra which appear to contain interpretable information on particle composition. The spectral lines occurring most consistently and pervasively are those of carbon and hydrogen.

Particles of differing composition are present. A plurality of particles appear to be of cosmic composition (major C, O, Mg, and Si; often with S and Fe, minor N, and sometimes Ca). These are termed "mixed" particles because they almost certainly contain more than a single chemical phase. Another group of particles consist of O, Mg, Si, and often Fe and Ca. These particles may well be silicate minerals. A final major group, with several possible subgroups, consists of particles predominantly of light elements. Such particles may be mostly or solely organic. The current analysis of this latter group will be emphasized in this communication.

---

\* PIA data analysis is supported in part by NASA, under contract JPL-956214.

## CHON Particles

The CHON particles contain the elements attributed in the name, with N sometimes higher and other times lower than O. The discovery spectra for CHON and mixed particles are shown in Figures 1 and 2, respectively. These are so-called mode-zero spectra, whereby the time-of-flight mass spectrum is sampled intensively, once each 66.7 ns. For the CHON spectra, it seems clear from this sampling that measured amplitudes from the nitrogen peak exceed the signal from the oxygen peak. Ion yield corrections have not been applied to these data, and must be done so before the relative atomic proportions of these two elements can be estimated. Another set of CHON spectra are shown in Figure 3. In this case, mode 1 data are shown, whereby only peaks and follow-up samples are shown. These particular spectra have been selected for N amplitudes less than O. A peak in the region 22-25, particularly at 23 or 24 AMU, is also often present, indicative of  $\text{Na}^+$ ,  $\text{Mg}^+$ , and/or  $\text{C}_2^+$  from this class of particle.

## (H,C,O) Particles

Many particles contain H, C, and O with no observed N. These (H,C,O) particles also typically contain a specie producing a peak in the 23-24 region, as seen in the examples of Figure 4 and 5. It has previously been shown that this particle classification is distinct from the CHON particles by virtue of variable relative occurrence patterns during the flythrough of the Halley coma (ref. 1, 2).

## (H,C,N) Particles

Assigned to another class are particles each of which contains H, C, and N, but with no observed O, as seen in Figure 6. Again, these particles were interpreted as a distinct class because of their relative occurrence. It can now be reported that these particles only rarely produce a peak at 23-24, providing an independent verification of their distinctness from the (H,C,O) class.

## (H,C) Particles

It should also be noted that many particles showing only evidence of hydrogen and carbon are present in the spectra. Further analysis will be required to explore the possibility that these grains might simply be a measurement artifact of one or more of the above light-element classes, but with N, O, or both elements not producing an observed peak. This is a possibility because of the fact that for all spectra other than the rare mode-zero samples, an automatic circuit within the PIA instrument must determine the presence of a peak at any given time before such peak is reported. Variability in peak shapes, not fully understood because of the difficulty in calibrating and characterizing the instrument in the laboratory environment, can cause peaks not to be detected. This is obvious in the occurrence of numerous spectra with only a single mass line and other spectra of doubtful chemical interpretation (e.g., a clearly silicate composition, but with the oxygen line missing).

## DISCUSSION

### Particle Characteristics

The discovery of jet patterns that imply gas-phase CN- correlated with a dust component not following the jets of the major dust pattern (A'Hearn et al., ref. 3), the so-called cyanojets, is presumably a result of volatilization or photo-release of from a minor particle component. The CHON particles were identified as the possible responsible agent. The (H,C,N) particles are, of

\*\*\* PIA 3 MODE 0 SPECTRA \*\*\* RUN ON: 30 Oct 1987  
 ONLY HIGHEST AMPLITUDE VALUE USED IN EACH MASS NUMBER  
 NO TIME SAMPLES USED ... NO ION YIELD CALCULATION  
 Rec: 167 Seq: 32770 Event: 31069 Class: 0 S/C time: -4:38.6

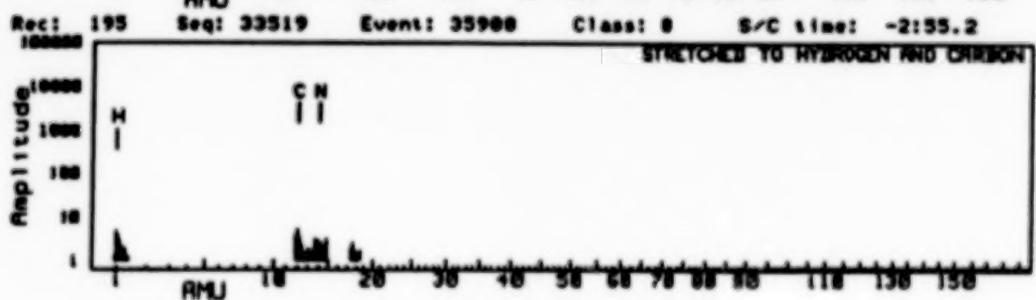
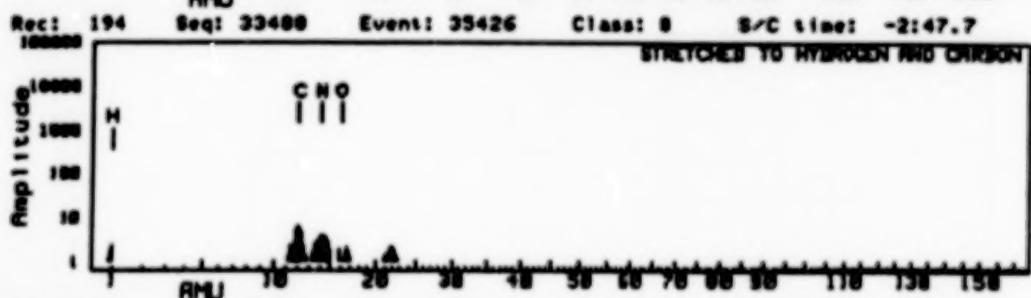
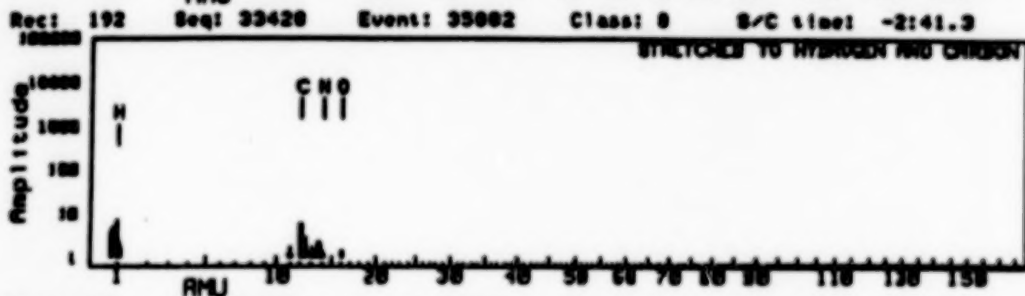
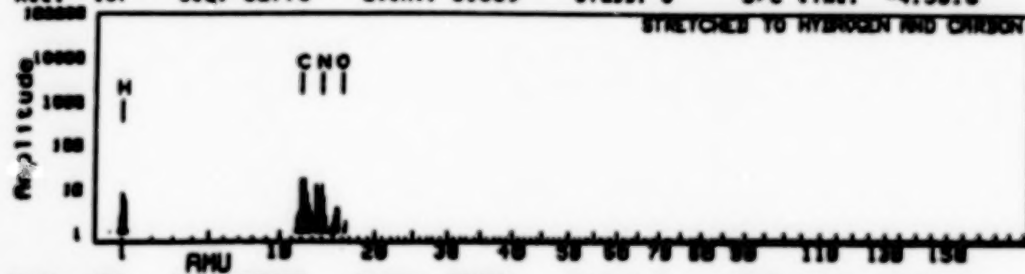


Figure 1. Selected CHON spectra from the mode zero data set.

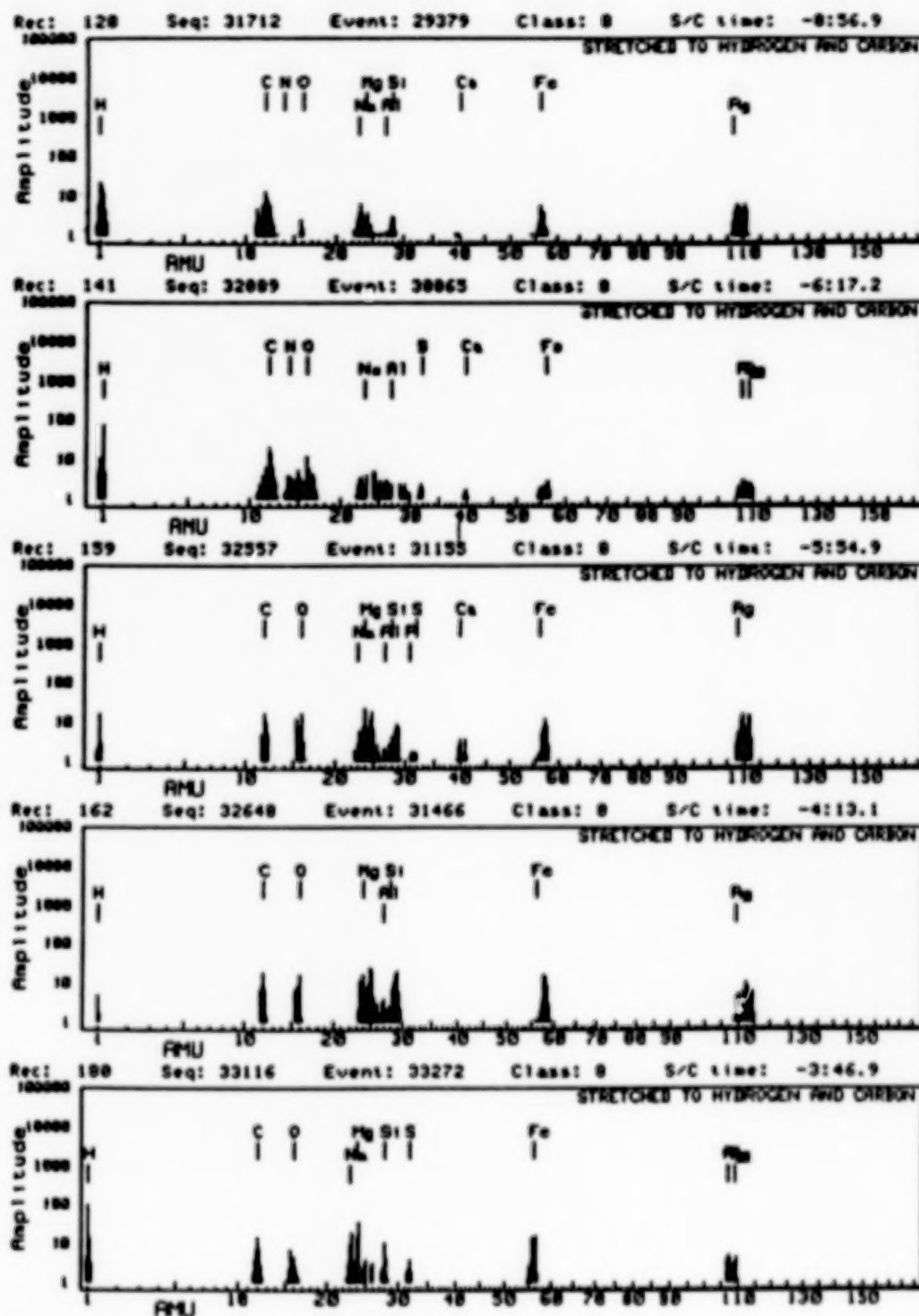


Figure 2. "Mixed" particles, mode zero data. Note the variation in distinctness of the peaks and the major variations of amplitude within a given element's mass range.

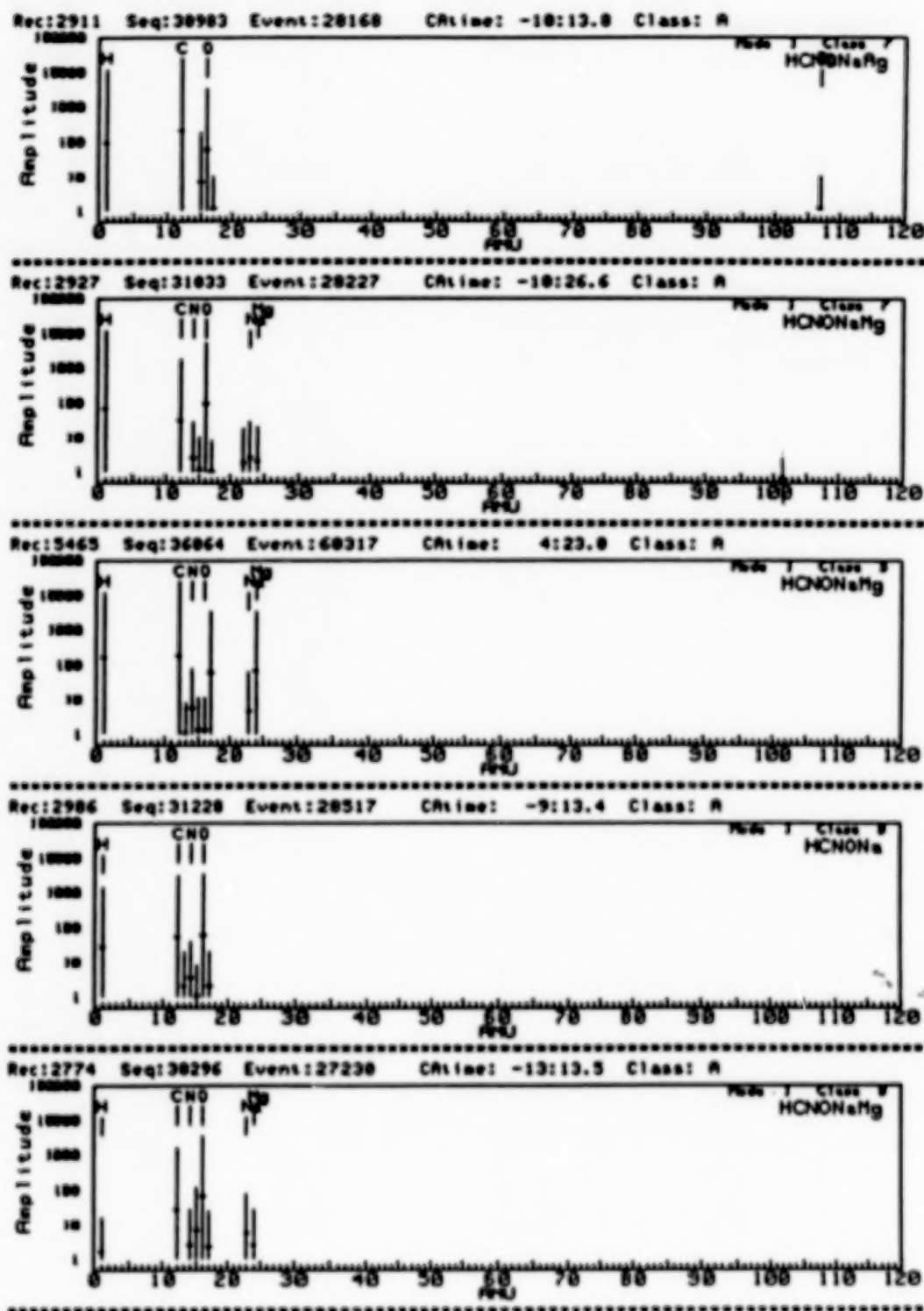


Figure 3. Selected mode 1 spectra showing large CHON particles. The topmost spectrum could also be classified as an (H,C,O) particle.

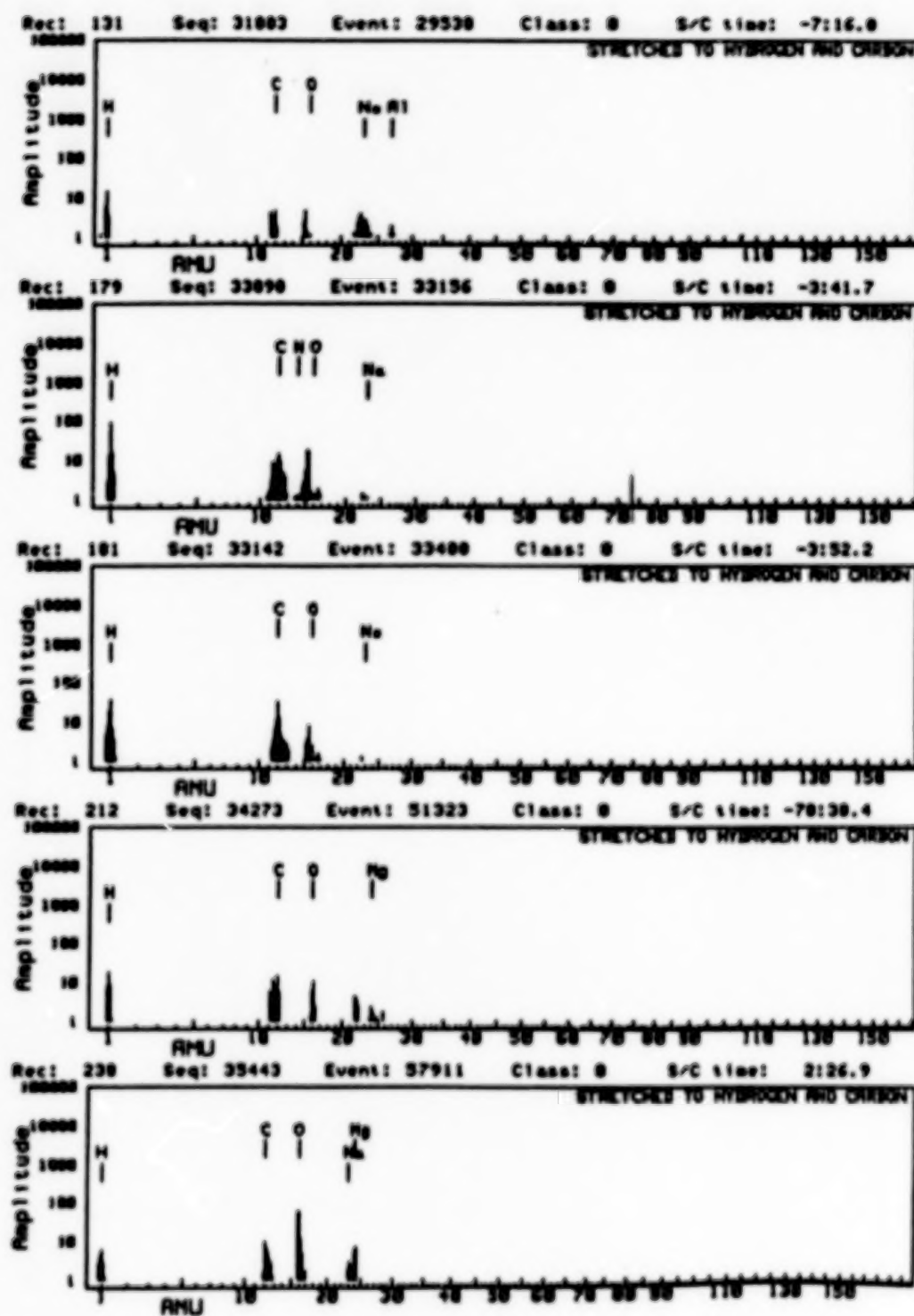


Figure 4. Mode zero spectra exhibiting the (H,C,O) classification.

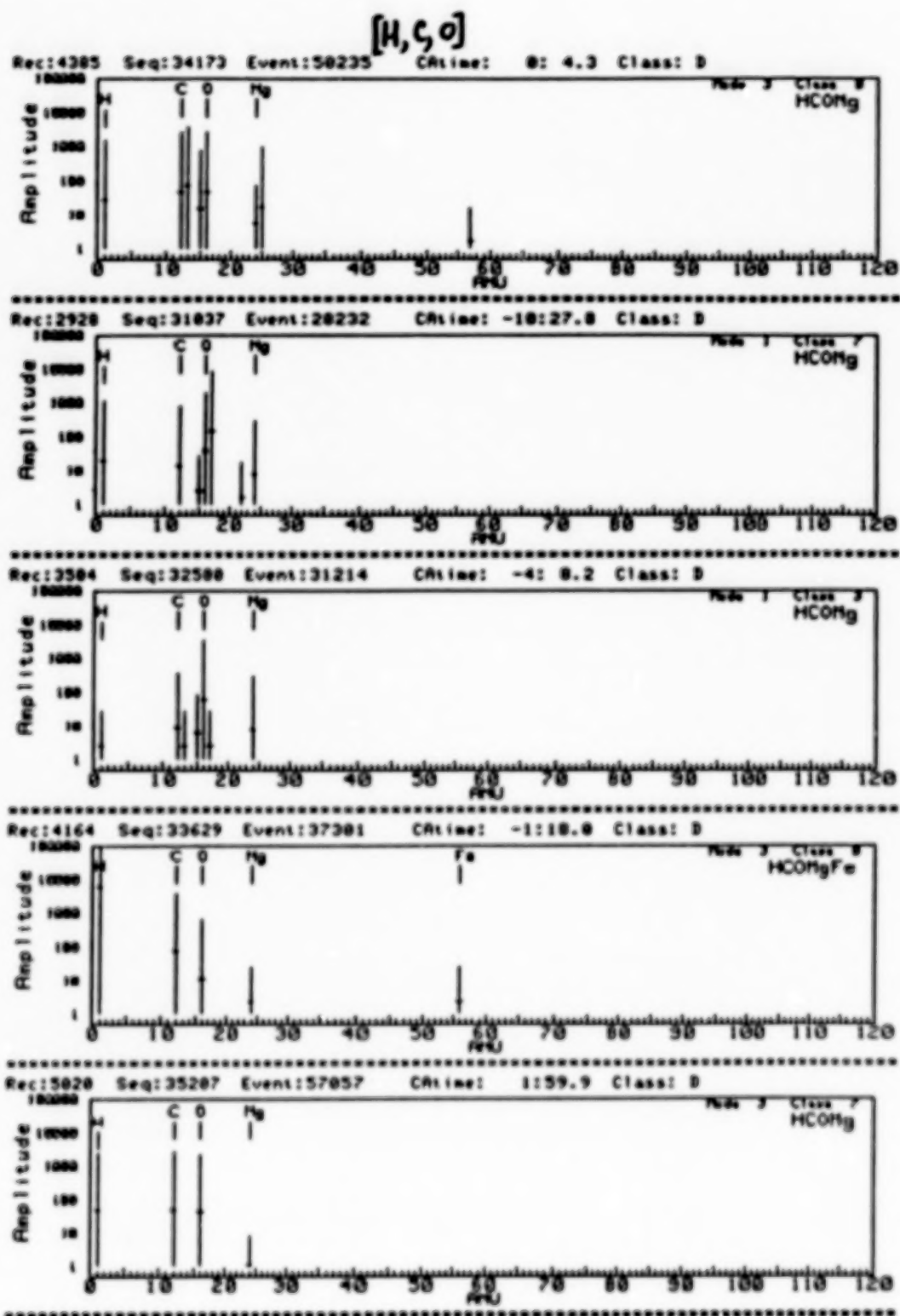


Figure 5. Additional examples of (H,C,O) particles. Note the occurrence of a peak in the 22-24 range in all of these spectra.

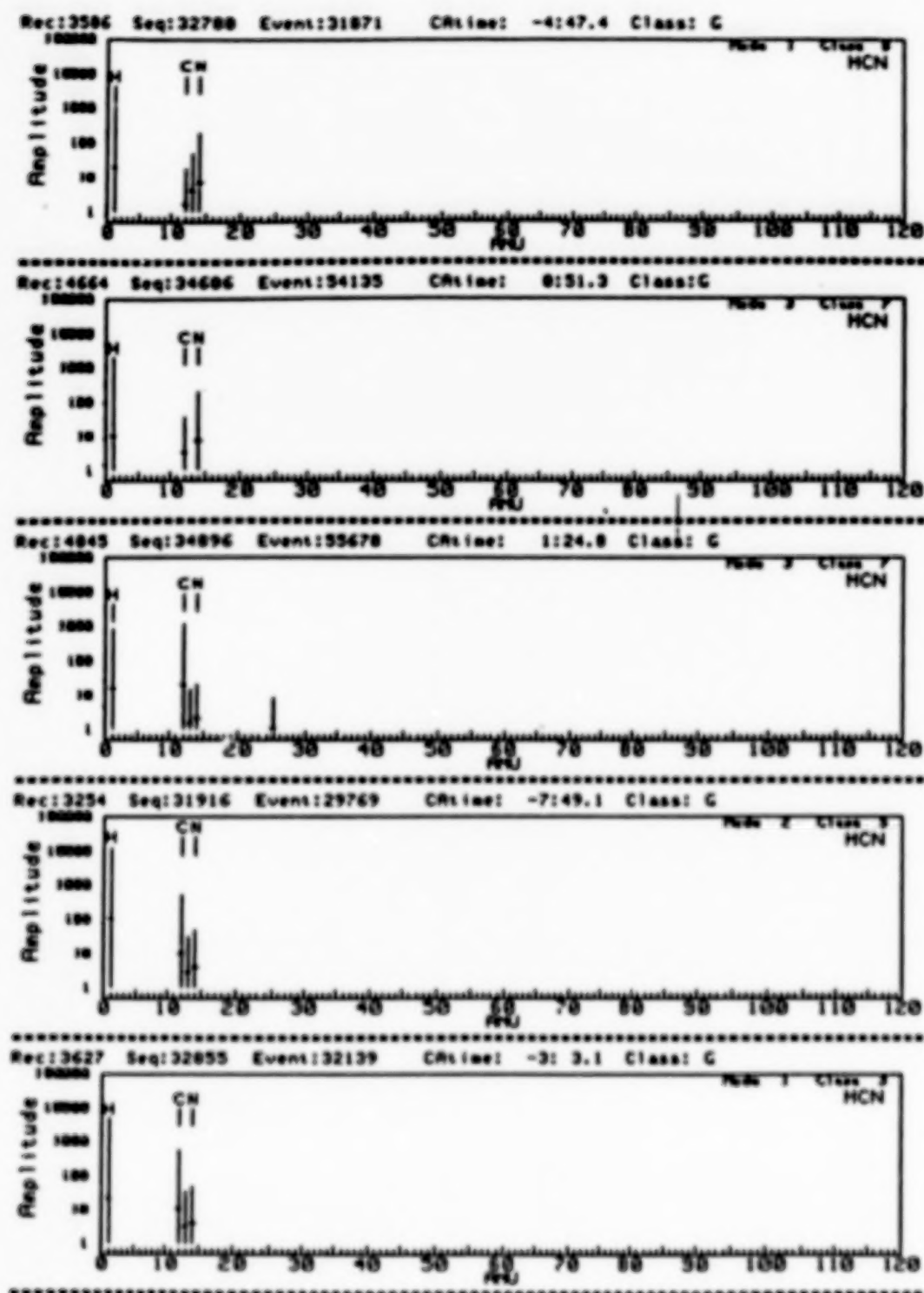


Figure 6. Examples of the (H,C,N) spectral class.

course, also a reasonable candidate. The possibility of polymerized hydrogen cyanide polymer in comets has been previously proposed (ref. 4).

Likewise, both CHON and (H,C,O) could release separately observable products. The recent recognition of polyoxymethylene (formaldehyde polymer) fragments in the gas phase (ref. 5, 6) opens the possibility that (H,C,O) grains could be the responsible source material.

The fact that the "23-24" peak occurrence pattern follows the relationship  $(H,C,O) > CHON > (H,C,N)$  is highly suggestive that CHON particles could be made up of (H,C,O) and (H,C,N) constituents, i.e., that CHON are also a mixture, or microconglomerate, or two or more particle types, just as are the "mixed" particles.

Kissel and Krueger (ref. 7) have inferred from minor peaks in spectra of the PUMA sister instrument flown on the Vega spacecraft during the Halley flyby missions that complex organic compounds may be present.

The overall impression is that comets are made up of a variety of primary grain types, each of which must have originated in separate times, places, and/or physicochemical conditions. As part of the accretion process, heterogeneous agglomeration on the particle-size scale anteceded formation of the macroscopic body we observe as the cometary nucleus.

### Implications for the Origin of Life

I have recently pointed out that the diversity in cometary particulate types may have allowed the formation of organized prebiotic chemical entities, which in turn facilitated or enabled the origin of life. Carbon, the quintessential element in life as we understand it, is likewise the touchstone of cometary matter in so far as regards the possible connection with life's origin. Carbon is extraordinarily ubiquitous in Comet Halley particulates, far exceeding its relative occurrence in any abiotic natural material so far detected on any of the rocky planetary bodies or meteorites. Of even greater significance, however, is the apparent diversity of organic solid phases within comets. The "mixed", CHON, (H,C,O), (H,C,N), and (H,C) classes provide the possibility of at least five importantly different particle types, each of which is available across a range of sizes. In an aqueous environment, many specialized and semi-compartmentalized microenvironments would be created due to physisorption and chemisorption processes as well as particle segregation according to size, density, and hydrophilic/hydrophobic tendencies.

Although rarely, *some* cometary nuclei (or fragments thereof) should survive accretive capture by planetary-sized bodies and thereby create a totally unique and localized, connected set of such microenvironments, providing one of the most favorable natural settings conceivable for the initiation of biogenic processes (Clark, ref. 8). The complexity of such an environment can only barely be imagined. Bulk, intact samples of cometary nucleus material will have to become available for direct laboratory analysis before the span of these possibilities can be comprehensively understood. Likewise, a retrieval and return to Earth of matter from a comet will permit a much richer understanding of the role of carbon in space chemistry and the anticipated multiphase distribution of this exceedingly important element.

### REFERENCES

1. Clark, B. C.; Mason, L. W.; and Kissel, J.: Systematics of the "CHON" and Other Non-silicic Particles in the Coma of Halley's Comet. 20th ESLAB Symposium on the Exploration of Halley's Comet (Abs. Poster), Oct. 1986, p. 466.

2. Clark, B. C.; Mason, L. W.; and Kissel, J.: Systematics of the "CHON" and Other Light-Element Particle Populations in Comet P/Halley. *Astronomy and Astrophysics*, vol. 187, 1987, pp. 779-784.
3. A'Hearn, M. F.; Hoban, S.; et al.: Cyanogen Jets in Comet Halley. *Nature*, vol. 324, 1986, pp. 649-651.
4. Matthews, C. N. and Ludicky, R.: The Dark Nucleus of Comet Halley: Hydrogen Cyanide Polymers. ESA SP-250, 20th Eslab Symposium on the Exploration of Halley's Comet. Dec 1986, pp. 273-277.
5. Huebner, W. F.: First Polymer in Space Identified in Comet Halley. *Science*, vol. 237, 1987, pp. 628-630.
6. Mitchell, D. L.; Lin, R. P.; et al.: Evidence for Chain Molecules Enriched in Carbon, Hydrogen, and Oxygen in Comet Halley. *Science*, vol. 237, 1987, pp. 626-628.
7. Kissel, J. and Krueger, F. R.: The Organic Component in Dust from Comet Halley as Measured by the PUMA Mass Spectrometer on board Vega 1. *Nature*, vol 326, pp. 755-760.
8. Clark, Benton C.: Primeval Procreative Comet Pond. *Origins of Life*, in press, 1988.

## **STUDIES OF CARBON IN INTERSTELLAR SPACE**

## ASTRONOMICAL OBSERVATIONS OF SOLID PHASE CARBON

M. Jura

University of California, Los Angeles

### I. INTRODUCTION

At least half of the material heavier than helium in the interstellar medium is contained within small ( $10^{-7}$  -  $10^{-4}$  cm) solid grains (see Spitzer 1978). The nature, composition, origin and evolution of this interstellar dust is still not fully known. Nevertheless, because it is so abundant in the Milky Way Galaxy, carbon is likely to be a major constituent of the interstellar solids. It seems that the solids do not form in the interstellar medium *in situ* because the densities are so low. Instead, the bulk of grain cores form in high density environments such as the envelopes of red giant stars; these nuclei are then expelled into the interstellar medium where the grains may undergo substantial processing (Seab 1987).

In the galaxy as a whole, about 90% by number of the material is hydrogen, nearly 10% is helium, and the rest is "minor constituents". In the standard or "cosmic abundances", oxygen is about twice as abundant as carbon. However, there are a few rare stars where carbon is more abundant than the oxygen, the carbon stars. In the late Bright Star Catalogue, the standard reference on the  $\sim 10^4$  optically brightest stars, about 20 carbon stars are listed. While carbon stars are quite rare, they are losing large amounts ( $>10^{-7} M_{\odot} \text{ yr}^{-1}$ ) of mass (Claussen *et al.* 1987). Therefore, a substantial fraction, perhaps half, of all the matter injected into the interstellar medium is produced in the carbon-rich environments of carbon stars (Zuckerman *et al.* 1977, Knapp and Morris 1985).

In the outer envelopes of red giants, when the gas cools sufficiently, molecules and solids form. Thermodynamically, the most stable molecule is CO, and it is usually assumed that all the available carbon and oxygen are consumed in the formation of this molecule (Salpeter 1977). If the carbon abundance is greater than the oxygen abundance, then the carbon left over after the formation of CO is available for solid grains. Because carbon is by far the most abundant species available for making solids in these environments, we anticipate that the grains are composed of nearly pure carbon in some form. Below, we discuss the observations which can be used to infer the nature of this solid phase carbon.

It is usually assumed that most of the carbon in any particular environment is  $^{12}\text{C}$ . In fact, in most carbon stars,  $^{12}\text{C}/^{13}\text{C} = 35$  (Lambert *et al.* 1986). However, about 15% of all carbon stars, the J-types, have  $^{12}\text{C}/^{13}\text{C}$  between 2 and 4 (Lambert *et al.* 1986, Jura, Kahane and Omont 1987). In these  $^{13}\text{C}$ -rich stars, the solid carbon might exhibit subtly different properties than the carbon-rich material around the more common carbon stars. However, this difference between the  $^{13}\text{C}$ -rich carbon stars and the more ordinary types has not yet been fully explored.

Once the grains are expelled from the carbon star into the interstellar medium, they may not remain intact as carbon-rich material because of the substantial processing that they undergo. However, there is good evidence for the widespread presence of interstellar PAH's, polycyclic aromatic hydrocarbons (see Leger, d'Hendecourt and Boccara 1986). These PAH's are carbon ring molecules containing at least 20 atoms. The relationships between the interstellar PAH's and carbon grains is still not clear.

Aside from carbon-rich red giants, there are other possible sites for the formation of carbon-rich grains. Some Wolf-Rayet (W-R) stars are also carbon-rich, and they might be appreciable sources of interstellar carbon (see Maeder 1983). Most W-R stars are thought to be quite massive ( $>20 M_{\odot}$ , Abbott and Conti 1987) as opposed to carbon-rich red giants which typically have masses of  $\sim 1.5 M_{\odot}$  (Claussen *et al.* 1987). However, only a few of the W-R stars show evidence for circumstellar grains in the sense that for most W-R stars, most of the infrared emission is produced by ionized gas in the hot wind (Abbott, Telesco and Wolff 1984). It is a subset of the W-R stars, the cool carbon-rich ones of type WC8, WC9 and WC10 which seem often to contain dust (Williams, van der Hucht and The 1987) since they display strong infrared excesses. For example, in the complete sample of 43 W-R stars north of  $-40^{\circ}$  declination and within 3 kpc of the Sun studied by Abbott *et al.* (1986), 2 are strong infrared sources in the sense that they have  $12 \mu\text{m}$  fluxes greater than 400 Jy in the IRAS catalog even though they are both more than 1 kpc from the Sun. In contrast to these two unusual stars, the other 41 stars all have  $12 \mu\text{m}$  fluxes in the IRAS catalog of less than 20 Jy and most are not detected at all.

At least some W-R stars actually are transition objects between red giants and planetary nebulae since the central stars of planetary nebulae sometimes have W-R spectra (Kaler 1985). That is, for some stars, there is some ambiguity about whether they are pre-planetary nebulae with a mass of  $\sim 1-2 M_{\odot}$  or are truly massive (see van der Hucht *et al.* 1981, 1985). It should be noted that Massey, Conti and Armandroff (1987) are unable to find WC8, WC9 and WC10 stars in nearby galaxies even though it is straightforward to find warmer W-R stars. One possible explanation for this result is that at least some of the very cool W-R stars are really just evolved from being red giants with luminosities of  $\sim 10^4 L_{\odot}$  instead of having luminosities  $>10^5 L_{\odot}$  that is characteristic of most W-R stars which are thought to be quite massive. In any case, except for the stars which are strong infrared sources, the typical dust loss rates are  $10^{-8} M_{\odot} \text{ yr}^{-1}$  (Williams, van der Hucht and The 1987), and this suggests that most carbon grains in the galaxy do not result from W-R stars. Therefore, because the evolutionary nature of the IR bright W-R stars is not certain, we do not discuss them in detail in this review. Also, carbon grains might be formed around some novae and even possibly around some supernovae; these processes are not described here because very little is known.

In Section II, we discuss the observations of the dust around carbon-rich red giants, while in Section III we place these results into their broader astrophysical context.

## II. Circumstellar Dust Around Carbon-Rich Red Giants

Carbon-rich red giants are thought to be on the Asymptotic Giant Branch with luminosities that are typically  $\sim 10^4 L_{\odot}$  (Iben and Renzini 1983). The evidence for mass loss from carbon-rich red giants is very strong. These stars exhibit "excess" infrared emission in the sense that the observed flux at infrared wavelengths is substantially greater than what one would expect on the basis of an extrapolation of their photospheric emission (Jura 1986a). Also, these stars are rich sources of molecular line emission (Olofsson 1985) which indicate typical outflow velocities of  $15 \text{ km s}^{-1}$ . As reviewed previously by Jura (1986b), there are a number of constraints on the nature of the circumstellar grains which are reviewed below.

### A.) Solid State Spectroscopy

For a number of years, low resolution spectra ( $\Delta\lambda/\lambda = 10^{-2}$ ) of mass-losing stars have been available (see Merrill 1979; Kleinmann, Gillett and Joyce 1981). Carbon-rich stars often display an SiC feature at  $11.3 \mu\text{m}$ , although there are some carbon stars where this infrared feature is very weak if it is present at all (Baron et al. 1987, Papoular 1988). For most carbon stars, in order to explain the strength of the SiC feature, it is necessary to argue that most of the silicon is contained in the solid phase within SiC (Pegourie 1987). In addition to the well-known SiC feature, there is evidence in the extensive IRAS data base for other features at  $8.6$ ,  $11.7$  and  $12.8 \mu\text{m}$  (Papoular 1988). The origin of these features is not known.

Recently, it has been discovered that some carbon-rich stars display silicate emission at  $9.7 \mu\text{m}$  that is characteristic of oxygen rich material in their circumstellar dust (Willems and de Jong 1986, Little-Marenin 1986), and some of these stars also have  $\text{H}_2\text{O}$  maser emission that is another characteristic of oxygen-rich gas (Benson and Little-Marenin 1987, Nakada et al. 1987). These oxygen-rich features are thought to be present either because in the last few decades these stars have just become carbon-rich from having been oxygen-rich, or, because they are interacting binary stars, one of which is the optically prominent carbon star and another is an oxygen-rich star. Whatever the correct explanation, the material in their outflows is not representative of most circumstellar gas from carbon stars.

Forrest, Houck and McCarthy (1981) have discovered a very broad feature near  $30 \mu\text{m}$  in the spectra of several carbon stars. It is now thought that this feature results from MgS (Goebel and Moseley 1985).

Finally, Draine (1984) has predicted that if graphite grains are present within the outflows from red giants, there should be a sharp, narrow feature at  $11.52 \mu\text{m}$ . No such feature is found suggesting that most of the dust grains in the outflows from carbon stars are not composed of graphite but rather carbon in some other form.

### B.) Broad-Band Colors

Another way to constrain the nature of the circumstellar grains is to study the emissivity and/or extinction as a function of wavelength. The infrared emission that results from reprocessing of the stellar light by the circumstellar dust can be modelled to infer the infrared emissivity of the circumstellar grains (see, for example, Rovin-Robinson and Harris 1983, Sopka et al. 1985, Jura 1986a). One

difficulty with this procedure is that the density distribution of the grains around the stars can also strongly affect the infrared colors because these colors depend upon the relative amounts of cold and warm grains (see, for example Harvey, Thronson and Gatley 1979). If we assume a constant mass loss rate,  $dM/dt$ , and a constant outflow velocity,  $v$ , then from the equation of continuity, we expect for the radial ( $r$ ) distribution of density,  $\rho$ , that:

$$\rho = (dM/dt)/(4\pi r^2 v)$$

Either by considering a few very well studied stars or by studying a large sample of stars where, on the average, we expect the density to vary as  $r^{-2}$ , we can derive the infrared emissivity as a function of wavelength. Note that if the grain density varied, say, as  $r^{-1}$ , the infrared colors would be very different from what is observed for envelopes where the density varies as  $r^{-2}$ .

Both analysis of the best-studied circumstellar shell around the star IRC+10216 (Campbell *et al.* 1976, Le Bertre 1987, Martin and Rogers 1987), and ensembles of carbon stars (Jura 1986a) indicates that a power law emissivity which varies as about  $\lambda^{-1.1}$  is a reasonable first approximation of the emissivity longward of  $1\mu m$ . However, there are differences in the broad-band colors between oxygen-rich and carbon-rich stars (Hacking *et al.* 1985, Zuckerman and Dyck 1986), and a single power law is not a perfect representation of the emissivity of the grains.

Shortward of  $1\mu m$ , the circumstellar grains are not significant emitters. Nevertheless, it is still possible to estimate the wavelength variation of the opacity both from direct observations of the light from the central star and indirect observations of molecules that are subject to photodissociation by the ambient interstellar ultraviolet radiation field. Observations of the Balmer decrement in the spectra of a number of dust-enshrouded carbon stars (Cohen 1979) show a continued rise in the grain opacity toward shorter wavelengths. Also, the large observed spatial extent of HCN around the well-studied carbon star IRC+10216 (Bieging, Chapman and Welch 1984) is most easily understood if the grain opacity continues to rise about as  $\lambda^{-1}$  into the ultraviolet (Jura 1983, Glassgold, Lucas and Omont 1986).

While it is straightforward to estimate the relative infrared emissivity as a function of wavelength, we do not know the absolute number of carbon grains. That is, with the information available, we do not know whether the infrared emission is produced by a few grains that are efficient emitters or many grains that are inefficient emitters. Experiments show that there is a range of at least a factor of 5 in the infrared emissivity of different sorts of solid carbon (Borghesi, Bussolletti and Colangeli 1985). It seems reasonable to adopt for amorphous carbon, the most likely candidate for the grain material, an opacity at  $60\mu m$  of  $150\text{ cm}^2\text{ gm}^{-1}$  (Borghesi *et al.* 1985). If  $\chi_{60}$  denotes the grain opacity ( $\text{cm}^2\text{ gm}^{-1}$ ) at  $60\mu m$ , then we have for the dust to gas ratio around most carbon stars within a factor of 3 that (Jura 1986a):

$$M_{\text{dust}}/M_{\text{gas}} = 4.5 \cdot 10^{-3} (150/\chi_{60})$$

All the data together indicate that the solid dust around mass-losing red giants is probably small particles of amorphous carbon (see, the detailed discussion by Martin and Rogers 1987).

### C.) Grain Sizes

There are some significant observational constraints on the size distribution of circumstellar grains around mass-losing red giants. Because we have less information than is available for interstellar extinction, we cannot argue as in the case of interstellar grains that the size distribution  $n(a)$  varies as  $a^{-3.5}$  (Mathis, Rumpl and Nordsieck 1977). Nevertheless, there are useful probes of the grain sizes: (i) As noted above, the extinction continues to rise approximately as  $\lambda^{-1}$  even into the ultraviolet. This implies (see, for example, Spitzer 1978) that at least some of the grains are relatively small compared to  $1000 \text{ \AA}$ . That is, grains with sizes large compared to the wavelength of the incident light tend to have a cross section equal to their geometric size and thus have an opacity independent of wavelength. (ii) Circumstellar grains scatter the light from the central star. This is sometimes seen directly as reflection nebulae (see, for example, Yusef-Zadeh, Morris and White 1984). Also, the integrated optical light from carbon stars typically exhibits some net polarization (Dyck, Forbes and Shavl 1971). These data are most easily understood as resulting from scattering by an anisotropic distribution of dust grains around the star (Daniel 1982). Because there is appreciable scattering of optical light, many of the grains cannot be much smaller than  $1000 \text{ \AA}$  (Spitzer 1978). That is, if the grains were all much smaller than the wavelength of the observed scattered light, the scattering cross section would be very small. (iii) A final constraint on the size of the grains is the heating of the circumstellar gas. Once the grains form, they stream supersonically through the gas, and this is the main source of gas heating. The amount of heating of the gas is sensitive to the grain size; the CO data for IRC+10216 are most easily understood if the grain size is  $\sim 400 \text{ \AA}$  (Kvan and Hill 1977, Kvan and Linke 1982). The thermal properties of circumstellar envelopes around other stars are also consistent with this value (Jura, Kahane and Omont 1988).

We conclude that there is good evidence that a number of circumstellar grains may have sizes of  $\sim 1000 \text{ \AA}$ . Like interstellar grains, there may be a wide range of sizes, but we know that many of these particles are submicron sized.

### III. ASTROPHYSICAL IMPLICATIONS

As reviewed by Jura (1987), stars of all different types are returning about  $10^{-3} M_{\odot} \text{ yr}^{-1} \text{ kpc}^{-2}$  into the local disk of the Milky Way Galaxy. Between 10% and 50% of this material results from carbon-rich red giants. Once the grains from carbon stars enter the interstellar medium, they undergo substantial processing. Therefore, even though we know that there are significant sources of carbon grains, we do not know how well this material keeps its identity as carbon-rich in the interstellar medium.

The strongest known feature in the interstellar extinction occurs near  $2200 \text{ \AA}$  (Savage and Mathis 1979). This feature is often attributed to carbon grains (Mathis, Rumpl and Nordsieck 1977). However, there is not universal agreement with this identification (Duley 1987), and there is no straightforward demonstration of the presence of carbon-rich grains within the interstellar medium itself.

There is an indirect argument that some interstellar carbon is contained within grains of some sort. First, as mentioned above, there is so much material within grains that it is almost certain that they must contain some carbon. Second, we know that the gas phase abundance of carbon is probably depleted by about a factor of 2 or

3 below its cosmic abundance (Hobbs, York and Oegerle 1982, Jenkins, Jura and Loevenstein 1983); it seems likely that there is as much interstellar carbon in the solid phase as there is in the gas phase.

Finally, it should be noted that there is evidence for the widespread presence throughout the interstellar medium of PAH's (Leger, d'Hendecourt and Boccarda 1987). These species may be either large molecules or very small grains. However, their origin and evolution within the interstellar medium are still very not well known (Omout 1986). It will be a matter of considerable concern for the future to develop a much deeper understanding of these carbon particles in the interstellar medium and their relationships with the larger dust grains.

#### References

- Abbott, D. C., Biegging, J. H., Churchwell, E., and Torres, A. V. 1986, Ap. J., 303, 239.
- Abbott, D. C., and Conti, P. S. 1987, Ann. Rev. Astr. Ap., 25, 113.
- Abbott, D. C., Telesco, C. M., and Wolff, S. C. 1984, Ap. J., 279, 225.
- Baron, Y., de Muizon, M., Papoular, R., and Pegourie, B. 1987, Astr. Ap., in press.
- Benson, P. J., and Little-Marenin, I. R. 1987, Ap. J. (Letters), 316, L37.
- Biegging, J. H., Chapman, B., and Welch, W. J. 1984, Ap. J., 285, 656.
- Borghesi, A., Bussoletti, E., and Colangeli, L. 1985, Astr. Ap., 142, 225.
- Campbell, M. F., Elias, J. H., Gezari, D. Y., Harvey, P. M., Hoffmann, W. F., Hudson, H. S., Neugebauer, G., Soifer, B. T., Verner, M. W., and Westbrook, W. E. 1976, Ap. J., 208, 396.
- Claussen, M. J., Kleinmann, S. G., Joyce, R. R., and Jura, M. 1987, Ap. J. Suppl., 65, 385.
- Cohen, M. 1979, M.N.R.A.S., 186, 837.
- Daniel, J. Y. 1982, Astr. Ap., 111, 58.
- Draine, B. T. 1984, Ap. J. (Letters), 277, L71.
- Duley, W. V. 1987, M.N.R.A.S., 229, 203.
- Dyck, H. M., Forbes, F. F., and Shavl, S. J. 1971, Astr. J., 76, 901.
- Forrest, W. J., Houck, J. R., and McCarthy, J. F. 1981, Ap. J., 248, 195.
- Glassgold, A. E., Lucas, R., and Omout, A. 1986, Astr. Ap., 157, 35.
- Goebel, J. H., and Moseley, S. H. 1985, Ap. J. (Letters), 290, L35.
- Hacking, P. et al. 1986, P.A.S.P., 97, 616.
- Harvey, P. M., Thronson, H. A., and Gatley, I. 1979, Ap. J., 231, 115.
- Hobbs, L. M., York, D. G., and Oegerle, W. 1982, Ap. J. (Letters), 252, L21.
- Iben, I., and Renzini, A. 1983, Ann. Rev. Astr. Ap., 21, 271.
- Jenkins, E. B., Jura, M., and Loevenstein, M. 1983, Ap. J., 270, 88.
- Jura, M. 1983, Ap. J., 267, 647.
- Jura, M. 1986a, Ap. J., 303, 327.

- Jura, M. 1986b, in Interrelationships Among Circumstellar, Interstellar, and Interplanetary Dust, J. Nuth and R. Stencel, eds. (NASA Conference Publication 2403), p. 3.
- Jura, M. 1987, P.A.S.P., in press.
- Jura, M., Kahane, C., and Omont, A. 1987, Astr. Ap., submitted.
- Kaler, J. B. 1985, Ann. Rev. Astr. Ap., 23, 89.
- Kleinmann, S. G., Gillett, F. C., and Joyce, R. R. 1981, Ann. Rev. Astr. Ap., 19, 411.
- Knapp, G. R., and Morris, M. 1985, Ap. J., 292, 640.
- Kvan, J., and Hill, F. 1977, Ap. J., 215, 781.
- Kvan, J., and Linke, R. A. 1982, Ap. J., 254, 587.
- Lambert, D. L., Gustafsson, B., Eriksson, K., and Hinkle, K. H. 1986, Ap. J. Suppl., 62, 373.
- Le Bertre, T. 1987, Astr. Ap., 176, 107.
- Leger, A., d'Hendecourt, L., and Boccarda, N. 1987, eds. Polycyclic Aromatic Hydrocarbons and Astrophysics, (D. Reidel :Dordrecht).
- Little-Marenin, I. R. 1986, Ap. J. (Letters), 307, L15.
- Maeder, A. 1983, Astr. Ap., 120,...
- Martin, P. G., and Rogers, C. 1987, Ap. J., 322, 374.
- Massey, P., Conti, P. S., and Armandroff, T. E. 1987, Astr. J., 94, 1538.
- Mathis, J. S., Rumpl, W., and Nordsieck, K. H. 1977, Ap. J., 217, 425.
- Merrill, K. M. 1979, Ap. Space Sci., 65, 199.
- Nakada, Y., Izumiura, H., Onaka, T., Hashimoto, O., Ukita, N., Deguchi, S., and Tanabe, T. 1987, Ap. J. (Letters), 323, L77.
- Olofsson, H. 1985, in Workshop on Submillimeter Astronomy, ed. P. A. Shaver and K. Kjar, (Garching:ESO), p. 535.
- Omont, A. 1986, Astr. Ap., 164, 186.
- Papoular, R. 1988, Astr. Ap., submitted.
- Pegourie, B. 1988, Astr. Ap., in press.
- Rovan-Robinson, M., and Harris, S. 1983, M.N.R.A.S., 202, 797.
- Salpeter, E. E. 1977, Ann. Rev. Astr. Ap., 15, 267.
- Savage, B. D., and Mathis, J. S. 1979, Ann. Rev. Astr. Ap., 17, 73.
- Seab, G. 1987, in Interstellar Processes, eds. D. J. Hollenbach and H. A. Thronson, (Reidel:Dordrecht), p. 491.
- Sopka, R. J., Hildebrand, R., Jaffe, D. T., Gatley, I., Roellig, T., Verner, M., Jura, M., and Zuckerman, B. 1985, Ap. J., 294, 242.
- van der Hucht, K. A., Conti, P. S., Lundstrom, I., and Stenholm, B. 1981, Space Science Reviews, 28, 227.
- van der Hucht, K. A., Jurriens, T. A., Olmon, F. M., The, P. S., Vesselius, P. R., and Williams, P. M. 1985, Astr. Ap., 145, L13.
- Williams, P. M., van der Hucht, K. A., and The, P. S. 1987, Astr. Ap., 182, 91.
- Villems, F. J., and de Jong, T. 1986, Ap. J. (Letters), 309, L39.
- Yusef-Zadeh, F., Morris, M., and White, R. L. 1984, Ap. J., 278, 186.
- Zuckerman, B., and Dyck, H. M. 1986, Ap. J., 311, 345.
- Zuckerman, B., Palmer, P., Morris, M., Turner, B. E., Gilra, D. P., Bovers, P. F., and Gilmore, W. S. 1977, Ap. J. (Letters), 211, L97.

## Survival of Carbon Grains in Shocks

C. Gregory Seab

Physics Department, University of New Orleans

### I. INTRODUCTION

The diffuse interstellar medium (ISM) is a hostile environment for all types of interstellar grains; it offers a variety of ways to destroy the grains. In the very hot ( $10^6$  K) phase, thermal sputtering will erode away grain material. In the warm ( $10^4$  K) phase, fast radiative shocks ( $30 < v_s < 150 \text{ km s}^{-1}$ ) can vaporize or shatter grains (Seab and Shull, ref. 1). Other destructive processes include astration, or incorporation into new formed stars; thermal sputtering in the galactic halo (Seab and Edgar, ref. 2), thermal evaporation in hot dense environments, and chemical sputtering of carbon grains (Barlow, ref. 3). Of all the grain destruction mechanism, grain destruction is supernova-driven shocks dominates (Draine and Salpeter, ref. 4; Dwek and Scalo, ref. 5). It is the purpose of this review to examine the processing of interstellar grains (carbon grain and other types) in interstellar supernova shock waves.

A typical interstellar grain will experience frequent shocks while it resides in the ISM. Seab (ref. 6) calculates the average shock time to be

$$\tau_{\text{sn}} = 10^8 v_7^2 \text{ years} \quad (1)$$

for a given grain being hit by a shock with velocity greater than  $v_7 = v/10^7 \text{ cm s}^{-1}$ . This average explicitly accounts for the different phases of the ISM in the McKee and Ostriker (ref. 7) model. For this shock frequency, the lifetime of a typical grain is approximately

$$\tau = \tau_{\text{sn}}/\epsilon \quad (2)$$

where  $\epsilon$  is the efficiency of grain destruction in a shock of a given velocity.

Section II briefly reviews the mechanisms of grain destruction in shocks; Section III describes the results of evaluating  $\epsilon$  for carbon grains specifically, while Section IV considers the possibility of producing small diamond particles from graphite grains subjected to grain-grain collisions. The final section summarizes these results and conclusions.

## II. GRAIN DESTRUCTION IN SHOCKS

The calculation of grain destruction in shocks divides into two parts depending primarily on the velocity. Shocks with  $v_s$  less than about 150 to 200 km s<sup>-1</sup> are radiative; the cooling time for the shocked gas is less than the evolution time of the shock. This evolution time is approximately given by the age of the supernova remnant (SNR) driving the shock. Shocks with velocity greater than 150 to 200 km s<sup>-1</sup> can be treated as adiabatic shocks, since the SNR expands significantly before the hot post-shock gas has a chance to cool by radiation. In the intermediate regime, and in some cases for slower shocks, at least a first-order time dependence correction to the shock structure must be done (McKee et al., ref. 8).

In radiative shocks, a cooling layer is established in the immediate postshock region. The shock layer itself can be treated as a thin discontinuity in which the gas temperature jumps from the ambient temperature up to 10<sup>4</sup> to 5 x 10<sup>5</sup> K, depending on the velocity, and the density jumps by about a factor of four in a strong shock. The gas is abruptly accelerated to about 0.75 $v_s$  in this layer. The grains, however, are sufficiently massive to go straight through the thin shock layer. In the shock frame, they are effectively injected into the gas with velocity 0.75 $v_s$  at the shock front. In addition to this initial velocity, the grains are also betatron accelerated (Spitzer, ref. 9). As the gas cools, it compresses; the frozen-in magnetic field is compressed along with the gas. Since the grains will normally be charged by up to several volts (McKee et al., ref. 8), they will gyrate around the magnetic field lines. As the field is compressed, the grains will spin up, attempting to conserve the magnetic moment  $\mu = qB/m$ . Calculations by Seab and Shull (ref. 1) show that they can reach velocities up to about twice the shock velocity before drag forces slow them to a halt. In radiative shocks, it is this velocity of the grains through the gas that powers the grain destruction.

As the grains move through the gas, they are gradually destroyed by non-thermal sputtering and by grain-grain collisions. Non-thermal sputtering is the erosion of surface layers of the grain by collision of the fast-moving grain with relatively stationary He atoms in the gas. Hydrogen, CNO group, and heavier elements contribute less than 10% of the He sputtering amount. Occasionally, the grains will collide violently with one another. The largest velocities are carried by the larger, more dense grains because they have greater mass per unit surface area than do the smaller, less dense grains. Collisional and plasma drag forces are less effective in decelerating these grains. Therefore the large grains are able to accelerate to higher gyration velocities and consequently suffer more destruction in radiative shocks, both from non-thermal sputtering and from grain-grain collisions. Note that the small grains continue to be destroyed in collisions as long as any of the grains are moving with high velocity.

In adiabatic shocks, in contrast, the primary destruction mechanism for grains is thermal sputtering in the hot postshock gas. The postshock tempera-

ture behind a  $250 \text{ km s}^{-1}$  shock, for example is about  $5 \times 10^5 \text{ K}$ . Thermal sputtering erodes away the outer layers of the grains in the same manner as non-thermal sputtering, except that here the collision velocities are due to the thermal motion of the gas rather than the gyration velocity of the grains. Figure 1 shows the thermal sputtering rates of silicate and graphite grains from Seab (ref. 6). Note that sputtering turns on rather steeply near  $3 \times 10^5 \text{ K}$ . Thermal sputtering in radiative shocks is not significant because the postshock temperatures are not high enough and because the gas quickly cools below the thermal sputtering threshold. In adiabatic shocks, the high temperatures persist in the SNR cavity roughly until the expanding SN bubble reaches pressure equilibrium with the general ISM. The smallest grains can be totally vaporized in this time, while the larger grains are merely pared down to a smaller radius. Preliminary calculations show that a  $250 \text{ km s}^{-1}$  shock removes about  $300 \text{ \AA}$  from each grain. Slower shocks hit more frequently according to equation (2) but destroy less grain material. We find that  $250 \text{ km s}^{-1}$  shock tend to dominate the grain destruction by thermal sputtering in adiabatic shocks.

McKee et al. (ref. 7) use a first order time dependent numerical hydrodynamic shock code to find the destruction efficiencies for silicate grains in radiative shocks from  $50$  to  $150 \text{ km s}^{-1}$ . The typical of destruction efficiency shocks in this range is on the order of  $10\%$ , down from the  $50\%$  typical efficiency found by Seab and Shull (ref. 1). With  $\epsilon = 0.10$ , the grain lifetime from equation (2) is on the order of  $10^6$  years for silicate grains.

This calculated lifetime for silicates poses a fundamental problem for grain evolution models. The formation time for new silicate grains in red giant winds is a few times  $10^6$  years. Since the destruction time is less than this, we would expect most of the silicon in the ISM to be in the gas phase. Instead, Si is found to be  $90\%$  or more depleted in most lines of sight (Shull and van Steenberg, ref. 10). Moreover, most of the depleted silicon must be in the form of silicates to give the observed strength of the  $10\mu$  feature (Tielens and Allamandola, ref. 11). The difficulty can be resolved if either the destruction rates are actually much lower than calculated, or if the grain formation rates are much higher than expected. The latter possibility would hold if a large fraction of the grain material is formed in the cloud phases of ISM itself, rather than exclusively in red giant atmospheres. At least some refractory grain material must necessarily form in the ISM to account for lines of sight with  $99\%$  or greater depletion of elements such as Si, Fe, and Ca. Greenberg and coworkers (Greenberg, ref. 12, 13) propose a mechanism for forming an organic refractory material in dark clouds. It therefore seems more likely that the classical formation rates are too low, rather than that the destructions rates are too high. It is not clear, however, just how a silicate material would form rather than an organic refractory material. Until this question is settled, some level of doubt must be attached to the whole issue of grain destruction.

### III. CARBON GRAINS

Carbon grains do not present the same problems as do silicate grains. The depletion of carbon in the ISM is on the order of 50% (Jenkins, ref. 14), much less than the depletion of silicon. These depletions can be reasonably explained with destruction rates approximately the same as the formation rates. Calculations of the destruction rates of graphite are in fact somewhat lower than for silicon because of the higher binding energy of graphite (7.5 eV for graphite versus about 5.35 eV for silicates). Graphite grains are accordingly expected to live longer than silicate grains. Unlike interstellar silicon, which must be in the form of silicates in order to produce the observed 10 and 20  $\mu$  features, carbon is not constrained to be in the form of graphite. Some or all of the carbon in grains might be in the form of amorphous carbon, glassy carbon, or an organic refractory material without violating the observations. The last form is easily grown in dark clouds in the interstellar medium. The primary question on carbon in grains is in what form the carbonaceous material exists. Whatever the form, shock processing of carbonaceous grains must still play a primary role in determining the structure of the grains.

The most popular candidate material has been graphite. Graphite has an absorption feature at about the right place and the right strength to explain the 2200 Å feature in the ultraviolet interstellar grain extinction curve (Savage and Mathis, ref. 15). Objections have been raised to this identification of the carbon grain material on the grounds that there is little correlation observed between the 2200 Å bump strength and the far-UV extinction rise (Greenberg and Chlewicki, ref. 16), and because the peak wavelength of the bump does not show any of the shifts that would be expected from variations in grain size (Massa and Fitzpatrick, ref. 17). For the present, graphite is still being used in destruction calculations because it remains a possible candidate for interstellar grain material (cf. Draine and Lee, ref. 18) and because at least some measured sputtering data is available.

The experimental data on graphite sputtering has been used to get a best fit sputtering curve (Seab, ref. 6; Tielens et al., in preparation) based on an empirical formula by Anderson and Bay (ref. 19). Agreement between experimenters is not good, even for supposedly similar samples of material. The worst case is for sputtering yield measurements of graphite by hydrogen, where there is nearly a factor of ten discrepancy between measurements by different groups (Anderson and Bay, ref. 19). Fortunately, hydrogen contributes less than 10% of the total sputtering rate. Agreement is better for sputtering by He, which contributes about 90% of the total. Overall, the adopted best fit sputtering parameters are uncertain by a factor of 2 to 3, only mildly worse than the uncertainties for silicate sputtering. It is reasonable that graphite should be harder to sputter than silicates since the binding energy per atom is 50% larger. The thermal sputtering curves shown in figure 1 reflect this conclusion.

In addition to being harder to sputter, graphite grains may also have a

very different size distribution than silicate grains. Basic information on the sizes of interstellar grains is deduced from the observed extinction curve, which measures the wavelength dependence of the attenuation of starlight due to the dust in the line of sight to a star. Mathis, Rumpl, and Nordsieck (ref. 20; hereinafter MRN) fit the average extinction curve very well with a combination of graphite grains and silicate grains, each with a power law size distributions of dex -3.5 and a range from 2500 Å to 50 Å grain radii. Graphite grain destruction calculations by Tielens et al. (ref. 21) use this sort of size distribution. However, the objections mentioned previously may restrict the sizes of graphite grains to less than about 200 Å in radius. Other types of carbonaceous grains may still exist in larger sizes.

Changing the size distribution of the carbon grains will have only a minor effect on the total destruction rate results. The non-thermal sputtering rates will be significantly decreased if smaller grains are used, since drag forces are more effective on small grains and consequently the betatron acceleration mechanism will be less effective. The effect of grain-grain collisions might be lessened by a factor of not more than 2 or 3. The decrease is not more because the large silicate grains will still be betatron accelerated to high velocities and will continue to collide energetically with smaller carbon grains. Smaller graphite grains will be more vulnerable to destruction by thermal sputtering behind adiabatic shocks since small grains have more surface area for their volume. Thus the total carbon grain destruction rate in the galaxy is not very sensitive to the size distribution chosen.

The results of a series of calculations on graphite grain destruction by Tielens et al. (ref. 21) are shown in figure 2. The sputtering process has a threshold just above 50 km s<sup>-1</sup> shock velocity, but increases steeply from there. The vaporization of material in grain-grain collisions has a lower threshold velocity than sputtering, but increases more slowly. The dominant process shown in Figure 2 is the shattering of grains in grain-grain collisions. Shattering has a lower threshold than both sputtering and vaporization since it must break atomic bonds only along the surfaces of the fragments, instead of having to break every bond in the solid.

If the carbon exists in forms other than graphite, as seems likely, then these results will be modified. Non-graphitic forms (other than diamond) are likely to be less tightly bound than graphite. The sputtering threshold for these materials will be correspondingly lower, so that the destruction rates will be higher. On the other hand, if the grain densities are also lower, then drag forces in radiative shocks will be more effective, so that grain velocities will be less and the destruction rates lower. Duley (ref. 22) proposes that the carbonaceous material is in the form of a thin layer covering a silicate type grain. In this case, the grain velocity will be determined by the bulk density of the grain, and the carbon material, being on the outside of the grain, will again be more readily destroyed. The resolution of this admittedly confusing situation depends on the careful evaluation of the destruction rates for the different grain models. Tielens et al. (in preparation) will present a more thorough analysis of the grain destruction rates and mechanisms. For the present, the calculations based on

an MRN graphite grain/ silicate grain model will be used as a guide to grain destruction rates.

In addition to shattering graphite grains, grain-grain collisions in radiative shocks can convert the shatter products into the high-pressure form of carbon: diamond. The diamond conversion process will be discussed in the next section.

#### IV. DIAMONDS IN THE SKY

Lewis et al. (ref. 23) found small ( $\approx 50 \text{ \AA}$ ) diamonds in the C6 phase of the Allende meteorite. These diamonds were associated with isotopic anomalies, indicative of an interstellar origin of the diamonds. They propose that the diamonds were formed by condensation in the outer atmosphere of a red giant which subsequently went supernova, thereby implanting additional isotopic anomalies in the circumstellar carbon grains.

Tielens et al. (ref. 21) propose that these small interstellar diamonds were produced by grain-grain collisions of graphitic or other carbonaceous grains in supernova-driven shocks.

When two grains collide at high velocities, they drive shock waves into the solid material of each grain. The shock wave heats and pressurizes the grain material. This high temperature and pressure can convert graphite into diamond. The process has been shown experimentally (cf. Tielens, this volume) to give high yields of small diamond particles when the shock pressure is greater than a threshold of about 0.7 eV per atom. This threshold is nearly the same as the shattering threshold, and both are a factor of ten less than the vaporization threshold of 7.5 eV per atom. Thus, the grain-grain collision will not only shatter part or all of the grain, but will convert the shatter products into diamond. The characteristic size of diamond produced by this process will be on the order of 30  $\text{\AA}$ , in reasonable agreement with the Allende diamond sizes. The microphysics of the diamond conversion is discussed more thoroughly by Tielens (this volume).

We can estimate the population of interstellar diamonds by balancing the formation and destruction rates to get

$$f_d = \frac{\epsilon_d/\epsilon_v}{\left[ 1 + \frac{r_{sn}}{\epsilon_v r_{sf}} \right] \left[ 1 + \left( \frac{\epsilon_v r_{sf}}{r_{sn}} \right) \right] \left[ 1 + \frac{\epsilon_d}{\epsilon_v} \right]} f_i \quad (3)$$

$$\approx 0.1 f_i$$

where  $f_d$  is the fraction of interstellar carbon in diamond form;  $f_i$  is the fraction of carbon injected into the ISM as graphite;  $\epsilon_d$  is the diamondization efficiency and  $\epsilon_v$  the vaporization efficiency including sputtering, both averaged over a distribution of shock velocities;  $\tau_{sf}$  is the star formation timescale, here taken to be the same as the destruction time for graphite grains; and  $\tau_{sn}$  is the time for a grain to be hit by a supernova shock with a velocity greater than the diamondization threshold. Figure 2 shows that the shock velocity corresponding to significant diamond conversion is about  $35 \text{ km s}^{-1}$ . Although  $\epsilon_d$  is larger than  $\epsilon_v$  for the radiative shocks shown in figure 2, it will drop to zero for shocks fast enough to be adiabatic ( $v > 200 \text{ km s}^{-1}$ ). The  $\epsilon_v$  efficiency also drops off as shock velocity approaches the adiabatic case, but then increases strongly as thermal sputtering turns on. Averaged over all shock velocities, we find  $\epsilon_d = \epsilon_v$  (Tielens et al., ref. 21).

Equation (3) is not very sensitive to the  $\epsilon_v$ ,  $\tau_{sf}$ , or  $\tau_{sn}$  parameters, since these appear both as  $(\epsilon_v \tau_{sf} / \tau_{sn})$  and as its inverse in the denominator. A wide range of values for these parameters yield values of about 0.1  $f_i$  for equation (3). Unfortunately  $f_i$  is not known. If we take an optimistic 50% of the fresh carbon injected into the ISM is in the form of graphite or amorphous carbon, then  $f_d = 0.05$ , or 5% of the interstellar carbon in the form of diamond.

This number is probably an upper limit to the actual diamond fraction of the ISM since we do not know the efficiency of diamondization of submicron-sized grains in shocks. The timescale for grain-grain collisions in the ISM is on the order of  $10^{-9}$  seconds, much shorter than the time for shocking graphite in the laboratory. The time required for conversion to diamond is not known; an upper limit has been set at  $10^{-6}$  seconds. It is not unreasonable to assume that diamond conversion can occur on the nanosecond timescale required for interstellar grain-grain collisions.

The diamond conversion process must start with something close to pure carbon. Some impurities can be tolerated, and will just add color to the diamond. The limit on the amount of impurities that can be tolerated and still yield a substantial conversion to diamond is not known; diamond conversion has been obtained with 10% oxygen impurity in glassy carbon (cf. Tielens this volume). The organic refractory material probably cannot be converted to diamond. Polycyclical aromatic hydrocarbons (PAHs) (Allamandola and Tielens, ref. 24) are too small for the conversion to work; the PAH will break apart before a shock front has time to fully develop. Graphite and amorphous or glassy carbon grains are likely candidates for conversion to diamond in the interstellar shocks. It is not known how much of the interstellar solid carbon is in these forms; the 50% figure used for  $f_i$  may be too high. The 5% figure derived above is again an upper limit to the expected amount of interstellar diamond.

Hecht (ref. 25) places an observational upper limit of 1% on the amount of carbon in diamond form, based on the absence of a diamond absorption edge starting at 7 eV (1430 Å in the far-UV extinction curve). This is not a hard upper limit because the absorption edge could be smoothed out by size effects in a distribution of diamond particle sizes. The small fraction of diamond

found in meteorites (Lewis et al., ref. 23) does not set an effective upper limit on the interstellar population because of the unknown amount of processing of the meteoritic material through the presolar nebula. Thus the 5% theoretical figure, regarded as a generous upper limit, is consistent with the little data available.

## V. SUMMARY AND CONCLUSIONS

Supernova shocks play a significant part in the life of an interstellar grain. In a typical  $10^8$  year lifetime, a grain will be hit by an average of 10 shocks of  $100 \text{ km s}^{-1}$  or greater velocity, and even more shocks of lower velocity. Evaluation of the results of this frequent shock processing is complicated by a number of uncertainties, but seems to give about 10% destruction of silicate grains and about half that for graphite grains. Because of the frequency of shocking, the mineralogy and sizes of the grain population is predominately determined by shock processing effects, and not by the initial grain nucleation and growth environment.

One consequence of the significant role played by interstellar shocks is that a certain fraction (up to 5%) of the carbon should be transformed into the diamond phase. Diamond transformation is observed in the laboratory at threshold shock pressures easily obtainable in grain-grain collisions in supernova shocks. Yields for transforming graphite, amorphous carbon, glassy carbon, and other nearly pure carbon solids into diamond are quite high. Impurities up to at least the 10% level (for oxygen) are tolerated in the process. The typical size diamond expected from shock transformation agrees well with the observed sizes in the Lewis et al. (ref. 23) findings in meteoritic material. Isotopic anomalies already contained in the grain are likely to be retained through the conversion process (Tielens, this volume), while others may be implanted by the shock if the grain is close to the supernova. The meteoritic diamonds are likely to be the results of transformation of carbon grains in grain-grain collisions in supernova shock waves.

## REFERENCES

1. Seab, C. G.; and Shull, J. M.: Shock Processing of Interstellar Grains. *Ap.J.*, vol. 275, 1983, pp.652-660.
2. Seab, C. G.; Edgar, R. J.: Galactic Fountains and Dust Grains. *Bull. Amer. Astron. Soc.*, vol. 18, 1985, p.960.
3. Barlow, M. J.: Observations of Dust in Planetary Nebulae. *IAU Symp. 103, Planetary Nebula*, D. R. Flower, ed., Reidel Pub. Co., pp.105-128.
4. Draine, B. T.; and Salpeter E. E.: Destruction Mechanisms for Interstellar Dust. *Ap.J.*, vol. 231, 199, pp.438-455.

5. Dwek, E.; and Scalo, J. M.: The Evolution of Refractory Interstellar Grains in the Solar Neighborhood. *Ap.J.*, vol. 239, 1980, pp.193-211.
6. Seab, C. G.: Grain Destruction, Formation, and Evolution. *Interstellar Processes*. D. J. Hollenbach and H. A. Thronson, eds., Reidel Pub. Co., pp.491-512.
7. McKee, C. F.; and Ostriker, J. P.: A Theory of the Interstellar Medium: Three Components Regulated by Supernova Explosions in an Inhomogeneous Substrate. *Ap.J.*, vol. 218, 1977, pp.148-169.
8. McKee, C. F.; Hollenbach, D. J.; Seab, C. G.; and Tielens, A. G. G. M.: The Structure of Time-Dependent Interstellar Shocks and Grain Destruction in the Interstellar Medium. *Ap.J.*, vol. 318, 1987, pp.674-701.
9. Spitzer, L.: High-Velocity Interstellar Clouds. *Comments Ap.*, vol. 6, 1976, pp.177-187.
10. Shull, J. M.; and van Steenberg, M.: *Ap.J.*, vol. 330, 15 July 1988 (in press).
11. Tielens, A. G. G. M.; and Allamandola, L. J.: Composition, Structure, and Chemistry of Interstellar Dust. *Interstellar Processes*. D. J. Hollenbach and H. A. Thronson, eds., Reidel Pub. Co., 1987, pp.397-469.
12. Greenberg, J. M.: Stars and Stellar Systems, B. Westerlund, ed., Reidel Pub. Co., 1979, p.155.
13. Greenberg, J. M.: Evolution of Interstellar Grains. *Laboratory & Observational Infrared Spectra of Interstellar Dust*, R. D. Wolstencroft and J. M. Greenberg, eds., Occasional Reports of the Royal Observatory, no. 12, 1984, pp.1-25.
14. Jenkins, E. B.: Element Abundances in the Interstellar Atomic Material. *Interstellar Processes*. D. J. Hollenbach and H. A. Thronson, eds., Reidel Pub. Co., 1987, pp.533-559.
15. Savage, B. D.; and Mathis, J. S.: Observed Properties of Interstellar Dust. *Ann. Rev. Astron. Ap.*, vol. 17, 1979, pp.73-111.
16. Greenberg, J. M.; and Chlewicki, G.: A Far-Ultraviolet Extinction Law: What Does It Mean? *Ap.J.*, vol. 272, 1983, pp.563-578.
17. Fitzpatrick, E. L.; and Massa, D.: An Analysis of the Shapes of Ultraviolet Extinction Curves II. The Far-UV Excess. *Ap.J.*, vol. 328, 1988 (in press).
18. Draine, B. T.; and Lee, H. M.: Optical Properties of Interstellar Graphite and Silicate Grains. *Ap.J.*, vol. 285, 1984, pp.89-108.

19. Anderson, H. H.; and Bay, H. L.: Sputtering Yield Measurements. Sputtering by Particle Bombardment I: Physical Sputtering of Single-Element Solids. R. Behrisch, ed., Springer-Verlag, 1981, pp.145-218.
20. Mathis, J. S.; Rimpl, W.; and Nordsieck, K. H.: The Size Distribution of Interstellar Grains. *Ap.J.*, vol. 217, 1977, pp.425-433.
21. Tielens, A. G. G. M.; Seab, C. G.; Hollenbach, D. J.; and McKee, C F.: Shock Processing of Interstellar Dust: Diamonds in the Sky. *Ap.J.*, vol. 319, 1987, pp.L109-L113.
22. Duley, W. W.: Interstellar Extinction and the Composition of Dust Grains. *Mon. Not. R. Astr. Soc.*, vol. 229, 1987, pp.203-212.
23. Lewis, R. S.; Ming, T.; Wacker, J. F.; Anders, E.; and Steel, E.: Interstellar Diamonds in Meteorites. *Nature*, vol. 326, 1987, pp.160-162.
24. Ailamandola, L. J.; Tielens, A. G. G. M.; Barker, J. R.: Infrared Absorption and Emission Characteristics of Interstellar PAHs. *Interstellar Processes*. D. J. Hollenbach and H. A. Thronson, eds., Reidel Pub. Co., 1987, pp.471-489.
26. Hecht, J. H.: Observations on Constraints on Interstellar Diamonds. *Nature*, vol. 326, 1988, p.765.

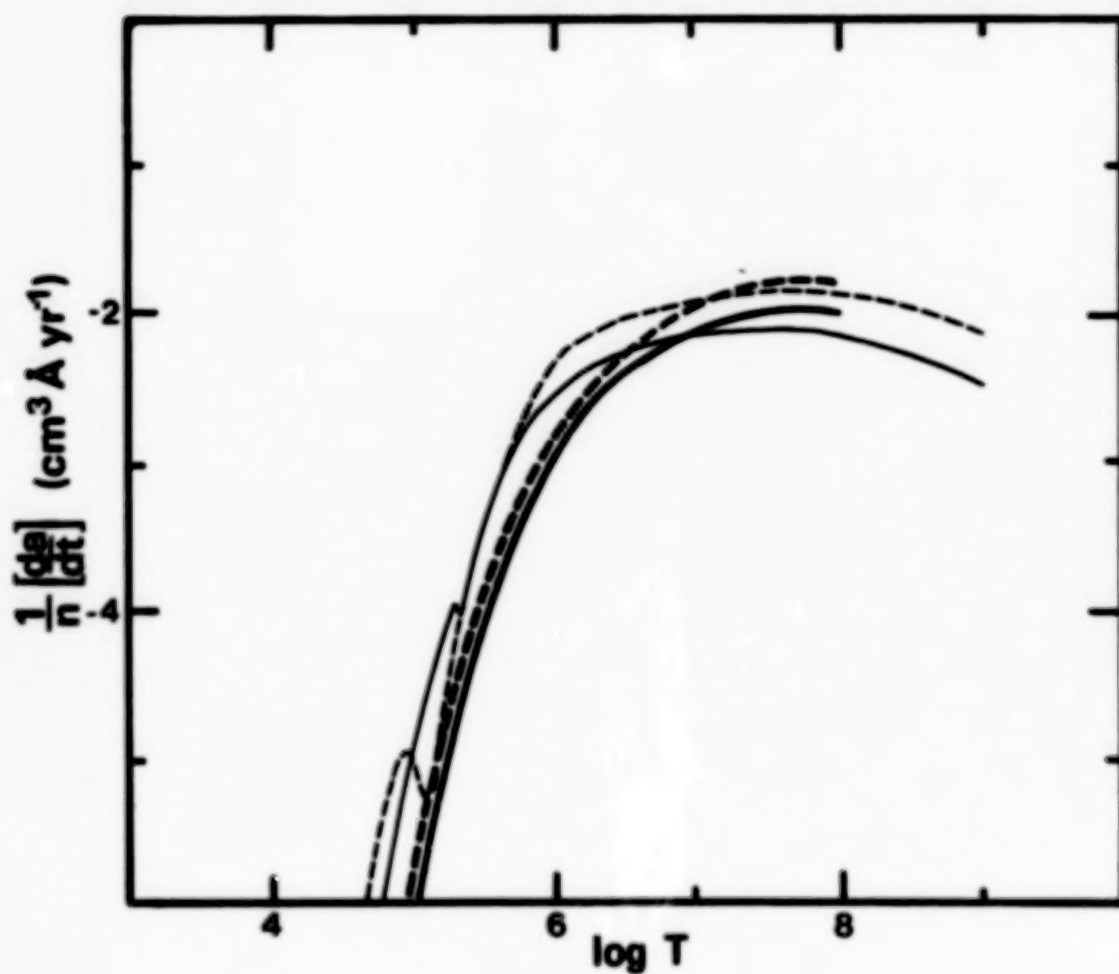


Figure 1.— Thermal sputtering rates for silicates (dashed curves) and graphite (solid curves). The thick lines represent the best fit to data from Seab (ref. 6), while the thin lines are from Draine and Salpeter (ref. 4).

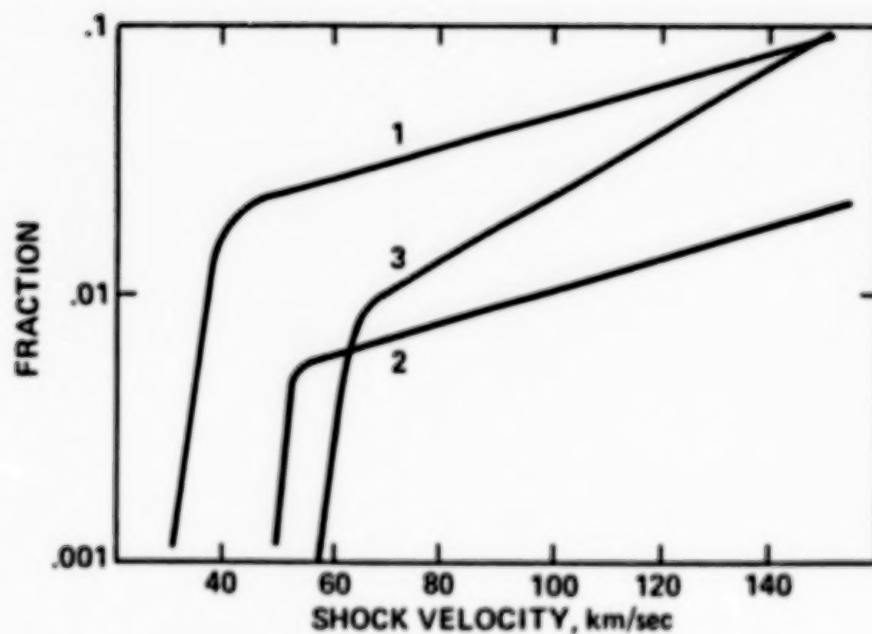


Figure 2.— Shock processing of graphite grains as a function of shock velocity. Curve (1) gives the fraction of total graphite grain material transformed into diamond; curve (2) gives the amount vaporized into gaseous carbon by grain-grain collisions, and curve (3) the amount sputtered off the grains. These curves are for radiative shocks only; for adiabatic shocks, thermal sputtering dominates the destruction, while the other processes are negligible.

# Carbon Stardust: From Soot to Diamonds

A.G.G.M. Tielens

MS 245-6  
Space Sciences Division  
NASA Ames Research Center  
Moffett Field  
CA 94035

and  
Space Sciences Laboratory  
University of California  
Berkeley  
CA 94720

*We are stardust*  
Joni Mitchell, 1969, Woodstock.

## Abstract

This paper reviews the formation of carbon dust in the outflow from stars and the subsequent evolution of this so-called stardust in the interstellar medium. The chemical and physical processes that play a role in carbon stardust formation are very similar to those occurring in sooting flames. Based upon extensive laboratory studies of the latter, the structure and physical and chemical properties of carbon soot are reviewed and possible chemical pathways towards carbon stardust are discussed. Grain-grain collisions behind strong interstellar shocks provide the high pressures required to transform graphite and amorphous carbon grains into diamond. This process is examined and the properties of shock-synthesized diamonds are reviewed. Finally, the interrelationship between carbon stardust and carbonaceous meteorites is briefly discussed.

## I Introduction

Interstellar dust is an important constituent of the interstellar medium. It absorbs efficiently visible and ultraviolet photons, which it reemits at IR wavelengths, and, thus, it regulates the spectral appearance of many dust-shrouded objects. It regulates the energy balance of the gas through the ejection of energetic electrons and gas-grain collisions. By attenuating the ambient interstellar UV radiation field, it allows (indirectly) the formation of quite complex molecules. Undoubtedly, the most abundant molecule,  $H_2$ , is formed directly on grain surfaces. The abundance of other molecules may also be influenced through grain-catalyzed reactions. Grains may also have played an important role in the cosmic history of the biogenic elements (Wood and Chang 1985). In fact, carbonaceous grains are thought to form an important component of interstellar dust (1).

In recent years, our understanding of interstellar carbonaceous dust has improved dramatically. Partly, this is a result of the opening up of the infrared

window. Infrared spectroscopy is a major tool for remote probing of the composition of interstellar dust (2). Indeed, most dust components thought to be present in the interstellar dust have been identified through infrared spectroscopy. The development of new techniques that allowed detailed analysis of microscopic amounts of stardust preserved in carbonaceous meteorites has also been instrumental in increasing our knowledge of interstellar dust (3).

The picture that arises from this new wealth of data is one where interstellar dust consists of many diverse components formed under a variety of conditions in many classes of objects. This varied background of interstellar dust makes the quotation from Woodstock particularly appropriate. A multitude of complex processes have been suggested to play a role in circumstellar dust formation and its modification in the interstellar medium. In view of the rapid developments, it has not yet been possible to weed out the unimportant processes and to concentrate on the few, more important ones. Lacking general consensus in the field, this review is an attempt to summarize my own views on these problems. Some of these seem to enjoy considerable following, others are more controversial. However, given the current large flux of ideas, any review has to be somewhat personal and dated anyway.

This review is organized as follows:

- I Introduction
- II Composition and Evolution of Interstellar Dust
- III The Structure of Carbonaceous Materials
- IV Carbon Injection into the Interstellar Medium
  - A) Sources
  - B) Carbon budget of the galaxy
  - C) The  $^{13}\text{C}$  budget
- V The Dust Condensation Zone
  - A) The photosphere
  - B) Structure of the outflow
  - C) Physical conditions in the dust condensation zone
  - D) Chemical composition
- VI Chemical Pathways to Carbon Stardust
  - A) Thermodynamics and carbon condensation
  - B) Soot formation
  - C) PAHs and the formation of carbon stardust
  - D) Non-LTE and the formation of carbon stardust
  - E) Carbon stardust formation around WC 8-10 and R Cr B stars
  - F) Carbon stardust formation in supernova ejecta
  - G) Summary
- VII Grains and Shocks in the Interstellar Medium
  - A) Grain-grain collisions
  - B) Diamond metamorphism
  - C) Diamonds in the sky
- VIII Interstellar Carbon Dust and Carbonaceous Meteorites
- IX Summary

## II Composition and Evolution of Interstellar Dust

Interstellar dust consists of many different components, including amorphous silicates, graphite, Polycyclic Aromatic Hydrocarbons (hereafter PAHs), amorphous carbon, icy grain mantles, and organic refractory grain mantles. Silicon carbide and magnesium sulfide, which have been identified in the outflow from carbon-rich giants and planetary nebulae might also be present in the interstellar medium. Our present astronomical knowledge on the composition of interstellar dust is summarized in table 1. For each component, this table gives the birth site(s), the fraction of the elemental abundance that it locks up, and the dust volume relative to that of the silicates. The spectral signatures that have been used to identify each dust component are also indicated. For a discussion of these the reader is referred to a recent review by us (1) as well as to earlier reviews (4,5,6).

One of the most interesting developments in recent years within the field of interstellar dust has been the realization that large polycyclic aromatic molecules form an ubiquitous component of the interstellar dust. A variety of objects show prominent emission features at 3.3, 6.2, 7.7, and 11.3  $\mu\text{m}$  (5,7,8), which are characteristic of PAHs either as free-flying molecules or in the form of soot particles (9,10,11). Figure 1 compares the IR spectrum observed towards the HII region in Orion with the Raman spectrum of auto soot (11). For a highly disordered material such as soot the infrared active and Raman active vibrational modes are similar in number and frequency. It is expected that a collection of free flying PAH molecules will have a similar IR spectrum. Although it is difficult to distinguish spectrally between a collection of large PAH molecules and solid soot particles, an analysis of the excitation mechanism shows that the carrier of these emission features contains only about 20 C atoms (10,11,12). Depending on the FUV absorption properties of the particular PAHs responsible for the IR emission, about 0.5-2% of the total available elemental carbon is locked up in this component (cf., table 1). Since in many objects the IR emission originates in material recently ejected from a star, PAHs probably are the extension of the grain size distribution of circumstellar carbon grains into the molecular domain and as such may shed light on the detailed formation mechanism of carbon stardust. This will be discussed in some detail in § VI.

About half of the volume of the interstellar dust is made up of silicate grains (c.f., table 1). The other half has to be in the form of a largely carbon-bearing dust component, either graphite or amorphous carbon stardust, or organic refractory grain mantles accreted on stardust in the interstellar medium. The latter component consists of a mixed organic polymer containing  $\text{CH}_3$ ,  $\text{CH}_2$ ,  $\text{C=O}$ , and possibly OH groups, which is formed by UV photolysis and (transient) heating of an icy (eg.,  $\text{H}_2\text{O}$ ,  $\text{NH}_3$ ,  $\text{CH}_3\text{OH}$  and CO) mixture. Current observations indicate that amorphous carbon particles seem to make up only a relatively minor fraction of the interstellar dust (c.f., table 1), although this value is somewhat uncertain. From table 1, one might get the impression that the carbon dust component is dominated by organic refractory grain mantles. This is somewhat misleading. First, large graphite particles ( $>1000\text{\AA}$ ) do not have readily discernable absorption features and they are, thus, not accounted for in table 1. Second, the relative volume of the organic refractory grain mantles, which has presently only been detected towards the galactic center, is uncertain by a factor of about two due to the uncertainty in the precise identification of the absorbing molecules. Moreover, the relative volume of this dust component in the local interstellar medium may be much less. In fact, observations towards nearby stars, yield an upper limit on the relative volume of organic grain mantles which is about half that quoted in table 1. In view of these uncertainties, the distribution of

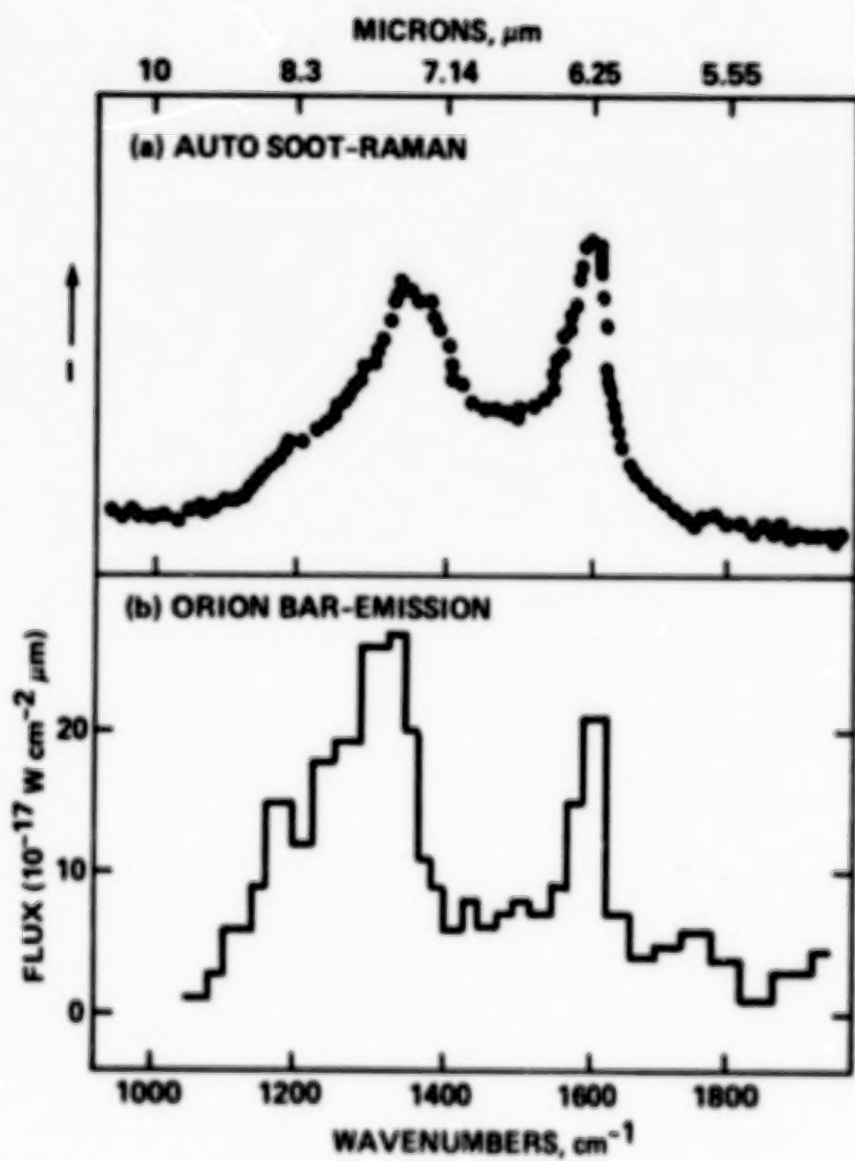


**Figure 1.** Comparison of the 5 to 8  $\mu\text{m}$  Raman spectrum of auto soot with the emission from the Orion Hill region.

Table 1: Interstellar Dust Components

COMPONENT	BIRTH SITE	ELEMENTAL ABUNDANCE <sup>a</sup>	REL VOL <sup>b</sup>	SPECTRAL SIGNATURE
Silicates	O-rich giants & Novae	100% Si 20% O (Mg & Fe ?)	1	10, 20 $\mu$ m features
Graphite	C-rich giants ?	>25% C	>0.25	2200Å bump <sup>f</sup>
PAHs	C-rich PN	1% C	0.01	3.3, 6.2, 7.7, 11.3 $\mu$ m emission features
Amorphous Carbon	C-rich giants, Novae, R Cr B & WC 8-10	5-10% C	~0.1	7.6 $\mu$ m absorption feature ?
Icy grain mantles <sup>d</sup>	molecular clouds	up to 40 % C and O	up to 3	3.1, 4.6, 6.0 and 6.85 $\mu$ m absorption features
Organic refractory grain mantles <sup>e</sup>	interstellar medium	24% C 6% O	0.8	3.4, 6.0 $\mu$ m absorption features
SiC	C-rich giants & Novae	.c	.c	11.4 $\mu$ m emission feature
MgS	C-rich Giants & PN	.c	.c	30 $\mu$ m emission feature

a) Percentage of cosmic abundance of element locked up in interstellar dust component.

b) Volume of dust component relative to that of silicates.

c) This dust component has not (yet) been detected in the interstellar medium.

d) Only observed in dense molecular clouds.

e) Only observed towards the galactic center.

f) Only graphite grains of 200Å contribute to this bump.

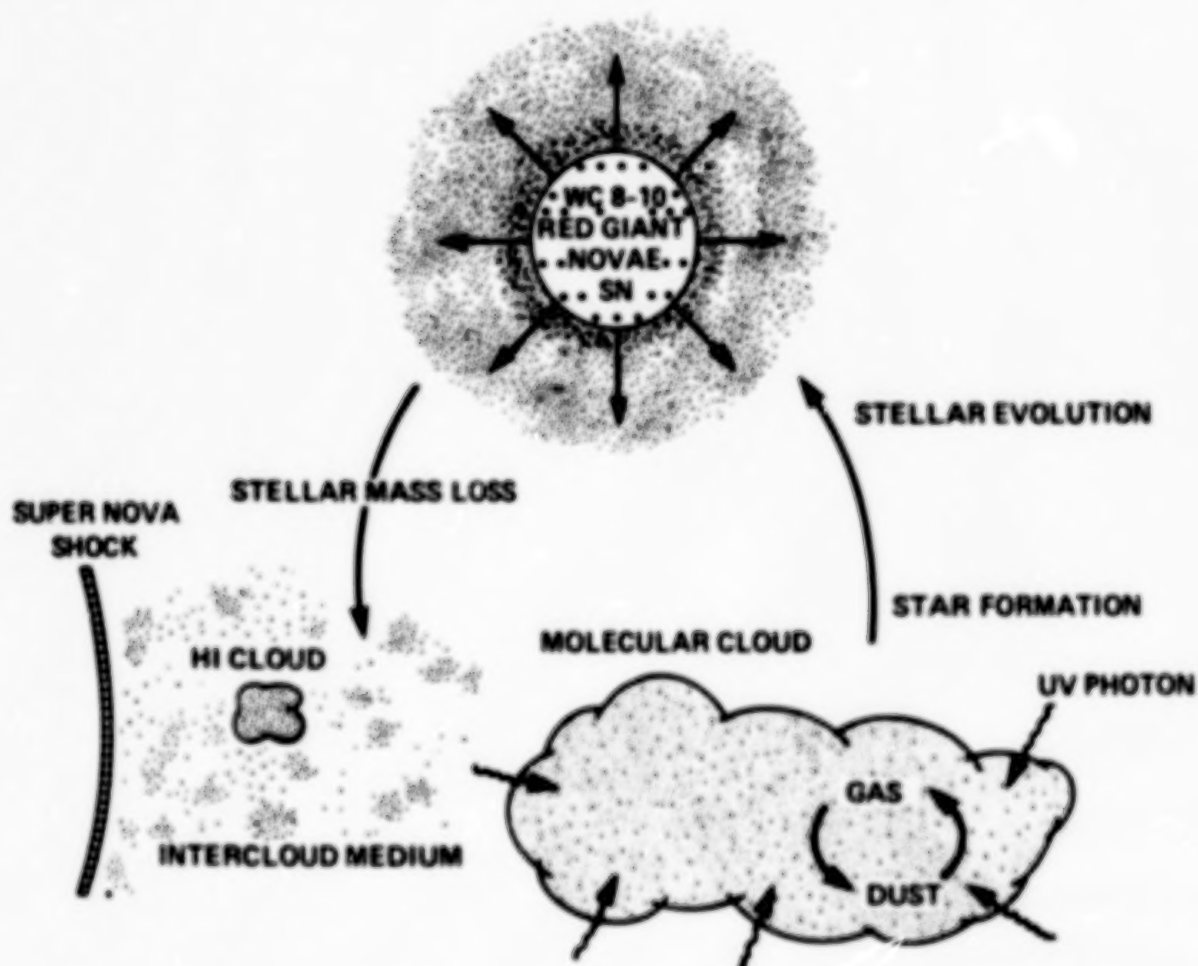
the carbon in the various carbon-bearing dust components in the interstellar medium should be considered approximate at this point.

Detailed models for the dust in the interstellar medium based on both premises - graphite and organic refractory grain mantles - have been developed (13-17). Using some combination of grain components, and a grain size (and shape) distribution, these models fit the visible and UV interstellar extinction curve, the linear and circular polarization, the visual extinction per hydrogen atom and, to some extent, the observed elemental depletions. Such an exercise is useful for the derivation of important quantities such as the grain size distribution within the framework of one particular model. However, these fits cannot be used to discriminate between

## EVOLUTION OF INTERSTELLAR DUST

**STARDUST:** SILICATES, GRAPHITE, AMORPHOUS CARBON, PAHs, SiC, MgS

**FORMATION PROCESSES IN CIRCUMSTELLAR SHELLS:** NUCLEATION, CONDENSATION, COAGULATION



**DUST IN THE INTERSTELLAR MEDIUM:** STARDUST, ICY GRAIN MANTLES, ORGANIC REFRACTORY MANTLES, DIAMONDS

**FORMATION PROCESSES IN MOLECULAR CLOUDS:** ACCRETION, REACTION, UV PHOTOLYSIS, TRANSIENT HEATING

**DUST MODIFICATION PROCESSES:** (DIAMOND) METAMORPHISM AND SHATTERING IN SHOCKS

**Figure 2.** A schematic representation of the evolution of interstellar dust, summarizing the processes that play a role in the formation, destruction and modification of interstellar dust. Stardust is formed in the outflow from stars in the late stages of their evolution and ejected into the interstellar medium. Interstellar medium dust is formed inside dense clouds. Dust is destroyed by strong shock waves and by incorporation into newly formed stars. Grain-grain collisions in shock waves can also transform graphite (or amorphous carbon) into diamonds. See text for details.

different grain models. The visible and UV interstellar extinction curves are notably insensitive to the exact grain composition because the amorphous structure of interstellar grains as well as the presence of a size distribution tend to smear out any identifiable structure in the electronic absorption properties of the materials (1). It is because of this that widely disparate models for the interstellar dust all yield reasonably good fits to the observed interstellar extinction curve. The presence of free parameters in the models such as the shape or surface structure of the grains, which have not yet been considered in such exercises, reinforces this point.

The evolution of interstellar dust is determined by many complex, interplaying processes whose details are not understood very well. Figure 2 gives a schematic overview of the evolution of interstellar dust. Some dust components -silicates, graphite, and amorphous carbon - are formed in the outflow from stars (i.e., stardust) by nucleation, condensation and coagulation processes and their composition and sizes reflect the chemical composition and physical conditions in the condensation zones. In contrast, other dust components -icy and organic refractory grain mantles - are formed by accretion, reaction, UV photolysis, and transient heating processes in the interstellar medium (i.e., ISM dust). Prolonged processing of such grain mantles may eventually lead to the formation of a highly disordered compound consisting mainly of carbon arranged in an aromatic network. This is akin to pyrolysis of hydrocarbons and will ultimately lead to an amorphous carbon dust component. Dust is also processed in the interstellar medium by strong supernova shock waves. High velocity ion-grain collisions behind a shock will lead to sputtering, ion-implantation, and radiation damage. These will also lead to an amorphization of the surface layers. High velocity grain-grain collisions send strong pressure waves into each grain which can lead to vaporization, shock metamorphism (eg., graphite  $\rightarrow$  diamond), and shattering. Since each of these processes will lead to a different grain material, the composition of the interstellar dust in a particular region will reflect the relative importance of these processes there. The composition of interstellar dust is therefore in some sense a misnomer since the dust composition is expected to vary with phase (eg., diffuse ISM versus dense cloud) as well as galactic radius (eg., local versus galactic center). A global outline of the physical processes playing a role in the formation and modification of interstellar dust has been given elsewhere (2). Here we will concentrate on the formation of carbon stardust and its subsequent evolution in the interstellar medium.

### III The Structure of Carbonaceous Materials

Carbon-rich materials show a wide range of behavior due to the diversity in chemical valence structure and bonding possible with carbon. These are referred to as  $sp$ ,  $sp^2$ , and  $sp^3$  hybridization, where the notation comes from the original carbon atomic orbitals involved in forming the molecular orbitals. In  $sp$  hybridization, the bond geometry is linear and two unequivalent bonds are formed, one triple and one single. An example of a simple organic compound with this structure is acetylene,  $H-C\equiv C-H$ . If only carbon is involved, an acetylene polymer (eg., polyynes) is formed, with a linear structure (cf., fig. 3). Note that polyacetylene is a polymer derived from acetylene by opening up of the triple bond and has an alternating double bond structure (eg.,  $sp^2$  bonding). In  $sp^2$  hybridization, the bond geometry is trigonal and all the bonds lie in a plane. In general only two of the three bonds are equivalent and two single bonds and one double bond characterize this configuration. A simple organic

## THE VARIETY OF CARBON SOLIDS



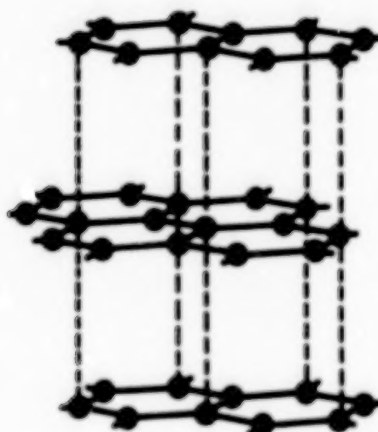
sp HYBRID



ACETYLENE POLYMER



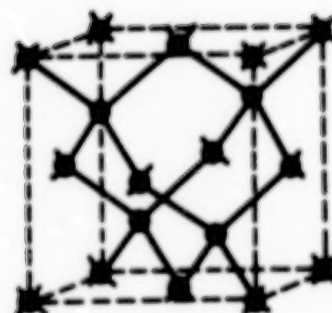
sp<sup>2</sup> HYBRID



GRAPHITE



sp<sup>3</sup> HYBRID



DIAMOND

**Figure 3.** A schematic representation of the chemical valence structures and bonding arrangements possible with carbon. Left: the orientation of the electron clouds in the different hybridizations. Right: the corresponding carbon solids. Solid lines indicate actual bonds, while dashed lines are intended to guide the eyes. Note that sp, sp<sup>2</sup>, and sp<sup>3</sup> hybridization lead to a linear, planar and three dimensional crystalline structure, respectively (see text for details).

compound with this structure is ethene,  $\text{H}_2\text{C}=\text{CH}_2$ . However, if only C is involved and there are enough atoms to form six-membered rings, all the bonds can become equivalent within the carbon framework. This results in an aromatic network as in graphite (cf., fig. 3). Hydrogen can bond to the external single bonds of the  $\text{sp}^2$  carbon atoms at the periphery of the aromatic structure. PAHs are molecular examples of such structures. In  $\text{sp}^3$  hybridization the bond geometry is tetrahedral and when only carbon is involved a diamond structure is produced (cf., fig. 3). Examples of simple molecules with this structure are methane ( $\text{CH}_4$ ) and ethane ( $\text{H}_3\text{C}-\text{CH}_3$ ).

Any realistic material will have some impurities, defects and dislocations and *pure* graphite, diamond or acetylene polymer materials do not exist in nature. In particular, a large variety of carbonaceous materials contain a mixture of C atoms with  $\text{sp}^2$  and  $\text{sp}^3$  bonding. These materials are all loosely called "amorphous carbon" in the astrophysical literature, although their physical properties can vary considerably. Hydrogenated amorphous carbon films are one example of such a mixed bonding structure and soot is another. Both materials contain large aromatic domains interspersed with tetrahedral C atoms which cross link aromatic planes. In hydrogenated amorphous carbon these tetrahedral C atoms are randomly distributed in between the aromatic C atoms. In soot they are more concentrated at the edges of aromatic planes (cf., § VIB). In both cases a large concentration of hydrogen atoms ( $\text{H/C}=0.1$ ) saturates the tetrahedrally carbon and is bonded to the edges of the aromatic domains. This difference in amorphous character is essentially that between a "truly" (random network) amorphous material and a polycrystalline material (cf., 1).

The physical and chemical properties of (hydro)carbons are largely determined by these bonding arrangements. For example, due to the conjugation of  $\pi$  electrons (eg., sharing of  $\pi$  electrons between different C atoms), graphite shows a metallic behavior within the basal (aromatic) plane (eg., graphite is a semi-metal). Its optical properties from the FUV throughout the IR are therefore dominated by interband and intraband transitions of these "free" electrons (18). When the aromatic structure is broken up by the presence of hydrogen atoms or tetrahedrally bonded C atoms, as in amorphous carbon, then the electrons will be more localized. As a result, amorphous carbon is a semi-conductor with a band gap up to 5 eV depending on the size of the largest aromatic domains. While its UV properties are still dominated by interband electronic transitions, its IR properties reflect now vibrations of the carbon (and hydrogen) skeleton (1). It should be emphasized that many of the properties of solid carbon, in particular the electronic structure, are dependent on the disorder and not the disordering agent present.

## IV Carbon Injection into the Interstellar Medium

### A Sources

There are many stellar sources that contribute to the carbon in the interstellar medium, including carbon-rich red giants, carbon-rich Wolf Rayet stars, and supernovae. The relative importance of these different types of objects is not well known. Even estimates of the relative importance of high mass stars versus low mass

Table 2: Stellar Mass-Loss Rates [ $M_{\odot} \text{ yr}^{-1} \text{ kpc}^{-2}$ ]

Object	$\dot{M}_H^a$	$\dot{M}_C^b$	$\dot{M}_d^c$	Observational evidence for dust
C-rich giants	5(-4)	5(-6)	2(-6)	1) featureless continuum: amorphous carbon 2) 11.3 $\mu\text{m}$ feature: SiC 3) 3.3,6.2,7.7,11.3 $\mu\text{m}$ features (in PN phase): PAHs
O-rich giants	5(-4)	2(-6)	-	1) 10 and 20 $\mu\text{m}$ features: silicates
Novae	6(-6)	4(-8)	1(-8)	1) 10 $\mu\text{m}$ feature: silicates 2) black body (marbles ?) 3) black body + 11 $\mu\text{m}$ feature (SiC ?)
OB stars	1-3(-4)	1(-6)	-	1) no dust
SN: Type I	-	3(-7)	-	1) no conclusive evidence for dust
Type II	2(-4)	2(-6)	1(-6)	
WR stars <sup>d</sup>	-	4(-6)	-	1) no dust
WC 8-10	-	2(-6)	5(-8)	1) featureless continuum + 7.7 $\mu\text{m}$ feature: amorphous carbon (+PAHs ?)
TOTAL	1.5(-3)	1.6(-5)	3(-6)	

notes:

- a) Hydrogen injection rate.
- b) Carbon injection rate.
- c) Carbon stardust injection rate.
- d) Excluding WC 8-10 stars.

stars vary continuously due to new developments in, for example, the determination of mass-loss rates (eg., IR studies) or nucleosynthetic reaction rates (eg.,  $^{12}\text{C}(\alpha, \gamma)^{16}\text{O}$ ). Thus, while 10 years ago high mass stars ( $M > 10 M_{\odot}$ ) were thought to be mainly responsible for the carbon in the interstellar medium (19), in more recent studies carbon-rich red giants seem to dominate (20,21). However, there are some indications that the pendulum is swinging back into the direction of the massive stars. In the remainder of this section, estimates of the carbon mass-loss rates of different types of objects are reviewed. These estimates are summarized in table 2.

**Red Giants:** The mass injection rate of gas in the interstellar medium is dominated by mass-loss from red giants. A rough estimate of the total mass injection rate can be determined from the white dwarf birth rates. Assuming that each white dwarf has lost about  $1 M_{\odot}$  during the red giant phase, we find from the birth rate of such objects

( $\sim 1 \text{ yr}^{-1}$ ; 22) a total mass injection rate of about  $1 M_{\odot} \text{ yr}^{-1}$ , corresponding to about  $10^{-3} M_{\odot} \text{ kpc}^{-2} \text{ yr}^{-1}$  (23). This is supported by IR and CO studies of the dust and gas mass-loss rate from these objects, which yield values between  $5$  and  $9 \times 10^{-4} M_{\odot} \text{ yr}^{-1} \text{ kpc}^{-2}$  (21,24-27). However, estimates of the mass injection rates due to C-rich and O-rich giants separately range from equal amounts by the two types of objects (21,26) to O-rich giants dominating by a factor ten (24). The giants with a high mass-loss rate ( $> 10^{-5} M_{\odot} \text{ yr}^{-1}$ ) dominate the total gas return to the galaxy and the above mentioned discrepancy centers on differences in the total number of such C-rich objects estimated to be present in the galaxy. It should be noted that all studies require large correction factors for sample incompleteness and the results are thus inherently uncertain. We will adopt a return rate by C-rich giants of  $5 \times 10^{-4} M_{\odot} \text{ yr}^{-1} \text{ kpc}^{-2}$ , which is about the maximum estimated (25,27). Estimates on the return rate by O-rich giants agree on approximately  $5 \times 10^{-4} M_{\odot} \text{ yr}^{-1} \text{ kpc}^{-2}$  (24,27). Using these gas return rates we have estimated the C return rates (cf., table 2) by assuming an elemental C abundance of  $5 \times 10^{-3}$  and  $10^{-2}$  by mass for O-rich and C-rich giants, respectively. The former corresponds to solar abundances, while the latter reflects the C enhancement due to dredge up of freshly synthesized material during the AGB phase (cf., § VA).

**OB stars:** Estimates of the total mass-loss rate of OB stars range from  $1$  to  $3 \times 10^{-4} M_{\odot} \text{ yr}^{-1} \text{ kpc}^{-2}$  (28,29). With a solar elemental C abundance this translates into about  $10^{-6} M_{\odot} \text{ yr}^{-1} \text{ kpc}^{-2}$ .

**Novae:** Nova events are generally interpreted as a thermonuclear runaway in an accreting hydrogen shell on top of a degenerate C-O-white dwarf in a binary system (30). With a nova rate of  $40 \text{ yr}^{-1}$  and an ejection of  $10^{-4} M_{\odot}$  per event, the total mass injection rate is about  $6 \times 10^{-6} M_{\odot} \text{ yr}^{-1} \text{ kpc}^{-2}$  (30). Typically H is depleted by a factor of about 3 with respect to He and little additional  $^{12}\text{C}$  and  $^{16}\text{O}$  have been synthesized (31-34). Assuming a C abundance of  $7 \times 10^{-3}$  by mass leads to  $4 \times 10^{-8} M_{\odot} \text{ yr}^{-1} \text{ kpc}^{-2}$  for the C ejection rate (cf., table 2).

**Supernovae:** There is little direct observational information on the carbon injection rate due to supernovae (35) and their contribution is largely guessed at. There are two types of SN, whose only connection is the large amount of energy released ( $\sim 10^{51}$  erg) and the explosive nucleosynthesis of heavy elements. Type II is generally believed to result from the gravitational collapse in massive stars ( $M > 8 M_{\odot}$ ). Type I's are thought to be due to a thermonuclear instability of an accreting white dwarf by the accumulation of a critical mass (36). The total supernova rate has been estimated to be about  $2 \times 10^{-5} \text{ kpc}^{-2} \text{ yr}^{-1}$  with about equal rates for type I and II (37). The typical type II supernova has a main sequence mass of  $25 M_{\odot}$ , of which about  $2 M_{\odot}$  remains behind in a neutron star (36), this yields a total H mass injection rate of about  $2 \times 10^{-4} M_{\odot} \text{ yr}^{-1} \text{ kpc}^{-2}$ . Such a supernova ejects about  $4 M_{\odot}$  in the form of freshly synthesized heavy elements, of which  $0.25 M_{\odot}$  is in the form of C (36). The C injection rate from type II supernovae is then about  $2 \times 10^{-6} M_{\odot} \text{ yr}^{-1} \text{ kpc}^{-2}$  (cf., table 2). This number is very uncertain since it depends critically on the somewhat uncertain  $^{12}\text{C}(\alpha, \gamma)^{16}\text{O}$  reaction rate and its effect on the presupernova convective shell structure (36,38).

Type I supernovae will contribute much less to the galactic enrichment of intermediate-mass elements such as C. Calculations typically yield a C/Fe mass fraction ratio of about  $3 \times 10^{-2}$  of the solar ratio (39). Since about  $0.5 M_{\odot}$  of Fe is required to explain the lightcurves of type I supernovae (36), this implies the

production of about  $2.5 \times 10^{-2} M_{\odot}$  of C per type I SN explosion. The resulting C ejection rate for type I supernovae is then about  $3 \times 10^{-7} M_{\odot} \text{ yr}^{-1} \text{ kpc}^{-2}$ .

**Wolf-Rayet stars:** Population I Wolf Rayet stars are the descendants of massive ( $M > 25-40 M_{\odot}$ ) OB stars where substantial mass-loss during the H burning phase as well as mixing processes have "uncovered" enriched stellar core material on the surfaces of these objects (40). The WC stars contain He, C and O and no evidence for H or N, while the WN have greatly enhanced He and N and no H (41). The total mass-loss rate of WC stars is estimated to be about  $3 \times 10^{-5} M_{\odot} \text{ yr}^{-1} \text{ kpc}^{-2}$  where about 25% is due to WC 8-10, which are associated with dust formation (42). Observations of the C/He abundance ratio in these stars lie in the range 0.1 to 2 by mass (41,43), while theoretical calculations yield about 0.5 (44). Assuming a conservative value (0.2) for this ratio yields a total C injection rate of  $6 \times 10^{-6} M_{\odot} \text{ yr}^{-1} \text{ kpc}^{-2}$  for all WC stars and about  $2 \times 10^{-6} M_{\odot} \text{ yr}^{-1} \text{ kpc}^{-2}$  for WC 8-10. The total mass-loss rate by WN is approximately  $2 \times 10^{-5} M_{\odot} \text{ yr}^{-1} \text{ kpc}^{-2}$  which with a C elemental abundance of about  $3 \times 10^{-4}$  by mass (41) translates into a negligible total C injection rate of  $6 \times 10^{-9} M_{\odot} \text{ yr}^{-1} \text{ kpc}^{-2}$  (cf., table 2).

## B) Carbon budget of the galaxy

From this discussion it is obvious that, although the mass return rate is dominated by red giants, many different object contribute substantially to the carbon budget of the galaxy. The uncertainty in these estimates should, however, once more be emphasized. While previously massive stars were thought to contribute mainly during the supernova phase (19), the upward revision in the  $^{12}\text{C}(\alpha, \gamma)^{16}\text{O}$  reaction rate makes this a less important source of C. Nevertheless, recent observations show that massive stars still contribute substantially albeit during the Wolf-Rayet phase. Essentially, during this phase they mix their helium-burning products to the surface and eject them in a strong wind before further nucleosynthetic burning can take place.

Elemental abundance studies of external galaxies may provide additional constraints on the type of objects that produce the C enrichment of the galaxy (45). For example, the low C/O ratios observed in the Large and Small Magellanic Clouds show that, since O is mainly synthesized in supernovae, C has to be formed mainly by other objects. Unfortunately, because of their low metallicity, the past contribution of both C-rich giants and WC stars to the elemental enrichment of these irregular galaxies has been small and thus these observations cannot be used to discriminate between these different types of stars.

The total C injection rate of  $1.6 \times 10^{-5} M_{\odot} \text{ yr}^{-1} \text{ kpc}^{-2}$  corresponds to a C-enrichment timescale of the ISM of about  $5 \times 10^9$  yrs. This may seem somewhat rapid, since the present C abundance in the ISM is very similar to the solar C abundance, which presumably reflects the C abundance in the ISM  $4.5 \times 10^9$  yrs ago. However, observations allow an infall rate of unprocessed extragalactic material (eg., no heavy elements) which is equal to the H injection rate by stars (23) and this could increase the C-enrichment lifetime of the ISM by an order of magnitude.

The last column in table 2 indicates the type of dust formed in the outflow of these objects. The best evidence for carbon stardust formation is for C-rich giants. Since about half of the carbon is tied up in gaseous CO in these objects, the carbon stardust

injection rate is about  $2 \times 10^{-6} M_{\odot} \text{ yr}^{-1} \text{ kpc}^{-2}$ . WC 8-10 stars also show evidence for circumstellar carbon stardust. The C fraction condensed in dust is however small ( $\sim 3 \times 10^{-2}$ ; 46). The contribution of these objects to the carbon stardust budget of the galaxy ( $5 \times 10^{-8} M_{\odot} \text{ yr}^{-1} \text{ kpc}^{-2}$ ) is thus minor. There is no conclusive evidence for dust formation in supernova ejecta (47). Assuming that half of the carbon in supernovae condenses out yields  $10^{-6} M_{\odot} \text{ yr}^{-1} \text{ kpc}^{-2}$  for these objects. There is observational evidence that suggests that some novae form SiC as well as amorphous carbon grains (48). Although silicates are not completely ruled out for the spectroscopic signatures observed, we note that studies of meteoritic carbon also strongly suggest that novae form carbon stardust (cf., § VIII). We will assume that 25% of the C condenses in the form of C stardust in novae. However, novae do not contribute much to the carbon (dust) budget of the galaxy. The total injection rate of C in solid form is then about  $3 \times 10^{-6} M_{\odot} \text{ yr}^{-1} \text{ kpc}^{-2}$ , which is about 20% of the total carbon injection rate. This rather small fraction results from the large C contribution by objects which do not produce carbon stardust (eg., O-rich giants, OB stars), the small fraction of C condensed in the outflows from WC stars, and from the substantial fraction of C locked up in CO in C-rich giants. It should also be emphasized that the dust formed by supernovae and WC stars is ejected at high velocities ( $\sim 1000 \text{ km s}^{-1}$ ). Appreciable destruction of this newly formed dust may take place during deceleration and mixing into the ISM due to sputtering and grain-grain collisions.

### C) The $^{13}\text{C}$ budget

It is of some interest to examine the  $^{13}\text{C}$  budget of the galaxy also. Here the situation is much less confused, since He burning does not produce much  $^{13}\text{C}$ . As a result supernovae and WC stars contribute negligibly to the  $^{13}\text{C}$  budget of the galaxy. Again C-rich red giants can be very important. The  $^{12}\text{C}/^{13}\text{C}$  ratio in those objects with the largest outflows (eg., IRC 10216) is typically 45 (49,50). The  $^{12}\text{C}$  injection rate (cf., table 2) translates then into a  $^{13}\text{C}$  mass-loss rate of  $10^{-7} M_{\odot} \text{ kpc}^{-2} \text{ yr}^{-1}$ . For O-rich giants and OB stars a solar  $^{12}\text{C}/^{13}\text{C}$  ratio is appropriate ( $\sim 89$ ), which leads to an injection rate of  $3 \times 10^{-8}$  and  $10^{-8} M_{\odot} \text{ kpc}^{-2} \text{ yr}^{-1}$ , respectively. The ejecta from novae are expected to be characterized by profoundly non-solar isotopic abundance patterns for the light elements C, N and O (30,51). Novae may indeed be an important source of  $^{13}\text{C}$ . Calculated  $^{12}\text{C}/^{13}\text{C}$  ratios range from 0.1 to 0.5 (52,53). Adopting 0.2 leads to a  $^{13}\text{C}$  mass-loss rate from novae of  $2 \times 10^{-7} M_{\odot} \text{ kpc}^{-2} \text{ yr}^{-1}$ . The total  $^{13}\text{C}$  injection rate is then about  $3 \times 10^{-7} M_{\odot} \text{ kpc}^{-2} \text{ yr}^{-1}$ .

This corresponds to an average  $^{13}\text{C}$  mass abundance in the ejecta of  $1.3 \times 10^{-4}$ , which is about 4 times solar. Again infall of metal-poor extragalactic material seems to be required to prevent rapid enrichment of the ISM. The  $^{13}\text{C}/^{12}\text{C}$  ratio in the injecta is about 0.02, which is about twice solar. As a result the  $^{13}\text{C}/^{12}\text{C}$  ratio in the ISM will slowly ( $\tau \sim 2 \times 10^{10} \text{ yrs}$ ) increase compared to solar abundances. This comparison is independent of the (uncertain) infall rate of metal-poor extragalactic material. Actually, observations of the  $^{12}\text{C}/^{13}\text{C}$  ratio in the interstellar medium indicate an enrichment by about a factor 2 since the solar system formed ( $\sim 4.5 \times 10^9 \text{ yrs}$ ; 54). However, since this enrichment timescale result from a comparison of two uncertain injection rates, this difference with observations may not be too worrisome. Observational studies of the  $^{12}\text{C}/^{13}\text{C}$  ratio as a function of galactic radius may be a very valuable tool in unraveling the contributions of different types of objects to the carbon budget of the galaxy. Preliminary observations indicate that there is no evident gradient in the  $^{12}\text{C}/^{13}\text{C}$  ratio in the solar neighborhood (55). This is somewhat surprising in view of the large contribution of "pure"  $^{12}\text{C}$  by WC stars, which show a

marked increase in surface density in the direction of the galactic center (42). This should be contrasted with the more even distribution of white dwarfs (eg., red giants descendants) and novae, which contribute most of the  $^{13}\text{C}$ . This might indicate that red giants actually dominate the carbon budget (56). We do note, however, that the O/H gradient in the galaxy is also fairly small (57) despite the large contribution from massive stars to the O budget and this argument may not be conclusive.

## V The Dust Condensation Zone

We will consider three different types of objects, characterized as carbon-rich (eg.,  $\text{C/O} > 1$ ), losing mass and showing evidence for dust formation. These are C-rich red giants, R Coronae Borealis (R Cr B stars), and late-type, carbon-rich Wolf Rayet stars (WC 8-10). Well studied prototypes of these stellar classes are IRC 10216, R Cr B itself and Ve 2-45, respectively. Each of these classes represents late stages in the evolution of stars of different mass (and evolution). C-rich giants are low mass stars ( $M < 8 M_{\odot}$ ) which have been (slightly) enriched in carbon through the dredge up of freshly synthesized material. The evolutionary status of R Cr B stars is not well understood. Presumably, these low mass stars ( $\sim 1 M_{\odot}$ ) have lost most of their H envelope due to H processing through the CNO cycle and possibly explosive ejection of their envelope and are now underway from a red supergiant stage to a white dwarf stage. These objects are very rare and have therefore been neglected in the C budget of the galaxy. As discussed in § IV, Wolf-Rayet stars are an advanced stage in the evolution of massive OB stars ( $M > 25 M_{\odot}$ ), where He burning products are exposed at the surface. Table 3 lists typical parameters for these prototypes and their circumstellar envelope. These have been compiled from the recent literature (41-43, 58-63). It should be emphasized that most of the parameters reported actually show a considerable spread within each class. A few of the reported parameters need some further clarification.

### A) The photosphere

The stellar radii have been calculated from the luminosities assuming that the stellar spectrum can be represented by a black body at the effective temperature,  $T_{\text{eff}}$  ( $R_{\star} = [L / 4\pi\sigma]^{1/2} T_{\text{eff}}^{-2}$ , where  $\sigma$  is Stefan-Boltzman's constant). The total pressure in the photosphere,  $P_{\text{tot}}$ , refers to the depth where the continuum emission originates. For the C giants it has been taken from model calculations (65) for  $\log g = 1$ . For the R Cr B stars it has been estimated assuming hydrostatic equilibrium and the Rosseland mean opacities appropriate for these stars (66). The total pressure in the photosphere is not a very meaningful concept for Wolf-Rayet stars where the continuum emission originates from a region well into the outflow and, thus, the stellar radius (defined this way) actually falls beyond the sonic point of the outflow (42).

The observed C/H and C/O ratios for an optically selected sample of C-rich giants are typically about  $6 \times 10^{-4}$  and 1.1, respectively (67). However, for our purposes the high mass-loss stars, which have been selected against in this sample, are of more interest. The quoted values seem reasonable and are also in agreement with abundances derived for planetary nebulae (58,67). The  $^{12}\text{C}/^{13}\text{C}$  ratio depends strongly on the amounts of He burning shell and equilibrium CNO cycle material mixed into the

**Table 3: Physical Conditions in the Carbon Dust Condensation Zone**

Type	C-rich Giant	R CrB	WC 8-10
<b>STELLAR PARAMETERS</b>			
$L_*$ ( $L_\odot$ )	$10^4$	$10^4$	$10^5$
$T_{\text{eff}}$ (K)	2500	7000	20000
$R_*$ ( $R_\odot$ )	530	67	25
$P_{\text{tot}}$ (dyn cm $^{-2}$ )	4 (3)	3 (3)	--
Period (days)	200	40	--
C/H	6 (-4)	300	--
C/He	7 (-3)	3 (-2)	8 (-2)
C/O	1-2	2	[10] <sup>a</sup>
$^{13}\text{C}/^{12}\text{C}$	3 (-2) <sup>b</sup>	<2 (-2)	[0] <sup>a</sup>
<b>CIRCUMSTELLAR SHELL: CONDITIONS AT THE CONDENSATION RADIUS</b>			
$\dot{M}_{\text{tot}}$ ( $M_\odot \text{ yr}^{-1}$ )	1 (-5)	1 (-6)	3 (-5)
$v_\infty$ (km s $^{-1}$ )	15	200	1500
$R_c$ ( $R_*$ )	5	10	500
$T_d$ (K)	~1000	~1000	~1000
$T_g$ (K)	~800	-	-
$P_{\text{tot}}^g$ (dyn cm $^{-2}$ )	6 (-5)	3 (-6) <sup>c</sup>	3 (-8) <sup>c</sup>
$P_{\text{carbon}}$ ("")	4 (-8)	1 (-7) <sup>c</sup>	2 (-9) <sup>c</sup>
$T_{\text{exp}}/T_{\text{col}}$	500	40 <sup>c</sup>	2 <sup>c</sup>
observed composition	molecular (see table 4)	C, C $_2$ , CN	C $^+$ , C $^{2+}$ , C $^{3+}$ , C

notes:

a) These abundance ratios refer to theoretical calculations rather than observations.

b) This ratio varies widely from object to object within the range 3.5-100.

c) These numbers have been calculated assuming a spherically symmetric outflow and the actual densities and pressures may be much higher (see text).

atmosphere by the dredge up process during the helium shell flash at the tip of the asymptotic giant branch (68). Observed values range from 3.5 to 100 (ie., solar). The value shown for IRC 10216 (cf., table 3) seems to be typical for high mass-loss C-rich giants (49).

## THE STRUCTURE OF C-RICH RED GIANTS

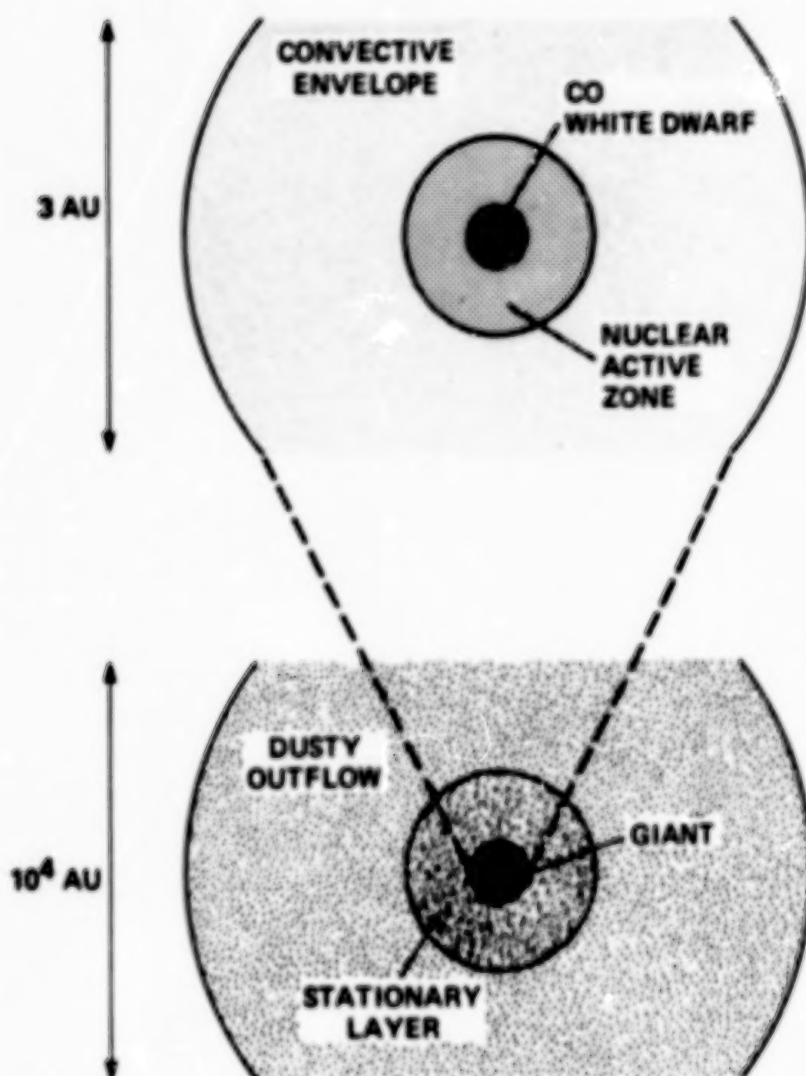


**Figure 4.** A schematic representation of the structure of red giants (top) and their surrounding circumstellar shells (bottom). 1 AU is the sun-earth distance  $\approx 1.5 \times 10^{13}$  cm. For clarity the various inner zones are not drawn to scale. A star on the asymptotic giant branch consists of a central, carbon-oxygen, white dwarf ( $\sim 10^{-3}$  AU) surrounded by a thin shell - in which nuclear burning takes place - and an extensive, convective envelope. Strong shock waves in the photosphere transport matter to large distances ( $\sim 5R_*$ ) where dust condensation takes place (stationary layer). Radiation pressure on the dust accelerates the dust outwards and the gas is dragged along.

## B) Structure of the outflow

A star on the asymptotic giant branch (AGB) has exhausted its hydrogen and helium nucleosynthetic fuel in the core, but is not massive enough ( $<8 M_{\odot}$ ) to explode as a supernova (type II). The core then collapses into a carbon-oxygen white dwarf ( $\sim 10^9$  cm), which is surrounded by a nuclear active zone in which alternately hydrogen and helium burns (cf., fig. 4). This core and nuclear active zone are embedded in an extensive ( $\sim 5 \times 10^{13}$  cm) convective envelope (68). The envelope is unstable and pulsations drive strong shock waves into the photosphere, transporting matter to large distances from the stellar surface. This material forms a (quasi) stationary layer at about  $5R_{\odot}$  ( $\sim 2 \times 10^{14}$  cm), where solid dust particles condense out. Radiation pressure on these dust grains leads then to the formation of an extensive ( $\sim 10^{17}$  cm), expanding ( $\sim 10$  km s $^{-1}$ ) dust shell. The gas is collisionally coupled to the dust and is dragged along. During the last part of this evolutionary phase of a low-mass star when the mass of the convective envelope becomes small ( $\sim 10^{-3} M_{\odot}$ ) a fast, low density wind (ie., "superwind") from the white dwarf compresses the surrounding gas and dust shell, which is ionized by UV photons from the white dwarf. The AGB star and its surrounding shell has become a planetary nebula. The nuclear fuel is exhausted and the white dwarf will eventually cool into oblivion. During the penultimate phase, some planetary nebula nuclei develop atmospheric characteristics of carbon-rich Wolf-Rayet stars (ie, population II WC stars; 69).

The mass-loss of population I Wolf-Rayet stars (ie.,  $M > 20 M_{\odot}$ ) is due to radiation pressure on atomic lines. Dust forms only at large distances from the stellar surface and, in contrast to red giants, plays no dynamic role in the outflow. These radiation driven winds from Wolf-Rayet stars are highly unstable and strong shocks are expected to develop (42). Velocity amplitudes may be as large as 500-1000 km s $^{-1}$ . For dust formation, the most important effect of these instabilities is perhaps the development of dense pockets of gas which can shield the budding molecule and soot formation processes from the disruptive effects of stellar and shock-produced UV photons. Indeed, the small fraction of C condensed in the form of dust and the absence of IR variability suggest that dust formation occurs in a large number of highly localized, dense regions in the outflow. The increase in dust mass towards later-type WC star is then attributed to a larger number of such regions, caused perhaps by a larger susceptibility to this instability.

In R Cr B stars, ejection from the pulsating stellar photosphere seems to take place in periodic, extremely dense, but localized, "puffs". During the expansion the temperature in these ejected gas blobs drops and dust is formed (62). Due to the localized nature of the ejection process, the stellar disk is only sporadically covered, giving rise to occasional deep minima in the observed light curves of these objects. Dust condensation takes therefore place at much higher densities than derived from the nominal mass-loss rates assuming spherical outflow at the terminal velocity.

## C) Physical conditions in the dust condensation zone

IR observations of the vibrational transitions of CO show that C-dust condensation in red giants takes place at a relatively large distance from the stellar photosphere ( $\sim 5R_{\odot}$ ; 63). This is in agreement with IR speckle measurements, which show similar inner shell radii (58). For R Cr B and WC stars the condensation radius has been estimated from the condensation temperature assuming reasonable absorption

properties for the dust (64,70). The derived inner radius for the WC stars is in good agreement with IR speckle studies of Ve 2-45. For red giants the gas temperature at the condensation radius is measured to be about 800 K (63). No measurements for WC and R Cr B stars are available. The total and partial carbon pressures,  $P_{\text{tot}}$  and  $P_{\text{C}}$ , at the condensation radius have been determined from the mass-loss rate, the outflow velocity (eg.,  $\rho = [4\pi R_c^2 v_{\infty}]$ ) and the (gas or dust) temperature. As remarked above, because of clumping, these values may not be very relevant for R Cr B and WC stars.

It is obvious from table 3 that carbon dust formation occurs under a wide variety of conditions. The effective temperature of the central star, for example, ranges from 2500 to 20000 K and this will have a profound influence on the chemical composition of the expanding shell (cf., below). The elemental composition of the outflow also varies dramatically from mainly hydrogen to mainly helium and carbon in the three classes of objects. However, dust formation always seems to occur at a condensation temperature of about 1000 K. An important parameter to consider in dust formation studies is the ratio of the expansion timescale,  $T_{\text{exp}}$ , to the collision timescale,  $T_{\text{col}}$  (71). The expansion timescale is approximately given by  $R_c/v_{\infty}$  (cf., table 3). Anticipating the discussion in § VI, dust formation is initiated by collisions with the most abundant, carbon bearing, gas phase molecule. For C-rich giants this is acetylene and, assuming a typical neutral-radical reaction rate ( $2 \times 10^{-11} \text{ cm}^3 \text{ s}^{-1}$ ), the calculated ratio is embarrassingly small (cf., table 3). This implies that kinetic effects (eg., activation barriers) are extremely important and that the dust formation process may be far from thermodynamic equilibrium. Essentially, the dust formation process has to be extremely efficient and should occur upon collision. Although grain growth probably occurs at this rate, such a high efficiency is difficult to understand for the initial nucleation step, which is probably inhibited by considerable activation barriers. On the other hand formation of the initial condensation nuclei (eg., PAHs; see § VI) in or slightly above the stellar photosphere, will be inhibited by the strong shock waves traversing this region (72). This presents an enigma for any stardust formation theory. It has been argued that the observation of a stationary layer and the IR speckle results are perhaps not in direct conflict with dust nucleation starting in the photosphere (58). Indeed, small PAH nuclei possess a large electronic band gap (cf., § III) and will not experience much radiation pressure until they have grown to about 50Å. Their dynamic influence on the outflow is therefore small. Likewise, if only a small fraction of the carbon is locked up in these species, they will not be detected in the IR (unless a bright FUV source is present as in planetary nebulae). The observations do imply, however, that further growth to dust particles is inhibited until about 5R<sub>\*</sub> above the photosphere. Since nucleation is the bottleneck to dust formation (further growth of nuclei into large dust grains is expected to be rapid), these observations do indirectly constrain nucleation to the stationary layer.

#### D) Chemical composition

The last row of table 3 summarizes the chemical composition in the outflows from these objects. For R Cr B stars only a few very simple carbon-bearing species have been observed. The winds from WC stars are completely ionized. The abundance of neutral carbon is about  $10^{-6}$  of the elemental carbon abundance in these stars. A wide variety of molecular species have been observed in C-rich late type giants. These are summarized in table 4. This data again refers specifically to the outflow from the well-studied C-rich giant, IRC 10216 (73-76). The IR observations refer to pencil beam observations against the IR stellar and dust continuum and are thus heavily weighted towards the high density region close to the star. Molecular abundances can

Table 4: Molecular Composition of Outflow from C-rich Giants

I. Infrared Observations <sup>a</sup>			II. Radio Observations <sup>b</sup>	
Species	$N_i$ [cm <sup>2</sup> ]	$X_i$	Species	$N_i$ [cm <sup>2</sup> ]
CO	2.0(20)	6(-4)	HCN	1.(16)
C <sub>2</sub> H <sub>2</sub>	3.0(18) <sup>c</sup>	9(-6)	HC <sub>3</sub> N	3.(15)
HCN	>1.5(18)	>5(-6)	HC <sub>5</sub> N	6.(14)
NH <sub>3</sub>	1.0(17) <sup>d</sup>	3(-7)	HC <sub>7</sub> N	3.(14)
CH <sub>4</sub>	1.8(16)	5(-8)	HC <sub>9</sub> N	2.(14)
SiH <sub>4</sub>	4.0(15)	2(-7)	HC <sub>11</sub> N	2.(14)
C <sub>2</sub> H <sub>4</sub>	4.0(15)	1(-8)	CH <sub>3</sub> ON	4.(12)
CS	6.0(19)	2(-4)	CN	9.(15)
			C <sub>3</sub> H	1.(14)
			C <sub>4</sub> H	3.(15)
			C <sub>5</sub> H	1.(14)
			C <sub>6</sub> H	2.(14)
			C <sub>3</sub> N	1.(15)
			C <sub>2</sub> H <sub>2</sub>	2.(14)
			SiC <sub>2</sub>	2.(15)
			SO	1.(16)
			SiS	7.(15)
			H <sub>2</sub> S	1.(13)
			CS	4.(15)
			C <sub>2</sub> S	1.(14)
			C <sub>3</sub> S	1.(14)
			NaCl	5.(12)
			AlCl	5.(12) <sup>e</sup>
			KCl	5.(12) <sup>e</sup>

notes:

a) Data taken from the compilation in reference (73). Abundances calculated assuming a CO/H<sub>2</sub> abundance of  $6 \times 10^{-4}$ .

b) Data taken from references (74-76).

c) 600K C<sub>2</sub>H<sub>2</sub> with N<sub>2</sub> 2.0(19) also present.

d) Cooler (<200K) NH<sub>3</sub> also observed.

e) Column densities assumed to be equal to that of NaCl.

be derived from the measured column densities, assuming a size scale (ie., the inner radius). The radio studies, in contrast, are dominated by the cooler, less dense material at large distances from the star. Since the observed intensity measures the total emitting volume, the column densities derived from the radio observations depend critically on the assumed (ie., unknown) inner radius (74). No direct comparison is therefore possible between the two sets of column densities given in table 4.

## COMPOSITION OF THE STATIONARY LAYER

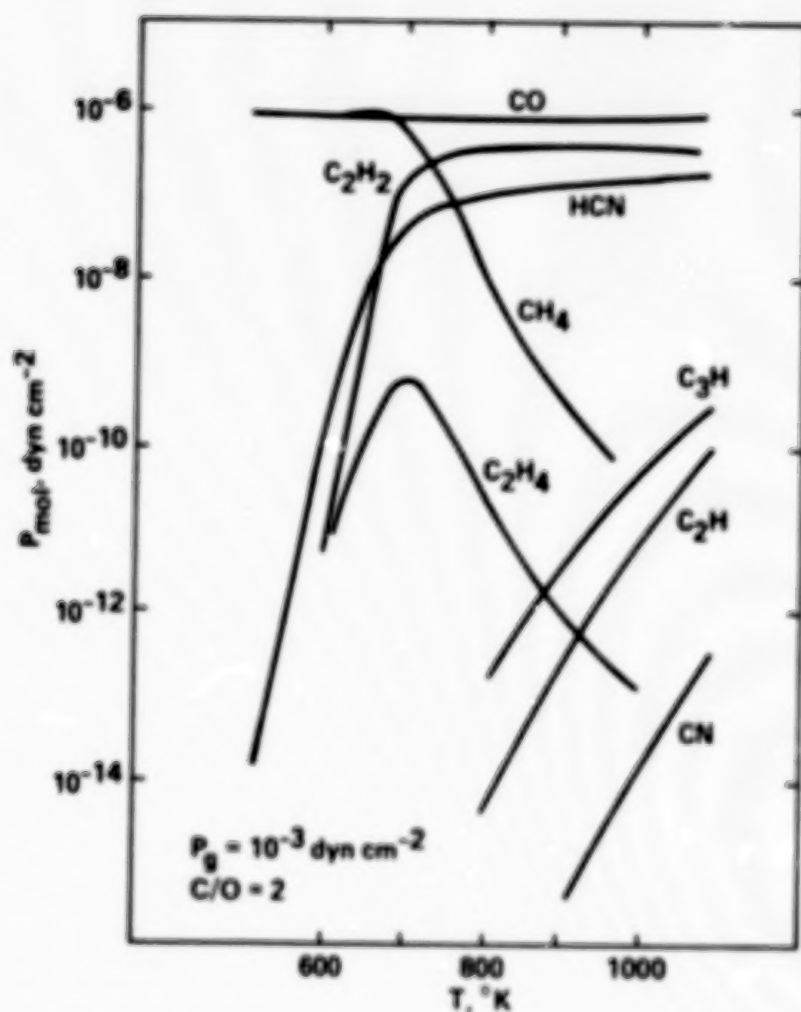


Figure 5. The chemical composition of the stationary layer calculated assuming thermodynamic equilibrium (adapted from reference 63).

A strikingly rich variety of molecules has been observed in IRC 10216, much more than in any other circumstellar shell. To a large extent, this is probably due to its proximity to the sun ( $d \approx 200$  pc) and other C-rich envelopes are likely to be as chemically diverse. The molecules in table 4 can be divided in four categories: 1) Simple and stable molecules expected in a C-rich environment (eg.,  $C_2H_2$ , HCN,  $CH_4$ ,  $C_2H_4$ ; see below). 2) A series of acetylenic chains (cyanopolyynes; eg.,  $HC_3N$ ,  $HC_5N$ ). 3) A series of reactive radicals (eg.,  $C_3H$ ,  $C_4H$ ). 4) A set of molecules involving S, Si and Cl. This diversity reflects the large number of chemical processes, which are of importance in circumstellar envelopes. These include (nearly) thermal equilibrium processes in the stellar photosphere and inner envelope, shock processes, UV photochemical processes, grain condensation and grain surface reactions (61). All of these can influence the chemical composition of the dust condensation zone. Figure 5 shows the abundance of some simple carbon bearing molecules as a function of gas temperature, calculated assuming thermal equilibrium at a total gas pressure of  $10^{-3}$  dyn  $cm^{-2}$  and a C/O ratio of 2 (63). This pressure is perhaps a little higher than expected for the dust condensation zone in C-rich giants (cf., table 3). At high temperatures, most of the carbon is locked up in CO and  $C_2H_2$ . At lower temperatures,  $CH_4$  becomes important and even some of the CO is converted, which results also in an increase of the abundance of other O-bearing molecules (eg., SiO,  $H_2O$ ; 63). Besides acetylene, attention should be drawn to the relatively high abundance of  $C_2H$  at high temperatures, which may play a key role in carbon dust condensation (cf., § VI). Note that these calculations ignore the dust condensation process. Similar calculations have been performed including dust condensation (again assuming thermal equilibrium), but for a high pressure ( $P_{tot} = 10^3$  dyn  $cm^{-2}$ ) more appropriate for the stellar photosphere rather than the condensation zone (77). Moreover all of these calculations ignore chemical kinetics which certainly plays an important role in determining the molecular composition and ultimately carbon dust formation (cf., § VI). Finally, atomic H may also play an important role in soot formation.  $H_2$  is the most abundant molecule in these equilibrium calculations and atomic H is a trace species. However, shocks driven into the extended photosphere by the stellar pulsations in red giants may actually lead to  $H_2$  dissociation and the H/ $H_2$  ratio may be far from equilibrium since  $H_2$  reformation will be slow under these conditions (78).

## VI Chemical Pathways to Carbon Stardust

In this section we will discuss the formation of carbon dust in the outflow from carbon-rich objects. We will concentrate on C-rich giants, since they dominate the carbon stardust budget (cf., § IV) and since the physical conditions in their outflows are much better determined than those in WC stars or R Cr B stars. Moreover, their chemical composition resembles that of sooting flames and we can draw on an immense chemical literature on soot formation under such conditions (79). Some of the differences that can be expected to be important in other objects will be pointed out.

### A) Thermodynamics and carbon condensation

Most studies of stardust formation are based on thermochemistry, which considers the condensation of solids out of a (slowly) cooling gas that originally contained no solids (71,80). The "condensation" sequence is then determined based on

## THERMODYNAMICS OF CARBON DUST FORMATION

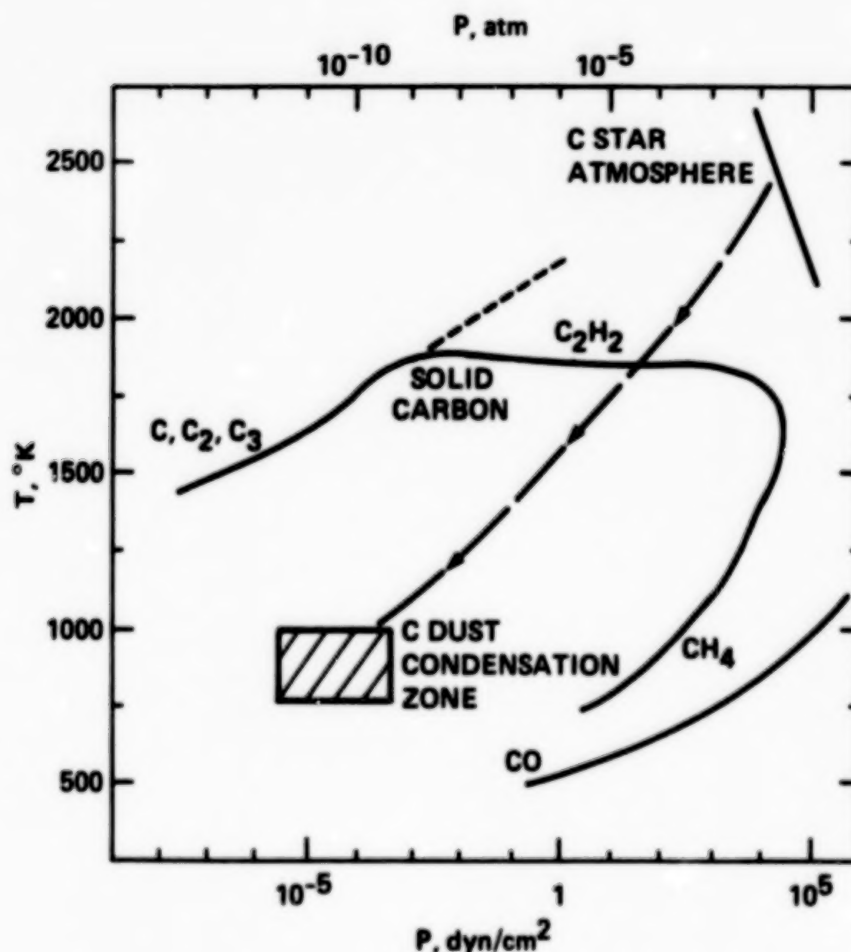


**Figure 6.** The phase diagram appropriate for C-rich red giants (adapted from reference 80). The line labeled solid carbon encloses the regime in which graphite is stable. Surrounding it, the position of the various, stable, carbon-bearing gas phase molecules are shown. To the left (right) of the dashed curve hydrogen is mainly atomic (molecular). The solid line in the lower right hand corner delineates the transition from the CO to the H<sub>2</sub>O dominated regime. The conditions appropriate for the photospheres and dust condensation zones of C-rich giants are also indicated. Due to the presence of strong shocks, the actual path of a cooling gas element in the outflow is far more complex than indicated. See text for details.

thermodynamic equilibrium. Essentially, the free energy of many atoms, molecules and solids are used to derive their relative abundances in equilibrium. Condensation sequences have been published for many different pressure, temperature, and elemental abundance regimes (71,80-82). Figure 6 shows the result for a C-rich (and H-rich) atmosphere (80). The thick solid curve encloses the regime where graphite is stable. Outside of it gas phase carbon species are more stable. Their relative abundance depends on the total (H) pressure. At the lowest pressures C, C<sub>2</sub> and C<sub>3</sub> are most important. Between 10<sup>-3</sup> and 10<sup>4</sup> dyn cm<sup>-2</sup> acetylene dominates, while at high pressures CH<sub>4</sub> ties up the carbon (80). To the left (right) of the dotted curve atomic H (H<sub>2</sub>) is most abundant. The conditions appropriate for the photosphere and the condensation zone in C-rich giants are also schematically indicated (cf., table 3). As expected from observations (59) the conditions in the stellar photosphere correspond to the acetylene dominated regime. Carbon stardust formation occurs in a regime where graphite is thermodynamically favored (cf., fig. 6). The long-dashed line schematically indicates the path of a cooling and expanding gas element. The actual path is, however, much more complex, due to the strong shocks traversing the extended photosphere (cf., § VB). Nevertheless, condensation does not seem to take place immediately upon passing the solid carbon stability line. The flow is, thus, highly supersaturated when the grains actually condense and an amorphous rather than crystalline material will form (cf., 1). The thermodynamic stability curve for such a material is, however, expected to be very similar to that of graphite (83). This late onset of condensation may reflect the importance of kinetics (eg., time-dependent nucleation) as well as other non-equilibrium effects.

The actual grain growth process is generally calculated using classical homogeneous nucleation theory (80,84). This assumes that the abundance of a cluster containing N atoms can be derived from the monomer concentration using the free energy of this cluster. The latter is often derived from the experimentally measured, bulk surface tension (84), although this may lead to large errors for small clusters (85). For small clusters, the surface free energy makes a large contributions to the total free energy. As a result, below a critical cluster size (which depends on the degree of supersaturation), clusters are more likely to evaporate than to grow. Statistical fluctuations are then responsible for producing clusters larger than this critical size, which can then grow on to actual dust grains (83,84). The formation of the critical cluster forms thus a bottleneck in the dust grain nucleation. Typical the final number of monomers in a grain is then approximately given by  $[\eta/\ln(\eta)]^{1/3}$  (80), where  $\eta$  is the number of monomer collisions within a relevant timescale (ie.,  $\tau_{\text{exp}}/\tau_{\text{col}}$ ). For the conditions in C-rich red giants (cf., table 3) this results in  $N=5 \times 10^5$  or a particle size of about 100Å. Since the initial steps are expected to be associated with considerable activation barriers, the actual grain size will be much smaller. This small expected grain size reemphasizes the dust nucleation problem alluded to in the previous section.

Chemical reaction rates are, to a large extent, governed by kinetic rather than thermodynamic factors, a point which has largely been ignored in stardust condensation studies. In particular, nucleation theory was developed for the formation and growth of liquid droplets where the bulk surface tension is more accurately known than for solid clusters. Indeed, the concept of a "surface" (or surface tension) is not even well determined for small molecular clusters (85) and such reasoning can easily lead to erroneous results. For example, it has been argued that, if the surface free energy of tetrahedrally-bonded carbon clusters is equal to



**Figure 7.** Transmission Electron Microscope photographs of a typical amorphous carbon sample produced by striking an arc between two carbon electrodes (courtesy of reference 92). Top: Carbon necklace. Bottom: a single grain.

that of aromatically-bonded clusters, diamond clusters would be favored over graphitic clusters in the carbon condensation route around stars, essentially due to the difference in volume density (86). However, aromatic clusters grow at the periphery of the aromatic planes and the surface free energy is associated with the dangling bonds of these peripheral carbon atoms. In contrast, diamond clusters grow three dimensionally. As a result the number of "surface" carbon atoms and their associated dangling bonds per carbon atom in the cluster is much larger in a "diamond" cluster than in a "graphite" cluster. It is only at high pressures, where volume plays a dominant role, that the high volume density of diamond favors diamonds over graphite. As a result aromatic clusters (eg., PAHs, see below) are expected to form around stars in agreement with astronomical observations and with laboratory studies of soot formation.

Although one may attempt to circumvent this problem in the definition of the cluster surface free energy in one way or another (84), the application of classical nucleation theory to stardust condensation is even more fundamentally flawed. In particular, the monomers (eg., atomic C) out of which graphite or amorphous carbon has to be formed do not even exist, as such, in the outflow from C-rich giants where most of the elemental carbon is in the form of CO and C<sub>2</sub>H<sub>2</sub> (87). A similar argument holds also for the condensation of silicates around O-rich giants. For a meaningful assesment of carbon dust formation, the chemical pathways which convert these molecules into solid dust grains has to be identified (79,88).

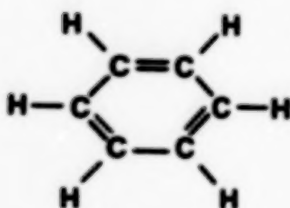
## B) Soot formation

The processes that convert C<sub>2</sub>H<sub>2</sub> into carbon grains in the outflow from C-rich red giants are probably very similar to those occurring during the gas phase pyrolysis of hydrocarbon molecules. There is an extensive literature on soot formation in combustion environments, in a large part driven by concerns on internal combustion engine efficiency, pollution, and health hazards (cf., 89-91 and references therein). Here we will briefly summarize the salient points.

Soot is a general side product of the combustion and pyrolysis of hydrocarbons. Morphologically, soot is independent of generation method and fuel type. Transmission electron microscopy shows that soot particles consist of a large number of small (100-1000Å) spherical particles arranged like pearls on a chain. Figure 7 shows a typical example generated by striking an arc between two amorphous carbon electrodes (taken from 92). Similar results are obtained when burning hydrocarbons such as methane, acetylene or benzene in air at room temperature and in pyrolysis studies in shock tubes and flow reactors (89-95). These particles are made up of microcrystallites with sizes in the range 10 to 25Å. X-ray analysis shows that the carbon atoms are arranged in a graphitic planar structure and thus such microcrystallites resemble large PAH molecules. Indeed, smaller members of the condensed aromatic ring compounds (eg., PAHs) are readily extracted from soot particles using organic solvents. Although the microcrystalline planes are parallel to each other, they are more randomly stacked in soot particles than in graphite (95).



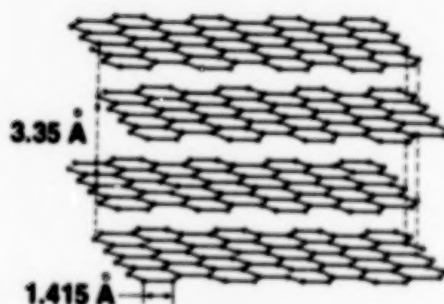
**ACETYLENE**



**BENZENE**



**POLYCYCLIC  
AROMATIC  
HYDROCARBON**



**PLATELET**



**SOOT PARTICLE**

**Figure 8.** The structure of the various molecules and particles involved in one possible carbon stardust formation scheme. Acetylene is the precursor gas phase molecule. Various chemical processes convert these molecules into benzene molecules. Further chemical growth involving acetylene leads to the formation of large polycyclic aromatic hydrocarbons. Several of these planar molecules stacked together form a platelet. These platelets are the building blocks of soot particles. These platelets as well as the layers within them are generally cross-linked by tetrahedrally bonded carbon atoms and chains (see text for details).

The chemical nature of the soot can vary within a flame. When first formed, the particles contain a large number of hydrogens ( $C/H=1$ , when  $a=50\text{\AA}$ ), which are distributed in between the aromatic layers. ESR studies show that these small particles have a pronounced free radical character and they continue to grow through surface reactions. Both the hydrogen content ( $C/H=0.1$ ) and radical nature decreases during this growth. At a size of about  $200\text{\AA}$  rapid surface growth stops and the particles aggregate in larger grains.

Three distinct steps can thus be discerned in the formation of soot (89-91): 1) the breakdown of fuel molecules to precursor molecules which react rapidly to form larger species; 2) chemical growth that results in the formation of numerous small particles ( $a>10\text{\AA}$ ); and 3) particle growth by surface reactions as well as by clustering and agglomeration. In flames these processes compete with oxidation processes. In the outflow from C-rich red giants, however, the C/O ratio is larger than 1 and essentially all of the oxygen is tied up in CO. In other words, all of the available carbon has already been burned in the stellar photosphere and the conditions resemble those of a fuel-rich flame. Thus, while the incandescent soot particles in flames, which give rise to its characteristic yellow color, will typically burn up quickly in the air at the top of the flame, this oxidation process will be of no importance in C-rich giants.

### C) PAHs and the formation of carbon stardust

The critical intermediates in the carbon condensation route have to be highly stable against dissociation and yet possess a high reactivity towards polymerization. Several different chemical pathways to soot formation have been proposed based on neutral radicals, ions, PAHs, poliacetylenic chains, or Buckminsterfullerene as intermediaries (89,90,96,97). The high tendency of aromatic fuels to soot, the high stability of PAHs as well as their structural similarity (the aromatic C backbone) has led to the notion that PAHs are the building blocks of soot particles. In the case of C-stardust formation around C-rich giants, the importance of PAHs is underscored by their ubiquitous presence in C-rich planetary nebula (7). Following references (79,88), we will identify PAHs as the key intermediates in C-stardust formation in these objects. The basic steps in soot formation in this scheme are schematically shown in figure 8. As remarked above, other pathways have been proposed in which PAHs are unreactive sidebranches (i.e., dead-ends), and the following discussion should be considered illustrative rather than authoritative. Moreover, as will be discussed in § E, it is likely that in different environments different mechanisms dominate C-stardust formation.

In the outflow from carbon-rich giants, acetylene and its radical derivatives are likely to be the precursor molecules from which soot is formed and the soot-limiting step is the formation of the first aromatic ring (cf., fig. 8). Rapid chemical growth of this ring then forms larger PAHs. At some stage clustering of PAHs becomes important and small platelets are formed in which small PAHs are randomly stacked. Simultaneously, further chemical growth will take place, in particular at the periphery of the aromatic planes. This may lead to cross-linking of the planes by tetrahedrally bonded carbon. Some crosslinking may also occur randomly dispersed in the aromatic planes. Finally, these platelets can cluster to form a spherical soot particle (cf., fig 8). In flames, these spherical soot particles cluster further to form a "pearl-like" necklace (cf., fig. 7).

# THE CHEMICAL PATHWAY FOR CARBON DUST FORMATION

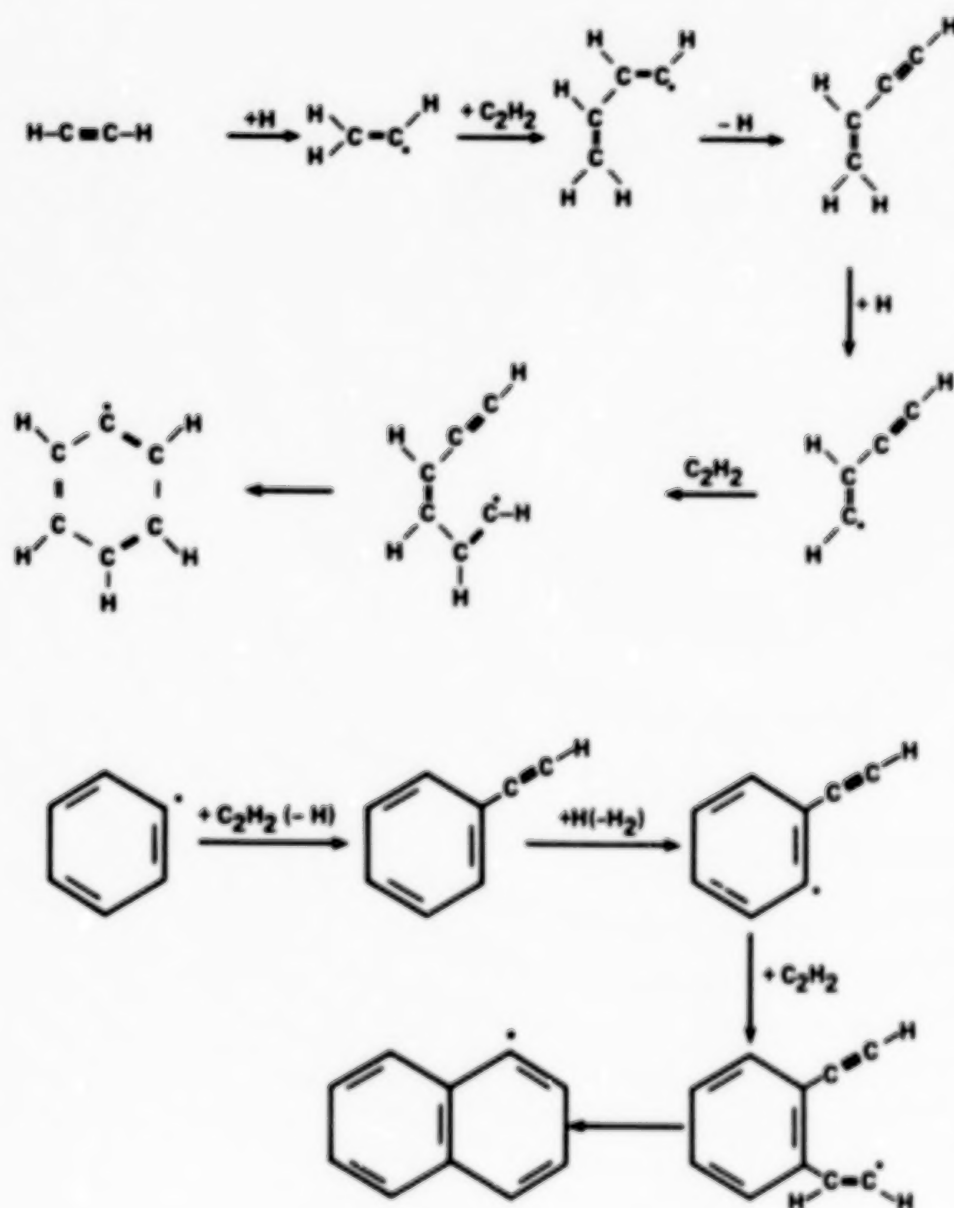


**Figure 9.** One possible chemical pathway towards soot (adapted from reference 103). Top: the formation of the first aromatic ring, starting from acetylene. Bottom: further chemical growth takes place through alternating steps of radical site formation and acetylene addition. Branching reactions have been omitted for clarity (see text for details).

The temperature and pressure history of a parcel of gas in the outflow of a carbon-rich giant is very complex due to the strong shock waves propagating through the extended photosphere which lead to large temperature and density excursions. Dust formation will then occur far above the photosphere ( $R \sim 5R_*$ ) where the activity generated by the shock waves has died down (72). PAH formation in flames starts typically when the temperature drops below about 2000K (98). The temperature of the extended red-giant photosphere is not determined by radiative equilibrium but by shock passage. A postshock temperature of 2000K corresponds to a shock velocity of a few  $\text{km s}^{-1}$  and shock calculations in Mira atmospheres indeed indicate a typical distance of about  $5R_*$  above the photosphere (99-102).

Figure 9 shows the first steps in one possible chemical pathway to soot derived from detailed kinetic model studies of shock-tube pyrolysis of acetylene at about 1700 K (78, 79, 103). A very similar cyclization model has been proposed to explain measured product distributions in sooting laminar flat flames with a variety of hydrocarbons (104). Many different branching reaction pathways are possible at all of the intermediate steps. For clarity, these have been ignored, since theoretical studies indicate that they are of lesser importance. There are two steps in this reaction scheme: a series of reactions describing the formation of the first ring out of acetylene and one describing further chemical growth. Formation of the first aromatic ring forms a bottleneck for the soot yield. It is started through the formation of the ethynyl radical ( $\text{C}_2\text{H}$ ) through H abstraction. This radical can then attack the triple bond in another acetylene molecule and react to form  $\text{C}_4\text{H}_5$ . Two steps of H abstraction by H atoms, followed by reaction with yet another acetylene yields  $\text{C}_6\text{H}_5$ . Cyclization of this radical via interaction of the unpaired electron with the triple bond leads then to the first aromatic ring. Once the first ring is formed subsequent chemical growth consists of (more or less) alternating steps of the formation of a radical site through H atom abstraction, acetylene addition and cyclization. This is illustrated for the formation of the small PAH, naphthalene. Further chemical growth will take place through the fused PAHs pyrene, coronene, and ovalene (105).

The stable molecular intermediates, including phenylacetylene ( $\text{C}_4\text{H}_4$ ), acenaphthalene ( $\text{C}_{12}\text{H}_8$ ) and the pericondensed PAH pyrene ( $\text{C}_{16}\text{H}_{10}$ ), present in this reaction scheme play an essential role. The reactions leading from one radical to another are reversible at these temperatures and quickly set up an equilibrium distribution. The reactions leading to these stable intermediates, however, are irreversible and thus "pull" the reaction sequence towards molecular complexity and soot formation. The importance of pericondensed aromatic hydrocarbons, such as pyrene, coronene and ovalene, in this scheme rest mainly in their high thermodynamic stability, resulting from their maximum resonance energy and minimal stress energy (105). The enthalpy of formation can also be maximized by minimizing the entropy change by returning as many  $\text{H}_2$  molecules as possible to the gas phase. This favors molecules with an as short as possible boundary structure and may actually lead to (smaller) aromatic molecules having pentagons or squares in their carbon skeleton (78). The molecule cyclopentanaphthalene is an example of this latter principle. The stresses due to the presence of pentagons in the carbon skeleton will lead to warping of the intrinsically planar structure of PAHs. If present in an ordered fashion this can even result in spheroidal molecules such as Buckminsterfullerene ( $\text{C}_{60}$ ; 106), which are closed upon

**Table 5: The most abundant PAHs in flames<sup>a</sup>**

Species	formula	abundance <sup>b</sup>
Naphthalene	C <sub>10</sub> H <sub>8</sub>	100
Acenaphthalene	C <sub>12</sub> H <sub>8</sub>	100
Phenanthrene	C <sub>14</sub> H <sub>10</sub>	30
Pyrene	C <sub>16</sub> H <sub>10</sub>	30
Benzo[g,h,i]fluoroanthene	C <sub>18</sub> H <sub>10</sub>	10
1,12-Benzperylene	C <sub>22</sub> H <sub>12</sub>	3
Coronene	C <sub>24</sub> H <sub>12</sub>	1
Soot <sup>c</sup>	--	1000 <sup>d</sup>

notes:

a) Taken from (98) and references therein.

b) Mass abundances in the burned gas normalized to coronene.

c) Typical soot diameter ~250Å, corresponding to about 10<sup>5</sup> C atoms.

d) Measured when chemical growth has stopped. However, further physical growth (ie., clustering) may increase this ratio further.

themselves and do not contain any hydrogen. When present in a disordered fashion, pentagons will lead to a curling of the aromatic planes without actual reconnection (96,97). However, cyclopenta groups are relatively unstable and may be partially lost along the reaction pathway (103). Whether they will persist in the carbon condensation route probably depends on the relative importance of thermodynamic and kinetic considerations.

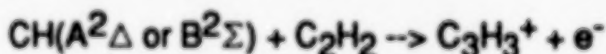
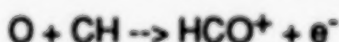
Table 5 list some typical PAHs detected in sooting flames with an estimate of their relative abundance (98). In the case of well-controlled combustion mainly the thermodynamically most stable PAHs are formed and survive in the burned gas. Although the absolute amount of PAHs formed depends critically on the physical and chemical conditions, the relative concentrations of these stable PAHs do not. This table is mainly concerned with the pericondensed PAHs which are thermodynamically favored (105). The abundance of hydrocarbons with the same number of carbon atoms but a larger hydrogen content and a less stable structure is much lower (98). For example, the abundance of the 5 ring, benzo[g,h,i]fluoroanthene and cyclopenta[c,d]pyrene is two orders of magnitude larger than that of triphenylene, chrysene, and benzoanthracene. Likewise, apart from coronene (C<sub>24</sub>H<sub>12</sub>), no isomers of this fully condensed benzonoid have been detected in sooting flames. Finally, the high abundance of species containing pentagons (eg., acenaphthalene) is not surprising in light of the discussion above. Searches for these PAHs in the outflow from C-rich giants will be very valuable to test the similarity of dust formation around C-rich giants with that of sooting flames, to elucidate the actual carbon condensation pathway and to determine the relative importance of different interstellar PAH species. Of course, the distribution of PAHs ejected by these objects will be further modified by processes in the diffuse interstellar medium. In particular, UV photodissociation and photoisomerization will play an important role in weeding out less stable as well as small PAHs in the diffuse interstellar medium (107).

The formation of carbon stardust in the outflow from carbon-rich red giants is, thus, expected to be alike to the formation of soot in flames. Numerous laboratory experiments suggest that PAHs are, if not an essential intermediate, at least an abundant side product of the soot formation process. The infrared spectra observed towards many planetary nebulae (the red giants "daughter") show emission features at 3.3, 6.2, 7.7, 11.3  $\mu\text{m}$  as well as broad underlying emission component (7). Although the observed spectra compare very well to that of carbon soot particles, energetic considerations imply that the species emitting the emission features are very small (20-50 carbon atoms; 10,11). They are, thus, a collection of free-flying molecules rather than clustered in soot particles. The broader emission components as well as the far infrared continuum is evidence for the presence of larger PAHs and soot particles (58, 108). Finally, we note that the ratio of C in PAHs relative to that in soot observed in planetary nebulae (~20; 108) is in reasonable agreement with that measured for sooting flames (cf., table 5).

#### D) Non-LTE and the formation of C stardust

The conditions in the outflow from carbon-rich objects are probably far from being in thermodynamic equilibrium and this should have a profound influence on the carbon dust condensation process. For example, the vibrational excitation temperature of molecules in the dust condensation zone may be higher than the kinetic gas temperature due to radiative excitation by stellar photons or the trapping of line radiation (109). Since reaction rate constants are often very sensitive to vibrational excitation, some reactions may proceed much faster than expected from the kinetic gas temperature. The chemical composition may also be far from equilibrium. This is in particular true for the expected H/H<sub>2</sub> ratio. In the photosphere H<sub>2</sub> is formed by three body reactions and the H/H<sub>2</sub> ratio freezes out when the density drops below about 10<sup>11</sup> cm<sup>-3</sup> (110). This results in a disproportionally large abundance of atomic H farther out in the flow. The atomic H abundance is also influenced by the strong shock waves in the extended photosphere. Shock velocities can be as high as 25 km s<sup>-1</sup> and H<sub>2</sub> dissociation will be important. Since the post shock density may be less than the freeze-out density, large deviations from the expected H/H<sub>2</sub> ratio may occur.

Finally, ionization may play an important role. Although no ionizing radiation is expected from a cool red giant, chromospheric radiation may play a (ionizing) role in supergiants. Moreover, chemiionization has been shown to be an important ionizing process in sooting flames. Of particular importance are the reactions



These ions are present in the reaction zone in sooting flames and their abundance falls off in the burnt gasses. Reactions between these ions and neutral molecules are rapid, as is isomerization into their most stable form (eg., PAH ions for the larger ones). They may actually play an important role in the soot nucleation and condensation process (90, 111). As for the neutral PAHs, pericondensed structures, such as C<sub>13</sub>H<sub>9</sub><sup>+</sup>, C<sub>17</sub>H<sub>11</sub><sup>+</sup> and C<sub>19</sub>H<sub>11</sub><sup>+</sup>, are thermodynamically favored and observed to be most abundant in flames. In the circumstellar case, however, oxidation occurs in the stellar photosphere and little atomic oxygen (or CH) is expected to be present in the outflow. Cosmic rays which have sometimes been considered as an ionizing agent

are unlikely to play a role, since they are tied to the galactic field (gyro radius  $\approx 10^{13}$  cm), which will be wrapped around the bubble blown by the stellar wind. Thus, ionization processes may be much less important in circumstellar shells around carbon-rich giants than in sooting flames.

#### E) Carbon stardust formation around WC 8-10 and R Cr B stars

The formation of carbon dust around R Cr B stars and WC 8-10 stars is expected to follow a completely different chemical pathway than in the outflow from C-rich giants. These objects have lost most of their H-rich envelope either through nuclear burning or through previous mass-loss. The reaction scheme derived above from experimental studies of the pyrolysis of hydrocarbons in sooting flames (cf., figure 8), which may be very relevant in the outflow from C-rich red giants, will play no role in the carbon dust formation in these objects, since no  $C_2H_2$ ,  $C_2H$  or H is present. Carbon soot formation is now expected to be initiated through the formation of polyynes (eg., acetylene-like C chains without H; ie.,  $C_2$ ,  $C_3$ ,  $C_4$ , etc). Large molecular structures of this kind ( $>20$  carbon atoms) are expected to be flexible enough to form an aromatic ring structure. One important difference between this soot formation scheme and that involving acetylene and PAHs discussed above is the presence of a large number of unfilled valences at the periphery of the planar aromatic structure. Therefore, even more than in pyrolysis of hydrocarbons where H can (temporarily) saturate these dangling bonds, minimizing this "surface free energy" is expected to be very important in soot formation in R Cr B and WC 8-10 stars. This may act to enhance the value of pentagons in the aromatic structure (eg., minimize the number of surface bonds). The introduction of pentagons induces warping and curling of the aromatic planes, which may lead to closure of the aromatic structure on itself, again minimizing the number of dangling bonds. Indeed, laser vaporization studies of graphitic materials under a H poor atmosphere clearly illustrate the importance of such considerations (96,97).

A second difference between the outflow from these objects and that from C-rich giants is the presence of ionizing radiation. WC 8-10 stars are very hot stars and most of their energy is emitted in the far ultraviolet. Indeed, the wind from these stars is highly ionized. The observed column density of neutral C is typically only  $10^{-6}$  of the elemental C. R Cr B stars are much cooler (cf., table 3), but they do possess an active chromosphere, emitting FUV radiation which may lead to ionization (as well as photodissociation). In this case simple, neutral, carbon bearing molecules do, however, dominate the composition of the envelope. Because ion-molecule reactions are much faster than neutral-radical reactions, ionization may play an important role in soot formation, in particular in WC 8-10 stars. The bottleneck in soot formation is now the formation of the first molecules. In view of the high degree of ionization, the absence of H, and the low pressure, radiative association of C with  $C^+$  and  $C_2^+$  are expected to be important reactions in the outflows from WC 8-10 stars. Dissociative recombination of  $C_3^+$  will lead to  $C_2$  which can then be used as a buildingblock towards larger acetylenic and aromatic species through ion-molecule reactions. Because of its low formation temperature, the carbon dust is expected to be highly disordered. Indeed, the IR spectrum of Ve 2-45 shows a weak emission feature at about  $7.7 \mu m$ , which is attributed to the C-C stretch of aromatic carbon (112). This feature is only expected in disordered carbon with an aromatic domain size less than about  $50 \text{ \AA}$  (1).

#### F) Carbon stardust formation in supernova ejecta

It is appropriate to consider briefly the formation of carbon dust in supernova ejecta both because of the (possible) contribution of supernovae to the carbon budget of the galaxy (cf., table 2) and the presence of a carbonaceous component in meteorites containing isotopic anomalies characteristic of supernovae (3,113). Although IR excess emission has been detected in several supernova remnants, this may actually result from preexisting dust which "lights" up due to the SN (eg., infrared echo) and there is presently no conclusive evidence for the formation of (carbon) stardust in SN ejecta (47). Because of its timely nature, this discussion will be mainly geared to the recent supernova in the Large Magellanic Clouds (SN 1987a).

Supernova 1987a in the LMC is thought to result from the explosion ( $\sim 10^{51}$  erg) of a slightly metal-poor star with an approximately  $6 M_{\odot}$  He core and a  $5-10 M_{\odot}$  H envelope (114,115). The main-sequence progenitor, SK-202-69, probably had a mass of about  $20 M_{\odot}$  and had undergone considerable mass-loss, presumably in a preceding red supergiant phase, as evidenced for example by the detection of a nitrogen-rich circumstellar shell (116). For our purposes we only need to consider the He core in which static He burning has produced a large mass fraction of  $^{12}\text{C}$ . Explosive nucleosynthesis following the passage of the shock front will convert a large fraction of this core into heavier elements, but a carbon-rich zone containing about  $2 M_{\odot}$  remains (115). The competition between different heat sources (diffusion of radioactive heat due to decay of freshly synthesized  $^{56}\text{Co}$ ; H recombination; possible pulsar) and sinks (adiabatic expansion; radiation) hampers an accurate prediction of the temperature-pressure history of the He core material. Uncertainties in the opacity due to velocity shearing, compositional gradients, as well as mixing of different zones due to Rayleigh-Taylor instabilities further compound this problem (115). Indeed, estimates of the gas pressure in supernova ejecta, when the kinetic temperature reaches the typical dust condensation temperature of about 1000K, vary by about 10 orders of magnitude (117). As a result of these uncertainties, predictions of grain formation in SN 1987a resemble a weather forecast: it may rain grains or it may not.

## G) Summary

This detailed examination of the chemical pathway towards soot has identified several important physical concepts and, although there is some "loose" correspondence, the distinct differences between the kinetical and thermodynamical approach should be stressed. Clearly, the role of hydrogen in soot condensation cannot be overemphasized. Hydrogen saturates the free valences at the periphery of the aromatic nucleation centers and thereby reduces its surface free energy. As a result surface free energy plays much less a role in dust formation than envisioned by classical nucleation theory. That  $\text{C}_2\text{H}_2$  rather than C is the gaseous precursor molecule to soot is a further distinction between the chemical and classical approach. The saturation with H implies that kinetic effects are very important, since a peripheral H has to be abstracted before further chemical growth can occur. Such kinetically controlled growth will lead to a highly disordered structure of the resulting condensates. The dominant role of H in soot formation is exemplified by the high abundance of PAHs as well as the high H content of soot. Physical growth (ie., clustering) can also play an important role in determining the final size and gross structure of the product (cf., fig. 7). At what point clustering of microcrystals overtakes chemical growth by monomer addition will depend on the detailed temperature and density history of the cooling gas. Finally, this discussion pertains

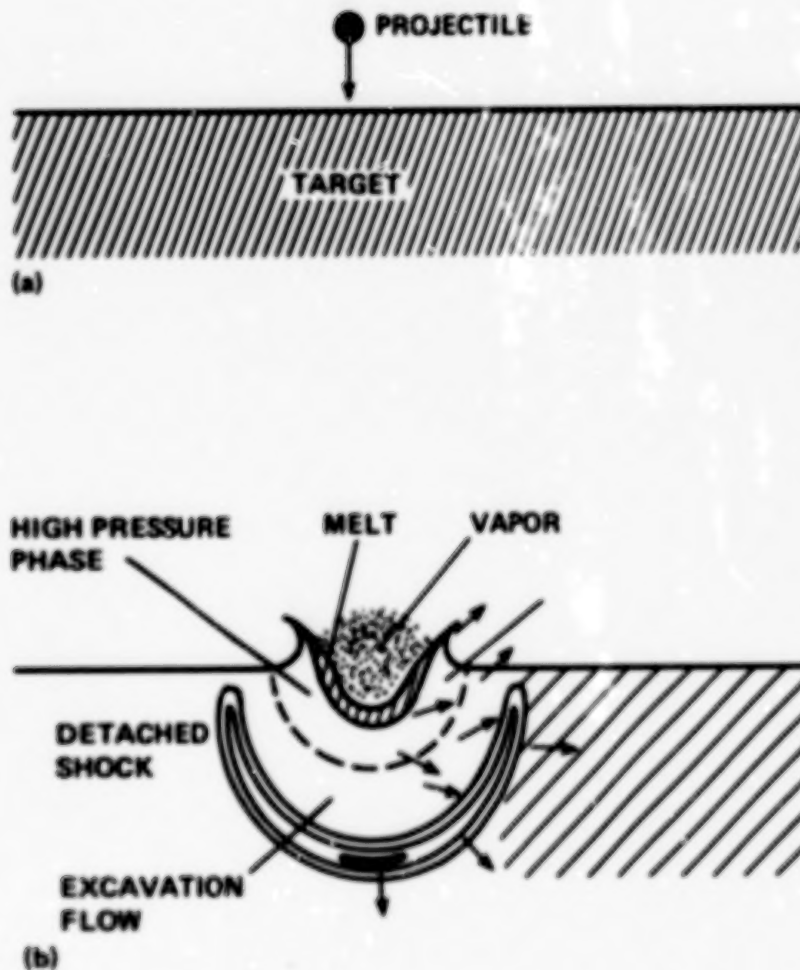


**Figure 10.** A schematic representation of the impact of a projectile on a target. The fate of the shocked target material depends strongly on the peak shock pressure. Since the strength of the shock wave driven into the target decays with distance, the impact point is surrounded by successive zones in which the target has been vaporized, molten, or converted into a high pressure phase (eg., diamonds). The arrows indicate the velocity vectors in the excavation flow which will carve out the final crater (see text for details).

to soot formation in a hydrogen-rich atmosphere. When H is absent, as in WC 8-10 stars, the chemical pathway toward dust will be quite different, leading perhaps to a different soot structure. Ions or Buckminsterfullerene rather than PAHs may be the reactive intermediaries. Nevertheless, it is expected that kinetic rather than thermodynamic effects will control soot formation and the structure of the resulting grains.

## VII Grains and Shocks in the Interstellar Medium

Strong shock waves generated by supernova explosions are the dominant destruction mechanism for interstellar dust grains (118-121). Behind the shock front, the charged grains gyrate at high velocities around the magnetic field lines. Impinging gas atoms can sputter atoms from the grain surface (non-thermal sputtering), while collisions with other grains can lead to partial and complete vaporization. Evidence for destruction of interstellar grains by shock waves is provided by the observation that high velocity ( $v \sim 100$  km/sec) interstellar gas (presumably recently shocked) has much higher elemental abundances in the gas phase than the general interstellar medium (122,123). Although grain destruction by sputtering and vaporization have received the greatest attention in the literature, shattering and phase transformations due to grain-grain collisions are equally important. The study of phase transformations due to grain-grain collisions in interstellar shocks has recently gotten additional impetus by the discovery of small ( $\sim 50$  Å) diamond grains in carbonaceous meteorites (124). This carbon phase (so-called C-8), which comprises about 2% of the elemental carbon, contains isotopic anomalies which presumably originated outside the solar system (3). These meteoritic diamond grains may result from shock processing of interstellar graphite or amorphous carbon grains. High velocity ( $> 8$  km s<sup>-1</sup>) grain-grain collisions behind strong supernova shock fronts are expected to produce the high pressures required to transform these carbonaceous materials into diamond. Such collisions are predicted to produce polycrystalline diamonds with microcrystal sizes ranging from about 5 to 100 Å, possibly intermixed with some highly disordered diamond (125).

Behind the shockfront small grains ( $< 500$  Å) are rapidly dragged to a halt through collisions with the gas. Essentially, because of their larger volume to surface ratio, large grains will not be stopped as quickly (cf., 121). Extinction observations show that interstellar grains have a steep size distribution ranging from about 3000 Å to molecular sizes (13-17). Most of the interstellar grain volume is in the large grains, but the surface area is in the small ones. The most important grain-grain collisions behind a shock are thus due to a large grain impacting a small grain at high velocity.

### A) Grain-Grain collisions

Initially, when a projectile impacts a target at high velocity, strong planar shock waves are driven into both target and projectile at nearly constant pressure and velocity as the kinetic energy of the collision is thermalized. This first stage ends when the shock wave in the projectile has reached the back surface and is reflected as a rarefaction wave which eventually reaches the target. These rarefaction waves as well as the expansion of the shock wave from the impact site will transform the planar shock in the target into a more or less hemispherical form (eg., the detached shock; see figure 10) and its strength will decrease with distance from the impact

site. In this second stage the shock pressure will drop approximately inversely with the engulfed volume ( $P \sim V^{-1.1}$ ) where the small deviations from the solution for a Sedov-Taylor blast wave are due to the back splash of ejected material which carries away energy and imparts momentum (126,127). The rarefaction waves from the free surfaces will set up a flow pattern for the shocked material upward and away from the impact site (eg., the excavation flow; see figure 10). During the excavation of the crater, some of this material reaches the free surface and can be ejected as small, shattered fragments. The remainder will line the crater. Shattering may also occur when the shock breaks through the backside of the target and is reflected backwards as a tensile wave (ie., spalling).

The rarefaction wave that follows the shock wave will release the compressed material and during this expansion the shocked material may undergo a phase transformation. For very strong shocks, the pressure is high enough to cause vaporization. For weaker shocks, the material can unload into the liquid phase, or into a high density solid phase such as diamond. A shock slows and weakens as it expands through a target, so that an initially very strong shock successively vaporizes, melts, transforms and shatters the target (cf., figure 10). Clearly, the process with the smallest threshold pressure will affect the largest volume. Assuming the experimentally measured threshold pressure for the graphite-diamond transition of 600 kbar (i.e., threshold energy  $\epsilon = 0.7 \text{ eV/C atom}$ ; cf., § B) and for vaporization of 5.7 Mbar (i.e., a binding energy  $\epsilon = 7.5 \text{ eV/C atom}$ ), the ratio of the volume of diamonds produced relative to that vaporized is about 7.5 for semi-infinite targets. Of course, for high velocity impacts of equal-sized grains both grains will be vaporized, but those collisions are fairly rare. Nevertheless, for interstellar grain-grain collisions a careful analysis has to be carried out taking into account the expansion of the shock wave in the target as well as the finite-size of the grains. The threshold collision velocity for diamond formation is the sum of the particle velocity behind the shock in the target and projectile ( $= 2(2\epsilon/m_c)^{1/2}$ ;  $m_c$  = mass of C atom), corresponding to  $6.8 \text{ km s}^{-1}$ . Likewise, the threshold collision velocity for vaporization is calculated to be about  $23 \text{ km s}^{-1}$  assuming a threshold energy equal to the binding energy. Actually, because of kinetic effects, the shock will have to supply several times the binding energy to cause appreciable vaporization (127,128) and this estimate as well as that of the relative volumes is only a lower limit.

In order to estimate the effects of grain-grain collisions in interstellar shock waves on interstellar grains several different steps have to be taken. First, for a given size ratio of projectile and target grain the diamondized volume (or vaporized/shattered) is calculated as a function of relative grain-grain collision velocity, taking the finite size of target (and projectile) into account. This volume is averaged over impact parameter, since glancing collisions couple less of the projectile's energy and momentum to the shock wave in the target (127). This is then used as input for a numerical code which calculates the structure of an interstellar supernova shock wave (120,129). Behind a supernova shock front different sized grains have a different velocity history and thus for each grain size at each spatial point in the postshock gas the collision rate with all other grains has to be weighted with the grain volume affected by such a collision. Integration over position behind the shock yields then the diamondized volume for each grain size. The total grain volume that is diamondized by a supernova shock at one particular shock velocity is then calculated by integrating over grain size. This calculation is repeated for several different supernova shock velocities. Finally, these volumes are convolved with the frequency a

grain is shocked by a supernova shock with a particular velocity to calculate the lifetime of a grain versus diamondization (or vaporization or shattering). This latter step requires a model for the interstellar medium. Evaluation of these integrals yields an expected fraction of elemental carbon in small diamond grains of about 5% (127). This fraction is not very dependent on the absolute supernova shock frequency since supernova shocks both form and destroy (through sputtering and vaporization) diamond grains. Of course, the large number of other steps required in the evaluation do make this number quite uncertain. Nevertheless, since observations of elemental depletions in high velocity gas testify to the destruction of interstellar grains by supernova shock waves, a small fraction of the elemental C (~5%) is expected to be in the form of interstellar diamonds produced by grain-grain collisions in the interstellar medium.

## B) Diamond metamorphism

Numerous laboratory experiments have shown that graphite and amorphous carbon transform into polycrystalline diamond (crystallite size ~200Å) by a diffusionless process when a shock wave traversing these solids drives the pressure above about 400 kbar. The transformation is complete when the pressure exceeds about 600 kbar (130-135). Experiments have been performed on fairly well ordered forms of pyrolytic graphite (i.e., polycrystalline carbon), on slightly disordered, natural graphite from Ceylon, as well as on highly disordered and porous forms of graphite. For the more disordered forms the threshold pressure for complete diamond transformation is actually somewhat lower (~400kbar). Because of the high activation energy (~7.5eV/C atom) for the diamond-graphite rearrangement, graphitization of newly formed diamond will not occur when the cooling behind the shock front is very rapid. Indeed, experiments have shown a high conversion efficiency. Even at shock pressures of only 250kbar, well below the complete transformation threshold, about 25% of diamonds have been recovered (135). A single, perfect crystal of graphite, when shocked along the c-axis, actually transforms into a hexagonal form of diamond (i.e., lonsdaleite) rather than the cubic form.

The carbon phase diagram: Figure 11 shows the high pressure phase diagram for carbon (136). Three different regimes can be discerned, where graphite, diamond and the liquid phase respectively are thermodynamically stable. The liquid-diamond transition has been shown with a positive slope, reflecting recent theoretical and experimental studies (137,138). Although diamond is thermodynamically favored at high pressures and temperatures, graphite is metastable in part of this regime, presumably because the transformation entails a complete rearrangement of the carbon lattice. Likewise, diamond is metastable in part of the graphite domain. Measurements of the metastable graphite melting curve within the diamond stability regime (eg., between about 2500 and 4000 K; 136) have been boldly linearly extrapolated to much lower temperatures in figure 11. Theoretical calculations show that a metallic carbon phase with a simple cubic structure is preferred at very high pressures (>10Mbar; 139). Although preferred at high temperatures and low pressures, the exact location of the vapor phase is not well known. Estimates of the solid-liquid-vapor triple point range from about 0.1 kbar and 4500K to about  $2 \times 10^{-4}$  kbar and 4000K (136). Essentially this uncertainty reflects a debate on the existence of a fourth polymorph of carbon which may have been detected in some carbonaceous meteorites and in chaotite from the Ries impact crater (140,141). In this solid, known as carbyne, the carbon is thought to be arranged in linear chains either with alternating triple and single bonds (acetylene polymer; cf., figure 2) or with

## CARBON PHASE DIAGRAM

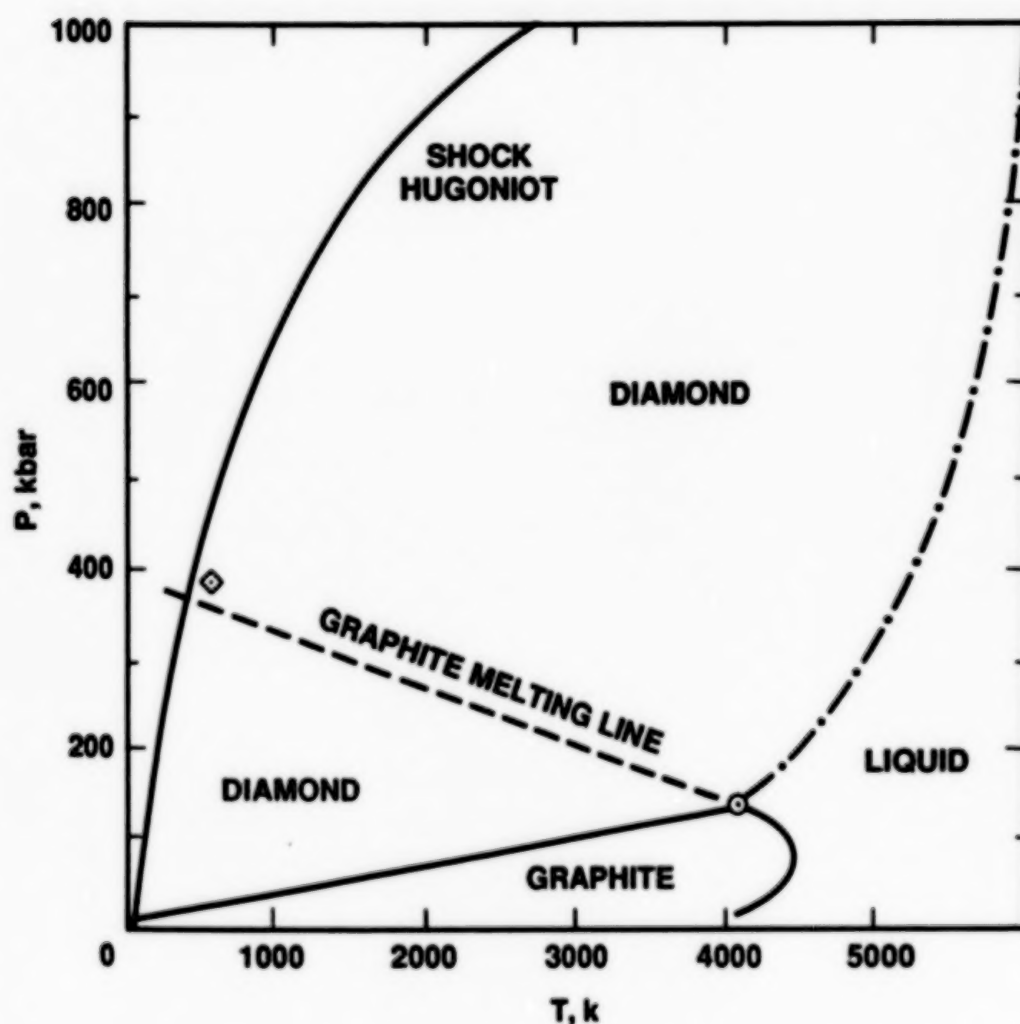


**Figure 11.** The carbon phase diagram at high pressures and temperatures (adapted from reference 136). The regimes in which graphite, diamond and liquid carbon are thermodynamically favored are indicated. Graphite is metastable below the graphite melting line within the diamond stability regime. Diamond is metastable below about 2000 K in the graphite stability field. The line labeled shock Hugoniot connects the loci of shock states accessible for graphite. The stronger the shock the further to the right the immediate post shock conditions will be. The diamond symbol indicates the experimentally determined threshold conditions required for the graphite  $\rightarrow$  diamond transformation.

cumulated double bonds (cumulene; 142). However, although carbon in the form of acetylene polymers could certainly be metastable in a large part of the phase diagram, the existence of this fourth stable carbon polymorph has never been shown directly. Moreover, the original discovery is very much in doubt, since later research on several of these samples either discovered impurity inclusions in these materials or could not repeat the earlier results (143).

The graphite shock Hugoniot (144) has been superimposed on the carbon phase diagram (cf., figure 11). The Hugoniot is the loci of shock states accessible for graphite. The higher the shock velocity, the higher the resulting postshock temperature and pressure will be and the farther to the right on the Hugoniot curve the material immediately behind the shockfront will find itself. After the passage of the shockfront the compressed material will expand again. This expansion is adiabatic and no entropy change will occur. For low postshock pressures, the expansion isotope will almost coincide with the shock Hugoniot. For the high shock pressures appropriate for this discussion, the material can still contain appreciable internal energy after expansion and the expansion isotope lies to the right of the Hugoniot. The approximate location of the shock conditions for which the graphite-diamond transition is first observed is indicated by a diamond in figure 11. Commercial production of (shocked) diamonds occurs typically up to about 1 Mbar and 3000 K (136,145).

The onset of the shock generated, graphite-diamond transformation occurs close to the extrapolated graphite melting line in the carbon phase diagram and is probably initiated by pseudo-melting of graphite and rapid recrystallization in the diamond phase (136,146). Extrapolation of these laboratory studies to interstellar grain collisions is somewhat hampered by the difference in scale size. Laboratory determined crystallization timescales are faster than  $10^{-8}$  s (135), but this may still be longer than the adiabatic shock cooling timescale in an interstellar grain ( $\Delta r/C_s \sim 10^{-12}$  s, where  $\Delta r$  ( $\sim 100$  Å) and  $C_s$  ( $\sim 5$  km s $^{-1}$ ) are the size and sound velocity in the compressed material) and the resulting crystal may be highly disordered. Note that although the shocked region may be optically thin at the small interstellar grain size scales, radiative losses due to electronic or vibrational transitions are not important since the radiative lifetimes (for aromatic molecules  $\sim 10^{-8}$  and 0.1 s, respectively; 147) are much longer than the adiabatic expansion timescale.

**Microcrystal sizes:** Near the melting line the structure of monatomic liquids is that obtained by dense random packing of hard spheres (148,149). Energy and strain considerations favor then a local liquid structure consisting of 20 tetrahedra arranged in clusters of icosahedral symmetry (containing 13 carbon atoms; 150,151). These abundant icosahedral clusters can act as nucleation centers for crystallization into an ordered crystal structure. The rate at which atoms in the liquid-solid interface move to lattice sites is limited by the sound velocity (eg., vibrational timescale,  $\sim 10^{-14}$  s). The advancing liquid-solid interface will be driven by the liberated latent heat of melting at velocities up to the sound velocity (explosive crystallization; 152). That is,

$$v_i = K \frac{dT}{dr} / \Delta H_m$$

where  $K$  is the heat conductivity ( $\sim 3 \text{ W cm}^{-1} \text{ K}^{-1}$  for diamond at 1000K; 153) and  $dT/dr$  is the temperature gradient ( $\sim 10^9 \text{ K cm}^{-1}$  for a 100Å compressed region). The latent heat of melting of diamond,  $\Delta H_m$ , is not known. Assuming it is the same as for graphite ( $\sim 25 \text{ kcal/mol}$ ; 136) yields  $v_i \sim 1 \text{ km s}^{-1}$ . Crystallization will stop when neighboring diamond crystals touch or when the heat loss to the surroundings becomes too large. The remainder of the carbon liquid will then cool so rapidly that it will solidify in a highly disordered diamond structure (c.f., 1). Probably, this will become important when the compressed material has expanded again due to the rarefaction wave. The diameter of the (ordered) diamond crystals grown this way will then be set by the crystal-liquid interface velocity,  $v_i$ , and the time available, (i.e.,  $\Delta a = 2v_i/C_s \Delta r$ ). This limits the size of a diamond microcrystal to the size of the expansion region behind the shock ( $\Delta r$ ), which is typically about 10% of the depth of the shock front in the target (154). For the formation of interstellar diamonds, collisions of small (100Å) grains with large carbon ( $a \sim 1000\text{Å}$ ) grains are most important resulting in a  $\Delta r$  of 100Å. For the parameters quoted above we find that  $\Delta a$  is typically 40Å. Note that this is to first order independent of the size of the expansion region, essentially because the crystal-liquid interface velocity adjusts itself to the size of the expansion region. It is therefore not very surprising that the sizescale of the microcrystallites in macroscopic experiments ( $\sim 100\text{Å}$ ; 135,145,155) is very similar to those expected in the collision of submicron particles.

Once the liquid has solidified, further rearrangement of the lattice will be inhibited by a considerable activation barrier. Therefore, the bonds between carbon atoms in the interfaces of neighboring microcrystals will be highly strained and distorted. As a result these interfacial carbon atoms will show some degree of  $sp^2$  bonding (cf., fig. 2). This will give an apparent "amorphous carbon" character to some types of spectra (cf., 124,156). Both laboratory produced diamonds as well as meteoritic diamond reveal the presence of such highly disordered interfacial carbon (156). Upon cooling and expansion, the shock synthesized diamond will enter the graphite stability regime. Graphitization of the newly formed diamonds will, however, be inhibited by a large energy barrier since all the bonds have to be broken and the lattice rearranged. Diamond is therefore metastable below 2000K in the graphite stability field. Since a large fraction of the carbon is recovered as diamonds in macroscopic shock experiments of graphite and since cooling will be even faster, graphitization is expected to be unimportant on the submicron sizescale of interstellar grains. We note, however, that ion-implantation during further shock processing will lead to an approximately 5Å thick, amorphous, surface layer in which the binding has an aromatic character (127).

Finally, in those cases where spalling is important (see below), a small fraction of the compressed material may be released during the spalling process. In that case, the sizes of the resulting fragments will be determined by the surface free energy of the high pressure carbon liquid and the resulting solidified droplets may be somewhat smaller.

**Shattering:** For the prediction of the structure of interstellar diamonds the effects of shattering must also be considered. The velocity associated with the excavation flow which carves out the crater in the target is much less than the velocity of the rarefaction wave and thus the molten material is expected to solidify long before

shattering at the free surface can occur. It is important to recognize that the fracture yield strength is highly size dependent (127,157,158). For macroscopic bodies shattering is due to the initiation, growth and coalescence of microscopic cracks, but these play no role at micron size scales where materials will show a ductile (fluid) rather than brittle behaviour. The dynamic yield strength of polycrystalline diamond is measured to be about 400 kbar (159,160). This is very similar to the minimum dynamic pressures required to form diamond by shock-metamorphism. Since the pressures associated with the excavation flow are much less than those of the shock and since most of the shock diamond synthesis occurs at the lowest pressures ( $V \sim P^{-0.9}$ ; cf., § VIIB), shattering during crater formation is expected to be of little importance. Shattering can also occur when the shock reaches the backside of the target and is reflected as a tensile wave (eg., spalling). However, in view of the increased tensile strength of materials at small sizescales, this plays much less a role than for macroscopic bodies. Indeed while "catastrophic destruction" of cm-sized glass spheres occurs for pressures of the order of one kbar (161-163), for submicron-sized glass spheres the critical pressure is of the order of 150 kbar (127). For shock synthesized diamonds this critical pressure is expected to be around 400 kbar. Assuming that the typical diamond forming collision occurs between a 100Å and a 1000Å grain, the minimum collision velocity for catastrophic destruction is then calculated to be about  $100 \text{ km s}^{-1}$  (127). Since diamond formation in the interstellar medium is dominated by low velocity shocks ( $V \sim 50 \text{ km s}^{-1}$ ; 125), shattering of newly formed diamonds is expected to be relatively unimportant.

**Impurities:** Interstellar graphite or amorphous carbon grains may contain considerable amounts of impurities, either interstitial or substitutional. In particular, stardust formed in the outflows from carbon-rich red giants may be heavily hydrogenated ( $H/C \sim 0.1$ ; cf., § VIB). Some impurities, such as N, can be substituted for C in the diamond lattice and their presence will not have a major effect. Hydrogen (or deuterium) atoms are small enough that they can be stored in interstitial diamond sites. Natural diamonds contain typically about 0.3% of substitutional nitrogen, which in fact gives them their striking colours. About 0.2% of interstitial and often a similar amount of chemically bonded hydrogen is also present (164). Small amounts of impurities will not affect the shock Hugoniot or the graphite-diamond transformation very much. Indeed, diamonds have been recovered from shock experiments on glassy carbon (highly disordered C resulting from heat treatment of furfural resins) containing up to 10% of oxygen, 3% of hydrogen and 0.2% of nitrogen (165). In principle, larger amounts of impurities might lead to different results. Nevertheless, theoretical and experimental studies of liquid benzene shocked to about 700 kbar indicate that some of the carbon is transformed into diamond, although no recovery studies have been performed (166). However, we do note that small diamonds have been recovered in static pressure/flash heating experiments on several organic compounds, including anthracene, naphthalene, chrysene and pyrene (167). The threshold conditions for diamond formation in these experiments seems to be somewhat higher than for pure graphite experiments (168). Thus, it is likely that even a fraction of "impure" amorphous carbon grains such as hydrogenated amorphous carbon formed around carbon-rich red giants will transform into diamonds under shock conditions.

In the context of the small diamonds discovered in carbonaceous meteorites, the fate of interstitial impurities such as Xe HL is of considerable interest. Pulsed laser

annealing studies of ion-implanted silicon layers show for example that, due to diffusion during the liquid phase, impurities are concentrated near the surface of the crystals (169). The measured crystal-liquid interface front velocity in these experiments is about  $1 \text{ m s}^{-1}$ , which is less than the effective "diffusion" velocity ( $\sim 10 \text{ m s}^{-1}$ ; 169). However, crystallization will occur much faster than diffusion in the interstellar case and (inert) impurities are expected to be incorporated into (and distort) the diamond structure.

### C) Diamonds in the sky

Since only a small fraction of the elemental C is expected to be in the form of diamond grains due to shock processing, it may be difficult to detect them in the interstellar medium. Small diamond grains will show a pronounced far ultraviolet absorption edge and may contribute to the far ultraviolet rise in the observed interstellar extinction curve (125). However, a size distribution of large (polycrystalline) diamond grains will produce a rather smooth extinction curve over the visible and UV (170). In that case, the presence of diamond grains will be difficult to prove (or negate), since the extinction will be dominated by other more abundant dust components (cf., table 1). The density of phonon states of diamond shows several peaks between  $4.5$  and  $5 \mu\text{m}$ , but these modes are IR inactive for a perfect monovalent crystal and thus for large, crystalline diamonds. However, some IR activity is induced by the disorder introduced by the presence of impurities, defects and particularly microcrystallite surfaces (1). Thus, highly disordered, interstellar, diamond grains, resulting from rapid quenching of the liquid (cf., § B), will show weak infrared signatures at the peaks of the phonon density of states.

The interlocking microcrystals in the polycrystalline diamond grains will be separated by highly disordered thin interface regions. The carbon atoms in these regions have a large  $\text{sp}^2$  character (eg., aromatic structure; cf., fig. 2) and their IR spectrum will resemble that of soot. These polycrystalline conglomerates might contribute to the widespread, near-infrared ( $12 \mu\text{m}$ ) cirrus observed by IRAS (125). Note that, in contrast to small PAH molecules, they absorb over a large part of the visible and UV region of the spectrum without showing distinct structure in the extinction curve. Moreover, their IR emission spectrum will be very similar to that of soot and is therefore likely to resemble that observed in reflection nebulae (8). Third, because most modes are IR inactive, these grains will radiate more easily in the mid IR than other materials with comparable sizes. A high temperature is also indicated by the high Debye temperature of diamonds. Moreover, due to the difference in structure and binding, it is perhaps possible to localize the excitation energy in a small (amorphous carbon) part of the polycrystalline grain, which will temporarily be excited enough to radiate through the near- and mid-infrared modes (171). Obviously, laboratory studies will be very important to study the reality of such energy localization effects.

## VIII Interstellar Carbon Dust and Carbonaceous Meteorites

One of the most interesting developments within the field of interstellar dust in recent years is the realization that some interstellar grains may have been incorporated into meteorites and interplanetary dust particles without totally losing their identity (3,113,172). Evidence for this rests on the measurement of isotopic

anomalies in meteorites and in particular in carbonaceous chondrites. Although the meteoritic composition is in a global sense remarkably homogeneous, non-mass-dependent isotopic anomalies do exist for many elements. These include the noble gases, the light elements (H, C, N, and O), and the heavy elements (e.g., Ca, Ti, Cr, Ni, Nd, Sm and others). Although some unusual processes in the solar nebula might have produced non-mass-dependent isotopic fractionation in some elements, it is unlikely that they could account for all of them. Moreover, the measured isotopic anomalies are very characteristic for a presolar origin of the material. For example, the Xe and Kr isotopic anomalies associated with one particular meteoritic carbon phase carry the signature of s processes in red giants, suggesting the presence of largely unmodified carbonaceous grains in meteorites which were produced in carbon-rich red giant outflows (17,25). Thus, meteoritic materials carry a nucleogenic record of the birth site of the dust grain, modified by processes which occurred in the interstellar medium as well as in the solar nebula or on planetary bodies. Consequently, laboratory analysis of meteoritic and interplanetary material may yield detailed microscopic information on interstellar dust, which is not obtainable by astrophysical observations. It should, however, be emphasized that meteoritic materials are very heterogeneous and contain dust grains from different origins; including star dust from many different birth sites, interstellar medium dust, and solar nebula condensates. Generally, the actual presolar carrier of the measured isotopic anomalies is not known. Such information is, however, of prime importance for our reading of this record and for our assessment of the implications for interstellar dust and its evolution.

Many different carbon phases with isotopically anomalous composition have been discovered in carbonaceous meteorites. Table 6 provides a summary of some relevant data on these phases (cf., 113). Each of these will be discussed in turn.

The C- $\alpha$  phase: This phase consists of turbostratic carbon, that is a carbon solid containing disoriented graphitic layers quite similar to soot. It contains almost pure  $^{22}\text{Ne}$ . Most of the  $^{22}\text{Ne}$  in the galaxy is produced by WC stars. These stars also produce minor amounts of carbon stardust (cf., table 2) and thus might be the origin of this carbon phase in carbonaceous meteorites (173). However, it is difficult to produce almost pure  $^{22}\text{Ne}$  this way. In particular, theoretical calculations of the nucleosynthesis in WC stars predict that the  $^{20}\text{Ne}/^{22}\text{Ne}$  ratio is about 0.02 (44). An alternative source of  $^{22}\text{Ne}$  is  $\beta$ -decay of  $^{22}\text{Na}$  and novae are then an attractive source for this carbon phase (174). The freshly synthesized  $^{22}\text{Na}$ , other Na isotopes (ie.,  $^{23}\text{Na}$ ), as well as other elements ( $^{25}\text{Mg}$ ,  $^{26}\text{Mg}$ ,  $^{26}\text{Al}$ ,  $^{27}\text{Al}$ ) must have been rapidly incorporated into the carbon stardust before the  $^{22}\text{Na}$  decayed ( $\tau \sim 2.5$  yrs) to  $^{22}\text{Ne}$ . We note that electron donors such as alkali, alkaline earth and transition metals, readily form intercalation compounds with graphitic and turbostratic carbon (175). Unlike the noble gases these metals are, however, difficult to measure in meteorites.

This meteoritic carbon phase component is also known to be enriched in  $^{13}\text{C}$  and  $^{15}\text{N}$  (cf., table 6). However, the  $^{13}\text{C}$  enrichment is less than one might expect from theoretical models for novae nucleosynthesis which predict  $^{12}\text{C}/^{13}\text{C}$  ratios less than unity (30,53). Also  $^{15}\text{N}$  overabundances of  $>10^3$  are predicted by some models. These predictions are quite sensitive to the details in the models (temperature; mixing; shell burning) and the problem may reside in the nucleosynthesis models rather than the identification of this meteoritic carbon phase with novae stardust. Alternatively,

**Table 6: Interrelationship of interstellar and solar system carbonaceous materials**

Carbon Phase	Isotopic Anomaly	concentration [ppm]	Birth Site
C- $\alpha$ (Ne-E)	pure $^{22}\text{Ne}$ $^{12}\text{C}/^{13}\text{C}=70$	5	-Novae
C- $\beta$	s process Xe $^{12}\text{C}/^{13}\text{C}=40$ $^{86}\text{Kr}$	<5	-C-rich Red Giants
C- $\delta$ (diamond)	Xe-HL $^{14}\text{N}/^{15}\text{N} > 400$ $^{12}\text{C}/^{13}\text{C}=90$	400	-graphite $\rightarrow$ diamond in ISM shock waves
C- $\epsilon$	$^{22}\text{Ne}$ $^{12}\text{C}/^{13}\text{C} < 10$	2	-Novae
soluble and dust	D/H up to $10^{-3}$	20,000	-pyrolysis of ISM
insoluble organic matter	mundane C and N		-PAHs (?)

the C- $\alpha$  phase may be contaminated with solar system carbon with a normal  $^{12}\text{C}/^{13}\text{C}$  ratio.

**The C- $\beta$  phase:** This carbon phase in carbonaceous meteorites consists of SiC grains which contain enriched s-process isotopes of Xe and Kr (cf., table 6). It is also enriched in  $^{13}\text{C}$ . It is generally accepted that this carbon phase represents stardust condensed out in the outflow from carbon-rich red giants (3,113,172), where we note that the  $11.4\mu\text{m}$  feature, characteristic for SiC, is often seen in such environments (cf., table 1 and 2). The  $^{14}\text{N}/^{15}\text{N}$  ratio in this carbon phase is solar, which is somewhat surprising since the same dredge-up episodes that enhance  $^{13}\text{C}$  also will produce  $^{14}\text{N}$  (176). Because of its refractory nature SiC is more readily detected in stepwise heating of carbonaceous meteorites than carbon dust. The latter is, however, more abundant in circumstellar and interstellar dust and a "pure" carbon phase with similar isotopic anomalies is expected to be present in carbonaceous meteorites at about the 50ppm level.

**The C- $\delta$  phase:** The C- $\delta$  phase in carbonaceous meteorites consists of small diamond ( $\sim 50\text{\AA}$ ) grains (124,156). Both the heavy and light isotopes of Xe are enriched compared to the sun, implying a presolar origin (3). It has been suggested that these isotopic anomalies reflect the effects of mixing of two different nucleosynthetic zones within one supernova. This may have occurred either before condensation or

after condensation in one zone by ion implantation of the products of the second zone. A variant of the latter is ion-implantation in grains formed in a precursor mass-loss phase by the overtaking high velocity, supernova ejecta (177). Recently, it has been suggested that these small diamond grains are the result of shock metamorphism of carbon stardust in the interstellar medium (125). In that model, the measured isotopic anomalies reflect the sum of the nucleosynthetic processes taking place in the various birth sites of the original carbon stardust. Both the small  $^{15}\text{N}$  and the absence of a  $^{13}\text{C}$  enhancement are difficult to understand in terms of a single circumstellar source (eg., supernovae or their red supergiant progenitors) of this meteoritic carbon phase but might conceivably result from averaging over many different carbon stardust sources. In the latter case, one might however expect isotopic variations on an individual interstellar grain basis ( $\sim 1000\text{\AA}$  scale). It should be emphasized that the measured abundances of the isotopically anomalous Xe are measured on  $\mu\text{g}$  samples and reflect thus an average over about  $10^{11}$  diamond microcrystals or about  $10^8$  typical interstellar dust grains ( $\sim 1000\text{\AA}$ ).

The surface layers of this meteoritic carbon phase seem to contain noble gases impurities with an isotopically anomalous composition (113). These might result from ion-implantation. For a typical gas-grain drift velocity due to radiation pressure in WC 8-10 and supernova ejecta of  $25\text{ km s}^{-1}$ , the ion range of Ar and Xe is 3 and  $7\text{\AA}$ , respectively. In this case, the implantation depth will, thus, depend to some extent on the mass of the element under consideration. Note that the drift velocity in red giant outflows is generally very small and ion implantation should be unimportant. Finally, appreciable drift velocities will also occur in interstellar shock waves and the resulting ion implantation will tend to dilute the nucleogenic record from the grain's birth site.

**The C- $\epsilon$  phase:** The C- $\epsilon$  phase consists of SiC grains carrying an almost pure  $^{22}\text{Ne}$  enrichment. As was the case for the C- $\alpha$  phase, this phase is thought to represent stardust condensed in nova ejecta. An  $11\mu\text{m}$  feature observed in nova Aquila has been attributed to SiC grains (48). Since the Si/C ratio in WC stars is expected to be very small, the identification of the carrier of this Ne E component with SiC provides an additional argument against an origin of the other Ne E component (the C- $\alpha$  phase) in WC stars, which have a very low Si abundance. The large enhancement of  $^{13}\text{C}$  in these grains (cf., table 6) supports an origin in novae (30,53). It makes the much higher  $^{12}\text{C}/^{13}\text{C}$  ratio in the C- $\alpha$  phase even more puzzling and suggests that the C- $\alpha$  phase is contaminated by solar system carbon with a normal  $^{12}\text{C}/^{13}\text{C}$  ratio.

**Organic matter:** Two components are lumped together under this nomenclature (3,113,172). First, the acid-soluble fraction ( $\sim 25\%$ ) contains such organic compounds as amino and carboxylic acids. Second, the acid-insoluble fraction ( $\sim 75\%$ ) consisting of aromatic moieties connected by short aliphatic bridges and sidechains (eg., kerogen). Both phases are heavily deuterated. Such chemical fractionation will only occur at very low temperatures ( $T < 100\text{K}$ ). Although the cooling solar nebula will have experienced such low temperatures, the timescale to reach this equilibrium is far too long to obtain a sizeable fractionation (3). High deuteration effects have been observed in many gas phase molecules in interstellar molecular clouds and are thought to originate from ion-molecule reactions (178). Large deuteration effects are also expected for icy grain mantles accreted in molecular clouds (179). These deuteration effects result from non-equilibrium chemistry driven by cosmic ray ionization and

equilibrium is readily established at interstellar timescales ( $\sim 10^7$  yrs). For this reason the hypothesis that interstellar, as distinct from circumstellar material, has been incorporated into carbonaceous meteorites without major modifications has been widely accepted (3, 172, 180). The actual deuterated carrier(s) into the solar nebula, whether gas phase or solid state, and the importance of the distinction between the soluble and insoluble phases is unknown. Possibly, the kerogen results from clustering of small interstellar PAH molecules and amorphous carbon grains, where the PAHs carried the deuteration effects due to photochemical processes in the interstellar medium (181). Alternatively, it may result from prolonged pyrolysis of (deuterated) interstellar molecules either in the solar nebula (3) or in the interstellar medium (2). In the latter model the acid-soluble phase may represent an intermediate step in the UV photolysis and transient heating of interstellar grain mantles. Indeed, laboratory studies show that carboxylic acids are readily formed from simple molecular ices (eg.,  $H_2O$  and  $CO$ ) by such processes (182, 183). Prolonged exposure to UV radiation and transient heating is expected to result eventually in the almost complete removal of elements other than C (and possibly H) and to lead to a structure similar to that of meteoritic kerogen.

## IX Summary

In summary, we conclude that interstellar dust is a collection of many different materials. There are many different stardust birth sites each with distinct physical and chemical conditions and elemental and isotopic composition. Many different types of objects contribute to the carbon budget of the galaxy, including WC stars, supernovae and carbon-rich red giants. Although the relative contribution of each of these is not well known, it is likely that both low mass and high mass stars contribute about equally. Astronomical evidence shows that carbonaceous stardust originates in WC 8-10 stars, C-rich red giants, and possibly supernovae. Studies of meteoritic carbon compounds strongly suggest that some novae produce SiC and amorphous carbon grains. Probably carbon-rich giants dominate the carbon stardust balance. About 20% of the elemental C is injected in the form of dust grains. Since extinction observations suggest that about half of the elemental C is locked up in dust grains, this implies the presence of an efficient formation mechanism for carbonaceous dust in the interstellar medium. One attractive mechanism is UV photolysis of accreted icy grain mantles, which may result in organic refractory grain mantles (polymeric carbon) or perhaps even amorphous carbon grain mantles.

The physical conditions in the stardust condensation zone around C-rich giants, R Cr B stars and WC stars have been reviewed. These objects span a wide range in physical and chemical conditions, yet carbon stardust seems always to form once the temperature drops to about 1000K. The typical densities inferred for the carbon condensation zone imply that dust nucleation has to occur essentially on a collision timescale. This will form a problem for any nucleation theory. Stardust formation has generally been modeled using thermochemistry (ie., condensation sequence) and classical nucleation theory. The problems with this approach have been pointed out and it is emphasized that any theory should start by identifying the chemical pathway to dust.

The chemical processes that convert  $C_2H_2$  into carbon stardust in the outflow from

carbon-rich giants are probably very similar to those occurring during the gas phase pyrolysis of hydrocarbon molecules in flames. PAHs may play an important role in this. Among the PAHs expected to be abundantly produced in such outflows are naphthalene, acenaphthalene, pyrene and coronene. Their detection in circumstellar shells will form an important confirmation of these chemical schemes as well as supporting the ubiquitous presence of PAHs in the interstellar medium. Photochemical processing as well as shock wave destruction will further influence the chemical composition of the *interstellar* PAH family. The carbon stardust formed in these outflows is expected to be very similar to soot and to consist of small aromatic moieties (ie., PAHs) clustered in larger units and connected by aliphatic bridges and side chains (ie., tetrahedral carbon). The hydrogen content of these platelets may be very high (~10%). These carbon platelets will be clustered in the form of larger spherical particles. The basic building blocks of carbon stardust will thus have a structure quite similar to that of hydrogenated amorphous carbon films (HAC).

The carbon stardust formation mechanism in WC 8-10 stars is not understood very well. It is likely that it starts with the formation of small acetylenic species such as  $C_2$ ,  $C_3$  and their ions. Indeed, ionization may play a dominant role. An important difference with carbon stardust formation around carbon-rich red giants is the absence of hydrogen and hydrogenated molecules in the outflow. Clearly, PAHs and HAC will not form a good model for this stardust. Actually, Buckminsterfullerene ( $C_{60}$ ) and its larger analogs, formed by laser vaporization of graphite targets in a hydrogen-poor atmosphere, may play an important role in the condensation processes around these objects.

High velocity ( $v \geq 7 \text{ km s}^{-1}$ ) grain-grain collisions drive strong shock in carbon stardust which provides the high pressures required to transform some of it into diamond. This supports the suggested interstellar origin for the recently discovered small diamonds in carbonaceous meteorites by providing a feasible interstellar formation mechanism. Shock metamorphism of carbon stardust is expected to produce polycrystalline diamond grains. The microcrystalline sizes are calculated to be about 40 Å, in good agreement with the measured ones in meteoritic carbon and shock experiments. Since the diamond formation is thought to go through a liquid precursor phase, the structure of the original carbon stardust grains is of little importance. Indeed, highly ordered graphite, amorphous carbon as well as glassy carbon containing substantial amounts of impurities will transform into diamonds under shock conditions.

A wide variety of isotopic anomalies have been detected in different carbon phases in carbonaceous meteorites. These carbon phases are thought to consist of interstellar or circumstellar dust grains which have been incorporated into the meteorite without major modifications. The isotopic anomalies reflect then the particular (nucleosynthetic) processes which played a role in the birth sites of these grains. Among the processes that may have been important in preserving this presolar (nucleosynthetic) record in these grains are (co)condensation (eg.,  $^{12}\text{C}/^{13}\text{C}$ ;  $^{14}\text{N}/^{15}\text{N}$ ;  $^{22}\text{Na}/^{22}\text{Ne}$ ), ion implantation (eg., Xe HL; Q phase), and photochemical processes in the ISM (eg., D/H). Because many different sources contribute, one of the characteristics of stardust preserved in carbonaceous meteorites is a widely varying isotopic composition on a submicron scale. In particular, the  $^{13}\text{C}/^{12}\text{C}$  ratio may vary dramatically on this scale depending on the source of the stardust ranging from about

zero for WC 8-10 and supernovae, solar ( $\sim 0.01$ ) for optically visible C-rich Miras, 0.3 for some C-rich giants, to  $>1$  for novae. In the protosolar nebula, stardust from different birthsites may have represented distinct, isotopically enriched reservoirs, which because of their different physical and chemical properties, may have been released at different times or in different parts of the nebula. Another signature of interstellar dust, which may help recognize presolar dust in meteorites or IDPs, is shock metamorphism on a submicron scale.

**Acknowledgments:** I thank Martin Cohen for hammering in the mystery of carbon dust formation around WC 8-10 stars during carpool hours, Helen Walker for a guided tour through the R Cr B phenomena, Mike Jura for helpful discussions on the carbon budget of the galaxy, and Stan Woosley for sharing his insight on supernova, in particular of SN 1987a. I thank Lou Allamandola and Dave Hollenbach for comments on an earlier version of this manuscript. Finally, I am indebted to Profs. E. Bussoletti and A. Borghesi for permission to show their beautiful carbon necklace.

## References

1. Tielens, A.G.G.M. and Allamandola, L.J. 1987, in Interstellar Processes, eds. D.J. Hollenbach and H.J. Thronson, (Reidel, Dordrecht), p.397.
2. Tielens, A.G.G.M. and Allamandola, L.J. 1987, in Physical Processes in Interstellar Clouds, eds. C.E. Morfill and M. Scholer, (Reidel, Dordrecht), p.333.
3. Lewis, R.S., and Anders, E., 1983, Sci. Am., 249, 66.
4. Merrill, K.M. 1977, in The Interaction of Variable Stars with their Environments, eds. R. Kippenhahn, J. Rahe and W. Strohmeyer, (veroff, Reineis Sternwarte, Bamberg), Bd. XI, nr 121, p.446.
5. Aitken, D.K. 1981, in IAU symp. no. 96, Infrared Astronomy, eds. G.C. Wynn Williams and D.P. Cruikshank (Reidel, Dordrecht), p.207.
6. Willner, S.P. 1984, in Galactic and Extragalactic Infrared Spectroscopy, eds. M.F. Kessler and J.P. Phillips, (Reidel, Dordrecht), p.37.
7. Cohen, M., Allamandola, L.J., Tielens, A.G.G.M., Bregman, J., Simpson, J.P., Witteborn, F., Wooden, D., and Rank, D., 1986, Ap. J., 302, 737.
8. Sellgren, K., Allamandola, L.J., Bregman, J., Werner, M.W., and Wooden, D., 1985, Ap.J., 299, 416.
9. Duley, W.W. and Williams, D.A., 1981, M.N.R.A.S., 196, 269.
10. Allamandola, L.J., Tielens, A.G.G.M., and Barker, J.B., 1985, Ap. J. Letters, 290, L25.
11. Leger, A., and Puget, J.L., 1984, Astr. Ap., 137, L5.
12. Barker, J.B., Allamandola, L.J., and Tielens, A.G.G.M., 1987, Ap. J. Letters, 315, L61.
13. Mathis, J.S., Ruml, W., and Nordsieck, K.H., 1977, Ap.J., 217, 425.
14. Mathis, J.S., and Wallenhorst, S.G. 1981, Ap.J., 244, 483.
15. Greenberg, J.M., and Chlewicki, G., 1984, Ap.J., 272, 563.
16. Greenberg, J.M., Hong, S.S., 1984, in Galactic Radio Astronomy, IAU symp. no. 60, eds. F.J. Kerr and S.C. Simonson, (Reidel, Dordrecht), p.155.
17. Draine, B.T., and Lee, H.M., 1984, Ap.J., 285, 89.
18. Kittel, C. 1976, Introduction to Solid State Physics, (Wiley and Sons, NY).
19. Audouze, J. and Tinsley, B.M., 1976, Ann. Rev. Astr. Ap., 14, 43.
20. Jura, M., 1988, elsewhere in this volume.
21. Knapp, G.R., 1987, in Late Stages of Stellar Evolution, eds. S. Kwok and S. Pottasch, (Reidel, Dordrecht), p.103.
22. Weidemann, V., and Koester, D., 1983, Astr. Ap., 121, 77.
23. Jura, M., 1987, in Interstellar Processes, eds. D.J. Hollenbach and H.J. Thronson, (Reidel, Dordrecht), p.3.

24. Thronson, J.A., Latter, W.B., Black, J.H., Bally, J., and Hacking, P., 1987, *Ap.J.*, 322, 770.
25. Clausen, M.J., Kleinmann, S.G., Joyce, R.R., and Jura, M., 1987, *Ap. J., Suppl.*, 65, 385.
26. Knapp, G.R., and Morris, M., 1985, *Ap. J.*, 292, 640.
27. Knapp, G.R., and Wilcots, E.M., 1987, in Late Stages of Stellar Evolution, eds. S. Kwok and S. Pottasch, (Reidel, Dordrecht), p.171.
28. Abbott, D.C., 1982, *Ap. J.*, 263, 723.
29. van Buren, D., 1985, *Ap. J.*, 294, 567.
30. Truran, J. W., 1986, in Nucleosynthesis and its Implications on Nuclear and Particle Physics, eds., J. Audouze and N. Mathieu, (Reidel, Dordrecht), p.97.
31. Ferland, G.J., and Shields, G.A., 1978, *Ap. J.*, 226, 172.
32. Gallagher, J.S., Hege, E.K., Kopriva, D.A., Williams, R.E., and Butcher, H.R., 1980, *Ap. J.*, 237, 55.
33. Tylenda, R., 1978, *Acta Astr.*, 28, 333.
34. Williams, R.E., Woolf, N.J., Hege, E.K., Moore, R.L., and Kopriva, D.A., 1978, *Ap. J.*, 224, 171.
35. Danziger, I. J., 1984, in Stellar Nucleosynthesis, eds. C. Choisi and A. Renzini, (Reidel, Dordrecht), p.35.
36. Woosley, S.E., and Weaver, T.A., 1986, *Ann. Rev. Astr. Ap.*, 24, 205.
37. Tammann, G.A., 1982, in Supernovae: A Survey of Current Research, eds. M. J. Rees and R.J. Stoneham, (Reidel, Dordrecht), p.371.
38. Woosley, S.E., 1987, private communications.
39. Thielemann, F.K., Nomoto, K., and Yokoi, K., 1986, in Nucleosynthesis and its Implications on Nuclear and Particle Physics, eds., J. Audouze and N. Mathieu, (Reidel, Dordrecht), p.131.
40. Chiosi, C., and Maeder, A., 1986, *Ann. Rev. Astr. Ap.*, 24, 329.
41. Willis, A.J., 1982, in Wolf Rayet Stars: Observations, Physics, Evolution, eds., C.W.H. de Loore and A.J. Willis, (Reidel, Dordrecht), p.87.
42. Abbott, D.C. and Conti, P.S., 1987, *Ann. Rev. Astr. Ap.*, 25, 113.
43. Nugis, T., 1982, in Wolf Rayet Stars: Observations, Physics, Evolution, eds., C.W.H. de Loore and A.J. Willis, (Reidel, Dordrecht), p.131.
44. Maeder, A., 1983, *Astr. Ap.*, 120, 113.
45. Torres-Peimbert, S. and Peimbert M., in Interstellar Processes, eds. D.J. Hollenbach and H.J. Thronson, (Reidel, Dordrecht), p.667.
46. van der Hucht, K.A., Williams, P.M., and Thé, P.S., *Q.J.R.A.S.*, 28, 254.
47. Dwek, E. et al., 1986, in Interrelationships Among Circumstellar, Interstellar, and Interplanetary Dust, ed., J.A. Nuth and R.E. Stencel, NASA CP 2403, WG-1.
48. Gehrz, R.D., Ney, E.P., Grasdalen, G.L., Hackwell, J.A., and Thronson, H.A., 1984, *Ap. J.*, 281, 303.
49. Knapp, G.R., and Chang, K.M., 1985, *Ap. J.*, 293, 281.
50. Zuckerman, B., 1980, *Ann. Rev. Astr. Ap.*, 18, 263.
51. Audouze, J., and Lazareff, B., 1977, in Novae and Related Stars, ed. M. Friedjung, (Reidel, Dordrecht), p.205.
52. Starrfield, S., Sparks, W.M., and Truran, J.W., 1985, *Ap.J.*, 291, 136.
53. Wiescher, M., Gorres, J., Thielemann, F.K., and Ritter, H., 1986, in Nucleosynthesis and its Implications on Nuclear and Particle Physics, eds., J. Audouze and N. Mathieu, (Reidel, Dordrecht), p.105.
54. Hawkins, and Jura, M., 1987, *Ap. J.*, 317, 374.
55. Hawkins, I., 1987, private communications.
56. Jura, M., 1987, private communications.
57. Pagel, B.E.J., and Edmunds, M.G., 1981, *Ann. Rev. Astr. Ap.*, 19, 77.
58. Martin, P.G., and Rogers, C., 1987, *Ap. J.*, 322, 374.
59. Lambert, D.L., 1986, in Hydrogen Deficient Stars and Related Objects, ed. K. Hunger, (Reidel, Dordrecht), p.127.
60. Lambert, D.L., 1987, in Astrochemistry, eds., M.S. Vardya and S.P. Tarafdar, (Reidel,

- Dordrecht), p.583.
61. Omont, A., 1987, in Astrochemistry, eds., M.S. Vardya and S.P. Tarafdar, (Reidel, Dordrecht), p.357.
  62. Feast, M.W., 1986, in Hydrogen Deficient Stars and Related Objects, ed. K. Hunger, (Reidel, Dordrecht), p.151.
  63. Tsuji, T., 1987, in Astrochemistry, eds., M.S. Vardya and S.P. Tarafdar, (Reidel, Dordrecht), p.409.
  64. Williams, P.M., van der Hucht, K.A., and Thé, P.S., 1987, *Astr. Ap.*, 182, 91.
  65. Querci, F., and Querci, M., 1974, in Highlights of Astronomy, 3, 341.
  66. Warner, 1967, *M.N.R.A.S.*, 137, 119.
  67. Lambert, D.L., Gustafsson, B., Erickson, K., and Hinkle, K.H., 1986, *Ap.J. Suppl.*, 62, 373.
  68. Iben, I., 1987, in Late Stages of Stellar Evolution, eds., S. Kwok and S.R. Pottasch, (Reidel, Dordrecht), p.175.
  69. Renzini, A., 1982, in Wolf Rayet Stars: Observations, Physics, Evolution, eds., C.W.H. de Loore and A.J. Willis, (Reidel, Dordrecht), p.413.
  70. Fadeyef, Y.A., 1986, in Hydrogen Deficient Stars and Related Objects, ed. K. Hunger, (Reidel, Dordrecht), p.441.
  71. Salpeter, E.E., 1974, *Ap. J.*, 193, 579.
  72. Tielens, A.G.G.M., 1983, *Ap.J.*, 271, 702.
  73. Betz, A., 1987, in Astrochemistry, eds., M.S. Vardya and S.P. Tarafdar, (Reidel, Dordrecht), p.327.
  74. Olofson, H., 1987, in Late Stages of Stellar Evolution, eds., S. Kwok and S.R. Pottasch, (Reidel, Dordrecht), p.149.
  75. Cernicharo, J., Guélin, M., Menten, K.M., and Walmsley, C.M., 1987, *Astr. Ap.*, 181, L1.
  76. Cernicharo, J., Guélin, M., Hein, H., and Kahane, C., 1987, *Astr. Ap.*, 181, L9.
  77. Tarafdar, S.P., 1987, in Astrochemistry, eds., M.S. Vardya and S.P. Tarafdar, (Reidel, Dordrecht), p.559.
  78. Gail, H.P., and Sedlmayr, E., 1987, in Physical Processes in Interstellar Clouds, eds. G.E. Morfill and M. Scholer, (Reidel, Dordrecht), p.275.
  79. Frenklach, M., elsewhere in this volume.
  80. Salpeter, E.E., 1977, *Ann. Rev. Astr. Ap.*, 15, 267.
  81. Grossman, L., and Larimer, J.W., 1974, *Rev. Geophys. Space Phys.*, 12, 71.
  82. Barshay, S.S. and Lewis, J.S., 1976, *Ann. Rev. Astr. Ap.*, 14, 81.
  83. Draine, B.T., 1986, in Interrelationships Among Circumstellar, Interstellar, and Interplanetary Dust, ed., J.A. Nuth and R.E. Stencel, NASA CP 2403, 19.
  84. Draine, B.T., 1979, *Astr. Space Sci.*, 65, 313.
  85. Donn, B. and Nuth, J., 1985, *Ap.J.*, 288, 187.
  86. Nuth, J., 1987, *Nature*, 329, 589.
  87. Donn, B., 1978 in Protostars and Planets, ed. T. Gehrels, (Univ. of Arizona Press, Tucson), p.100.
  88. Keller, R., 1987, in Polycyclic Aromatic Hydrocarbons and Astrophysics, eds., A. Leger, L.B. d'Hendecourt, and N. Bocarra, (Reidel, Dordrecht), p. 327.
  89. Hucknall, D.J., 1985, Chemistry of Hydrocarbon Combustion, (Chapman and Hall, New York).
  90. Barnard, J.A., and Bradley, J.N., 1985, Flame and Combustion, (Chapman and Hall, New York).
  91. Smyth, K.C., and Miller, J.H., 1987, *Science*, 236, 1540.
  92. Bussoletti, E., Colangeli, L., Borghesi, A., 1987, in Polycyclic Aromatic Hydrocarbons and Astrophysics, eds., A. Leger, L.B. d'Hendecourt, and N. Bocarra, (Reidel, Dordrecht), p. 63.
  93. Borghesi, A., Bussoletti, E., and Colangeli, L., 1985, *Astr. Ap.*, 142, 225.
  94. Koike, C., Hasegawa, H., and Manabe, A., 1980, *Ap. Space Sci.*, 67, 495.
  95. Palmer, H.B., and Cullis, C.F., 1965, in Chemistry and Physics of Carbon vol.1, ed., J. Walker, (Marcel Dekker, New York), p.265.
  96. Smalley, 1988, elsewhere in this volume.
  97. Kroto, H., 1988, elsewhere in this volume.

98. Homann, K.H., 1984, in Twentieth Symp. (Int.) on Combustion, 857.
99. Willson, L.A., and Hill, S.J., 1979, Ap.J., 228, 854.
100. Wood, P.R., 1979, Ap.J., 227, 220.
101. Willson, L.A., 1987, in Late Stages of Stellar Evolution, eds., S. Kwok and S.R. Pottasch, (Reidel, Dordrecht), p.253.
102. Bowen and Beach, 1987, in Late Stages of Stellar Evolution, eds., S. Kwok and S.R. Pottasch, (Reidel, Dordrecht), p.275.
103. Frenklach, M., Clary, D.W., Gardiner, W.C., and Stein, S.E., 1984, in Twentieth Symp. (Int.) on Combustion, 887.
104. Bockhorn, H., Fetting, F., and Wenz, H.W., 1983, Ber. Buns. Phys. Chem., 87, 1067.
105. Stein, S.E., 1978, J. Phys. Chem., 82, 566.
106. Kroto, H.W., Heath, J.R., O'Brien, S.C., Curl, R.F., and Smalley, R.E., 1985, Nature, 318, 162.
107. Crawford, M.K., Tielens, A.G.G.M., Allamandola, L.J., 1985, Ap.J. Letters, 293, L45.
108. Allamandola, L.J., Tielens, A.G.G.M., and Barker, J.R., in Physical Processes in Interstellar Clouds, eds. G.E. Morfill and M. Scholer, (Reidel, Dordrecht), p.305.
109. Goldreich, P., and Scoville, N., 1976, Ap.J., 205, 144.
110. Clegg, R.S., and Wootten, A., 1980, Ap. J., 240, 828.
111. Caloote, H.F., 1981, Comb. Flame, 42, 215.
112. Cohen, M., et al. 1988, in preparation.
113. Kerridge, J.F., elsewhere in this volume.
114. Woosley, S.E., Pinto, P.A., and Ensman, L., 1987, Ap. J., 324, 466.
115. Woosley, S.E., 1987, preprint.
116. Kirshner, R.P., 1987, IAU colloq. 108, in press.
117. Lattimer, J.M., Schramm, D.N., and Grossman, L., Ap. J., 219, 230.
118. Draine, B.T., and Salpeter, E.E., 1979, Ap.J., 231, 438.
119. Shull, J.M., 1978, Ap.J., 226, 858.
120. Seab, C.G., and Shull, J.M., 1983, Ap. J., 275, 652.
121. Seab, C.G., 1987, in Interstellar Processes, eds., D.J. Hollenbach and H.J. Thronson, (Reidel, Dordrecht), p.491; and elsewhere in this volume.
122. Routly, P.M., and Spitzer, L., 1952, Ap. J., 115, 227.
123. Cowie, L.L., 1978, Ap. J., 225, 887.
124. Lewis, R.S., Tang, M., Wacker, J.F., Anders, E., and Steel, E., 1987, Nature, 326, 160.
125. Tielens, A.G.G.M., Seab, C.G., Hollenbach, D.J., and McKee, C.F., 1987, Ap.J. Letters, 319, L109.
126. Rae, W.J., 1970, in High Velocity Impact Phenomena, ed. R. Kinslow, (Acad. Press, New York), p.214.
127. Tielens, A.G.G.M., McKee, C.F., Seab, C.G., and Hollenbach, D.J., 1988, in preparation.
128. Zel'dovich, Ya.B., and Raizer, Yu.P., 1966, Physics of Shock Waves and High Temperature Hydrodynamic Phenomena, vol 2, (Acad. Press, New York).
129. McKee, C.F., Hollenbach, D., Seab, C.G., and Tielens A.G.G.M., 1987, Ap. J., 318, 674.
130. De Carli, P.S., and Jamieson, 1961, Science, 133, 1821.
131. Alder, B.J., and Christian, R.H., 1961, Phys. Rev. Lett., 7, 367.
132. McQueen, R.G., and Marsh, S.P., 1968, in Behavior of Dense Media under High Dynamic Pressures, (Gordon and Breach, New York), p207.
133. Pavlovskii, M.N., Sov. Phys. Solid State, 13, 741.
134. Gust, W.H., and Young D.A., 1979, in High Pressure Science and Technology. vol I, eds. K.D. Timmerhaus and M.S. Barter, (Plenum Press, New York), p944.
135. De Carli, P.S., 1979, in High Pressure Science and Technology. vol I, eds. K.D. Timmerhaus and M.S. Barter, (Plenum Press, New York), p940.
136. Bundy, F.P., 1985, Solid State Physics under Pressure, ed., S. Minomura, (Terra Sci. Publ. Co.), p.1.
137. Gold, J.S., Bassett, W., Weathers, M.S., and Bird, J.M., 1984, Science, 225, 921.

138. Young, D.A. and Grover, R., 1988, preprint.
139. Yin, M.T., and Cohen, M.L., 1983, *Phys. Rev. Letters*, 50, 2006.
140. Whittaker, A.G., 1978, *Science*, 200, 763.
141. Whittaker, A.G., Watts, E.J., Lewis, R.S., and Anders, E., 1982, *Science*, 209, 1512.
142. Heimann, R.B., Kleiman, J., and Slansky, N.M., 1983, *Nature*, 306, 164.
143. Smith, P.P.K. and Buseck, P.R., 1982, *Science* 216, 984.
144. Shaner, J.W., Brown, J.M., Swenson, C.A., and McQueen, R.G., 1984, *J. Phys.*, C8, 235.
145. Bergmann, O.R., 1983, in Shock Waves in Condensed Matter, eds., J.R. Asay, R.A. Graham, and G.K. Straub, (Elsevier, Amsterdam), p.429.
146. Bundy, F.P., Strong, H.M., and Wentorf, R.H., 1973, in Chemistry and Physics of Carbon, 10, eds. P.L. Walker and P.A. Thrower, (M. Dekker, New York), p213.
147. Turro, N.J., 1978, Modern Molecular Photochemistry, (Benjamin/Cummins, Menlo Park).
148. Frank, F.C., 1952, *Proc. Roy. Soc. London, Ser. A*, 215, 43.
149. Bernal, J.D., 1960, *Nature*, 185, 68.
150. Anderson, J.F., 1975, Structure of Metallic Catalysts, (Acad. Press, New York).
151. Nelson, D.R., 1983, *Phys. Rev. B*, 28, 5515.
152. Galvin, G.J., Thompson, M.O., Mayer, J.W., Hammond, R.B., Poulter, N., Peercy, P.C., 1982, *Phys. Rev. Letters*, 48,33.
153. Berman, R., 1979, The Properties of Diamonds, ed. J.E. Field (Acad. Press, New York), p.3.
154. Dienes, J.K., and Walsh, J.M., 1970, in High Velocity Impact Phenomena, ed. R. Kinslow, (Acad. Press, New York), p46.
155. Trueb, L.F., 1968, *J. Appl. Phys.*, 39, 4707.
156. Blake, D., Freund, F., Krishnan, K., Echer, C., Sipp, R., Bunch, T., Tielens, A., Lipari, R.J., Hetherington, C. and Chang, S., 1988, *Nature* in press.
157. Griffith, A.A., 1920, *Phil. Trans. R. Soc.*, A221, 163.
158. Kendall, K., 1978, *Nature*, 272, 710.
159. Ruoff, A.L., 1979, 1979, in High Pressure Science and Technology, vol I, eds. K.D. Timmerhaus and M.S. Barter, (Plenum Press, New York), p.525..
160. Gigl, P.D., 1979, 1979, in High Pressure Science and Technology, vol I, eds. K.D. Timmerhaus and M.S. Barter, (Plenum Press, New York), p915.
161. Gault, D.E. and Wedekind, J.A., 1969, *J. GeoPhys. Res.*, 74, 6780.
162. Matsui, T., Waza, T., Kani, K., and Suzuki, S., 1982, *J. Geophys. Res.*, 87, B10,968.
163. Takagi, Y., Mizutani, H., and Kawakami, S., 1984, *Icarus*, 59, 462.
164. Bibby, D.M., 1982, in Chemistry and Physics of Carbon, 18, ed. P.A. Thrower, (Dekker, New York), p1.
165. Setaka, N., and Sekikawa, Y., 1981, *J. Mat. Sci.*, 16,1728.
166. Ree, F.H., Nellis, W.J., Trainor, R.J., Mitchell, A.C., and Boslough, M.B., 1983, in Shock Waves in Condensed Matter, eds., J.R. Asay, R.A. Graham, and G.K. Straub, (Elsevier, Amsterdam), p.42.
167. Wentorf, R.H., 1965, *J. Phys. Chem.*, 69, 3063.
168. Bundy, F.P., 1963, *J. Chem. Phys.*, 38, 618.
169. Appleton, B.R., and Celler, G.K., 1982, Laser and Electron Beam Interaction with Solids, (Elsevier, Amsterdam).
170. Landau, R., 1970, *Nature*, 226, 924.
171. Allamandola, L.J., 1987, in Polycyclic Aromatic Hydrocarbons and Astrophysics, eds. A. Leger, L.B. d'Hendecourt, and N. Bocarra, (Reidel, Dordrecht), p339.
172. Kerridge, J.F., and Chang, S., 1986, in Protostars and Planets II, eds. D.C. Black and M. Mathews, (Univ. Arizona Press, Tucson), p.738.
173. Maeder, A., 1983, *Astr. Ap.*, 120, 130.
174. Clayton, D.D., *Nature*, 257, 36.
175. Herold, A., in Intercalated Layered Materials, ed. F. Levy, (Reidel, Dordrecht), p. 321.
176. Renzini, A., 1984, in Stellar Nucleosynthesis, eds. C. Chiosi and A. Renzini, (Reidel Dordrecht), p.99.

177. Clayton, D.D., 1981, Proc. Lun. Plan. Sci. Conf., 12B, 1781.
178. Watson, W.D., 1976, in Atomic and Molecular Physics and the Interstellar Matter, eds. R. Balian, P. Encrenaz, and J. Lequeux, (Elsevier, Amsterdam), p.177.
179. Tielens, A.G.G.M., 1983, Astron. Astr., 119, 177.
180. Geiss, J., and Reeves, H. 1981, Astron. Astr., 93,189.
181. Allamandola, L.J., Tielens, A.G.G.M., and Barker, J.B., 1988, in preparation.
182. d'Hendecourt, L.B., Allamandola, L.J., Grim, R.J.A., and Greenberg J.M., 1986, Astron. Astr., 158, 119.
183. Agarwal,V.K., Schutte, W., Greenberg, J.M., Ferris, J.P., Briggs, R., Connor, S., van de Bult, C.E.P.M., and Baas, F., 1985, Origins of Life, 16, 21.

## INTERSTELLAR GRAIN CHEMISTRY AND ORGANIC MOLECULES

L. J. Allamandola and S. A. Sandford,  
NASA-Ames Research Center, Moffett Field, CA 94035

### ABSTRACT

The detection of prominent infrared absorption bands at 3250, 2170, 2138, 1670 and 1470  $\text{cm}^{-1}$  (3.08, 4.61, 4.677, 5.99 and 6.80  $\mu\text{m}$ ) associated with molecular clouds shows that mixed molecular ("icy") grain mantles are an important component of the interstellar dust in the dense interstellar medium. These ices, which contain many organic molecules, may also be the production site of the more complex organic grain mantles detected in the diffuse interstellar medium.

Theoretical calculations employing gas phase as well as grain surface reactions predict that the ices should be dominated only by the simple molecules  $\text{H}_2\text{O}$ ,  $\text{H}_2\text{CO}$ ,  $\text{N}_2$ ,  $\text{CO}$ ,  $\text{O}_2$ ,  $\text{NH}_3$ ,  $\text{CH}_4$ , possibly  $\text{CH}_3\text{OH}$ , and their deuterated counterparts. However, spectroscopic observations in the 2500-1250  $\text{cm}^{-1}$  (4-8  $\mu\text{m}$ ) range show substantial variation from source to source, implying a far richer chemistry than expected from surface reactions alone. By comparing these astronomical spectra with the spectra of laboratory-produced analogs of interstellar ices, one can determine the composition and abundance of the materials frozen on the grains in dense clouds.

The 2170  $\text{cm}^{-1}$  (4.61  $\mu\text{m}$ ) band is attributed to the CN stretching vibration in an unidentified grain constituent designated X(CN), while the 2138  $\text{cm}^{-1}$  (4.677  $\mu\text{m}$ ) band is attributed to solid CO. Comparison of the CO band with laboratory data shows that there are two distinct chemical regimes in clouds, one dominated by atomic hydrogen, the other by molecular hydrogen.

The 1670  $\text{cm}^{-1}$  (5.99  $\mu\text{m}$ ) feature is assigned primarily to the HOH bending mode in  $\text{H}_2\text{O}$ , in line with the identification of the 3250  $\text{cm}^{-1}$  (3.08  $\mu\text{m}$ ) band as the OH stretching mode. Source-to-source variation on the high frequency side of this band is quite likely due to the C=O stretch in organic species such as ketones, aldehydes, esters, and carboxylic acids. The 1470  $\text{cm}^{-1}$  band is largely due to the CH deformation modes, possibly in alcohols. The source-to-source variations in this band are probably due to differences in the amounts of unsaturated hydrocarbons, or saturated hydrocarbons which contain strongly electro-

negative groups, in different clouds. These variations suggest that energetic processing, such as by ultraviolet photolysis and cosmic ray bombardment, is important in determining the grain mantle composition.

In addition to reviewing the above, experiments are described in which the chemical evolution of an interstellar ice analog is determined during irradiation and subsequent warm-up. Particular attention is paid to the types of moderately complex organic materials produced during these experiments which are likely to be present in interstellar grains and cometary ices.

## I. INTRODUCTION: CARBON AND ICY GRAIN MANTLES IN DENSE MOLECULAR CLOUDS

Dense interstellar clouds are comprised of gas and dust. The gas is a mixture of many different atoms, ions, radicals, and molecules. (see Irvine et al., 1985, and references therein). Interspersed with the gas, at lower abundance, are small, cold ( $\sim 10$  K) dust particles. The refractory component of these grains is thought to consist of silicates and amorphous carbon.

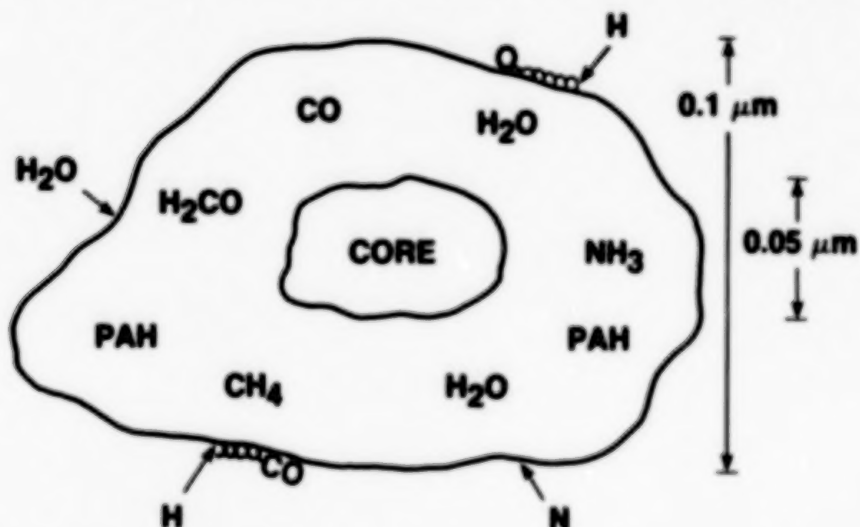
Because the grains are cold, most gaseous species (except H and  $H_2$ ) striking the grains will stick, forming a mixed molecular ice mantle (see Greenberg, 1977, and references therein). The accreting species include atoms and radicals as well as molecules. At this point in our understanding of chemistry in clouds, two general types of molecular mantle are envisioned. One type is comprised largely of relatively simple species. The other consists of a chemically more complex mixture (Figure 1).

The simpler mantles are produced during the accretion of gas phase components. Chemical reactions, which are not possible in the gas phase, can occur between neighboring reactive components on grain surfaces during accretion. Consequently, the mantle will not simply reflect the gas phase composition, but can also contain other species. Since atomic H is very abundant during a significant fraction of a cloud's lifetime, atoms on the surface such as C, N, or O will quickly become hydrogenated and produce species such as  $CH_4$ ,  $NH_3$ , and  $H_2O$ . Polar molecules such as  $H_2O$  and  $NH_3$  will certainly remain on the surface and the mantle will become enriched in them. Non-polar molecules such as  $CH_4$  may or may not stick upon formation. The first attempts to integrate gas and grain chemistry into a single model predicted that grain mantles produced in this way should fall into two categories depending on the  $H/H_2$  ratio (Tielens and Hagen, 1982; d'Hendecourt, Allamandola, and Greenberg, 1985). If the  $H/H_2$  ratio is large, reactions with H atoms are important and simple hydrides dominate the ice. If, on the other hand, it is substantially less than one, reactions involving species such as O and N become important and form molecules such as  $O_2$  and  $N_2$ . Thus, two qualitatively different categories of mantle may be produced by grain surface reactions, one characterized by polar, H-bonded molecules and the other characterized by non-polar or only slightly polar, highly unsaturated molecules. Recently, more sophisticated models have been developed which examine the effects of additional surface reactions (Williams, 1987, 1988). Millar (1988) and Brown (1988), describe some of the more recent results using these models and show that slightly more complex species than simple hydrides, diatomics and triatomics can be produced by surface reactions.

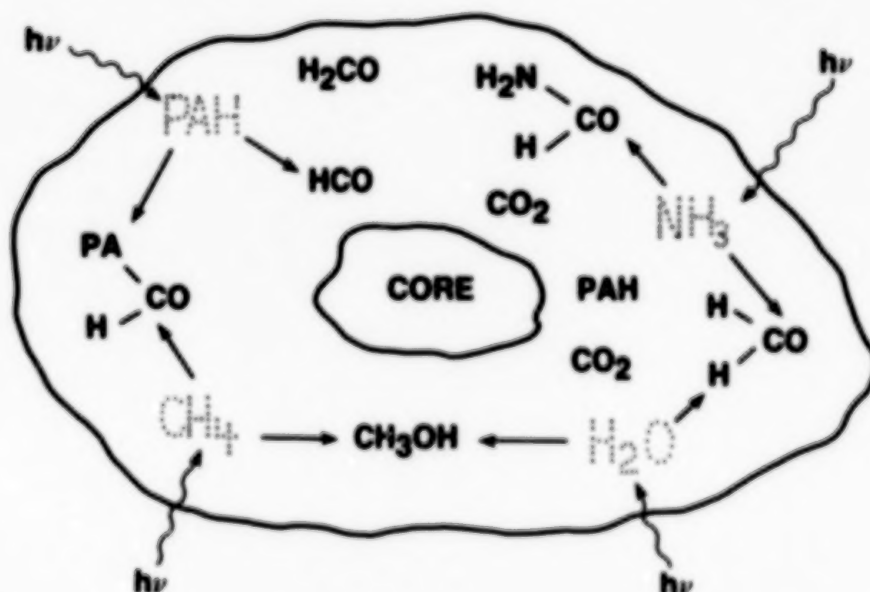
Significantly more complex ice mantles should be produced by energetic processing with ultraviolet radiation and cosmic rays. In 1976 Greenberg suggested that the ultraviolet irradiation of grains in dense clouds would produce chemically complex molecules within ice

mantles. The photoproducts of irradiation span a broad range in number and complexity, starting with molecules as "simple" as  $\text{CO}_2$  and  $\text{H}_2\text{CO}$ , and extending to large, poorly characterized species. As an example of the complexity in number, the many reaction pathways involving CO and the simple photoproducts of an ice made of  $\text{H}_2\text{O}$ ,  $\text{CH}_4$ , and  $\text{NH}_3$  is shown in Figure 2.

### GRAIN SURFACE REACTIONS PRODUCE SIMPLE MOLECULES



### UV IRRADIATION PRODUCES COMPLEX MOLECULES



**WITHOUT SOME FORM OF ENERGETIC PROCESSING, MANTLES  
WILL BE MADE UP PRIMARILY OF SIMPLE MOLECULES**

Fig. 1. Grain mantle growth and evolution.

Thanks to the development of powerful infrared observational tools and the persistence of infrared astronomers, high quality infrared spectra are available for a small number of sources in dense clouds. These spectra have revealed more about the composition of dust in molecular clouds than all of the previous observations combined because the infrared spectrum of a substance gives more information about its structure than any of its other properties (Figure 3). As discussed in the following sections, these spectra, interpreted in the light of laboratory analog experiments, are now beginning to provide compelling evidence for a broad range of organic molecules in grain mantles.

Sections II and III, which discuss ice analog production and the comparison of laboratory spectra with interstellar spectra, have been largely reproduced from Sandford and Allamandola, 1988. Sections IV and V discuss the photochemical and thermal evolution of ice analogs and astrophysical implications and are largely reproduced from Allamandola, Sandford and Valero, 1988.



Fig. 2. Possible reaction pathways involving CO in an interstellar grain mantle illustrating how the intermediates H, OH,  $\text{CH}_3$ , and  $\text{NH}_2$  can add to CO and produce a very rich chemical mixture.

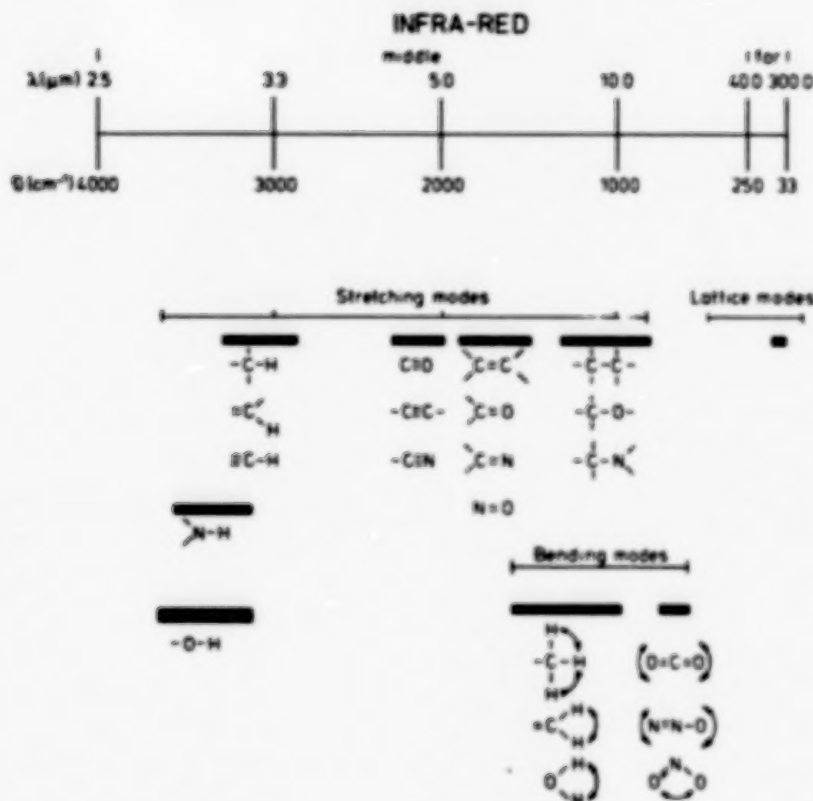


Fig. 3. Vibrational frequency ranges of various molecular groups.

## II. INTERSTELLAR ICE ANALOG PRODUCTION

Mid-infrared absorption spectroscopy of ices in dense interstellar clouds generally depends on the presence of embedded or background radiation sources (Figure 4). Radiation from the source heats the immediately surrounding dust. This hot dust emits an infrared pseudo-blackbody continuum like that shown in the inset close to the protostar in Figure 4. As this radiation passes through the cloud, molecules along the line-of-sight absorb at their fundamental frequencies. This produces a spectrum which has absorption features diagnostic of the material along the line of sight (lower inset in Figure 4). Ice features generally dominate this type of absorption spectrum. The key features shown in Figure 4 (infrared source, absorbing material, and detection) must be mimicked in laboratory studies of ice analogs. The specific conditions within the cloud which must be duplicated to create interstellar ice analogs vary widely. Composition, temperature, and exposure to radiation can be duplicated reasonably well in the laboratory.

The general laboratory procedure consists of slowly flowing the gas from which the ice is made into a high-vacuum chamber. This gas, which can be a pure substance or a mixture of substances, is directed to and

## MOLECULAR CLOUD WITH COLD (10K) DUST

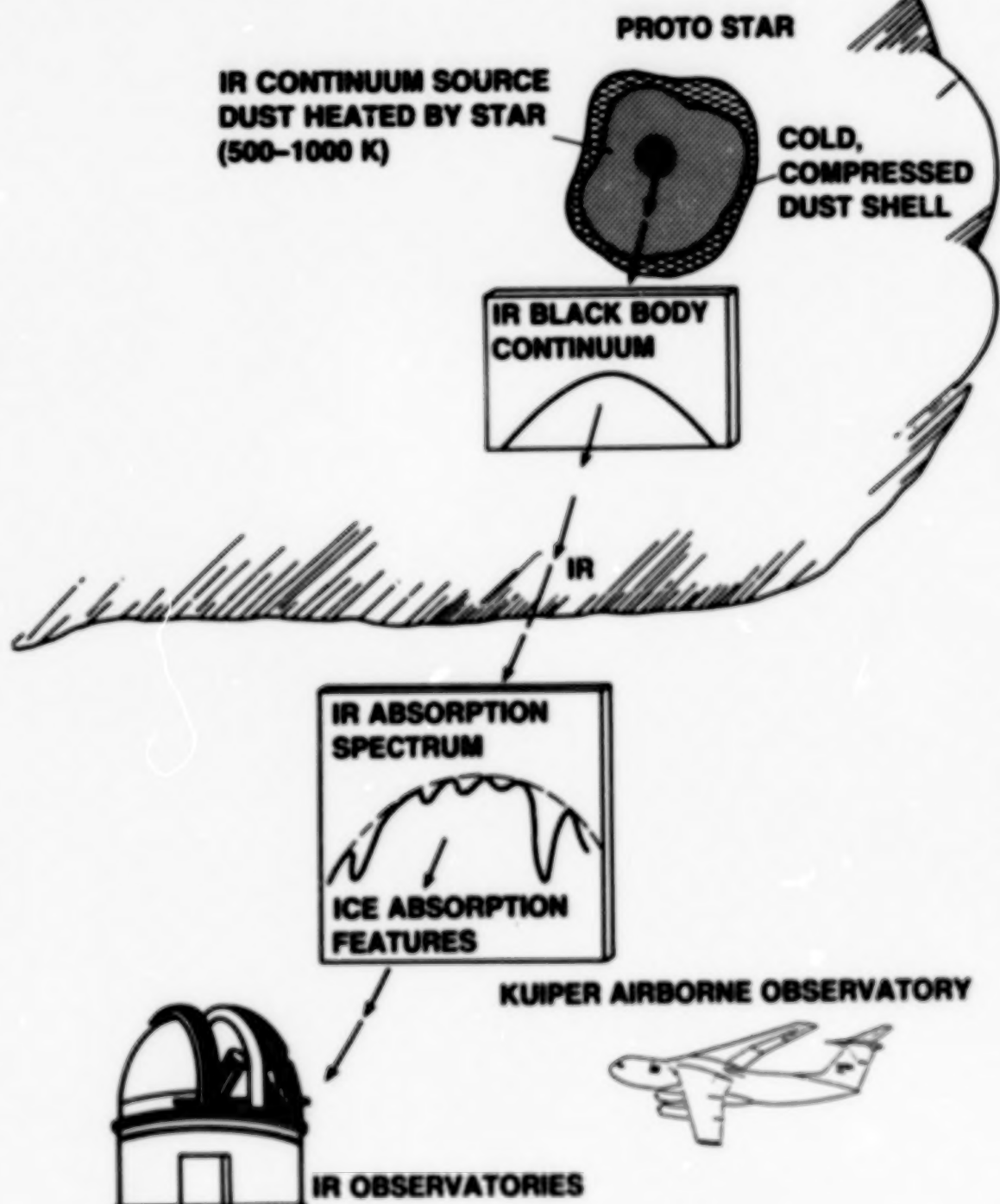


Fig. 4. Schematic illustration of how one obtains absorption spectra of interstellar ices.

condenses on the surface of a substrate cooled by a closed-cycle helium refrigerator or by a cryogen such as liquid helium. A schematic drawing of a typical sample chamber in various configurations is shown in Figure 5 and a photograph of the apparatus at Ames is given in Figure 6. Substrate temperature can generally be maintained anywhere from 10 K (4 K with liquid helium) to room temperature. The substrate is interchangeable. For infrared studies it is generally a cesium iodide window. The substrate is rotatable and is suspended in the center of a sample chamber with gas inlet tubes and several larger ports. The larger openings can be fitted with windows, lamps, ion sources, ovens, pressure gauges, mass spectrometers, phototubes, etc., depending upon the particular properties under study. Generally, the substrate is initially positioned to face the gas inlet tube for the preparation of the ice and then rotated to face the other ports as needed. Radiation processing of the sample can be carried out with ultraviolet lamps or ion sources. Subsequently, the evaporation characteristics of the ice can be studied by measuring spectra during warm-up of the substrate.

The column density of an individual component or molecular subgroup in an interstellar ice can only be determined for species in which the integrated absorbance,  $A$ , has been measured in the appropriate solid. The column density of any solid state species can be estimated by

$$N = \frac{\tau \Delta\nu_{1/2}}{A} \quad (1)$$

where  $\tau$  is the optical depth of the band at maximum absorbance,  $\Delta\nu_{1/2}$  is the full-width-at-half-maximum in  $\text{cm}^{-1}$ , and  $A$  is the integrated absorbance in  $\text{cm molecule}^{-1}$ . The integrated absorbances for the vibrational transitions of a number of astrophysically interesting materials are listed in Table 1.

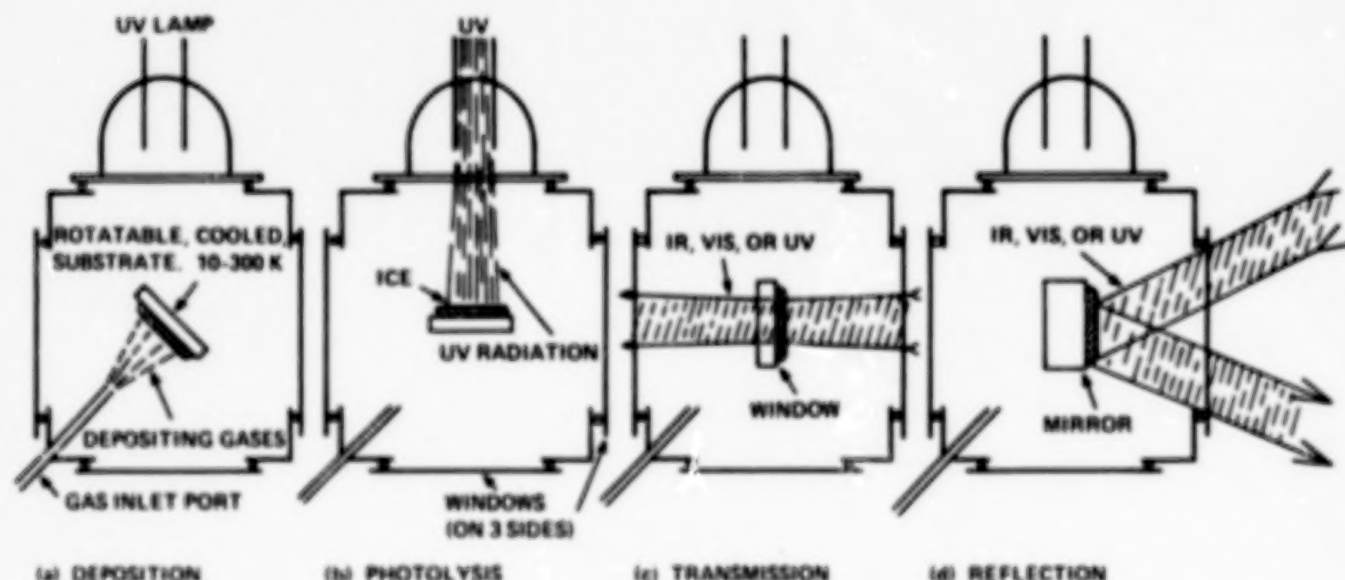


Fig. 5. Common configurations of a low temperature ice sample chamber.

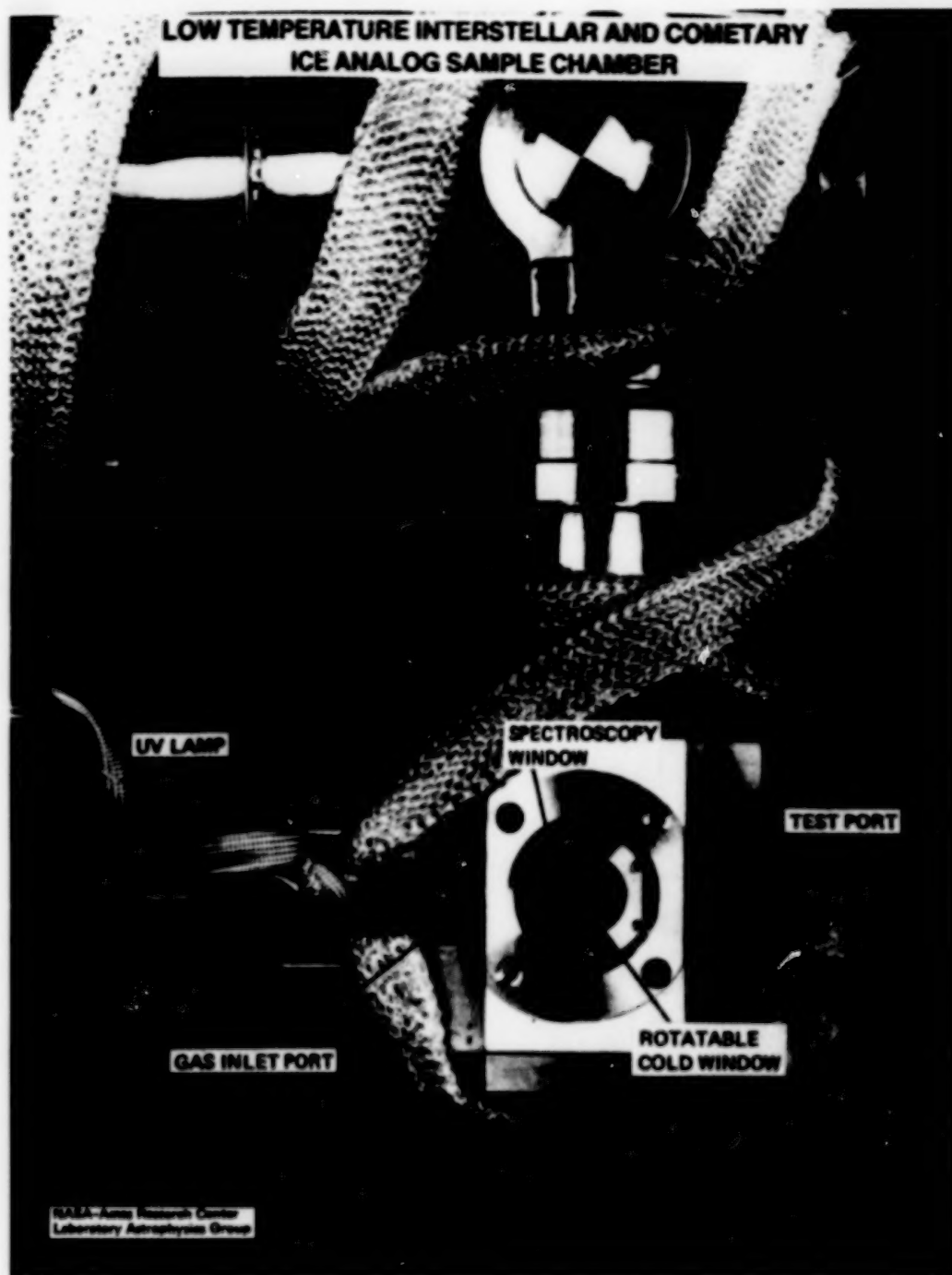


Fig. 6. Photograph of an Ice Analog sample chamber at NASA Ames Research Center. The base is approximately 10 cm on a side and the cold window is about 2 cm in diameter.

Table 1. Absorbance Values for Molecules in the Solid State

Molecule	Mode	Frequency ( $\text{cm}^{-1}$ )	$\lambda$ ( $\mu\text{m}$ )	A ( $\text{cm}/\text{molecule}$ )
$\text{H}_2\text{O}^{\text{a}}$	OH-stretch	3275	3.053	$2 \times 10^{-16}$
	OH-bend	1670	5.988	$8 \times 10^{-18}$
	libration	750	13.33	$3 \times 10^{-17}$
CO	stretch in $\text{CO}^{\text{b}}$	2139	4.675	$1 \times 10^{-17}$
	stretch in $\text{H}_2\text{O}^{\text{c}}$	2137	4.680	$2 \times 10^{-17}$
$\text{CO}_2^{\text{c}}$	CO-stretch	2342	4.270	$2 \times 10^{-16}$
	CO-bend	653	15.31	$4 \times 10^{-17}$
$\text{CH}_4^{\text{d}}$	CH-stretch	3010	3.322	$6 \times 10^{-18}$
	CH-deformation	1300	7.692	$6 \times 10^{-18}$
$\text{NH}_3^{\text{d}}$	NH-stretch	3375	2.963	$1 \times 10^{-17}$
	umbrella mode	1070	9.346	$2 \times 10^{-17}$
$\text{CH}_3\text{OH}^{\text{d}}$	OH-stretch	3250	3.077	$1 \times 10^{-16}$
	CH-stretch	2982	3.354	$2 \times 10^{-17}$
	CH-stretch	2828	3.536	$8 \times 10^{-18}$
	CH-deform. \	"1450"	6.897	$1 \times 10^{-17}$
	and OH-bend /			
	CO-stretch	1026	9.747	$2 \times 10^{-17}$
$\text{CH}_3(\text{CH}_2)_4\text{CH}_3^{\text{d}}$	CH-stretch <sup>e</sup>	2955	3.384	$1 \times 10^{-17}$
		2870	3.484	$2 \times 10^{-18}$
	CH-stretch <sup>f</sup>	2921	3.424	$5 \times 10^{-18}$
		2858	3.499	$1 \times 10^{-18}$
	CH-sciss. \	"1465"	6.826	$1 \times 10^{-18}$
	and deform. <sup>g</sup> /			
	$\text{CH}_3$ -deform.	1370	7.299	$2 \times 10^{-19}$
$\text{CH}_3\text{CN}^{\text{d}}$	CN-stretch	2270	4.405	$2 \times 10^{-18}$
$\text{C}_4\text{H}_8\text{O}_2^{\text{d}}$	C=O stretch	1738	5.754	$4 \times 10^{-17}$
	CH stretch <sup>e</sup>	2986	3.349	$2 \times 10^{-18}$
	$\text{CH}_2$ deform. <sup>f</sup>	1450	6.897	$8 \times 10^{-18}$
	$\text{CH}_3$ deform. <sup>e</sup>	1375	7.273	$4 \times 10^{-18}$

a) Hagen, Tielens, and Greenberg (1981, 1983); b) Jiang, Person, and Brown (1975); c) Sandford et al. (1988); d) d'Hendecourt and Allamandola (1986); e) per  $-\text{CH}_3$  group; f) per  $-\text{CH}_2-$  group; g) per  $-\text{CH}_3$  and  $-\text{CH}_2-$ .

**Note:** Integrated absorbance values often depend on neighboring groups and solid-state interactions. See original references for detailed discussion of each absorbance value and range of applicability.

The infrared transmission spectrum through a sample of known thickness is measured when optical constants ( $n$  and  $k$ ) or integrated absorbance values ( $A$ ) are to be determined. Sample thickness is determined by monitoring the temporal development of the thin film interference pattern of a He-Ne laser beam reflected off or transmitted through the sample during deposition. The infrared spectrum is measured and plotted as  $\log \{I_0(\nu)/I(\nu)\}$  versus frequency ( $\text{cm}^{-1}$ ), where  $I_0(\nu)$  is the single beam spectrum measured through the substrate before sample deposition and  $I(\nu)$  the spectrum measured after deposition. For a description of the technique and its application to astrophysics as well as a discussion of how to derive  $n$  and  $k$  values and  $A$  values, see Hagen, Tielens, and Greenberg (1981) and d'Hendecourt and Allamandola (1986), respectively.

One can generally ignore the effects of scattering in the analysis of interstellar infrared absorption spectra because throughout most of the mid-infrared the wavelength is significantly greater than the diameter of the dust grains. In this "Rayleigh limit" the pure absorption term dominates. Scattering becomes important at shorter wavelengths and, under certain conditions, may contribute to the profile of the  $3250 \text{ cm}^{-1}$  ( $3.08 \text{ }\mu\text{m}$ )  $\text{H}_2\text{O}$  ice band (cf. Allamandola, 1984, and references therein).

### III. COMPARISON OF INTERSTELLAR SPECTRA WITH THE SPECTRA OF ICE ANALOGS

In this section interstellar spectra will be directly compared with ice analog spectra. Figure 7 shows one of the earliest direct comparisons of the entire mid-infrared spectrum of an interstellar protostar with the spectrum of a laboratory analog. W33 A is an intense infrared source deeply embedded in a molecular cloud. Estimates of the value of  $A_V$  range from 50 to over 100 magnitudes (Capps, Gillett, and Knacke, 1978; Willner et al., 1980). The principle features in both spectra agree reasonably well except in the region around  $10 \text{ }\mu\text{m}$  where the SiO absorption due to silicates dominates the interstellar spectrum. In the interstellar case, the ice features near  $10 \text{ }\mu\text{m}$  are presumably so badly blended with the silicate band that they are indiscernable. Carefully measuring the spectral profile of the silicate feature in objects with deep ice bands may reveal some discrepancies with pure silicate profiles (Day, 1979; Knacke and Krätschmer, 1980; Koike et al., 1981). A search for such substructure would be particularly helpful in constraining some of the ice band identifications.

The ice bands will each be discussed in turn, starting with those near  $2140 \text{ cm}^{-1}$  ( $4.67 \text{ }\mu\text{m}$ ). Extensive discussion of the  $3250 \text{ cm}^{-1}$  ( $3.10 \text{ }\mu\text{m}$ )  $\text{H}_2\text{O}$  band can be found elsewhere (Hagen, Tielens, and Greenberg, 1981; Leger et al., 1983) and it will not be treated further here. We restrict this discussion to the spectroscopic aspects of the comparisons between interstellar and laboratory spectra. See Whittet (1988), for a more general description of the astrophysical implications. A detailed

spectroscopic discussion of many of the bands can be found in Tielens and Allamandola (1987).

The 2500-2000  $\text{cm}^{-1}$  (4-5  $\mu\text{m}$ ) Region:

Infrared spectroscopy in the 2500-2000  $\text{cm}^{-1}$  (4-5  $\mu\text{m}$ ) region is a particularly important diagnostic of organic molecules in the interstellar medium because it probes the  $\text{C=O}$ ,  $\text{C=C}$ , and  $\text{C}\equiv\text{N}$  triple-bond

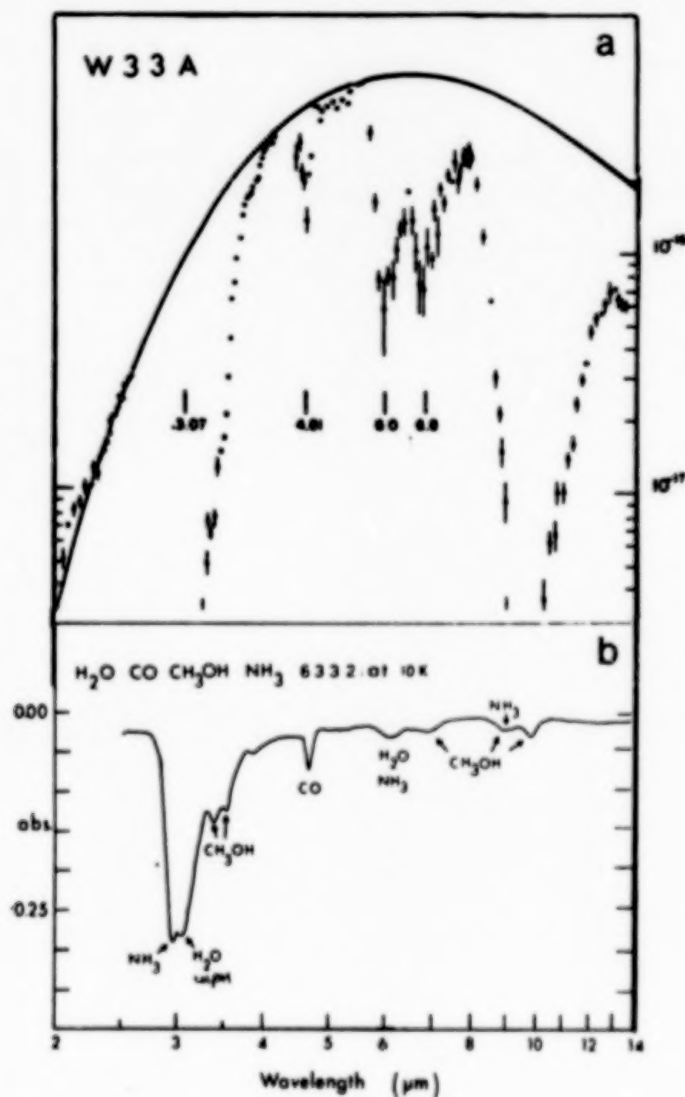


Fig. 7. Comparison of the entire mid-infrared spectrum from W33 A with the spectrum of a laboratory analog. The W33 A spectrum is reproduced from Willner et al. (1980) and the laboratory spectrum from Hagen, Allamandola, and Greenberg (1979).

stretching modes of most molecules (see Figure 3). In interstellar spectra this region is often dominated by a feature near  $2138\text{ cm}^{-1}$  ( $4.667\text{ }\mu\text{m}$ ). In several objects there is also an additional band at  $2165\text{ cm}^{-1}$  ( $4.619\text{ }\mu\text{m}$ ). The narrow band near  $2138\text{ cm}^{-1}$  is due to solid state CO, while the broader feature at  $2165\text{ cm}^{-1}$  has been attributed to the CN stretching vibration in an unknown molecule designated X(CN) (Lacy et al., 1984). These two features will be treated separately in the discussion that follows.

Of the 27 objects for which published spectra are available in this region, 16 show a band attributable to frozen CO. The spectral properties of the interstellar solid CO band and derived column densities are listed in Table 2. The width of the interstellar CO band implies that it is present in mixed molecular icy grain mantles (Allamandola, 1984). The position, profile, and cross-section of the CO fundamental for CO in mixed ices depends sensitively on the nature of the ice (Sandford et al., 1988). Figure 8 shows the large spectral variation this band exhibits when the CO is suspended in different solids. The crosshatched areas in the figure indicate the position and full-width-at-half-height (FWHH) of the interstellar CO and X(CN) features. In some sources the CO band seems to consist of a strong, narrow component ( $5\text{ cm}^{-1}$  FWHH) peaking at about  $2140\text{ cm}^{-1}$  ( $4.673\text{ }\mu\text{m}$ ) and a broader component ( $\sim 10\text{ cm}^{-1}$  FWHH) which peaks at about  $2135\text{ cm}^{-1}$  ( $4.684\text{ }\mu\text{m}$ ) (Lacy et al., 1984). Comparison of the interstellar spectra with the laboratory spectra shows that the broader  $2135\text{ cm}^{-1}$  band in most objects is probably due to CO frozen in an  $\text{H}_2\text{O}$ -rich mantle with an  $\text{H}_2\text{O}/\text{CO}$  ratio in the 5-20 range. The narrower band at  $2140\text{ cm}^{-1}$  cannot be matched with laboratory spectra of CO intimately mixed with  $\text{H}_2\text{O}$  or any other polar mantle species likely to be important in a molecular cloud. The peak position and width of the narrower band can, however, be matched by CO frozen in a  $\text{CO}_2$ -rich ice (Sandford et al., 1988). NGC 7538 provides a good example (Figure 9). This is an extremely important result as it provides the first evidence that there are ice mantles which are not dominated by  $\text{H}_2\text{O}$  or other hydrogenated polar species, but rather by non-polar or only slightly polar, non-hydrogenated species. These are precisely the sort of mantles which were predicted to be present in cloud regions where the  $\text{H}/\text{H}_2$  ratio is substantially less than one (Tielens and Hagen, 1982; d'Hendecourt, Allamandola and Greenberg, 1985).

NGC 7538 is also unique in that the optical depth of the CO feature is exceedingly high. Other objects similar to NGC 7538 may have recently been found. Eiroa and Hodapp (1988), report a source in which the solid state CO band optical depth exceeds that of the  $3250\text{ cm}^{-1}$  ( $3.07\text{ }\mu\text{m}$ ) O-H stretch band in  $\text{H}_2\text{O}$ . Preliminary analysis indicates that the CO peak position in this object is also close to  $2140\text{ cm}^{-1}$  ( $4.673\text{ }\mu\text{m}$ ), again indicating the dominance of non-polar mantles.

It is important to realize that being able to determine the peak position to an accuracy of about  $0.2\text{ cm}^{-1}$  at a frequency of  $2140\text{ cm}^{-1}$  implies that an observational resolution of 1 part in  $10^4$  is required to fully extract the information carried by this band. No other

Table 2. Solid State CO Towards Embedded Objects (from Sandford et al. 1988)

Source Name	Peak Pos. (cm <sup>-1</sup> )	Optical Depth ( $\tau$ )	FWHM (cm <sup>-1</sup> )	N(CO)-solid $\times 10^{17}$ (cm <sup>-2</sup> )	Ref.
W33 A					
Narrow	2139.1 <sup>d</sup>	0.56	(5)( $\tau/2$ )	3.0	a
Broad	2134.8	0.58	(12)( $\tau/2$ )	4.4	a
NGC 7538/IRS9					
Narrow	2139.9 <sup>d</sup>	2.09	5.0 ( $\tau/2$ )	11.0	a
Broad	2134.9	0.46	(12)( $\tau/2$ )	3.5	a
NGC 7538/IRS1	2139.9 <sup>d</sup>	0.24	3.5 ( $\tau/2$ )	0.76	a
W3/IRS 5	2140 <sup>d</sup>	0.20	4.6 ( $\tau/2$ )	0.83	a
Elias 1	2135 $\pm$ 2	0.10	-10-20 ( $\tau/2$ )	0.9	b
Elias 7	2135 $\pm$ 2	0.13	-12 ( $\tau/2$ )	0.9	b
Elias 13	2136 $\pm$ 2	0.22	-10 ( $\tau/2$ )	1.3	b
Elias 16	2141 $\pm$ 2 <sup>d</sup>	0.96	-5 ( $\tau/2$ )	4.5	b
Elias 18	2140 $\pm$ 2 <sup>e</sup>	0.35	-11 ( $\tau/2$ )	2.9	b
GL 2136	2137 $\pm$ 2	0.15	-7	0.62	c
OMC-2/IRS3	2137 $\pm$ 2	0.10	-10	0.59	c
GL 490	2140 $\pm$ 2	0.15	-5	0.68	c
NGC 2024/IRS2	2137 $\pm$ 2	0.35	7	1.4	c
GL 961	2137 $\pm$ 2	0.30	11	1.9	c
GL 989	2137 $\pm$ 2	0.35	9	1.9	c
Mon R2/IRS2	2137 $\pm$ 2	0.30	9	1.6	c

a) Lacy et al. (1984)

b) Whittet, Longmore, and McFadzean (1985)

c) Geballe (1986)

d) For these features,  $A = 1.0 \times 10^{-17}$  cm/molecule for pure CO was used rather than  $A = 1.7 \times 10^{-17}$  cm/molecule, the value for CO in water ice.

e) The profile of this feature indicate that it is comprised of comparable amounts of the broad and narrow solid CO bands. N(CO) was determined by arbitrarily assuming that half the band area was due to the narrow component and half to the broad component.

interstellar ice feature we are presently aware of requires such resolution for analysis. In most cases 1 part in  $10^3$  is sufficient. The unique combination of the ability to measure the interstellar CO feature with such precision, in conjunction with the high sensitivity of the solid state CO band position and profile to the nature of the solid, provides far more insight into the nature of the cloud (solid state properties as well as gas phase chemistry) than even the most optimistic analog aficionados anticipated a few years ago.

While the observed CO band profiles can be explained by simple accretion and grain surface chemistry, the X(CN) band at  $2165\text{ cm}^{-1}$  ( $4.619\text{ }\mu\text{m}$ ) indicates that processing by radiation also occurs. Laboratory studies carried out by van de Bult in 1982 and 1983 (Leiden University, unpublished results) showed conclusively that the  $2165\text{ cm}^{-1}$  feature could be produced in ices comprised of species expected on the basis of accretion only if they were irradiated and if they contain

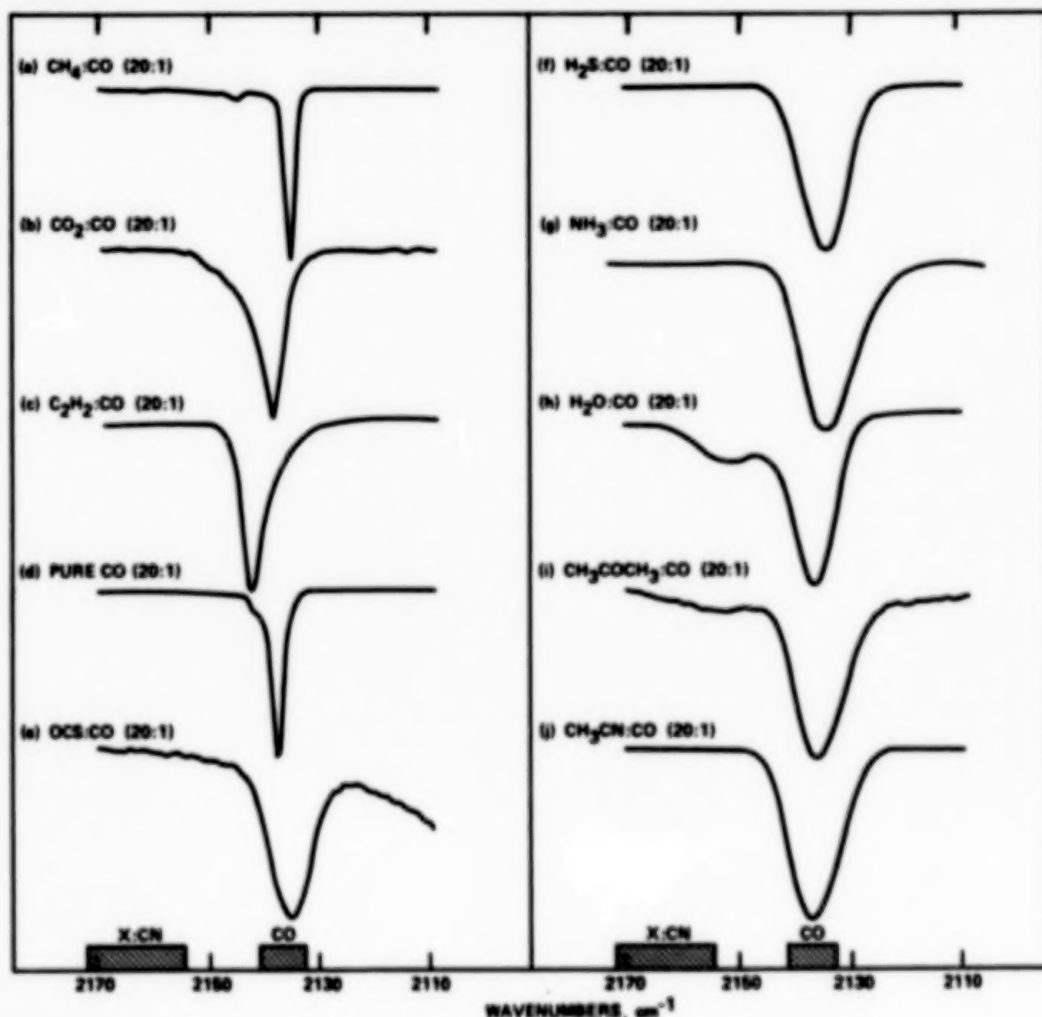


Fig. 8. The CO absorption band for CO suspended in various ices at 10 K. Figure adapted from Sandford et al. (1988).

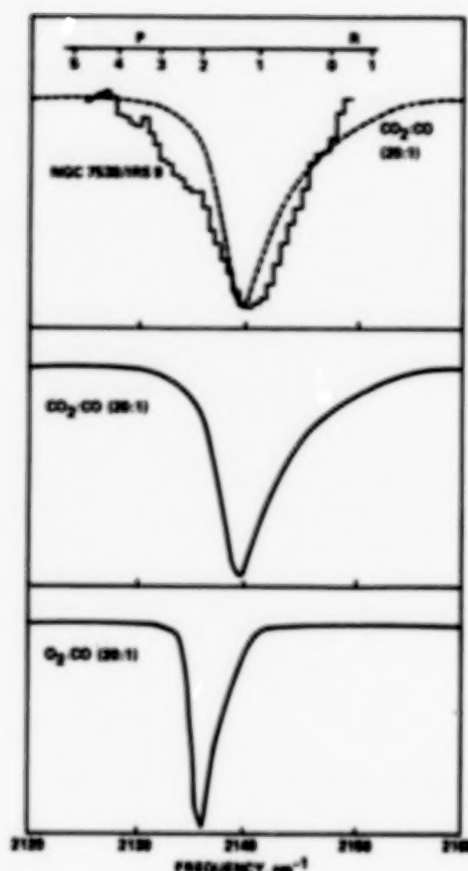


Fig. 9. The solid CO absorption feature in NGC 7538/IRS 9 compared to the bands produced when CO is suspended in solid CO<sub>2</sub> (middle) and O<sub>2</sub> (bottom) at 10 K. Figure adapted from Sandford et al. (1988)

sources of C and N atoms which can be freed from their parent species by energetic processes. Several of these experiments are described in Lacy et al. (1984). Further photochemical studies regarding this band are described in d'Hendecourt et al. (1986) and Grim and Greenberg (1987). This band is also produced in ices bombarded by ions (Moore et al., 1983). Figure 10 shows a comparison of the spectrum of W33 A with the laboratory spectrum of an irradiated ice which had been warmed to eliminate most of the more volatile CO. The X(CN) feature at 2165 cm<sup>-1</sup> provides a good fit to the astronomical data and was originally thought to be due to a nitrile or isonitrile. Recently, however, it has also been suggested that the band is produced by the CN stretch of the OCN<sup>-</sup> ion (Grim and Greenberg, 1987). The ion assignment must be tested further in the laboratory. Until it is, the exact identification of this band remains somewhat uncertain. In any event, it appears that the source of the interstellar 2165 cm<sup>-1</sup> band contains a CN bond and is produced by the energetic processing of pre-existing ice mantles.

In addition to the 2140 and 2165 cm<sup>-1</sup> features, the spectrum of W33 A also shows two weak bands at 2525 and 2043 cm<sup>-1</sup> (3.960 and 4.895 μm) which are thought to be associated with the ice mantles (Geballe et al., 1985; Larson et al., 1985). The former band has been attributed to H<sub>2</sub>S. Candi-

dates proposed for the identification of the latter band include a sulfur-containing compound like OCS (Geballe et al., 1985), methanol (CH<sub>3</sub>OH), and the radicals C<sub>3</sub> and CN (Larson et al., 1985).

#### The 2000-1250 cm<sup>-1</sup> (5-8 μm) Region:

Infrared spectroscopy in the 2000-1250 cm<sup>-1</sup> (5-8 μm) region is important because it probes the C-H, N-H, and O-H bending and deformation modes as well as the C=O, C=C, and C=N double-bond stretching modes of most molecules. It is the only part of the spectrum where the types of molecule which contain carbonyl groups (C=O) can be

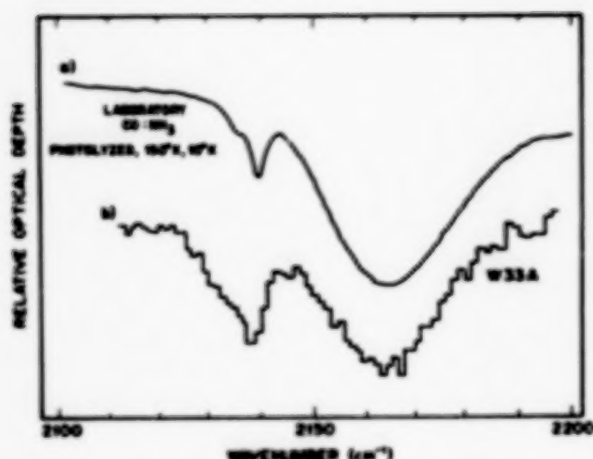


Fig. 10. The laboratory spectrum in the 2100-2200  $\text{cm}^{-1}$  (4.5-4.8  $\mu\text{m}$ ) region of an  $\text{NH}_3/\text{CO}$  ice which has been photolyzed and warmed up to 150 K compared to the spectrum of W 33A. Figure adapted from Lacy et al. (1984).

classified. The importance of this spectral region is amplified in the interstellar case because strong, broad absorption features in the 3 and 10  $\mu\text{m}$  regions, due to the O-H stretch in  $\text{H}_2\text{O}$  and the Si-O stretch in silicates, respectively, considerably hamper the detection of other absorption features. The discussion in this section relies heavily on the previous review by Tielens and Allamandola (1987).

Figure 11 shows a number of 2000-1250  $\text{cm}^{-1}$  (5-8  $\mu\text{m}$ ) spectra of embedded protostars taken using the Kuiper Airborne Observatory (Tielens and Allamandola, 1987; Tielens et al., 1988). All the spectra show prominent absorption features peaking around 1670 and 1460  $\text{cm}^{-1}$  (5.99 and 6.85  $\mu\text{m}$ ). The signal-to-noise in these spectra is sufficiently

high to permit a comparison of the profiles and substructures of these features. They show a continuous variation from relatively narrow bands like those in W33 A to much broader ones. The apparent increase in the width of some of the bands is caused by the increasing importance of additional absorption features near 1720, 1500, and 1410  $\text{cm}^{-1}$  (5.81, 6.67, and 7.09  $\mu\text{m}$ ). The 1670 and 1460  $\text{cm}^{-1}$  features are treated separately in the discussion that follows.

The 1670  $\text{cm}^{-1}$  (5.99  $\mu\text{m}$ ) band is generally attributed to the H-O-H bending mode of  $\text{H}_2\text{O}$ . In fact, the relatively narrow feature in W33 A (as well as in NGC 7538-IRS 9 and AFGL 2136) can be well matched by simple  $\text{H}_2\text{O}$  ice spectra (Figure 12a). The objects with a wider 1670  $\text{cm}^{-1}$  feature require that additional components be present, however. The short wavelength wing on the 1670  $\text{cm}^{-1}$  feature, which is not prominent in the W33 A spectrum, is attributed to absorption by the C=O stretching mode in carbonyl-bearing molecules. Possible identifications include ketones like acetone ( $\text{CH}_3\text{COCH}_3$ ) and aldehydes like formaldehyde ( $\text{H}_2\text{CO}$ ). The presence of formaldehyde is supported by the suggestion of substructure at 1500 and 1410  $\text{cm}^{-1}$  (6.67 and 7.09  $\mu\text{m}$ ) in some of the spectra. Higher resolution studies are needed to verify the presence of these features.

It has also been suggested that the 1670  $\text{cm}^{-1}$  (5.99  $\mu\text{m}$ ) feature could be due to the H-O-H bending mode of  $\text{H}_2\text{O}$  molecules adsorbed or

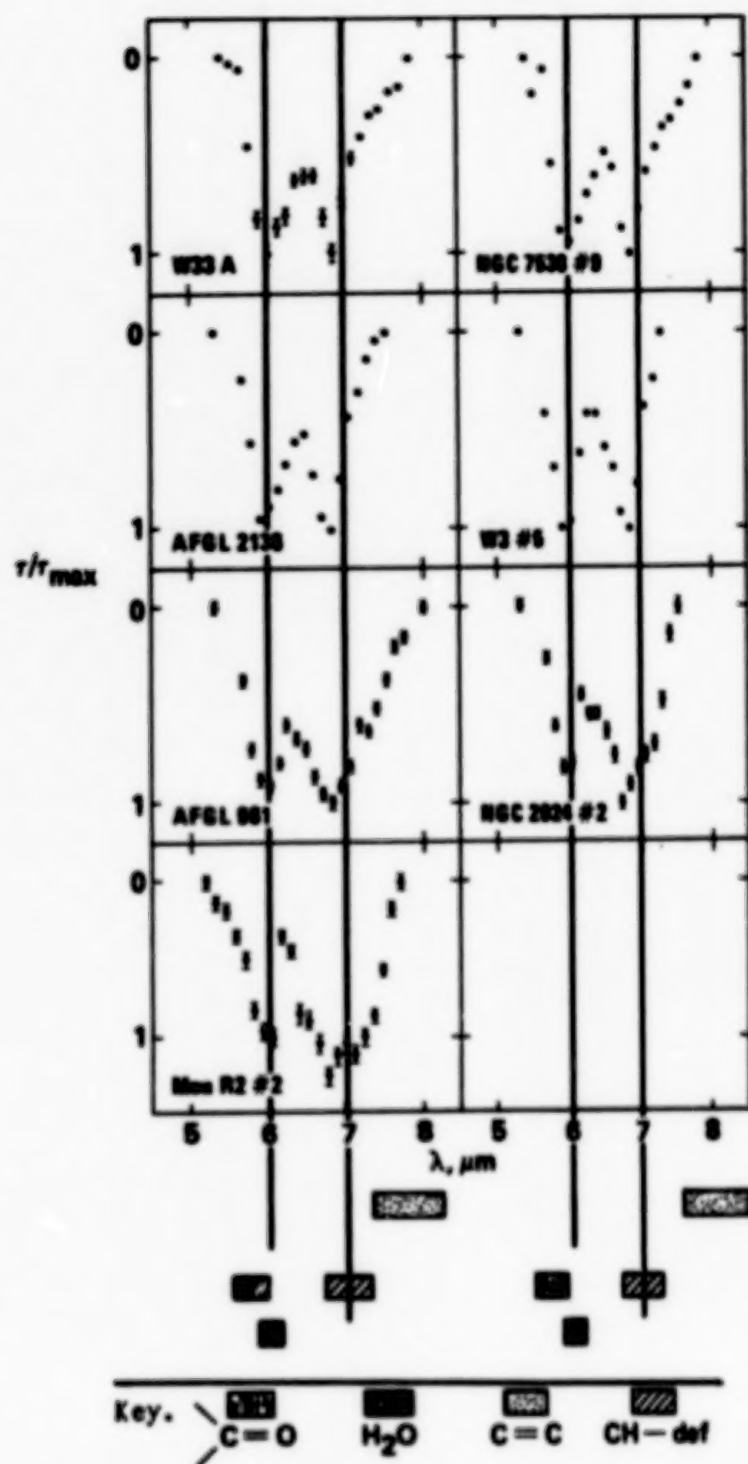


Fig. 11. The  $2000\text{--}1250\text{ cm}^{-1}$  ( $5\text{--}8\text{ }\mu\text{m}$ ) spectra of several protostars obtained with the Kuiper Airborne Observatory. Spectra taken from Tielens et al. (1988). The spectral ranges indicated by the various shaded boxes below the figure indicate the vibrational frequency regions appropriate for each molecular subgroup.

absorbed in hydrated or layer-lattice silicates (Knacke and Krätschmer, 1980; Sandford and Walker, 1985; Hecht et al., 1986). For example, strong "hydration" bands are seen in the spectra of many interplanetary dust particles (Sandford and Walker, 1985) which are known to contain interstellar components (McKeegan et al. 1985). However, the O-H deformation modes in such materials usually peak between 1640 and 1600  $\text{cm}^{-1}$  (6.09 and 6.25  $\mu\text{m}$ ), i.e. at too low a frequency to match the deepest part of the interstellar feature, and they produce bands that are too narrow. These materials, however, may contribute to the long wavelength wing seen in many of the 1670  $\text{cm}^{-1}$  features. Thus, although hydrated silicates may well be present, it appears that they are not the dominant source of the interstellar 1670  $\text{cm}^{-1}$  feature.

The major feature at 1460  $\text{cm}^{-1}$  (6.85  $\mu\text{m}$ ) has been the recipient of a number of identifications. At present, this band is generally attributed to the C-H deformation mode in simple alcohols like methanol ( $\text{CH}_3\text{OH}$ ) (Tielens and Allamandola, 1987; Tielens et al., 1988). The laboratory spectra of these molecules agree quite well with the feature in W33 A and NCC 7538 (Figure 12a). Figure 12b provides an illustration that the C-H deformation modes of pure hydrocarbons (in this case hexane,  $\text{C}_6\text{H}_{14}$ ) do not provide a satisfactory match to the interstellar feature. The position of the C-H deformation mode in methyl ( $-\text{CH}_3$ ) and methylene ( $-\text{CH}_2-$ ) groups depends on the species to which they are attached, an effect illustrated in Figure 13. Thus, the change in the peak position and profile of the "1470"  $\text{cm}^{-1}$  band shown in Figure 11 indicates a wide variation in the relative importance of different types of hydrocarbons from one cloud to another.

Another identification of the 1460  $\text{cm}^{-1}$  (6.85  $\mu\text{m}$ ) feature has also been suggested. Knacke and Krätschmer (1980) and Sandford and Walker

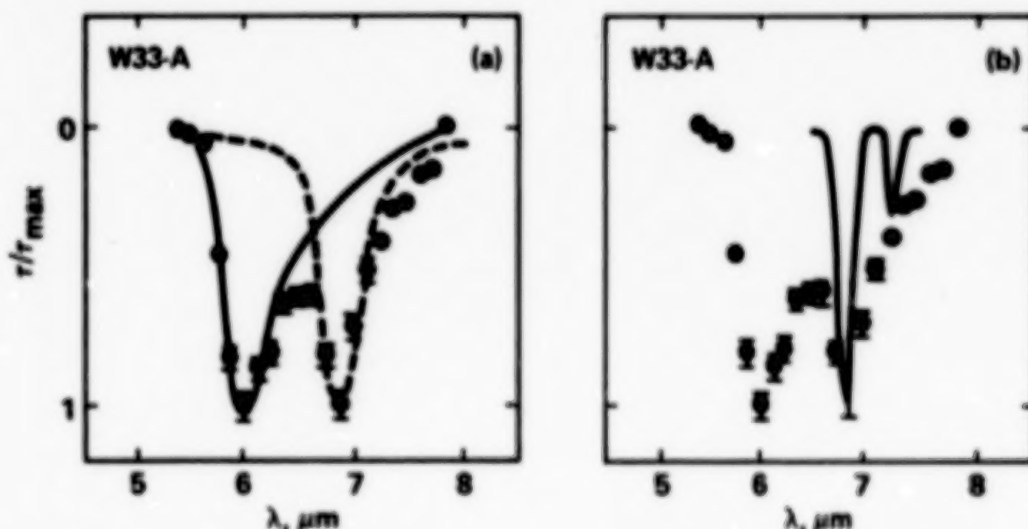


Fig. 12. Comparison between the 2000-1250  $\text{cm}^{-1}$  (5-8  $\mu\text{m}$ ) spectrum of W33 A (dots) with (a) the laboratory spectrum of  $\text{H}_2\text{O}$  (solid line) and  $\text{CH}_3\text{OH}$  (dashed line) ices at 10 K, and with (b) the laboratory spectrum of  $\text{C}_6\text{H}_{14}$  (solid line).

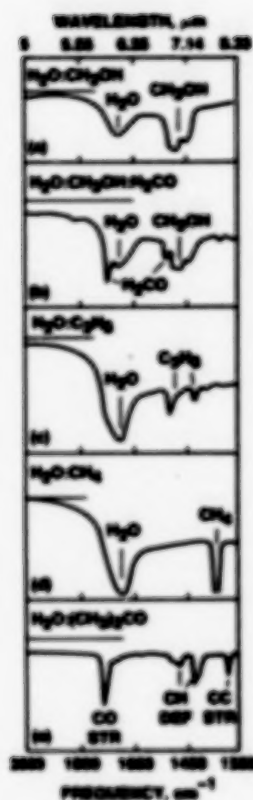


Fig. 13. Laboratory spectra of several  $\text{H}_2\text{O}$ -rich ices containing different hydrocarbons illustrating that the C-H deformation falls at different frequencies in the  $1500\text{--}2000\text{ cm}^{-1}$  ( $6.6\text{--}8.3\mu\text{m}$ ) region.

clouds, a significant fraction of the PAH population is expected to be frozen in grain mantles. High resolution searches for absorption by the  $1610\text{ cm}^{-1}$  ( $6.21\mu\text{m}$ ) aromatic CC stretch feature is very important to test this identification in these sources.

Thus, while the absorption in the  $2000\text{--}1250\text{ cm}^{-1}$  ( $5\text{--}8\mu\text{m}$ ) spectral region probably contains contributions from a wide variety of materials,

(1985) have suggested that the asymmetric stretch of the  $\text{CO}_3$  anion in carbonates may be responsible for some of this feature. This possibility is worth considering since carbonates are known to exist in many interplanetary dust particles (Sandford, 1986; Tomeoka and Buseck, 1986). Many of these same particles contain isotopic anomalies, demonstrating that at least some of their material has an interstellar origin (McKeegan et al., 1985). The feature produced by carbonates in IDPs provides a good match to that seen in the W33 A spectra. However, while carbonates can provide a broad feature in the correct region of the spectrum, they cannot easily reproduce the details of the subfeatures and profile variations seen in the more complex astronomical spectra (cf. NCC 202402 in Figure 11). Thus, we are led to conclude that, while other components may well be present, ices are largely responsible for the  $1460\text{ cm}^{-1}$  feature.

There are also two weak features in the spectrum of NCC 7538-IRS 9, a relatively narrow one ( $\text{FWHM} = 35\text{ cm}^{-1}$ ) at  $1820\text{ cm}^{-1}$  ( $5.49\mu\text{m}$ ) and a much broader one ( $\text{FWHM} = 85\text{ cm}^{-1}$ ) at about  $1310\text{ cm}^{-1}$  ( $7.63\mu\text{m}$ ). The presence of the  $1310\text{ cm}^{-1}$  feature in NCC 7538 has been confirmed by a higher resolution study (Tielens et al., 1988). This band is also present in the spectrum of W33 A. The  $1820\text{ cm}^{-1}$  feature is attributed to the C=O stretch in organic peroxides or carbonyl-containing radicals like HCO or HOCO. The  $1310\text{ cm}^{-1}$  ( $7.63\mu\text{m}$ ) feature may be the absorption counterpart of the  $1300\text{ cm}^{-1}$  ( $7.7\mu\text{m}$ ) emission feature, attributed to polycyclic aromatic hydrocarbons (PAHs) and related materials. This feature can be used to set an upper limit on the amount of PAHs and amorphous carbon absorbing along the lines of sight to these sources. In

it appears that ices are responsible for the majority of the absorption. Certainly a reasonably good fit to most of the interstellar absorption features can be obtained using only icy materials. While it may seem a bit premature to consider some band carriers as identified and attempt to quantify their relative abundances and column densities, it is nonetheless a useful exercise since the admittedly tentative results can provide important insights into the nature of dust in dense clouds and establish a framework on which to base future work. It is in this spirit that Table 3 is presented, assuming only icy materials are present. Table 3 contains estimates of the relative amounts of the various interstellar ice components in different clouds. The reader should see Tielens and Allamandola (1987) for a detailed discussion of the limitations and assumptions that went into producing this table. In considering this listing, bear in mind that the data on which these values are based are obtained by viewing through a cloud, and projection effects are important. For example, the presence of much more CO frozen in non-polar ices (possibly  $\text{CO}_2$ ) than in  $\text{H}_2\text{O}$ -rich ices in W33 A and NCC 7538 (Sandford et al., 1988) and perhaps in the Serpens cloud (Eiroa and Hodapp, 1988) seems to indicate that the  $\text{H}/\text{H}_2$  ratio can vary substantially from one cloud to another. At present there is no way to determine the relative importance of polar versus non-polar ices in clouds apart from the CO band. In this respect, high resolution spaceborne studies of  $\text{CO}_2$  (and perhaps  $\text{O}_3$ , as this is the other major non-polar mantle constituent predicted by the models) in interstellar ices should prove very informative.

It is difficult to understand how the processes which led to the relatively simple  $2000\text{--}1250\text{ cm}^{-1}$  ( $5\text{--}8\text{ }\mu\text{m}$ ) spectra exhibited by W33 A and NCC 7538-IRS 9 could be modified by changing only cloud density and opacity and produce the variations in band breadth and substructure shown by the other sources. Thus the richness of compositional variation implied by the differences in the interstellar spectra suggests that energetic processing of the ices is the rule rather than the exception.

#### IV. PHOTOCHEMICAL AND THERMAL EVOLUTION OF INTERSTELLAR AND PROTOPLANETARY ICE ANALOGS

Infrared spectra of several energetically processed ices are now available for comparison with the astrophysical data. To date most studies have focused on polar ices (Hagen, Allamandola, and Greenberg, 1979; Moore et al., 1983; Strazzulla et al., 1984; Strazzulla, 1985; Agarwal et al., 1985; Allamandola, Sandford, and Valero, 1988; Khare et al. 1988; Schutte, 1988), while only a few studies have included non-polar, mixed molecular ices (Strazzulla et al., 1984; d'Hendecourt et al., 1986). In general, most of the carbon in these experiments has been provided by  $\text{CH}_4$ . In view of the arguments in favor of  $\text{CH}_3\text{OH}$  in interstellar ices, it is important to carry out a similarly thorough experimental program on ices containing this molecule. In particular, it will be interesting to find out if the relative amounts of the various products formed by high energy particle bombardment differ

Table 3. Composition of Interstellar Grain Mantles<sup>a,b</sup>

Species	W3 IRS 5	MCC2024 IRS2 <sup>c</sup>	MonR2 IRS2 <sup>c</sup>	AFGL 961	W33 A	AFGL 2136	MCC7538 IRS9
H <sub>2</sub> O	1.	1.	1.	1.	1.	1.	1.
CH <sub>3</sub> OH <sup>d</sup>	0.81	1.75	3.0	0.87	0.55	0.66	0.65
CO	0.05	0.22	0.20	0.06	0.02	0.04	0.16
Carbonyl	0.05	0.15	0.64	0.04	--	0.04	0.01 <sup>e</sup>
Aldehyde	0.05	0.35	0.55	0.13	--	--	--
Ketones	--	0.65	1.3	0.21	--	--	--
CH <sub>4</sub>	--	--	0.05	0.015	0.005	--	0.01
NH <sub>3</sub>	<0.10	--	--	0.10	0.10	0.10	0.10

a) Taken from Tielens and Allamandola (1987)

b) All abundances normalized to H<sub>2</sub>O

c) H<sub>2</sub>O and CH<sub>3</sub>OH abundance not well determined [see Tielens et al. (1988)]

d) Abundance of CH<sub>2</sub> and CH<sub>3</sub> groups based on the A value of the combination C-H deformation and O-H bending modes in methanol

e) Determined from the 1820 cm<sup>-1</sup> (5.49 μm) feature

significantly from those produced by ultraviolet irradiation. A difference might be expected since CH<sub>3</sub>OH is very sensitive to ultraviolet radiation (it dissociates upon absorption of photons out to wavelengths of about 2000 Å, in contrast to species like H<sub>2</sub>O and CH<sub>4</sub> which have photo-dissociation thresholds that require shorter wavelength radiation), whereas high energy particles deposit sufficient energy for dissociation in a non-selective manner.

We present the following example as an illustration of the processes which occur upon ultraviolet irradiation of CH<sub>3</sub>OH containing ices. A more detailed discussion of these experiments and the astrophysical implications can be found elsewhere (Allamandola, Sandford, and Valero, 1988).

$\text{H}_2\text{O}:\text{CH}_3\text{OH}:\text{NH}_3:\text{CO}$  (100:50:1:1)

Figure 14 shows the spectral development of a long duration photolysis of an  $\text{H}_2\text{O}:\text{CH}_3\text{OH}:\text{NH}_3:\text{CO}$  (100:50:1:1) ice mixture. Infrared spectra were taken after 1, 9, and 37 hours of irradiation. The photochemical evolution of this mixture is shown graphically in Figure 15 where the abundance of each molecule is plotted versus photolysis time. Inspection of Figures 14 and 15 show that  $\text{H}_2\text{CO}$ ,  $\text{CH}_4$ ,  $\text{CO}_2$ , and  $\text{HCO}$  are produced, largely at the expense of  $\text{CH}_3\text{OH}$ . Very long irradiation (37 hours) destroyed nearly all the  $\text{CH}_3\text{OH}$  and it appears that some of the  $\text{H}_2\text{CO}$  produced during the early irradiation stage (10 hours) was photo-oxidized to  $\text{CO}$  and  $\text{CO}_2$ . The later oxidation of  $\text{H}_2\text{CO}$  is probably due to reduced screening of ultraviolet photons by  $\text{CH}_3\text{OH}$  which absorbs more strongly across the ultraviolet than does  $\text{H}_2\text{CO}$  (Calvert and Pitts 1966).

Blending of the C-H stretching bands in the  $3000\text{--}2900\text{ cm}^{-1}$  ( $3.3\text{--}3.4\text{ }\mu\text{m}$ ) region with the O-H stretching band produces a false continuum which leads to underestimates of the abundances of hydrocarbons present if this region alone is analyzed.

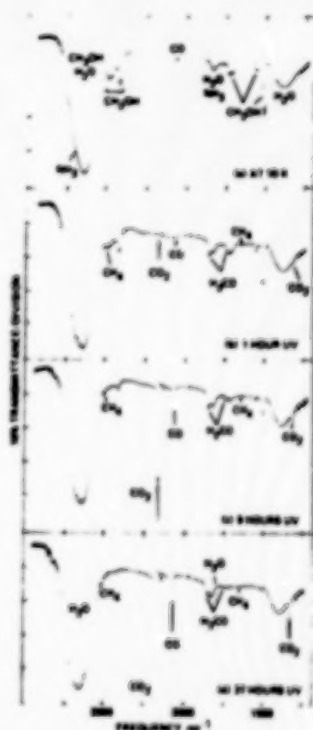


Fig. 14. The infrared spectra of an  $\text{H}_2\text{O}:\text{CH}_3\text{OH}:\text{NH}_3:\text{CO}$  (100:50:1:1) ice taken at 10 K (a) before and after (b) 1, (c) 9, and (d), 37 hours of ultraviolet photolysis.

A similar mixture ( $\text{H}_2\text{O}:\text{CH}_3\text{OH}:\text{NH}_3:\text{CO} = 100:50:10:10$ ) was also deposited and irradiated in order to study the low volatility material produced by photolysis. Figure 16 shows the spectra (each taken at 10 K) of this residual material after the substrate was temporarily warmed to 200, 250, and 300 K under vacuum. The figure shows that, while the bulk of the low volatility material produced by photolysis leaves between 250 and 300 K, some remains at 300 K.

$\text{H}_2\text{O}:\text{CH}_3\text{OH}:\text{NH}_3:\text{CO}:\text{C}_3\text{H}_8$  (100:50:10:10:10)

Figures 17 and 18 present spectra of an  $\text{H}_2\text{O}:\text{CH}_3\text{OH}:\text{NH}_3:\text{CO}:\text{C}_3\text{H}_8$  (100:50:10:10:10) ice sample taken at 10 K and after 1, 6, 9, and 15 hours of ultraviolet photolysis followed by warm-ups to 30, 55, and 100 K. The photochemical evolution of molecular abundances in this sample is shown graphically in Figure 19. This and the following experiment were done to determine how the nature of a hydrocarbon initially present in the ice affects the character of the hydrocarbons in the resulting resi-

dues. The major difference between the spectra in Figures 14a and 17a is the addition in the latter of the C-H stretch and deformation bands of  $C_3H_8$  ( $H_3C-CH_2-CH_3$ ) in the 2900-2800 and 1500-1400  $cm^{-1}$  regions, respectively. The photochemical behavior of this mixture is similar to that in the previous experiment in that  $H_2CO$ ,  $CH_4$ ,  $CO_2$ ,  $CO$ , and  $HCO$  are produced, while  $CH_3OH$  is destroyed. The spectrum taken after 9 hours of irradiation (Figure 17d) is very similar to the 9 hour irradiation spectrum of the  $H_2O:CH_3OH:NH_3:CO$  (100:50:1:1) ice shown in Figure 14c. The major difference between these two 9 hour irradiation spectra is that bands due to unconsumed  $C_3H_8$  and weak  $X(CN)$  and residue bands (at 2160 and 1580  $cm^{-1}$ , respectively), are only present in Figure 17d. Note again the blending of the C-H stretch bands in the 3000-2900  $cm^{-1}$  region with the strong O-H band.

The spectra shown in Figure 18 illustrate several interesting points. Between 10 and 30 K the spectra are virtually unchanged, indicating that the volatile species  $CO$  and  $CH_4$  are tightly trapped in the ice. Between 30 and 55 K the bands due to both  $CO$  and  $CH_4$  diminish while the rest of the spectrum remains unchanged. This occurs because

PHOTOCHEMICAL EVOLUTION OF  
 $H_2O:CH_3OH:NH_3:CO$   
 100:50:1:1

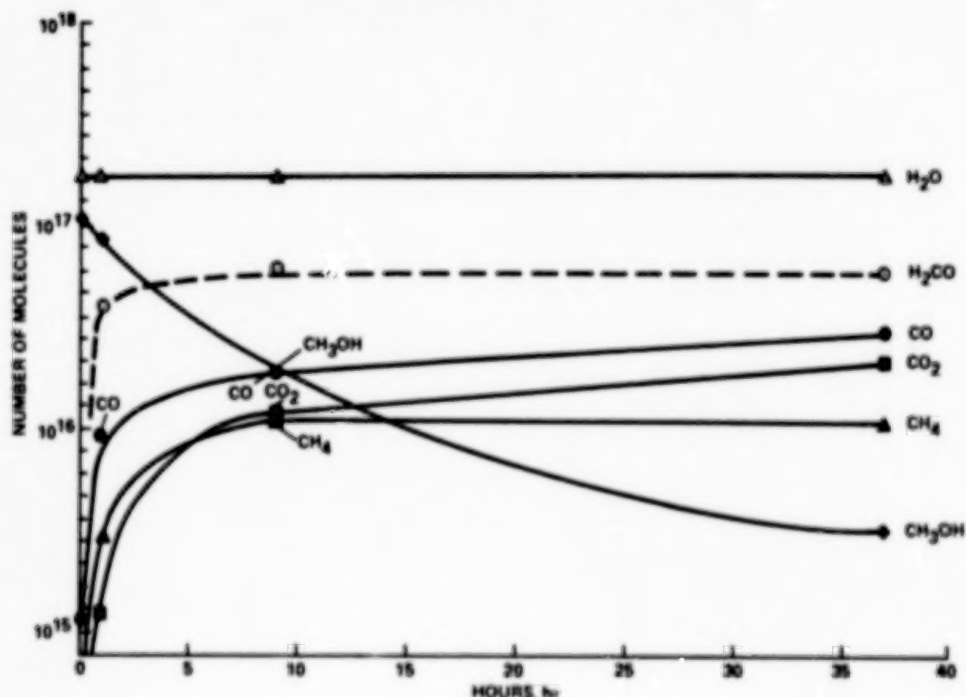


Figure 15. The abundance of parent and product molecules in the  $H_2O:CH_3OH:NH_3:CO$  (100:50:1:1) sample as a function of photolysis time. The  $H_2CO$  abundance is given as a dashed line since its  $A$  value in  $H_2O$ -rich ices is only estimated. The ultraviolet photon flux striking the sample area is about  $5 \times 10^{17} \text{ hr}^{-1}$ .

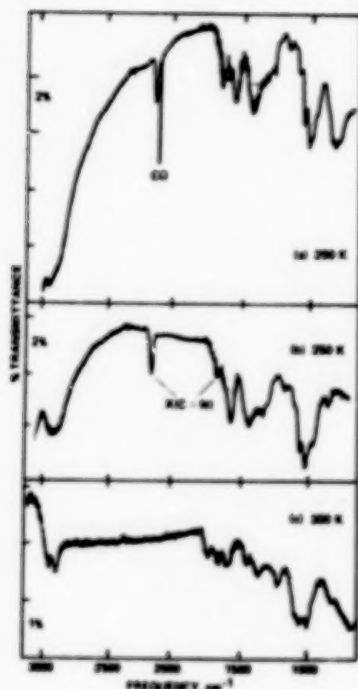


Fig. 16. The infrared spectra (taken at 10 K) of the low vapor pressure materials produced by the 9 hour photolysis of an  $\text{H}_2\text{O}:\text{CH}_3\text{OH}:\text{NH}_3:\text{CO}$  (100:50:10:10) ice after temporary warm-up to (a) 200, (b) 250, and (c) 300 K.

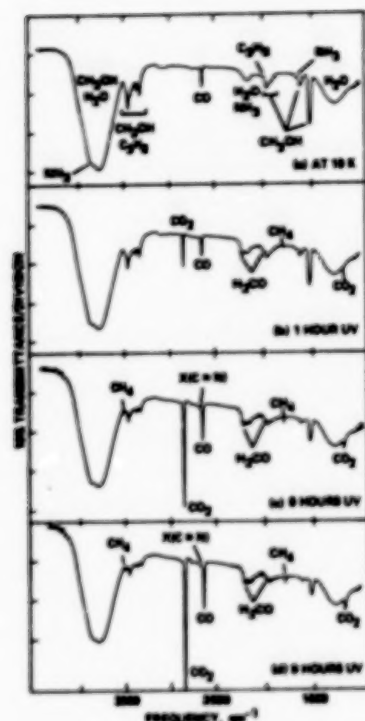


Fig. 17. The infrared spectra of an  $\text{H}_2\text{O}:\text{CH}_3\text{OH}:\text{NH}_3:\text{CO}:\text{C}_3\text{H}_8$  (100:50:10:10:10) ice taken at 10 K (a) before and after (b) 1, (c) 6 and (d) 9 hours of photolysis.

$\text{CO}$  and  $\text{CH}_4$  can migrate slowly through the ice in this temperature range and can escape (see Sandford and Allamandola 1988 for a discussion of  $\text{CO}$  loss from  $\text{H}_2\text{O}$  ice). At 100 K, only 23% of the  $\text{CO}$  and 28% of the  $\text{CH}_4$  initially present just before warm-up remains. The profile of the  $3275\text{ cm}^{-1}$   $\text{H}_2\text{O}$  band becomes asymmetric and narrower in the 100 K spectrum, indicating that the solid  $\text{H}_2\text{O}$  is transforming from the amorphous to cubic form. Apart from  $\text{CH}_4$ , there is no other loss of hydrocarbons up to 100 K.

Warm-up to 200 K was sufficient to remove most of the parent molecules from the sample, leaving a mixture comprised primarily of low volatility photoproducts. Spectra of these materials taken at 10 K after temporary warm-up to 200, 250, and 300 K are shown in Figure 20. The bulk of the residue sublimates away between 200 and 250 K. The

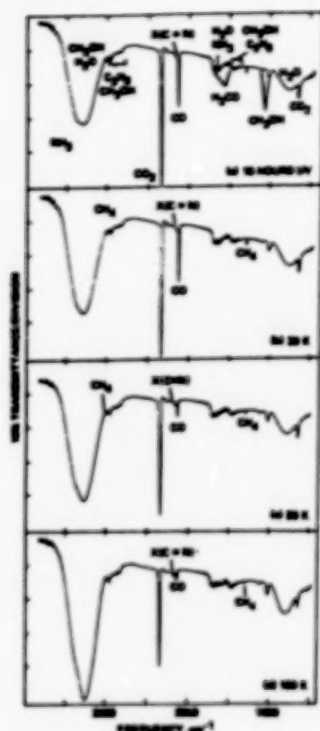


Fig. 18 The infrared spectra of an  $\text{H}_2\text{O}:\text{CH}_3\text{OH}:\text{NH}_3:\text{CO}:\text{C}_3\text{H}_8$  (100:50:10:10:10) ice irradiated for 15 hours taken at 10 K (a) after temporary warm-up to (b) 30, (c) 55 and (d) 100 K.

spectral evolution in the C-H stretching region from  $3100\text{--}2600\text{ cm}^{-1}$  is presented on an expanded scale in Figure 21. The C-H stretching band profile indicates that the residue contains both methyl ( $-\text{CH}_3$ ) and methylene ( $-\text{CH}_2-$ ) groups. Figure 21 shows that there are at least two components in the residue. The first is principally responsible for the  $-\text{CH}_3$  stretching bands at about  $2960$  and  $2870\text{ cm}^{-1}$  which largely disappear by 250 K, behavior similar to that of the  $\text{C}\equiv\text{N}$  band at  $2158\text{ cm}^{-1}$  (Figure 20). There are at least two  $-\text{CH}_2-$  components, one giving rise to the bands at about  $2925$  and  $2850\text{ cm}^{-1}$ , and the other producing bands at about  $2910$  and  $2840\text{ cm}^{-1}$ . The first pair is largely gone by 250 K and thus may be related to the  $-\text{CH}_3$ , and possibly the  $\text{C}\equiv\text{N}$ , carrier. The second  $-\text{CH}_2-$  carrier remains to 300 K. The band profile and position of the 300 K fraction is quite similar to that of the residue produced in the previous experiment in which  $\text{CH}_3\text{OH}$  was the only hydrocarbon present in the initial ice. The relative intensities of the  $-\text{CH}_3$  and  $-\text{CH}_2-$  bands in the 300 K spectra indicate that  $-\text{CH}_2-$  groups dominate the structure of this fraction of the residue. This implies long hydrocarbon chains are responsible. A chain structure is consistent with the observed low volatility of this material and represents a significant change from the  $-\text{CH}_3$  dominated parent molecules,  $\text{C}_3\text{H}_8$  ( $\text{H}_3\text{C}-\text{CH}_2-\text{CH}_3$ ), and  $\text{CH}_3\text{OH}$ .

Additional experiments, where the  $\text{C}_3\text{H}_8$  was replaced by  $\text{C}_6\text{H}_{14}$  (hexane), yielded similar results. The strong similarity between the residue spectra and warm-up behavior of these two experiments indicates that the  $-\text{CH}_3/-\text{CH}_2-$  ratio of the complex molecules formed by photolysis does not depend strongly on the  $-\text{CH}_3/-\text{CH}_2-$  ratio of the parent

hydrocarbon in the ice prior to photolysis (Allamandola, Sandford and Valero, 1988).

#### V. THE NATURE OF THE COMPLEX MOLECULES PRODUCED BY PHOTOLYSIS AND ASTROPHYSICAL IMPLICATIONS.

The richness of the 200 K spectra shown in Figures 16 and 20, and the changes in relative band strengths which occur upon warm-up from 200 to 300 K, indicate that species of varying complexity have been produced. Apart from being important in the chemical evolution in the

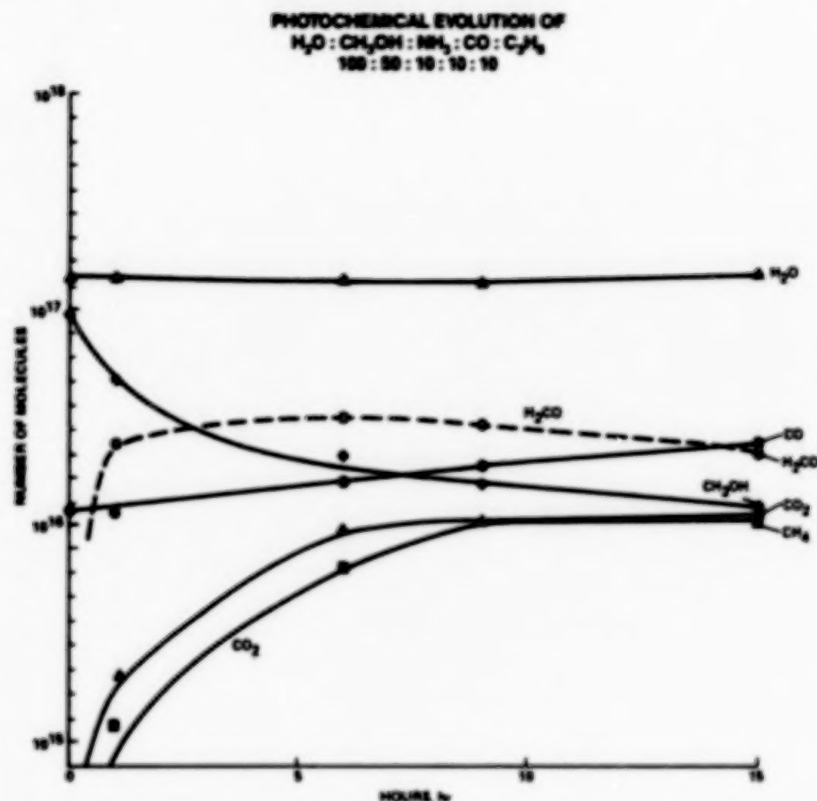


Fig. 19. The abundance of parent and product molecules in the  $\text{H}_2\text{O}:\text{CH}_3\text{OH}:\text{NH}_3:\text{CO}:\text{C}_2\text{H}_6$  (100:50:10:10:10) sample as a function of photolysis time. The  $\text{H}_2\text{CO}$  abundance is given as a dashed line since its A value in  $\text{H}_2\text{O}$ -rich ices is only estimated. The ultraviolet photon flux striking the area sampled by the infrared spectrometer is about  $5 \times 10^{17} \text{ hr}^{-1}$ .

interstellar medium, these results have applications to solar system processes as well. For example, the observed differential sublimation of these moderately volatile compounds may regulate the scale heights of some of the molecular photo-fragments seen in cometary comae (Delsemme and Miller, 1971).

All the 200 K spectra have a prominent band at  $1580 \text{ cm}^{-1}$ . This band and the one at  $2168 \text{ cm}^{-1}$  are the only "residue" features evident before warm-up. The  $2168 \text{ cm}^{-1}$  band, which we identify with a nitrile or iso-nitrile ( $-\text{C}\equiv\text{N}$  or  $\text{C}\equiv\text{N}-$ ) bearing compound, leaves between 200 and 250 K, suggesting that it is part of a small molecular species. These molecules may be similar to those ejected in ice particles, freed by sublimation, and processed by solar photons to produce the  $\text{C}\equiv\text{N}$  jets observed in Comet Halley (A'Hearn et al., 1986).

The presence of several different types of  $-\text{CH}_3$  and  $-\text{CH}_2-$  bearing molecules in the residues is shown by the spectral structure in the  $3000\text{--}2700 \text{ cm}^{-1}$  region in Figure 21. As just pointed out, the similar

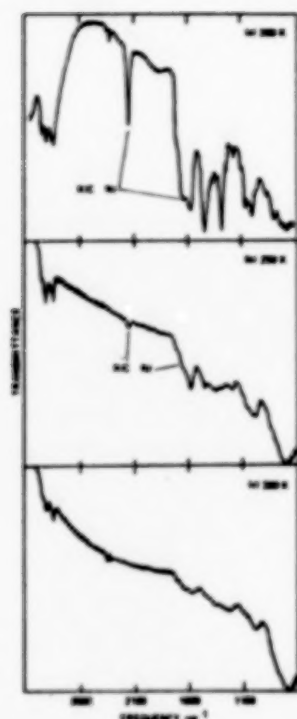


Fig. 20. The infrared spectra taken at 10 K) of the low vapor pressure materials produced by the 15 hour photolysis of an  $\text{H}_2\text{O}:\text{CH}_3\text{OH}:\text{NH}_3:\text{CO}:\text{C}_2\text{H}_6$  (100:50:10:10:10) ice after temporary warm-up to (a) 200, (b) 250, and (c) 300 K.



Fig. 21. The infrared spectra (taken at 10 K) in the C-H stretch region of the low vapor pressure materials produced by the 15 hour photolysis of an  $\text{H}_2\text{O}:\text{CH}_3\text{OH}:\text{NH}_3:\text{CO}:\text{C}_2\text{H}_6$  (100:50:10:10:10) ice. The data are identical to those in Figure 20, but are plotted on an expanded scale to demonstrate the behavior of the various hydrocarbon components upon warm-up.

evaporation behavior of some of the bands indicates that they may be related. In particular, the simultaneous loss of the bands assigned to  $\text{C}\equiv\text{N}$ ,  $-\text{CH}_3$ ,  $\text{C}=\text{O}$ , and one of the  $-\text{CH}_2-$  components suggests the possibility of a common carrier.

The spectra of the residues remaining at 300 K show that they are  $-\text{CH}_2-$  rich, independent of the  $-\text{CH}_2-/-\text{CH}_3$  ratio in the original ice. The relatively non-volatile behavior of this component is consistent with the molecular structures implied. Because methyl ( $-\text{CH}_3$ ) groups are chain terminating, while methylene ( $-\text{CH}_2-$ ) groups are chain lengthening,  $-\text{CH}_3$  rich compounds either consist of shorter hydrocarbon chains or are

highly branched, while  $-\text{CH}_2-$  rich compounds contain longer hydrocarbon chains. Chain-like structures interact more strongly with their environment than do more compact structures. Consequently, all other interactions being equal,  $-\text{CH}_2-$  rich hydrocarbons have lower vapor pressures than  $-\text{CH}_3$  rich hydrocarbons.

The peak position and profile of the C-H stretching feature in the spectrum of dust toward the galactic center shows that it is  $-\text{CH}_2-$  rich (Allen and Wickramasinghe, 1981; Jones et al., 1983). The grains along this line-of-sight are thought to be representative of interstellar dust in diffuse, highly photo-processed regions. The observation of a  $-\text{CH}_2-$  rich hydrocarbon is therefore consistent with a non-volatile, complex material in the diffuse interstellar medium. This is similar to the aliphatic hydrocarbon component found in interplanetary dust particles (Swan et al., 1987).

In contrast, the profile and peak position of the emission feature near  $2990\text{ cm}^{-1}$  ( $3.34\text{ }\mu\text{m}$ ) observed in the spectra of Comets Halley and Wilson imply that the cometary carrier(s) are dominated by  $-\text{CH}_3$  groups (Wickramasinghe and Allen, 1986; Tokunaga et al., 1986; Baas, Geballe, and Walther, 1986; Danks et al., 1987; Knacke, Brooke, and Joyce, 1986). Our most refractory material provides a better match to the interstellar spectra than the cometary spectra. The apparent mismatch between our 300 K residue spectra and the cometary data suggests that either (i) the  $-\text{CH}_3$  rich material that leaves between 200 and 300 K is more representative of the cometary materials responsible for the emission, or (ii) that our original samples lack an important component.

The peak position of the observed cometary feature falls at the high frequency extreme of the normal spectral range for saturated aliphatic hydrocarbons, implying that the  $-\text{CH}_2-$  and  $-\text{CH}_3$  groups are attached to strongly electronegative moieties. The recent proposal that polycyclic aromatic hydrocarbons (PAHs) and related materials are ubiquitous and abundant in space (Duley and Williams, 1981; Leger and Puget, 1984; Allamandola, Tielens, and Barker, 1985) suggests that PAHs may be a component of interstellar and cometary ices. PAHs, which are very electronegative, could be present with abundances as high as about 10% that of  $\text{H}_2\text{O}$  and still not be detectable in protostellar absorption spectra since these molecules are poor absorbers in the infrared. In fact, there is a broad, weak absorption centered near  $1300\text{ cm}^{-1}$  in the spectra of the protostellar objects W33A and NGC 7538 which is consistent with PAHs or amorphous carbon (see Section III and Tielens and Allamandola, 1987). Certainly aromatic moieties are present in the carbonaceous components of primitive meteorites and interplanetary dust particles (Hayatsu and Anders, 1981; Allamandola, Sandford, and Wopenka, 1987), both of which may have a cometary origin.

Finally, it is interesting to consider these results in light of the recent suggestion that polyoxymethylene (POM), a polymer of formaldehyde  $[-(\text{CH}_2-\text{O})_n-]$ , may exist in comets (Huebner, Boice, and Sharp, 1987). The work reported here, as well as that of others, shows that  $\text{H}_2\text{CO}$  is readily produced during the irradiation of ice analogs.

Irradiation of  $\text{H}_2\text{CO}$ -rich residues might well produce some POM. However, the observed differential evaporation implies that the residue material is not dominated by a simple repeating structure like that of POM.

## VI. CONCLUSIONS

Infrared absorption spectra of dense molecular clouds, when compared with laboratory spectra of interstellar ice analogs, provide a powerful means of probing the chemical composition of interstellar, pre-cometary dust and the physical and chemical nature of the various environments in which it is found. This comparison indicates that the bulk of the interstellar absorption features are due to mixed molecular ices containing many organic molecules.

The  $2138\text{ cm}^{-1}$  ( $4.677\text{ }\mu\text{m}$ ) band is due to solid CO. Analysis of the different profiles and positions of this feature provides strong evidence that clouds contain two distinct types of ice: one characterized by polar, hydrogen-bonding molecules like  $\text{H}_2\text{O}$ , and the other characterized by non-polar, or only slightly polar, species such as  $\text{CO}_2$ . The first type of ice is thought to be produced in areas where the majority of the available hydrogen is in atomic form and the second is produced in environments in which the hydrogen is predominantly in molecular form. The  $2165\text{ cm}^{-1}$  ( $4.619\text{ }\mu\text{m}$ ) band is attributed to the CN stretch in an unidentified ice constituent designated X(CN). The initial assignment to a nitrile ( $-\text{C}\equiv\text{N}$ ) or iso-nitrile ( $\text{C}\equiv\text{N}-$ ) has been recently questioned and the suggestion made that it is due to the CN stretch in the ion  $\text{OCN}^-$ . Although the  $1670\text{ cm}^{-1}$  ( $5.99\text{ }\mu\text{m}$ ) feature is due mainly to the HOH bend in  $\text{H}_2\text{O}$ , source-to-source profile variations on the high frequency side of the absorption band are attributed to organic carbonyls, implying the presence of ketones, aldehydes, esters, and carboxylic acids. The  $1470\text{ cm}^{-1}$  ( $6.80\text{ }\mu\text{m}$ ) band is largely attributed to the CH deformation modes of aliphatic hydrocarbons. While alcohols, such as methanol, are strongly implied by the currently available data, source-to-source spectral variations in this band are almost certainly due to variations in the amounts of different types of aliphatic hydrocarbons in the ices. These differences provide strong evidence that energetic processing, such as by ultraviolet photolysis and/or cosmic ray bombardment is an important and common process in the chemical evolution of grain mantles.

Experimental investigations of the photochemical and thermal evolution of laboratory analogs containing  $\text{H}_2\text{O}$ ,  $\text{CH}_3\text{OH}$ ,  $\text{NH}_3$ , CO, and saturated hydrocarbons were also described. These experiments, relevant to both interstellar and cometary ices, are the first in which  $\text{CH}_3\text{OH}$  is a major constituent. Ultraviolet photolysis of these analogs invariably produces  $\text{H}_2\text{CO}$ ,  $\text{CO}_2$ , CO,  $\text{CH}_4$ , and HCO, largely at the expense of photolyzed  $\text{CH}_3\text{OH}$ . Photolysis also produces a mixture of more complex molecules, some of which contain nitrile or iso-nitrile and carbonyl groups. Most of the parent ice molecules sublime upon warm-up to 200 K, leaving behind a mixture of refractory substances. Warm-up to 250 K

liberates a component rich in  $-\text{CH}_3$  groups which may correlate with the carrier(s) of the C=O and C $\equiv$ N bonds. A residue rich in  $-\text{CH}_2-$  groups remains even after warm-up to 300 K. The final residue is rich in  $-\text{CH}_2-$  groups, independent of the  $-\text{CH}_2-/-\text{CH}_3$  ratio of the hydrocarbons in the parent ice and residue components of intermediate volatility. The infrared spectrum of dust towards the galactic center, dust which is probably highly photoprocessed, shows that it is  $-\text{CH}_2-$  rich, whereas the emission spectrum from Comets Halley and Wilson, which is presumably much less processed, implies that  $-\text{CH}_3$  rich organics are present.

#### REFERENCES

- A'Hearn, M. F., Hoban, S., Birch, P. V., Bowers, C., Martin R., and Klinglesmith III, D. A. (1986). Nature, 324, 649-651.
- Agarwal, V. K., Schutte, W., Greenberg, J. M., Ferris, J. P., Briggs, R., Connor, S., van de Bult, C. E. P. M., and Baas, F. (1985). Origins of Life, 16, 21-40.
- Allamandola, L. J. (1984). In Galactic and Extragalactic IR Spectroscopy, (M. Kessler and P. Phillips, eds.), D. Reidel, Dordrecht, pp. 5-35.
- Allamandola, L. J., Sandford, S. A., and Wopenka, B. (1987). Science, 237, 56-59.
- Allamandola, L. J., Tielens, A. G. G. M., and Barker, J. R. (1985). Astrophys. J. 290, L25-L28.
- Allamandola, L. J., Sandford, S. A., and Valero, G. J. (1988). Icarus, submitted.
- Allamandola, L. J., and Sandford, S. A. (1988), in Dust in the Universe, (D. A. Williams and M. E. Bailey eds.), Cambridge University Press, Cambridge, in press.
- Allen, D. A. and Wickramasinghe, D. T. (1981). Nature, 294, 239-240.
- Baas, F., Geballe, T.R., and Walther, D. M. (1986). Astrophys. J., 311, L97-L101.
- Brown, P. D. (1988) in Dust in the Universe, (D. A. Williams and M. E. Bailey), Cambridge University Press, Cambridge, in press.
- Calvert, J. G., and Pitts, J. N., Jr. (1966). Photochemistry, John Wiley and Sons, New York.
- Capps, R. W., Gillett, F. C., and Knacke, R.F. (1978). Astrophys. J. 226, 863-868.

- d'Hendecourt, L. B., and Allamandola, L. J. (1986). Astron. Astrophys. Suppl. Ser., 64, 453-467.
- d'Hendecourt, L. B., Allamandola, L. J., and Greenberg, J. M. (1986). Astron. Astrophys., 152, 130-150.
- d'Hendecourt, L. B., Allamandola, L. J., Crim, R. J. A., and Greenberg, J. M. (1986). Astron. Astrophys., 158, 119-134.
- Danks, A. C., Encrenaz, T., Bouchet, P., Lew Bertre, T., and Chalabaev, A. (1987). Astron. Astrophys., 184, 329-332.
- Day, K. L. (1979). Astrophys. J., 234, 158-161.
- Delsemme, A. H., and Miller, D. C. (1971). Planet. Space Sci. 19, 1259-1274.
- Duley, W. W., and Williams, D. A. (1981). Mon. Not. R. Astron. Soc., 196, 269-274.
- Eiroa, C., and Hodapp, K. W. (1988). In Dust in the Universe, (D. A. Williams and M. E. Bailey, eds.), Cambridge University Press, Cambridge, in press.
- Geballe, T. R. (1986). Astron. Astrophys., 162, 248-252.
- Geballe, T. R., Baas, F., Greenberg, J. M., and Schutte, W. (1985). Astron. Astrophys., 146, L6-L8.
- Greenberg, J. M. (1977). In Comets, Asteroids, and Meteorites, (A. H. Delsemme, ed.), University of Toledo Press, Toledo, pp. 491-497.
- Crim, R. J. A., and Greenberg, J. M. (1987). Astrophys. J., 321, L91-L96.
- Hagen, W., Allamandola, L. J., and Greenberg, J. M. (1979). Astrophys. Spa. Sci., 65, 215-240.
- Hagen, W., Tielens, A. G. G. M., and Greenberg, J. M., (1981). Chem. Phys., 56, 367-379.
- Hagen, W., Tielens, A. G. G. M., and Greenberg, J. M. (1983). Astron. Astrophys. Suppl. Ser., 51, 389-416.
- Hayatsu, R., and Anders, E. (1981). Topics of Current Chemistry 99, 1-37.
- Hecht, J. H., Russell, R. W., Stephens, J. R., and Grieve, P. R. (1986). Astrophys. J., 309, 90-99.
- Huebner, W. F., Boice, D. C., and Sharp, C. M. (1987). Astrophys. J. 320, L149-L152.

- Irvine, W. M., Schloerb, F. P., Hjalmarsen, A., and Herbst, E. (1985). In Protostars and Planets II, (D. C. Black and M. S. Matthews, eds.), Univ. Ariz. Press, Tucson, pp. 579-620.
- Jiang, G. J., Person, W. B., and Brown, K. G. (1975). J. Chem. Phys., 62, 1201-1211.
- Jones, T. J., Hyland, A. R., and Allen, D. A. (1983). Mon. Not. R. Astron. Soc. 205, 187-190.
- Khare, B. N., Thompson, W. R., Murray, B. G. J. P. T., and Sagan, C. (1988) Icarus, in press.
- Knacke, R. F., Brooke, T. Y., and Joyce, R. R. (1986). Astrophys. J. 310, L49-L53.
- Knacke, R. F., and Krätschmer, W. (1980). Astron. Astrophys., 92, 281-288.
- Koike, C., Hasegawa, H., Asada, M., and Hattori, T. (1981). Astrophys. Spa. Sci., 79, 77-85.
- Lacy, J. H., Baas, F., Allamandola, L. J., Persson, S.E., McGregor, P. J., Lonsdale, C. J., Geballe, T. R., and van der Bult, C. E. P., (1984). Astrophys. J., 276, 533-543.
- Larson, H. P., Davis, D.S., Black, J. H., and Fink, U. (1985). Astrophys. J., 299, 873-880.
- Leger, A., and Puget, J. L. (1984). Astron. Astrophys., 137, L5-L8.
- Leger, A., Gauthier, S., Defourneau, D., and Rouan, D. (1983). Astron. Astrophys., 117, 164-169.
- McKeegan, K. D., Walker, R. M., and Zinner, E., (1985). Geochim. Cosmochim. Acta, 49, 1971-1987.
- Millar, T. J. (1988). In Dust in the Universe, (D. A. Williams and M. E. Bailey, eds.), Cambridge University Press, Cambridge, in press.
- Moore, M. H., Donn, B., Khanna, R., and A'Hearn, M. F. (1983). Icarus, 54, 388-405.
- Sandford, S. A., and Allamandola, L. J. (1988). Icarus, submitted.
- Sandford, S. A. (1986). Science, 231, 1540-1541.
- Sandford, S. A., and Walker, R. M. (1985). Astrophys. J., 291, 838-851.
- Sandford, S.A., Allamandola, L. J., Tielens, A. G. G. M., and Valero, G. J., (1988). Astrophys. J., in press (June 1, 1988).

- Schutte, W. A. (1988). Ph. D. Dissertation, Leiden University.
- Strazzulla, G. (1985). Icarus, 61, 48-56.
- Strazzulla, G., Cataliotti, R. S., Calcagno, L., and Foti, G. (1984). Astron. Astrophys., 133, 77-79.
- Suan, P., Walker, R. N., Wopenka, B., and Freeman, J. J. (1987). Meteoritics 22, 510-511.
- Tielens, A. G. G. M., and Hagen, W. (1982). Astron. Astrophys., 114, 245-260.
- Tielens, A. G. G. M., and Allamandola, L. J. (1987). In Physical Processes in Interstellar Clouds, (G. E. Morfill and M. Scholer, eds.), D. Reidel, Dordrecht, pp. 333-376.
- Tielens, A. G. G. M., Allamandola, L. J., Bregman, J. D., Witteborn, F. C., Wooden, D., and Rank, D. M. (1988). Astrophys. J., submitted.
- Tokunaga, A. T., Smith, R. C., Nagata, T., DePoy, D. L., and Sellgren, K. (1986). Astrophys. J. 310, L45-L48.
- Tomoka, K., and Buseck, P. R. (1986). Science, 231, 1544-1546.
- Whittet, D. C. B. (1988). In Dust in the Universe, (D. A. Williams and M. E. Bailey, eds.), Cambridge University Press, Cambridge, in press.
- Whittet, D. C. B., Longmore, A. J., and McFadzean, A. D. (1985). Mon. Not. R. Astro. Soc., 216, 45p-50p.
- Wickramasinghe, D. T., and Allen, D. A. (1986). Nature, 323, 44-46.
- Williams, D. A. (1988). In Dust in the Universe, D. A. Williams and M. E. Bailey eds.), Cambridge University Press, Cambridge, in press.
- Williams, D. A. (1987). In Physical Processes in Interstellar Clouds, (G. E. Morfill and M. Scholer, eds.), D. Reidel, Dordrecht, pp. 337-388.
- Willner, S. P., Puetter, R. C., Russell, R. W., and Soifer, B. T. (1980). In Interstellar Molecules, (B. H. Andrew, ed.), D. Reidel, Dordrecht, pp. 381-386.

# Carbon Chemistry of Circumstellar Envelopes

John H. Bieging

University of California, Berkeley

## ABSTRACT

The chemical composition of envelopes surrounding cool evolved stars, as determined from microwave spectroscopic observations, is reviewed. Emphasis is placed on recent observations with the new large mm-wavelength telescopes and interferometer arrays, and on new theoretical work, especially concerning ion-molecule chemistry of carbon-bearing species in these envelopes. Thermal (as opposed to maser) emission lines are discussed. Much progress has been made in the past few years in the theoretical understanding of these objects. It is already clear, however, that observations with the new generation of mm-telescopes will require substantial improvements in the theoretical models to achieve a thorough understanding of the data now becoming available.

## INTRODUCTION

This paper reviews our understanding of the circumstellar molecular envelopes of evolved, late-type stars in terms of their envelope chemical composition. There have been several good reviews of this general topic in the last few years (refs. 1-7) so in this paper I will emphasize the results of recent observations and theoretical work on the subject, especially with the new instruments for millimeter wavelengths which provide significant improvements in sensitivity and angular resolution compared with past work. I will deal largely with the microwave "thermal" line emission in the envelopes with emphasis on molecules containing carbon, and will largely neglect masers, which are worth a separate review (see refs. 8 and 9).

The chemistry of circumstellar envelopes (CSE's) of evolved stars are of interest for several reasons.

First, they offer us the possibility of constraining theoretical models for the rapid phase of stellar evolution which must occur in the interiors of stars in the mass range  $\sim 1-10 M_{\odot}$ , as these stars evolve into white dwarfs. The elemental and isotopic composition of the CSE must reflect the surface composition of the star at the time that the matter was ejected from the photosphere. The surface composition must in turn be determined by the nuclear processing in the interior coupled with the convective dredge-up of processed material to the surface (ref. 10). Consequently one might hope to use the envelope composition to help understand the rapid post-AGB evolution to the white dwarf stage. Indeed, since observed envelopes generally have relatively constant outflow velocities, spatially-resolved information on isotope and element abundances could, in principle, be read as a chronology of the stellar photospheric composition.

CSE's are also a major source of element enrichment and of dust grains in the interstellar medium (ISM). Current estimates of the rate of mass returned from stars in the initial mass range 1-10  $M_{\odot}$  are of the order one solar mass per year averaged over the whole galaxy. This rate, with the element enrichment as a result of nuclear burning, is large enough to imply that mass loss from AGB stars must play a major role in galactic chemical evolution. In particular, carbon in the ISM is probably produced and returned mainly by the red giants. The  $^{12}\text{C}/^{13}\text{C}$  isotope ratio in the ISM must also be affected by the nucleosynthesis processes in these stars, in which  $^{13}\text{C}$  may become strongly enriched compared to the solar abundance. It is therefore important to quantify as accurately as possible the rate of return to the ISM of matter and of nucleosynthesis products.

Microwave spectroscopic imaging of CSE's is now increasing our understanding of these issues by providing detailed information on the elemental, isotopic, and chemical composition; the temperature and density structure; and the composition and abundance of the dust component. The gas composition and structure are obtainable more or less directly from the observations while dust properties can to some extent be inferred from observations of the gas.

#### ENVELOPE CHEMICAL COMPOSITION DEDUCED FROM MICROWAVE SPECTROSCOPY

##### Thermodynamic Equilibrium Models

The simplest picture of a CSE is that of a spherical uniformly-expanding wind of material ejected from the star by a process not yet well understood. Provided that the rate at which material leaves the star is constant over time (clearly an untenable assumption over long timescales), the CSE then has a density varying as  $1/r^2$  with distance from the star. In the simplest picture, the composition of the envelope is assumed to be determined by chemical reactions at or just above the photosphere. The reactions occurring in this region have been modelled on the assumption of chemical equilibrium (refs. 11-16). It has been argued that, once material has been ejected from the star, the rapid decrease in gas density with increasing radius will cause the "freezing out" of molecular abundances once the dynamical timescale (the time in which the density changes by a significant amount) is less than the chemical reaction timescale (i.e., the inverse of the important reaction rates). Freeze-out is generally expected to occur close to the star, compared with the observed extent of CSE's (up to  $\sim 0.1$  pc), so that the chemical composition is predicted to be determined chiefly by the equilibrium chemical composition near the photosphere.

The most important predictions of the chemical equilibrium models are:

1. Hydrogen is almost entirely converted to molecular form by three-body reactions as long as the gas density exceeds  $10^{11} \text{ cm}^{-3}$  and the photospheric temperature is less than 2500 K (ref. 16). These conditions are expected to hold for most late-type giants, and in fact H I is generally undetected in CSE's (ref. 2), except for the recent observation of H I in  $\alpha$  Ori (ref. 17), a star whose photospheric temperature is well above 2500 K.

2. Abundances of molecules other than  $H_2$  depend critically on the C/O ratio. If there are more carbon than oxygen atoms ( $C/O > 1$ ) essentially all the available O is tied up in CO, with the remaining C divided between HCN and  $C_2H_2$ . If  $C/O < 1$ , all C goes into CO and the remaining O is in the form of  $H_2O$ . Nitrogen is predominantly in the form of  $N_2$  in either case.

3. Second-row elements like Si and S are predicted to form molecules with relatively large abundances, e.g., SiO and SiS (see ref. 15). In fact, grain formation is thought to alter dramatically the gas phase abundance of elements such as Si and Al. Grain formation is poorly understood, however, and is generally not included in chemical equilibrium models. (For example, the models of Tsuji (ref. 13) were computed for gas temperatures down to 500 K, low enough that grain formation is likely to be important, but this process is not included in the model calculations.) The form in which Si is incorporated into grains may depend on the C/O ratio. If  $C/O > 1$ , silicon carbide may be formed, while if  $C/O < 1$ , the dominant form may be silicates.

Of the most abundant predicted species,  $H_2$ ,  $N_2$ , and  $C_2H_2$  have no microwave transitions, while  $H_2O$  is detected as a maser, making column density determinations very uncertain. ( $C_2H_2$  is detected by its mid-IR ro-vibrational transitions--see the review by Wannier in reference 18). CO and HCN are detected by their mm-wavelength emission lines in many CSE's, and the line intensities confirm in a rough way that both molecules are abundant. However, the spectra often indicate large optical depths in the lines, especially for CO, so that accurate CO column densities are not always reliably determined. In fact, the CO profiles have been used to derive total mass loss rates by assuming a CO/ $H_2$  abundance ratio, guided by expectations from chemical equilibrium models (see refs. 19-21).

For HCN, large abundances are also implied by the line intensities. In one case, the C-rich envelope of IRC+10216, HCN excitation has been modelled to derive the space density of HCN as a function of radius (ref. 22). However, since the molecule is radiatively excited, one cannot infer a total gas density from the observations, so as for CO, the absolute HCN abundance is not well-known. HCN has been detected in more than 20 C-rich CSE's, but in only a few O-rich cases (ref. 4).  $H_2O$  is found as maser emission (in the 22.3 GHz line) in ~150 O-rich envelopes, but in none of the C-rich objects. These figures are largely in accord with the predictions of the chemical equilibrium models, although the presence of HCN in O-rich CSE's is difficult to explain in that context.

Equilibrium chemistry may be a reasonable approximation for the few most abundant species, which are closed-shell, stable molecules. However, the equilibrium models are clearly inadequate to explain the observations of the less-abundant species. Some of the most obvious failures of the chemical equilibrium picture are:

1. OH must be present in the envelopes of the O-rich stars with maser emission (the OH/IR stars), but OH is not predicted in any significant amount.

2. SiS and SiO are detected in their thermal (non-maser) emission lines in many CSE's, but the observed abundances derived from observations are 100-1000 times less than predicted by equilibrium chemistry.

3. Complex organic species are not predicted but are observed. The most

notable case is IRC+10216, in which many such molecular species have been detected. These include

a. Long carbon chain molecules ( $\text{HCN}$ , with odd  $x$  up to 11;  
 $\text{C}_x\text{H}$  species, with integer  $x$  up to 6).

b. Organic rings like  $\text{C}_3\text{H}_2$  and  $\text{SiC}_2$ .

4. Ammonia ( $\text{NH}_3$ ) is detected with an abundance much larger than predicted by equilibrium chemistry.

The shortcomings of the equilibrium models have led to the consideration of other mechanisms for producing the observed abundances of the rarer species. These mechanisms include photon and cosmic ray initiated chemical reactions; and grain processes.

#### Photochemical Processes

Two kinds of processes are of interest:

1. Direct photodissociation or ionization by the interstellar UV field, which can penetrate the CSE by an amount depending on the dust optical depth and molecular column densities as seen from the outside. This mechanism was first proposed by Goldreich and Scoville (ref. 23) to explain the presence of OH in O-rich envelopes. Further calculations have been made by Huggins and Glassgold (ref. 24). The reaction of interest is simply  $\text{H}_2\text{O} + h\nu \rightarrow \text{OH} + \text{H}$ , yielding the OH needed for maser emission. The predicted UV penetration depth seems to be in agreement with the observed sizes of OH masers (refs. 25-27).

A similar mechanism has been proposed to explain the large abundance and extent of CN emission toward IRC+10216 (ref. 28). In this case, the abundant species HCN is photodissociated to  $\text{H} + \text{CN}$ . In fact, essentially all molecular species are expected to be dissociated at sufficiently large radii, though the quantitative effect depends on the details of the dissociation mechanism. In particular, CO is believed to be dissociated from UV lines, rather than the continuum (cf. refs. 29, 30). This effect, coupled with the large abundance of CO, implies that CO is self-shielding to much larger radii than most other species (ref. 31), a conclusion which is consistent with the much larger extent of CO emission ( $\sim 6'$ ) than of HCN ( $\sim 45''$ ) in IRC+10216.

Glassgold (ref. 31) and Glassgold and Huggins (ref. 32) have also considered the effects of UV photons produced in a stellar chromosphere. They find that for  $\alpha$  Orionis, chromospheric radiation can play a significant role in determining the ionization structure of the CSE.

2. A second process is reaction between neutrals and ionic molecules. The molecular ions may be produced by interstellar UV ionization of the abundant species ( $\text{CO}$ ,  $\text{H}_2\text{O}$ ,  $\text{N}_2$ ,  $\text{C}_2\text{H}_2$ ) yielding  $\text{HCO}^+$ ,  $\text{H}_3\text{O}^+$ , or  $\text{N}_2\text{H}^+$ . These ions may then react with other molecules to produce a variety of products. Another source of ionization is cosmic rays which penetrate throughout the envelope to ionize  $\text{H}_2$ , leading to the formation of  $\text{H}_2^+$ , which in turn can produce the molecular ions mentioned above (see ref. 30).

Chromospheric UV may also be capable of generating molecular ions in the inner CSE, if the star possesses a chromosphere. In some cases, a nearby hot star (a binary companion or a nearby O-star) may produce UV sufficient to influence the envelope chemistry (ref. 24).

Theoretical models for ion-neutral chemistry in molecular CSE's have been calculated by various authors. For the O-rich ( $C/O < 1$ ) case, early work by Goldreich and Scoville (ref. 23) dealt mainly with reactions of  $H_2$  and  $H_2O$ . Related calculations were made by Huggins and Glassgold and by Scalo and Slavsky (refs. 24 and 33), who extended the models to include S and Si chemistry. More recently, Slavsky and Scalo (ref. 34) and Mamon, Glassgold, and Omont (ref. 30) have presented more refined and extensive calculations which attempt to incorporate all important physical effects. Slavsky and Scalo (ref. 34) employ some 135 reactions among 45 species and 8 elements.

For the carbon-rich CSE's, detailed photochemically-initiated ion-neutral reaction networks have been calculated by Nejad, Millar, and Freeman (ref. 35), Glassgold, Lucas, and Omont (ref. 36), Nejad and Millar (ref. 37), and Glassgold et al. (ref. 38). Nejad and Millar (ref. 37) include 270 reactions with 85 species and although these authors note that nearly all the important reaction rates are laboratory measurements, about 50% of all the rates used are only estimates. Moreover, Glassgold et al. (ref. 38) have pointed out that the temperature dependence of ion-molecule reactions may differ from assumptions commonly made in extrapolating laboratory values to the lower temperatures found in CSE's. Thus, despite the increase in model sophistication, there is evidently some room for improvement in precision.

#### Comparison of Chemical Models with Observations

##### Carbon-rich CSE's

The archetypical example of a carbon-rich CSE is the carbon star IRC+10216. It has a large mass loss rate and hence a dense envelope, and it is relatively nearby ( $\sim 200$  pc), so that trace molecules are more easily detected than in more distant CSE's. Its proximity to us also makes possible spatially-resolved studies of the envelope structure with a fair amount of detail at a resolution of a few arcseconds, now attainable at mm-wavelengths. Moreover, the envelope of IRC+10216 appears to be basically spherical, so that spherically-symmetric models (which are universally assumed) should bear some resemblance to reality.

Evidence for photochemical reactions in IRC+10216 was found by Wootten et al. (ref. 28) in the large abundance (and apparent angular size) of CN, which they interpreted as a result of photodissociation of HCN. Further evidence was given by Bieging, Chapman, and Welch (ref. 22), based on interferometric mapping of HCN, which shows a cutoff in the HCN emission at a radius of  $\sim 10^{17}$  cm. The photochemical models of Glassgold et al. (refs. 36, 38) predict that the HCN abundance falls to 10% of its initial value at  $R = 7 \times 10^{16}$  cm, while CN reaches a maximum abundance at  $6 \times 10^{16}$  cm. Similar results were obtained by Truong-Bach et al. (ref. 39) in their analysis of data from the 20-m Onsala telescope. Thus, photodissociation models seem to account for the observed size of the HCN emission as well as the product CN molecule.

A second molecule detected in IRC+10216 is  $C_2H$ , which is almost certainly a photodissociation product of acetylene ( $C_2H_2$ ) (see ref. 40). Truong-Bach et al. (ref. 39) have mapped  $C_2H$  with the Onsala telescope and modelled the  $C_2H_2$  photodissociation. Their model predicts that  $C_2H$  is distributed in a shell with a peak abundance of  $5 \times 10^{16}$  cm radius. However, they could not resolve the shell structure with the 45" telescope beamwidth. More recently, Bieging and Rieu (ref. 41) have mapped the  $C_2H$  emission at 87 GHz toward IRC+10216, using the U.C. Berkeley mm-interferometer. With a synthesized beam of  $\sim 8''$ , they clearly resolve the  $C_2H$  emission into a ring-like structure as expected for a spherical shell distribution. The observed size of  $C_2H$  emission is in good agreement with the predictions of Nejad and Millar (ref. 37) and of Glassgold et al. (ref. 36) in that the observed radial extent is as predicted; however, the absolute abundances are discrepant by factors of 2 to 5. Considering the model uncertainties, this should be considered rather good agreement.

Other molecular species for which both theoretical predictions and high-resolution observations have recently been made include HNC and  $HCN$ . Both are predicted to form in sequences of photon-initiated ion-molecule reactions (refs. 36-38, 43). Mapping of HNC and  $HCN$  (J=10-9) by Bieging and Rieu (ref. 41) with the Berkeley interferometer and of  $HCN$  (J=12-11) by Likkell et al. (ref. 42) with the Caltech instrument, all show the predicted shell structure with approximately the expected dimensions.

Although detailed excitation calculations have not yet been completed for these species, the observed lines are optically thin. Therefore, since the molecules are linear rotors, the emission intensity can be used to derive total column densities directly, so long as the level populations approximately follow a Boltzmann distribution at some reasonable temperature. Assuming a "standard" mass loss rate for IRC+10216, one can derive molecular abundances for comparison with the published theoretical values. For HNC, the calculations of Glassgold and Mamon (ref. 43) are in excellent agreement with the observations, while Nejad and Millar (ref. 37) predict a size  $\sim 2$  times larger than observed.

For  $HCN$ , the results of Bieging and Rieu (ref. 41) show a ring-like distribution with a filled center--i.e., at the position of the star the line brightness temperature at line center is not zero, but is reduced to  $\sim 40\%$  of the value at the peak of the ring. Likkell et al. (ref. 42) do not detect emission in the J=12-11 line at the stellar position at line center. This result may be a consequence of more limited sampling of spatial frequencies in their data. The overall size and morphology of the  $HCN$  ring are otherwise in good agreement for the two transitions, which suggests that real abundance effects, not excitation, are responsible for the ring-like brightness distribution. By way of comparison with theoretical models, the work of Glassgold and Mamon (ref. 43) is in good agreement in radial distribution, but their predicted  $HCN$  abundance is  $\sim 5$  times too low. Nejad and Millar (ref. 37) predict too-extended a distribution and an abundance  $\sim 15$  times too low. Glassgold and Mamon, by including the effects of cosmic ray ionization in the interior envelope, can reproduce the "filled center" seen by Bieging and Rieu (ref. 41) with rather good agreement in molecular abundances. This agreement suggests that the reaction



followed by dissociative recombination to yield  $\text{HC}_2\text{N}$  may be an important pathway to producing  $\text{HC}_2\text{N}$  in the inner envelope, where  $\text{H}_2\text{CN}^+$  is produced from reactions initiated by cosmic rays. Since  $\text{HC}_2\text{N}$  is the simplest of the cyanopolyynes ( $\text{HC}_n\text{N}$ ), whose remarkably large abundances have been a puzzle (see ref. 4), these results suggest that cosmic ray-initiated chemistry may be important in forming the longer carbon chains as well.

Although the rather good agreement between recent observations and photochemical models implies that molecular ions play an important role in CSE chemistry, detection of the ions has proved elusive. For IRC+10216, Lucas et al. (ref. 44) have set a low upper limit on the emission of  $\text{HCO}^+$ . The model of Glassgold et al. (ref. 38) is just consistent with this limit, although subject to assumed model parameters such as the rates of mass loss and cosmic ray ionization.  $\text{HCO}^+$  has recently been detected in several other CSE's (ref. 45 and Omont, private communication), but these objects all have evidence for shocked winds or internal sources of ionization, so that the photochemical models may not be directly applicable in predicting the  $\text{HCO}^+$  abundance.

#### Oxygen-rich CSE's

Comparison of observations with chemical model predictions for the O-rich envelopes is hampered by a lack of quantitative observational data. Emission lines of OH,  $\text{H}_2\text{O}$ , and SiO have been detected from a large number of stars, but virtually all of these are masers. Since the maser excitation and amplification processes are poorly understood, it is not possible to get reliable column densities or abundances of these molecules for comparison with theoretical chemical models. Relatively few other, non-maser, lines have been detected toward O-rich CSE's, although that situation is now improving with the operation of the new large mm-wavelength telescopes of IRAM and Nobeyama. One species of interest is  $\text{NCO}^+$ , which Mamon et al. (ref. 30) have argued should be fairly abundant in O-rich CSE's. However, the excitation conditions and other envelope properties of known CSE's make the predicted emission from  $\text{NCO}^+$  very weak. As noted above, the objects in which  $\text{NCO}^+$  has so far been detected have anomalous properties which may make photochemical models inappropriate for comparison.

Neutral species whose thermal line emission has been observed include SO and SiO. Sahai and Howe (ref. 46) have detected SO in several O-rich CSE's. They derived abundances of  $\sim 10^{-5}$ , much higher than equilibrium chemical models predict ( $\sim 10^{-8}$ ). They argue that the high SO abundance supports the non-equilibrium chemical models of Scalo and Slavsky (refs. 33, 34), in which SO is a product of reactions with OH produced by photodissociation of  $\text{H}_2\text{O}$ . Thermal SiO emission has been detected now in more than 20 O-rich CSE's<sup>2</sup>, and shows abundances which are inconsistent with equilibrium chemical models. However, the SiO gas phase abundance is probably strongly affected by grain processes, which we consider briefly in the next section.

#### Grain Processes

Circumstellar envelopes are important sources of dust grains for the interstellar medium. Most of our information about the grain component in CSE's is obtained from infrared observations, since the thermal dust emission

at microwave frequencies is very weak (though detectable--e.g. ref. 47). However, it has been possible to draw certain conclusions about the grains and gas-grain processes from microwave spectroscopic observations.

In the case of oxygen-rich CSE's, the presence of strong SiO maser emission from vibrationally excited states implies a large abundance of gas-phase SiO close to the star. Morris and Alcock (ref. 48) pointed out that emission from ground state SiO is also detected, with intensities which imply abundances of SiO 100 to 1000 times less than predicted by chemical equilibrium models. This discrepancy suggests that SiO is quickly depleted onto grains from the gas relatively close to the star ( $R < 10^{15}$  cm), possibly just outside the zone of SiO maser action. The form which the Si takes is not entirely certain, but the presence of the 9.7  $\mu$ m feature (usually in absorption) in spectra of many OH/IR stars (ref. 49) suggests that the Si is predominantly in silicates.

For the C-rich envelopes, SiO maser emission is not observed, so there is no comparable constraint on the gas phase abundance of Si close to the star. Even so, observations of SiS toward IRC+10216 (ref. 50) implied an abundance of SiS some two orders of magnitude less than predicted by chemical equilibrium models. Sahai et al. argued that since sulfur appears to be relatively undepleted, it is the silicon which has been removed from the gas phase, probably in the form of SiC, and incorporated into grains.

Recent interferometer maps of the SiS and SiO distributions toward IRC+10216 (refs. 41, 42) show that these species are spatially extended, but with intensities corresponding to molecular abundances about 100 times lower than predicted from chemical equilibrium. Bieging and Rieu (ref. 41) find that the SiS abundance as a function of radius is roughly constant, though possibly showing some (factor of 5) enhancement at  $R = 3 \times 10^{16}$  cm, and with a cutoff for  $R > 6 \times 10^{16}$  cm. This abundance variation is consistent with a large initial depletion of Si onto grains for  $R < 10^{15}$  cm, and some chemical production of SiS in the outer envelope, followed by UV photodissociation at large  $R$ . This picture is consistent with some of the chemical models of Scalo and Slavsky (refs. 33 and 34).

#### CONCLUDING REMARKS

In this review, I have tried to summarize the ways in which microwave spectroscopic observations of circumstellar envelopes can give us essential information on the processes of stellar evolution at the end of the asymptotic giant branch and on the enrichment of the interstellar medium in elements and in grains. There has been much progress recently in both the observations and their theoretical interpretation. Photochemical models for CSE's can now account at least in a rough way, and sometimes with remarkable accuracy, for both the distribution and abundances of a number of molecular species which have been observed with high angular resolution. Much of the theoretical effort has focussed on the C-rich envelope of IRC+10216, and a desirable goal would be a comprehensive, fully self-consistent model that can explain all observations at once. The extension of such modelling to other CSE's will also be important as the quality of the observational data continues to improve. As we have seen, this improvement in the data is especially striking for the O-rich CSE's. An increasing number of such objects are now

detected in a growing list of molecules--some of which (for example, C-bearing species like HCN) are not expected on theoretical grounds. The presence of these species is a challenge to the chemical model-builders. A point perhaps worth noting again is the need for better chemical rate coefficients. Most important reactions are probably adequately understood over a limited range of temperatures, but in extrapolating to the wide range of conditions possible in CSE's, there is some room for improvement.

Finally, the increases in resolution and sensitivity which are now becoming possible with the new large single-dish telescopes and with interferometer arrays will require improvements in analysis. To do justice to the observational data, one may be forced to abandon the usual assumptions of spherical symmetry, uniform outflow velocity, and constant mass loss rate, at least in specific cases. As a consequence, the calculations of radiative transfer and of molecular excitation may be significantly complicated, raising the need for improved computer codes to handle more realistic cases than have been treated in the past. It seems clear, though, that the improvements in observational data already appearing in print will warrant such a computational effort. Further progress in understanding CSE's and the physical processes associated with them will depend on both new observations and their careful analysis.

#### References

1. Glassgold, A.E., and Huggins, P.J. 1987, in "The M, S, and C Stars", eds. H.R. Johnson and F. Querci (NASA/CNRS), in press.
2. Knapp, G.R. 1987, in "Late Stages of Stellar Evolution", eds. S. Kwok and S. Pottasch (Dordrecht: Reidel), p. 103.
3. Morris, M. 1985, in Mass Loss from Red Giants, eds. M. Morris and B. Zuckerman (Dordrecht: Reidel), p. 129.
4. Olofsson, H. 1987, in "Late Stages of Stellar Evolution", eds. S. Kwok and S. Pottasch (Dordrecht: Reidel), p. 149.
5. Omont, A. 1985, in Mass Loss from Red Giants, eds. M. Morris and B. Zuckerman (Dordrecht: Reidel), p. 269.
6. Omont, A. 1987, in IAU Symp. 120, Astrochemistry, eds. M.S. Vardya and S.P. Tarafdar (Dordrecht: Reidel), p. 357.
7. Zuckerman, B. 1987, in IAU Symp. 120, Astrochemistry, eds. M.S. Vardya and S.P. Tarafdar (Dordrecht: Reidel), p. 345.
8. Chapman, J. 1988, P.A.S.P, in press for January.
9. Walmsley, C.M. 1987, in IAU Symp. 120, Astrochemistry, eds. M.S. Vardya and S.P. Tarafdar (Dordrecht: Reidel), p. 369.
10. Iben, I., and Renzini, A. 1983, Ann. Rev. Astr. Ap., 21, 271.
11. Tsuji, T. 1964, Ann. Tokyo Astr. Obs., 9, 1.
12. Tsuji, T. 1973, Astr. Ap. 23, 411.

13. Tsuji, T. 1987, in IAU Symp. 120, Astrochemistry, eds. M.S. Vardya and S.P. Tarafdar (Dordrecht: Reidel), p. 409.
14. McCabe, E.M., Smith, R.C., and Clegg, R.E.S. 1979, *Nature*, 281, 263.
15. Lafont, S., Lucas, R., and Omont, A. 1982, *Astr. Ap.*, 106, 201.
16. Glassgold, A.E., and Huggins, P.J. 1983, *M.N.R.A.S.*, 203, 517.
17. Bowers, P.F., and Knapp, G.R. 1987, *Ap. J.* 315, 305.
18. Wannier, P. 1985, in *Mass Loss from Red Giants*, eds. M. Morris and B. Zuckerman, D. Reidel, p. 65.
19. Knapp, G.R., and Morris, M. 1985, *Ap. J.*, 292, 640.
20. Zuckerman, B., and Dyck, H.M. 1986a, *Ap. J.*, 304, 394.
21. Zuckerman, B., Dyck, H.M., and Claussen, M.J. 1986, *Ap. J.*, 304, 401.
22. Bieging, J.H., Chapman, B., and Welch, W.J. 1984, *Ap. J.*, 285, 656.
23. Goldreich, P., and Scoville, N.Z. 1976, *Ap. J.*, 205, 144.
24. Huggins, P.J., and Glassgold, A.E. 1982, *A.J.*, 87, 1828.
25. Bowers, P.F., Johnston, K.J., and Spencer, J.H. 1983, *Ap. J.*, 274, 733.
26. Diamond, P.J., Norris, R.P., Rowland, P.R., Booth, R.S., and Nyman, L.-A. 1985, *M.N.R.A.S.*, 212, 1.
27. Engels, D., Kreysa, E., Schultz, G.V., and Sherwood, W.A. 1983, *Astr. Ap.*, 124, 123.
28. Wootten, A., Lichten, S., Sahai, R., and Wannier, P. 1982, *Ap. J.*, 257, 151.
29. Morris, M., and Jura, M. 1983, *Ap.J.*, 264, 546.
30. Mamon, G.A., Glassgold, A.E., and Omont, A. 1987, *Ap. J.*, 323, 306.
31. Glassgold, A.E. 1987, in IAU Symp. 120, Astrochemistry, eds. M.S. Vardya and S.P. Tarafdar (Dordrecht: Reidel), p. 379.
32. Glassgold, A.E., and Huggins, P.J. 1986, *Ap. J.*, 306, 605.
33. Scalo, J.M., and Slavsky, D.B. 1980, *Ap.J.(Letters)*, 239, L73.
34. Slavsky, D.B., and Scalo, J.M. 1987, preprint.
35. Nejad, L.A.M., Millar, T.J., and Freeman, A. 1984, *Astr. Ap.*, 134, 129.
36. Glassgold, A.E., Lucas, R., and Omont, A. 1986, *Astr. Ap.*, 157, 35.
37. Nejad, L.A.M., and Millar, T.J. 1987, *Astr. Ap.*, 183, 279.

38. Glassgold, A.E., Mamon, G.A., Omont, A., and Lucas, R. 1987, *Astr. Ap.*, 180, 183.
39. Truong-Bach, Nguyen-Quang Rieu, Omont, A., Olofsson, H., and Johansson, L.E.B. 1987, *Astr. Ap.*, 176, 285.
40. Huggins, P.J., and Glassgold, A.E. 1982b, *Ap. J.*, 252, 201.
41. Biegging, J.H., and Nguyen-Quang Rieu 1987, *Ap. J.* (Letters), submitted.
42. Likkell, L., Morris, M., Masson, C., and Wootten, A. 1987, *Bull. Amer. Astron. Soc.*, 19, 755.
43. Glassgold, A.E., and Mamon, G.A. 1987, paper presented at Haystack Observatory Symposium, 10-12 June 1987.
44. Lucas, R., Omont, A., Guilloteau, S., and Nguyen-Quang Rieu 1986, *Astr. Ap.* 154, L12.
45. Morris, M., Guilloteau, S., Lucas, R., and Omont, A. 1987, *Ap. J.*, 321, 888.
46. Sahai, R., and Howe, J. 1987, in "Late Stages of Stellar Evolution", eds. S. Kwok and S. Pottasch (Dordrecht: Reidel), p. 167.
47. Neilligan, G. et al. 1986, *Ap. J.*, 308, 306.
48. Morris, M., and Alcock, C. 1977, *Ap. J.*, 218, 687.
49. Jones, T.J. 1987, in "Late Stages of Stellar Evolution", eds. S. Kwok and S. Pottasch (Dordrecht: Reidel), p. 3.
50. Sahai, R., Wootten, A., and Clegg, R.E.S. 1984, *Ap. J.*, 284, 144.
51. Mamon, G.A., Glassgold, A.E., and Huggins, P.J. 1988, *Ap. J.*, in press for 15 May.

## CARBON CHEMISTRY IN DENSE MOLECULAR CLOUDS: THEORY AND OBSERVATIONAL CONSTRAINTS

Geoffrey A. Blake  
Division of Geological and Planetary Sciences  
California Institute of Technology

**ABSTRACT.** For the most part, gas phase models of the chemistry of dense molecular clouds predict the abundances of simple species rather well. However, for larger molecules and even for small systems rich in carbon these models often fail spectacularly. We present a brief review of the basic assumptions and results of large scale modeling of the carbon chemistry in dense molecular clouds. Particular attention will be paid to the influence of the gas phase C/O ratio in molecular clouds, and the likely role grains play in maintaining this ratio as clouds evolve from initially diffuse objects to denser cores with associated stellar and planetary formation.

Recent spectral line surveys at centimeter and millimeter wavelengths along with selected observations in the submillimeter have now produced an accurate "inventory" of the gas phase carbon budget in several different types of molecular clouds, though gaps in our knowledge clearly remain. The constraints these observations place on theoretical models of interstellar chemistry can be used to gain insights into why the models fail, and show also which neglected processes must be included in more complete analyses. Looking toward the future, larger molecules are especially difficult to study both experimentally and theoretically in such dense, cold regions, and some new methods are therefore outlined which may ultimately push the detectability of small carbon chains and rings to much heavier species.

### I. INTRODUCTION

In the short span of less than two decades molecular astrophysics, the observational and theoretical examination of molecules in extraterrestrial environments, has grown from a small field of limited importance to one of the most active and innovative branches of many disciplines. Work in this area has literally revolutionized our understanding of the interstellar medium in general, and star formation in particular. An entirely new type of object - the dense molecular cloud - has been discovered, which we now know to be the birthplace of stars, some of them like our own sun. Over ninety atomic and molecular species have been identified in these clouds, a richness and complexity unexpected even a decade ago. Table 1 presents a listing of the currently observed interstellar molecules, and as may be immediately seen the vast majority of these species contain carbon. Indeed, nearly every functional group in organic chemistry may be found in the interstellar medium!

The dust in molecular clouds renders them opaque at optical and near infrared wavelengths. Because of this the gas and dust in "typical" molecular clouds have temperatures on the order of 10-100 K, and the bulk of their radiation is emitted throughout the millimeter (10-1 mm), submillimeter (1-0.2 mm), and far-infrared (200-30  $\mu$ m) regions of the spectrum where the inter-

Table 1  
Interstellar Molecules (as of 1/88)

<u>Simple Inorganic Molecules:</u>			
H <sub>2</sub>	CH <sub>4</sub> *	CS	NaCl*
HCl	SiH <sub>4</sub> *	SiS	AlCl*
H <sub>2</sub> O	C <sub>2</sub> H <sub>4</sub> *	OCS	KCl*
H <sub>2</sub> S	CO	SO <sub>2</sub>	AlF*
NH <sub>3</sub>	SiO	HNO ?	
<u>Nitriles, Acetylene Derivatives, &amp; Related Molecules:</u>			
PN	HC <sub>3</sub> N	CH <sub>3</sub> CN	C <sub>2</sub> H <sub>3</sub> CN
HCN	HC <sub>5</sub> N	CH <sub>3</sub> C <sub>2</sub> CN	C <sub>2</sub> H <sub>5</sub> CN
HNC	HC <sub>7</sub> N	CH <sub>3</sub> C <sub>4</sub> CN	HNCO
HCCH*	HC <sub>9</sub> N	CH <sub>3</sub> CCH	HNCS
CCCO	HC <sub>11</sub> N	CH <sub>3</sub> C <sub>4</sub> H	CCCS
<u>Aldehydes, Alcohols, Esters, and Amides:</u>			
H <sub>2</sub> CO	CH <sub>3</sub> OH	HCOCH <sub>3</sub>	HCONH <sub>2</sub>
H <sub>2</sub> CS	CH <sub>3</sub> SH	HCOOH	H <sub>2</sub> CNH
H <sub>2</sub> CCO	CH <sub>3</sub> CH <sub>2</sub> OH	HCOOCH <sub>3</sub>	H <sub>2</sub> NCN
HCOCH <sub>3</sub>	(CH <sub>3</sub> ) <sub>2</sub> O ?	HCOC <sub>2</sub> H <sub>2</sub> ?	CH <sub>3</sub> NH <sub>2</sub>
<u>Cyclic Molecules:</u>		<u>Ions:</u>	
C <sub>3</sub> H		CH <sup>+</sup>	HN <sub>2</sub> <sup>+</sup>
C <sub>3</sub> H <sub>2</sub>		H <sub>2</sub> D <sup>+</sup> ?	HOCO <sup>+</sup>
SiC <sub>2</sub>		H <sub>3</sub> O <sup>+</sup> ?	HCNH <sup>+</sup>
		HCO <sup>+</sup>	HCS <sup>+</sup>
		HOC <sup>+</sup> ?	SO <sup>+</sup>
<u>Radicals:</u>			
CH	C <sub>3</sub> H	CN	CCS
OH	C <sub>4</sub> H	C <sub>3</sub> N	SO
HCO	C <sub>5</sub> H	NO	
CCH	C <sub>6</sub> H	NS	

\* Detected only in the envelope around IRC+10216.  
? Claimed but not yet confirmed.

action of electromagnetic radiation with the rotational motion of simple molecules and with the vibration-rotation interactions of larger molecules is at a maximum. The millimeter and submillimeter bands are therefore key windows to the universe, as the composite spectrum in Figure 1 demonstrates. At longer wavelengths the rotational envelopes of heavy molecules dominate the spectra of dense molecular clouds, but in the submillimeter region the lowest transitions of molecular hydrides, the fine structure transitions of low  $Z$  atoms, and the lowest vibrational transitions of long chain hydrocarbons begin to appear.

In addition to producing some of the most accurate estimates of the chemical abundances, temperatures, densities, and velocity structures within molecular clouds, millimeter and submillimeter-wave spectral lines also contribute substantially to the energy balance in these objects. The amount of energy released by rotational and fine structure emission determines, in part, the rates of collapse and ultimately the efficiency of star formation in molecular clouds, and is very sensitive to the exact chemical composition of the gas and dust.

Observations over the last several years have established similarities in the chemical composition of many molecular clouds, but several fundamental problems, such as the large differences in the abundances of key species, remain. For example, it is not known whether the observed differences between the chemical composition of giant molecular cloud complexes and smaller dark clouds is purely a result of the different physical conditions within these objects or whether evolutionary patterns exist.

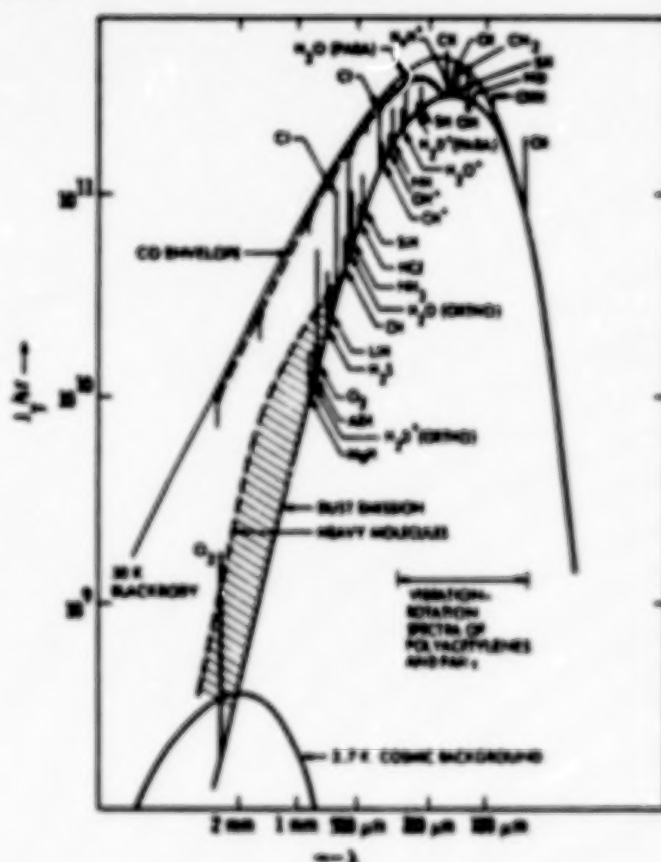


Figure 1.- Composite spectrum of a 30 K molecular cloud. Only a few of the most fundamental of the host of spectral features have been included.

Considerable progress has also been made theoretically since the first discovery of complex organic molecules in interstellar space. Several different hypotheses about the nature of chemical synthesis in the interstellar medium have been brought forward, and have been shown to contribute to the extraordinary richness observed. Models of the gas phase and surface chemical reactivity of matter in non-terrestrial environments have become commonplace. As with observational work, however, basic questions still surround the formation of molecular species in the galaxy.

We shall attempt in this paper to outline what is currently known both theoretically and observationally about the formation of complex carbonaceous molecules in dense interstellar clouds and their possible relation to organic material found in primitive relics of the presolar nebula. For fuller explanations of the details of various processes outlined here, more comprehensive reviews of molecular cloud chemistry by Herbst<sup>1</sup> and Prasad *et al.*<sup>2</sup>, and observational aspects of molecular astrophysics by Irvine *et al.*<sup>3</sup>, are recommended. The chemistry within shocks and within outflows from evolved stars can also contribute to the observed chemical composition of dense molecular clouds, but shall not be explicitly addressed here (contributions by Seab and Bieging in this volume describe the important aspects of such environments to the galactic carbon budget). A tutorial style will be used throughout, with illustrative, but not comprehensive, references.

## II. CHEMICAL PROCESSES IN THE INTERSTELLAR MEDIUM

The often harsh environment of interstellar space led early investigators of the chemical content of the interstellar medium to conclude that the gas would be composed entirely of atoms, throughout which was dispersed a family of small ( $\leq 0.1 \mu\text{m}$ ) dust grains. Even now, our understanding of the processing of material from atomic to more complex species in space is hindered by a lack of experimental data. Just what sort of processes are important in molecular clouds? Even in the densest cloud cores, the density is sufficiently low that only bimolecular reactions need be considered in the gas phase; any intermediate complex has sufficient time to react or break up before a third body can carry away excess energy. Temperatures are sufficiently low in most regions of dense molecular clouds to preclude any reactions with even small activation barriers. Gas phase modeling may therefore be confined principally to exothermic binary reactions. Reactions on grain surfaces may also be invoked, although little experimental data is available on the catalytic potential of cosmochemical surfaces at relevant temperatures. Thus, there are really two separate camps: Gas phase processing and catalysis on grain surfaces. Each camp has its own set of defenders and detractors, and, unfortunately, little collaborative work has so far been accomplished. The importance of each to the overall chemistry in dense molecular clouds and in protostellar nebula are beyond question, however.

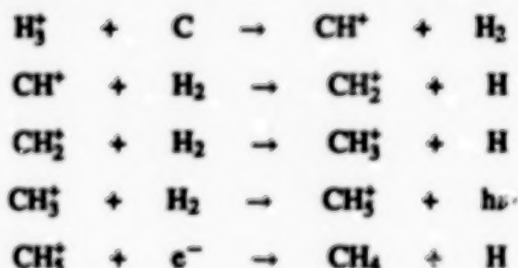
For example, molecular hydrogen is known to be the dominant form of hydrogen in the cores of dense molecular clouds, yet no adequate scheme for its formation in the gas phase has been found. Observational limits as to the required formation efficiencies on grain surfaces are high, but not excessive<sup>4</sup>. The importance of  $\text{H}_2$  bond formation to the subsequent chemistry cannot be overestimated, for it is this initial molecular linkage which breaks the bottleneck to the further synthesis of complex species. Conversely, the abundances of molecular ions such as  $\text{HCO}^+$ , of highly unsaturated polyacetylene chains such as  $\text{C}_4\text{H}$ , and certain isomeric behavior in dense clouds are quite difficult to reconcile with formation on grain surfaces, but are quite well predicted by gas phase models of interstellar chemistry incorporating ion-molecule reactions. Relevant aspects of gas phase chemistry are better understood at present, and we begin accordingly with a discussion of what has been discovered about such processes in dense molecular clouds.

### Gas Phase Chemistry in Dense Clouds

As noted above, the low densities and temperatures in dense molecular clouds restricts viable gas phase mechanisms to exothermic reactions without activation barriers. Except for certain radical-radical reactions, nearly all exothermic reactions between neutral species possess substantial activation energies and may be safely neglected. Ion-molecule reactions, on the other hand, often proceed at the collision rate - any activation barrier is overcome by the gain in kinetic energy of the collision complex as reaction occurs<sup>5</sup>. The long range nature of the ion/induced dipole force also creates significantly larger rate constants than those for even the fastest neutral-neutral reactions. Further, it has recently been discovered that certain exothermic ion-molecule reaction rates involving highly polar species *increase* dramatically at lower temperatures due to dipole locking and tunneling effects<sup>6</sup>. All of these factors combine to make ion-molecule reactions the dominant driver of gas phase chemistry in cold, dense clouds.

Many different types of reactions are important to molecular cloud chemistry. These include purely chemical processes such as hydrogenation, proton transfer, condensation, electron recombination, fixation, etc. in which particles are used to carry away the excess reaction energy; and radiative association reactions in which the collision complex emits radiation to stabilize itself. All of these reactions, and several radical-radical steps, are essential to the formation of the simplest carbon containing molecules in dense clouds, CH<sub>4</sub>, C<sub>2</sub>H<sub>2</sub>, and CO:

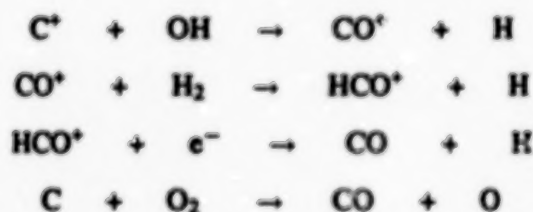
CH<sub>4</sub>:



C<sub>2</sub>H<sub>2</sub>:



CO:



on so on. Radiative association reactions are especially important for the production of larger molecules, as we shall see later.

One of the most important aspects of homogeneous gas phase chemistry is the ease with which it may be modeled theoretically. A glance at the many reactive species listed in Table 1, and the high degree of unsaturation found despite the overwhelming H<sub>2</sub> abundance, drives home

the essential point of interstellar chemistry - kinetic factors dominate thermodynamics. The result is a highly non-equilibrium chemical composition that is very sensitive to physical properties of the environment, time scales, and initial conditions. Once appropriate rate constants have been measured or estimated, however, large scale kinetic modeling of the chemistry is possible. The temporal behavior of the concentration  $X$  of a chemical species in the gas phase is given by the sum of three terms:

$$(dX_k/dt)_t = (dX_k/dt)_g + (dX_k/dt)_p + (dX_k/dt)_d \quad k = 1, \dots, s$$

where

$(dX_k/dt)_g$  = rate of change due to gas phase reactions

$(dX_k/dt)_p$  = rate of change due to physical motions (collapse, outflow)

$(dX_k/dt)_d$  = rate of change due to interaction with dust grains

$s$  = total number of chemical species.

Mathematically, the chemistry is modeled using matrix methods and a master equation for the total rate of change of the concentration of a species  $X_k$ , namely

$$(dX_k/dt) = \sum_{j=1}^q \nu_{ij} ( \alpha_j \prod_{i=1}^s X_i^{\alpha_{ij}} ) \quad k = 1, \dots, s$$

over all  $i, j$ .  $\nu_{ij}$  are the stoichiometric coefficients of a given reaction channel, and  $\alpha_j$  are the reaction rates. The resulting equations are stiff, that is the rates of change  $(dX_k/dt)$  vary by orders of magnitude, necessitating involved differential equation solvers such as the Gear's method. Nevertheless, modern supercomputer technology allows time dependent calculations with as many as several hundred reactants and several thousand reactions to be performed.

Initial conditions for the differential equations are selected from observations of diffuse clouds, with incremental numerical integration of the total reaction matrix producing the abundances of selected species as a function of time. The most recent calculations have included cosmic ray ionization, positive and negative ion-molecule reactions, radiative association, electron recombination, photoprocessing, etc. Some models incorporating crude dynamical effects have also been reported, but none of these large time dependent models have addressed, in a realistic way, the nature of gas-grain interactions<sup>7,8</sup>. Another major limitation of gas phase modeling is a lack of experimental measurements of some crucial reaction rates and their branching ratios, most notably those involving the neutral atomic species C, N, and O, and electron recombination processes involving molecular ions.

A simplified view of the ion-molecule chemistry in dense molecular clouds as determined by such large scale models is shown in Figure 2<sup>9</sup>. In diffuse clouds, the vast majority of the gas phase carbon is present as  $C^+$  (C II) due to the permeation of energetic UV photons throughout the cloud. In denser clouds, the UV flux is reduced markedly, and impact by cosmic rays becomes the primary ionization mechanism for cloud column densities up to  $10^{25} \text{ cm}^{-2}$ . At higher column densities the cosmic rays no longer penetrate to the center of the cloud. Initial products of the cosmic ray bombardment are energetic  $H_2^+$  and  $He^+$  ions.  $H_2^+$  then reacts upon every collision with neutral molecular hydrogen to produce  $H_3^+$ , which along with  $He^+$  then leads to a wide variety of reaction paths among the first and second row elements. In this way, the energy deposited within the cloud by the cosmic rays is converted into chemical complexity, thereby providing the continual input required to maintain the chemical disequilibrium.

## DENSE CLOUDS: FLOW OF IONIZATION

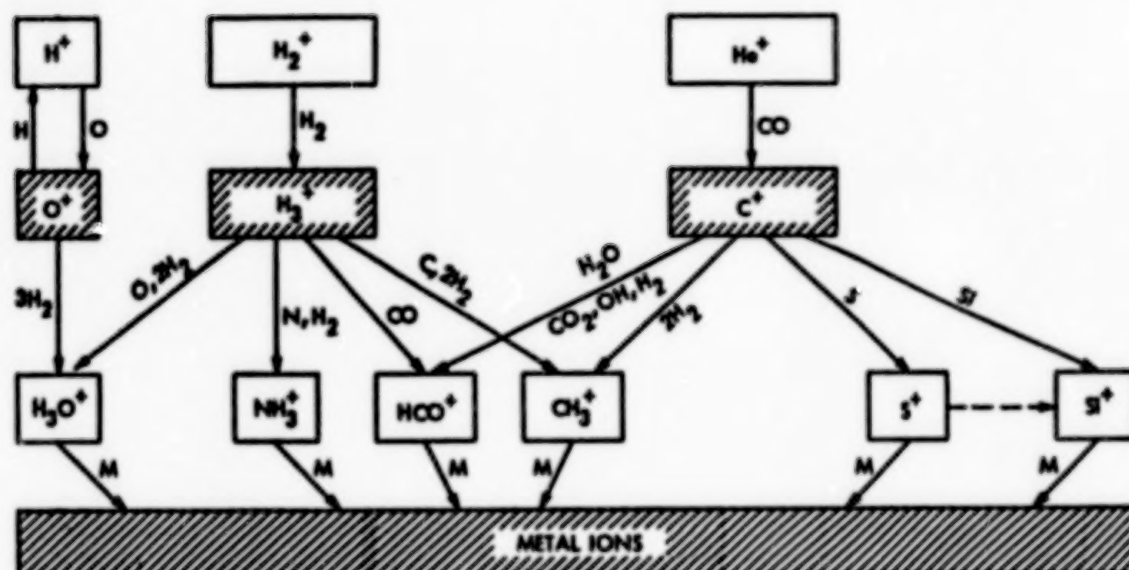


Figure 2.- Flow of ionization in dense clouds and the initiation of gas phase chemistry<sup>9</sup>.

The lack of intense UV sources within most molecular clouds and the large attenuation caused by dust leads to a dramatic drop in the ionization fraction in dense clouds as compared with more diffuse objects. Whereas in diffuse clouds the fractional ionization is near  $10^{-4}$  (from the photoionization of atomic carbon), in dense clouds it is closer to  $10^{-8}$ . Accordingly, the ionized carbon becomes gradually neutralized. Reactions of C II and C I with species such as O,  $O_2$ , or OH then form CO, while reactions with  $H_3^+$  or  $H_2$  begin the hydrocarbon chemistry. A schematic outline of the coupling of the carbon and oxygen chemistry in dense clouds is presented in Figure 3. The great stability of CO is such that this channel dominates over the hydrocarbon routes. Indeed, the only important *chemical* reaction of CO is with cosmic ray induced  $He^+$ , which regenerates  $C^+$ . Without this "leak", the C II  $\rightarrow$  C I  $\rightarrow$  CO conversion sequence would completely dominate the carbon chemistry in dense clouds. For example, even when material is driven into the hydrocarbon channels, oxidation still remains the primary limitation to the evolution of molecular complexity. The close coupling of complex molecules with the atomic carbon/CO network is most clear in time dependent calculations of the carbon chemistry, where the C I abundance climbs early in the cloud lifetime but then drops as steady state is approached. Similar curves are observed for more complex species such as  $CH_3OH$ , but with a considerable time lag<sup>1</sup>. A more thorough discussion of C II  $\rightarrow$  C I  $\rightarrow$  CO sequence and its impact on the carbon budget in molecular clouds is presented in the accompanying review by J. Keene.



scale kinetic modeling of interstellar chemistry beyond the formation of the initial  $H_2$  bond. Nevertheless, it is clear from numerous experiments, principally those performed by Greenberg and co-workers<sup>10,11</sup>, that grains will not be chemically inert in the interstellar medium.

Even if grains were chemically inert, however, they would still influence the chemical composition of molecular clouds through selective depletion processes. Indeed, following diffuse cloud observations gas phase models of dense cloud chemistry assume that 80-90% of the cosmically available C, N, and O atoms are depleted onto grains. "Metals" such as Si, S, or Fe are depleted by factors exceeding 100. To see why, consider a molecular cloud with a central density of  $10^5 \text{ cm}^{-3}$  and a kinetic temperature of 20 K with a "standard" gas-to-dust ratio. Simple calculations show that the time required for complete depletion of the condensable gas phase material onto grains to be

$$\tau_{\text{depletion}} = 10^9 / n_{H_2} y_s \quad \text{yr},$$

where  $y_s$  is the sticking coefficient, or about  $10^5$  years even for models where only one collision in ten results in adsorption. Direct evidence of molecules trapped on grains is provided through the observations of solid state vibrational features of CO,  $H_2O$ ,  $NH_3$ , etc. in the mid-infrared<sup>12</sup>. This depletion time scale is much less than estimated cloud lifetimes of nearly  $10^7$  years, and implies that at the very least some efficient desorption mechanism must exist for returning grain mantles into the gas phase. Several such mechanisms have been suggested, ranging from shocks, spot heating by cosmic rays and X-rays, or grain-grain collisions to grain mantle chemical explosions, but none have been definitively established<sup>13,14</sup>.

Estimates of the chemical reactivity of grains must include several processes: collisional capture of gas phase atoms and molecules, migration of trapped species over the grain surface, reaction between species on the grain surface (including photo-processing of the grain mantle) and ejection of reaction products into the gas phase. All of these factors are very sensitive to the exact nature of the grain surface, and may vary widely depending on the reacting species and the substrate. Nevertheless, certain general features have become clear from recent experiments. For a more complete review of these processes, see the contributions from M. Greenberg, L. Allamandola, and A. Tielens in these proceedings. Basically, it has been determined theoretically that even at the low temperatures characterizing interstellar grains, H and  $H_2$  (and some heavier atoms as well) can "scan" the grain surface rapidly and react with heavier or more strongly bound species. This produces primarily heavily hydrogenated species such as  $NH_3$ ,  $H_2CO$ ,  $CH_3OH$ , etc. Exposure of such an icy grain mantle to UV radiation creates energetic radicals within the matrix, which when heated sufficiently can explosively drive off much of the mantle leaving behind an organic refractory residue. In this way, molecules are returned to the gas phase while organic grain mantles continue to grow. The only drawbacks of these otherwise elegant experiments are the difficulty of simulating hydrogen rich grain mantles, and the lack of detailed kinetic data necessary to produce realistic models of the chemical potential of grains in molecular clouds.

As previously noted, models to date have really concentrated on either only gas phase or surface processes. That is to say, large models of the gas phase chemistry have not dealt with depletion onto and chemical modification within grain mantles, and grain mantle models have not incorporated realistic models of the gas phase chemistry. A limited set of calculations by d'Hendecourt *et al.*<sup>15</sup> have shown, however, that plausible desorption mechanisms can prevent a complete removal of the gas phase component of dense molecular clouds. In this calculation, the abundances of a small set of molecules, constrained to be identical in the gas phase and in grain mantles for computational stability, were examined using grain-grain collisions and subsequent

chemical explosions as the desorption scheme. The requirements for computational stability also underline a second problem with comparing the relative importance of gas phase and surface chemistry to observations, namely, the similarity of simple molecules produced. For example, both gas phase and grain chemistry can produce the observed quantities of  $\text{H}_2\text{O}$ ,  $\text{CH}_3\text{OH}$ ,  $\text{HCN}$ , etc., and it is not possible based on the observations of such species to conclude which process, if either, dominates. The real key is to find "signposts" of each which may be unambiguously assigned to either process given large observational uncertainties. Molecular ions and reactive isomers like  $\text{HNC}$  or  $\text{CH}_3\text{NC}$  are probably such molecules for gas phase chemistry, neither can be convincingly produced on grain surfaces. Likewise, the observations of significant enhancements of saturated molecules such as  $\text{C}_2\text{H}_3\text{CN}$  or  $\text{C}_3\text{H}_3\text{CN}$  in the warmest regions of active star forming clouds (see next section) are powerful arguments for the pervasiveness of surface catalysis. The most pressing need in grain chemistry models at the moment is experimental measurement of the mobility and reactivity of simple molecules on realistic cosmochemical substrates. We note that such measurements are now feasible using state-of-the-art surface science instruments.

### III. OBSERVATIONAL CHARACTERIZATION OF DENSE CLOUD CHEMISTRY

Due to the opaque nature of the atmosphere in many wavelength regions and the relatively insensitive nature of early receiver/telescope combinations, most of the previous observational work on the chemistry of dense molecular clouds has proceeded through a biased selection of molecules on a line-by-line basis. Nevertheless, a marvelous pattern of great chemical complexity has emerged from these observations, with both familiar species such as  $\text{CO}$ ,  $\text{H}_2\text{O}$ , or  $\text{CH}_3\text{OH}$  and highly unusual molecules like  $\text{HCO}^+$ ,  $\text{HC}_3\text{N}$ , or  $\text{SiC}_2$  present in considerable abundance. Although most of the detected molecules have low lying transitions in the microwave range, for accurate measurements of their excitation and abundance it is necessary to examine higher  $J$  levels whose transitions occur most prominently in the millimeter and submillimeter regimes. Indeed, the rotational envelope maxima of most molecules in dense clouds lie between 200 and 600 GHz where only a small amount of research has been performed.

Recent developments in receiver and telescope technology have allowed unbiased surveys of small regions in the millimeter-wave spectrum below 200 GHz to be recorded for the brightest objects in the sky such as the Orion and Sagittarius giant molecular clouds at the Onsala Radio Observatory and at AT&T Bell Laboratories<sup>16,17</sup>. Advantages of line surveys versus selected observations include completeness, better calibration, certainty of identification, and measurement of the total integrated line flux. Construction of higher frequency superconductor-insulator-superconductor (SIS) receivers at Caltech, and the improved performance possible with the large 10.4m telescopes of the Owens Valley Radio Observatory (OVRO), permitted a high sensitivity survey of the Orion molecular cloud (OMC-1) between 208-263 GHz<sup>18,19</sup>. This survey was conducted, in part, as an attempt to preview the millimeter and submillimeter wave spectra of dense molecular clouds obtainable with the new generation of submillimeter telescopes now becoming operational worldwide. A compressed view of the spectrum is presented in Figure 4. Nearly 900 resolved spectral features, arising from some thirty species in sixteen varying isotopic substitutions, have been detected. Of these, less than 15 remain currently unidentified! Analyses of the intensities of the emission features after a deconvolution of their line profiles have resulted in accurate estimates of the abundances of the molecular species in different regions of the cloud, and have shown that the tremendously heterogeneous composition of the Orion cloud core may be simply interpreted in the framework of the interaction between a quiescent molecular cloud chemistry and that induced by massive star formation within the cloud core. At the noise level

of the OVRO survey (0.2 K) roughly 50% of the 1.3 mm spectrum contains detectable emission, with the integrated molecular line flux accounting for at least 40% of the total radiative output of the cloud at these wavelengths.

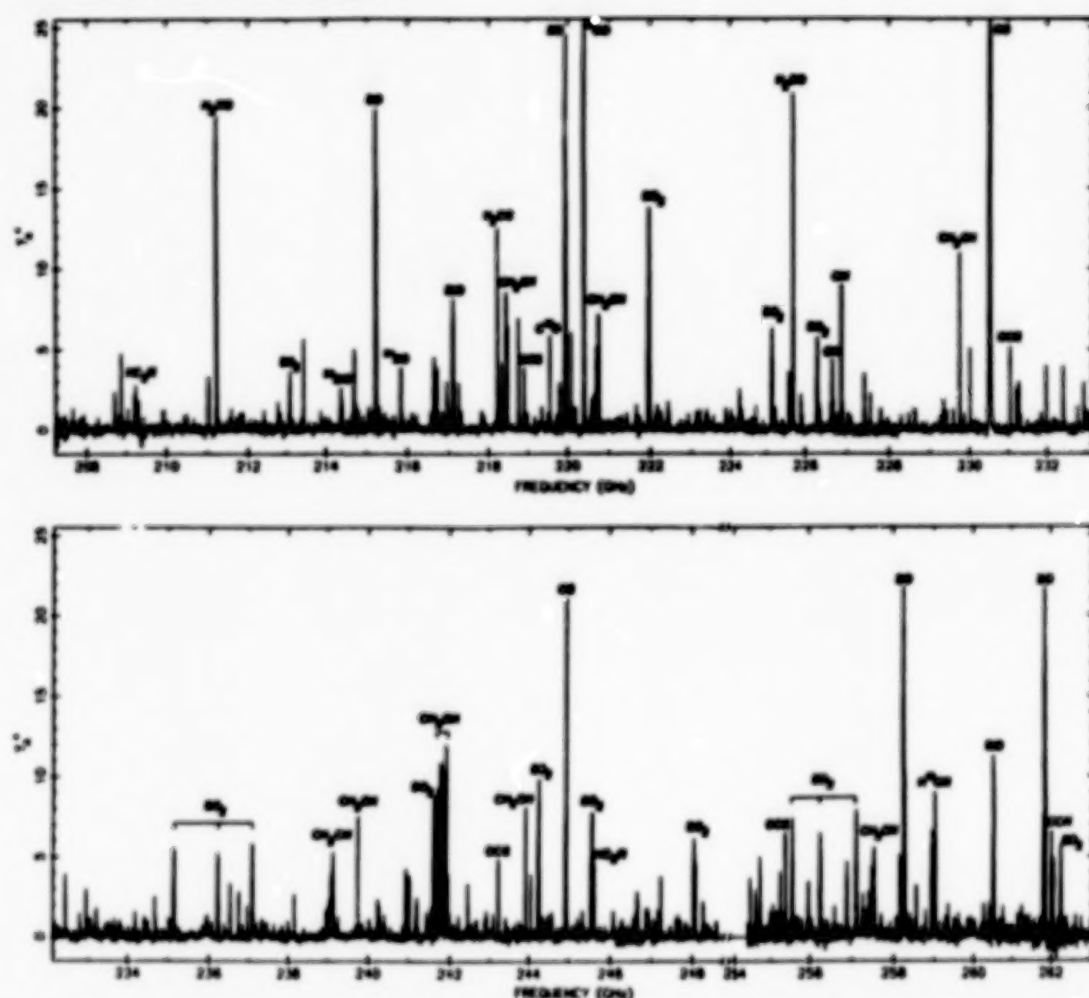


Figure 4.- Compressed millimeter-wave survey of OMC-1 near 1.3 mm. Nearly 900 resolved features have been detected, all but 13 of which are identified.

The total observing time required for this spectrum was approximately 28 nights during which the average optical depth at the zenith was 0.3. Data reduction took several hundred hours of computer time and months of human analysis. Indeed, identifications of the many lines left after comparison with publicly available spectral line catalogs would not have been possible without a vigorous, complementary laboratory program carried out at Duke University and the Jet Propulsion Laboratory. Catalog incompleteness will continue to be a problem, especially as new line searches move into the submillimeter region where laboratory observations are sparse, and an essential part of future programs must be continued close ties and access to state-of-the-art laboratory spectrometers. The improved sensitivity of the new telescopes will give roughly a factor of ten increase in speed, and will enable the chemical composition of many interstellar objects to be determined for the first time.

### The Caltech OVRO 1.3mm Survey of OMC-1

A major goal of such surveys will be an assessment of the influence of the chemistry which occurs in diffuse and dense molecular clouds on the formation of stars and planets. That is to say, does the star formation process completely erase the chemical history of matter used to build, for example, the solar system, or is memory significant? The Orion-Monoceros complex, of which OMC-1 is but a small part, lies only 500 pc from the sun. Due to its proximity and brightness, it has become the prototypical star formation region. Here, we use the studies of this cloud to outline the tremendous chemical heterogeneity of star forming clouds and the impact of this heterogeneity on the evolution of early bodies in the solar system. A more complete description of the OVRO linesearch and its chemical implications has been presented by Blake *et al.*<sup>20</sup>

The cool and extended gas of the Orion-Monoceros complex is visible in observations of OMC-1 as a strip or "ridge" of material running roughly N-S. A velocity gradient exists across the cloud, with the southern section appearing at  $8 \text{ km s}^{-1}$  and the northern section appearing at  $10 \text{ km s}^{-1}$ . In the center of the cloud several compact sources dominate the spectral appearance of this source in both continuum and spectral line observations, associated primarily with IRc 2; a young, massive star which is in the process of disrupting the cloud core. Most prominent among these sources is the "plateau" feature, so named for the broad lines which emanate from this region. First observed as very high velocity wings of  $\text{CO}^{21}$ , this source has since been observed in many molecules and seems to possess two distinct signatures. The first is a high velocity outflow with speeds of up to  $100 \text{ km s}^{-1}$ , and the second is a "low" velocity outflow with linewidths closer to  $20 \text{ km s}^{-1}$ .

The supersonic velocities in the plateau gas drive shocks into the surrounding medium, compressing and heating the gas. A particularly interesting region of this type in OMC-1 has been labelled the "compact ridge" source, and lies slightly south of IRc 2 on the edge of the  $8 \text{ km s}^{-1}$  ridge cloud. As its name implies, it is unresolved in single dish maps. It is slightly warmer than the extended ridge ( $100\text{--}150 \text{ K}$  versus  $40\text{--}50 \text{ K}$ ) and it also has a noticeably different chemistry. Closer to IRc 2 itself is a large clump, or set of clumps, known as the "hot core", with temperatures and densities approaching  $300 \text{ K}$  and  $10^8 \text{ cm}^{-3}$ . Unlike either the plateau or compact ridge sources, it is heated passively by radiation from the young star(s). Differences in the spectral line profiles of these sources must be used to deconvolve their individual contributions in single dish surveys of OMC-1 because they are often superposed along the line of sight. With recently developed millimeter wave interferometers, however, it has been possible to examine the chemical variations within this surprising source at high angular resolution.

Many different models of the Orion cloud core have been presented, but all boil down to essentially this: Outflow from IRc 2 creates directly the low and high velocity plateau sources. Where these winds strike the surrounding cloud shocks are created. In the shock front themselves the temperatures are very high, but regions close to and not in direct contact with the shock will be heated and compressed (the compact ridge). The high velocity plateau is formed along the most rapid density gradients in the cloud, while the low velocity plateau is created where the outflowing wind strikes the densest parts of the surrounding medium. Material left over from the formation of IRc 2 but not yet disrupted by the outflow is observed as the hot core. We now examine the chemical content of these four regions, starting first with the extended ridge clouds.

Early observations of simple species such as  $\text{H}_2\text{CO}$  and  $\text{HCN}$  in molecular clouds showed a strong correlation of abundance with density, an effect ascribed to the depletion of molecules onto grain mantles. A major result of more recent observations, especially the accurately calibrated spectral line surveys from Onsala, OVRO, and Bell Labs, is that the abundances of simple species

appear to be rather constant not only in dense clouds, but in other sources as well. Table 2 presents a listing of some of the more abundant molecules in the Orion, Sagittarius, and Taurus molecular clouds in addition to their predicted abundances in the gas phase model of Herbst and Leung<sup>22</sup>. The two predictions refer to gas phase C/O ratios of 0.4 (solar) and 1.3. As may be seen, the abundances of species like CO, CS, and HCO<sup>+</sup> are roughly constant, and their abundance is well predicted by the gas phase model.

Table 2  
MOLECULAR ABUNDANCES IN QUIESCENT CLOUDS

SPECIES	ABUNDANCE RELATIVE TO H <sub>2</sub>			Herbst and Leung <sup>a</sup>	
	OMC-1 <sup>b</sup>	Sgr B2 <sup>c</sup>	TMC-1 <sup>d</sup>	Model 1 <sup>e</sup>	Model 2 <sup>f</sup>
CO	$5.0 \times 10^{-5}$	$6.0 \times 10^{-5}$	$5.8 \times 10^{-5}$	$1.5 \times 10^{-4}$	$3.4 \times 10^{-4}$
CN	$3.3 \times 10^{-9}$	$3.4 \times 10^{-10}$	$3.0 \times 10^{-9}$	$3.2 \times 10^{-9}$	$2.4 \times 10^{-9}$
CS	$2.5 \times 10^{-9}$	$3.0 \times 10^{-9}$	$2.0 \times 10^{-9}$	$4.8 \times 10^{-9}$	$1.5 \times 10^{-9}$
SO	$\leq 9.3 \times 10^{-10}$	$1.5 \times 10^{-10}$	$5.0 \times 10^{-9}$	$1.2 \times 10^{-9}$	$4.5 \times 10^{-11}$
SO <sub>2</sub>	$< 3.3 \times 10^{-9}$	$2.0 \times 10^{-9}$	---	$4.8 \times 10^{-9}$	$1.3 \times 10^{-12}$
C <sub>2</sub> H	$5.3 \times 10^{-9}$	---	$8.4 \times 10^{-9}$	$2.4 \times 10^{-10}$	$2.7 \times 10^{-6}$
HCH	$5.0 \times 10^{-9}$	$\sim 3.0 \times 10^{-9}$	$1.2 \times 10^{-9}$	$5.5 \times 10^{-9}$	$1.0 \times 10^{-6}$
HNC	$5.3 \times 10^{-10}$	$\sim 3.0 \times 10^{-9}$	$8.0 \times 10^{-9}$	$5.5 \times 10^{-9}$	$1.0 \times 10^{-6}$
HCO <sup>+</sup>	$2.3 \times 10^{-9}$	$2.3 \times 10^{-9}$	$8.0 \times 10^{-9}$	$1.0 \times 10^{-8}$	$7.3 \times 10^{-8}$
HCS <sup>+</sup>	$5.3 \times 10^{-11}$	$3.0 \times 10^{-11}$	$5.0 \times 10^{-10}$	$1.4 \times 10^{-11}$	$5.3 \times 10^{-11}$
H <sub>2</sub> D <sup>+</sup> <sup>g</sup>	$\sim 1.0 \times 10^{-10}$	---	$< 3.0 \times 10^{-9}$	---	$\sim 1.1 \times 10^{-10}$
HC <sub>3</sub> N	$1.3 \times 10^{-10}$	$3.8 \times 10^{-10}$	$6.0 \times 10^{-9}$	$3.5 \times 10^{-12}$	$9.2 \times 10^{-8}$
HC <sub>4</sub> N	$\leq 2.3 \times 10^{-11}$	---	$1.0 \times 10^{-9}$	$8.9 \times 10^{-12}$	$6.2 \times 10^{-10}$
CH <sub>3</sub> CN	$3.2 \times 10^{-10}$	$2.0 \times 10^{-10}$	$5.0 \times 10^{-10}$	$1.5 \times 10^{-11}$	$8.5 \times 10^{-8}$
H <sub>2</sub> CO	$1.7 \times 10^{-8}$	$3.0 \times 10^{-9}$	$1.2 \times 10^{-8}$	$7.7 \times 10^{-9}$	$5.7 \times 10^{-8}$
CH <sub>3</sub> OH	$1.2 \times 10^{-7}$	$2.0 \times 10^{-8}$	---	$5.6 \times 10^{-10}$	$1.6 \times 10^{-8}$

<sup>a</sup> Derived from this work and Johansson *et al.* (16)

<sup>b</sup> Derived from Cummins, Link, and Thaddeus (17)

<sup>c</sup> From the data compilation in Leung, Herbst, and Huerber (23)

<sup>d</sup> Ref. 22.

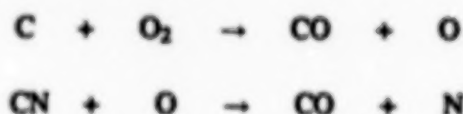
<sup>e</sup> Model results for C/O = 0.4,  $n_{H_2} = 10^5 \text{ cm}^{-3}$ ,  $t = 10^5 \text{ yr}$ .

<sup>f</sup> Model results for C/O = 1.3,  $n_{H_2} = 10^5 \text{ cm}^{-3}$ ,  $t = 10^5 \text{ yr}$ .

<sup>g</sup> Abundances derived by Phillips *et al.* (24)

To a great extent, the agreement between observation and gas phase theory must be considered coincidental. For example, many of the reactions used in the model have not been measured experimentally; and as we have noted earlier gas-grain interactions have not been taken into account. The lack of abundance correlations with density does suggest, however, that for many species gas phase processes dominate their chemistry and also that an efficient grain desorption mechanism must exist which either does not significantly chemically process material or which produces species similar to those inferred from ion-molecule reaction networks.

The most glaring deficiencies in the model involve atomic carbon and related molecular species such as CCH and the polyacetylenes. This problem is especially severe in cold clouds like TMC-1, as Table 2 demonstrates. At steady state most gas phase models predict little C I or other carbon rich radicals because reactions like



convert most of these species into more stable forms ( $O_2$  is predicted to be a major oxygen reservoir). Thus, for molecular species other than CO these models predict that the observable C and O inventories should reflect the total C/O ratio. Of all the species studied to date, C I shows the greatest discrepancy; and several mechanisms have therefore been brought forward to explain the high observed abundance. These proposals are discussed more fully by J. Keene in this volume. We simply wish to note here that although most of the abundances of simple closed shell species are well predicted by gas phase models, abundances of reactive hydrocarbon radicals are not. A related problem, discussed in more detail later, is the high abundances of complex species like  $CH_3OH$  and  $HCOOCH_3$  also observed in clouds like OMC-1. The basic question is how clouds can simultaneously be rich in reactive carbon rich radicals like CCH and also in stable oxygen containing species like  $HCOOCH_3$ . As might be expected, the answer most likely lies in the complex physical variations of molecular clouds along a given line of sight and the finite spatial resolution that characterizes any observational study of dense cloud chemistry.

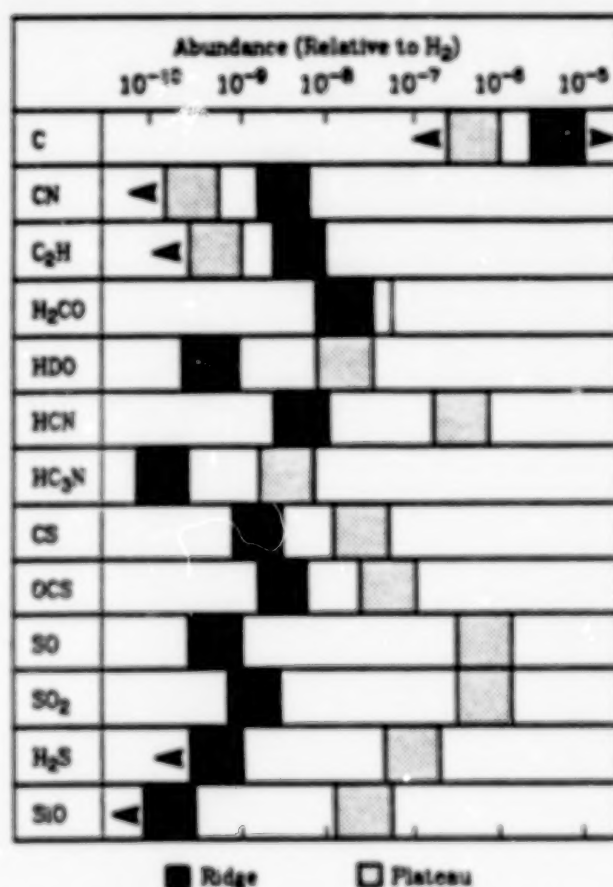


Figure 5.- Graphical comparison of the OMC-1 ridge and plateau fractional abundances.

For example, outflowing gas from IRc 2 lies along the same line of sight as much of the surrounding quiescent cloud, and signals from each region will be detected simultaneously by millimeter-wave telescopes. Whereas gas in the exterior regions appears to be controlled primarily by ion-molecule chemistry and depletion effects, the chemical composition of the plateau material is dominated by high temperature chemistry induced by shocks. A graphical demonstration of

the differences between the quiescent ridge chemistry and that of the plateau source is depicted in Figure 5. The most striking result is the tremendous drop in the abundances of carbon rich species like C, CCH, and CN and the concomitant rise in the abundance of species such as H<sub>2</sub>O, SiO, H<sub>2</sub>S, and SO<sub>2</sub>. While the extended ridge clouds appear observationally to have a deficit of oxygen in the gas phase, the plateau gas seems to have a gas phase C/O ratio that is solar or lower. Indeed, whereas the extended ridge C/O ratio in forms other than CO is much greater than unity, in the plateau source it is much smaller than unity. The higher oxygen fugacity and the very high temperatures behind the shock front drive most of the carbon into stable forms such as CO, but also enhance the abundances of more refractory species such as sulfur and silicon via grain disruption or evaporation.

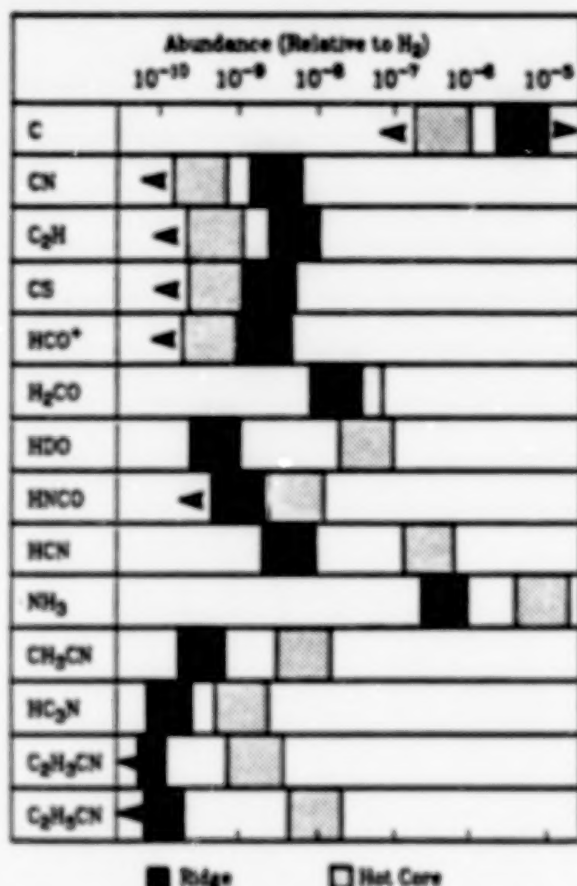


Figure 6.- Graphical comparison of the OMC-1 ridge and hot core abundances.

High temperature chemistry is also evident in observations of the hot core, but with a considerably different signature. Here the critical importance of gas-grain interactions become apparent as is shown graphically in Figure 6. Again, the abundances of reactive, carbon rich species like C, CCH, and CN are significantly reduced, with the observed C/O ratio in molecular form less than unity. Because the heating is passive, however, grain vaporization does not occur and the abundances of the refractory sulfur and silicon species remain low. The high densities and temperatures in this source shut down ion-molecule networks, and are sufficient to release much of the material stored over the cloud lifetime in grain mantles. Indeed, the composition of the hot

core is most consistent with chemistry that is dominated by kinetic equilibrium and evaporation from grains. For example, water and ammonia are observed to be tremendously enhanced in the hot core to levels near that observed in near infrared absorption bands of water ice mantles on interstellar grains. The water observations are especially noteworthy as they are carried out using HDO, which seems to have retained significant deuterium fractionation even though the source kinetic temperature is well above 100 K. The most likely explanation is therefore that the observed HDO is "fossil" water trapped onto grains throughout the cloud lifetime and released when star formation has raised the grain temperatures sufficiently to release their icy mantles<sup>25</sup>. Further, the conversion of polyacetylenes into more hydrogenated species like  $\text{HC}_3\text{N} \rightarrow \text{C}_2\text{H}_3\text{CN}$  must occur on grains because reactions such as



are highly endothermic, while hydrogenation on surfaces is known to be fairly efficient, at least in the laboratory.

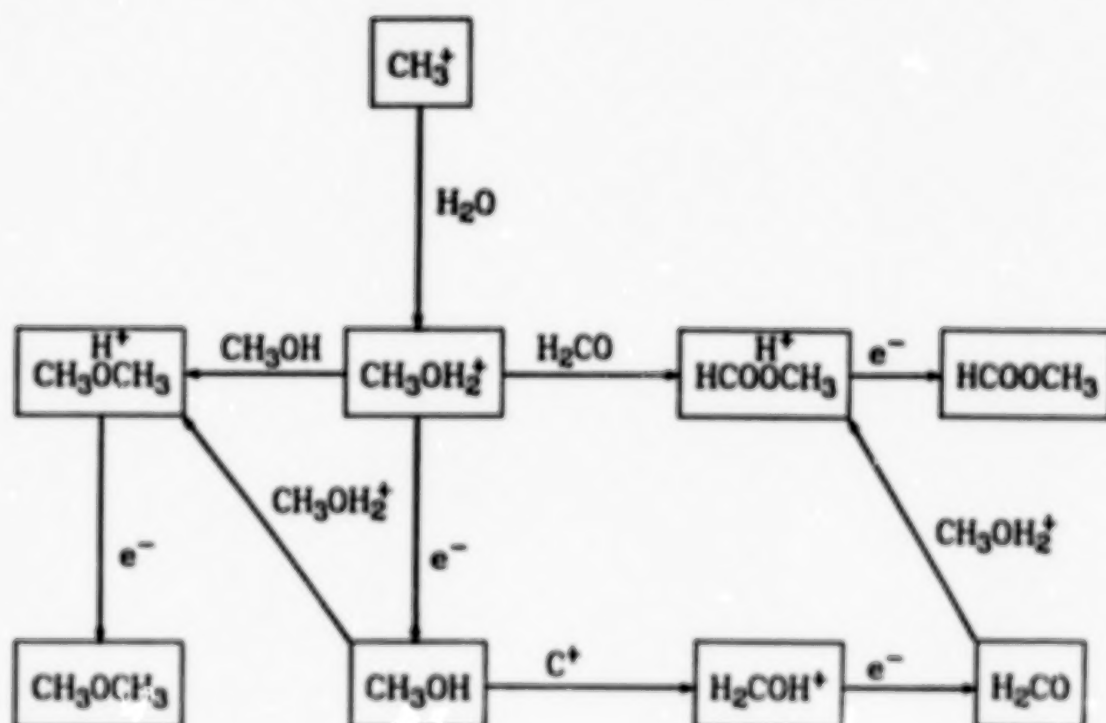


Figure 7.- Schematic outline of the proposed ion-molecule network responsible for the formation of complex molecules in the OMC-1 compact ridge.

Finally, the importance of mixing in active cores like that in OMC-1 is demonstrated by the composition of the compact ridge source. It is here that the abundances of complex oxygen containing organics such as  $\text{CH}_3\text{OH}$  and  $\text{HCOOCH}_3$  peak. These species could either

be produced by grain mantle hydrogenation of CO, etc., or by gas phase routes. A possible gas phase scenario is presented in Figure 7 which relies heavily on radiative association reactions of the type originally outlined by Herbst<sup>1</sup>. Theoretical predictions of the rates of such reactions, tested experimentally only for the  $\text{CH}_3^+ + \text{H}_2$  system<sup>26</sup>, indicate that they can become quite fast for large complexes - with some reactions occurring at the collision rate even in the presence of exothermic bimolecular channels! In this model, mixing of oxygen and water rich gas from the plateau with ion rich gas from the extended clouds is predicted to form the ionic precursor to methanol and methanol itself via the reactions



The resulting products then synthesize a variety of *isomerically specific* molecules such as dimethyl ether and methyl formate through reactions with other hydrocarbons. Larger species should also be formed by such networks, but their abundances will lie below that detectable with current instrumentation. The resulting C/O ratio in these larger species is near unity.

A major point in favor of the gas phase model versus grain mantle synthesis is the observational selectiveness of interstellar chemistry. Namely, dimethyl ether and methyl formate are found to be much more abundant than their isomers ethanol and acetic acid. A simple steady state solution to the chemistry outlined in Figure 7 reproduces the observed abundances in OMC-1 to within a factor of a few, and, while most likely fortuitous, is probably indicative of the dominance of a gas phase synthesis of these molecules.

Further evidence for the gas phase scheme is provided by recent high angular resolution observations of methanol in OMC-1 by Plambeck and Wright<sup>27</sup>. If methanol and the other related species were produced primarily by grain mantle catalysis, then they should show observational correlation with other grain mantle products. For example, ammonia, ethyl cyanide and water show striking observational similarities in Orion. Methanol, however, appears to be *anticorrelated* with these species. These and other observations are most consistent with a general model of active cloud cores in which the surrounding, cooler medium contains the bulk of the observed reactive hydrocarbons while the cloud cores have liberated the more refractory elements and driven the chemistry towards *kinetic equilibrium*.

#### Studies of the Chemical Evolution of Protostars

The Orion cloud core is an example of massive star formation, and a natural question is just how applicable the results from high mass sources are to the formation of lower mass stars like our own sun. In massive star forming clouds, clustering appears to be common, resulting in significant alteration of the overall cloud chemistry. It is generally accepted that, as single low mass stars condense out of molecular clouds, the circumstellar gas will gradually become flattened so that eventually the remnant cloud around the protostellar object will have a disk-like morphology, and that the gas surrounding the protostar need only represent a small fraction of the total cloud mass. With the advent of interferometric techniques at millimeter and infrared wavelengths it has recently become possible to identify such *disks* directly. Around the objects HL Tauri, L1551 IRS5 and IRAS 16293-2422, for example, are extended, flattened structures with radii of order a few hundred AU<sup>28,29</sup>. Because of the parallels with our own solar system, it is important to investigate such putative proto-planetary disks in considerable detail. While dynamical studies ultimately require the resources of instruments capable of higher resolution, single telescopes can explore the chemical nature of these disks. Broadband surveys such as

those outlined above may no longer be possible due to sensitivity limitations, but deep searches for selected species should give decent estimates of the chemical environment of circumstellar material.

Indeed, the necessity for chemical analyses of the immediate circumstellar environment of young stellar objects and protostars has already been highlighted by the case of IRAS 16293-2422. OVRO maps of this object in the lines of CO and its isotopes and VLA maps in  $\text{NH}_3$ , although at similar resolution, are markedly different. The OVRO  $\text{C}^{18}\text{O}$  and 2.7 mm continuum measurements suggest a disk of size  $1800 \times \leq 800$  AU. This disk is aligned perpendicular to the direction of a high velocity molecular outflow and the magnetic field. The  $\text{NH}_3$  maps show an elongated structure, with similar orientation, but considerably greater in extent, 7200 AU. In addition, at 2 cm the VLA indicates the presence of two compact continuum sources in the central core, separated by 800 AU and lying along the major axis of the disk. Obviously the  $\text{NH}_3$  is tracing different gas than the  $\text{C}^{18}\text{O}$ , but it is not clear without further analysis in different molecules precisely how to characterize the size and structure of the disk.

Numerical simulations of such disk like structure have now determined the likely temperature and density gradients in these objects. One finds that only in the inner few A.U. of the disk do temperatures climb high enough to vaporize the dust. At the distances of the major planets the temperatures have dropped sufficiently low that degassing of even the grain mantles becomes unlikely in the bulk gas. Models of the transport properties of accretion disks show that it is very difficult to move matter from large radii into smaller radii and back out again. The major result is thus that it is kinetically impossible to transform stable species such as CO and  $\text{N}_2$ , the dominant interstellar forms of carbon and nitrogen, into complex hydrocarbons via homogeneous gas phase chemistry at radii beyond 5-10 A.U. As such, one expects considerable persistence of memory in these objects, at least in the outer portion of the disk where major planets and comets form. The observations of significant fractionation effects in meteoritical and cometary particles as well as in planetary atmospheres may well be due to the preservation of primarily interstellar material.

Several processes will act to alter the composition from a pristine interstellar signature, however. Most of these effects are similar to those operating in massive molecular cloud cores, but on a much smaller scale. For example, as matter rains onto the disk from the surrounding molecular cloud, it experiences a discontinuous velocity change at the disk. This so called accretion shock front processes all of the infalling material through the high temperature environment of a roughly  $10 \text{ km s}^{-1}$  shock, although the effect drops sharply at larger radii. The investigation of shock chemistry and sputtering effects in this regime is therefore of the utmost importance. Secondly, although it is true that homogeneous gas phase conversion of CO and  $\text{N}_2$  into organics is prohibited in the bulk gas, in the regions around large gaseous protoplanets the increased temperatures and densities may be sufficient to drive such conversions<sup>30</sup>. As in the Orion hot core region, the high densities and temperatures reduce the effectiveness of ion-molecule chemistry, but enable new neutral-neutral pathways to emerge. Surface catalysis will also become considerably more active in such environments. Since comets have been hypothesized to arise from these regions, the alteration of protosolar gas and dust during planetary and cometary formation must be addressed in the future. Ideally, one would ultimately like to construct a kinetic model incorporating dynamical effects and heterogeneous catalysis in a realistic fashion. Before this can occur, however, increasingly rigorous theoretical calculations on the dynamics of the accretion process and experimental work on shock chemistry and surface catalysis must be performed.

#### IV. INTERSTELLAR SPECTROSCOPY OF LARGE MOLECULES

Recently, it has become clear that small carbonaceous "grains" of approximately 20-50 atoms may be responsible for much of the near infrared emission from reflection nebulae and also the unidentified IR emission features found throughout the galaxy. Indeed, many reviews at this conference addressed the importance of such small grains to the total carbon budget in the interstellar medium. The apparent lack of molecules between the 10-13 atom limit found by millimeter-wave astronomy and the  $0.1 \mu\text{m}$  grains detectable in the IR (about  $10^7$  atoms) is therefore most likely an observational selection effect. One of the important properties of the latest generation of precision radiotelescopes will be their ability to search for "large" molecules in dense clouds through their rotation-vibration bands in the submillimeter.

For example, microwave spectroscopy has detected long chain cyanopolyacetylenes of the form  $\text{H}-(\text{C}-\text{C})_x-\text{CN}$ , where the largest detected value of  $x$  is 6. Larger molecules simply have to many rotational states populated to be detected, that is, they are too large. The drop off in the abundance as successive acetylene units are attached is only a factor of three or so, implying that heavier chains are, in fact, present. Radicals like  $\text{C}_6\text{H}$  have also been detected, and it is likely that pure polyacetylene chains ( $\text{H}-(\text{C}-\text{C})_x-\text{H}$ ) and bare carbon clusters are also formed.

The latter species do not possess permanent dipole moments and are therefore undetectable in the microwave region regardless of their abundance or the sensitivity of the receivers employed. However, the lowest bending modes of such long chains begin in the far-infrared near  $45 \mu\text{m}$  for cyanoacetylene, and for chains longer than  $\text{HC}_9\text{N}$  or  $\text{HC}_{10}\text{H}$  these lowest modes appear in the range of ground-based telescopes. An important point is that even for totally symmetric species like  $\text{C}_{10}$  or  $\text{HC}_{10}\text{H}$  bending modes do possess finite dipole derivatives that make them, in principle, observable. A further advantage of these modes is the presence of Q-branch features at the band origin whose lines are split only by centrifugal distortion effects. At the low temperatures characterizing dense clouds, these Q-branch features, which are highly diagnostic, will be heavily blended. Many lines will therefore be superposed to create a much stronger central feature than is possible in pure rotational spectroscopy. Even in cold regions such as dark cloud cores the lowest bending states are sufficiently low in energy to be significantly populated. Previous laboratory work on these compounds will be essential, as theoretical models are clearly incapable of predicting the rotation-vibration spectra of such large chains with anything approaching the required accuracy. Indeed, one of the goals of the laboratory spectroscopy programs such as that described by Prof. Saykally in these proceedings is the analysis of the vibration-rotation modes of carbonaceous clusters. Once these bands have been detected and analyzed in the laboratory, searches for larger chains, and more condensed species as well, in opaque sources such as circumstellar envelopes and dense molecular clouds may begin.

#### V. CONCLUSIONS

A tremendous amount of both observational and theoretical progress has been made in the analysis of interstellar chemistry since the discovery of OH in dense clouds some twenty-five years ago. Plausible formation mechanisms in the gas phase and on grain surfaces now exist for most of the observed species, and models of their abundances can be performed. Observational work has given us not only estimates of the chemical composition of objects ranging from diffuse interstellar clouds to the extended atmospheres of evolved stars, but also significant constraints on the physical conditions there. While the general picture is fairly clear, for further progress to be made much more detailed work must be performed.

Observationally, we are now in a position to examine directly molecular cloud cores similar to that which formed the solar system. It will therefore be possible to probe, for the first time, changes which occur in the speciation of matter associated with the star formation process. In the laboratory, state-of-the-art experiments in laser spectroscopy and in surface science are in a position to examine processes directly relevant to the formation of gas and dust in the interstellar medium and their assembly into stars and planets. Only through a combination of such efforts will the true details of our origins be revealed.

## REFERENCES

- [1] Herbst, E., *Interstellar Processes*, Hollenbach, D.J. and Thronson, H.A., Jr. eds., D. Reidel Publ., 1987, pp. 611-630.
- [2] Prasad, S.S. *et al.*, *Interstellar Processes*, Hollenbach, D.J. and Thronson, H.A., Jr. eds., D. Reidel Publ., 1987, pp. 631-667.
- [3] Irvine, W.M., Goldsmith, P.F., and Hjalmarsen, A., *Interstellar Processes*, Hollenbach, D.J. and Thronson, H.A., Jr. eds., D. Reidel Publ., 1987, pp. 561-610.
- [4] Spitzer, L., Jr., *Physical Processes in the Interstellar Medium*, John Wiley and Sons, Inc.
- [5] *Gas Phase Ion Chemistry*, M.T. Bowers, ed., Academic Press, 1979.
- [6] Clary, D.C., *Mol. Phys.* **54**, 1985, p. 605.
- [7] Boland, W. and de Jong, T., *Astr. Ap.* **134**, 1984, p. 87.
- [8] Tarafdar, S.P. *et al.*, *Ap. J.* **289**, 1985, p. 220.
- [9] Prasad, S.S. and Huntress, W.T., Jr., *Ap. J. Suppl.* **43**, 1980, p. 1.
- [10] Hagen, W., Tielens, A.G.G.M., and Greenburg, J.M., *Astr. Ap.* **117**, 1983, p. 132.
- [11] Greenburg, J.M., *Workshop on Laboratory and Observational Infrared Spectra of Interstellar Dust*, Wolstencroft, R.D. and Greenburg, J.M., eds., Royal Observatory of Edinburgh Publ., 1983, pp.1-25.
- [12] Gillet, F.C. and Forrest, W.J., *Ap. J.* **179**, 1973, p. 483.
- [13] Williams, D.A. and Hartquist, T.W., *Mon. Not. Roy. Astr. Soc.* **210**, 1984, p. 41.
- [14] Leger, A., Jura, M., and Omont, A., *Astr. Ap.* **144**, 1985, p. 147.
- [15] d'Hendecourt, L.B., Allamandola, L.J., and Greenburg, J.M., *Astr. Ap.* **152**, 1985, p. 130.
- [16] Johansson, L.E.B. *et al.*, *Astr. Ap.* **130**, 1984, p. 227.
- [17] Cummins, S.E., Linke, R.A., and Thaddeus, P., *Ap. J. Suppl.* **60**, 1986, p. 819.
- [18] Sutton, E.C. *et al.*, *Ap. J. Suppl.* **58**, 1984, p. 341.

- [19] Blake, G.A. *et al.*, *Ap. J. Suppl.* 60, 1986, p. 357.
- [20] Blake, G.A. *et al.*, *Ap. J.* 315, 1987, p. 621.
- [21] Wilson, R.W., Jefferts, K.B., and Penzias, A.A., *Ap. J.(Letters)* 161, 1970, p. L43.
- [22] Herbst, E. and Leung, C.M., *Ap. J.* 310, 1986, p. 378.
- [23] Leung, C.M., Herbst, E., and Huebner, W.F., *Ap. J. Suppl.* 56, 1984, p. 231.
- [24] Phillips, T.G. *et al.*, *Ap. J.(Letters)* 294, 1985, p. L45.
- [25] Plambeck, R.L. and Wright, M.C.H., *Ap. J.(Letters)* 317, 1987, p. L101.
- [26] Barlow, S.E., Dunn, G.H., and Schauer, K., *Phys. Rev. Lett.* 52, 1984, p. 902.
- [27] Plambeck, R.L. and Wright, M.C.H., *Ap. J.(Letters)*, submitted.
- [28] Sargent, A.I. and Beckwith, S., *Ap. J.* 323, 1986, p. 294.
- [29] Mundy, L.G., Wilking, B.A., and Myers, S., *Ap. J.(Letters)* 311, 1986, pp. L75-L79.
- [30] Prinn, R.G. and Fegley, B., *Origin and Evolution of Atmospheres*, University of Arizona Press, 1988, in press. dvips

## C I, C II, AND CO AS TRACERS OF GAS PHASE CARBON

Jocelyn Keene

California Institute of Technology

In this talk I will be discussing the form of gas phase carbon in the dense interstellar medium. Since this is a very mixed audience, I will make this talk more of a tutorial, using illustrative references only, than a comprehensive review. Some relevant questions for this discussion are:

1. What are the major forms of gas phase carbon in the dense interstellar medium?
2. What are their abundances relative to hydrogen?
3. How are the major components related?
4. What controls their relative abundances and distribution?

I will try to answer the first two of these questions and will only briefly touch on the last two.

The discussion will center on dense molecular clouds for two reasons: *a*) molecular clouds are the sites of most of the interesting chemical processes in the interstellar medium and *b*) gaseous carbon in the diffuse interstellar medium is thought to be almost entirely singly ionized. Typical molecular clouds have kinetic temperatures of 10–100 K, depending on whether they are associated with star-formation regions. Average densities for giant molecular clouds are  $n(\text{H}_2) \gtrsim 10^2 \text{ cm}^{-3}$ , but this discussion will be slanted toward smaller and denser condensations,  $n(\text{H}_2) \gtrsim 10^4 \text{ cm}^{-3}$ , often associated with star formation.

It is thought that molecular clouds contain approximately half of the Galaxy's total gaseous mass although they occupy only a small fraction of the volume of the Galaxy. The imbalance between mass and volume occurs because, except for dense self-gravitating clouds, the general interstellar medium is approximately in pressure equilibrium and the other gas phases have higher temperatures and lower densities. Another small volume is occupied by cool neutral atomic gas,  $T \lesssim 100$ , concentrated in structures called "diffuse clouds" which may be associated with molecular clouds. About half of the volume of the Galaxy is occupied by neutral atomic and ionized gas components with temperatures  $T \lesssim 8000\text{K}$  and rest of it is occupied by a very hot,  $T \sim 10^6 \text{ K}$ , highly ionized gas component.<sup>1</sup>

### FUNDAMENTAL DATA

Table 1 is a list of the most abundant elements, with their ionization potentials.<sup>2</sup> It is important to notice three things:

1. carbon is the fourth most abundant element in the universe, with an abundance relative to hydrogen of  $3.3 \times 10^{-4}$ .
2. carbon's ionization potential, 11.26 eV, is the only one of the first 6 elements in this table lower than that of hydrogen. Not until iron, which is a factor of 8 less abundant, do you find a lower ionization potential. This means that, among atoms, carbon has virtually no competition for the interstellar ultraviolet radiation with photon energy between 11.26 and 13.6 eV and it will be easily ionized unless it is shielded by dust, an efficient continuum absorber of radiation.
3. the dissociation potential for the carbon monoxide molecule, listed at the bottom of the table, is very close to the ionization potential for carbon. Carbon monoxide is a very stable molecule, not highly reactive. In a shielded environment in which chemical reactions can occur it is the endpoint of these reactions. Also, oxygen, which is the other component of carbon monoxide, is twice as abundant as carbon. Therefore in a shielded environment it would be reasonable to expect most of the carbon to be in the form of CO.

TABLE I  
COSMIC ABUNDANCES

Element	Abundance	Ionization Potential (eV)
H	1.0	13.60
He	$8.5 \times 10^{-2}$	24.59
O	$6.6 \times 10^{-4}$	13.62
C	$3.3 \times 10^{-4}$	11.26
N	$9.1 \times 10^{-5}$	14.53
Ne	$8.3 \times 10^{-5}$	21.56
Fe	$4.0 \times 10^{-5}$	7.87
Si	$3.3 \times 10^{-5}$	8.15
Mg	$2.6 \times 10^{-5}$	7.65
S	$1.6 \times 10^{-5}$	10.36
Molecule		Dissociation Potential (eV)
CO		11.09

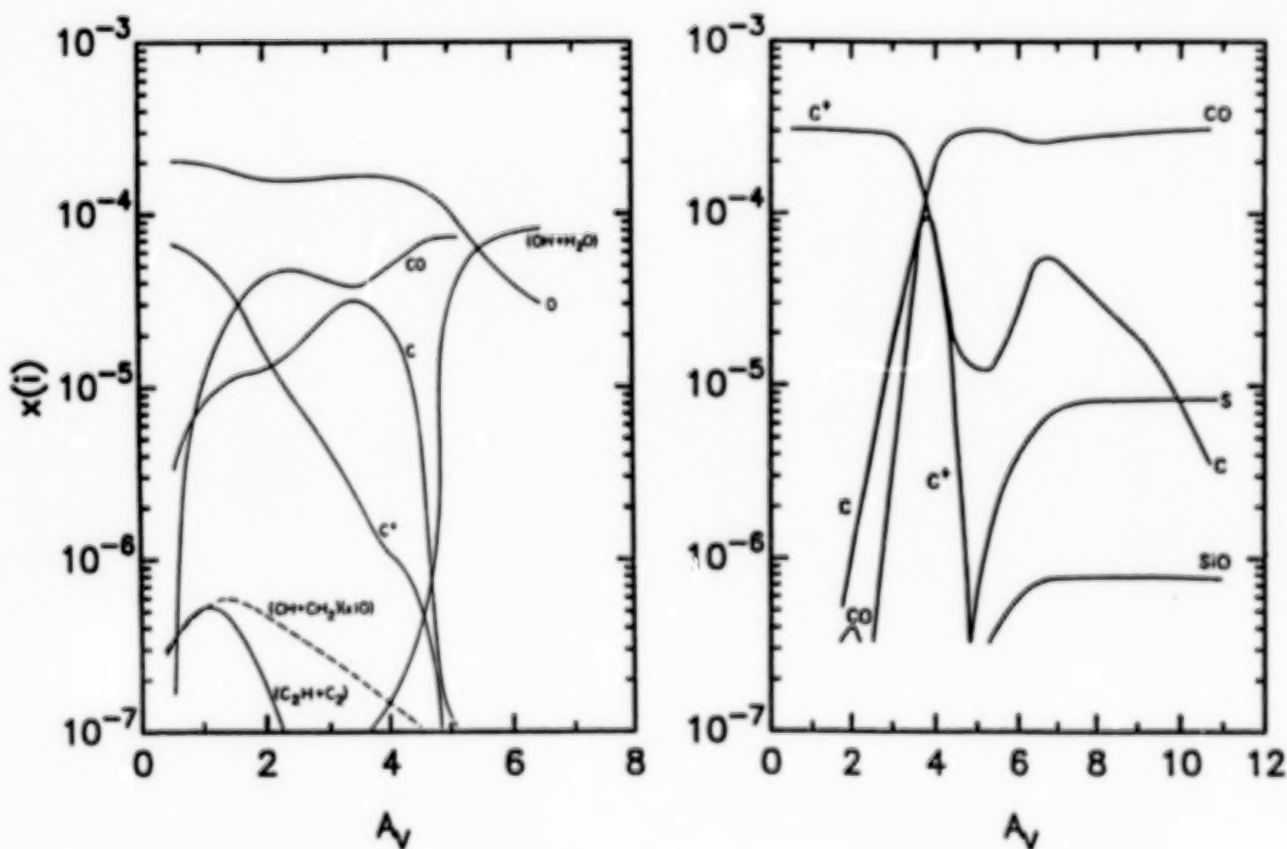


FIG. 1. - Fractional abundances as a function of visual extinction into a cloud *left*) from Langer,<sup>3</sup> with  $T = 20$  K,  $n(\text{H}) = 10^3 \text{ cm}^{-3}$ ,  $G = G_0$ ; *right*) from Tielens and Hollenbach,<sup>4</sup> with  $T = T(A_V)$ ,  $n(\text{H}) = 2.3 \times 10^5 \text{ cm}^{-3}$ ,  $G = 10^5 G_0$ .

## RESULTS OF CALCULATIONS

Steady state calculations, including the effects of the ultraviolet radiation field and chemical reactions, show that one might expect most of the carbon outside dense clouds to be ionized (hereafter C II), most of it within dark clouds to be in the form of carbon monoxide (CO), and, at the edges of clouds between these two regions, a fraction of it to be in a thin layer of neutral atomic carbon (C I). All other gas phase forms of carbon should be negligible compared with these. Figure 1 shows the results of two calculations on the abundances of carbon species near the edge of a cloud under different sets of conditions: *left*) a calculation for the case of a cool (20 K) cloud immersed in the general interstellar radiation field, and *right*) the Orion Molecular Cloud which lies just behind the Orion Nebula. The ultraviolet field illuminating the cloud ( $G$ , measured in units of  $G_0 = 1.6 \times 10^{-3} \text{ ergs cm}^{-2} \text{ s}^{-1}$ , the average intensity of the interstellar field) in the Orion model is enhanced by a factor of  $10^5$  because of the presence of the hot stars which produce the ionized nebula. Both these calculations show the qualitative results discussed above, i.e., that the carbon is expected to be mostly in the form of C II outside the cloud ( $A_V < 1$  to 2) and in the form of CO within the cloud. The exact dividing line between these two regimes and the position of the anticipated narrow shell of C I is determined by the amount of ultraviolet radiation illuminating the cloud.

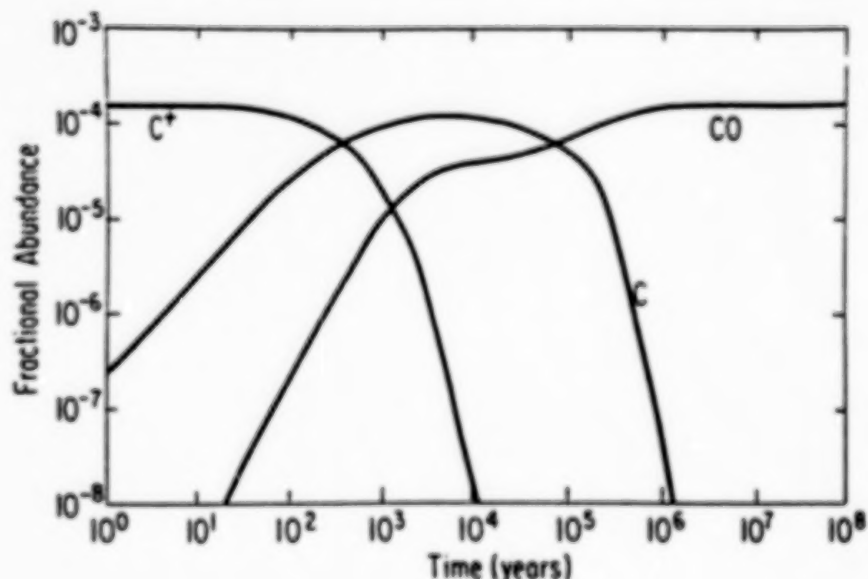


FIG. 2. - Fractional abundances as a function of time at the center of a well shielded cloud of density  $n(\text{H}_2) = 2 \times 10^4 \text{ cm}^{-3}$  from Leung, Herbst, and Heubner.<sup>5</sup>

Other calculations which follow the chemical time evolution of clouds show analogous effects. Figure 2 shows the results of an evolutionary model which at its origin in time had all the carbon in the form of C II, as a cloud would have before its collapse from the diffuse interstellar medium.<sup>5</sup> Since this calculation did not include the effects of ultraviolet radiation, these results are valid only for a region at the center of a cloud which is completely shielded from the ultraviolet radiation field at the edge. The calculation illustrates the point that  $\sim 10^6$  years after the initial collapse of a cloud there should be no C I left in the shielded cloud interiors. Since molecular clouds are thought to exist for at least  $10^7$  years, shown by the presence of young stars within many of them, the endpoint of this calculation should be relevant for the interiors of most molecular clouds today.

## SPECTRA OF CARBON SPECIES

C I, C II, and CO all have transitions in the far-infrared to millimeter wavelength region of the spectrum. This is important because only long wavelengths can pass through the dense material which makes up molecular clouds. They also have transitions in the ultraviolet to infrared spectral region that are useful for studying their abundances

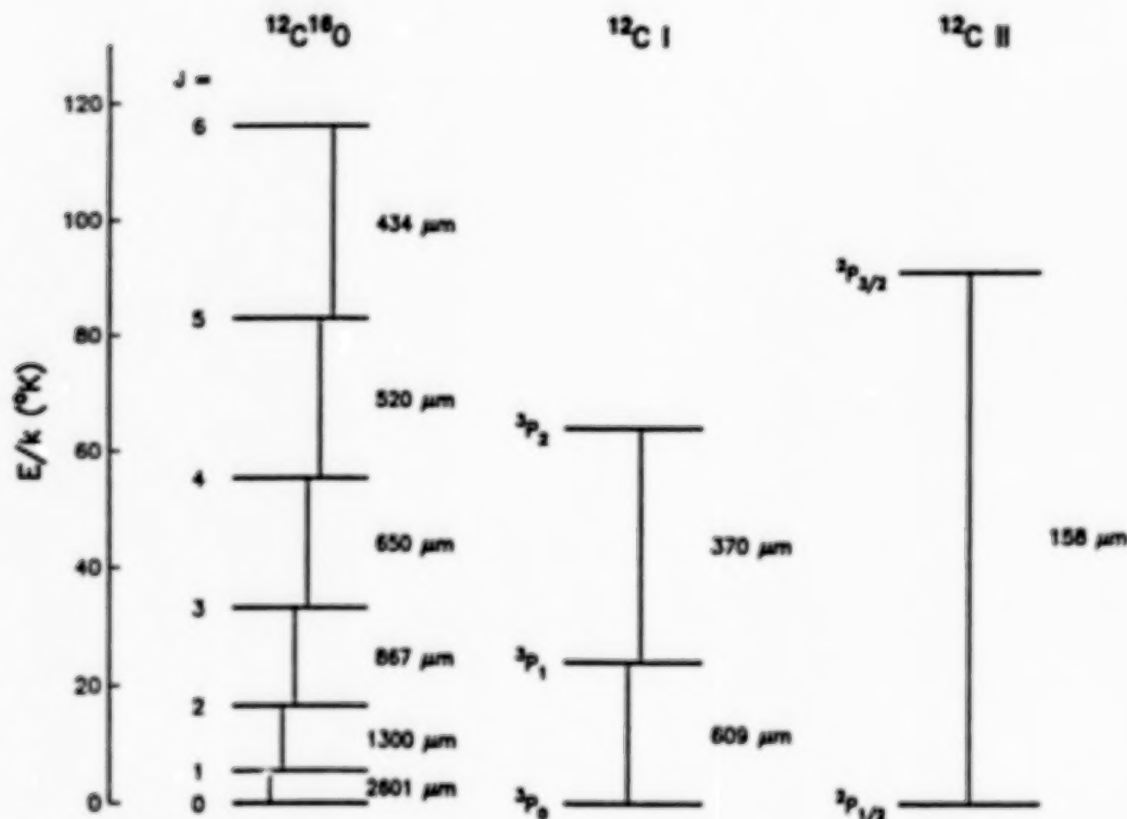


FIG. 3. – Energy levels of the three most common species of gas phase carbon and their transition wavelengths. The lowest transitions of these species all lie in the millimeter to far-infrared wavelength region. The energy levels are appropriate for excitation in typical interstellar clouds ( $T \approx 10\text{--}100\text{ K}$ ).

in more diffuse matter. Figure 3 shows the low-lying transitions for all three species and the energy of the upper states in units of  $E/k$ . The transitions of both C I and C II are magnetic-dipole fine-structure transitions, whereas those of CO are electric-dipole rotational transitions. The C I and CO transitions are well suited to studying both the cold ( $T < 20\text{ K}$ ) and the warm ( $T > 50\text{ K}$ ) interstellar media because of the presence of energy levels only 10's of degrees above the ground state, as well as higher levels. Unfortunately, the only C II ground state transition is quite high in energy (91 K) and is easily observed only in warm objects.

### CO ABUNDANCES

We would like to estimate the abundance of CO relative to hydrogen. This ratio is most often calculated by comparing the line of sight abundance of CO (column density) with the visual extinction ( $A_V$ ) from dust grains in the same line of sight. It is commonly assumed that the dust to hydrogen mass ratio is constant throughout the Galaxy so the column ratio of CO to hydrogen can be derived.

In order to compute column densities of CO, we have to understand its distribution among the available excitation levels and the photon propagation processes for individual clouds. The lines of the most common form of CO,  $^{12}\text{C}^{16}\text{O}$ , are usually optically thick, so that they cannot be used to measure the column density. Luckily both carbon and oxygen have isotopes which, although rare, are observable. In the Solar system the abundance ratios of the main isotopes to the rarer ones are:  $^{12}\text{C}/^{13}\text{C} = 89$ ,  $^{16}\text{O}/^{18}\text{O} = 500$ , and  $^{16}\text{O}/^{17}\text{O} = 2750$ .<sup>6</sup> The ratios in the interstellar medium are different from the Solar System values and are a function of position in the Galaxy.<sup>7</sup> Of course the isotopes can also be found in combinations, such as  $^{13}\text{C}^{18}\text{O}$ . (Hereafter, I will use the atomic mass superscript only when referring to one of the rare isotopes of carbon or oxygen.)  $^{13}\text{CO}$  is usually only moderately optically thick ( $\tau \approx 1$  in many sources), and  $\text{C}^{18}\text{O}$  is usually optically thin so that radiative transfer problems are minimized. These, as well as the even rarer forms, can be used to determine the abundance in one of the levels

of the observed transition along a line of sight. One must then correct for both the ratio of the main isotope of CO to the rare species and also for the population which is in other energy levels. One commonly used method for finding the column density of CO, the LTE method, is discussed in the Appendix.

Visual extinction in large areas of clouds is most often measured by the star-counting method in which comparisons of the number of stars in obscured and unobscured regions of sky in the vicinity are used to deduce the amount of extinction.<sup>8,9</sup> Measurements of the ultraviolet H I and H<sub>2</sub> line absorption in the light from hot, bright stars compared with measurements of the visual extinction towards the same stars show that the ratio of hydrogen column density to visual extinction is  $1.9 \times 10^{21}$  atoms cm<sup>-2</sup>.<sup>10</sup>

#### RESULTS FROM CO

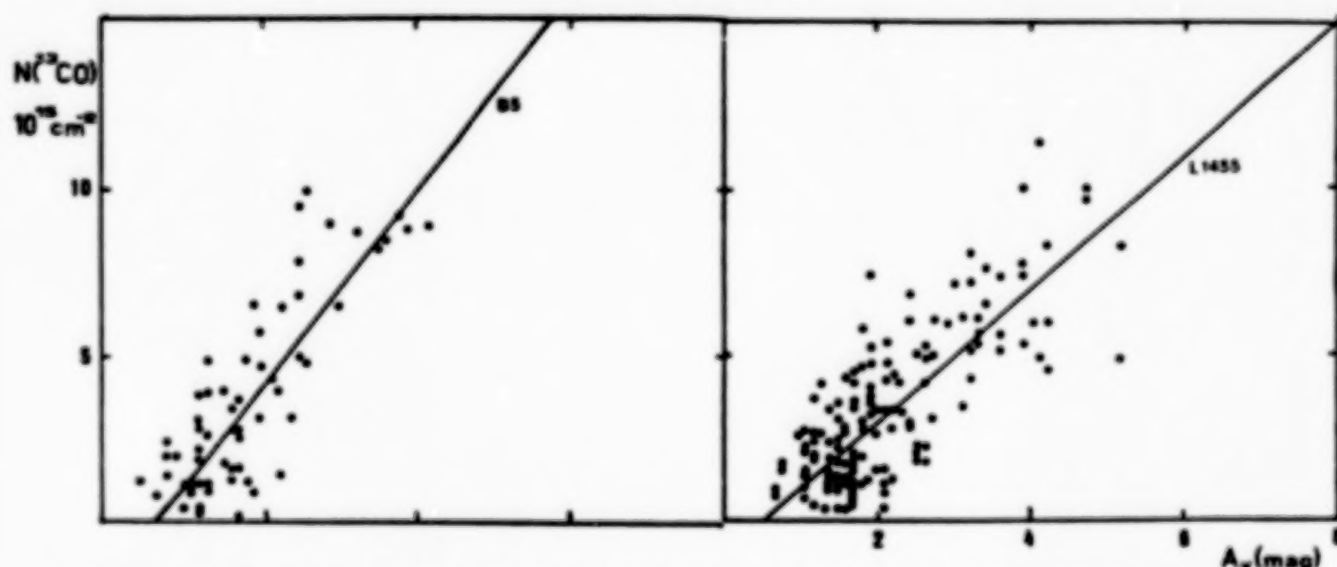


FIG. 4. - The LTE derived column density of <sup>13</sup>CO vs  $A_V$  in two dark clouds, from Bachiller and Cernicharo.<sup>11</sup>

Figure 4 shows some results for the relation between  $N(^{13}\text{CO})$  and  $A_V$  in two different molecular clouds. Table 2 contains a summary of many such studies adapted from Bachiller and Cernicharo.<sup>11</sup> Typically the slope of the relation between  $N(^{13}\text{CO})$  and  $A_V$  is  $2 \times 10^{15}$ . Since  $N(\text{CO})/N(^{13}\text{CO}) \approx 60$  in the solar neighborhood<sup>7</sup> and since  $N(\text{H} + 2\text{H}_2)/A_V \approx 1.9 \times 10^{21}$  atoms cm<sup>-2</sup>, the ratio between CO and total hydrogen abundance is approximately  $6.3 \times 10^{-5}$ . It is possible to use observations of C<sup>18</sup>O rather than <sup>13</sup>CO; the results are similar. Referring back to Table 1 we see that this implies that within molecular clouds about 20% of the carbon is in the form of CO.

#### PROBLEMS WITH CO

There are several problems associated with deriving the ratio of CO column density to H<sub>2</sub> via visual extinction.

1. The ratio of H I plus H<sub>2</sub> column density to visual extinction has been measured only in lines of sight with less than 2 mag of extinction.<sup>10</sup> Even at such low extinctions some clouds have a law for extinction as a function of wavelength that is different from that of the average. The implications of this are that such clouds, for example the one near the star  $\rho$  Ophiuchi, contain dust grains which differ from grains in more diffuse clouds, most probably in the grain size distribution. For the same total mass of dust, a cloud which has large dust grains will have less extinction than one with small grains. This means that  $N(\text{H} + 2\text{H}_2)/A_V$  may vary from cloud to cloud and even from center to edge of the same cloud.
2. Over large areas of sky only small values of visual extinction can be measured reliably. At positions of large extinction no background stars are visible and thus the extinction is not measurable. For this reason,

TABLE 2  
RELATION BETWEEN CO ABUNDANCE AND  $A_V$

Cloud	$N(^{13}\text{CO})$ ( $\text{cm}^{-2}$ )	$N(\text{C}^{18}\text{O})$ ( $\text{cm}^{-2}$ )	Comments	Reference
$\rho$ Oph	$2.5 \times 10^{15} A_V$			14
L134	$3.8 \times 10^{15} A_V$			15
many	$2.0 \times 10^{15} A_V$			16
L43	$1.5 \times 10^{15} A_V$			17
Taurus	$1.4 \times 10^{15} (A_V - 1.0)$	$0.7 \times 10^{14} (A_V - 1.9)$	$2 < A_V < 4$	18
Taurus		$2.4 \times 10^{14} (A_V - 2.9)$	$5 < A_V < 11$	18
$\rho$ Oph	$2.7 \times 10^{15} (A_V - 1.6)$	$1.7 \times 10^{14} (A_V - 3.9)$		18
Heiles # 2	$1.3 \times 10^{15} (A_V - 0.5)$	$2.5 \times 10^{14} (A_V - 1.5)$		19
L1495	$2.0 \times 10^{15} (A_V - 0.5)$	$2.2 \times 10^{14} (A_V - 1.1)$		20
Perseus	$2.5 \times 10^{15} (A_V - 0.8)$			11
L1506	$1.4 \times 10^{15} (A_V - 0.6)$			21
L1529	$0.9 \times 10^{15} (A_V - 0.9)$			21

measurements of CO column density versus visual extinction have generally been limited to visual extinctions less than 8 mag.

3. The ratio of CO to  $^{13}\text{CO}$  is not well known and may be variable. In cold clouds ( $T < 20$  K) the abundance of  $^{13}\text{CO}$  is enhanced by chemical fractionation. That is, it is energetically more favorable to form  $^{13}\text{CO}$  than CO ( $\Delta E/k \approx 35$  K), so that an atom of  $^{13}\text{C}$  will preferentially exchange with  $^{12}\text{C}$  in CO. In cold clouds there is not enough kinetic energy available to reverse the exchange and the abundance of  $^{13}\text{CO}$  will eventually be enhanced.<sup>12</sup>
4. On the edges of clouds  $^{13}\text{CO}$  and  $\text{C}^{18}\text{O}$  are selectively photodissociated because their abundances are not high enough for self-shielding from the ambient interstellar radiation field. Thus at low extinctions, the column density derived from these species underestimates the total abundance of CO.<sup>13</sup>

### C I ABUNDANCES

Since we have established the CO to  $\text{H}_2$  relation, it is now only necessary to compare C I and CO directly.<sup>22,23,24</sup> Again the LTE method of abundance calculation is discussed in the Appendix. Unfortunately, the collisional excitation of C I by  $\text{H}_2$  is not well understood. A recent estimate gives  $\sim 10^4 \text{ cm}^{-3}$  for the critical density of the  $^3P_1 \rightarrow ^3P_0$  transition.<sup>25</sup> If the new estimate is correct the validity of the LTE method of abundance determination is questionable. Earlier estimates were  $\sim 2000 \text{ cm}^{-3}$ , approximately the same as  $^{13}\text{CO}$ .<sup>26</sup>

### RESULTS FROM C I

In many cases it has been found that the spectral lines of the  $^3P_1 \rightarrow ^3P_0$  transition of C I strongly resemble the  $J = 1 \rightarrow 0$  lines of  $^{13}\text{CO}$  (e.g., see Figure 5), particularly the observed linewidths and lineshapes. The line intensities are also often similar. This implies that the optical depth of the C I lines is moderate and is similar to that of  $^{13}\text{CO}$  and that the C I and  $^{13}\text{CO}$  emission lines arise in areas of similar density and temperature.

Comparing Equations (9) and (11) in the Appendix we see that in a region in LTE with  $T_{\text{ex}} = 30$  K having lines of C I and  $^{13}\text{CO}$  of equal integrated intensity and optical depth the ratio  $N(\text{C I})/N(^{13}\text{CO}) = 7.5$ . Since  $N(\text{CO})/N(^{13}\text{CO}) \approx 60$  in the Solar neighborhood that would imply that  $N(\text{C I})/N(\text{CO}) \approx 0.13$  or that about 3% of the total carbon abundance is in the form of C I in molecular clouds.

Figures 6 and 7 show that the situation is somewhat more complex than outlined above. These figures combine submillimeter and millimeter wavelength observations of C I and CO in the dense cloud associated with the star

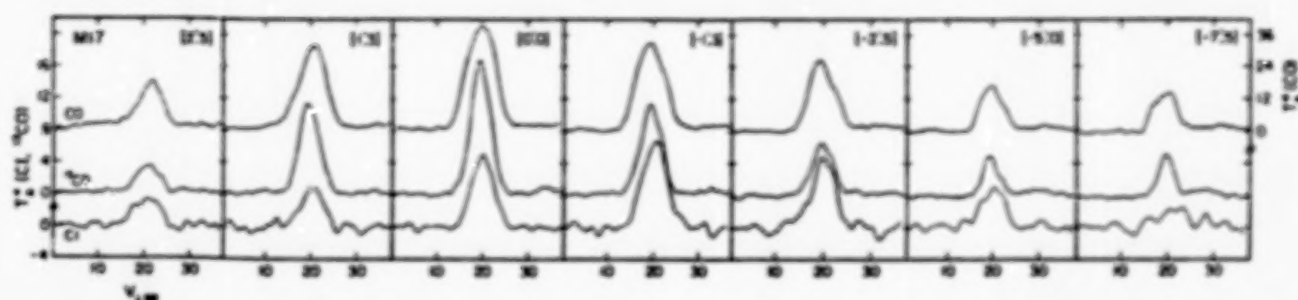


FIG. 5. — A comparison of the lines of CO,  $^{13}\text{CO}$  and C I across the ionization front in M17.<sup>23</sup> The ionization front is at position 2.5 and the dense molecular cloud lies to the right. The intensity scale of the CO line is a factor of 3 smaller than the C I and  $^{13}\text{CO}$  scales in the plot. The C I line bears a strong resemblance to the  $^{13}\text{CO}$  line at most of these positions.

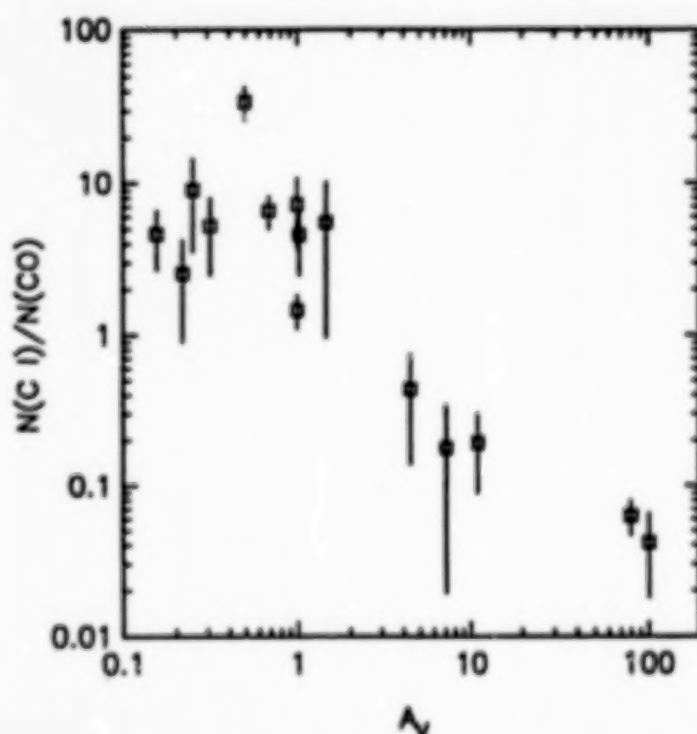


FIG. 6. — The ratio of  $N(\text{C I})$  to  $N(\text{CO})$  as a function of  $A_V$ . In diffuse clouds the ratio generally has values of 2–10; within moderately opaque dense clouds,  $4 < A_V < 30$  mag, the ratio decreases from about 0.5 to 0.1; at higher  $A_V$ 's the ratio appears to drop further but this effect may be due to strong self-absorption in the C I line. At  $A_V < 2$  the data are from ultraviolet absorption observations,<sup>27,28</sup> at higher  $A_V$ 's they are from millimeter and submillimeter emission line observations.<sup>24</sup>

$\rho$  Ophiuchi with ultraviolet observations of C I and CO in diffuse clouds.<sup>24,27,28</sup> It can be seen in Figure 6 that the ratio  $N(\text{C I})/N(\text{CO})$  decreases from about 5 to 0.1 as the extinction increases from  $A_V$  of about 1 to 30. At higher  $A_V$ 's the ratio appears to decrease further but, as discussed in the next section, that conclusion is confused by the high opacity and resultant self-absorption of the C I lines at large  $A_V$ .

Figure 7 shows the results of comparing  $N(\text{C I})$  with  $N(\text{H} + 2\text{H}_2)$ . The interesting points are that the fractional abundance of C I is low outside dense clouds ( $A_V < 1$ ), is fairly constant within dense clouds ( $4 < A_V < 30$ ) at  $10^{-3}$  relative to hydrogen, i.e. 3% of the total abundance of carbon, and may decrease in the centers of dense clouds ( $A_V > 30$ ), but the behavior at the largest extinctions is not yet well established.

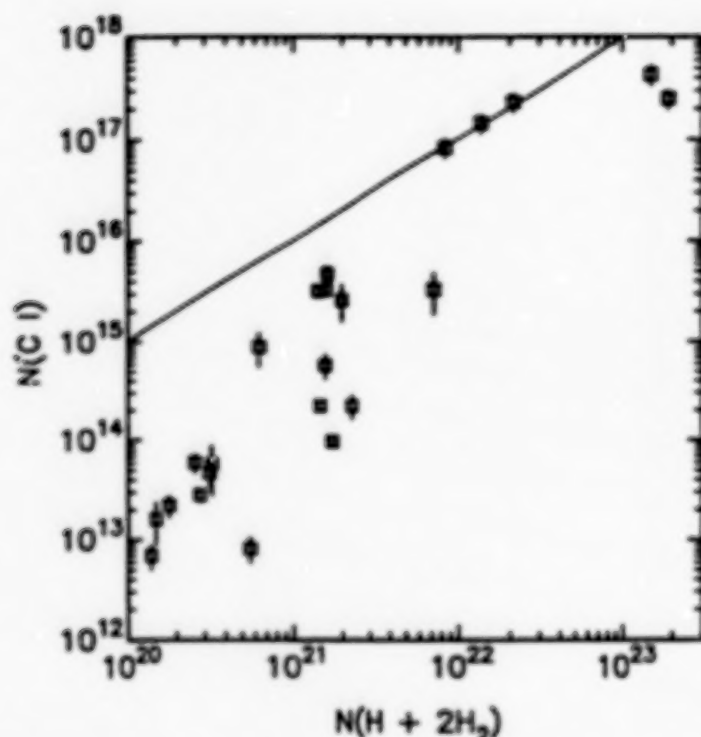


FIG. 7. - The column density of C I as a function of total hydrogen column density. The line indicates a constant  $N(\text{C I}) / N(\text{H} + 2\text{H}_2)$  ratio of  $10^{-5}$  or 3% of the cosmic abundance of carbon in the form of C I. The data for  $N(\text{C I}) < 10^{16}$  are from ultraviolet observations of diffuse clouds<sup>27</sup> and for higher values from submillimeter observations of the dense dark cloud associated with  $\rho$  Ophiuchi. It can be seen that the fractional abundance of C I reaches a peak in moderately opaque clouds,  $8 \times 10^{21} < N(\text{H} + 2\text{H}_2) < 4 \times 10^{22}$  or  $4 < A_V < 20$ . It may decrease at higher opacities but that conclusion is as yet uncertain.

Figures 5-7 show that the simple picture of C I distribution developed by the classical photodissociation models (Fig. 1) does not match the observations. The abundance of C I is higher throughout molecular clouds than is predicted by such models. The generally high abundances observed via the  $^3P_1 \rightarrow ^3P_0$  line have been confirmed recently by observations of the  $^3P_2 \rightarrow ^3P_1$  line.<sup>29,30</sup> Many models have been produced to explain these observations (see the review by Keene *et al.*<sup>23</sup>). An attractive model has been proposed in connection with C I and C II line observations of M17.<sup>29</sup> In this model the molecular cloud is assumed to be clumpy, allowing ultraviolet radiation from exterior and interior sources to reach most parts of the molecular cloud, producing C I (and C II) throughout the cloud.

#### PROBLEMS WITH C I ABUNDANCE DETERMINATIONS

The problems associated with determining the abundance of C I are similar to those associated with CO.

1. The excitation temperature is unknown and is often assumed to be same as the CO excitation temperature. Knowledge of the temperature is necessary to calculate the partition function, correcting for the population in unobserved energy levels. The level populations depend on the critical density for excitation by  $\text{H}_2$  which has not yet been calculated.
2. The optical depth of the C I lines is also unknown. The lines usually appear to be of moderate optical depth so opacity corrections are not unreasonable. However, at large extinctions, the C I lines are seen to be optically thick and occasionally display symptoms of self-absorption similar to that often seen in CO and, less commonly, in  $^{13}\text{CO}$ . Figure 8 contains an example of a high-extinction region in the  $\rho$  Oph dark cloud which has both strong CO and  $^{13}\text{CO}$  self-absorption. This is evident in the high degree of asymmetry of the lines and the displacement of their peak velocities relative to the more optically thin  $\text{C}^{18}\text{O}$ . It is clear

from Figure 8 that C I also shows effects of self-absorption. Unfortunately, measuring the optical depth of the C I transitions, independent of CO observations, is difficult. It is not possible to observe the  $^3P_1 \rightarrow ^3P_0$  transition of  $^{13}\text{C I}$  because the brightest hyperfine component is separated from the C I line by only about 3 MHz ( $1.8 \text{ km s}^{-1}$ ), less than the linewidth in a typical warm cloud. Although it should be possible to observe the  $^3P_2 \rightarrow ^3P_1$  transition of  $^{13}\text{C I}$  – the  $F = 5/2 \rightarrow 3/2$  hyperfine component of the  $^{13}\text{C I } ^3P_2 \rightarrow ^3P_1$  line is separated from the C I line by about 153 MHz ( $57 \text{ km s}^{-1}$ )<sup>31</sup> – it has not yet been done. Since the optical depths are often only moderate in both the C I lines the corresponding  $^{13}\text{C I}$  lines will be difficult to detect.

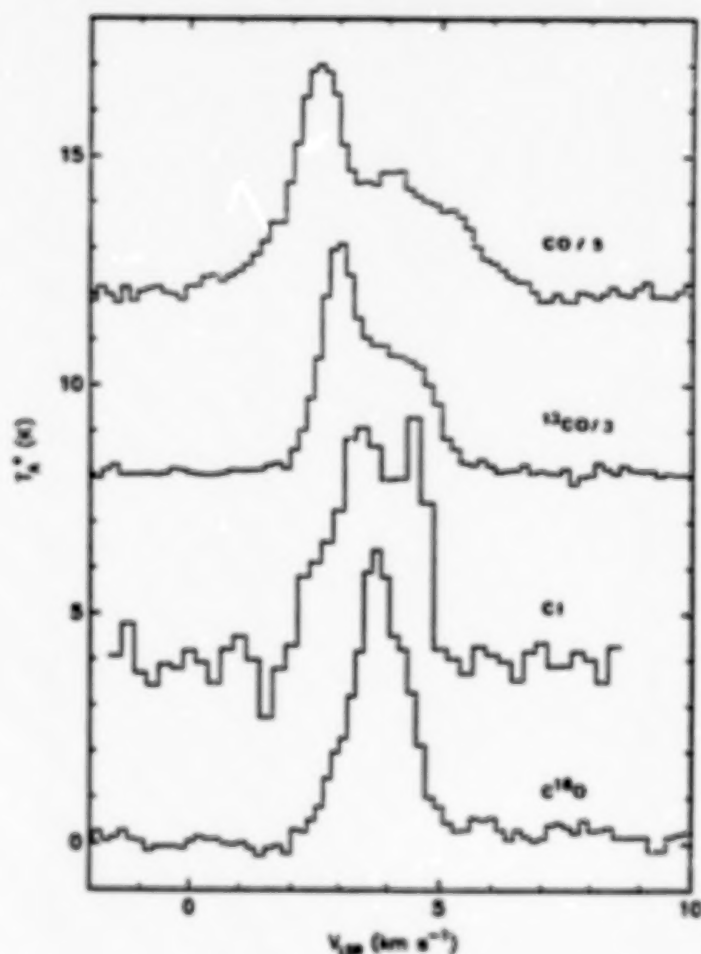


FIG. 8. – A comparison of the spectral lines of CO and its rarer isotopes with C I in the  $\rho$  Oph dark cloud.

#### OPPORTUNITIES FOR FUTURE WORK ON C I

Although there remain problems with the C I observations and unanswered questions about the abundance of C I, the hopes for future work are high. Submillimeter emission from the  $^3P_1 \rightarrow ^3P_0$  transition of C I was first observed in 1979 and the  $^3P_2 \rightarrow ^3P_1$  transition was first observed in 1985.<sup>32,33</sup> There has not yet been a systematic program to observe both of these transitions at the same positions with the same angular resolutions. When this is done the results should place constraints on the temperature and optical depths of the regions. Also, the earth's atmosphere is partially transparent (from very dry sites) at the wavelengths of both the  $^3P_1 \rightarrow ^3P_0$  and  $^3P_2 \rightarrow ^3P_1$  transitions. This means that the new submillimeter wavelength telescopes which are just being commissioned at the Mauna Kea Observatory and other places will be useful for making such studies of C I.

High spatial resolution observations will enable us to study the detailed distribution of C I, and to determine whether it has a smooth or clumpy distribution. If there are strong localized abundance peaks we will have to interpret them as being caused by localized sources of C I, such as embedded stars or nearby H II regions. It is also important to determine whether the C I fractional abundance decreases at the densest positions in molecular cloud cores or whether that apparent effect is an artifact of high opacity in the C I  $^3P_1 \rightarrow ^3P_0$  line.

### C II ABUNDANCES

The  $^2P_{3/2} \rightarrow ^2P_{1/2}$  transition of C II lies in an opaque region of the atmosphere and can only be observed from above most of the earth's atmospheric water vapor, i.e., from an airplane, balloon, or spacecraft. This limits the spatial resolution with which it can be observed and the length of time spent observing it. Also until very recently it had been observed only at low spectral resolution with either grating or Fabry-Perot spectrometers.<sup>34,35</sup> Even with the relatively low resolution available ( $200 < \nu/\Delta\nu < 1.2 \times 10^4$ ;  $1500 > \Delta V > 25 \text{ km s}^{-1}$ ) it was obvious that C II emission is related to CO  $J = 1 \rightarrow 0$  emission.

### RESULTS FROM C II

The distribution of C II emission across the Galactic plane resembles that of CO, not in detail but enough to see that it is closely associated with molecular clouds.<sup>36</sup> Also, over two orders of magnitude and in many different objects, the C II line intensity has been observed to be proportional to the intensity of the  $J = 1 \rightarrow 0$  line of CO (Figure 9).<sup>35</sup> These observations similarly imply that the C II emission is intimately associated with molecular clouds. Since the presence of C II emission necessarily indicates that ultraviolet radiation is present, these results have been interpreted in terms of warm,  $T \approx 300 \text{ K}$ , photodissociation regions lying at the interfaces between bright H II regions and molecular clouds.<sup>4,35</sup> At such a high temperature the emission from such regions would be optically thin.

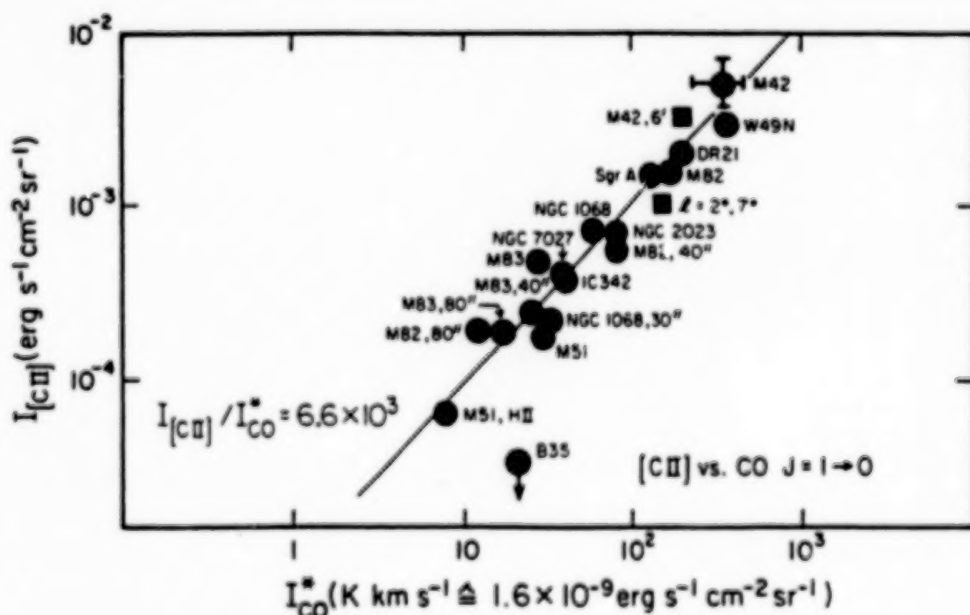


FIG. 9. - Correlation between C II and CO integrated line intensities for Galactic molecular clouds and other galaxies.<sup>35</sup>

Extensive observations of C II in the M17 region have shown that the emission is spread widely through the entire cloud, not just concentrated at the H II region, molecular cloud interface.<sup>37</sup> In fact the C II line intensity away from the interface follows the CO intensity and is a factor of 20 higher than predicted by photodissociation models. This has been interpreted as being due to a possible clumpy structure of the M17 molecular cloud which

allows ultraviolet radiation from *a*) luminous, hot, young stars within the H II region, *b*) less luminous and hot stars embedded within the molecular cloud, and *c*) the general interstellar radiation field to penetrate the entire molecular cloud, producing C II (and also C I) throughout the cloud.

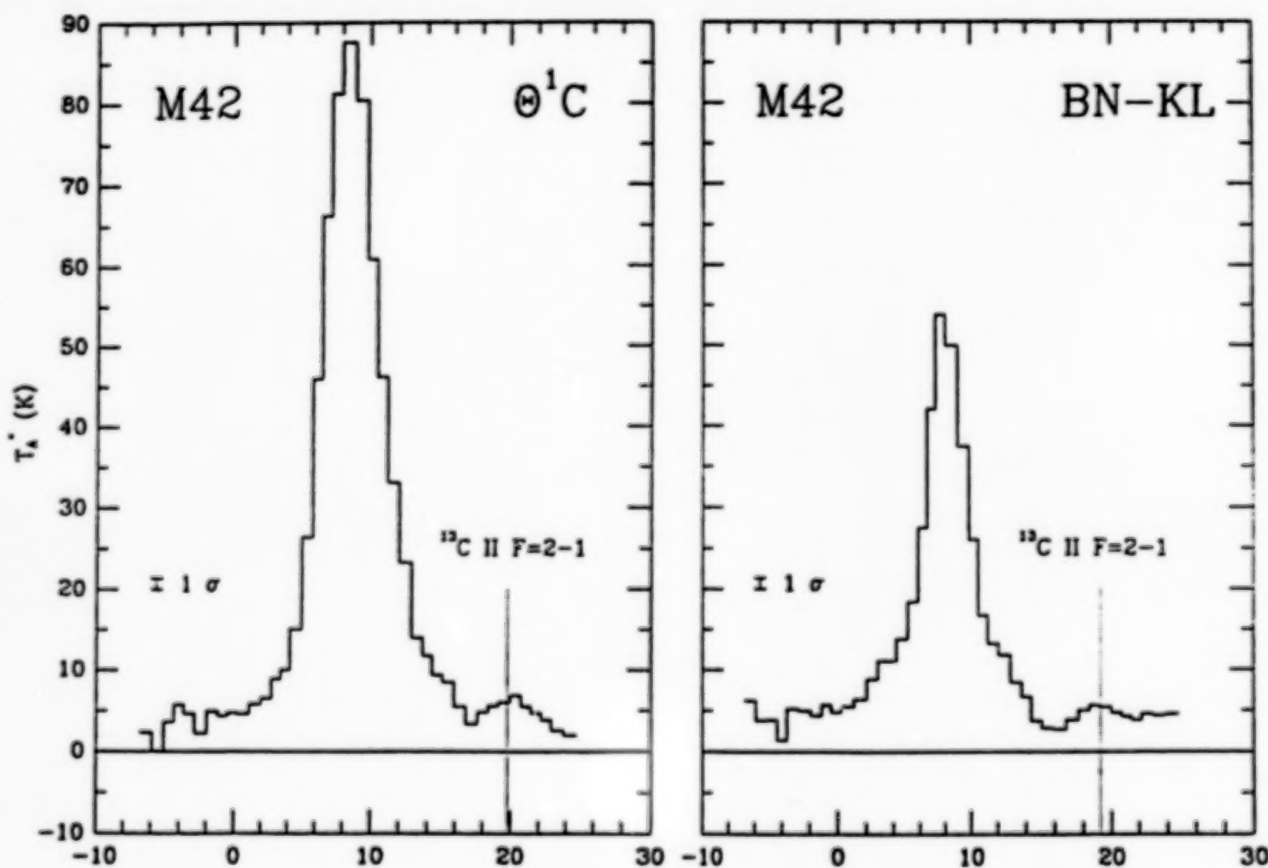


FIG. 10. - Spectra of the  $2P_{3/2} \rightarrow 2P_{1/2}$  line of C II from two positions in the Orion Nebula.<sup>38</sup>

Recent heterodyne observations have modified the above interpretations somewhat. Figure 10 shows the results of observations of C II at two positions in the Orion Nebula.<sup>38</sup> The main line in each spectrum, of course, is that of C II; about 11 km s<sup>-1</sup> toward higher velocity is a feature which possibly is the  $F = 2 \rightarrow 1$  hyperfine line of  $^{13}\text{C II}$ . If the feature is real it implies that the optical depth in the main line is high,  $\tau \approx 5$ . In addition, since the optical depth is probably large and the critical density of C II is small ( $10^3 \text{ cm}^{-3}$ ), the observed brightness temperature is equal to the excitation temperature unless there is a non-unity beam filling factor. In OMC-1 the Planck corrected brightness temperature is in the range 90–130 K, thus the emission originates from regions closer to 100 K than 300 K in temperature, similar to the temperature in the molecular region.

It is difficult, without the benefit of large Galactic surveys, to calculate the total amount of C II. We can nevertheless get some idea of the amount of C II from surveys of many objects. Assuming that the C II emission is optically thin and originates in high temperature regions where all the carbon is in the form of C II, Crawford *et al.*<sup>35</sup> have calculated that the ratio of mass in C II regions to that in molecular clouds, H<sub>2</sub> regions, is at least 3%. The heterodyne spectroscopy by Boreiko, Betz, and Zmuidzinas<sup>38</sup> show that this estimate may be low by a factor of as much as 5 (cf. eq. [14] in the Appendix). Therefore probably about 5–15%, say 10%, of the Galactic carbon associated with molecular clouds may be found in the form of C II.

#### PROBLEMS WITH AND OPPORTUNITIES FOR C II ABUNDANCE DETERMINATIONS

Because the excitation energy of the  $2P_{3/2}$  level is high it is difficult to observe in cold regions. Thus the estimate given above, 10% of Galactic carbon in molecular clouds in the form of C II, really only refers to high-

temperature regions associated with star formation where the levels of ultraviolet radiation are enhanced. We have not yet measured the possibly much lower abundance of C II associated with dark molecular clouds.

As is the case with C I, the determinations of the kinetic temperature of emission regions and line optical depths present problems for the interpretation of C II observations. Luckily, with the advent of sensitive far-infrared heterodyne spectrometers that problem is ripe for solving. The  $^2P_{3/2} \rightarrow ^2P_{1/2}$  line of C II is considerably brighter than either the  $^3P_1 \rightarrow ^3P_0$  or  $^3P_2 \rightarrow ^3P_1$  line of C I so that observations of the  $F = 2 \rightarrow 1$  hyperfine component of the  $^{13}\text{C II } ^2P_{3/2} \rightarrow ^2P_{1/2}$  line are possible. Measurement of the brightness of that line in many sources will lead to a better determination of the overall C II abundance.

Also with the high sensitivity and frequency resolution of heterodyne receivers now available we can begin to develop an understanding of the relative kinematics of the C II and various atomic and molecular components of the dense gas.

## SUMMARY

In the dense interstellar medium, we find that about 20% of the total carbon abundance is in the form of CO, about 3% in C I, and 10% in C II with uncertainties of factors of order 2. The abundance of other forms of gaseous carbon is negligible. CO is widespread throughout molecular clouds as is C I. C II has only been observed near bright star-formation regions so far because of its high excitation energy. Further from ultraviolet sources it may be less abundant. Altogether we have accounted for about 1/3 of the total carbon abundance associated with dense molecular clouds. Since the other gaseous forms are thought to have negligible abundances the rest of the carbon is probably in solid form.

## APPENDIX

### CO COLUMN DENSITIES

CO is an example of the most common type of diatomic molecule, in its ground electronic state it has no net electronic angular momentum, i.e., the ground electronic state is  $^1\Sigma$ . This greatly decreases the number of available energy levels and facilitates the calculation of their energies and transition probabilities. The rotational states in the ground vibrational state (displayed for CO in Figure 3) have energies above the  $J = 0$  ground state which are given to first order by  $E_J = J(J+1)hB$ , where  $J = 0, 1, 2, \dots$  is the rotational quantum number (actually the total angular momentum quantum number) and  $B$  is the rotational constant. For CO,  $hB/k = 2.77$  K, for  $^{13}\text{CO}$ , 2.64 K and, for  $\text{C}^{18}\text{O}$ , 2.63 K. The statistical weights of the levels are given by  $g_J = 2J + 1$ .

If the emission lines under consideration are optically thin, which is almost certainly the case for  $^{13}\text{C}^{18}\text{O}$  and  $\text{C}^{17}\text{O}$ , is often the case for  $\text{C}^{18}\text{O}$ , is sometimes the case for  $^{13}\text{CO}$ , and is almost never the case for CO, the calculation of column densities is relatively straightforward. The average column density of molecules in the telescope beam in upper level  $J$ ,  $N_J$ , is simply related to the energy intensity averaged over the telescope beam,  $I_\nu$ , as

$$N_J = \frac{4\pi}{A_{J,J'} h\nu} \int I_\nu d\nu. \quad (1)$$

$A_{J,J'}$  is the Einstein coefficient for spontaneous emission in the  $J \rightarrow J'$  transition.

In millimeter-wave astronomy the energy intensity is more conveniently expressed in temperature units proportional to the average energy intensity in the beam. The "antenna temperature" corrected for all telescope losses,  $T_A^*$  also sometimes called  $T_R^*$ , is such a unit. Its definition is

$$\frac{kT_A^*}{h\nu} = \frac{c^2 I_\nu}{2h\nu^3}. \quad (2)$$

In the long-wavelength or high-temperature limit,  $T_A^*$  is the temperature of a blackbody with intensity  $I_\nu$ , but in the submillimeter and far-infrared wavelength regions the Planck corrections are usually not negligible.

In terms of the observed antenna temperature, the average column density of molecules in state  $J$  observed via the optically thin  $J \rightarrow J'$  emission line is

$$N_J = \frac{8\pi k\nu^2}{A_{J,J'}hc^3} \int T_A^* dV, \quad (3)$$

where the integral is taken over all velocities in the line.

The Einstein  $A$  coefficient for any transition is related to the dipole matrix element,  $|\mu_{J',J}|$ , by

$$A_{J,J'} = \frac{64\pi^4 \nu^3}{3h c^3} \frac{g_{J'}}{g_J} |\mu_{J',J}|^2. \quad (4)$$

For a molecule with a  $^1\Sigma$  electronic ground state, the dipole matrix element is given by

$$|\mu_{J-1,J}|^2 = \mu^2 \frac{J}{2J-1} \quad (5)$$

and radiative transitions other than  $\Delta J = \pm 1$  are forbidden. The dipole moment,  $\mu$ , for CO (as well as all its isotopes) is 0.11 Debyes ( $0.11 \times 10^{-18}$  cgs), thus the Einstein  $A_{1,0}$  coefficient for CO is  $7.2 \times 10^{-8} \text{ s}^{-1}$ , for  $^{13}\text{CO}$  is  $6.3 \times 10^{-8} \text{ s}^{-1}$ , and for  $\text{C}^{18}\text{O}$  is  $6.2 \times 10^{-8} \text{ s}^{-1}$ .

To calculate the total abundance of molecules we must correct for those in levels other than the observed one. The distribution of molecules among the various levels is commonly parameterized by the "excitation temperature",  $T_{\text{ex}}$ . The ratio of the population in level  $J$ ,  $n_J$ , to that in the level  $J'$ ,  $n_{J'}$ , is given by the Boltzmann equation,

$$\frac{n_J}{n_{J'}} = \frac{g_J}{g_{J'}} \exp\left(-\frac{E_J - E_{J'}}{kT_{\text{ex}}}\right), \quad (6)$$

which is actually the definition of excitation temperature. The "partition function" is the function that is needed to correct the abundance calculation in equation (1) to the total abundance. For a molecule with only angular momentum states  $J$  available the partition function,  $f$ , is

$$f = \sum_J g_J \exp(-E_J/kT_{\text{ex}}). \quad (7)$$

A good approximation to this function (for a  $^1\Sigma$  electronic ground state molecule at high  $T_{\text{ex}}$ ) is  $f = kT_{\text{ex}}/hB$ .<sup>39</sup>

The expression for the partition function given above has made use of a very common approximation, i.e., that all the CO energy levels are characterized by the same excitation temperature which is the local gas kinetic temperature. This approximation is described by the term "local thermodynamic equilibrium" (LTE). The kinetic temperature of isothermal gas in LTE is equal to the brightness temperature of an optically thick emission line, in this case the CO  $J = 1 \rightarrow 0$  emission line. This LTE assumption is approximately valid for the following reason.

At densities higher than the "critical density" for a given molecular transition, the excitation temperature approaches the kinetic temperature of the gas. In the limit of zero optical depth the critical density is the space density at which the rate of collisional de-excitations of a given energy level is equal to the rate of radiative de-excitations. However, if the emission lines resulting from radiative de-excitation are optically thick then the critical density is decreased by a factor of about  $\tau$ , the optical depth.<sup>40</sup> In dense clouds, low-lying transitions of CO are optically thick and easily excited – the critical density of the  $J = 1 \rightarrow 0$  transition is  $n(\text{H}_2) \approx 2500 \text{ cm}^{-3}$ . Since  $\tau(\text{CO})$  is typically 50 to 100, it is obvious that these low energy states of CO should be thermalized, i.e., in LTE, in dense clouds. It is less clear that the states of the rare CO isotopic species will be in LTE. The assumption of LTE for these species is likely to overestimate their abundance since the upper energy levels are probably underpopulated relative to their lower ones.

The total number of molecules is related to the integrated antenna temperature of an optically thin line as

$$N_T \approx \frac{1}{g_J} \exp\left(\frac{E_J}{kT_{\text{ex}}}\right) f \frac{8\pi k\nu^2}{A_{J,J'}hc^3} \int T_A^* dV. \quad (8)$$

If the line used in the above analysis has moderate optical depth, i.e.,  $\tau \sim 1$ , we can multiply the result by  $\tau_0/(1 - e^{-\tau_0})$ , where  $\tau_0$  is the optical depth at the center of the line, as an approximate correction. The central optical depth can be derived from comparison of the line brightness with the brightness in an optically thick line, i.e., CO  $J = 1 \rightarrow 0$ .

For the  $J = 1 \rightarrow 0$  line of both  $^{13}\text{CO}$  and  $\text{C}^{18}\text{O}$  the final result for the total isotopic abundance is

$$N_T \approx 4.7 \times 10^{13} T_{\text{ex}} \exp\left(\frac{5.3}{T_{\text{ex}}}\right) \frac{\tau_0}{(1 - e^{-\tau_0})} \int T_A^* dV, \quad (9)$$

where  $\int T_A^* dV$  is measured in units of  $\text{K km s}^{-1}$ .

Finally the abundance must be corrected to the main isotope by using the isotopic abundance ratios. These are typically taken to be  $N(\text{CO})/N(^{13}\text{CO}) \approx 60$  and  $N(\text{CO})/N(\text{C}^{18}\text{O}) \approx 500$ .<sup>7</sup>

### C I COLUMN DENSITIES

We analyze the C I column density as we did that of CO, making use of the same definitions for excitation temperature and partition function. The carbon atom has a  $^3P$  ground term, split by spin-orbit coupling into three levels. The total electronic angular momentum quantum number, called  $J$ , has the values 0, 1 and 2 resulting in ground term levels  $^3P_0$ ,  $^3P_1$  and  $^3P_2$ . The statistical weights,  $g_J$ , of these lowest three energy levels are again equal to  $2J + 1$ .

Because C I has only three accessible energy states at temperatures common in the interstellar medium ( $T < 100$  K), with energies  $E_0 = 0$ ,  $E_1/k = 23.6$  K and  $E_2/k = 62.5$  K, the partition function is given by

$$f = 1 + 3 \exp\left(-\frac{23.6}{T_{\text{ex}}}\right) + 5 \exp\left(-\frac{62.5}{T_{\text{ex}}}\right). \quad (10)$$

The total number of atoms of atomic carbon observed in an optically thin line is given by equation (8). The Einstein  $A_{1,0}$  coefficients for C I are  $A_{1,0} = 7.9 \times 10^{-8} \text{ s}^{-1}$  and  $A_{2,1} = 2.7 \times 10^{-7} \text{ s}^{-1}$ .<sup>41</sup> Inserting the numerical constants for the  $^3P_1 \rightarrow ^3P_0$  line of C I in equation (8) and including the correction for finite optical depth, we obtain for the total number of C I atoms

$$N_T = 1.9 \times 10^{15} \left[ \exp\left(\frac{23.6}{T_{\text{ex}}}\right) + 3 + 5 \exp\left(-\frac{38.0}{T_{\text{ex}}}\right) \right] \frac{\tau_0}{(1 - e^{-\tau_0})} \int T_A^* dV, \quad (11)$$

where again  $\int T_A^* dV$  is measured in  $\text{K km s}^{-1}$ .

The collisional cross sections for C I with  $\text{H}_2$  have not been calculated, so the critical density for excitation of C I by  $\text{H}_2$  is not well known. However, Monteiro and Flower<sup>25</sup> estimate that the cross section for excitation of the  $^3P_1$  level from the  $^3P_0$  level by  $\text{H}_2$  is about 0.1 times the cross section for excitation by atomic hydrogen calculated by Launay and Roueff.<sup>42</sup> That makes the critical density for the  $^3P_1 \rightarrow ^3P_0$  transition  $\sim 10^4 \text{ cm}^{-3}$ . With such a high critical density the LTE assumption may be questionable. Luckily the  $^3P_2 \rightarrow ^3P_1$  transition is observable and seems to have a smaller critical density for excitation by  $\text{H}_2$  than does the  $^3P_1 \rightarrow ^3P_0$  transition.

### C II COLUMN DENSITIES

Singly ionized carbon, C II, has a  $^2P$  ground state term, split by spin-orbit coupling into the levels  $^2P_{1/2}$  and  $^2P_{3/2}$ . Again, the statistical weight of each level is  $2J + 1$  where  $J$  has the values  $1/2$  and  $3/2$ . The energies of the levels are  $E_{1/2} = 0$  and  $E_{3/2}/k = 91.2$  K. In the dense interstellar medium only these two levels have significant populations.

To solve for the number of ionized carbon atoms we once again assume that the population distribution of the C II energy levels can be described by LTE. The partition function is then

$$f = 2 + 4 \exp\left(-\frac{91.2}{T_{\text{ex}}}\right). \quad (12)$$

The value of the Einstein A coefficient for the  $^2P_{3/2} \rightarrow ^2P_{1/2}$  transition is  $2.4 \times 10^{-6} \text{ s}^{-1}$ . The total number of atoms of ionized carbon is

$$N_T \approx 1.5 \times 10^{15} \left[ \exp\left(\frac{91.2}{T_{\text{ex}}}\right) + 2 \right] \frac{\tau_0}{(1 - e^{-\tau_0})} \int T_A^* dV, \quad (13)$$

where the correction factor for finite optical depth has been included.

In the past it has not been common to express the intensity of C II emission in terms of antenna temperature because the lines are generally not spectrally resolved. In terms of energy intensity equation (13) can be written (as in eq. [1]),

$$N_T \approx 2.1 \times 10^{20} \left[ \exp\left(\frac{91.2}{T_{\text{ex}}}\right) + 2 \right] \frac{\tau_0}{(1 - e^{-\tau_0})} \int \bar{I}_\nu d\nu \quad (14)$$

where  $\int \bar{I}_\nu d\nu$  is in units of  $\text{ergs s}^{-1} \text{ cm}^{-2} \text{ sr}^{-1}$

## REFERENCES

1. Kulkarni, S. R., and Heiles, C. 1987, in *Interstellar Processes*, eds D. Hollenbach and H. Thronson (Dordrecht: Reidel), p. 87.
2. Allen, C. W. 1973, *Astrophysical Quantities*, (London: Athlone Press).
3. Langer, W. D. 1976, *Ap. J.*, **206**, 699.
4. Tielens, A. G. G. M., and Hollenbach, D. 1985, *Ap. J.*, **291**, 722.
5. Leung, C. M., Herbst, E., and Heubner, W. F. 1984, *Ap. J. Supp.*, **56**, 231.
6. Audouze, J. 1977, in *CNO Isotopes in Astrophysics*, ed. J. Audouze (Dordrecht: Reidel), p. 3.
7. Wannier, P. G. 1980, *Ann. Rev. Astr. Ap.*, **18**, 399.
8. Bok, B. J., and Cordwell, C. S. 1973, in *Molecules in the Galactic Environment*, eds. M. Gordon and L. Snyder (Wiley-Interscience: New York), p. 53.
9. Dickman, R. 1978, *A. J.*, **83**, 363.
10. Bohlin, R. C., Savage, B. D., and Drake, J. F. 1978, *Ap. J.*, **224**, 132.
11. Bachiller, R., and Cernicharo, J. 1986, *Astr. Ap.*, **166**, 283.
12. Watson, W. D., Anicich, V. G., and Huntress, W. T. 1976, *Ap. J. (Letters)*, **205**, L165.
13. Bally, J., and Langer, W. D. 1982, *Ap. J.*, **255**, 143.
14. Encarnaz, P. J., Falgarone, E., Lucas, R. 1975, *Astr. Ap.*, **44**, 73.
15. Tucker, K. D., Dickman, R. L., Encarnaz, P. J., Kutner, M. L. 1976, *Ap. J.*, **210**, 679.
16. Dickman, R. 1978, *Ap. J. Supp.*, **37**, 407.
17. Elmegreen, D. M., and Elmegreen, B. G. 1979, *A. J.*, **84**, 615.
18. Frerking, M. A., Langer, W. D., and Wilson, R. W. 1982, *Ap. J.*, **262**, 590.
19. Cernicharo, J., and Guélin 1987, *Astr. Ap.*, **176**, 299.
20. Duvert, G., Cernicharo, J., Baudry, A. 1986, *Astr. Ap.*, **164**, 2.
21. Nercissian, E., Castets, A., Cernicharo, J., and Benayoun, J. J. 1988, *Astr. Ap.*, **189**, 207.
22. Phillips, T. G., and Huggins, P. J. 1981, *Ap. J.*, **251**, 533.
23. Keene, J., Blake, G. A., Phillips, T. G., Huggins, P. J., and Beichman, C. A. 1985, *Ap. J.*, **299**, 967.
24. Frerking, M. A., Keene, J., Blake, G. A., and Phillips, T. G. 1988, submitted to *Ap. J.*
25. Monteiro, T. S., and Flower, D. R. 1987, *M. N. R. A. S.*, **228**, 101.
26. Flower, D. R., Launay, J. M., and Roueff, E. 1978, in *Les Spectres des Molecules Simples au Laboratoire et en Astrophysique* (Liège: Université de Liège), p. 137.
27. Jenkins E. B., and Shaya, E. J. 1979, *Ap. J.*, **231**, 55.
28. Federman, S. R., Glassgold, A. E., Jenkins, E. B., and Shaya, E. J. 1980, *Ap. J.*, **242**, 545.
29. Genzel, R., Harris, A. I., Jaffe, D. T., and Stutzki, J. 1988, preprint.
30. Zmuidzinas, J., Betz, A. L., Boreiko, R. T., and Goldhaber, D. M. 1988, preprint.
31. Cooksy, A. L., Saykally, R. J., Brown, J. M., and Evenson, K. M. 1986, *Ap. J.*, **309**, 828.

32. Phillips, T. G., Huggins, P. J., Kuiper, T. B. H., and Miller, R. E. 1980, *Ap. J. (Letters)*, 238, L103.
33. Jaffe, D. T., Harris, A. I., Silber, M., Genzel, R., and Betz, A. L. 1985, *Ap. J. (Letters)*, 285, L59.
34. Russell, R., Melnick, G., Smyers, S. D., Kurtz, N. T., Gosnell, T. R., Harwit, M., and Werner, M. W. 1980, *Ap. J. (Letters)*, 250, L35.
35. Crawford, M. K., Genzel, R., Townes, C. H., and Watson, D. M. 1985, *Ap. J.*, 291, 755.
36. Stacey, G. J., Viscuso, P. J., Fuller, C. E., and Kurtz, N. T. 1985, *Ap. J.*, 289, 803.
37. Stutzki, J., Stacey, G. J., Genzel, R., Harris, A. I., Jaffe, D. T., and Lugten, J. B. 1988, preprint.
38. Boreiko, R., Betz, A., and Zmuidzinas J. 1988, *Ap. J. (Letters)*, 325, L47.
39. Goldreich, P., and Kwan, J. 1974, *Ap. J.*, 189, 441.
40. White, R. E. 1977, *Ap. J.*, 211, 744.
41. Nussbaumer, H. and Rusca, C., *Astr. Ap.*, 72, 129.
42. Launay, J. M. and Roueff, E. 1977, *Astr. Ap.*, 56, 289.

**LABORATORY STUDIES OF CARBON**

## DOWN-TO-EARTH STUDIES OF CARBON CLUSTERS \*

R. E. Smalley

Rice University

### ABSTRACT

Recent advances in supersonic beam experiments with laser-vaporization sources of clusters have provided some interesting new insights into the nature of the small clusters of carbon, and the processes through which carbon condenses. One cluster in particular,  $C_{60}$ , appears to play a central role. It is argued that this cluster takes the shape of a soccerball: a hollow sphere composed of a shell of 60 carbon atoms connected by a lattice of hexagonal and pentagonal rings, in a pattern of overall icosahedral symmetry. Although  $C_{60}$  appears to be uniquely stable due to its perfect symmetry, all other even-numbered carbon clusters in the 32-100+ atom size range seem to favor similar closed spheroidal forms. These species are interpreted as relatively unreactive side products in condensation reactions of carbon vapor involving spiraling graphitic sheets. The prevalence of  $C_{60}$  in laser-vaporized carbon vapors and sooting flames suggests that it may be formed readily whenever carbon condenses. Such ready formation and extraordinary stability may have substantial astrophysical implications.

### I. INTRODUCTION

Development of laser techniques with supersonic molecular beams has stimulated a flurry of new results from earth-based, laboratory measurements on carbon. Although these new results are still in the process of verification, extension, and further interpretation, a rather remarkable new picture is beginning to emerge as to the processes of carbon condensation and the nature of the species involved. Perhaps the most concise way to introduce this subject is simply to list the key features of this new picture.

(1) Carbon nucleates to form small clusters far more readily than any other element in the periodic table (including such refractory elements as tungsten and tantalum).

(2) The smallest clusters ( $C_2$  through  $C_9$ ) are most stable in the form of linear chains.

-----  
\* Research on carbon clusters in author's group has been supported by the National Science Foundation and the Robert A. Welch Foundation.

- (3) Clusters in the 10-29 atom size range take the form of monocyclic rings.
- (4) Even-numbered clusters in the 32--100+ atom size range take the form of closed spheroidal shells (the "fullerenes").
- (5) Odd-numbered clusters in the 33-101+ atom size range take the form of nearly-closed spheroidal shells (the "semifullerenes").
- (6)  $C_{60}$  ("buckminsterfullerene") prefers the shape of a soccerball. Because of its size and perfect symmetry, it is extremely stable (chemically, thermodynamically, photophysically).
- (7) A spiral shell is a good model for the active nucleus involved in carbon grain growth (and soot formation).
- (8) The fullerenes are side products (dead ends) in the process of soot formation.
- (9) The fullerenes are made whenever carbon condenses, including sooting flames.
- (10) Metal atoms may be trapped inside completely closed fullerene shells.

When compared to the view prevalent in the carbon literature only a few years ago, these 10 points (with the possible exception of the first two or three) are quite divergent. Nonetheless, my colleagues and I have found the new experimental evidence compelling. To our knowledge this picture is the only one consistent with all experimental results, both new and old. This is intellectually quite an exciting time in carbon cluster research since in many essential aspects the new view is still rather controversial. We believe the evidence is strong, although in a few remaining cases the definitive experiment has yet to be done.

In most areas of cluster science new insights and observations are of fairly esoteric interest. But carbon is special. If the above points are correct there are major implications both in the fields of combustion and astrophysics. So it is well to review what is now quite an extensive body of experimental evidence, and let each observer come to her/his own conclusions.

## II. LASER VAPORIZATION CLUSTER BEAMS & ABUNDANCE DISTRIBUTIONS

Figure 1 shows a schematic of the sort of laser- vaporization cluster source used for the new carbon cluster experiments. This new technique was developed at Rice particularly for the study of small clusters of transition metals, but turned out to be rather general in scope (refs. 1-4). Here a pulsed laser is directed at the surface of the material to be studied. With currently available pulsed lasers one can easily generate temperatures on the target material in excess of 10,000K in this apparatus, readily vaporizing any known substance in such a short period of time that the rest of the source can operate at room temperature. The cool,

high density helium flowing over the target then serves as a buffer gas in which clusters of the target material form, thermalize to near room temperature, and then cool to near 0 K in the subsequent supersonic expansion as this helium emerges into a well-pumped vacuum chamber. Collimated beams skimmed from these supersonic cluster expansions then provide useful sources for detailed study of a vast set of fascinating new cluster species.

The first such experiment on carbon was performed by a group at Exxon (ref. 5) using an apparatus originally developed and built at Rice. As shown in Figure 2, a rather dramatic result is obtained in such an apparatus: there are two distinct cluster distributions. In the higher mass distribution only even-numbered clusters are observed. The Exxon group was uncertain as to the reason for the prominence of this second, even-numbered distribution, although they suggested it may be evidence for the formation during vaporization of a hypothetical "carbyne" form of carbon consisting of linear chains of triply-bonded carbon, much as had been reported previously (see ref. 6 and references therein). As it turned out, the real reason for this bizarre bimodal distribution appears to be even more interesting.

The key to unraveling this mystery appeared in experiments at Rice in the late summer of 1985 while my colleagues and I were exploring the chemical reactivity of the smaller-sized side of the bimodal carbon cluster distribution. Incidentally we noticed that one particular member of the large cluster distribution,  $C_{60}$ , often appeared significantly more intense in the supersonic beam than any other. Upon further study we found that the relative abundance of this special cluster was sensitive to the detailed clustering and reaction conditions in the supersonic nozzle (ref. 7). This is most clearly seen in Figure 3, which compares the cluster distribution obtained under two extremes. In each the abundance of each cluster is being monitored as a function of cluster size by direct 1-photon ionization with an  $F_2$  excimer laser (photon energy 7.9 eV) followed by time-of-flight (TOF) mass analysis of the cluster photoions. The bottom half of Fig. 3 shows the TOF spectrum of the clusters made by laser vaporization very early in the supersonic gas pulse when there is very little helium buffer gas present over the graphite target. Ordinarily under these conditions very little if any clusters are produced -- even with such refractory elements as tungsten, molybdenum, tantalum, and platinum. But carbon is by far the most facile at cluster formation of any element we have yet examined in such an apparatus. As shown in the bottom panel of Figure 3 these mild clustering conditions readily produce an abundance of large clusters of carbon. Note that there is no significant even-odd alternation in abundance, and no single cluster dominates the distribution.

However, the top panel of Figure 3 shows that a dramatic change in the cluster distribution occurs when more extreme clustering conditions are used in the nozzle. Here the vaporization laser was fired at the peak of the helium carrier gas pulse, when the effective helium pressure above the graphite target was roughly 1 atmosphere. At this higher pressure the laser-induced carbon vapor plume is more rapidly cooled, it is more effectively confined to a small volume in flowing gas during the subsequent passage out the rest of the supersonic nozzle, and diffusional loss to the nozzle walls is minimized. The result is that these high-pressure nozzle conditions are far more conducive to cluster growth, both by carbon atom addition and by reaction with small carbon radicals. In order to push this cluster growth and aging process to an extreme, a small reservoir was added to the down-stream section of the nozzle to prolong the reaction time prior to

formation of the free supersonic expansion. As shown by the top panel of Fig 3, these extreme clustering conditions leave primarily just one cluster behind in this size range: the remarkable  $C_{60}$ .

To us the most striking aspect of this prominence of  $C_{60}$  was the fact that none of the clusters of similar mass showed any suggestion that a particularly stable cluster was nearby: clusters of 52, 54, 56, 58, 62, 64, 68 carbon atoms all seemed to behave about the same. Upon a bit of reflection it occurred to us that this may be due to the fact that 60 is the number of vertices of a truncated icosahedron (ie. a soccer ball). Carbon with such a bonding structure would have its bonding needs met in a beautifully symmetrical fashion. The direct correspondence of this figure and the geodesic domes of R. Buckminsterfuller led us to suggest the rather tortuous name of "buckminsterfullerene" for this hypothetical form of carbon (ref. 7).

The likely stability of such a spheroidal 60-atom molecule of carbon had in fact been predicted before the new beam experiments (refs 8-10). In the two years since our original realization of the special aspect of  $C_{60}$ , a flood of calculations have appeared with successively higher level predictions of the stability and electronic structure of this icosahedral form of carbon (refs 11-40). Regardless of the theoretical approach used, there is now general agreement that this structure for  $C_{60}$  should be expected to result in a strongly bound, electronically closed shell, highly stable molecule.

### III. REACTIVITY STUDIES

Shortly after the initial realization that  $C_{60}$  was very special, and an early indication that a metal atom such as lanthanum could be put inside its spheroidal cage (ref. 41), we used a rapid flow reactor technique (ref. 42) to measure the reactivity of these carbon clusters toward various reagents (ref. 43). The principal result of this study is shown in Figure 4. Here again the TOF mass spectrum is shown of carbon cluster species in the supersonic beam as probed by direct photoionization with an  $F_2$  excimer laser. The top mass spectrum is a control showing the cluster distribution prior to reaction, the bottom panel shows the mass spectrum obtained after a flow of nitric oxide (NO) had been added to the fast-flow reactor. Under the conditions used the average carbon cluster received on the order of 10,000 potential reactive hard sphere collisions with the NO reactant molecules during passage at near 300 K through the reactor.

As expected,  $C_{60}$  was found to be effectively inert under these reaction conditions even with such active reagents as NO,  $SO_2$ ,  $O_2$ ,  $NH_3$ , and  $H_2O$ . As can be readily seen in Fig. 4, the odd-numbered clusters, and all clusters smaller than  $C_{36}$  were found to react readily -- just as would be expected if these species possessed one or more active carbon sites with effectively "dangling" bonds. The most striking result, however, was that not only  $C_{60}$ , but all even-numbered clusters of size greater than (roughly)  $C_{40}$  appeared to be almost as inert as  $C_{60}$  itself. They are far more inert than one would expect for any sort of open graphitic sheet.

This observation led to the suggestion that all these large even-numbered clusters may have tied up all their dangling bonds by taking the form of closed

spheroidal shells. As with  $C_{60}$  it is generally possible to construct many such closed nets of pentagonal and hexagonal rings. Figure 5 shows one possibility for  $C_{72}$ . Using Euler's theorem it is rather straightforward to prove that all such closed nets of  $n$  atoms have exactly 12 pentagons and  $n/2 - 10$  hexagons (refs. 12, 22, 23). Therefore only even-numbered clusters are capable of closing -- a fact providing a ready explanation of the measured higher reactivity of the odd-numbered carbon clusters. The smallest closed shell possibility would be  $C_{20}$  in the form of a dodecahedron (12 pentagons, 0 hexagons), although this species would almost certainly be far too strained to be stable. The saturated analog, dodecahedrane,  $C_{20}H_{20}$  has almost perfect tetrahedral bond angles and is a known and quite stable molecule (ref. 44). With the exception of  $C_{22}$  all larger even-numbered clusters may assume the form of one of these geodesically rigid, closed spheroidal shells. The architectural parallel has led us to refer to these species in general as the "fullerenes" of which  $C_{60}$ , "buckminsterfullerene", is the prototypical example.

#### IV. SYMMETRY, STRAIN CONCENTRATION, AND THE ADJACENCY OF PENTAGONS

The number 60 is rather extraordinary. It was the base of the Babylonian number system, from which we derive the current convention of dividing hours and minutes into 60ths, and the circle into 360 degrees. Continued use of this ancient practice likely stems from the ready factorability of the number 60: it and its multiples are the most highly factorable of all integers (eg. all members of the series {1,2,3,4,5,6} are factors simultaneously only for 60 and its multiples). A related, but more important property of 60 in the current context is that it is the number of proper rotations in the largest point group, the icosahedral group,  $I_h$ . As a direct consequence, 60 is the largest number of objects that can be arranged on the surface of a sphere such that each is exactly equivalent to every other.

As a side point, it is reasonable to argue that 120 is even more special since there are actually 120 elements in the icosahedral group, and one could arrange 120 objects on a sphere with each related to every other by an element in the group (for an example see ref 12). But only 60 of these 120 symmetry elements are proper rotations, the rest either involve inversion, reflection, or improper rotations -- symmetry operations which interconvert left and right-handedness. The 120 equivalent objects then fall in two sets of 60: one left-handed, the other right-handed.

In the case of spheroidal networks of 60 vertices, there are two distinct ways of generating an icosahedral structure: the truncated icosahedron consisting of 12 pentagons and 20 hexagons, and the truncated dodecahedron, consisting of 20 triangles and 12 decagons. Although each of these is equivalently symmetrical, due to bond strain and resonance effects carbon far prefers forming 5 and 6 membered aromatic rings over any other possibility. Electronic structure calculations for these structures have been compared using simple Huckel techniques by Fowler and Woolrich (ref. 16), by Klein, Seitz, and Schmaltz (ref. 22), and most recently with a somewhat higher level INDO procedure by

Shibuya and Yoshitani (ref. 35). All agree the truncated icosahedron is by far the most stable possible structure.

Given this soccerball structure for  $C_{60}$  as a starting point, one can begin to look for predictions of the relative stability of the other even-numbered  $C_n$  "fullerenes". Based on the overwhelming dominance of 5 and 6-membered aromatic carbon ring systems in nature, one expects these will be the most stable forms for all even-numbered carbon clusters. Each will assume the form of the most stable possible closed spheroidal net made up of 12 pentagons and  $n/2 - 10$  hexagons such as shown in Figure 4 for the case of  $C_{72}$ .

In examining such structures it is easy to imagine why  $C_{60}$  should be uniquely unreactive. Because of the symmetry properties of the number 60, only for this cluster is the strain of closure distributed perfectly over all atoms. In all other clusters the strain tends to localize. For example the structure shown in Figure 4 clearly has concentrated the strain on the vertices of the pentagons, leaving fairly flat regions in the top and bottom hexagonal nets. This is a general phenomenon in the larger carbon clusters: strain concentrates at the pentagons. Kroto (ref. 45) has recently discussed this issue in some detail.

For clusters smaller than  $C_{70}$  there is another factor to consider in addition to strain. It is reasonable to expect that structures having two or more adjacent pentagons will be less stable than those where the pentagons are isolated by intervening hexagonal rings. In all known naturally occurring or synthetic carbon molecules there is no known example of a stable species having two fused 5-membered aromatic carbon rings. Interestingly, Smaltz et. al. (ref. 38) have been able to show that  $C_{60}$  is the smallest fullerene which can avoid having two or more adjacent pentagons, and  $C_{70}$  is the next. The smallest cluster that can avoid having more than two pentagons adjacent turns out to be  $C_{50}$ , and the smallest that can avoid more than three adjacent is  $C_{32}$ . As can be seen in the cluster beam TOF mass spectra of Figs 1-3, clusters with 70, 60, or 50 atoms do, in fact, turn out to be specially abundant. Evidence for the special behavior of  $C_{32}$  has been found in fragmentation experiments (refs 46, 47) as will be discussed below when we consider the photophysics of the fullerenes and their observation in sooting flames (ref.48).

## V. NEGATIVE CARBON CLUSTER UPS

Cluster beam TOF abundance distributions and cluster reactivity studies have therefore provided reasonably impressive evidence for the spheroidal carbon shell model of large carbon clusters. But for many observers such data can never be completely adequate as proof of a structural assignment. As is true with research in all areas of both metal and semiconductor clusters, a direct spectral probe of these carbon species would be highly valuable.

Since these clusters are produced cold in a supersonic beam, one might suspect that high-resolution laser probes of the electronic spectrum in the visible and ultraviolet would be an excellent general tool. In fact quite powerful techniques have been developed and applied to supersonic beams of small

clusters involving resonant 2-photon ionization (R2PI) with mass-selective detection. The published studies of the vanadium dimer (ref. 49), the copper trimer (ref 50), and the triangular SiC<sub>2</sub> cluster (ref. 51) are a few of the many excellent examples of the power of this R2PI spectral technique -- when it works. Unhappily, this R2PI technique generally does not work well for clusters containing more than a few atoms. In the larger clusters radiationless decay processes are generally far too fast to permit detection of the upper level before the electronic excitation is degraded into the vibrational quasicontinuum. In the case of C<sub>60</sub> extensive R2PI probes have been carried out in our laboratory over large regions of the visible and ultraviolet spectrum without success. Electronic excitation in C<sub>60</sub> simply does not last long enough to detect by the R2PI technique.

One general way of overcoming such difficulties is to go after a different type of electronic spectroscopy, one that works equally well for bulk materials as it does for atoms and small molecules. Such a procedure is UPS, ultraviolet photoelectron spectroscopy. Recently we have been able to implement such probes of supersonic cluster beams in a general way by developing a magnetically-focussed time-of-flight electron spectrometer which measures the energy spectrum of photoelectrons detached by pulse UV laser irradiation of mass-selected negative ions of the desired cluster (refs 52,53).

#### V.1 Small Carbon Cluster UPS (Linear Chains and Monocyclic Rings)

The electronic and geometrical structure of small carbon clusters has been a topic of interest for molecular calculations over many years. In an early paper Pitzer and Clementi (ref. 54) used an elementary semi-empirical version of molecular orbital theory to conclude that linear chains should be the dominate form in carbon vapors. For such linear chains they found there should be a pronounced even-odd alternation in electronic structure: the even-numbered chains having open shell structures with a  $^3\Sigma^-$  ground state (except for C<sub>2</sub> where  $^3\Pi$  is lowest), and the odd-numbered chains having closed shell structures with  $^1\Sigma^+$  ground state. The even numbered clusters were predicted to be somewhat more strongly bound and have considerably higher electron affinity than the neighboring odd clusters.

These calculations were refined a bit later by Strictler and Pitzer (ref 55) where the possibility of monocyclic ring structures were considered more extensively. For such rings there is also an even-odd alternation in the electronic structure, except now it is the even-numbered clusters (and particularly those with 4n+2 carbon atoms, n=1,2,3,...) that are particularly strongly bound, with closed-shell singlet ground states and low electron affinities. In the early years of development of extended Huckel theory, Roald Hoffmann considered these small carbon clusters in detail (ref. 56). Generally, his results were consistent with those of Pitzer and his co-workers. His prediction was that the linear chains would be the favored form up through C<sub>9</sub>. At C<sub>10</sub> and above, however, Hoffmann predicted that monocyclic rings would be most stable.

Now we are in a position to test such theories using the new UPS cluster beam apparatus -- at least for the structures preferred by the negative cluster

ions. Figure 6 shows the UPS patterns for the small carbon cluster negative ions in the 2-9 atom range (ref. 57). The photoelectrons were detached here using a  $F_2$  excimer laser which has a photon energy of 7.9 eV. Note that the original prediction of Pitzer and Clementi is perfectly well born out by these data. The arrows in each panel of the figure mark our estimate to the vertical photodetachment threshold from the negative cluster ion, approximately corrected for thermal and instrument resolution effects. This corresponds to the vertical electron affinity (EA) of the neutral cluster, evaluated at the geometrical configuration of the negative cluster ion. Note that the even-numbered clusters in the left-hand panels exhibit electron affinities starting near 3.2 eV for  $C_2$  and increasing smoothly to nearly 4.4 eV for  $C_8$ . The odd-numbered clusters on the right-hand panels have considerably lower electron affinities, starting near 2.0 eV for  $C_3$  and increasing smoothly to 3.6 eV for  $C_9$ . In addition, note that there is substantial gap between the first peak in the UPS pattern of the odd-numbered clusters and the next major feature, and that the relative intensity of this first peak compared to the second decreases steadily as a function of cluster size. This is the expected behavior of a species which as a neutral has a tightly-bound closed shell electronic structure with a large HOMO-LUMO gap -- just as predicted by Pitzer and Clementi for odd-numbered linear carbon chains.

Figure 7 show the UPS patterns for negative carbon clusters in the 6 through 29 atom size range. Here it is clear that an abrupt change in the simple even-odd alternation of the linear chains has occurred starting at  $C_{10}$ . Here again arrows have been placed at the estimated vertical photodetachment onset, giving a measure of the vertical electron affinity of the neutral form of each cluster. Instead of having an EA of over 4.5 eV as would be expected from extrapolation of the EA trend of the smaller even-numbered clusters,  $C_{10}$  clearly has an EA closer to 2.3 eV. Furthermore, starting with  $C_{10}$  the simple even-odd alternation in UPS patterns has been replaced by a period of 4, as emphasized by the arrangement of the spectra in the figure. Note that these periods of 4 begin at 10, 14, 18, 22, and 26 -- just the numbers expected from the predictions of extra stability of  $(4n+2)$ -membered monocyclic rings.

Close examination of these UPS patterns shows one particularly glaring anomaly:  $C_{11}$ . For this cluster there appear to be two overlapping small features where one larger peak is expected at the photodetachment threshold. Figure 8 resolves this mystery. Here it is seen that there really are two distinct types of negative  $C_{11}$  clusters. Here we have been able to selectively prepare one or the other by varying the method of generating the negative cluster beam. For the bottom panel the nozzle was run in such a way that a portion of the carbon cluster ions resulting from the original laser-induced plasma survived passage through the supersonic nozzle and subsequent expansion, much as has been done by other workers in this field who have studied negative carbon clusters (refs 58, 59). In contrast, the UPS data of the top panel was taken using cluster ions prepared by directing an excimer laser (ArF, 6.4 eV) into the throat of the supersonic nozzle just as the neutral clusters emerged. Slow electrons produced by photoionization of some of the carbon clusters effectively attach to other members of the neutral cluster distribution under these conditions, producing an intense cluster ion beam (see refs 60-63 for more details). The UPS patterns taken under these two conditions are quite different -- and different in an interesting way. The top UPS panel is in excellent agreement with the pattern one would have expected for a linear  $C_{11}$  chain, based on extrapolation from the  $C_9$  UPS pattern and those of the smaller odd-numbered clusters. The bottom panel of Figure 8 is just what one would have expected for a monocyclic ring form of  $C_{11}$ , based on back-extrapolation

from the UPS patterns of  $C_{15}$ ,  $C_{19}$ ,  $C_{23}$ , and  $C_{27}$ . The cluster beam used to obtain the  $C_{11}$  UPS pattern in Figure 7 had been prepared using the excimer laser re-ionization technique, but apparently for that particular run the timing and laser intensity was such that an approximately 1:1 mixture of the two forms of  $C_{11}^-$  was produced.

This linear chain / monocyclic ring transition in the UPS patterns is particularly graphic in the electron affinity plot shown in Figure 9, where the EA values for each cluster were taken from the UPS data of Figures 6 and 7 at the positions of the arrows. Note that there are two points plotted for  $C_{11}$ .

The notion that carbon clusters in this size range may take the form of monocyclic rings is hardly new. The 4-fold periodicity seen in the early mass spectroscopy of carbon vapors from spark discharges (ref. 64) was used to reach this conclusion very early on in the history of carbon cluster research (refs 54,56). Recently, quite high level *ab initio* calculations have concluded that cyclic structures may be preferred for very small even-numbered clusters, eg. a rhombus for  $C_4$  (ref. 65), and a slightly distorted hexagon for  $C_6$  (ref 66). The UPS data shown here in Figs 6-8, and particularly the smooth EA trends, seems quite conclusive that the negative carbon clusters with <10 atoms prefer the linear chain geometry. Of course, it is likely that there is a minimum in the potential surface corresponding to a cyclic structure, and this minimum for some clusters such as  $C_4$  and  $C_6$  may be lowest for the neutral charge state of the cluster. These new UPS data only probe the favored geometry of the negative cluster ions.

For positively charged small carbon clusters there has been recently a very impressive determination that  $C_3^+$  is a monocyclic ring ( a triangle ) by measurement of the "coulomb explosion" this cluster undergoes as its electrons are stripped by passage at high velocity through a target foil (ref. 67). Photodissociation cross-section measurements (ref. 68) and reactivity measurements in an FT-ICR apparatus (ref 69-71) indicate that  $C_{10}^+$  behaves as a monocyclic ring.

The initial impetus for carbon cluster work at Rice was the question of whether the long carbon chain species so abundant in the interstellar medium could be produced effectively in condensing carbon vapors. Reaction studies performed with various reagents mixed in the helium carrier gas prior to laser generation of the carbon plasma provided a clear demonstration that long linear carbon chains can indeed be produced in this way (refs 72, 73). However, in light these new UPS results and the uniform results of quantum chemical calculations, it is now clear that carbon clusters substantially longer than 9 atoms will take the form of linear chains only in reactive conditions where the ends can be terminated by such groups as -H or -CN.

## V.2 Intermediate Size Carbon Cluster UPS (Open Polycyclic Nets and Highly-Strained Cages)

Above the high twenties there is a region in the carbon cluster distribution extending up to near  $C_{40}$  that is quite difficult to study. The clusters in this intermediate region appear to be far more reactive than either the small or large

carbon clusters, so that unusually when one samples carbon clusters from a vapor-phase distribution the concentration of these active species is abnormally low. This effect can be seen in the TOF cluster mass spectrum shown in Figure 2. It was first pointed out by Rohlfsing, Cox, and Kaldor in their original supersonic carbon cluster study (ref 5). These intermediate range clusters are difficult to generate, and thus far we have been unable to obtain repeatable, dependable UPS data for them. In order to generate useable cluster beams in this mass region, the cluster source must be run such that growth reactions in the nozzle are abruptly terminated, and there is little opportunity for the most stable form of a particular cluster to dominate the population. As a result, the cluster beam always appears to contain a mixture of closed- and open-shell species, and the resultant UPS patterns are ill-defined.

We suspect it is in this 28-40 atom cluster size range that the switch in cluster growth occurs from 2-dimensional monocyclic rings to polycyclic (quasi-graphitic) nets, to growing 3-dimensional spirals and highly strained cages.

### V.3 Large Carbon Cluster UPS (C<sub>60</sub> and the Fullerenes)

As shown in the bimodal distribution that generally characterizes carbon cluster distributions from these high pressure supersonic nozzle sources, above C<sub>40</sub> cluster abundance grows again, and there is a dramatic even-odd alternation in the cluster reactivities and intensities. Figure 10 shows the UPS patterns obtained for selected even-numbered clusters in the 48-84 atom size range (ref. 63). The odd-numbered clusters throughout this region display only broad, featureless UPS pattern characteristic of open-shell species. As is evident from the figure, the even-numbered clusters in this region generally do not have highly structured UPS patterns either. However, there are a few clear exceptions to this rule of little structure: C<sub>50</sub>, C<sub>60</sub>, and C<sub>70</sub>. Note that of all the clusters in this 48-84 region, C<sub>60</sub> has the lowest photodetachment onset (therefore the lowest EA) and the clearest initial peak, with the broadest gap to the next feature. This low electron affinity and substantial gap in the UPS pattern is indicative of a tightly bound, electronically closed shell molecule.

The UPS data of Figure 10 were taken with an ArF excimer laser (6.4 eV photon energy) used to produce the photoelectrons. Recently, we have begun re-examining these clusters with the new, higher photon energy F<sub>2</sub> excimer laser. Qualitatively the results are unchanged, except that now the difference between C<sub>60</sub> and the other clusters is far more pronounced. Figure 11 shows the most recent picture of the UPS pattern for C<sub>60</sub> taken with the F<sub>2</sub> laser at 7.9 eV. Sufficient structure is now resolved that detailed comparison with electronic structure calculations begins to be reasonable.

As mentioned earlier, C<sub>60</sub> has been the subject of many calculations over the past few years (refs 11-40). One interesting result emerging from these calculations is that the molecular orbitals near the top of the valence band of this cluster are almost purely made up of radially directed 2p atomic orbitals with a small amount of 2s hybridization on each of the 60 carbon atoms. The result is that even simple Huckel MO treatments which neglect the tangentially-directed orbitals will be fairly good approximations near the HOMO-LUMO region of the cluster. This point was first clearly made by Newton and Stanton based on

MNDO calculations (ref. 24), and independently confirmed by LMTD studies of Satpathy (ref. 25), the PRDDO work of Marynick and Estreicher (ref. 28), the DV-Xalpha calculations of Hale (ref. 27), and the CNDO/S method of Larsson, Volosov, and Rosen (ref. 35). A portion of the high-lying molecular orbital energy levels predicted by a simple Huckel calculation of icosahedral  $C_{60}$  is shown on the right hand side of Figure 11.

For the neutral  $C_{60}$  cluster the HOMO is (as shown in Fig. 11) an orbital of  $h_u$  symmetry; it is filled with 10 electrons, giving a closed-shell electronic ground state of  $^1A_g$  symmetry. The  $C_{60}^-$  negative ion ground state is then produced by adding one electron to the next highest orbital, the  $t_{1u}$  symmetry level marked in the figure as the LUMO of the neutral molecule, producing a state of overall  $^2T_{1u}$  symmetry. The first peak in the UPS spectrum for such a molecule would then arise from the photodetachment of the lone electron in the  $t_{1u}$  orbital. The binding energy of this orbital (approximately the vertical electron affinity) has been estimated to be 2.4 eV in the recent CNDO/S calculations of Rosen and coworkers (ref. 35). As seen in the UPS data of the figure, this is in fairly good agreement with measured value of roughly 2.8 eV.

The next lowest level, the  $h_u$  orbital that is the HOMO of the neutral cluster, is estimated in this same CNDO/S calculation to have a binding energy of 7.55 eV -- also in excellent agreement with the measured ionization potential of  $C_{60}$  which is known to lie in the range between 6.4 and 7.9 eV (refs. 43, 74). From the fact that the  $F_2$  laser is able to directly photoionize weakly-bound van der Waals adducts of  $C_{60}$  without fragmentation (ref. 75), we suspect the IP threshold is quite sharp, and located only slightly below the 7.9 eV photon energy of this laser. The agreement with the calculated 7.55 eV IP value of Rosen et. al. is therefore quite impressive.

Since the  $t_{1u}$  LUMO is calculated at 2.4 eV binding energy and seen in the UPS at roughly 2.8 eV, one might expect the next feature in the UPS spectrum would arise from removal of electrons from the  $h_u$  HOMO level and appear near the calculated 7.5 eV binding energy for this orbital. However, there is a detail here: these are 1-electron molecular orbitals, and the energy levels calculated by simply adding the orbital energies of all electrons corresponds to the energy of a single Slater determinant (single configuration) multielectron wavefunction for  $C_{60}$ . While the electronic ground states of  $C_{60}$ ,  $C_{60}^+$ , and  $C_{60}^-$  will be fairly well approximated by these single-determinant wavefunctions, the excited electronic states of  $C_{60}$  will not. IP and EA estimates from the HOMO and LUMO binding energy calculations should therefore be fairly accurate, but calculations of the excited electronic states of  $C_{60}$  must consider configuration interaction. This is true for simple aromatic molecules like benzene and naphthalene, it will certainly be true here for  $C_{60}$ .

In the absence of configuration interaction, predicted UPS pattern for  $C_{60}^-$  would show a peak due to removal of electrons from the  $h_u$  HOMO orbital shifted  $7.5 - 2.4 = 5.1$  eV higher in binding energy than the first peak arising from removal of the  $t_{1u}$  LUMO electron. Since there are 10 electrons in the  $h_u$  orbital, this second feature in the UPS spectrum should be roughly ten times more intense than the first (assuming, as is the case here, that the same type of atomic orbitals are involved in each molecular orbital). Removal of an electron from the  $h_u$  orbital of  $C_{60}^-$  gives rise to 8 excited electronic states with a configuration of  $(h_u)^9(t_{1u})^1$ :  $^1,^3T_{1g}$ ,  $^1,^3T_{2g}$ ,  $^1,^3G_g$ , and  $^1,^3H_g$ . Since these states are all of different symmetries, they will not mix through configuration interaction. But at

higher energy there are many excited states of these same symmetries arising from other orbital configurations (for example:  $(h_u)^9(t_{1g})^1$ ). The result of configuration interaction will then be to mix in these higher configurations, pushing the excited electronic states with  $(h_u)^9(t_{1g})^1$  parentage down in energy. As a consequence what would have been a sharp single peak in the UPS spectrum associated with removal of 1 of the 10 electrons in the  $h_u$  HOMO will now appear as an extensively broadened photodetachment band at considerably lower binding energy. Although a definite assignment must await comparison to a detailed calculation, the broad band appearing in the UPS data between 4 and 5 eV binding energy is a reasonable candidate. In fact the integrated area under this band does turn out to be roughly ten times larger than the first band at 2.8 eV.

The UPS data shows there is another, more intense band of excited states in the region of 6.5 to 5.5 eV. Referring to the predicted molecular orbital pattern, it is reasonable to tentatively assign this band to the states over overall ungerade symmetry arising from generation of a hole in the nearly degenerate  $g_u$  and  $h_u$  orbitals. Here the integrated intensity is about 1/80 of that expected for the 18 electron occupancy of these orbitals. Intensity in the UPS data then drops off sharply in the 6-7 eV region, as would be expected from the calculated molecular orbital pattern: the next available orbital ( $g_u$ ) is far deeper.

In summary, the new UPS data make it clear that the electronic structure of  $C_{60}$  is much like that expected of the soccerball geometry. As expected for such a well-bound closed shell molecule, the electron affinity is low -- much lower than any other carbon cluster in this size range, and quantitatively in agreement with the best calculations. In addition, the  $C_{60}^-$  UPS pattern is far more highly structured than any other carbon cluster in the region. For such a huge, highly unsaturated molecule it is hard to imagine such a simple UPS pattern arising from anything but the sort of rigid, highly symmetrical structure proposed. In addition, the details of this pattern appear consistent with theoretical expectations.

Of course the assignments of the excited state structure in the  $C_{60}^-$  UPS data postulated above can only be considered tentative at this point. Larsson, Volosov, and Rosen have calculated the excited electronic states of  $C_{60}$  allowing for interaction between 250 configurations of lowest energy (ref. 35). Such calculations can provide the sort of information needed for a detailed comparison with the new UPS data.

## VI. PHOTOPHYSICS OF THE POSITIVE CARBON CLUSTER IONS

Regardless of the ultimate answer to the question of the structure of  $C_{60}$ , it is by far the most stable small cluster of carbon. As such it may be made in abundance wherever carbon condenses. From the standpoint of astrophysics, one of the most significant aspects of this molecule is its photophysics: how much excitation can  $C_{60}$  withstand? How efficient is  $C_{60}$  at re-radiating excitation energy? What are its photofragmentation products? Since in most astrophysical environments of interest carbon is ionized, these questions on the photophysics of  $C_{60}$  are particularly relevant for the positive ion,  $C_{60}^+$ . And, of course, it would be nice to know how the answers to these questions compare with those for all other clusters of carbon.

Using tandem time-of-flight techniques (ref. 76) a good deal of progress has been made in understanding the photophysics of mass-selected carbon cluster positive ions over the past several years. For the small positive cluster ions (up to  $C_{20}^+$ ) Geusic and co-workers at Bell Labs (ref. 68) found that laser excitation in the visible or ultraviolet resulted in only a single fragmentation pathway: successive loss of  $C_3$ . This was true both of even-numbered and odd-numbered clusters. More recently we have reproduced and extended these studies to larger clusters (ref. 46). Two distinct photophysical regimes were found. The first applies to all positive carbon clusters of 31 atoms or less. As found by the Bell Labs group for the smaller members of this set, all these clusters photodissociate exclusively by the loss of a neutral  $C_3$  fragment. Dominance of this fragmentation channel over that for the loss of C or  $C_2$  is easy to rationalize since  $C_3$  is far more stable. For the reasons first put forward by Pitzer and Clementi (ref. 54) the even-numbered small carbon clusters such as  $C_2$  are not as strongly bound as is  $C_3$ . The cohesive energy of the diatomic  $C_2$ , for example is only 3.1 eV/atom, while that of  $C_3$  is 4.2 eV/atom (see ref. 77 for the most recent estimate of small carbon cluster binding energies). Raghavachari and Binkley have recently considered the photofragmentation of these small carbon clusters in detail. They concluded that the  $C_3$  loss channel is energetically preferred for all carbon clusters at least up to  $C_{10}^+$  -- even when one considers the possibility that some of the even clusters may be monocyclic rings (ref. 77). The uniform observation of  $C_3$  loss from the small carbon clusters is therefore unsurprising.

The second distinct photophysical regime for positive carbon clusters applies to the most stable (unreactive) forms of all clusters larger than 33 atoms. The qualifier here about the most stable forms is necessary since many valence isomers of these larger carbon clusters are possible, and the presence of the more reactive, less well-bound versions is sometimes detected in the supersonic beams (see ref. 46 for details). For the most stable forms of the even-numbered clusters in this  $>33$  cluster size range the photophysics is again simple, but is also quite surprising: these even "fullerenes" are extremely difficult to photodissociate, and when at sufficiently high laser excitation they do ultimately fragment, they do so by the loss of  $C_2$ . For example, Figure 12 shows the result of a tandem-TOF photodissociation experiment on  $C_{60}^+$  irradiated by a  $2 \text{ mJ cm}^{-2}$  pulse of ArF excimer laser radiation (6.4 eV). As is evident in the figure,  $C_{58}^+$  is the primary photoproduct. As the laser fluence is increased the smaller even numbered fullerenes are produced by successive  $C_2$  loss.

Figure 13 shows the photodissociation laser fluence dependence on the observed primary ( $C_{58}^+$ ) and secondary ( $C_{56}^+$ ) photoproduct from  $C_{60}^+$  mass-selected in the tandem-TOF apparatus and irradiated with a single 10 nsec pulse of ArF radiation (1930 Å, 6.4 eV) with a fluence per pulse which was varied under computer control and measured for each shot (ref. 46). Note that there is a minimum fluence below which no significant fragment signal is seen, and that this critical minimum fluence is greater for the  $C_{56}^+$  photoproduct. This proves that dissociation of  $C_{60}^+$  is a multiphoton process at this wavelength, and that  $C_{56}^+$  is a secondary photoproduct.

It is difficult in such experiments to obtain an accurate measure of the photon order of a dissociation process once this order is greater than one. Inhomogeneities in the laser beam profile, imperfect overlap between laser beam

and target beam, and temporal irregularities in the laser pulse all have the effect of making the apparent photon order seem much lower than it really is (see the appendix of ref. 76 for a numerical example). In addition, the  $C_{60}^+$  supersonic cluster ion source used for these experiments is now known not to have cooled the internal degrees of freedom of the carbon clusters completely. It is possible the species studied had internal temperatures in excess of 400K. Given the predicted vibrational frequencies of  $C_{60}$  (refs. 34,39), one can calculate that a 400K vibrational temperature means the average cluster starts off the photodissociation experiment with 3.7 eV internal energy even before the first photon is absorbed.

By careful fitting of photofragmentation fluence measurements such as that shown in Figure 12, we are confident that the  $C_{60}^+ \rightarrow C_{58}^+ + C_2$  primary fragmentation event is at least a 3 photon process at 1930 Å. Because of the photon order measurement difficulties mentioned above, it is likely that the real photon order for  $C_{60}^+$  fragmentation is even higher. The main point here is that  $C_{60}^+$  is an extremely photoresistant molecule, requiring more than 12.8 eV to dissociate, and probably much more. In fact it is the most photoresistant positive cluster ion we have ever encountered in such an experiment, including such extremely tightly bound clusters as  $Ta_{10}^+$ .

Similar photodissociation experiments to those shown in Figure 12 have been carried out for a wide range of the large even carbon cluster "fullerenes". All behave essentially the same way: they are all highly resistant to fragmentation, and when they do, they do so by the loss of  $C_2$ . As the photodissociation laser fluence is increased, the successive  $C_2$  loss process generates successively smaller even numbered cluster ion products. But, as shown in Figure 14, this  $C_2$  loss process does not go on forever. The  $C_2$  loss continues down until  $C_{32}^+$  is formed. At this point, instead of losing  $C_2$  to become  $C_{30}^+$ , this critical cluster virtually explodes in to small pieces, most of which are smaller than  $C_{20}^+$ .

As discussed a bit earlier,  $C_2$  is a very strange fragment to find coming out of any large cluster of carbon;  $C_3$  or virtually any other larger fragment would be energetically far more favorable. After extensive consideration over the past year in our laboratory and others, only one mechanism has been advanced which can successfully explain this  $C_2$  loss. It involves the concerted removal of  $C_2$  from a closed fullerene net. As the top panel of Figure 15 shows, it is possible to extract a  $C_2$  unit from such a closed net while at the same time beginning to form the next smaller fullerene whenever two pentagons are adjacent in the net. This mechanism has the advantage that it readily explains why the sequential photodissociation process senses that  $C_{70}^+$ ,  $C_{60}^+$ , and  $C_{50}^+$  are particularly stable as high order grand-daughters (ref. 46). As shown in the lower two panels of Fig. 15, concerted mechanisms for loss of longer even-numbered chains are available for the fullerenes as well. Dissociation by these longer chain pathways appears to be necessary in order to explain certain observations in the long-term decay of intensely irradiated fullerenes (see ref. 46 for details). Such processes may be a significant source of the long carbon chain species in the interstellar medium.

The only alternatives to the closed fullerene net model for these clusters would have to involve either interlinked polyacetylene chains or open graphitic sheets. From the measurements on the <32 atom clusters which we know are linear chains and monocyclic rings, all these species fragment readily at low laser

fluence, and they do so by the very sensible path of  $C_3$  loss. For any open graphitic net it is easy to see that  $C_3$  loss from one of the edges is always available, and involves no more bond breakage or rearrangement than would  $C_2$  loss. Since  $C_3$  removal is by far the lowest energy channel, there is no reason to expect  $C_2$  loss to occur.

On the other hand, a closed, edgeless carbon network such as that postulated for the fullerenes has a far more difficult time producing any fragments. This, we believe, is why the photophysics of these species is so difficult to activate, and why the  $C_2$  loss channel suddenly becomes important. Incidentally, this model also naturally explains why the  $C_2$  loss terminates abruptly at  $C_{32}^+$  and why this last cluster dissociates explosively. Each  $C_2$  loss from a fullerene produces the next smaller fullerene. Schmaltz et. al. have shown (ref. 38) that the total out-of-plane angle strain necessary to close a graphitic sheet into a fullerene shell is to first order independent of the size of the cluster. As the cluster gets smaller, the strain per carbon atom increases, until at some point the fullerene shell will be too unstable to survive. Apparently the smallest viable fullerene shell is  $C_{32}$ .

### VI.1 The Semifullerenes

The only remaining well-defined carbon cluster species to be discussed are the large odd-numbered species,  $C_n^+$ , where  $n$  is an odd number  $> 33$ . The photophysics of these is quite simple. The primary photoprocess is loss of a single C atom, or in some cases loss of a single  $C_3$ . After this initial loss the resultant even-numbered daughter ion will (if sufficiently excited) begin losing  $C_2$  pieces just as if it had begun as a member of the even-numbered fullerene family. The fact that the high-order grand-daughters in this successive  $C_2$  loss process appear to sense the special nature of the "magic" fullerene numbers (70,60,50) indicates that these grand-daughters are, in fact, fullerenes themselves (see ref. 46 for details). Since it is impossible to generate a closed fullerene net with an odd number of carbon atoms, they must originally be open. But the fact that the primary photoprocess is often loss of a single C atom strongly suggests that these species are nearly as close to closure into a fullerene net as they can get -- hence the name "semifullerene".

Very similar results have been obtained by Bowers and coworkers by examining the fragmentation routes of metastable carbon cluster ions produced by laser vaporization of a graphite target in a vacuum (ref. 47) although their explanation of these fragmentation pathways is completely different.

## VII. PHOTOPHYSICS OF METAL-CONTAINING FULLERENES

There is one other class of photophysical experiments that have recently provided further indication that the fullerenes are in fact closed, hollow shells. Shortly after our first realization that  $C_{60}$  may have the form of a hollow sphere, we published evidence that a single metal atom could be trapped inside (ref. 41). The key experimental result was that shown in Figure 16. This shows the TOF mass spectrum of large clusters in a supersonic beam made by laser-vaporization of a graphite disc which had been impregnated with  $LaCl_3$ . There are two mass spectra shown here, both obtained using an ArF excimer laser to photoionize the species in

the beam. The bottom panel shows the spectrum obtained at very low probe laser fluence ( $<0.01 \text{ mJ cm}^{-2}$ ) such that multiphoton excitation and fragmentation of the clusters was minimized as much as possible. As seen in the figure, the TOF mass spectrum obtained in this way was highly complicated, containing features due to bare carbon clusters and clusters containing one La atom which each peak broadened to the high mass side and the whole spectrum riding on a broad, unresolved baseline. In a TOF mass spectrometer such asymmetrically broadened peaks and underlying baseline signal are a signature of extensive fragmentation of the parent ions during the initial acceleration process in the sample region of the spectrometer. In fact the baseline signal was considerably worse than shown here; most has been cut out in the figure in order to get the partially resolved peaks on the same scale as the top panel.

This top panel, on the other hand, was taken at a much higher ArF excimer laser fluence ( $1\text{--}2 \text{ mJ cm}^{-2}$ ). Previous experience with ordinary organometallic complexes in this group (refs 78,79) had led us to expect that even strongly bound complexes would be readily fragmented at these laser fluence, resulting in a complete loss of ligands, leaving only the charged (often multiply charged) bare metal atom or metal oxide. As a group organometallic complexes are not particularly photoresistant. So it is quite impressive to see in the top panel of Figure 15 that large organometallic clusters survive high laser excitation. Not only do they survive, but (aside from  $\text{C}_{60}^+$  and  $\text{C}_{70}^+$ ) species of the form  $\text{C}_n\text{La}^+$  are the only ions detected in this mass range. Furthermore, there is no evidence of clusters surviving with more than one La atom, suggesting that there is only one strong binding site. Similar results were obtained with Ca, Sr, and Ba when the corresponding chloride was incorporated in the graphite disc.

Kaldor and co-workers have cautioned that due to photoionization artifacts this early evidence that the clusters have only a single strong metal atom binding site may be misleading (ref. 74). They have shown that in some cases such as potassium, carbon clusters with 2 or 3 metal atoms can be detected in the supersonic beam (refs. 80, 81). However, their own experiments show that only  $\text{C}_n\text{K}^+$ , the clusters with a single metal atom, are sufficiently stable to survive at high laser fluences (ref. 81).

One test of the hypothesis that the metal atom in these complexes is trapped inside a closed fullerene shell is to examine the photophysics. If the M in the  $\text{C}_n\text{M}^+$  complexes is completely surrounded by an edgeless carbon net, then such complexes should be at least as photoresistant and the bare  $\text{C}_n^+$  clusters, and when they fragment they should do so by the loss of  $\text{C}_2$ , leaving the metal atom still trapped inside a now somewhat smaller fullerene shell. As shown in Figure 17, this is exactly what happens.

Here the  $\text{C}_{60}\text{La}^+$  and  $\text{C}_{72}^+$  clusters were extracted from a supersonic beam and injected into an ion cyclotron resonance apparatus (refs. 82, 83). The ions are trapped in a high vacuum in the analysis cell of this apparatus by the combination of a strong (6 Tesla) axial magnetic field and an electrostatic barrier. After exposure to roughly  $10^4$  thermalizing collisions with a neon buffer gas to cool the translational and internal degrees of freedom of the clusters to near the 120K wall temperature of the trap, these clusters were subjected to 50 shots of an ArF laser at roughly  $4 \text{ mJ cm}^{-2}$  fluence per shot. Detection of the contents of the analysis cell was accomplished by coherent RF excitation of the cyclotron motion of the ions, followed by amplification and digitization of the oscillating image charge currents in the side electrodes of the cell. The Fourier transform of this

time-dependent signal then provides a sensitive, non-destructive measure of the contents of the cell at extremely high mass resolution. This technique, known as Fourier transform ion cyclotron resonance (FT-ICR) is one of the most promising new probes for cluster ions.

As is evident from comparison of the top panel where no laser excitation was used, the result of such intense laser irradiation has been to fragment a portion of both the original types of clusters in the cell. As expected, both show exactly the same photophysical pathway: successive loss of  $C_2$ . Also as expected, the metal-containing cluster is a bit more photoresistant than the bare fullerene (although part of this extra stability is due in this case to the fact that a  $C_{60}M^+$  cluster is being compared to one of the less stable fullerenes,  $C_{72}^+$ ).

These experiments have been extended to a wide variety of the  $C_nLa^+ / C_{n+12}^+$  metal complex / bare cluster pairs with similar results. FT-ICR photolysis experiments have also been done with  $C_nK^+$  clusters. They too are extremely photoresistant, and ultimately fragment by the  $C_2$  loss route. One particularly intriguing result is that the  $C_2$  loss process for  $C_nK^+$  breaks off abruptly at  $C_{44}K^+$ . Just as  $C_{32}^+$  is the last fullerene seen in the high order photofragmentation of the bare carbon clusters,  $C_{44}K^+$  appears to be the smallest viable potassium-containing carbon cluster.

Computer modeling of the  $C_nK^+$  clusters reveals a very simple explanation for this break off at 44. The ionic radius of  $K^+$  is 1.33 Å. Assuming a 1.45 Å carbon-carbon bond length and a 1.6 Å carbon van der Waals radius, these modeling tests show that there is plenty of room for the electronically closed shell  $K^+$  atom to fit inside the closed  $C_n$  fullerene net as long as  $n > 44$ . For  $C_{44}K^+$  a few bonds need to be lengthened to roughly 1.5 Å to permit the  $K^+$  atom to fit. But for  $C_{42}$  smaller fullerenes the amount of bond stretching required becomes quite prohibitive. Experiments are currently in progress to see if this critical  $C_nM^+$  cluster size scales correctly with the size of the alkali ion.

### VIII. STATISTICAL FRAGMENTATION & RADIATIVE COOLING

In the course of these FT-ICR photolysis experiments an observation was made that is particularly relevant to the question of survival of these carbon cluster ions in the interstellar medium. The fluence dependence of the fragmentation process shown in Figure 17 was the same as that found in the tandem TOF experiments (Fig. 13) where only a single laser shot could be used prior to monitoring the fragments. In the ICR apparatus the carbon cluster ions can be exposed to many laser pulses over an extended time period (over 30 seconds) while the background pressure is so low ( $< 10^{-8}$  torr) that the only de-excitation pathway is radiative. Under these conditions when the fluence per 10 nsec pulse of the ArF laser was less than  $0.5 \text{ mJ cm}^{-2}$ , no fragmentation whatever was seen from  $C_{60}^+$  -- even when the repetition rate of the laser pulses was raised to 50 Hz and the clusters were irradiated for over 30 seconds.

From measurements to be described below in the section on optical spectroscopy of fullerenes, we know that the absorption cross-section of  $C_{60}^+$  at the 1930 Å wavelength of the ArF laser is roughly  $5 \times 10^{-16} \text{ cm}^2$ . At a fluence of  $0.5 \text{ mJ cm}^{-2}$  the probability of a 1-photon excitation event in any particular  $C_{60}^+$  cluster is then roughly 1/20. Without radiative cooling the typical  $C_{60}^+$  cluster

would then receive  $0.2 \times 1500 = 300$  ArF laser photons of excitation. The fact that no dissociation was observed indicates that  $C_{60}^+$  is very efficient in radiating away excitation energy on a millisecond timescale.

Given the absence of and C-H oscillators in this molecule, it is initially rather surprising that radiative cooling is so efficient. But here the key feature is that the molecule is so large (174 vibrational modes) that for a statistical dissociation process with even a moderate activation barrier, an extreme amount of superexcitation is required to produce fragmentation on a relevant time scale. If  $C_{60}^+$  has the icosahedral structure we have suggested, any UV photoexcitation will initially be globally distributed over the cluster. Since electronic radiationless energy decay is fast in  $C_{60}$  (otherwise R2PI would work), it will certainly have to dissociate starting from a statistical distribution of the available energy among the 174 vibrational modes. This is a nearly macroscopic bath of vibrational states. For example, given the recent estimates for the vibrational frequencies of  $C_{60}$  (ref. 34,39), one can readily calculate that even at only 1.0 eV vibrational energy in the cluster there are over  $6 \times 10^{18}$  vibrational states per  $cm^{-1}$ .

If one accepts the closed carbon net structure for the fullerenes, it is easy to find on energetic grounds alone that the dissociation barrier of  $C_{60}^+$  to form  $C_{58}^+ + C_2$  will be at least 4 eV (reference to Figure 15 shows that 2 carbon-carbon bonds are lost in this process, each worth over 2 eV). In addition, the concerted loss process of Fig. 15 is orbitally-forbidden in the Woodward-Hoffmann sense (ref. 84), and should therefore have a substantial activation barrier. So it is difficult to imagine the barrier to  $C_2$  loss from  $C_{60}^+$  being less than something like 5 eV. Even with optimistic assumptions as to the nature of the activated process, a crude RRKM calculation of the unimolecular fragmentation rate of  $C_{60}^+$  shows that the average cluster would require over 26 eV excitation energy in order to dissociate over such a barrier in less than 0.1 second.

While radiative cooling should be very slow for moderate levels of excitation, 26 eV is not moderate -- it is equivalent to the average thermal excitation of  $C_{60}^+$  at 1800K. Approximated simply as a black body, the radiative cooling rate of  $C_{60}^+$  would be extremely fast at these levels of excitation. However,  $C_{60}^+$  will not act as a black body at these temperatures, even though the high excitation will certainly speed the radiative cooling rate considerably. The lowest excited electronic state of  $C_{60}^+$  capable of emitting electric dipole radiation is likely to be above 1 eV, and there will be little weight for such excited electronic states in the typical quasicontinuum wavefunction even at 26 eV. Vibrational excitation of the ground electronic state will dominate, with an average of 2-3 quanta in each of the 174 vibrational modes. Excited  $C_{60}^+$  will therefore be a poor black body emitter. The bulk of the radiation from the superheated molecule should still be expected to be emitted in the infrared at frequencies near each of the four ir-active  $t_{1u}$  modes (calculated frequencies: 1628, 1353, 718, and 577  $cm^{-1}$  -- see refs. 34, 39). The highest two of these have been calculated to have large dipole moment derivatives (3.1 and 2.0 debye  $\text{\AA}^{-1}$ , respectively for the 1628, and 1353  $cm^{-1}$  modes) and should therefore be particularly effective IR emitters (ref. 39). This fact coupled with the high degree of vibrational excitation make the result of millisecond (or faster) radiative cooling times seem reasonable, although it would be interesting to see a detailed calculation.

Regardless of the explanation for the efficient radiative cooling, the clear experimental result is that excitation energy sufficient to fragment  $C_{60}^+$  must be pumped in within considerably less than 20 milliseconds in order to be effective. In low flux astrophysical environments where the highest energy photon is insufficient to fragment  $C_{60}^+$  in a single step, this molecule should therefore be quite stable. Because of its unique symmetry, its size, and the perfect absence of edges providing easy, low energy fragmentation pathways,  $C_{60}^+$  may be the most photoresistant of all possible molecules. Because of its ability to cool by infrared emission, it may be able to survive unshielded in the interstellar medium for very long periods of time.

Interestingly, there appears to be a close agreement between the calculated frequency of the two most intense IR active modes in  $C_{60}$  and two of the more intense interstellar IR emissions in the 6 to 8 micron region (see, for example, ref. 85).

## IX. OPTICAL SPECTROSCOPY

Direct optical probes of  $C_{60}$  and similar large clusters have proved difficult. Due to the low densities of the cluster species in the supersonic beam and the need to distinguish the spectrum of one cluster from all others, direct absorption methods are generally not applicable. The principal techniques of obtaining electronic spectra of clusters in supersonic beams rely either on resonant photoionization (R2PI) or fluorescence detection, both of which effectively require the excited electronic states of the cluster to live for a nanosecond or more. Neither  $C_{60}$ , nor any of the other clusters of carbon beyond  $C_3$  seem to have such long-lived excited states -- at least none have been found in the extensive surveys carried out thus far.

### IX.1 Neutral $C_{60}$

In spite of these difficulties, one moderately successful spectral experiment has recently been reported for  $C_{60}$  using a van der Waals probe technique (ref. 75). Here  $C_{60}$  was cooled in a supersonic helium jet which had been seeded with a few percent concentration of a small closed shell molecule -- benzene, for example. By arranging for a particularly intense expansion, some of the  $C_{60}$  molecules were cooled sufficiently that a benzene molecule became attached to the surface, held only by weak van der Waals bonds. In the subsequent supersonic beam the concentration of this  $C_{60}$ -benzene complex was detected by direct 1-photon ionization with a  $F_2$  excimer laser at 1570 Å (7.9 eV), followed by TOF mass spectrometric detection of the  $C_{60}^+$ -benzene ion. One of the virtues of this approach is that one is guaranteed to be dealing with an extremely cold molecule. Based on other known van der Waals complexes, the  $C_{60}$ -benzene van der Waals bond is unlikely to be stronger than 1500  $cm^{-1}$ . Vibrational predissociation of such van der Waals complexes generally proceeds readily on a microsecond timescale, so that only those  $C_{60}$ -benzene complexes with less than 1500  $cm^{-1}$  internal energy are likely to last the 700 microsecond flight time from the source in this beam apparatus to the detection chamber. In the case of  $C_{60}$ -benzene, this implies the effective vibrational temperature of the complex in the beam must be less than 30 K.

Since the  $C_{60}$ -benzene van der Waals complex is so weakly bound, its spectrum may be probed simply by passing a tuneable laser down the axis of the molecular beam. The result of absorption of a laser photon is inevitably dissociation of the van der Waals complex, and this fact may be sensed as a depletion of the van der Waals complex concentration in the beam. Such depletion spectroscopies are notoriously insensitive since they try to detect a small change in a large, erratic signal. Nonetheless, it was successful in this case. Figure 17 shows a single, isolated absorption feature detected by this van der Waals probe technique. It is roughly 50  $cm^{-1}$  wide, located near 3860 Å, and rides on an underlying absorption continuum. The estimated absorption cross-section at the peak is  $1.2 \times 10^{-17} cm^2$ , while that of the underlying continuum is 2-4 times smaller. The top spectrum was recorded for the  $C_{60}$ -benzene complex, the bottom for the methylene chloride complex,  $C_{60} \cdot CH_2Cl_2$ . The fact that this absorption feature appears only slightly shifted in both complexes, and the fact that neither benzene nor methylene chloride have absorptions anywhere close to this wavelength proves that this isolated absorption band is due to the cold  $C_{60}$  molecule. Since the shift is so slight when such a drastic change is made in the type of van der Waals probe molecule, one expects the corresponding absorption feature in the bare  $C_{60}$  molecule will be close to this same wavelength.

The assignment of this 3860 Å band of  $C_{60}$  is not yet certain. Based on its position (3.22 eV) and the fact that it appears alone, it has been tentatively assigned as the 0-0 band of the first electric dipole allowed electronic transition of icosahedral  $C_{60}$  ( ${}^1T_{1u} \leftarrow {}^1A_g$ ). The calculations of Rosen and coworkers predict this transition should be found at 3.6 eV, and have an oscillator strength of 0.08. The fact that the observed transition has an oscillator strength of only 0.004 gives reason to suspect the assignment may be in error (see ref. 75). Due to difficulties in laser technology and apparatus time, the spectral search was completed only over the regions 3350 -- 3450 Å, 3650 -- 4000 Å, 4350 -- 4450 Å, and 5750 -- 5900 Å. Although the 3860 Å band was the only spectral feature observed in these regions, given the rather poor sensitivity of the technique other weaker transitions might have been missed. It is quite possible that the real  ${}^1T_{1u} \leftarrow {}^1A_g$  origin lies in one of the as yet unscanned regions. Regardless of the final assignment of the 3860 Å band, it is impressive that such a relatively narrow, isolated absorption feature exists in a carbon cluster this large.

Perhaps more interesting is where this  $C_{60}$  molecule does not absorb: it is nearly transparent in the visible. Even with a 200 mJ  $cm^{-2}$  laser pulse, the 5320 Å green output of a doubled Nd:YAG laser produced no noticeable fragmentation of the  $C_{60}$ -benzene van der Waals complex. The absorption cross-section of  $C_{60}$  at this wavelength is less than  $2 \times 10^{-19} cm^2$ . Furthermore, careful spectral scans in the regions of the strongest known diffuse interstellar bands (4428, 5780, 5797 Å -- ref. 86) showed conclusively that neutral  $C_{60}$  is not responsible.

## IX.2 Optical Spectroscopy of $C_{60}^+$

The positive ion of  $C_{60}$  is likely to be the most abundant form in the interstellar medium. Unlike the closed-shell icosahedral neutral molecule where the first dipole-allowed transition is not expected until the ultraviolet, the open-shell  $C_{60}^+$  is expected to have 10 - 15 allowed electronic origins sprinkled throughout the visible spectrum. Given the rigidity of the icosahedral net, and the small change in net bonding produced by promotion of 1 out of 239 bonding

valence electrons, these 10-15 electronic bands are expected to be confined mostly to just the 0-0 vibrational origins, with small splittings due to Jahn-Teller effects. In other words,  $C_{60}^+$  is an outstanding candidate for the carrier of the diffuse interstellar lines (refs. 7, 86).

An attempt has been made to record the spectrum of  $C_{60}^+$  by an extension of the way the neutral molecule was done: using a van der Waals probe. However, the interaction between benzene and  $C_{60}^+$  is considerably stronger than between benzene and neutral  $C_{60}$ . This becomes vastly more of a problem in the excited electronic states of the complex since configuration interaction with the  $C_{60}$ -benzene<sup>+</sup> charge transfer states is strong. The  $C_{60}^+$ -CH<sub>2</sub>Cl<sub>2</sub> complex should be somewhat better in this regard, but we have found the spectrum of both complexes to be structureless. Either there are no sharp spectral features for  $C_{60}^+$ , or the benzene and methylene chloride probes cause too much of perturbation. Efforts are underway to use a more innocent probe such as neon, although this will require a major change in cluster source technology.

Although the benzene and methylene chloride probes have not provided any sharp spectral features, they have permitted estimates of the absorption intensity over broad wavelength regions. As with the neutral  $C_{60}$ , the cold positive ion is effectively transparent in the visible (cross section  $< 2 \times 10^{-19} \text{ cm}^2$ ). In the ultraviolet, preliminary absorption cross-section estimates were roughly the same as those measured for the neutral:  $2 \times 10^{-16} \text{ cm}^2$  at 248 nm,  $7 \times 10^{-16} \text{ cm}^2$  at 1930 Å. Considering the significant possibility that  $C_{60}^+$  or some of the other fullerenes may be responsible for the interstellar UV extinction feature (ref. 87), these absorption cross-section measurements should be extended and performed with care. Again, it would be best to complete these only after the technology is in hand to study less perturbed complexes such as  $C_{60}^+$ -neon.

## X. ASTROPHYSICAL $C_{60}$

Granting the fact that  $C_{60}$  is so special and so readily produced in the laser-produced carbon vapor of these supersonic nozzles, it is still by no means obvious that it should be generated in significant quantities in any astrophysical environment. When considering why such spheroidal nets should form spontaneously, my colleagues and I proposed a mechanism in which a growing graphitic sheet incorporates pentagons on its periphery so as to minimize the dangling bonds (ref. 43). For each new pentagon included, a few new carbon-carbon bonds could be made from what were previously dangling bonds on the hexagonal lattice. Each added pentagon causes further curling of the growing sheet, but the instability associated with adjacent pentagons tends to keep them isolated from each other by an intervening hexagon. The result is a propensity for a graphite sheet to curl with a curvature that is exactly that of  $C_{60}$ . Once the growth has gone far enough that the opposite edges approach, there is a possibility that the spheroidal net will close, thereby producing a fullerene. However, most such growing imperfect nets would be expected to overlap the opposite edge, burying it inside, and continuing to grow in spiralling shells around a central core. Figure 19 shows an idealized image of such a growing spiral particle. Sumio Iijima has reported evidence for such spiralling carbon particles visualized in an electron microscope (see ref. 88 and references therein).

While this is a topologically appealing mechanism, it depends for its driving force on the presence of dangling bonds on the periphery of the growing

nets. In the more relevant environment of a sooting flame -- or the outer atmosphere of a carbon-rich red giant -- there is plenty of hydrogen around to tie up these dangling bonds. Why would there be any tendency to curl then? We suspect the answer is the same as it is to the question of why carbon nets grow at all under these conditions: at these high temperatures carbon-carbon bonds are preferred over carbon-hydrogen bonds. At high temperatures in hydrocarbon systems, carbon is most stable as graphite; hydrogen is most stable as  $H_2$ .

Regardless of the reasons advanced pro and con for the likelihood of  $C_{60}$  formation in sooting environments, there has now been a direct measurement of its presence in high abundance along with the other fullerenes in acetylene-oxygen and benzene-oxygen flames (ref. 48). If  $C_{60}$  is formed in these sooting flames, it is almost certainly formed in abundance also in carbon-rich red giants, since the temperatures and compositions are quite similar. Given the unique photophysical stability of  $C_{60}^+$ , it appears possible that this molecule may be able to survive migration far away from its original star. It may therefore be both very abundant and very important in the interstellar medium.

The list of possible astrophysical implications of abundant circumstellar and interstellar  $C_{60}$ , the fullerenes in general, and the spiral graphitic objects of the sort shown in Fig. 19, is long and (by now) widely known. Given sufficient funding and sustained interest, the combination of laboratory experiments of the sort described here and the new generation of space-based spectral probes may be able to settle most (if not all) of these conjectures within the next decade.

#### REFERENCES

1. Dietz, Thomas G; Duncan, Michael A.; Powers, David E; and Smalley, Richard E.: Laser Production of Supersonic Metal Cluster Beams. *J. Chem. Phys.*, vol. 74, 1981, pp 6511-6512.
2. Powers, David E; Hansen, Steven G.; et. al.: Supersonic Metal Cluster Beams: Laser Photoionization Studies of  $Cu_2$ . *J. Phys. Chem.*, vol. 86, 1982, pp 2556-2560.
3. Hopkins, John B; Langridge-Smith, Patrick R. R.; Morse, Michael D., and Smalley, Richard E.: Supersonic Metal Cluster Beams of Refractory Metals: Spectral Investigations of Ultracold  $Mo_2$ .
4. O'Brien, Sean C.; Liu, Yuan; et. al.: Supersonic III-V Semiconductor Cluster Beams:  $Ga_xAs_y$ . *J. Chem. Phys.*, vol. 84, 1986, pp 4074-4079.
5. Rohlfing, Eric A.; Cox, Donald M.; and Kaldor, Andrew: Production and Characterization of Supersonic Carbon Cluster Beams. *J. Chem. Phys.*, vol. 81, 1984, pp 3322-3330.
6. Heimann, R. B.; Kleiman, J.; and Salansky, N. M.: A Unified Structural Approach to Linear Carbon Polytypes, *Nature*, vol 306, 1983, pp 164-167.
7. Kroto, Harry W.; Heath, James R.; O'Brien, Sean C.; Curl, Robert F., and Smalley, Richard E.:  $C_{60}$ : Buckminsterfullerene. *Nature*, vol. 318, 1985, 162-163.

8. Osawa, Eiji: Superaromaticity, Kagaku, vol.25, 1970, pp 854-855.
9. Bochvar, D. A.; and Gal'pern, E. G.: Hypothetical Systems: Carbondodecahedron, s-Icosahedron, and Carbon-s-icosahedron. Dokl. Akad. Nauk. SSSR vol. 209, 1973, pp 239-241.
10. Davidson, R. A.: Theoret. Chim. Acta, vol. 58, 1981, pp 193-195.
11. Stanlevich, I. V.; Nikerov, M. V.; and Bochvar, D. A.: The Structural Chemistry of Crystalline Carbon: Geometry, Stability, and Electronic Spectrum. Russian Chem. Rev., vol. 53, 1984, pp 640-655.
12. Haymet, Anthony D. J.:  $C_{120}$  and  $C_{60}$  Archimedean Solids Constructed from  $sp^2$  Hybridized Carbon Atoms, Chem. Phys. Lett., vol. 122, 1985, pp 421-424.
13. Haymet, Anthony D. J.: Footballene: A Theoretical Prediction for the Stable, Truncated Icosahedral Molecule  $C_{60}$ . J. Am. Chem. Soc., vol. 108, 1986, pp 319-321.
14. Haddon, R. C.; Brus, Louis E.; and Ragavachari, Krishnan: Electronic Structure and Bonding in Icosahedral  $C_{60}$ , Chem. Phys. Lett., vol. 125, 1986, pp 459-464.
15. Disch Raymond L. and Schulman, Jerome M.: On Symmetrical Clusters of Carbon Atoms:  $C_{60}$ , Chem. Phys. Lett., vol. 125, 1986, pp 455-456.
16. Fowler, P. W.; and Woolrich, J.:  $\pi$ -Systems in Three Dimensions. Chem. Phys. Lett., vol. 127, 1986, pp 78-83.
17. Ozaki, Masa-aki; and Takahashi, Akira: On Electronic States and Bond Lengths of the Truncated Icosahedral  $C_{60}$  Molecule, Chem. Phys. Lett., vol. 127, 1986, pp 242-244.
18. Stone, A. J. and Wales, D. J.: Theoretical Studies of Icosahedral  $C_{60}$  and Some Related Species, Chem. Phys. Lett., vol. 128, 1986, pp 501-503.
19. Fowler, P. W.: How Unusual is  $C_{60}$ ? Magic Numbers for Carbon Clusters, Chem. Phys. Lett., vol. 131, 1986, pp 444-450.
20. Hess, Jr., B. Andres; and Schaad, L. J.: The Stability of Footballene. J. Org. Chem., vol. 51, 1986, 3902-3903.
21. Klein, Douglas J.; Schmalz, Thomas G.; Hite, G. E.; and Seitz, William A.: Resonance in Buckminsterfulleren. J. Am. Chem. Soc., vol. 108, 1986, pp 1301-1302.
22. Klein, D. J.; Seitz, W. A., and Schmalz, T. G.: Icosahedral Symmetry Carbon Cage Molecules. Nature, vol. 323, 1986, pp 703-706.
23. Schmaltz, Thomas G.; Seitz, William A.; Klein, Douglas J.; and Hite, George E.:  $C_{60}$  Carbon Cages, Chem. Phys. Lett., vol. 130, 1986, pp 203-207.

24. Newton, Marshall D. and Stanton, Richard E.: Stability of Buckminsterfullerene and Related Carbon Cluster, J. Am. Chem. Soc., vol. 108, 1986, pp 2469-2470.
25. Satpathy, Sashi: Electronic Structure of the Truncated-Icosahedral C<sub>60</sub> Cluster, Chem. Phys. Lett., vol. 130, 1986, pp 545-550.
26. Haddon, R. C.; Brus, L. E.; Raghavachari, Krishnan: Rehybridization and PI-Orbital Alignment: The Key to the Existence of Spheroidal Carbon Clusters. Chem. Phys. Lett., vol. 131, 1986, pp. 165-169.
27. Hale, Paul D.: Discrete-Variational-Alpha Electronic Structure Studies of the Spherical C<sub>60</sub> Cluster: Prediction of Ionization Potential and Electronic Transition Energy, J. Am. Chem. Soc., vol. 108, 1986, pp 6087-6088.
28. Marynick, Dennis S. and Estreicher, Stephen: Localized Molecular Orbitals and Electronic Structure of Buckminsterfullerene, Chem. Phys. Lett., vol. 132, 1986, pp 383-386.
29. Harter, William G.; and Weeks, David E.: Rovibrational Spectral Fine Structure of Icosahedral Molecules, Chem. Phys. Lett., vol. 132, 1986, pp 387-392.
30. Kataoka, Masahiro; and Nakajima, Takeshi: Geometrical Structures and Spectra of Carannulene and Icosahedral C<sub>60</sub>. Tetrahedron, vol. 42, 1986, pp 6437-6442.
31. Luthi, Hans Peter; and Almlof, Jan: Ab Initio Studies on the Thermodynamic Stability of the Icosahedral C<sub>60</sub> Molecule "Buckminsterfullerene", Chem. Phys. Lett., vol. 135, 1986, pp 357-360.
32. Laszlo, I.; and Udvardi, L.: On the Geometrical Structure and UV Spectrum of the Truncated Icosahedral Sixty-Atom Carbon (C<sub>60</sub>) Molecule. Chem. Phys. Lett., vol. 136, 1987, pp 418-422.
33. Shibuya, Tai-Ichi; and Yoshitani, Masaaki: Two Icosahedral Structures for the C<sub>60</sub> Cluster, Chem. Phys. Lett., vol. 137, 1987, pp 13-16.
34. Wu, Z. C.; Jelski, Daniel A.; and George, Thomas F.: Vibrational Motions of Buckminsterfullerene, Chem. Phys. Lett., vol 137, 1987, pp 291-294.
35. Larsson, Sven; Volosov, Andrey; and Rosen, Arne: Optical Spectrum of the Icosahedral C<sub>60</sub> -- "Follene-60", Chem. Phys. Lett., vol. 137, 1987, pp. 501-503.
36. Elser, V.; and Haddon, R. C.: Icosahedral C<sub>60</sub>: An Aromatic Molecule with a Vanishingly Small Ring Current Magnetic Susceptibility. Nature, vol. 325, 1987, pp. 792-794.
37. Schulman, Jerome M.; Disch, Raymond L.; Miller, Mitchell A.; and Peck, Rosalie C.: Symmetrical Clusters of Carbon Atoms: The C<sub>24</sub> and C<sub>60</sub> Molecules, Chem. Phys. Lett., vol. 141, 1987, pp 45-48.
38. Schmaltz, Thomas G.; Seitz, William A.; Klein, Douglas J.; and Hite, G. E.: "Elemental Carbon Cages", J. Am. Chem. Soc., vol. 110, 1988, (in press).

39. Stanton, Richard E.; and Newton, Marshall D.: Normal Vibrational Modes of Buckminsterfullerene. *J. Phys. Chem.*, vol. 92, (to be published).
40. Hayden, G. W.; and Mele, E. J.: The  $\pi$  Bonding in the Icosahedral Carbon ( $C_{60}$ ) Cluster. *Phys. Rev. B: Condens. Matter.*, vol. 36, 1987, pp 5010-5015.
41. Heath, J. R.; O'Brien, S. C.; et. al.: Lanthanum Complexes with Spheroidal Carbon Shells. *J. Am. Chem. Soc.*, vol. 107, 1985, pp. 7779-7780.
42. Morse, M. D.; Geusic, M. E.; Heath, J. R.; and Smalley, R. E.: Surface Reactions of Metal Clusters II: Reactivity Surveys with  $D_2$ ,  $N_2$ , and CO. *J. Chem. Phys.*, vol. 83, 1985, pp 2293-2304.
43. Zhang, Qing-Ling, O'Brien, S. C.; et. al.: The Reactivity of Large Carbon Clusters: Spheroidal Carbon Shells and Their Possible Relevance to the Formation and Morphology of Soot. *J. Phys. Chem.*, vol. 90, 1986, pp 525-528.
44. Paquette, Leo. A.; Ternansky, R. J.; Balogh, D. W.; and Kentgen, G.: *J. Am. Chem. Soc.*, vol. 105, 1983, pp 5445-.
45. Kroto, H. W.: The Stability of the Fullerenes  $C_n$  ( $n = 28, 32, 36, 50, 60$  and  $70$ ), *Nature*, vol. 329, 1987, pp 529-531.
46. O'Brien, S. C.; Heath, J. R.; Curl, R. F.; and Smalley, R. E.: Photophysics of Buckminsterfullerene and other Carbon Cluster Ions, *J. Chem. Phys.*, vol. 88, 1988, (in press).
47. Radi, Peter P.; Bunn, Thomas L.; Kemper, Paul R.; Molchan, Michele E.; and Bowers, Michael T.: A New Method for Studying Carbon Clsters in the Gas Phase: Observation of Size Specific Neutral Fragment Loss from Metastable Reactions of Ma Selected  $C_n^+$ ,  $n < 60$ , *J. Phys. Chem.* vol. 30, 1988, (in press).
48. Gerhardt, Ph.; Loffler, S.; and Homann, K. H.: Polyhedral Carbon Ion in Hydrocarbon Flames, *Chem. Phys. Lett.*, vol. 137, 1987, pp 306-310.
49. Langridge-Smith, Patrick R. R.; Morse, M. D.; Hansen, G. P.; Smalley, R. E., and Merer, Anthony J.: The Bond Length and Electronic Structure of  $V_2$ . *J. Chem. Phys.*, vol. 80, 1984, pp 593-600.
50. Morse, M. D.; Hopkins, J. B.; Langridge-Smith, P. R. R.; and Smalley, R. E.: Spectroscopic Studies of the Jet-Cooled Copper Trimer. *J. Chem. Phys.*, vol. 79, 1983, pp 5316-5328.
51. Michalopoulos, D. L.; Geusic, M. E.; Langridge-Smith, P. R. R.; and Smalley, R. E.: Visible Spectroscopy of Jet-Cooled  $SiC_2$ : Geometry and Electronic Structure.
52. Cheshnovsky, O.; Yang, S.; Pettiette, C. L.; Craycraft, M. J.; Liu, Y.; and Smalley, R. E.: Ultraviolet Photoelectron Spectroscopy of Semiconductor Clusters: Silicon and Germanium. *Chem. Phys. Lett.*, vol. 138, 1987, pp. 119-124.

53. Cheshnovsky, O.; Yang, S.; Pettiette, C. L.; Craycraft, M. J.; and Smalley, R. E.: Magnetic Time-of-Flight Photoelectron Spectrometer for Mass-Selected Negative Cluster Ions. *Rev. Sci. Instrum.*, vol. 58, pp. 2131-2137.
54. Pitzer, K. S.; and Clementi, E.: Large Molecules in Carbon Vapor, *J. Am. Chem. Soc.*, vol. 81, 1959, pp 4477-4485.
55. Strickler, S. J.; and Pitzer, K. S.: Energy Calculations for Polyatomic Carbon Molecules. in Molecular Orbitals in Chemistry, Physics, and Biology ed. by P. O. Lowdin and B. Pullman (Academic Press, New York, 1964), pp 281-291.
56. Hoffmann, Roald: Extended Huckel Theory -- V: Cumulenes, Polyenes, Polyacetylenes and  $C_n$ . *Tetrahedron*, vol. 22, 1966, pp 521-538.
57. Yang, S.; Taylor, K. R.; et. al.: UPS of 2-30 Atom Carbon Clusters. *Chem. Phys. Lett.*, (to be published).
58. Bloomfield, Louis; Geusic, Michael E.; Freeman, Richard R.; and Brown, W. L.: Negative and Positive Cluster Ions of Carbon and Silicon. *Chem. Phys. Lett.*, vol. 121, 1985, pp 33-37.
59. Hahn, M. Y.; Honea, E. C.; Paguia, A. J.; Schriver, K. E.; Camerena, A.M.; and Whetten, Robert L.: Magic Numbers in  $C_n^+$  and  $C_n^-$  Abundance Distributions. *Chem. Phys. Lett.*, vol. 130, 1986, pp 12-16.
60. O'Brien, Sean C.; Heath, James R.; Kroto, Harry W.; Curl, Robert F.; and Smalley, Richard E.: A Reply to "Magic Numbers in  $C_n^+$  and  $C_n^-$  Abundance Distributions" Based on Experimental Observations. *Chem. Phys. Lett.*, vol. 132, 1986, pp 99-102.
61. Zheng, L-S.; Brucat, P. J.; Pettiette, C. L.; Yang, S. and Smalley, R. E.: Formation and Photodetachment of Cold Metal Cluster Negative Ions. *J. Chem. Phys.*, vol. 83, 1985, pp. 4273-4274.
62. Liu, Yuan; O'Brien, Sean C.; et. al.: Negative Carbon Cluster Ion Beams: New Evidence for the Special Nature of  $C_{60}$ . *Chem. Phys. Lett.*, vol. 126, 1986, pp 215-217.
63. Yang, S.; Pettiette, C. L.; et. al.: UPS of Buckminsterfullerene and Other Large Clusters of Carbon. *Chem. Phys. Lett.*, vol. 139, 1987, pp. 233-238.
64. Hintenberger, H.; and Dornenburg, E.: Das Auftreten Vielatomiger Kohlenstoffmolekule in Hochfrequenzfunken Zwischen Graphitelektroden. *Z. Naturforsch.*, vol. 14a, 1959, pp 765-767.
65. Magers, David H.; Harrison, Robert J.; and Bartlett, Rodney, J.: Isomers and Excitation Energies of  $C_4$ . *J. Chem. Phys.*, vol. 84, 1986, pp 3284-3290.
66. Ragavachari, Krishnan; Whiteside, R. A.; and Pople, John A.: Structure of Small Carbon Clusters: Cyclic Ground State of  $C_6$ . *J. Chem. Phys.*, vol. 85, 1986, pp 6623-6628.
67. Faibis, A.; Kanter, E. P.; Tack, L. L.; Bakke, E.; and Zabransky, B. J.: Geometry and Structure of  $C_3^+$ . *J. Phys. Chem.*, vol. 91, 1987, pp 6445-6447.

68. Geusic, M. E.; Jarrold, M. E.; McIlrath, T. J.; Freeman, R. R.; and Brown, W. L.: Photodissociation of Carbon Cluster Cations. *J. Chem. Phys.*, vol. 86, 1986, 3862-3869.
69. O'Keefe, A. O.; Ross, M. M.; and Baronovski, A. P.: Production of Large Carbon Cluster Ions by Laser Vaporization. *Chem. Phys. Lett.*, vol. 130, 1986, 17-19.
70. McElvany, S. W.; Creasy, W. R.; and O'Keefe, A. O.: Ion-Molecule Reaction Studies of Mass-Selected Carbon Cluster Ions Formed by Laser Vaporization. *J. Chem. Phys.*, vol. 85, 1986, pp. 632-633.
71. McElvany, Stephen, Nelson, H. H.; Baronovski, Andrew P.; Watson, Clifford H.; and Eyler, John R.: FTMS Studies of Mass-Selected Large Cluster Ions Produced by Direct Laser Vaporization.
72. Heath, J., R.; Zhang, Q.; et. al.: The Formation of Long Carbon Chain Molecules during Laser Vaporization of Graphite. *J. Am. Chem. Soc.*, vol. 109, 1987, pp. 359-363.
73. Kroto, H. W.; Heath, J. R.; et. al.: Long Carbon Chain Molecules in Circumstellar Shells. *Ap. J.*, vol. 314, 1987, pp. 352-355.
74. Cox, Donald M.; Trevor, Dennis J.; Reichmann, Kenneth C.; Kaldor, Andrew:  $C_{60}$  La: A Deflated Soccerball?. *J. Am. Chem. Soc.*, vol. 108, 1986, pp 2457-2458.
75. Heath, James R.; Curl, Robert F.; and Smalley, Richard E.: The UV Absorption Spectrum of  $C_{60}$  (Buckminsterfullerene): A Narrow Band at 3860 Å. *J. Chem. Phys.*, vol. 87, 1987, pp. 4236-4238.
76. Brucat, Phillip J.; Zheng, Lan-Sun; Pettiette, Claire L.; Yang, Shihe, and Smalley, Richard E.: Metal Cluster Ion Photo-fragmentation. *J. Chem. Phys.*, vol. 84, 1986, pp 3078-3088.
77. Raghavachari, Krishnan; and Brinkley, J. S.: Structure, Stability, and Fragmentation of Small Carbon Clusters. *J. Chem. Phys.*, vol. 87, 1987, pp. 2191-2197.
78. Duncan, Michael A.; Dietz, Thomas G.; and Smalley, Richard E.: Laser Synthesis of Metal Clusters from Metal Carbonyl Microcrystals. *J. Am. Chem. Soc.*, vol. 103, 1981, pp. 5245-5246.
79. Dietz, Thomas G.; Duncan, Michael A; et. al.: Spectral Narrowing and Infrared Laser Fragmentation of Jet-Cooled  $UO_2(hfaa)_2TMP$  and  $UO_2(hfaa)_2THF$ : Volatile Uranyl Compounds. *J. Chem. Phys.*, vol. 77, 1982, pp. 4417-4426.
80. Kaldor, A.; Cox, D. M.; Trevor, D. J.; and Zakin, M. R.: The Chemistry and Physics of Molecular Surfaces. *Z. Physik D.*, vol. 3, 1986, pp. 195-204.
81. Cox, D. M.; Reichmann, K. C.; and Kaldor, A.: Carbon Clusters Revisited: Comments on the "Special" Behavior of  $C_{60}$  and Other Large Carbon Clusters. *J. Chem. Phys.*, vol. 88, 1988, (to be published).

82. Elkind, J. L.; Alford, J. M.; Weiss, F. D.; Laaksonen, R. T.; and Smalley, R. E.: FT-ICR Probes of Silicon Cluster Chemistry. *J. Chem. Phys.*, vol. 87, 1987, pp 2397-2398.
83. Elkind, J. L.; Weiss, F. D.; Alford, J. M.; Laaksonen, R. T.; and Smalley, R. E.: FT-ICR Studies of H<sub>2</sub> Chemisorption on Niobium Cluster Cations. *J. Chem. Phys.*, (to be published).
84. Woodward, R. B.; and Hoffmann, R.: The Conservation of Orbital Symmetry (Verlag Chemie Academic Press, Weinheim, 1971).
85. Allamandola, L. J.; Sandford, S. A.; and Wopenda, B.: Interstellar Polycyclic Aromatic Hydrocarbons and Carbon in Interplanetary Dust Particles and Meteorites. *Science*, vol. 237, 1987, no. 4810, pp. 56-59.
86. Herbig, G. H.; and Soderblom, R. R.: ... *Astrophys. J.*, vol. 252, 1982, pp 610- .
87. Rabilizirov, R.: The Role of Cavities and Mantles in the Ultraviolet Extinction Peak of Graphite spheres with Particular Reference to a Possibly Discovered C<sub>60</sub> Structure. *Astrophys. Space Sci.*, vol. 125, 1986, pp 331-339.
88. Iijima, Sumio: The 60-Carbon Cluster has been Revealed!. *J. Phys. Chem.*, vol. 91, 1987, pp 3466-3469.

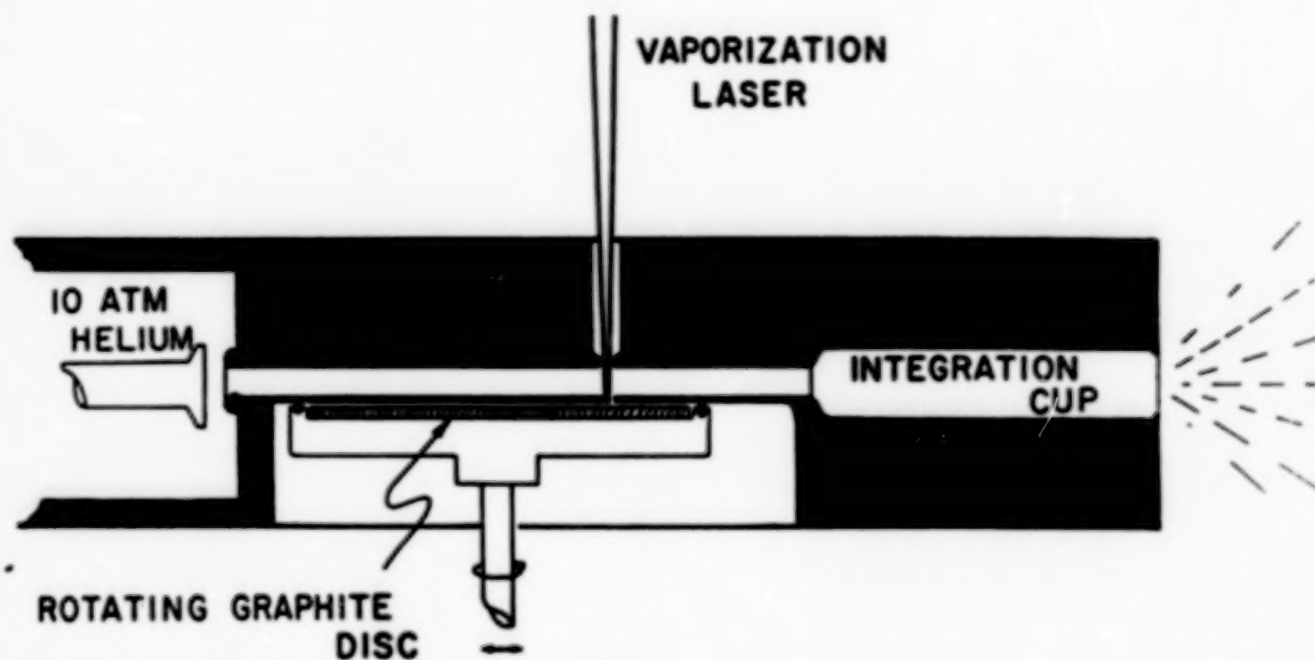


Figure 1.— Schematic of pulsed laser vaporization nozzle source for production of supersonic beams of carbon clusters.

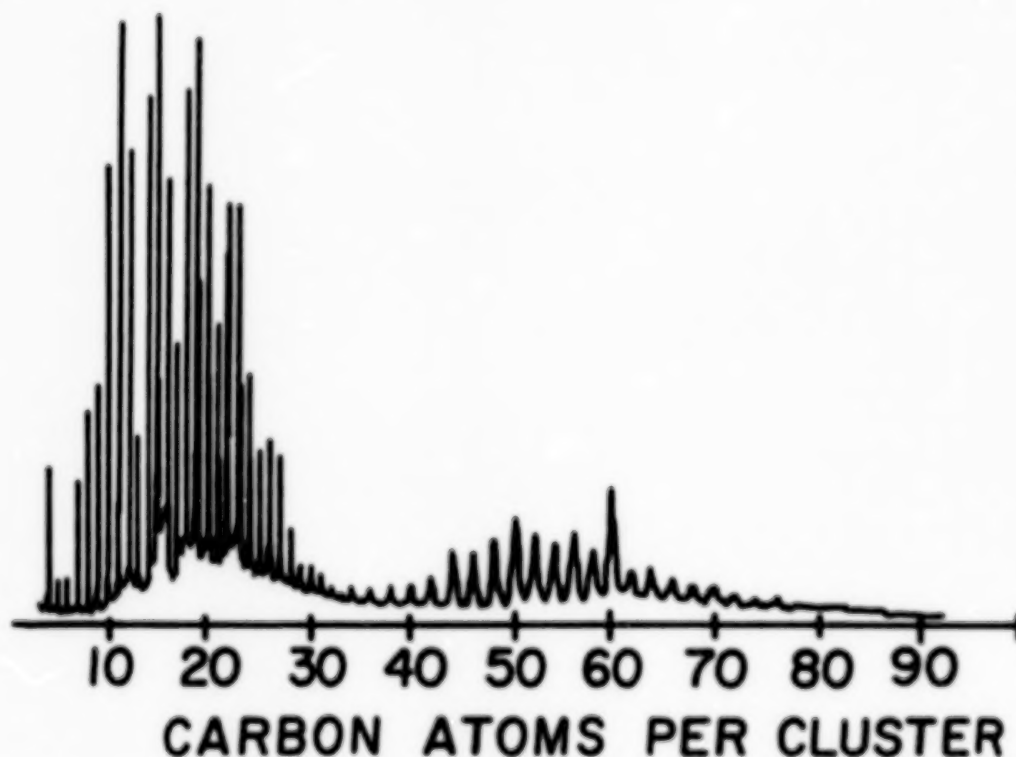


Figure 2.— Time of Flight (TOF) mass spectrum of carbon clusters prepared in a supersonic beam by laser vaporization of a graphite disc in the nozzle device of the type shown in Fig. 1. Ionization of the neutral clusters was done by photoionization with an ArF excimer laser beam (1930 Å, 6.4 eV).

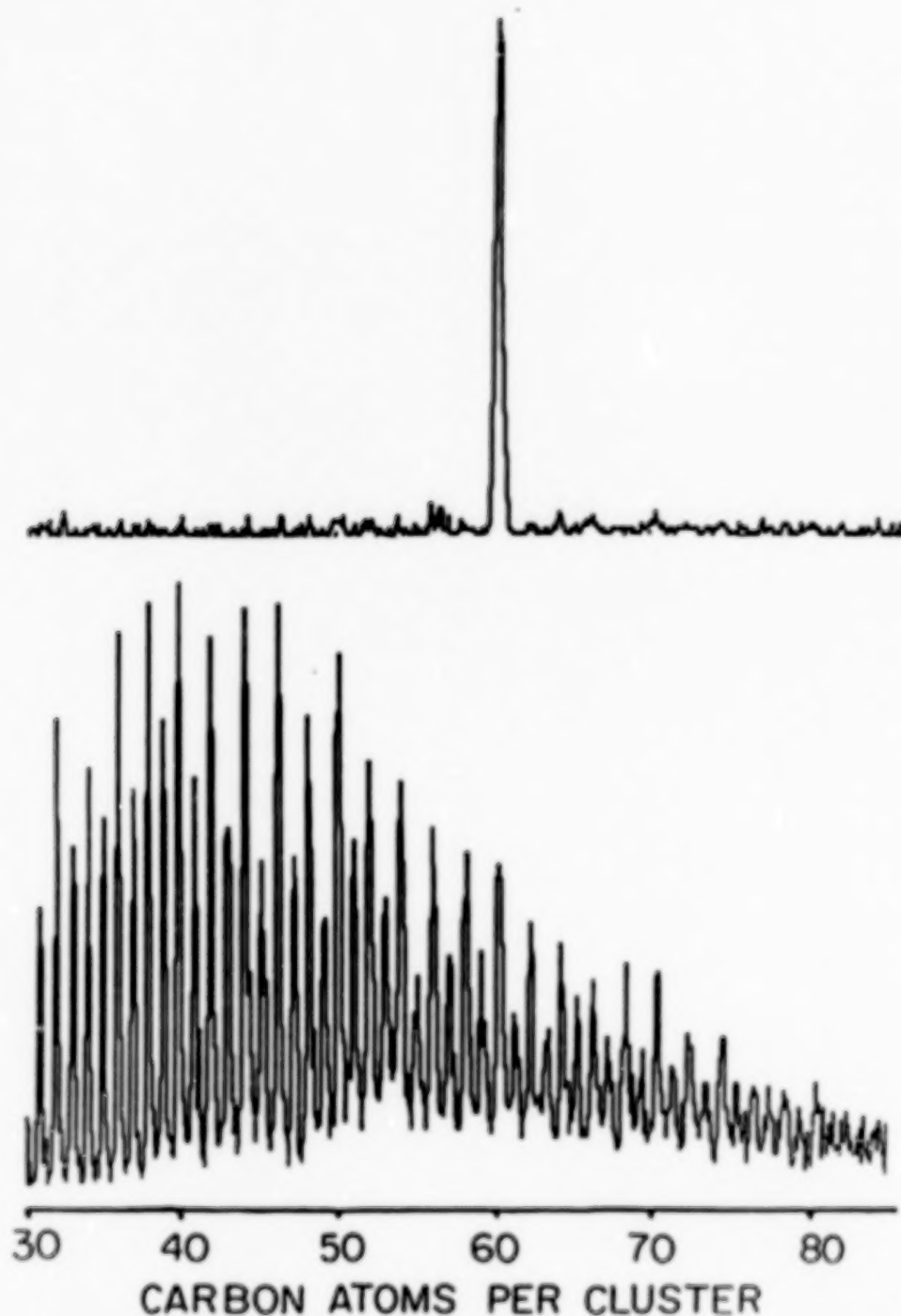


Figure 3.- Time of flight mass spectrum of carbon clusters in a supersonic beam when the nozzle source was operated under minimal clustering/reaction conditions (bottom panel), and maximum clustering/reaction conditions (top panel). Ionization was accomplished by direct one-photon photoionization with a F<sub>2</sub> excimer laser (1570 Å, 7.9 eV). Note that only C<sub>60</sub> survives. It has not grown in intensity, rather the other clusters have dropped in intensity due to cluster growth reactions in the nozzle.

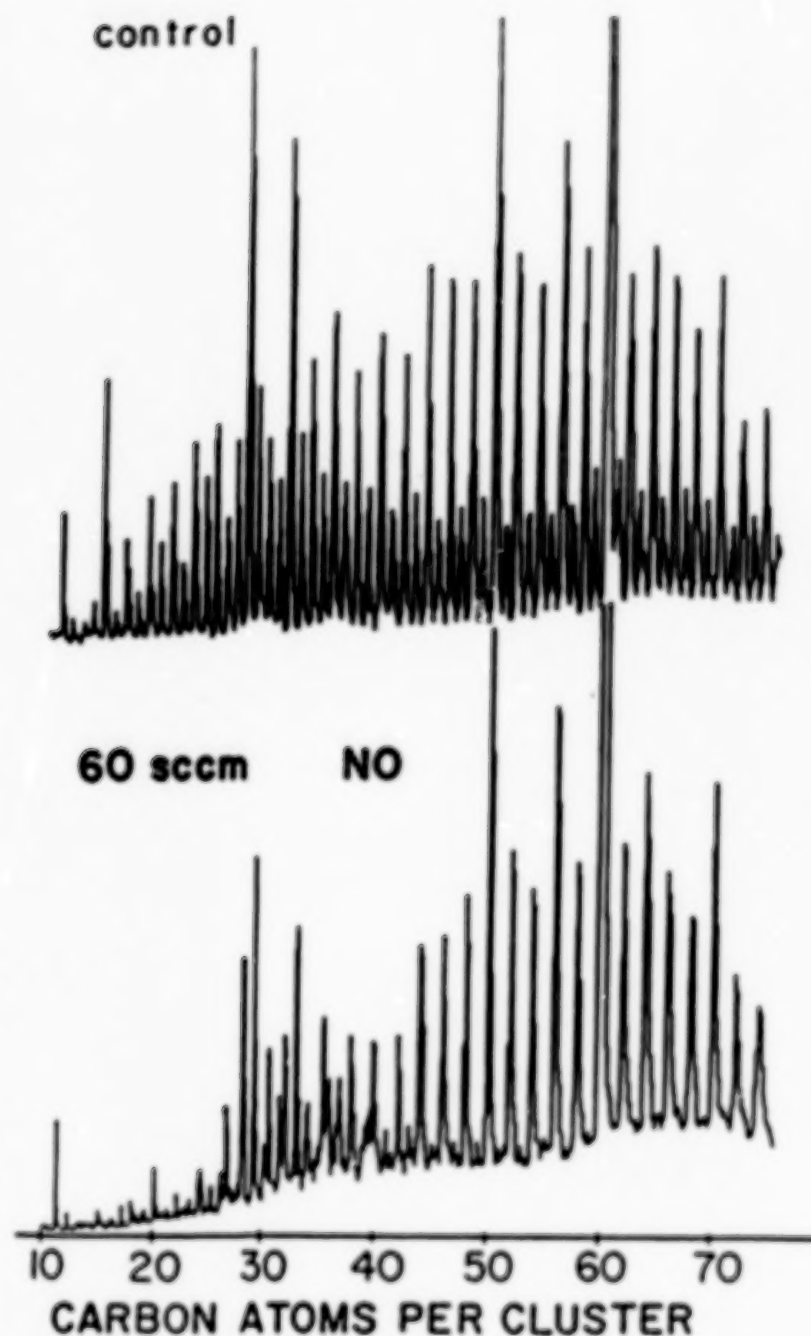


Figure 4.— Reactivity study with NO on carbon clusters. The top panel shows the cluster distribution prior to injection of the reactant ( an F<sub>2</sub> excimer laser was used for ionization). The bottom panel shows this distribution after 170 microseconds of exposure to NO in a helium buffer gas at near room temperature in a fast flow reactor.

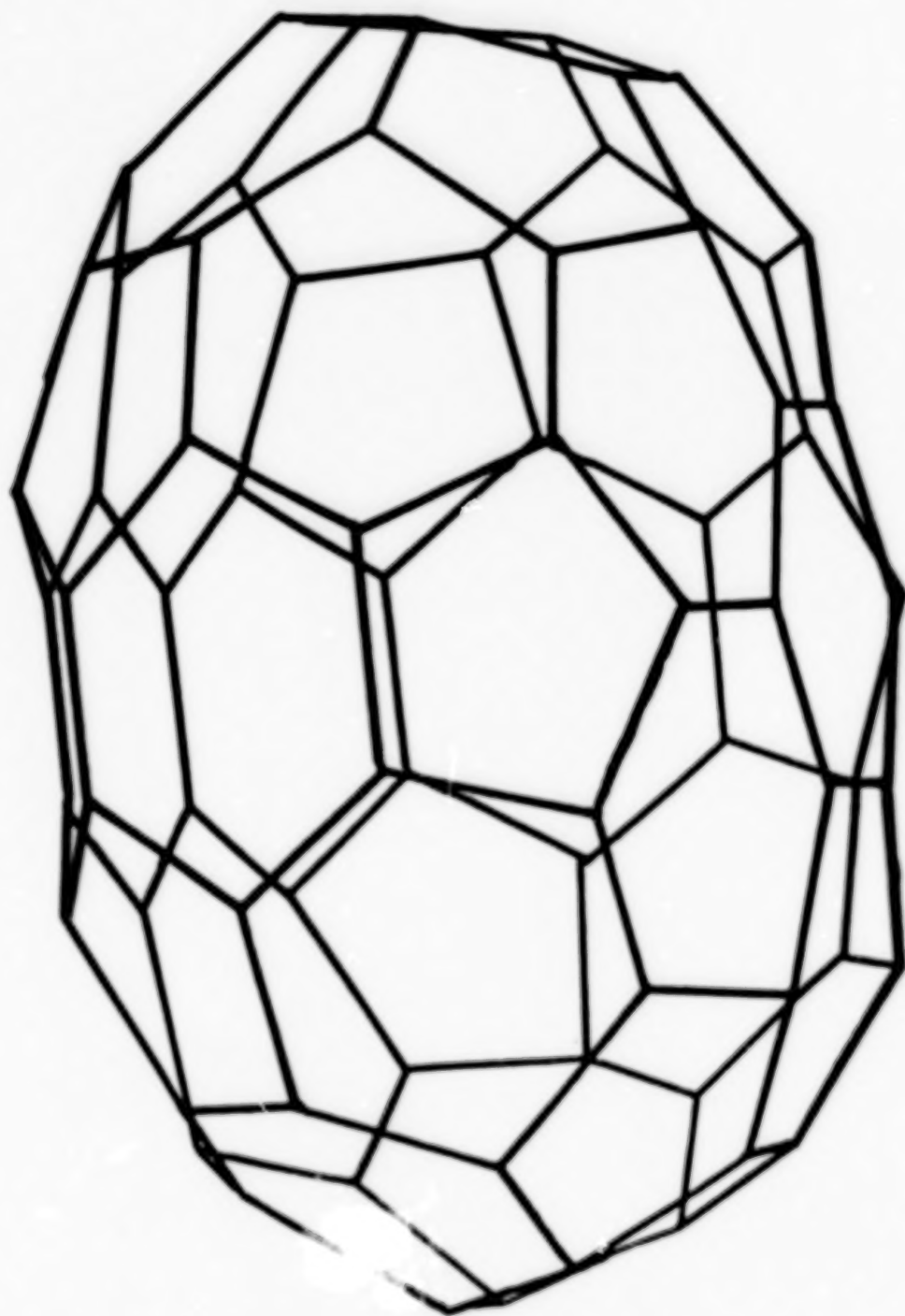


Figure 5.— One possible closed spheroidal network structure for the  $C_{72}$  fullerene. All fullerene structures are closed nets containing 12 pentagons and  $n/2-10$  hexagons. Note the concentration of strain at the pentagons. These sites are suspected to be the most reactive. Due to its perfect symmetry,  $C_{60}$  is the only fullerene with perfectly distributed (and therefore minimized) strain.

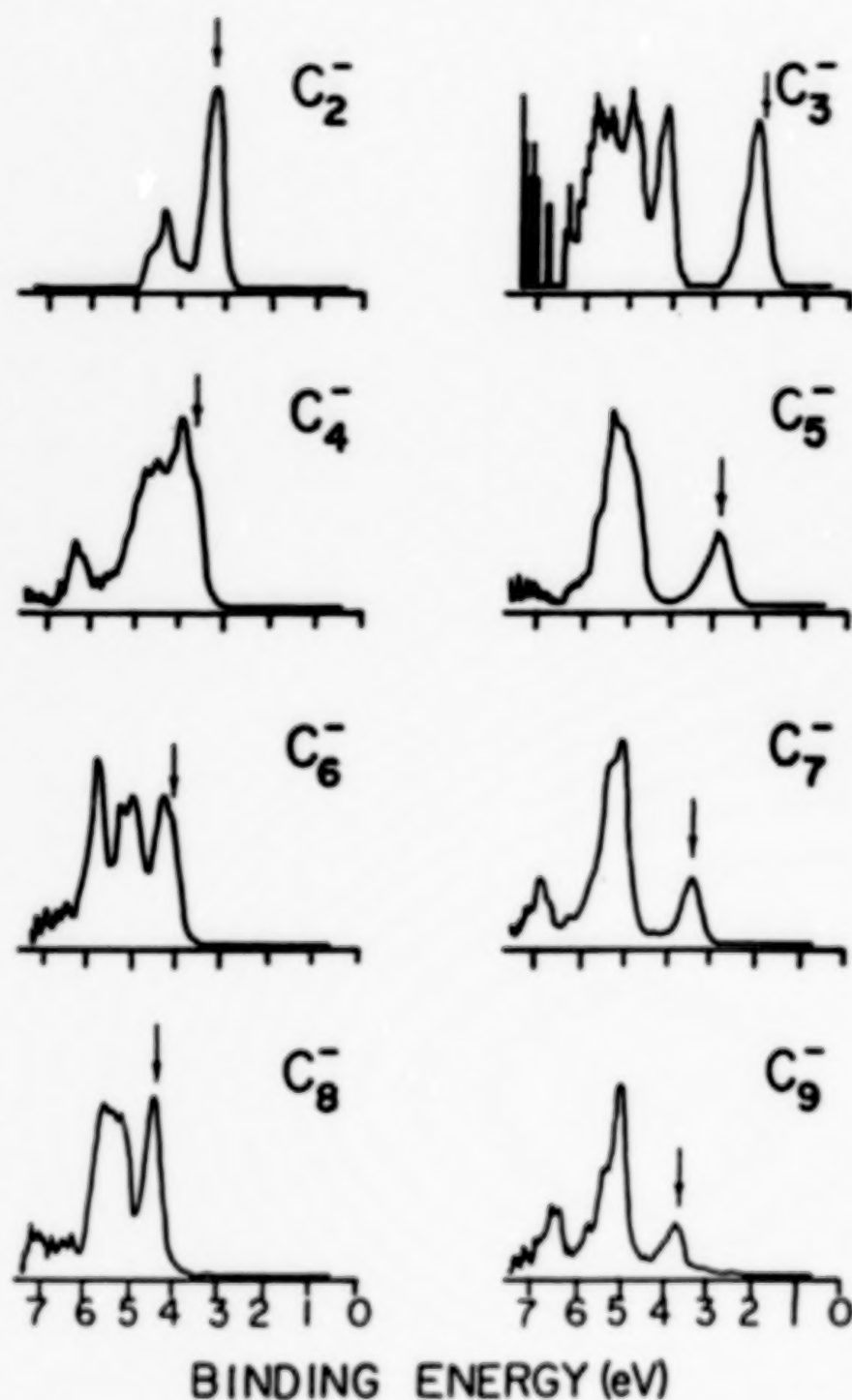


Figure 6.— Ultraviolet Photoelectron Spectrum (UPS) of  $C_n^-$  in the  $n=2$  to 9 region. An  $F_2$  excimer laser (7.9 eV) was used for photodetachment of the appropriate mass-selected negative cluster ion. The arrow in each panel is an estimate of the vertical photodetachment threshold energy roughly corrected for thermal effects and instrument resolution.

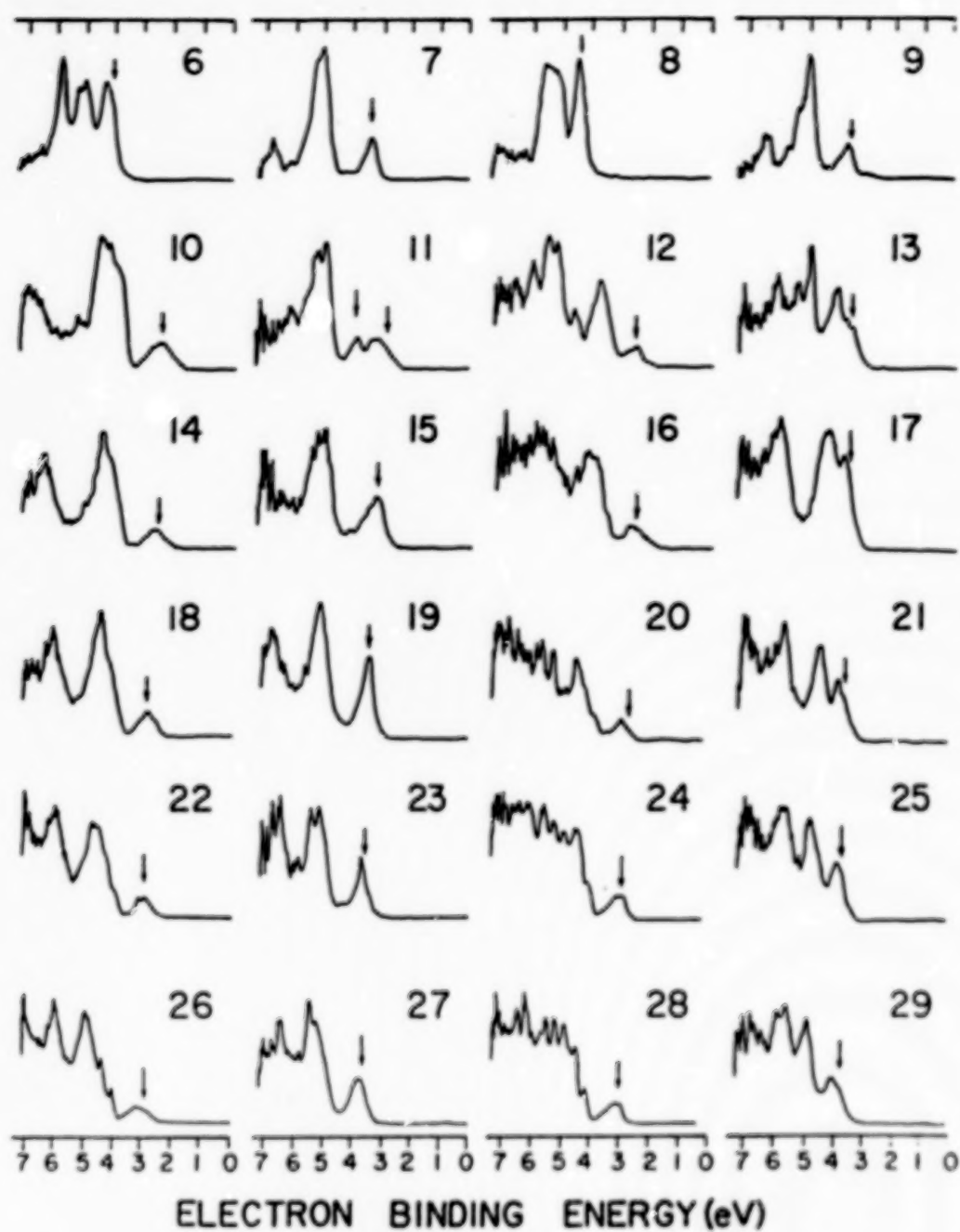


Figure 7.— UPS of negative carbon clusters in the 6-29 atom region.

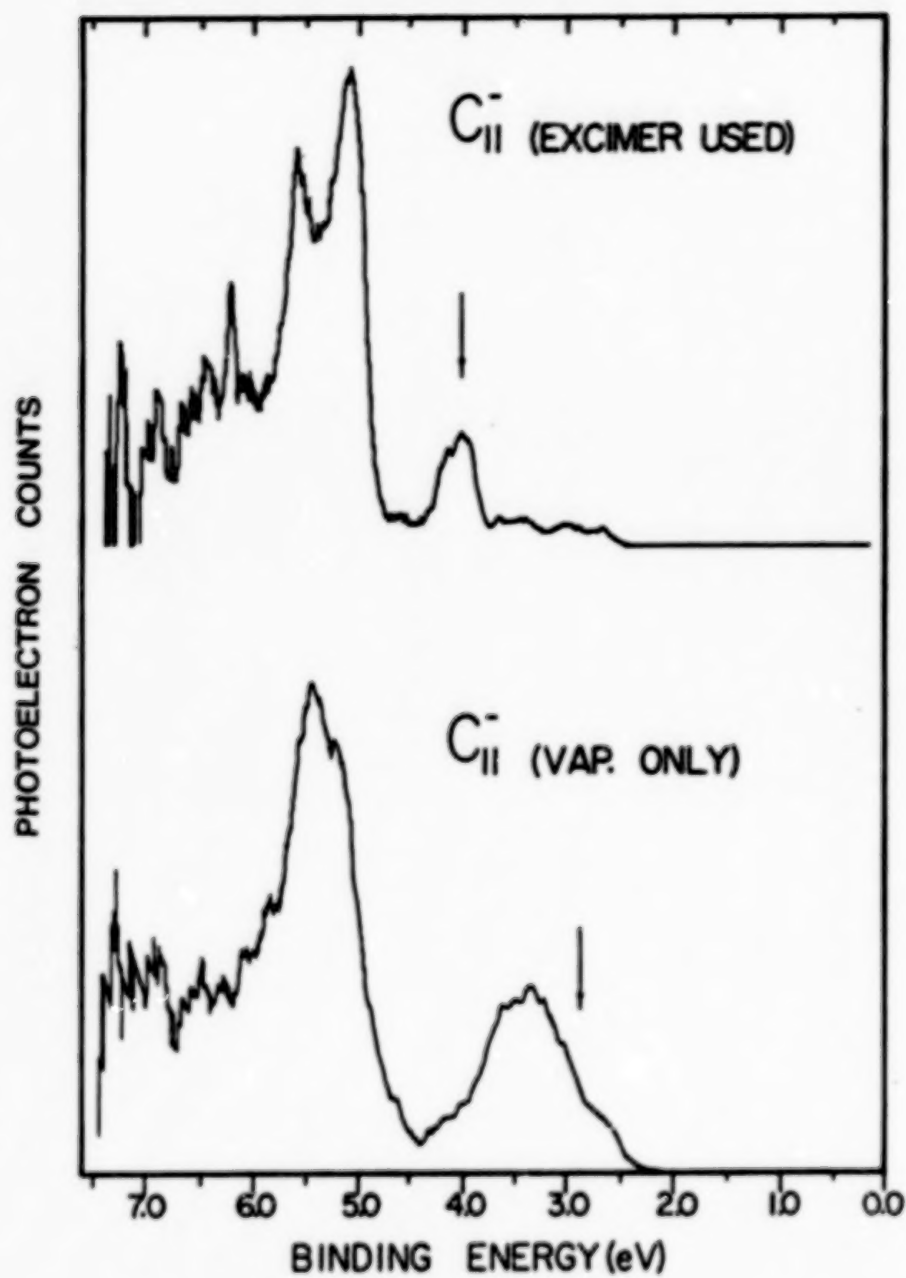


Figure 8.— UPS of  $C_{11}^-$  under two conditions which favor different geometrical forms of the cluster.

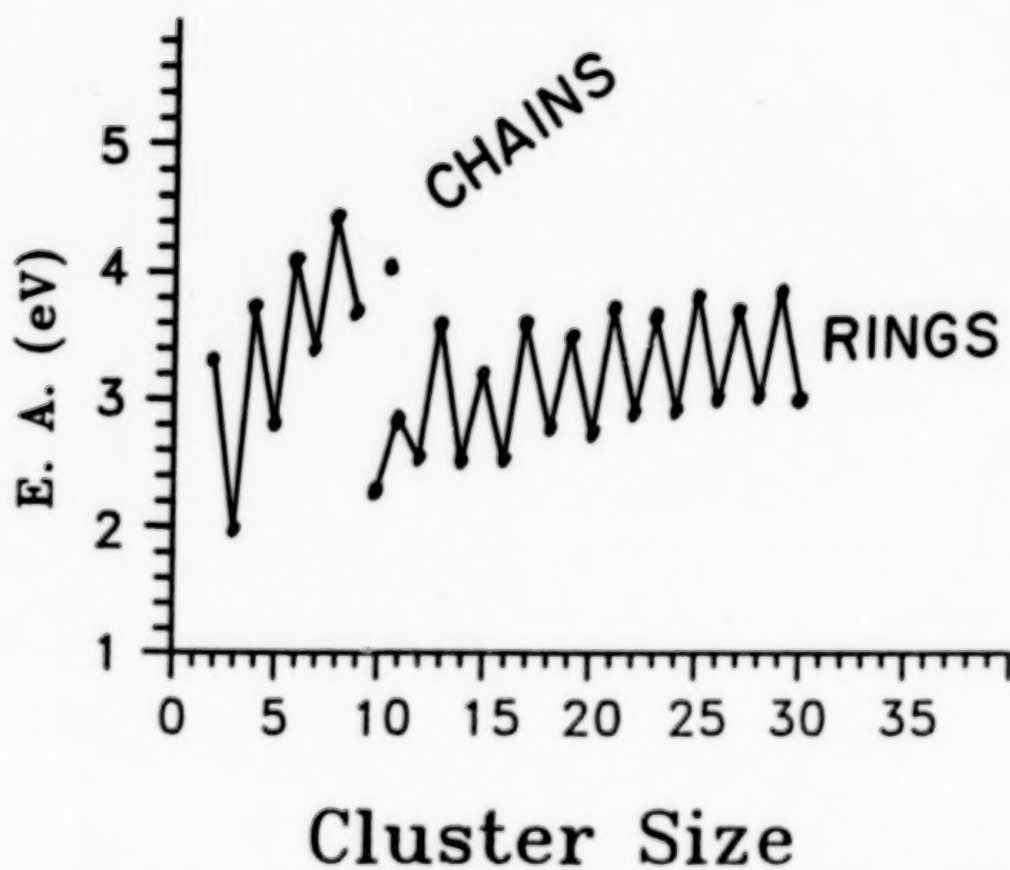


Figure 9.— Electron Affinity of carbon clusters in 2-29 region. The measured values were taken from the estimated photodetachment thresholds in the UPS data of Figs. 5-7. Note there are two values plotted for  $C_{11}$ .

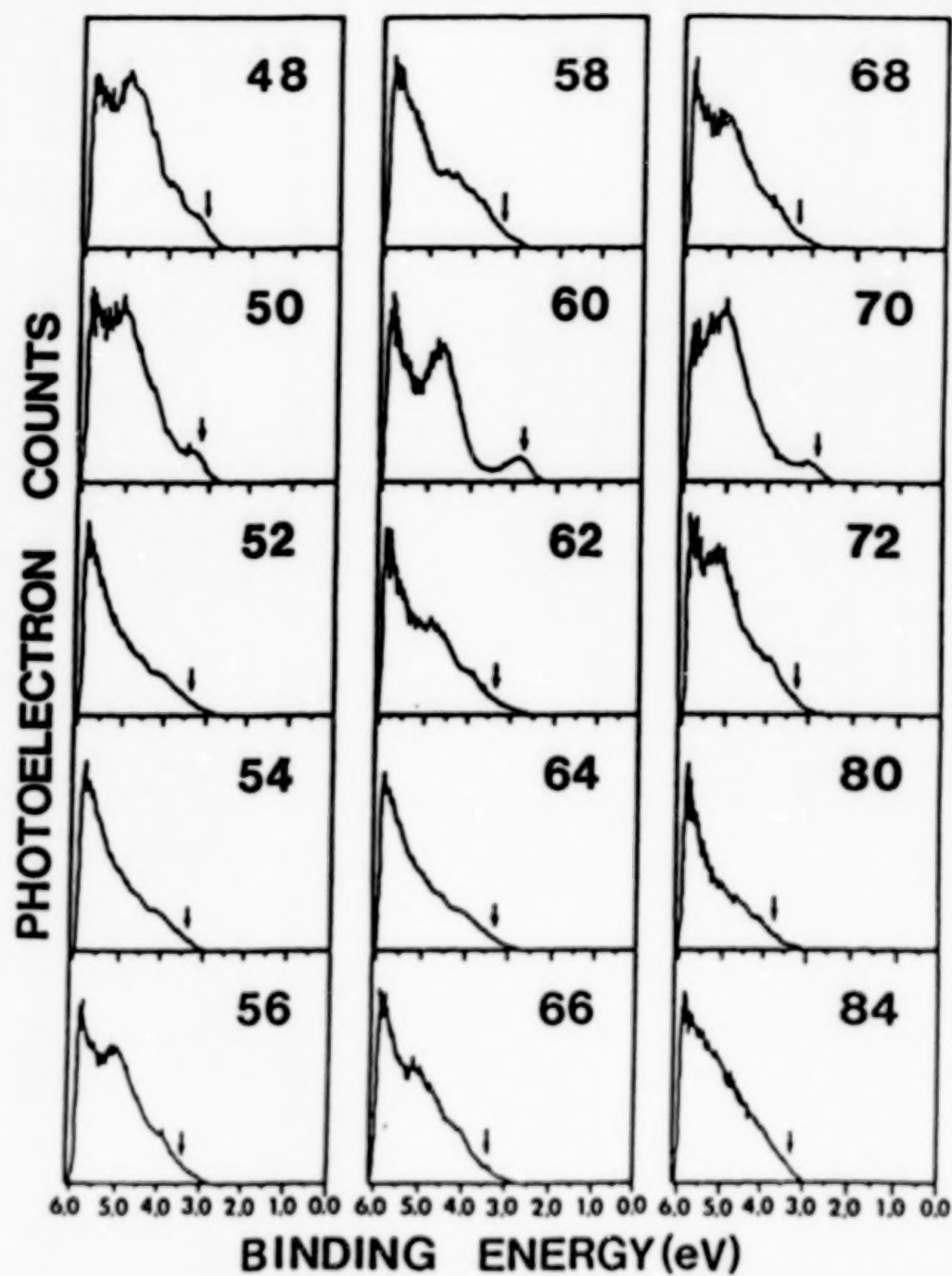


Figure 10.— Carbon cluster UPS in the 48-84 size range taken with an ArF excimer laser (6.4 eV).

$C_{60}^-$  UPS

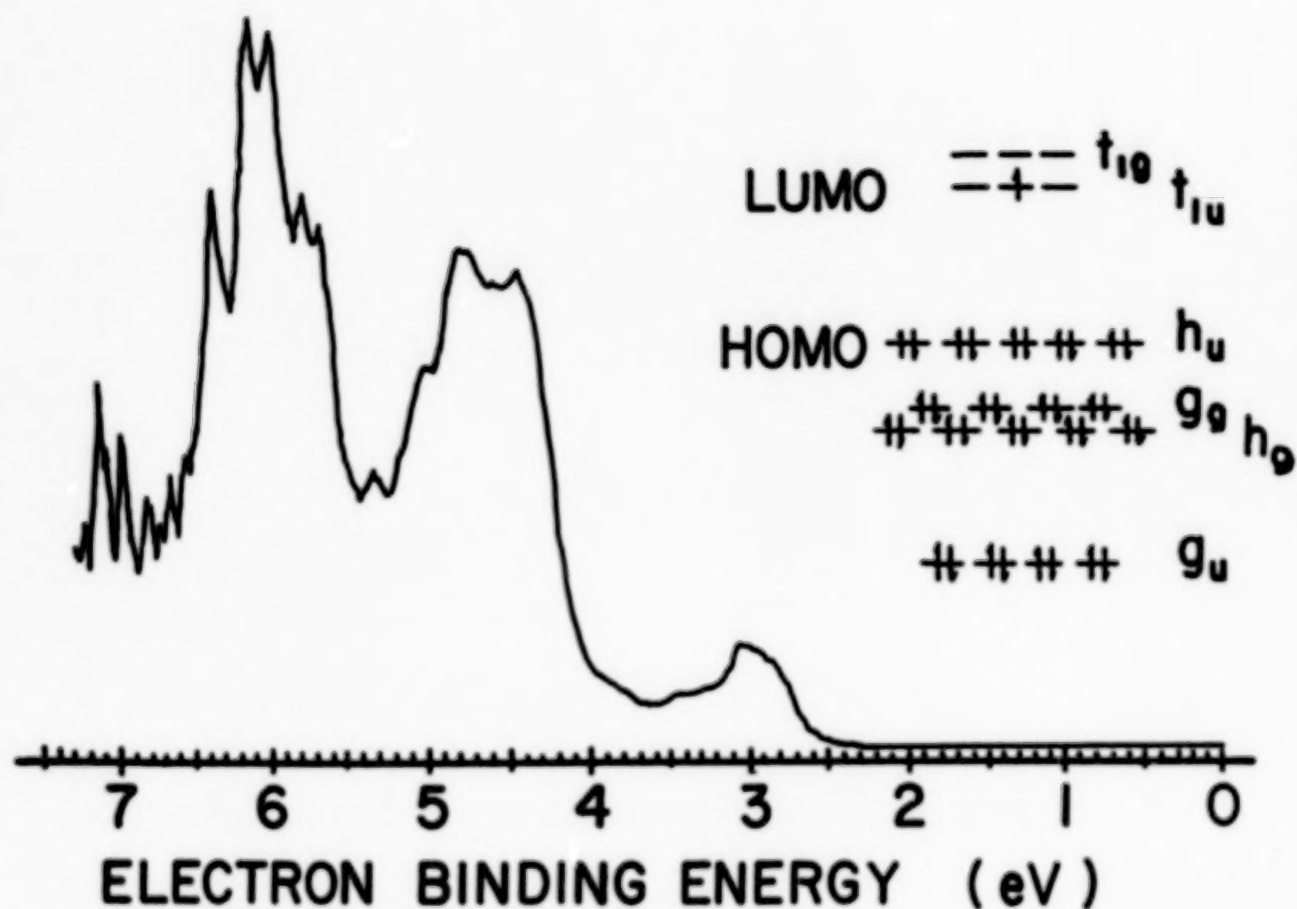


Figure 11.— $C_{60}^-$  UPS taken with a  $F_2$  excimer laser. The right side of the figure shows an approximate molecular orbital diagram for  $C_{60}$  assuming a truncated icosahedral (buckminsterfullerene) structure.

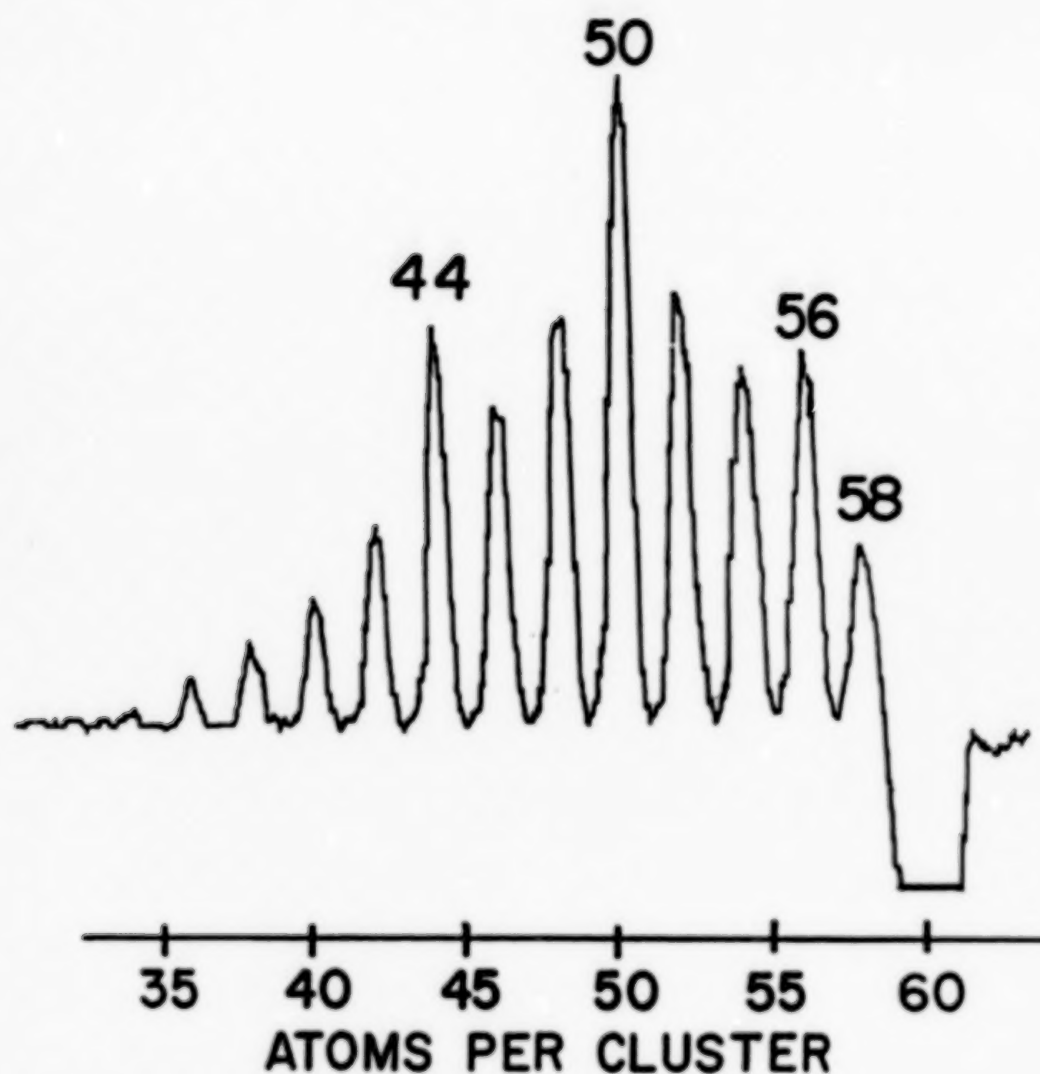


Figure 12.— $C_{60}^+$  photofragmentation showing  $C_2$  loss to produce first  $C_{58}^+$ , then  $C_{56}^+$ , etc. These data were obtained by mass-selecting  $C_{60}^+$  with an initial TOF mass spectrometer, and analyzing the parent and product ions with a second TOF mass spectrometer.

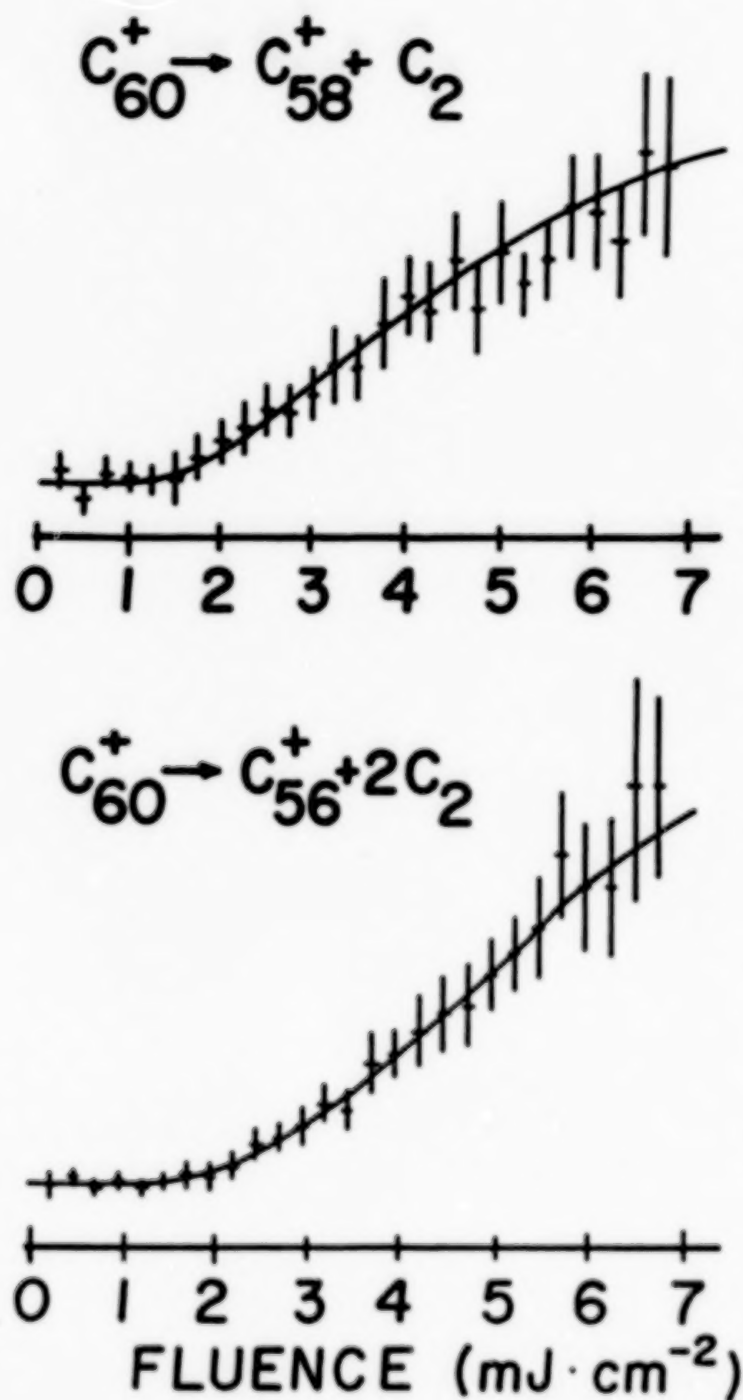


Figure 13.— Laser fluence dependence of  $C_{58}^+$  and  $C_{56}^+$  daughter ions fragmented from an initially mass-selected  $C_{60}^+$  using a single shot of the 1930 Å (6.4 eV) ArF excimer laser.

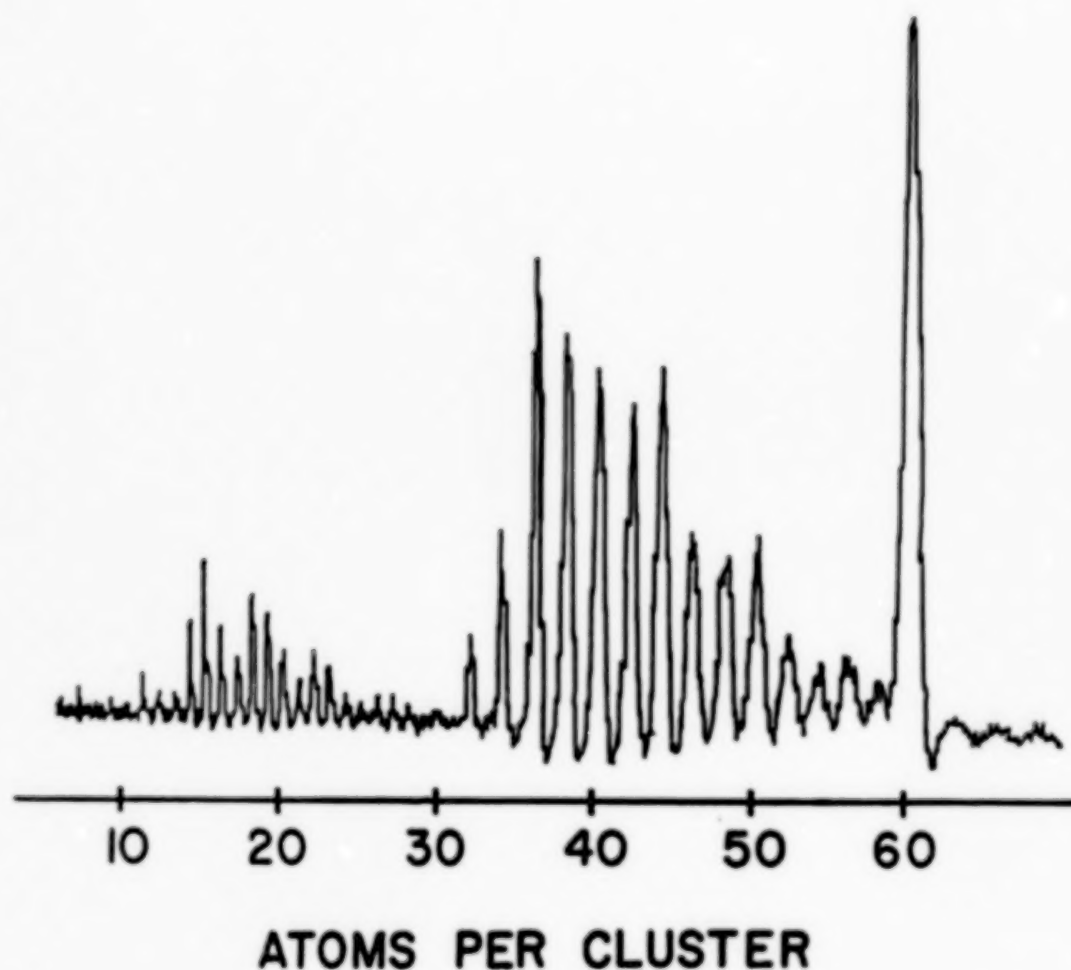


Figure 14.— Photofragmentation pattern for very highly excited  $C_{60}^+$  showing high-order granddaughter fragments. Note the abrupt breakoff in the  $C_2$  loss process at  $C_{32}^+$ . This is believed to be the smallest viable fullerene.

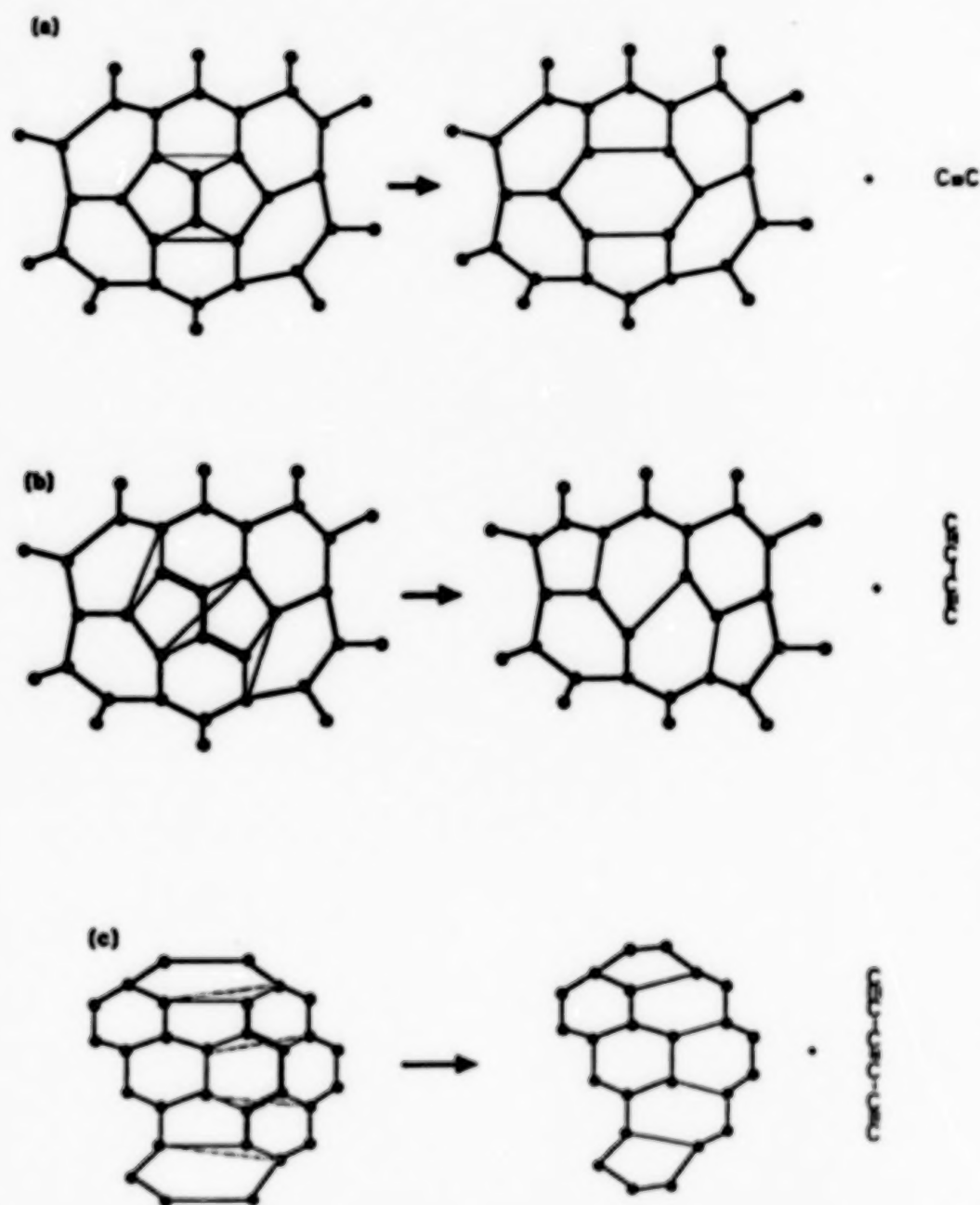


Figure 15.—Concerted fragmentation mechanism postulated to be responsible for (TOP panel) the  $C_2$  loss from a closed fullerene net upon intense laser excitation. The middle and bottom panels depict higher-order concerted mechanisms which result in the loss of successively longer even-numbered carbon chains from the closed net. Note that all of these processes conserve the number of pentagons in the net. In contrast, all open nets, chains, and rings are expected to fragment by the loss of  $C_3$ .

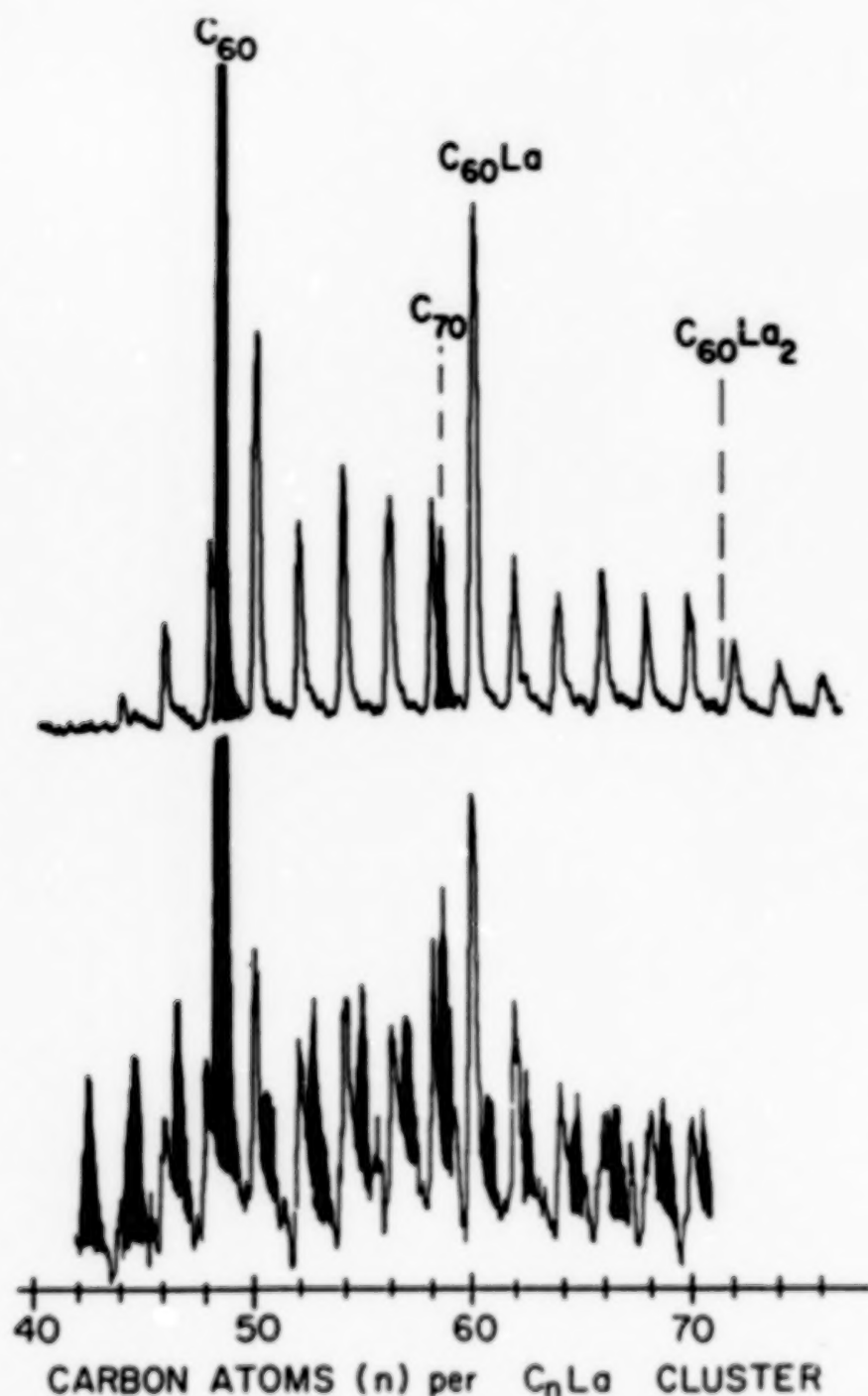


Figure 16.- TOF mass spectrum of  $C_nLa^+$  cluster complexes (open peaks) and  $C_n^+$  bare fullerene clusters (blackened peaks) produced by laser vaporization of a  $LaCl_3$  impregnated graphite disk in a pulsed supersonic nozzle, followed by ionization with an ArF excimer laser as the neutral clusters passed through the TOF spectrometer. The bottom spectrum was taken at low ArF laser fluence ( $<0.01 \text{ mJ cm}^{-2}$ ) much of an extensive unresolved baseline due to dissociating metastable ions has been subtracted here. The top spectrum was taken with an intense ArF excimer ( $1-2 \text{ mJ cm}^{-2}$ ) sufficient to dissociate all weakly bound complexes.

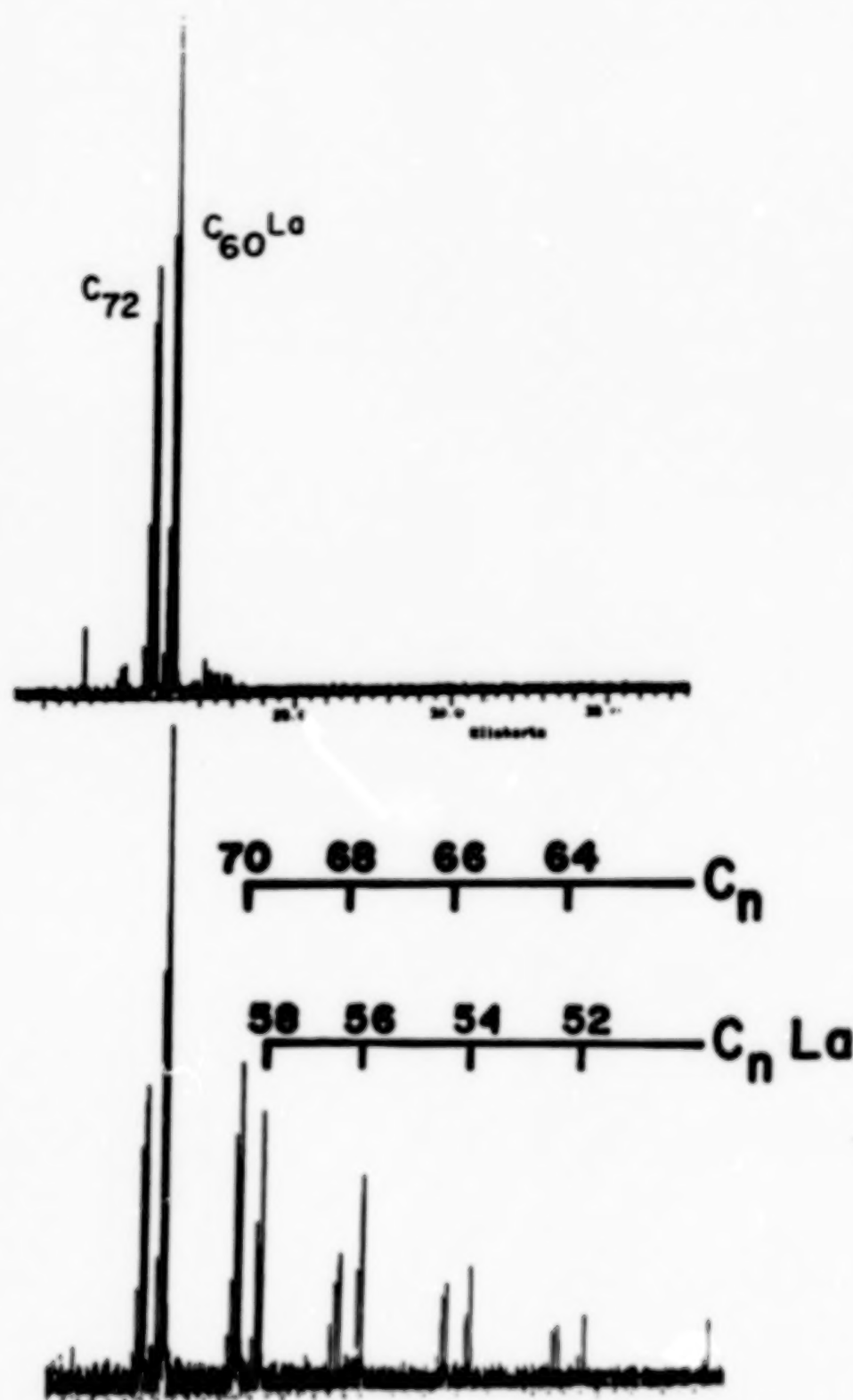


Figure 17.— ArF excimer laser photolysis experiment on  $C_{72}^+$  and  $C_{60}La^+$  trapped in an ion cyclotron resonance cell by the combination of a 6 tesla magnetic field and a weak electrostatic saddle potential. The top trace shows the Fourier transform mass spectrum before irradiation. The bottom shows the results of 50 shots of an ArF excimer laser operating at 10 Hz with a pulse fluence in the ICR cell of  $4 \text{ mJ cm}^{-2}$  per shot. Note that the fragmentation mechanism of  $C_{60}La^+$  is the same as that of all the bare fullerenes:  $C_2$  loss.



Figure 18.— Spectrum of  $C_{60}$  van der Waals complexes prepared and cooled in a supersonic beam, showing an isolated absorption band near 3860 Å.

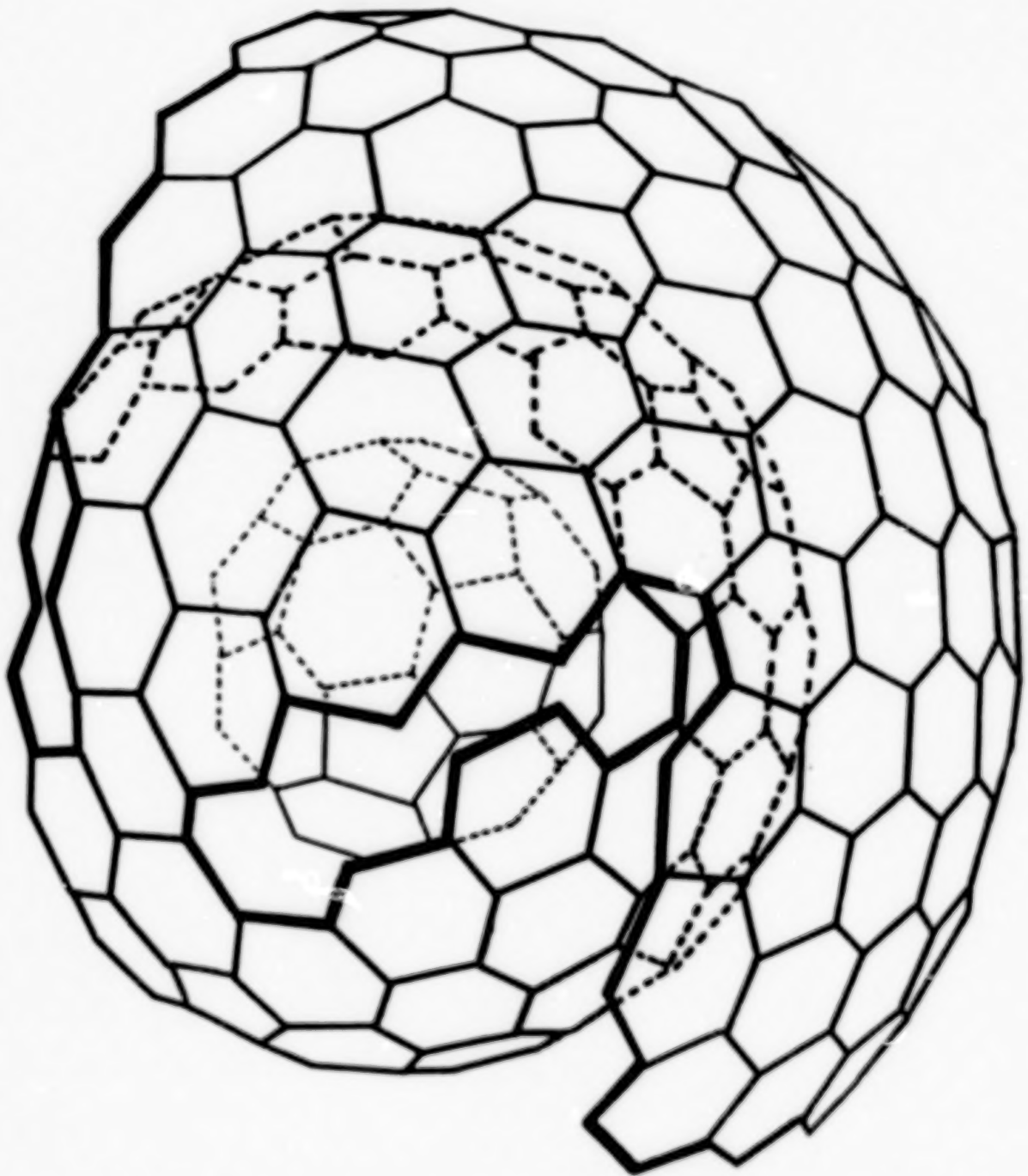


Figure 19.— Spiral carbon network structure believed to be a reasonable model for a growing carbon grain. Growth is thought to proceed from an original small carbon net which curls by the incorporation of pentagons so as to minimize dangling bonds.

# ELECTRONIC AND MOLECULAR STRUCTURE OF CARBON GRAINS\*

Jan Almlöf and Hans-Peter Löthi

Minnesota Supercomputer Institute

Clusters of carbon atoms have been studied with large-scale *ab initio* calculations. Planar, single-sheet graphite fragments with 6 - 54 atoms were investigated, as well as the spherical C<sub>60</sub> "Buckminsterfullerene" molecule. Polycyclic aromatic hydrocarbons (PAHs) have also been considered. Thermodynamic differences between diamond- and graphite-like grains have been studied in particular. Saturation of the peripheral bonds with hydrogen is found to provide a smooth and uniform convergence of the properties with increasing cluster size. For the graphite-like clusters the convergence to bulk values is much slower than for the three-dimensional complexes.

## Introduction.

Due to their scientific and technical importance, carbon clusters have long been subject to a variety of experimental[1-24] and theoretical[25-51] investigations. The areas of interest are of great diversity, including heterogeneous catalysis, the composition of graphite vapor, soot formation during combustion[15] and early stages of synthetic natural gas production from coal. Several small clusters have been identified spectroscopically in the atmospheres of red giant stars and in comet tails[6-9].

The experimental work reported for carbon clusters ranges from the early investigations of Honig and Drowart et al on small clusters[1-3] to the recent studies in the groups of Smalley and Kaldor[10-16] on larger clusters with up to 200 atoms.

A striking observation that lacks a satisfactory explanation is the existence of 'magic numbers', i.e. the fact that in a distribution of clusters some species with a certain number of carbon atoms are much more abundant than others. The exact clustering mechanisms are not completely understood, and, as noted by e.g. Rohlfing et al.[10], the origin of the observed distribution of clusters may depend upon instrumental factors. Accounting for this fact, however, there still seems to be a preference for clusters with certain numbers of atoms which cannot be explained solely as due to the experimental conditions.

Evidently, several aspects of this exciting area are difficult to study with experimental techniques. The different species are short-lived, reactive, and exist only under rather extreme conditions. These are conditions under which theoretical studies can contribute a lot to our understanding. Theoretical work has indeed been reported on smaller clusters with  $n=2-10$ [42-50] as well as on some of the larger ones[25-41]. The present work reports *ab initio* calculations for a number of large carbon clusters of relevance for the chemical problems addressed above.

\* Work supported by the National Science Foundation, grant #CHE-8610809.

*Ab initio* investigations on systems of the size considered here are usually not considered a routine procedure. Calculations which account for electron correlation in a meaningful fashion are still beyond reach for most of these molecules. With recent progress in hardware and software development it is now technically and economically feasible to study quite large molecules using the Hartree-Fock method. That approach has also the advantage of being size consistent, which is a necessity for this type of study when results for molecules of vastly different size are to be compared. This allows for the selection of study species which may at first be relatively small, but which may be gradually increased to sizes that eventually strain the capacity of the computing equipment. Size-consistency allows for an extrapolation of these results to even larger molecules, eventually to bulk systems, which are far beyond reach for a direct application of these computational methods.

### Graphite-like Fragments

Due to the enormous number of possible structures for all but the few smallest clusters, quite restrictive assumptions about their geometry have to be made. For those clusters where well-defined equilibrium structures do exist, these are likely to possess a non-trivial point group symmetry (in many cases the highest possible symmetry). It therefore seemed justified to focus the study on high-symmetric systems. Symmetry can also be used to simplify the calculation of electronic structure, and reduces the number of geometrical degrees of freedom to be optimized. In order to further confine the study, only graphite-like systems consisting of pericondensed aromatic six-rings are considered.

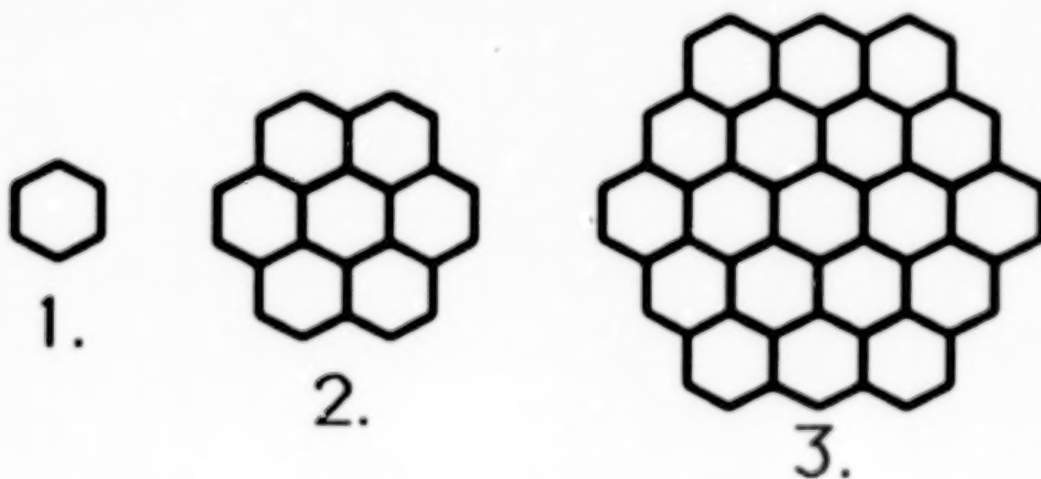


Figure 1. Graphite-like fragments of  $D_{6h}$  symmetry.  $C_6$ (1),  $C_{24}$ (2) and  $C_{54}$ (3).

In an initial series of calculations, the systems  $C_6$ ,  $C_{24}$  and  $C_{54}$  ( $D_{6h}$  symmetry, 1, 2 and 3 in Fig. 1) were computed in a high spin form with all unpaired electrons having parallel spins (Total spin  $S=3, 6$ , and  $9$ ). All carbon-carbon bond distances were kept equal at  $1.42 \text{ \AA}$ , the distance experimentally found in bulk graphite(55). The total energies computed,  $-226.5321$  Hartree for  $C_6$ ,  $-907.0085$  Hartree for  $C_{24}$  and  $-2041.5720$  Hartree for  $C_{54}$ , can be interpreted in terms of cohesive energies of  $71.0$ ,  $97.1$  and  $106.5 \text{ kcal/mol}$  per carbon atom, respectively.

Apparently, the cohesive energy of these clusters shows a very slow convergence with the size of the molecule. This should not be surprising, since the number of unsaturated valences "dangling bonds" per carbon atom is one in 1, one-half in 2 and one-third in 3.

Assuming an approximately constant energy per C-C bond, the above trend is understandable. With clusters on the above general type, the number of carbon atoms is  $6N^2$ , the number of dangling bonds is  $6N$  and the number of C-C bonds is  $9N^2 - 3N$ . The energy per bond shows a smoother trend, the numbers being 71.0, 77.6 and 79.9 kcal/mol, respectively. Alternatively, the energies can be fitted to a two-parameter expression of the form

$$E_{\text{tot}} = 6N^2 E_C + 6NE_{\text{db}} \quad (1)$$

where  $E_C$  (energy per carbon atom) and  $E_{\text{db}}$  (energy per dangling bond) are adjustable parameters. The optimum coefficients are  $E_C = -37.8366$  Hartree and  $E_{\text{db}} = +0.0891$  Hartree. For large values of  $N$  the total energy per carbon atom will converge towards  $E_C$ , and accordingly the cohesive energy per carbon atom in graphite can be expressed as the difference between  $E_C$  and the atomic energy of carbon ( $-37.6371$  Hartree), leading to a value of  $0.1995$  Hartree or  $125$  kcal/mol. (i.e.  $83.3$  kcal/mol per C-C bond, since in graphite there are  $3/2$  bonds per carbon atom). The parameter  $E_{\text{db}}$ , for which a value of  $+0.0891$  Hartree is derived, can be interpreted as the energy loss (note the positive sign of  $E_{\text{db}}$ ) for introducing a dangling bond in a graphite-like sheet of carbon atoms. Since breaking a C-C bond would result in two dangling bonds, the value of  $E_{\text{db}}$  corresponds to a loss of bond energy of  $112$  kcal/mol per bond, somewhat higher than the bond energy derived from  $E_C$ . One might have expected the electrons unpaired by the bond-breaking to redistribute into other bonding orbitals, or, in valence-bond language, that the broken peripheral bonds would rehybridize to minimize the destabilization of the framework. The opposite turns out to be true, though; breaking some bonds weakens others due to an interrupted electron delocalization, a phenomenon illustrated by the fact that the C-C bond in cyclic  $C_6$  is considerably weaker than in graphite.

For the larger clusters  $C_{24}$  and  $C_{54}$  all carbon atoms are not symmetry equivalent, and fluctuations in the local properties from atom to atom may occur. It is of some interest to study the details of that fluctuation. For instance, it is important to know how large the molecule needs to be before its interior is reasonably close to that of a single-sheet graphite. The population analysis for  $C_{24}$  shown in Fig. 2 demonstrates that the charge originating from the unpaired electrons is located to a large extent in the peripheral carbon sigma-bonding orbitals.

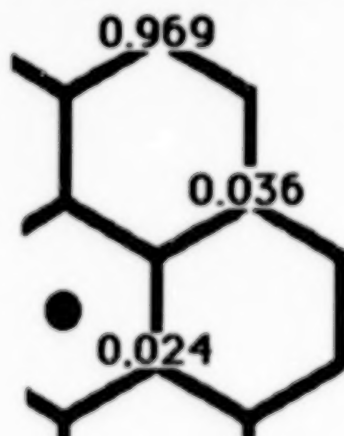


Figure 2. Spin-density populations for  $C_{24}$  in a high-spin form ( $S=6$ ).

So far, only high-spin systems have been considered. However, when neighboring dangling bonds interact, spin-pairing may occur and lead to the formation of new bonds, and hence to a lower

energy. In the case of  $C_{24}$  all adjacent dangling bond electrons can be paired up, which would result in a singlet state of the molecule. A partial structure optimization on this state leads to very short peripheral carbon-carbon bonds (1.20 Å) with essentially triple bond character. All other bond lengths change very little despite the strain introduced by shortening one bond of the outer six-membered ring by more than 0.2 Å. For  $C_{54}$  a similar structure may be obtained. Pairing up electrons from adjacent carbon atoms of the same six-membered ring, and leaving all the other (isolated) dangling bond electrons with parallel spins, a low spin state ( $S=3$ ) would be obtained. This mechanism is supported by an actual calculation on the low spin form, in which the spin density is almost entirely localized on the carbon atom that would carry the dangling bond in a simple valence orbital picture. (see Fig 3).

### low-spin ( $S=3$ )

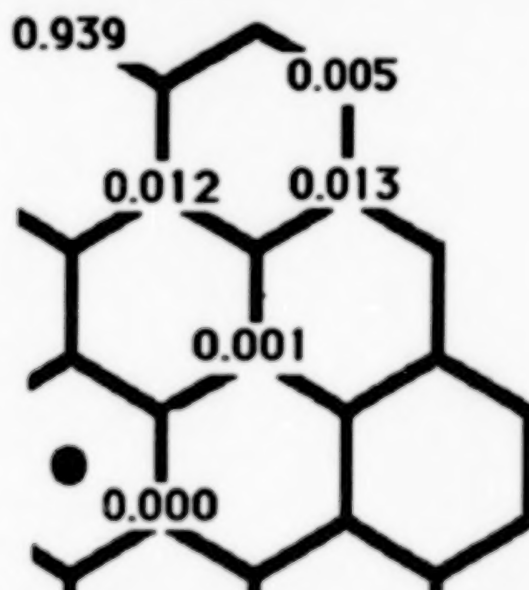


Figure 3. Spin density distribution for  $C_{54}$  in a low-spin form ( $S=3$ ).

Energy calculations show that the low spin state of  $C_{54}$  is indeed about 1.3 eV lower in energy than the high spin state, at least for the molecular geometries used here, whereas for  $C_{24}$  nearly identical energies for the two states are found. Inclusion of electron correlation would favor the low spin form further, though hardly enough to significantly affect a comparison of cohesive energies between various forms of carbon.

The ionization potentials (Koopmans' values) for the high spin and the low spin form of  $C_{54}$  are 6.8 and 7.3 eV respectively, values that would both fit into the bracket of IP's reported for carbon clusters with 40 to 100 atoms[11]. The corresponding values for  $C_{24}$  are higher, 8.0 and 8.3 eV respectively.

### Polycyclic Aromatic Hydrocarbons.

The above studies show that properties in the interior of the graphite-like clusters do not converge readily to bulk values. Even for the  $C_{54}$  cluster, the populations in the center show a significant deviation from neutrality. Despite the possibility of exploiting the high point-group symmetry of these systems, the complicated open-shell structure places severe limits on the maximum

size of the clusters that can be studied. Therefore, the calculation of a graphite cluster large enough to ensure that the calculated properties have converged to bulk values would be computationally unfeasible.

If the focus of interest is on the carbon clusters themselves, then of course no substitute system can be used. However, for studying the convergence of properties one can minimize the termination effects by saturating the dangling bonds in the simplest possible way, i.e. with hydrogen. By that approach one can both avoid the problem of handling an excessive number of open shells, and obtain a series of molecules that converge towards bulk properties more smoothly than the bare carbon clusters.

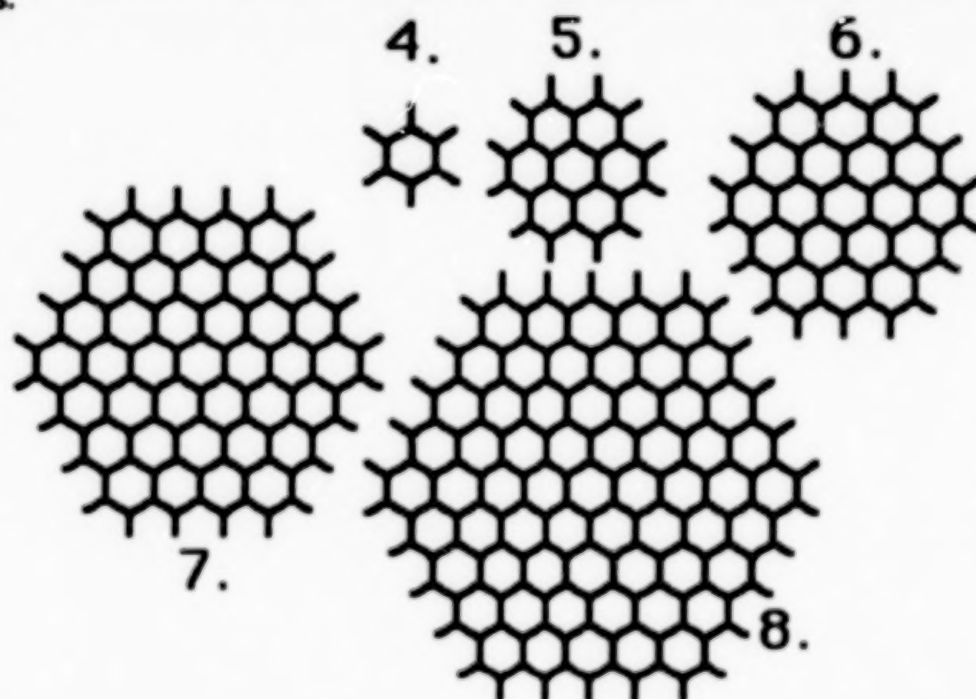


Figure 4. The PAHs  $C_6H_6$ (4),  $C_{10}H_8$ (5),  $C_{14}H_{10}$ (6),  $C_{96}H_{24}$ (7), and  $C_{150}H_{30}$ (8)

The series of PAHs shown in Fig. 4 have been studied in the present work, and should allow for an extrapolation towards an infinite single layer of graphite. The total energies of these systems with the general formula  $C_{6N}H_{6N}$  are presented in Table 1. For all molecules except 8 an overall C-C bond distance was optimized. This seems to converge smoothly towards 1.406 Å, a value somewhat shorter than that experimental distance of 1.421 Å found in bulk graphite[52]. The Hartree-Fock approximation is the main source of this discrepancy. It should be noted, however, that the bond distance in a graphite mono-layer is expected to be somewhat shorter than the bulk value[53].

The total energy of these molecules can be accurately fitted with a two-parameter expression similar to that given in Equation 1:

$$E_{\text{tot,est}} = 6N^2E_C + 6NE_H \quad (2)$$

Table 1 shows that the total energies of the systems studied here are reproduced by Eq. 2 with an error smaller than 0.2 kcal/mol per carbon atom.

The optimum coefficients in Equation 2 are  $E_C = -37.8363$  and  $E_H = -0.5685$  Hartree.  $E_C$  is very close to the value -37.8366 found for the pure graphite clusters.

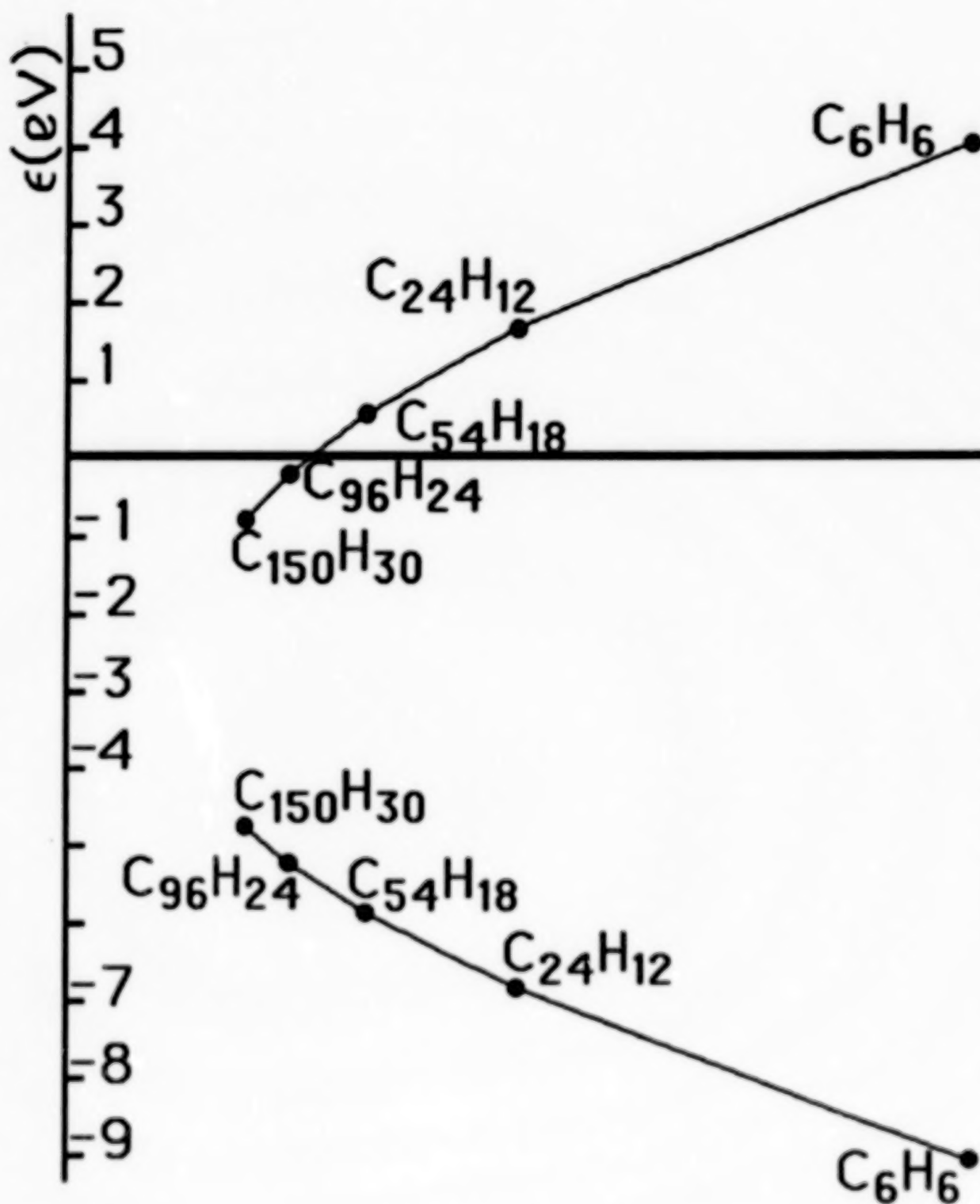


Figure 5. HOMO and LUMO orbital energies for  $C_6N_2H_6N$ , plotted vs  $1/N$ .

The value of  $E_H$  corresponds to a contribution of 47.1 kcal/mol to the total energy of  $C_6N_2H_6N$  for each bonded H-atom (the hydrogen atom has an energy of -0.4935 Hartree in the basis set used).

Alternatively, the parameter values can be interpreted as 83.3 kcal/mol per C-C bond, 88.7 kcal/mol per C-H bond.

The value 125 kcal/mol represents an upper bound to the cohesive energy per carbon atom in graphite, since the interaction between layers in the bulk has not been accounted for. Given the relatively large distance and the physical properties of graphite, the inter-layer interaction energy is estimated to be < 5 kcal/mol.

This leaves us with a computed result in less than satisfactory agreement with the experimental value of about 170 kcal/mol[54]. The neglect of electron correlation and the limited basis set used are the most important sources of the discrepancy. In a previous study on mono-layer graphite[53], basis set effects were found to lead to a significant underestimation of the cohesive energy.

The orbital energies show a surprisingly slow convergence as the size of the molecule increases. Even for the largest system studied, the HOMO-LUMO gap is about 4 eV. From the values shown in Fig. 5 one may expect semiconducting behavior to occur at N=8-10, i.e. for clusters with 400-600 atoms. At that point a conventional Hartree-Fock approach would of course break down.

The HOMO and LUMO orbital energies seem to converge towards a value of about -4 eV, which would be an estimate of the work function for single-sheet graphite. This is in reasonable agreement with the work function of 4.9 eV experimentally found for bulk graphite[52].

### Diamond-like Clusters.

From the two-dimensional, graphite-like clusters, the extension to three-dimensional structures is obvious. Symmetric structures developed in a similar fashion to the planar systems would grow in three dimensions with increasing N, and the number of atoms would increase faster. In this work clusters of  $T_d$  symmetry were studied, resembling a small fragment of a diamond structure. Only systems with saturated external bonds were considered. The number of carbon and hydrogen atoms in such a structure is given by

$$N_C = N(4N^2 - 1)/3$$

$$N_H = 4N^2$$

Here we present some results from studies on systems with N=2,3, and 4. (N=1 would correspond to the methane molecule). The molecules are shown in Fig. 6

For all three molecules, an overall C-C distance was optimized. The values obtained for the three systems are 1.542Å, 1.540Å and 1.539Å, smoothly converging to a value slightly shorter than the equilibrium distance in diamond.

Fitting the energies to an expression similar to Eq 2 gives  $E_C = -37.8360$ ,  $E_H = -0.5732$  for the tertiary hydrogens, and  $E_H = -0.5742$  for methylene carbons. The extrapolated cohesive energy is 125 kcal/mol, the same as for graphite. A breakdown of the bond energies per bond gives a C-C bond energy of 62 kcal/mol. The C-H bond energies are 82 and 81 kcal/mol for the methylene and the tertiary hydrogens, respectively.

The convergence pattern for the orbital energies is quite different from that found in the graphite-like clusters as shown in Fig. 7. The extrapolated band gap is somewhat uncertain but seems to lie around 10 eV, and is definitely larger than the experimental value of about 4.6 eV. This difference is mainly due to neglect of electron correlation in our calculations.

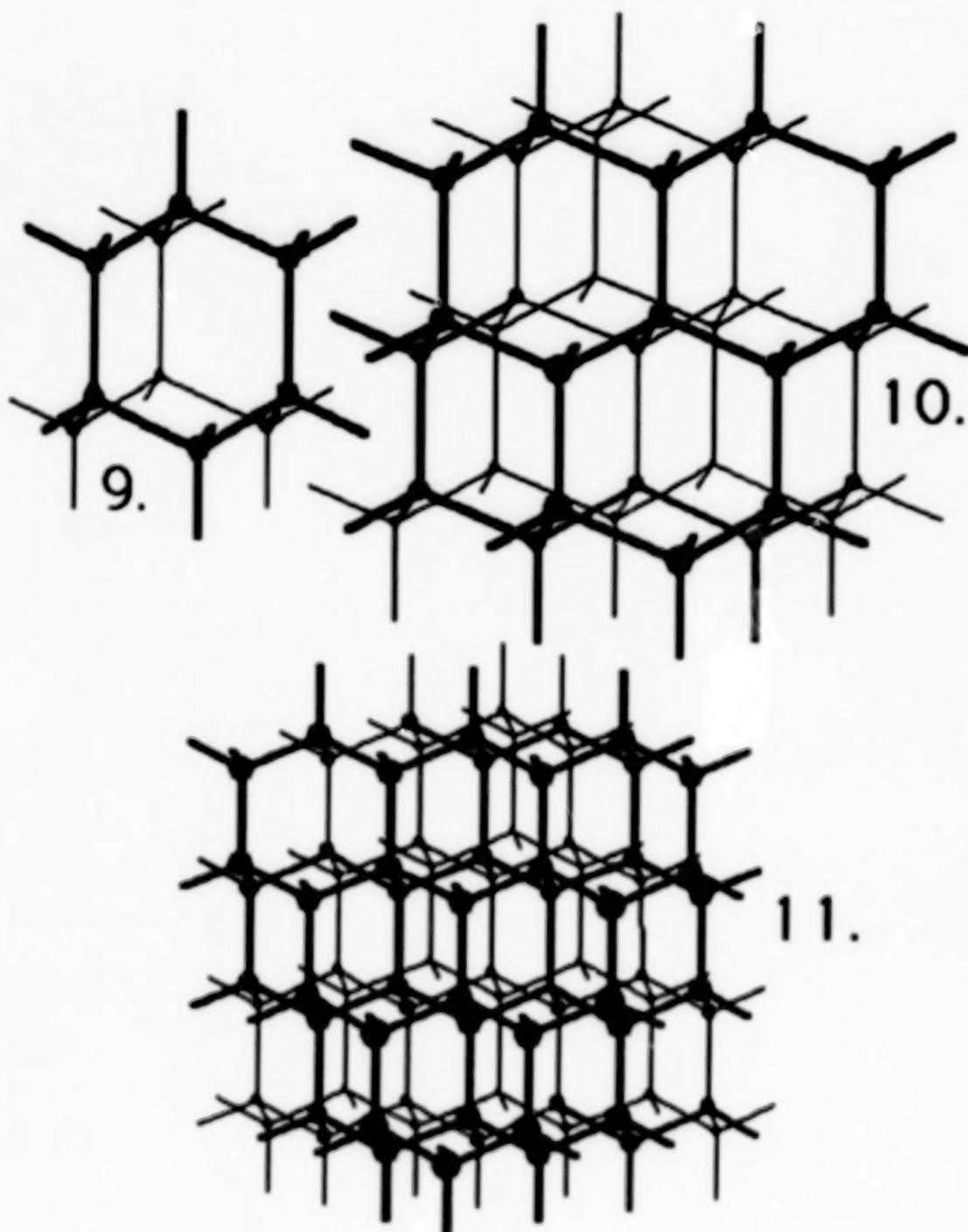


Figure 6. The diamond-like systems  $C_{10}H_{16}$ (9),  $C_{35}H_{36}$ (10) and  $C_{84}H_{64}$ (11).

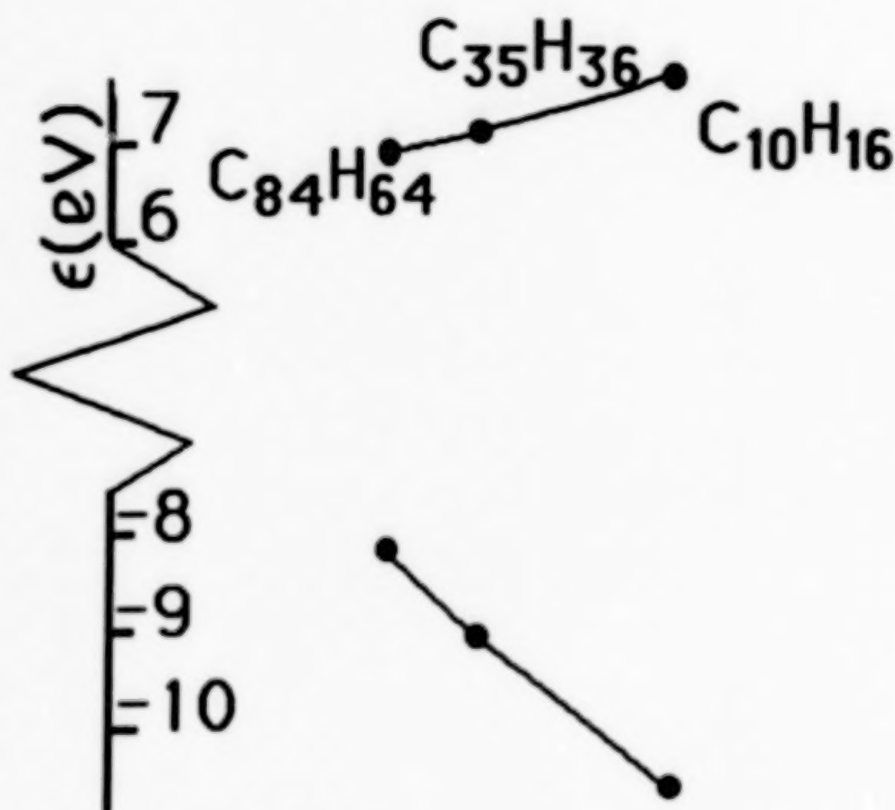


Figure 7. HOMO and LUMO energies for the diamond-like clusters, plotted vs  $1/N$ .

### Linear Carbon Chains.

Another, simple form of elemental carbon would be chains formed from carbon atoms. As a prototype model a single-stranded chain is most suitable. If branching were to be considered, all intermediate forms up to and including the diamond- and graphite-like clusters would be included. For non-branched chains, the two variants to choose from are a system of alternating singly and triply bonded carbon atoms (poly-yne), and a system with all double bonds (cumulenes). Cumulene structures are assumed to be the preferred ones for odd-membered chains, whereas the even ones may have some poly-yne character. Recent studies on linear  $C_6$  show that a cumulene-like structure is preferred, both at the SCF level and when correlation is accounted for[50].

As an alternative to linear chains, a simple ring-shaped molecule should also be considered. Regardless of whether poly-yne or cumulenes are considered, the gain in bond energy due to the new bond formed should be relatively independent of the size of the chain. In contrast, the strain involved in forming a ring is inversely proportional to the number of atoms, assuming a harmonic C-C-C bending potential. Clearly, ring structures should be thermodynamically preferred for chains above a certain size (even though their formation might be kinetically or statistically unfavorable). In fact, already for as small a system as  $C_6$  the ground state structure is found to be cyclic, although the omission of electron correlation would predict a linear, cumulene-like geometry to be marginally lower in energy[50].

We have chosen to study the  $C_{20}$  poly-yne ring assuming it to be a reasonable representative for a large chain molecule. The bond lengths optimized at the Hartree-Fock level are 1.37 Å and

1.20 Å, respectively. The same values are found for the experimental bond lengths in 1,3-butadiene  $\text{CH}_3\text{-C}=\text{C}-\text{C}=\text{C}-\text{H}$ , indicating that there is very little  $\pi$  conjugation in the system.

The cohesive energy per carbon atom in a poly-yne ring is only 99.1 kcal/mol, clearly lower than the value in e.g. planar  $\text{C}_{54}$ . In addition to the unfavorable energy one would anticipate a long and complicated route of formation for a chain-like molecule when starting from graphite, and it does not seem likely that any of the larger clusters observed experimentally would have a linear or cyclic chain structure.

### Non-planar Clusters Containing Five-membered Rings.

The existence of a stable  $\text{C}_{60}$  molecule, *Buckminsterfullerene* was recently proposed[14]. In the suggested structure, twelve regular pentagons and twenty hexagons are connected to form an almost perfectly spherical pattern of icosahedral symmetry.

Previous theoretical work seems to support the existence of this amazing molecule. Several calculations[25-41] on *Buckminsterfullerene* at various degree of approximation find a resonance stabilization larger than in benzene, and only slightly smaller than in graphite. From these calculations it has been concluded that the molecule is likely to exist. A recent MNDO study[41] concludes that large polyhedral complexes (> 40 atoms) are more stable than the corresponding graphite-like ones. However, the predictive power of these approximate methods is limited, in particular for problems where planar and non-planar systems are compared. The interpretation of the original experiment postulating the existence of *Buckminsterfullerene* has recently been challenged[11], and *ab initio* calculations of the relative energies involved could be used to resolve some of the controversy.

The optimized geometry has twelve regular five-membered rings with an edge of 1.453 Å. Each of the thirty hexagons shares three sides with pentagons, whereas the three others, shared with adjacent hexagons, are substantially shorter (1.369 Å). Our calculated HOMO-LUMO splittings are around 8 eV, both at the minimal-basis and double-zeta level. The results of our calculations on *Buckminsterfullerene* were reported fully in Ref 39, and are summarized in Table 3.

The ionization potential (7.9 eV) falls right outside the bracket of experimental IP's reported for carbon clusters with 40 to 100 atoms ( $6.42 \text{ eV} \leq \text{IP} \leq 7.87 \text{ eV}$ [11]). Inclusion of correlation effects will lower the calculated  $\Delta\text{SCF}$  IP by 0.25 to 0.50 eV, so that the corrected IP will be at the upper end of the experimental IP-bracket. Due to the diffuseness of the  $\pi$  orbital from which an electron is removed, the correlation error in the  $\Delta\text{SCF}$  value will be smaller than in cases where an electron is removed from a well localized bond. In those cases a correction of 1 eV is usually applied.

The cohesive energy per carbon atom in *Buckminsterfullerene*, 114 kcal/mol, is 11 kcal/mol lower than the value extrapolated for graphite, but 7 kcal/mol higher than the value computed for the  $\text{C}_{54}$  graphite-like sheet or 14.5 kcal/mol higher than for the  $\text{C}_{20}$  poly-acetylene ring. Accordingly, the heat of formation for *Buckminsterfullerene* is 650 kcal/mol, suggesting a high degree of instability with respect to graphite.

At the Hartree-Fock level, comparisons between systems with very different molecular and electronic structures have to be made with some care. Strained geometries of the type found in  $\text{C}_{60}$  are usually difficult to describe without polarization functions. The basis set used is therefore expected to slightly favor the planar systems. Repeating the calculations with d-functions added would be unnecessarily time-consuming, and another approach has instead been used. The bowl-shaped corannulene molecule ( $\text{C}_{20}\text{H}_{10}$ ) has a geometry resembling a fragment of a  $\text{C}_{60}$  ball, and the strain in the C-framework ought to be similar as well.

To investigate the basis set effect in connection with geometric strain in *Buckminsterfullerene*, we have performed calculations with and without d-type functions on corannulene. The d-functions

improve the binding with about 10 kcal/mol per C-atom in  $C_{20}H_{10}$ ; the corresponding improvement in coronene ( $C_{24}H_{12}$ ) is 8 kcal/mol. Within reasonable limits, these numbers are not crucially dependent on the d-exponents used (0.4-0.6). One can therefore estimate that the inclusion of d-orbitals in *Buckminsterfullerene* would decrease the calculated heat of formation by about 120 kcal/mol.

Even though the predicted relative instability of *Buckminsterfullerene* would be somewhat diminished by such an extension of the basis, the main conclusion remains; the  $C_{60}$  molecule is still about 530 kcal/mol higher in energy than a corresponding fragment of bulk graphite.

Another conclusion that can be drawn from the calculations on corannulene is an estimate of the loss of energy due to incorporation of a five-membered ring into a structure of condensed six-rings. Eq. (2) predicts a total energy of -762.4110 Hartree. for  $C_{20}H_{10}$ , the energy actually computed is -762.2656 Hartree., and the loss due to a five-membered ring is thus about 0.14 Hartree. This is significantly larger than loss of 0.09 Hartree. predicted from Eq. (1) due to the occurrence of a dangling bond in the structure. It can therefore be concluded that the reducing the number of dangling bonds in 2 and 3 above by introducing five-membered rings on the periphery is not likely to lead to more stable structures.

In conclusion, these calculations suggest that the *Buckminsterfullerene* molecule is thermodynamically unstable with respect to graphite by about 23 eV. In general, thermodynamically unstable molecules can often be readily synthesized, and frequently exist with virtually infinite lifetimes. The unusually large instability observed in this case might seem almost prohibitive, however no other good candidate for the pronounced peak seen at  $n=60$  in the reported mass spectra has been found. Apparently, the bond strain in *Buckminsterfullerene* is still more favorable than a situation with 20 unpaired electrons. Multiple-sheet models have not been considered in this work, since the number of dangling bonds in these would be even larger.

### Conclusions.

We have demonstrated that new and unique information about large molecular systems can be achieved by using computational methods on a large scale. In many cases, that information would have been very difficult to obtain with other means.

Even though our calculations on PAHs show a fairly slow convergence of properties, they allow for an extrapolation on the cohesive energy per carbon atom in bulk graphite. The data obtained from the Mulliken population analysis further show that the inner parts of the larger molecules studied have a domain with little total charge or spin density, which may mimic a graphite surface rather well. Since the problem of dealing with a large number of open shells can be circumvented by these calculations, the approach offers an attractive way of modeling a graphite surface as well as a way to study graphite intercalation compounds.

The fact that pairing up dangling bond electrons may lead to more stable graphite fragments is somewhat surprising. This suggests that the edge of a graphite fragment may look different from what is commonly assumed. This observation may have far-reaching consequences for the understanding of the chemistry and reactivity of large carbon clusters.

Energetically, the lively debated soccerball-form of  $C_{60}$  compares very favorably with a graphite-like sheet of carbon atoms. This, of course, does not prove that *Buckminsterfullerene* really is (fully or partly) responsible for the  $C_{60}$  peak observed. Due to the large number of degrees of freedom, a study of all plausible isomers would be a prohibitively cumbersome task. Even if such a complete coverage were possible the existence of different molecular species at these conditions is not likely to be governed by thermodynamic stabilities only.

## References

1. R.E. Honig, J. Chem. Phys. 1954, **22**, 126.
2. J. Drowart, R.P. Burns, G. DeMaria and M.G. Inghram, J. Chem. Phys. 1959, **31**, 1131.
3. J. Berkowitz and W.A. Chupka, J. Chem. Phys. 1964, **40**, 2735.
4. N. Fürstenau, F. Hillenkamp and R. Nitsche, Int. J. Mass Spectr. Ion Phys. 1979, **31**, 85.
5. N. Fürstenau and F. Hillenkamp, Int. J. Mass Spectr. Ion Phys. 1981, **37**, 135.
6. A. McKellar, Astrophys. J. 1948, **108**, 453.
7. P. Swings, Rev. Mod. Phys. 1942, **14**, 190.
8. P. Swings and A. McKellar, Astrophys. J. 1948, **108**, 458.
9. W.R.M. Graham, K.I. Dismuke and W. Weltner, Jr., Astrophys. J. 1976, **204**, 301.
10. E.A. Rohlfing, D.M. Cox and A. Caldor, J. Chem. Phys. 1984, **81**, 3322.
11. D.M. Cox, D.J. Trevor, K.C. Reichmann and A. Caldor, J. Amer. Chem. Soc. 1986, **108**, 2457.
12. Y. Liu, S.C. O'Brien, Q.L. Zhang, J.R. Heath, F.K. Tittel, R.F. Curl, H.W. Kroto and R.E. Smalley, Chem. Phys. Lett. 1986, **126**, 215.
13. J.R. Heath, Q.L. Zhang, S.C. O'Brien, R.F. Curl, H.W. Kroto, and R.E. Smalley, J. Am. Chem. Soc. 1987, **109**, 359.
14. H.W. Kroto, J.R. Heath, S.C. O'Brien, R.F. Curl and R.E. Smalley, Nature 1985, **318**, 162.
15. Q.L. Zhang, S.C. O'Brien, J.R. Heath, Y. Liu, R.F. Curl, H.W. Kroto and R.E. Smalley, J. Phys. Chem. 1986, **90**, 525.
16. J.R. Heath, S.C. O'Brien, Q.L. Zhang, Y. Liu, R.F. Curl, H.W. Kroto, F.K. Tittel and R.E. Smalley, J. Am. Chem. Soc. 1985, **107**, 7779.
17. L.A. Bloomfield, M. Geusic, R.R. Freeman and W.L. Brown, Chem. Phys. Letters 1985, **121**, 33.
18. M.E. Geusic, T.J. McIlrath, M.F. Jarrold, L.A. Bloomfield, R.R. Freeman and W.L. Brown, J. Chem. Phys. 1986, **84**, 2421.
19. R.D. Knight, R.A. Walsh, S.C. Foster, T.A. Miller, S.L. Mullen and A.G. Marshall, Chem. Phys. Letters 1986, **129**, 331.
20. S.W. McElvany, W.R. Creasy and A. O'Keefe, J. Chem. Phys. 1986, **85**, 632.
21. A. O'Keefe, M.M. Ross and A.P. Baronavski, Chem. Phys. Letters 1986, **130**, 17.
22. M.Y. Hahn, E.C. Honea, A.J. Paguia, K.E. Schriver, A.M. Camarena and R.L. Whetten, Chem. Phys. Letters 1986, **130**, 12.
23. S.C. O'Brien, J.R. Heath, H.W. Kroto, R.F. Curl, and R.E. Smalley, Chem. Phys. Letters 1986, **132**, 99.
24. J. Bernholc and J.C. Phillips, Phys. Rev. B 1986, **33**, 7395.
25. R.L. Disch and J.M. Schuiman, Chem. Phys. Letters 1986, **125**, 465.
26. A.J. Stone and D.J. Wales, Chem. Phys. Letters 1986, **128**, 50.
27. D.S. Marynick and S. Estreicher, Chem. Phys. Letters 1986, **132**, 383.
29. D.J. Klein, T.G. Schmatz, G.E. Hite and W.A. Seitz, J. Amer. Chem. Soc. 1986, **108**, 1301.
30. T.G. Schmatz, W.A. Seitz, D.J. Klein and G.E. Hite, Chem. Phys. Letters 1986, **130**, 203.
31. P.D. Hale, J. Amer. Chem. Soc. 1986, **108**, 6087.
32. P.W. Fowler and J. Woolrich, Chem. Phys. Letters 1986, **127**, 78.
33. P.W. Fowler, Chem. Phys. Letters 1986, **131**, 444.
34. M. Ozaki and A. Takahashi, Chem. Phys. Letters 1986, **127**, 242.
35. A.D.J. Haymet, Chem. Phys. Letters 1985, **122**, 421.
36. A.D.J. Haymet, J. Amer. Chem. Soc. 1986, **108**, 319.
37. R.C. Haddon, L.E. Brus and K. Raghavachari, Chem. Phys. Letters 1986, **125**, 459.

38. R.C. Haddon, L.E. Brus and K. Raghavachari, Chem. Phys. Letters, 1986, **131**, 165.
39. H.P. Lüthi and J. Almlöf, Chem. Phys. Letters 1987, **135**, 357.
40. S. Satpathy, Chem. Phys. Lett. 1986, **130**, 545.
41. M.D. Newton and R.E. Stanton, J. Amer. Chem. Soc. 1986, **108**, 2469..
42. J.P. Ritchie, H.F. King and W.S. Young, J. Chem. Phys. 1986, **85**, 5175
43. R.A. Whiteside, R. Krishnan, D.DeFrees, J.A. Pople and P.v.R. Schleyer, Chem. Phys. Lett. 1981, **78**, 538.
44. R.A. Whiteside, R. Krishnan, M.J. Frisch, J.A. Pople and P.v.R. Schleyer, Chem. Phys. Lett. 1981, **80**, 547.
45. K. Raghavachari and J.S. Binkley, J. Chem. Phys., in press.
46. P. Joyes and M. Leleuter, J. Phys. 1984, **45**, 1681..
47. K.S. Pitzer and E. Clementi, J. Amer. Chem. Soc. 1959, **81**, 4477
48. R. Hoffmann, Tetrahedron, 1966, **22**, 521.
49. D.W. Ewing and G.V. Pfeiffer, Chem. Phys. Lett. 1982, **86**, 365.
50. K. Raghavachari, R.A. Whiteside and J.A. Pople, J. Chem. Phys. 1986, **85**, 6623
51. J.R. Dias, J. Mol. Structure Theochem, 1986, **137**, 9.
52. J.D. Donohue, The Structure of the Elements Wiley; New York, 1974.
53. W. Weinert, E. Wimmer and A.J. Freeman, Phys. Rev. B 1982, **26**, 4571.
54. P.D. Zavitsanos and G.A. Caruso, J. Chem. Phys. 1973, **39**, 2966.
55. R.F. Willis, B. Fuebacher and B. Fritton, Phys. Rev. B 1971, **4**, 2441.

Table 1: Total energies and C-C bond distances computed for  $C_{6n}2H_{6n}$  and energies estimated using expression (2) with the parameters  $E_C = -37.8363$ ,  $E_H = -0.5685$  Hartree. The C-H distances were kept fixed at 1.10Å.

n	system	-E <sub>tot,calc</sub>	-E <sub>tot,pred</sub>	Δ	R <sub>CC</sub> (Å)
1	C <sub>6</sub> H <sub>6</sub>	230.4320	230.4288	0.0032	1.384
2	C <sub>24</sub> H <sub>12</sub>	914.8938	914.8932	0.0006	1.401
3	C <sub>54</sub> H <sub>18</sub>	2053.3942	2053.3932	0.0010	1.404
4	C <sub>94</sub> H <sub>24</sub>	3645.9003	3645.9288	-0.0285	1.406
5	C <sub>150</sub> H <sub>30</sub>	5692.4981	5692.5000	-0.0019	1.406 <sup>a</sup>

<sup>a</sup>assumed without geometry optimization.

**Table 2: Total computed energies and distances for the diamond-like clusters.**  
**The C-H distances were kept fixed at 1.09 Å.**

n	system	-E <sub>tot</sub> (a.u.)	R <sub>CC</sub> (Å)
2	C <sub>10</sub> H <sub>16</sub>	387.54332	1.542
3	C <sub>35</sub> H <sub>36</sub>	1344.90665	1.540
4	C <sub>84</sub> H <sub>64</sub>	3214.91903	1.539

**Table 3: Computed properties for Buckminsterfullerene.**

**Bond lengths:**

R1 1.453 Å

R2 1.369 Å

**Ionization potential:**

ΔSCF 7.92 eV

HOMO energy 8.24 eV

**Electron affinity:**

ΔSCF 0.80 eV

LUMO energy 0.60 eV

**Cohesive energy/carbon atom:** 114 kcal/mol

## A UNIFYING PICTURE OF GAS-PHASE FORMATION AND GROWTH OF PAH, SOOT, DIAMOND AND GRAPHITE\*

Michael Frenklach

The Pennsylvania State University  
University Park, PA 16802

*A variety of seemingly different carbon formation processes -- polycyclic aromatic hydrocarbons and diamond in the interstellar medium, soot in hydrocarbon flames, graphite and diamond in plasma-assisted-chemical vapor deposition reactors -- may all have closely related underlying chemical reaction mechanisms. Two distinct mechanisms for gas-phase carbon growth are discussed. At high temperatures it proceeds via the formation of carbon clusters. At lower temperatures it follows a polymerization-type kinetic sequence of chemical reactions of acetylene addition to a radical, and reactivation of the resultant species through H-abstraction by a hydrogen atom.*

### INTRODUCTION

Carbonaceous solids -- like amorphous carbon, carbon black, soot and graphite -- are known to be structurally related materials (refs. 1-3). They are composed of polycyclic aromatic planes. The arrangement of the planes is what distinguishes these materials: hexagonal crystal lattice in graphite (refs. 2,4) and turbostratic layers of crystallines in soot and carbon blacks (refs. 1,5,6). The turbostratic structures can be transformed into the graphitic lattice with the increase in temperature (ref. 2). Graphite is found to be in equilibrium with diamond at very high pressures, 20 to 80 kbar at temperatures from 1000 to 3000 K (refs. 3,7).

All of these materials can be formed in gas-phase processes at near-atmospheric or lower pressures (refs. 3,5,7-10). It is suggested in this article that the mechanisms of formation and growth under these conditions are closely related to each other. Furthermore, it is suggested that a similar mechanism may be responsible for the formation of polycyclic aromatic hydrocarbons (PAH) and diamonds observed in the interstellar medium (refs. 11-16).

The following discussion is organized in four parts: soot formation in hydrocarbon pyrolysis and oxidation, and the chemical reaction mechanism advanced to explain the observed experimental phenomena; numerical results for the formation of PAH in carbon-rich circumstellar envelopes; mechanism of vapor-deposited diamond; and homogeneous nucleation of diamond at near-atmospheric pressures.

---

\* The work was supported in part by NASA-Lewis Research Center and the Office of Naval Research

## SOOT IN HYDROCARBON PYROLYSIS AND OXIDATION

Soot production in flame environment has long been a focus of combustion research and a great deal of data have been accumulated. The present knowledge on the global picture of soot formation can be summarized as follows (see references 1,2,5,6,8,17-21 for details). High-temperature gas-phase reactions lead to the production of two-dimensional PAH. These planar molecules then "adhere" to each other forming multi-layered "sandwiches". The PAH planes in these three-dimensional crystallines are arranged without any specific order, and thus they are called turbostratic layers. The crystallines coalesce forming spherical particles, reaching typically an average diameter of 20 to 40 nm, which then agglomerate into chain-like aggregates of the order of 1  $\mu\text{m}$ . In addition to coagulation and agglomeration there is also particle growth due to chemical deposition (of acetylene) on the particle surface, a surface reaction (refs. 22,23). The formation of primary spherical particles takes place on the time scale of a millisecond at flame temperatures, about 1300 to 2000 K (ref. 24).

Of particular interest to the present symposium are the results obtained in high-temperature near-atmospheric hydrocarbon pyrolysis (refs. 25-33), especially those obtained in shock tubes, i.e. under the conditions free of transport phenomena. In the initial work, Graham and co-workers (refs. 25,26) demonstrated that under similar experimental conditions aromatic fuels produce more soot than non-aromatic ones. They also observed that soot yield from aromatic fuels exhibit a bell-like dependence on temperature, i.e., the amount of soot formed increases with temperature, reaches a maximum (at about 1800 K) and then decreases. Further experimental data obtained (refs. 32-35) showed that the bell-like dependence of soot yield on temperature is characteristic of all the hydrocarbon fuels studied. An example of such a dependence obtained for soot formation in pyrolysis of acetylene is shown in figure 1. The soot-yield bell appeared to be a function of reaction time, initial fuel concentration, pressure, absorption wavelength, presence of oxygen, addition of hydrogen, and fuel molecular structure:

- With an increase in reaction time, the soot bell is shifted to lower temperatures with an increase in the absolute yield values (see fig. 1);
- Higher initial fuel concentrations, within the range tested, increase the soot yields with a slight shift to higher temperatures;
- Lowering the total pressure shifts the soot bell to higher temperatures with an increase in the bell width. The effect is more pronounced at lower pressures;
- With changing the probe beam wavelength from the visible to the infrared the soot bell, as determined by light absorption, appears at higher temperatures;
- The addition of small amounts of molecular oxygen shifts the soot bell to lower temperatures. Large amounts of oxygen completely suppress the formation of soot;
- The addition of molecular hydrogen strongly suppresses soot formation (ref. 36); this is demonstrated in Fig. 2.

At very high temperatures, above approximately 2500 K, soot yield begins to increase again, which can be seen in figures 1 and 2 for the pyrolysis of acetylene. This second rise in soot yield is thought to have a mechanism different from that responsible for the soot bell observed at lower temperatures and will be discussed later in the text.

The results obtained in shock-tube experiments were interpreted in light of the following phenomenological description (refs. 32,33). Formation of the first aromatic ring (e.g., phenyl radical or benzene molecule) is the process bottleneck starting with a non-aromatic fuel. Once the aromatic ring is

formed, it reacts with a non-aromatic species (e.g., acetylene molecule or vinyl radical) initiating a polymerization reaction sequence leading to the formation of polycyclic aromatic hydrocarbons. Starting with an aromatic fuel, the process rate is determined by the rate of fragmentation of the aromatic ring. The fragments formed react with the intact rings thus initiating the polymerization sequence of PAH. Addition of oxygen accelerates fuel pyrolysis, which results in a shift of soot formation to lower temperatures; on the other hand, it removes aromatic rings and active intermediates by oxidation, thus suppressing soot formation at high oxygen concentrations (ref. 34).

This phenomenological description was generally supported by the results of detailed chemical kinetic modeling (refs. 36-41). A mechanism of approximately a thousand elementary reversible chemical reactions was generated according to the physical organic chemistry principles. The rate coefficients of these reactions were for the most part estimates. Computer experimentation with the composed mechanism identified the principal reaction pathways leading to the formation of particular stable fused polycyclic aromatics, like acenaphthalene, pyrene, coronene, etc. -- their formation reactions are essentially irreversible and have an effect of pulling chains of reversible reactions. Hydrogen atoms reactivate aromatic molecules to radicals by H-abstraction reactions. The principal reaction pathway for PAH growth in acetylene pyrolysis is depicted in figure 3. As can be seen in this figure, the reaction pathway is essentially a sequence of alternating acetylene additions to aromatic radicals and H-abstractions by hydrogen atoms from forming aromatic molecules.

A detailed analysis of the computational results lead us to conclude that it is superequilibrium of hydrogen atoms which is a driving kinetic force for PAH growth (refs. 37-41). Reactions of class



are highly reversible and the net mass flux through them is determined by the degree of superequilibrium of hydrogen atoms (with respect to the local concentration of molecular hydrogen). Thus, the addition of  $\text{H}_2$  decreases the degree of superequilibrium and thus suppresses the growth of PAH. This phenomenon is important for understanding the conditions of PAH growth in the interstellar environment, which is discussed in the next section.

Acetylene addition, following reaction (1), is also a reversible step and, therefore, thermodynamic stability of forming intermediates play an important role in PAH growth. Analysis of this factor (ref. 42) presents arguments against the proposed role of spheroidal carbon clusters in soot particle inception under the conditions of hydrocarbon combustion and pyrolysis suggested by Smalley and co-workers (ref. 43).

The main effects of the presence of oxygen on the polymeric-type growth of PAH were identified to be (ref. 39): (a) promotion of fuel decomposition, which has an effect on the initiation of the reaction route to PAH and soot; (b) additional, rapid production of hydrogen atoms in the initial, small-molecule branching-chain reactions, which drives their concentration above the equilibrium value and thus enhances the polymeric growth of PAH; and (c) oxidation of aromatic radicals by molecular oxygen, which removes them from the polymeric growth process.

An additional factor found to be important in a sooting premixed acetylene flame, i.e. under the conditions of large temperature and concentration gradients, is diffusion of hydrogen atoms from the hot, main reaction zone upstream, into a cooler environment, where they add to acetylene molecules,



thus initiating the formation and growth of PAH (ref. 40).

The reaction pathways to soot in the pyrolysis of individual hydrocarbons other than acetylene were found to relax to the acetylene-addition mechanism initially identified for high-temperature acetylene

pyrolysis (ref. 41). Fuel molecular structure influences the growth process only at its early stages: first, by providing more (or less) efficient reaction partners for the formation of aromatic molecules; and, second, by affecting the generation of hydrogen atoms. Similar behavior was computed for binary hydrocarbon mixtures (ref. 36).

## PAH IN THE INTERSTELLAR MEDIUM

There have been recent proposals that previously unidentified near infra-red emission of the Interstellar Medium (ISM) originates from vibrationally excited PAH (refs. 11-14,44). It is actually suggested that PAH may be the most abundant organic molecules present in ISM (ref. 45). The question, therefore, is whether PAH can be formed in such large quantities under the conditions of ISM. Applying a general non-homogeneous nucleation theory, Keller recently argued the importance of non-equilibrium factors for the PAH production (ref. 46). The analysis lead him to predict that "A small number of very large PAH's, containing a considerable amount of the condensable carbon" should be produced.

In an attempt to address the question on the grounds of a more rigorous model, Frenklach and Feigelson (ref. 47) investigated gas-phase PAH production under conditions found in dense C-rich circumstellar envelopes, a possible formation site, using the approach of detailed kinetic modeling. The chemical reaction mechanism, initially developed to describe PAH formation in terrestrial flames and discussed in the previous section, was used in the study. The rate coefficients were modified to fit the ranges of temperature and pressure in circumstellar envelopes. The temperature, pressure and velocity gradients were drawn from a number of literature models as well as a grid of constant-velocity-wind models for a parametric sensitivity study.

Starting with a mixture of H, H<sub>2</sub> and C<sub>2</sub>H<sub>2</sub>, the dominant reaction pathways were found to be sequential acetylene additions and H-abstractions, as in the terrestrial case. Addition of CO reactions did not result in any change. An example of the numerical results obtained for one of the more successful simulations is given in figure 4. As can be seen in this figure, there is no significant PAH production at high temperatures (above 1100 K) and its rate peaks at about 1000 K. This temperature dependence was found to be characteristic to all conditions tested, the peak rate appears within a range of 800 to 1000 K.

The lack of PAH production at high temperatures is the result of high concentration of H<sub>2</sub> in the mixture; and it does not matter much what initial ratio of H to H<sub>2</sub> is assumed -- at the initial temperature of 1600 to 2000 K a partial equilibrium between them is established quickly. In other words, at the high-temperature range of a circumstellar envelope there is no hydrogen atom superequilibrium and hence, as was discussed for the terrestrial case, there is no PAH production. The appearance of measurable quantities of PAH coincides with the growth of H-superequilibrium.

Due to the large hydrogen concentration in the system, both forward and reverse reactions of (1) are fast compared to the acetylene addition reactions. The latter, therefore, are the main "bottleneck" in the PAH production pathway. Since the rate of each of these addition steps is proportional to acetylene concentration, the rate of PAH production becomes strongly, more than linearly, dependent on the initial concentration of acetylene. This dependence on acetylene concentration can be generalized to state that the amount of PAH formed in an circumstellar envelope should depend on the *total* amount of hydrocarbons (or, perhaps, total amount of carbon) present in the wind, since at the initial temperature on the order of 2000 K and the time scale of 10<sup>8</sup> to 10<sup>11</sup> s acetylene is the dominant hydrocarbon species present in the mixture.

Another parameter to which PAH production showed a large sensitivity is the time gas spends at temperatures of about 1100 to about 900 K, while expanding. In other words, PAH production is strongly dependent on wind velocity at the above temperature range and larger amounts of PAH are

computed for very slow winds, with velocities below 1 km/s. For conditions tested, however, even those producing above 1% conversion of acetylene carbon to PAH, the computed average size for PAH distribution is relatively small. This is in disagreement with the prediction of Keller (ref. 46), but in accord with the suggestions of Leg r and d'Hendecourt (ref. 45) and Allamandola, Tielens and Barker (refs. 44,48). Further details can be found in reference 47.

## LOW-PRESSURE VAPOR-DEPOSITED DIAMOND

Synthetic diamond is known to be formed at extremely high pressures -- at such pressures diamond is the most thermodynamically stable form of carbon (ref. 7). It has been demonstrated in recent years that diamond (and diamond-like carbon) can be also produced at low, near- or sub-atmospheric, pressures when diamond is thermodynamically metastable with respect to graphite (refs. 3,7,9,10). Crystalline diamond is shown to be formed in a number of chemical vapor deposition (CVD) techniques: microwave, RF, DC, and UV created plasmas as well as using hot-filament thermal reactors. Both thin films and single crystals can be grown. A variety of initial hydrocarbons were used, however most results have been reported using methane-hydrogen mixtures. Best quality diamond has been obtained using low concentrations (below 1%) of methane. A major problem is the formation of graphite, which kinetically competes with the production of diamond. The details on the apparatus used and the product analysis can be found in recent reviews, references 7 and 10. The focus of the present discussion is on the mechanism of diamond growth.

Induced plasma or hot filament "activates" gas and the formed "active" species then nucleate and are deposited on the substrate surface (refs. 3,9). The question is what are these critical "active" species and what are the elementary steps responsible for nucleation and surface deposition? Several hypotheses have been recently advanced. Tsuda *et al.* (refs. 49,50), based on their quantum computations, proposed a two-step mechanism assuming  $\text{CH}_3^+$  to be the key precursor. In the first step, the (111) plane of the diamond surface is covered by methyl groups via methylene insertion or hydrogen atom abstraction followed by methyl radical addition; then, three neighboring groups created on the (111) plane are spontaneously bound to form the diamond structure following the single attack of a methyl cation and the subsequent loss of three hydrogen molecules. The problem with this mechanism is that it cannot explain diamond growth in ion-free environment, whereas such growth has been observed, for example, in hot-filament apparatus.

Mitsuda *et al.* (ref. 51) monitored ultraviolet emission spectra during synthesis of diamond in a low-pressure microwave plasma reactor with a  $\text{CH}_4\text{-H}_2$  mixture. These authors noted that "When the spectra of  $\text{C}_2$  radicals were too high as compared with those of CH radicals, graphite was mainly formed. So,  $\text{C}_x$  radicals were considered to be responsible for the formation of graphite." Similarly, they concluded that " $\text{CH}_x$  radicals are related to the diamond formation." However, it is well known that  $\text{C}_2$  and CH have extremely high emission efficiencies as compared to those of other radicals and molecules possibly present in the mixture. In fact,  $\text{C}_2$  and CH have strongest emission lines in flame spectra (ref. 52), yet it is well established that these radicals do not play any significant role in flame dynamics since their concentrations and hence the associated reaction rates are too low. Analogously, since Mitsuda *et al.* did not determine the absolute concentrations of species they monitor nor they examine other hydrocarbon species present, their conclusions may be circumstantial.

Frenklach and Spear (ref. 53) proposed an elementary-reaction mechanism of diamond growth by a vapor deposition method. The central postulate is that the main monomer growth species is acetylene. The mechanism basically consists of two alternating steps: surface activation by H-abstraction of a hydrogen atom from a surface carbon,



followed by the addition of acetylene. During the addition reaction cycle a number of solid C-C bonds is formed and hydrogen atoms migrate from a lower to an upper surface layer. This mechanism is in general agreement with macroscopic views developed by the Russian school of Derjaguin, Fedoseev and co-workers (refs. 3,9, and cited in 53) and is consistent with major, undisputable experimental evidence:

- a) *Independence on starting material* - Acetylene is produced rapidly in hydrocarbon plasma and high-temperature pyrolysis and is the most abundant gaseous hydrocarbon species present in these harsh environments. Since acetylene is assumed to be the main surface building block, this explains the independence of the growth process from the nature of the hydrocarbon source.
- b) *Hydrogen effect* - Surface reaction (3) is very much similar to its gas-phase counterpart, reaction (1), and, hence, in accordance with the discussion of reaction (1), the net rate of reaction (3) should depend on superequilibrium of hydrogen atoms. The dependence of diamond growth rate on H-superequilibrium was suggested by the Russian researchers based on their experimental findings (ref. 9).
- c) *Co-existence and competition between diamond and graphite growth* - Derjaguin, Fedoseev and co-workers (refs. 9,54) provide a persuasive argument, based on an extensive experimental base, that the growth of diamond and graphite and the close competition between the two are controlled by kinetics. There are two possibilities for the production of graphite along with the growth of diamond: first, formation of graphite precursors in the gas phase followed by surface deposition and further growth and, second, initiation and growth directly on the surface. The gas-phase process would follow the mechanism of PAH formation discussed above. The surface growth of graphite can be envisioned to proceed along similar lines, initiated by structural deviations from the epitaxial growth of diamond (ref. 53). Since the mechanism of diamond growth is also very similar to that of the gas-phase PAH production, the co-existence of the two carbon forms, diamond and graphite, and the specific results obtained under different experimental conditions should be determined by the close kinetic competition between the very similar reaction mechanisms.
- d) *Substrate temperature effect* - The temperature dependence of the rate of diamond growth exhibits a maximum; that is, it initially increases with the substrate temperature and then decreases (refs. 9,55). This phenomenon can be explained as follows. At low temperatures, the growth rate is kinetically limited -- it is controlled by the rate of the H-abstraction, reaction (3), which increases with temperature. As temperature increases, the superequilibrium of hydrogen atoms and the thermodynamic stability of the reaction intermediates both decrease, eventually causing a decline in the growth rate. Graphite formation rates also exhibit a temperature maximum, but at higher temperatures than that of diamond; so are the soot formation rates. Since the intermediates in the growth reaction sequences leading to graphite and soot are more thermodynamically stable than those leading to diamond, the maximum rates of the former should be shifted to higher temperatures compared to that of the latter, as observed in experiment.

The discussed mechanism can also predict some facts of morphology; this and other details can be found in Ref. 53.

## INTERSTELLAR DIAMOND

Two recent reports presented evidence that the C<sub>8</sub> component of the Allende meteorite is diamond (refs. 15,16). There is a disagreement, however, as to the origin of this diamond. Blake *et al.* (ref.16,

see also reference 56) proposed that "C $\delta$  diamond results from high velocity grain-grain collisions behind a supernova shock front in the interstellar medium," whereas Lewis *et al.* (ref. 15) suggested that "part or all of C $\delta$  diamond -- not shock-produced but primary, formed by stellar condensation as a metastable phase." One of the arguments of Lewis *et al.* was that diamond is known to be formed in low-pressure CVD processes, as discussed in the previous section; for example, Mitura (ref. 57) reports on gas-phase formation of fine-crystalline diamond powders in an RF plasma. Recent near-atmospheric shock-tube pyrolysis results (ref. 35) may provide additional evidence in support of the "condensation" hypothesis.

As discussed above, soot production in shock-tube pyrolysis of acetylene exhibits a maximum and then a second rise with the increase in temperature (figs. 1 and 2). This second increase coincides with "soot formation" from chloroform and carbon tetrachloride (fig. 2). The product obtained in the pyrolysis of carbon tetrachloride, however, is very different from what is typically known as soot: it looks white (and hence was termed by us as "white soot", see reference 35); on the transmission electron microscope (TEM) appears as shapeless particles with the size on the order of a micrometer; electron diffraction shows a clear single-crystal pattern with an unidentified d-spacing; and the results of the wet oxidation, performed by Freund and co-workers at NASA-Ames Research Center following the procedures used for C $\delta$  analysis of reference 16, indicate that a sizable fraction of the "white soot" has chemical resistance similar to that of diamond.

It was proposed (ref. 35) that the mechanism of "white soot" formation is a clustering-type growth. The formation of the interstellar diamond can be explained as follows. At high temperatures, when the aromatic ring is thermodynamically unstable, yet not too high, so that C-C bonds can still exist, dehydrogenated carbon clusters begin to be formed. Some of them may assume the diamond structure. As the gas expands and the temperature decreases to the point where acetylene becomes a dominant gaseous carbon-containing species, the cluster growth switches to an acetylene-addition mechanism, of the type discussed above, producing amorphous and later sootlike carbon. This would explain the findings of Blake *et al.* (ref. 16) that "the C $\delta$  diamond is single phase, but surface and interfacial carbon atoms ... impart an 'amorphous' features to some spectral data." Also, since the nucleation of carbon clusters should be slow in mostly atomized environment and the time spent by the gas within the favorable temperature range should be short, the size of the diamond crystallines should be rather small, as indeed reported in references 15 and 16.

## SUMMARY

There appear to be two distinct mechanisms of carbon growth in the gas phase. At high temperatures it is clustering, which may be responsible for the presence of diamond particles in carbonaceous meteorites. At lower temperatures the growth follows sequential H-abstraction and acetylene addition. The general pattern of the two-step reaction sequence, although slightly varying in the specific form it takes, appears to be remarkably similar in such seemingly different processes as soot production in hydrocarbon combustion, PAH formation in carbon-rich circumstellar envelopes, and growth of vapor-deposited diamond and graphite films.

## REFERENCES

1. Donnet, J. B.: Structure and Reactivity of Carbons: From Carbon Black to Carbon Composites. *Carbon*, vol. 20, no. 4, 1982, pp. 266-282.
2. Marchand, André: Various Kinds of Solid Carbon: Structure and Optical Properties. In *Polycyclic Aromatic Hydrocarbons and Astrophysics*, Léger, A.; d'Hendecourt, L.; and Boccara, N., Eds., D. Reidel Publishing Co., 1987; pp. 31-54.
3. Derjaguin, B. V.; and Fedoseev, D. V.: Growth of Diamond and Graphite from the Gas Phase. Nauka, Moscow, 1977 (in Russian).
4. Walker, P. L., Jr.: Structure of Graphites. *Nature*, vol. 180, Nov. 1957, pp. 1184-1185.
5. Palmer, Howard B.; and Cullis, Charles F.: The Formation of Carbon from Gases. In *Chemistry and Physics of Carbon*, Walker, P. L., Jr., Ed., Marcel Dekker, vol. 1, 1965, pp. 265-325.
6. Ebert, L. B.; Scanlon, J. C.; and Clausen, C. A.: Combustion Tube Soot from a Diesel Fuel/Air Mixture. Preprints of 194th ACS National Meeting, vol. 32, no. 3, Aug. 1987, pp. 440-447; also *Energy & Fuels*, 1988 (to be published).
7. DeVries, R. C.: Synthesis of Diamond Under Metastable Conditions. Report No. 86CRD247, General Electric, Schenectady, New York, March 1987.
8. Haynes, B. S.; and Wagner, H. Gg.: Soot Formation. *Prog. Energy Combust. Sci.*, vol. 7, 1981, pp. 229-273.
9. Fedoseev, D. V.; Derjaguin, B. V.; Varshavskaya, I. G.; and Semenova-Tyan-Shanskaya, A. S.: Crystallization of Diamond. Nauka, Moscow, 1984 (in Russian).
10. Messier, R.; Badzian, A. R.; Badzian, T.; Spear, K. E.; Bachmann, P.; and Roy, R.: From Diamond-Like Carbon to Diamond Coatings. *Proc. Int. Conf. on Metallurgical Coatings*, San Diego, March 1987; also *Thin Solid Films* (to be published).
11. Léger, A.; and Puget, J. L.: Identification of the Unidentified IR Emission Features of Interstellar Dust? *Astron. Astrophys. Lett.*, vol. 137, 1984, pp. L5-L8.
12. Allamandola, L. J.; Tielens, A. G. G. M.; and Barker, J. R.: Polycyclic Aromatic Hydrocarbons and the Unidentified Infrared Emission Bands: Auto Exhaust Along the Milky Way! *Astrophys. J.*, vol. 290, 1985, pp. L25-L28.
13. Allamandola, L. J.; Sanford, S. A.; and Wopenka, B.: Interstellar Polycyclic Aromatic Hydrocarbons and Carbon in Interplanetary Dust Particles and Meteorites. *Science*, vol. 237, July 1987, pp. 56-59.
14. Léger, A.; d'Hendecourt, L.; and Boccara, N.; Eds.: *Polycyclic Aromatic Hydrocarbons and Astrophysics*. D. Reidel Publishing Co., 1987.
15. Lewis, Roy S.; Ming, Tang; Wacker, John F.; Anders, Edward; and Steel, Eric: Interstellar Diamonds in Meteorites. *Nature*, vol. 326, March 1987, pp. 160-162.
16. Blake, David; Freund, Friedemann; Krishnan, Kannan; Echer, Charles; Shipp, Ruth; Bunch, Ted; Tielens, Alexander; Lipari, Robert, J.; and Chang, Sherwood: The Nature and Origin of Interstellar Diamond. *Nature* (to be published).

17. Calcote, H. F.: Mechanisms of Soot Nucleation in Flames - A Critical Review. *Combust. Flame*, vol. 42, 1981, pp. 215-242.
18. Siegl, Donald C.; and Smith, George W.; Eds.: *Particulate Carbon: Formation During Combustion*. Plenum Press, 1983.
19. Lahaye, J.; and Prado, G.; Eds.: *Soot in Combustion Systems and Its Toxic Properties*. Plenum Press, 1983.
20. Homann, R. H.: Formation of Large Molecules, Particulates and Ions in Premixed Hydrocarbon Flames; Progress and Unresolved Questions. Twentieth Symposium (International) on Combustion, The Combustion Institute, Pittsburgh, 1985, pp. 857-870.
21. Proceedings of the Symposium on Advances in Soot Formation Chemistry, Energy & Fuels, 1988 (to be published).
22. Wagner, Heinz G.: Mass Growth of Soot. *Soot in Combustion Systems and Its Toxic Properties*. Lahaye, J.; and Prado, G.; Eds., Plenum Press, 1983, pp. 171-195.
23. Harris, Stephen J.; and Weiner, Anita M.: Chemical Kinetics of Soot Particle Growth. *Ann. Rev. Phys. Chem.*, vol. 36, 1985, pp. 31-52.
24. Glassman, Irvin: *Combustion*. Second ed., Academic Press, Inc., 1987.
25. Graham, S. C.; Homer, J. B.; and Rosenfeld, J. L. J.: The Formation and Coagulation of Soot Aerosols Generated by the Pyrolysis of Aromatic Hydrocarbons. *Proc. R. Soc. Lond. A.*, vol. 344, 1975, pp. 259-285.
26. Graham, S. C.; Homer, J. B.; and Rosenfeld, J. L. J.: The Formation and Coagulation of Soot Aerosols. *Proc. 10th Int. Shock Tube Symp.*, Kyoto, Japan, 1975, pp. 621-631.
27. Fussey, D. E.; Gosling, A. J.; and Lampard, D.: A Shock Tube Study of Induction Times in the Formation of Carbon Particles by Pyrolysis of the C<sub>2</sub> Hydrocarbons. *Combust. Flame*, vol. 32, 1978, pp. 181-192.
28. Evans, Margaret; and Williams, Alan: Shock Tube Studies on the Formation of Soot from the Combustion and Pyrolysis of Some Hydrocarbons. *Fuel*, vol. 60, 1981, pp. 1047-1056.
29. Prado, G.; Lahaye, J.: Physical Aspects of Nucleation and Growth of Soot Particles. In *Particulate Carbon: Formation During Combustion*. Siegl, Donald C.; and Smith, George W., Eds., Plenum Press, 1983, pp. 143-164.
30. Wang, T. S.; Matula, R. A.; and Farmer, R. C.: Combustion Kinetics of Soot Formation from Toluene. Eighteenth Symposium (International) on Combustion, The Combustion Institute, Pittsburgh, 1981, pp. 1149-1158.
31. Rawlins, W. T.; Cowles, L. M.; and Krech, R. H.: Spectral Signatures (0.2-5  $\mu$ m) of Soot Initiation in the Pyrolysis of Toluene Near 2000 K. Twentieth Symposium (International) on Combustion, The Combustion Institute, Pittsburgh, 1985, pp. 879-886.
32. Frenklach, M.; Taki, S.; and Matula, R. A.: A Conceptual Model for Soot Formation in Pyrolysis of Aromatic Hydrocarbons. *Combust. Flame*, vol. 49, 1983, pp. 275-282.

33. Frenklach, M.; Taki, S.; Durgaprasad, M. B.; and Matula, R. A.: Soot Formation in Shock-Tube Pyrolysis of Acetylene, Allene, and 1,3-Butadiene. *Combust. Flame*, vol. 54, 1983, pp. 81-101.
34. Frenklach, M.; Ramachandra, M. K.; and Matula, R. A.: Soot Formation in Shock Tube Oxidation of Hydrocarbons. Twentieth Symposium (International) on Combustion, The Combustion Institute, Pittsburgh, 1985, pp. 871-878.
35. Frenklach, M.; Hsu, J. P.; Miller, D. L.; and Matula, R. A.: Shock-Tube Pyrolysis of Chlorinated Hydrocarbons: Formation of Soot. *Combust. Flame*, vol. 64, 1986, pp. 141-155.
36. Frenklach, M.; Yuan, T.; and Ramachandra, M. K.: Shock-Tube and Modeling Study of Soot Formation in Mixtures of Hydrocarbons. Preprints of 194th Amer. Chem. Soc. Nat. Meeting, vol. 32, No. 3, 1987, pp. 467-473; also, Soot Formation in Binary Hydrocarbon Mixtures. *Energy & Fuels* (to be published).
37. Frenklach, Michael; Clary, David W.; Gardiner, William C., Jr.; and Stein, Stephen E.: Detailed Kinetic Modeling of Soot Formation in Shock-Tube Pyrolysis of Acetylene. Twentieth Symposium (International) on Combustion, The Combustion Institute, Pittsburgh, 1985, pp. 887-901.
38. Frenklach, M.; Clary, D. W.; Gardiner, W. C., Jr.; and Stein, S. E.: Shock-Tube Pyrolysis of Acetylene: Sensitivity Analysis of the Reaction Mechanism for Soot Formation. *Proc. 15th Int. Symp. Shock Waves and Shock Tubes*, Bershader, D.; and Hanson, R., Eds., Stanford University Press, 1986, pp. 295-301.
39. Frenklach, M.; Clary, D. W.; Yuan, T.; Gardiner, W. C., Jr.; and Stein, S. E.: Mechanism of Soot Formation in Acetylene-Oxygen Mixtures. *Combust. Sci. Technol.*, vol. 50, 1986, pp. 79-115.
40. Frenklach, Michael; and Warnatz, Jürgen: Detailed Modeling of PAH Profiles in a Sooting Low-Pressure Acetylene Flame. *Combust. Sci. Technol.*, vol. 51, 1987, pp. 265-283.
41. Frenklach, Michael; Clary, David W.; Gardiner, William C., Jr.; and Stein, Stephen E.: Effect of Fuel Structure on Pathways to Soot. Twenty-First Symposium (International) on Combustion, The Combustion Institute, Pittsburgh (to be published).
42. Frenklach, Michael; and Ebert, Lawrence, B.: Comment on the Proposed Role of Spheroidal Carbon Clusters in Soot Formation. *J. Phys. Chem.*, 1988 (to be published).
43. Zhang, Q. L.; O'Brien, S. C.; Heath, J. R.; Liu, Y.; Curl, R. F.; Kroto, H. W.; and Smalley, R. E.: Reactivity of Large Carbon Clusters: Spheroidal Carbon Shells and Their Possible Relevance to the Formation and Morphology of Soot. *J. Phys. Chem.*, vol. 90, no. 4, 1986, pp. 525-528.
44. Allamandola, L. J.; Tielens, A. G. G. M.; and Barker, J. R.: Infrared Emission from Interstellar PAHs. In *Physical Processes in Interstellar Clouds*, Morfill, G. E.; and Scholer, M.; Eds., D. Reidel Publishing Co., 1987, pp. 305-331.
45. Léger, A.; and d'Hendecourt, L.: Identification of PAHs in Astronomical IR Spectra - Implications. In *Polycyclic Aromatic Hydrocarbons and Astrophysics*, Léger, A.; d'Hendecourt, L.; and Boccara, N.; Eds., D. Reidel Publishing Co., 1987, pp. 223-254.
46. Keller, Rudolf: Polyaromatic Hydrocarbons and the Condensation of Carbon in Stellar Winds. In *Polycyclic Aromatic Hydrocarbons and Astrophysics*, Léger, A.; d'Hendecourt, L.; and Boccara, N.; Eds., D. Reidel Publishing Co., 1987, pp. 387-397.

47. Frenklach, M.; and Feigelson, E. D.: PAH Formation in Carbon-Rich Circumstellar Envelopes. Amer. Astro. Soc. Meeting, Austin, Texas, January 1988.
48. Barker, John R.; Allamandola, L. J.; and Tielens, A. G. G. M.: Anharmonicity and the Interstellar Polycyclic Aromatic Hydrocarbons Infrared Emission Spectrum. *Astrophys. J.*, vol. 315, 1987, pp. L61-L65.
49. Tsuda, Minoru; Nakajima, Mitsuo; and Oikawa, Setsuko: Epitaxial Growth Mechanism of Diamond Crystal in  $\text{CH}_4\text{-H}_2$  Plasma. *J. Am. Chem. Soc.*, vol. 108, 1986, pp. 5780-5783.
50. Tsuda, Minoru; Nakajima, Mitsuo; and Oikawa, Setsuko: The Importance of the Positively Charged Surface for the Epitaxial Growth of Diamonds at Low Pressures. *Japn. J. Appl. Phys.*, vol. 26, No. 5, May 1987, pp. L527-L529.
51. Mitsuda, Y.; Kojima, Y.; Yoshida, T; and Akashi, K.: The Growth of Diamond in Microwave Plasma under Low Pressure. *J. Mater. Sci.*, vol. 22, 1987, pp. 1557-1562.
52. Gaydon, A. G.: *The Spectroscopy of Flames*. Second Ed., Chapman and Hall, 1974.
53. Frenklach, Michael; and Spear, Karl E.: Growth Mechanism of Vapor-Deposited Diamond. *J. Mater. Res.*, February 1988 (to be published).
54. Varnin, V. P.; Fedoseev, D. V.; and Teremetskaya, I.G.: Kinetics of Diamond Growth from Activated Gas. *Arch. Nauki Mater.*, vol. 7, 1986, pp. 121-125 (in Russian).
55. Derjaguin, B. V.; Bouilov, L. L.; and Spitsyn, B. V.: Crystallization and Some Properties of Diamond Films. *Arch. Nauki Mater.*, vol. 7, 1986, pp. 111-119 (in Russian).
56. Tielens, A. G. G. M.; Seab, C. G.; Hollenbach, D. J.; and McKee, Christopher F.: Shock Processing of Interstellar Dust: Diamonds in the Sky. *Astrophys. J.*, vol. 319, Aug. 1987, pp. L109-L113.
57. Mitura, Stanislaw: Nucleation of Diamond Powder Particles in an RF Methane Plasma. *J. Crystal Growth*, vol. 80, 1987, pp. 417-424.

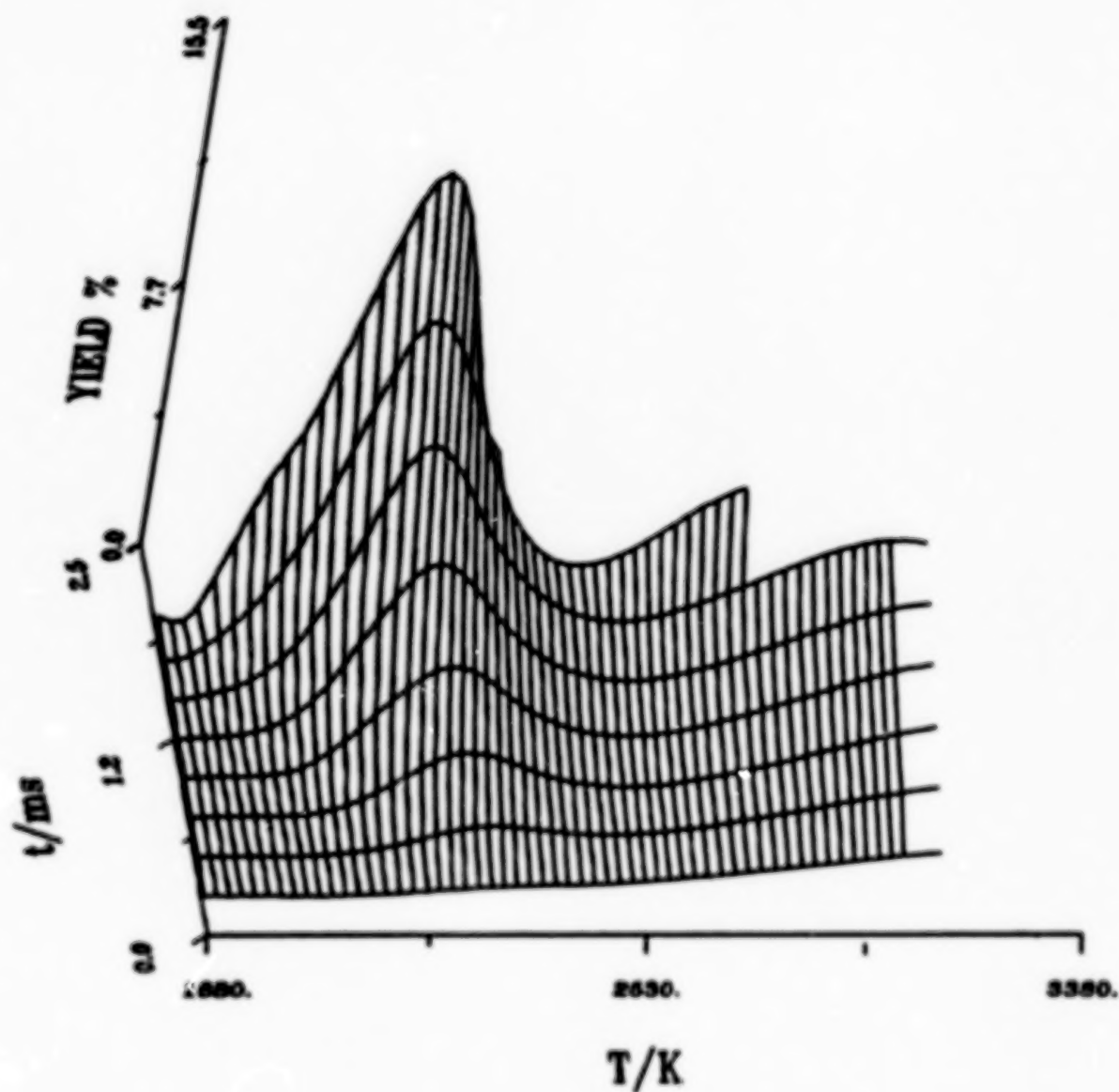


Figure 1.— Soot yield versus temperature and reaction time in shock-tube pyrolysis of a 4.25% acetylene-argon mixture at near-atmospheric pressures; the data are from reference 33, Series D.

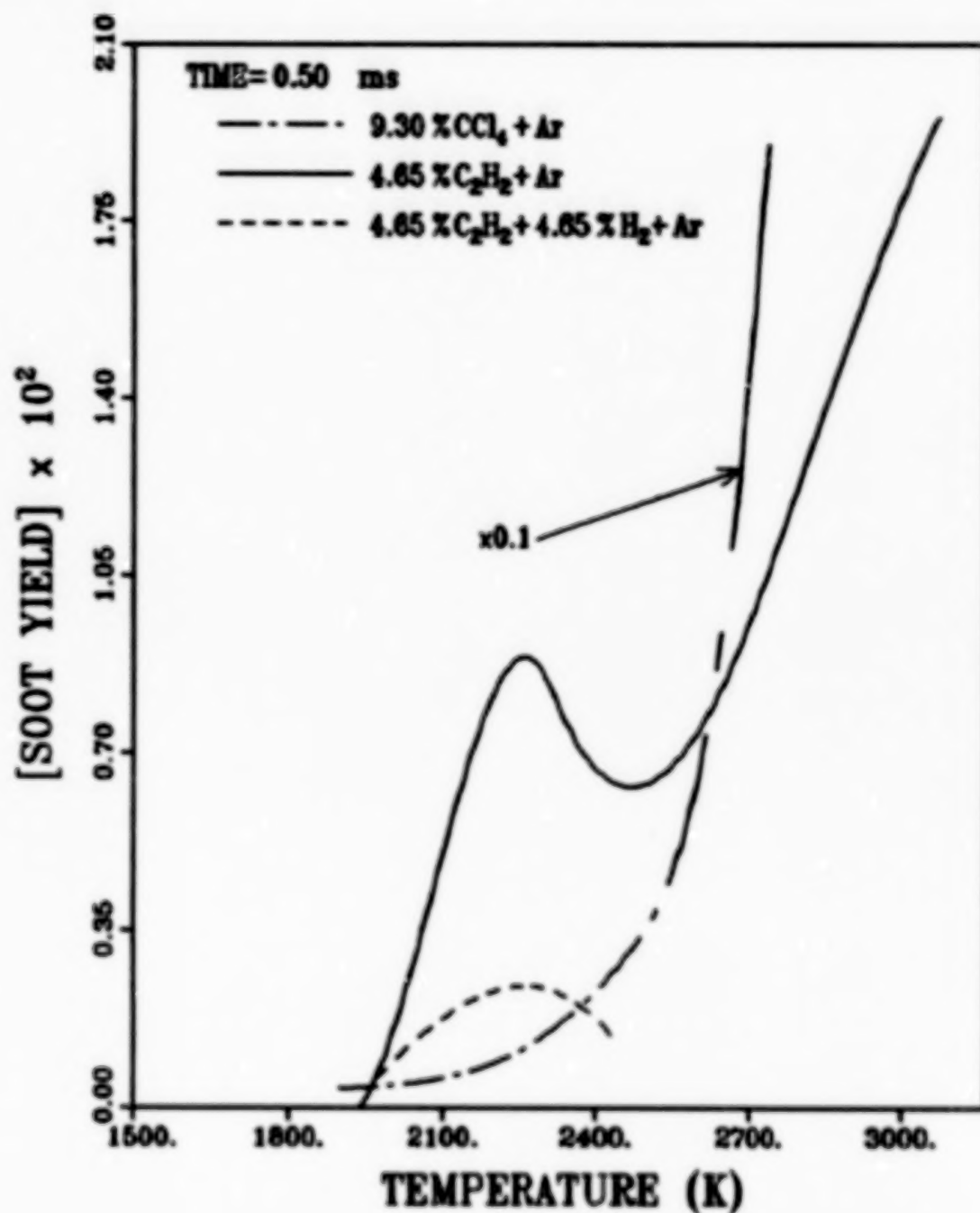


Figure 2.- Soot yields versus temperature in shock-tube pyrolysis of acetylene, acetylene-hydrogen, and carbon tetrachloride argon-diluted mixtures at a reaction time of 0.5 ms; the data are from references 33, 35 and 36.

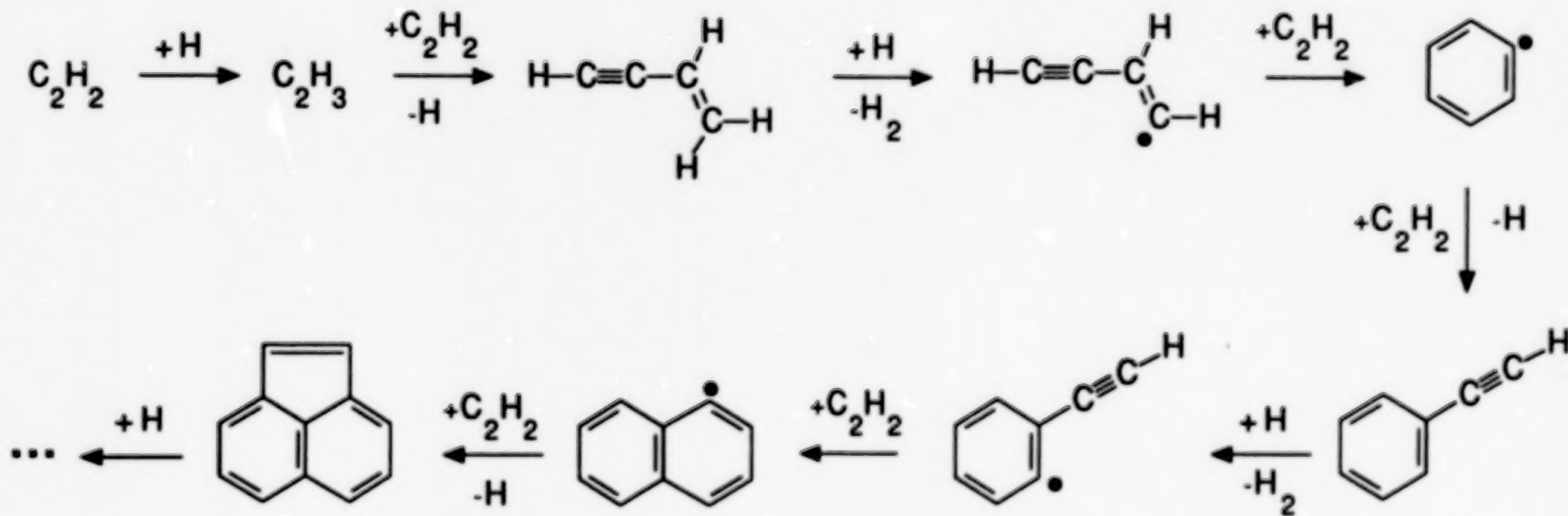


Figure 3.- The dominant reaction pathway for the formation of PAH in acetylene pyrolysis.

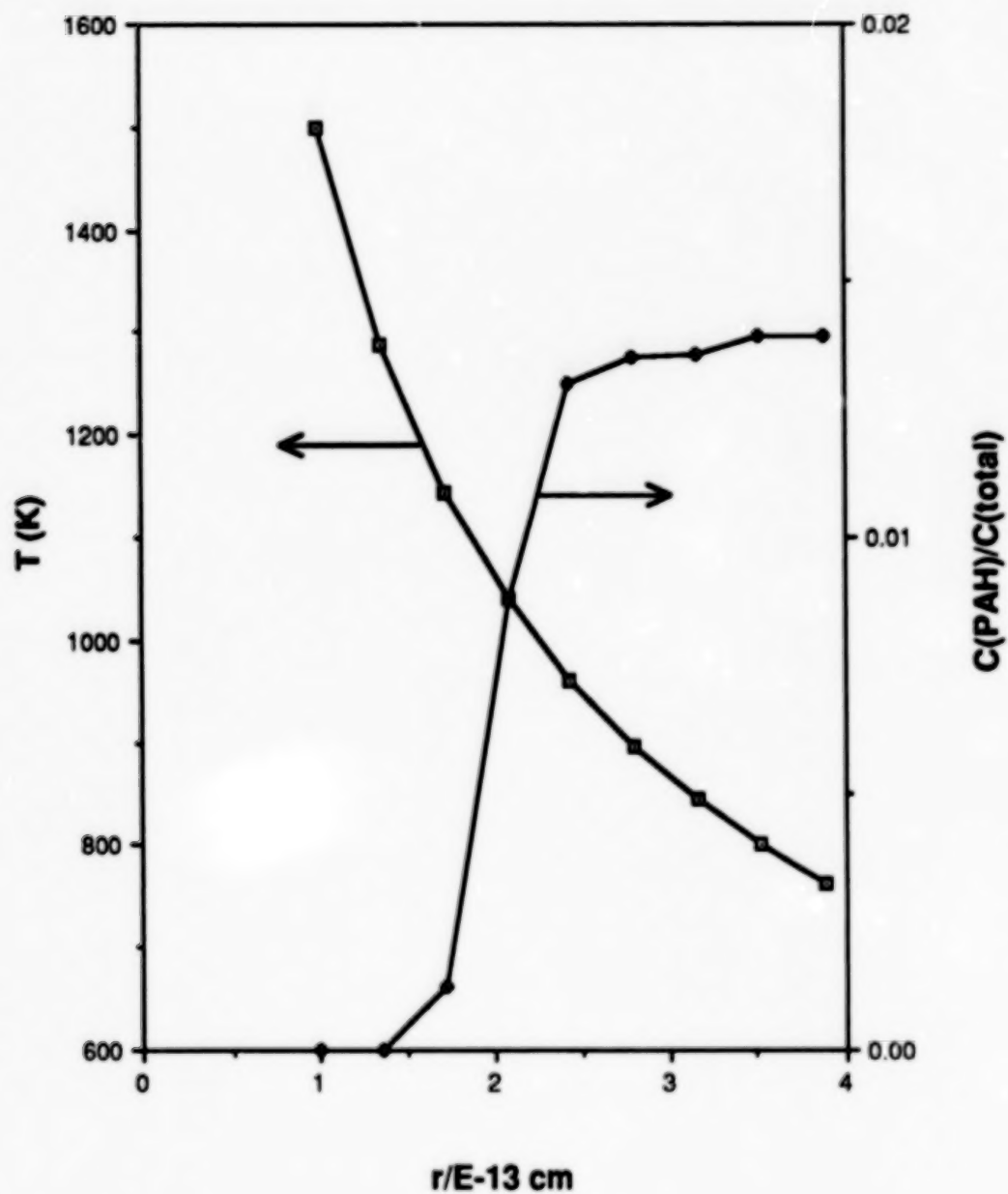


Figure 4.— Computed fractional conversion of acetylene carbon to PAH and assumed temperature profile for a constant-velocity slow wind model:  $\dot{M} = 1 \times 10^{-5} M_{\odot}/\text{yr}$ ;  $v = 0.05 \text{ km/s}$ ;  $T = (1500/\text{K}) (r/1 \times 10^{13} \text{ cm})^{-1/2}$ ;  $[C_2H_2]_0 = 0.12\%$ ;  $[H_2]_0 = 99.88\%$

# THE FORMATION AND STRUCTURE OF CIRCUMSTELLAR AND INTERSTELLAR DUST

H.W Kroto

School of Chemistry and Molecular Sciences  
University of Sussex,  
Brighton, BN1 9QJ, U.K.

## ABSTRACT.

The intriguing abundance of long linear carbon chain molecules in some dark clouds and in circumstellar shells is still not well understood. Recent laboratory studies which have probed this problem indicate that when carbon vapour nucleates to form particles, linear chains and hollow cage molecules (fullerenes) also form at more-or-less the same time. The results have consequences for the formation, structures and spectroscopic properties of the molecular and dust components ejected from cool carbon-rich stars. A most interesting result of the experimental observations relates to the probability that a third character in addition to the chains and grains, the  $C_{60}$  molecule probably in the form of the ion  $C_{60}^+$  in the less shielded regions, is present and perhaps responsible for some of the ubiquitously observed interstellar spectroscopic features such as the Diffuse Interstellar Features, the 2170Å UV Absorption or perhaps some of the Unidentified Infrared Bands. Further study of small carbon particles which form in the gas phase has resulted in the discovery that they have quasi-icosahedral spiral shell structures. The rôle that such species may play in the interstellar medium as well as that played by  $C_{60}$  (or  $C_{60}^+$ ) should soon be accessible to verification by a combination of laboratory experiment and astronomical spectroscopy.

## INTRODUCTION

In 1975 the polyyne  $H-C\equiv C-C\equiv C-C\equiv N$  was synthesised and studied by microwave spectroscopy (ref. 1) and the resulting laboratory frequency was then used to detect this species in space by radioastronomy (ref. 2). Subsequently the combined synthetic/microwave/ radioastronomy approach resulted in the discovery of even longer carbon chains in space. The molecules  $HC_7N$  (refs 3, 4) and  $HC_9N$  (ref. 5) were detected and laid the basis for the detection of even longer chains such as  $HC_{11}N$  (ref. 6). More recent work has aimed at an understanding of the formation of chains in space (refs 7-9) and has focused attention on the possibility that they are produced at the same time as dust in carbon-rich red giant stars (refs 10-14).

In order to explore the high temperature stellar route to carbon chain molecules experimentally, a project to study the reactions and spectra of carbon clusters in a beam produced by laser vapourisation was initiated. These experiments successfully confirmed that very long carbon chains (Fig 1) are indeed produced in a plasma when carbon particles form (refs 15, 16). During these experiments a most exciting discovery was made; that a single molecule,  $C_{60}$ , was spectacularly resistant to further growth<sup>17</sup>. Indeed it has subsequently been shown that under conditions where almost all the carbon vapour has nucleated

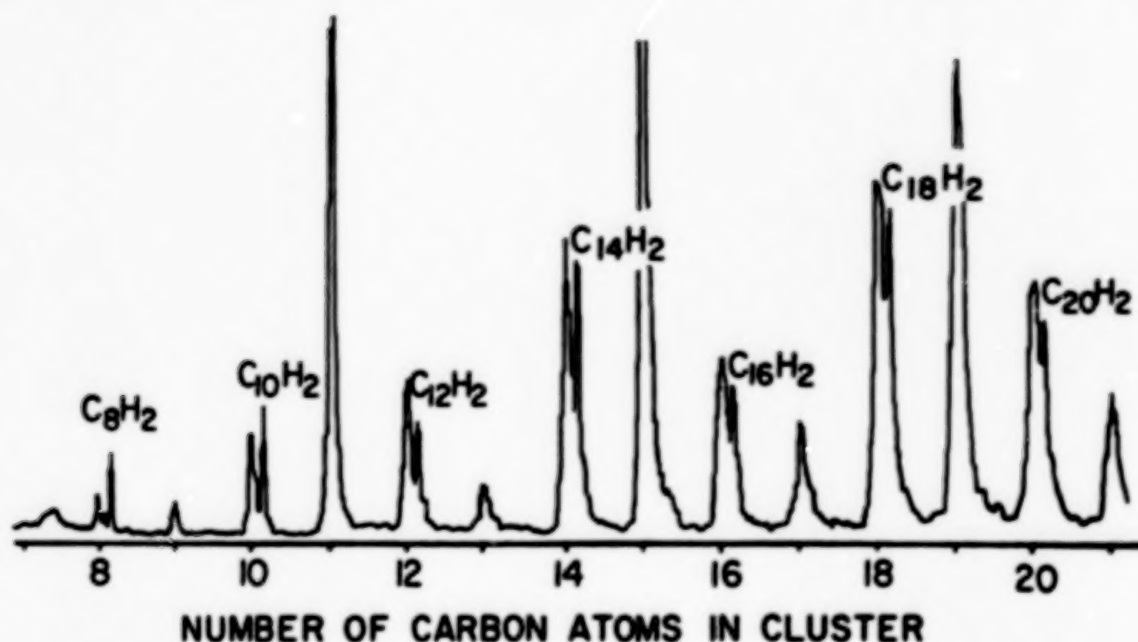


Fig 1 Mass spectrometric detection of species  $H-(C_nH)_n-H$  produced by the reaction of  $H_2O$  with a beam of carbon clusters.  $C_n$  peaks ( $n$  even) are accompanied by +2 mass unit satellites.

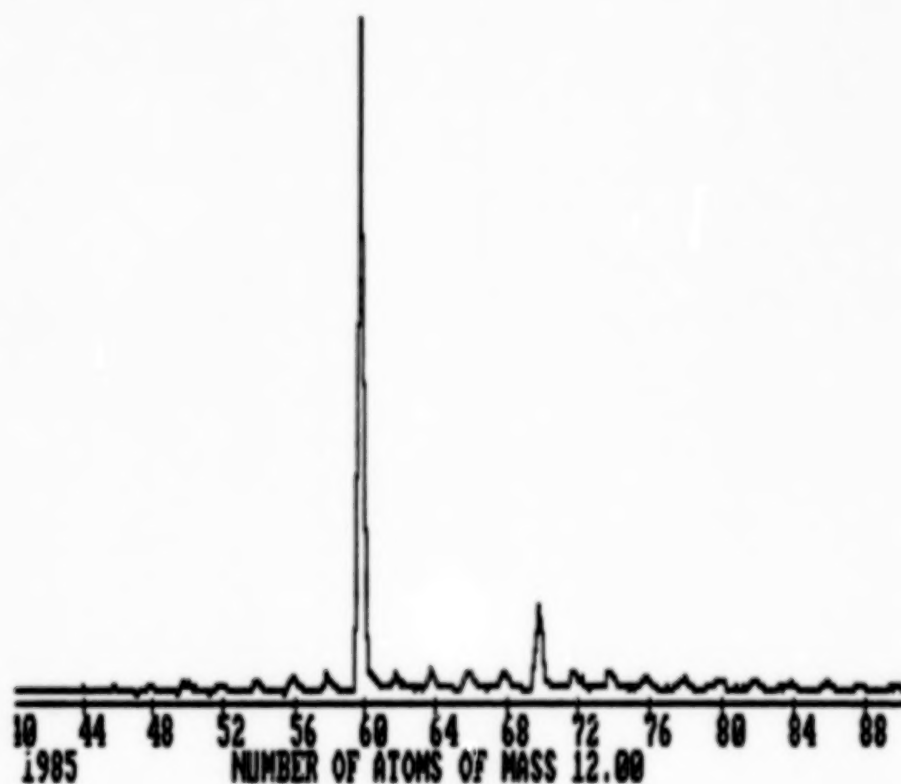
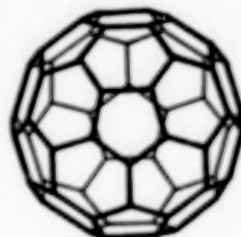


Fig 2 Mass Spectrum of the carbon clusters which remain after particle formation has taken place in the gas phase. Note that under these conditions  $C_{60}$  and  $C_{70}$  are dominant because they are inert to growth.

to form large particles,  $C_{60}$  remains together with some  $C_{70}$  as shown in the mass spectrum, Fig. 2. The formation of a specific large molecule in dominant abundance in a chaotic chemical system is a unique observation with many consequences.

The properties of this carbon molecule have been rationalised on the basis of a closed carbon cage with truncated icosahedral symmetry, similar to that of a football, Fig 3. Geodesic and

**Fig 3** The proposed truncated icosahedral structure of  $C_{60}$  buckminsterfullerene.



aromaticity factors can account readily for the stability of such a molecule. Several further experiments have been carried out relating to the formation of  $C_n$ -metal complexes (ref. 18) the reactivity and clustering (ref. 19), negative ion formation (ref. 20) and the relation between the ionic and neutral clusters and their nucleation rates (ref. 21). The results of this programme have recently been reviewed (refs 22, 23). A study of the geodesic and chemical properties of cage structures of various sizes has produced significant support for the buckminsterfullerene  $C_{60}$  structure proposal by showing that the magic numbers observed in the carbon nucleation experiments are entirely consistent with the formation of a family of closed fullerene cages (ref. 24). The basic nucleation mechanism (ref. 19) has recently been refined resulting in a detailed new picture of the structure of small carbon particles that nucleate in the gas phase (ref. 25)

The first stages in the hypothetical nucleation mechanism are shown schematically in Fig 4. It is proposed that the mechanism is

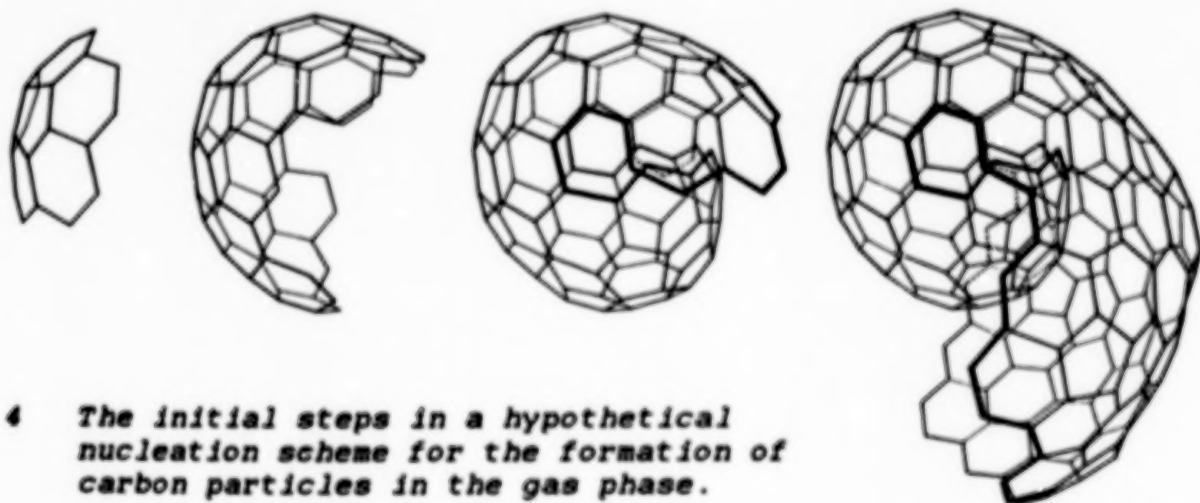
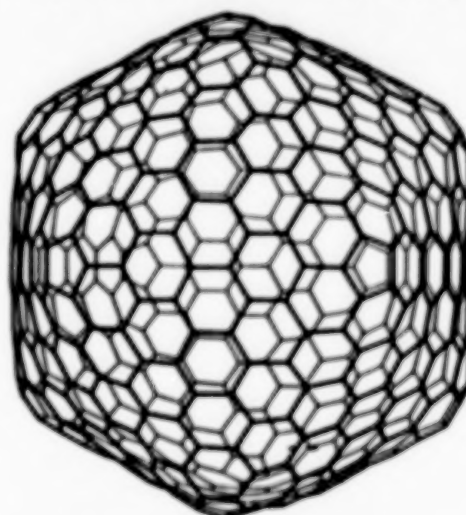


**Fig. 4** The initial steps in a hypothetical nucleation scheme for the formation of carbon particles in the gas phase.

governed by two straight-forward principles: 1) Graphitic network formation, in the gas phase, follows a low energy route involving curved, rather than flat, sheets so that edge dangling bonds are

eliminated, and 2) epitaxial factors control the subsequent structure of new network. The initial embryos have shell-like shapes, Fig. 4, in which the network involves both 5- and 6-membered rings. The network has bond lengths and angles consistent with those of an extended polyaromatic hydrocarbon in which isolated corannulene segments play key rôles. As the shell grows larger, fresh network forms at an altitude close to 3.4Å (the graphite interlayer separation) above the previous surface. This is achieved most readily by locating the twelve necessary and sufficient pentagons in each turn of the spiral directly over those in the previous segment. This epitaxial growth pattern results in a single particle with structural integrity. As it grows the structure should approximate that of a large closed cage which has been shown to be quasi-icosahedral, Fig 5 (ref. 25). The pentagons in

*Fig 5 Large particles consist of concentric spiral shells. The shapes of the larger ones are more-or-less icosahedral, like larger closed cages. The highly symmetric fullerene ( $I_h$ )C<sub>540</sub> is depicted here.*



spiral shell particles will be located along twelve radii resulting in a single quasi-crystal consisting effectively of 20 pyramidal micro-crystallite segments. In cross-section such a particle should exhibit a concentric spiral polygonal "ring" pattern. In Fig. 6 is shown one of

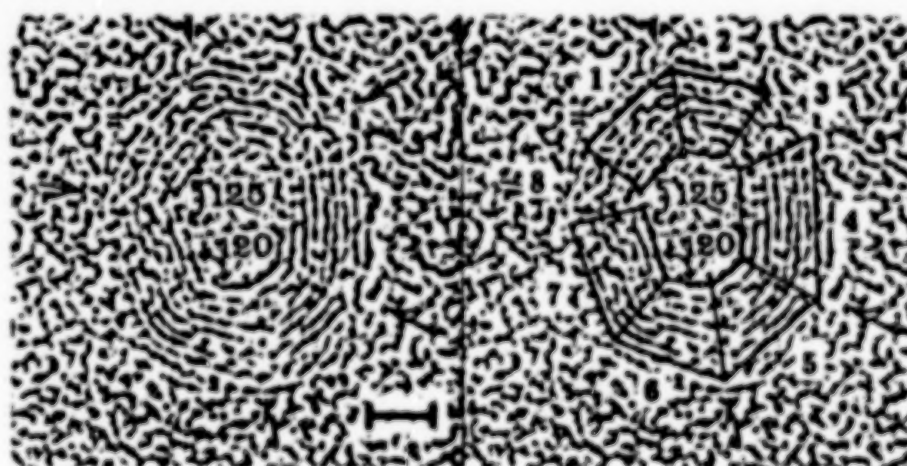


*Fig 6 Electron microscope picture of a particle from a carbon arc. The concentric polyhedral shells are clearly evident. The folds in the shells are delineated in RH figure. The similarity in shape with C<sub>540</sub>, Fig 5, is striking. The marker indicates 20Å and the interlayer spacing is 3.4Å.*

the beautiful transmission electron microscope pictures of carbon particles taken by Iijima (ref. 26), is shown. Iijima was able to show clear evidence of such concentric polyhedral shells and the present work has yielded a simple explanation (ref. 25).

In this model, it is clear, that occasionally the pentagons will occur at just the right places for  $C_{60}$  to form. When this happens however the reactive edge is lost and further growth cannot occur. Thus  $C_{60}$  is predicted to be a by-product of the general carbon nucleation process. Just how much carbon, in general, ends up in this cul-de-sac is an interesting and important question. The mechanism thus accounts for  $C_{60}$  and also, for the first time, the detailed structures of macroscopic carbon particles. The mechanism also appears to have the basic ingredients necessary for the solution the old problem of soot (ref. 19, 25). This proposal has recently gained significant support from the discovery by Gerhardt, Löffler and Homann that  $C_{60}^+$  is a dominant ion in a sooting flame (27).

#### ASTROPHYSICAL IMPLICATIONS OF THE DETECTION OF $C_{60}$

As far as interstellar problems are concerned it is likely that in the circumstellar shells of carbon stars, processes similar to those in the vapourisation experiments occur and the solid particles known to be ejected from such objects may have similar structures. Such quasi-icosahedral particles may thus be the primary refractory cores which are the nucleation sites for further particle growth in the interstellar medium. Intermingled with these particles will be some  $C_{60}$  itself. How prevalent the t-icosahedral  $C_{60}$  molecule is likely to be in interstellar space is a most intriguing question, however it must be present whenever carbon particles form as it is a survivor of the clustering process, detected at the same time as chains and carbon particles. Large carbon particles are relatively sensitive to photoionisation laser power as they readily shake down to produce smaller daughter fragments ( $n < 100$ ). On the other hand  $C_{60}$  appears to be astonishingly resistant (ref. 18). This behaviour is unique as no other cluster species has shown anything like this level of stability. Indeed most other clusters dissociate at relatively modest photon flux.

From these observations we can draw a number of conclusions that are likely to be significant as far as the structure and properties of carbonaceous interstellar grains are concerned. First of all the results indicate that chains and carbonaceous grains form at the same time and in those regions (such as TMC1 and IRC+10216) where they are both detected the grains are likely to have quasi-icosahedral spiral shell structures. It is possible that the presence of hydrogen will obscure this basic pattern producing perhaps a more spheroidal (less obviously polyhedral) structure. We know that chains and grains are forming in the shells surrounding IRC+10216 and other similar objects from where they are continually being ejected into the interstellar medium. Once in the general interstellar medium they are subjected to the ambient stellar flux and occasional shock waves which are the main agents of molecule destruction. On the basis of these arguments we can draw some interesting conclusions about the astrophysical significance of  $C_{60}$  buckminsterfullerene itself.

We know that the resilience of CO is a major reason for its abundance and the fact that it is so much more widespread than other molecules, extending significantly further into unshielded (by grains) regions of space than any other molecule so far detected. It is worth remembering that this widespread abundance only became obvious with the advance in the radioastronomy techniques. The present observations indicate that after ejection  $C_{60}$  should be an outstanding survivor in the general interstellar medium, probably as the ion,  $C_{60}^+$ , protected by its unique ability to withstand shock-wave and photodissociative processes so drastic that most, if not all, other known molecules are destroyed.

As neither  $C_{60}$ , nor  $C_{60}^+$  have dipole moments they cannot be detected by radioastronomy which is the most specific of interstellar analytic techniques.  $C_{60}$  has however four ir active fundamental vibrational frequencies though others may become active through resonances and it is likely that the modes will be similar to those of corannulene or coronene which do not involve C-H bonds. During nucleation in the presence of hydrogen, partially hydrogenated quasi-icosahedral spiral shell particles should form and such species will also possess vibrational modes of similar frequency, including the C-H modes. Thus such species are likely to give rise to emission similar to that of the Unidentified Infrared Bands for the same reasons that these features have been ascribed to hydrogenated amorphous carbon by Duley and Williams (ref. 28) and to polyaromatic hydrocarbons by Leger and Puget (ref. 29) and Allamandola et al (ref. 30). Soot will give rise to similar emission spectra. The pure carbon species  $C_{60}$  and  $C_{60}^+$  should also be extensively distributed and their emission, which will lie at similar frequencies, should be excited by the processes that dissociate all other species.

It is possible to generate complexes of the form  $C_{60}X$  in which the atom X appears to reside inside the carbon shell (ref. 18) and during the circumstellar carbon dust formation it is likely that many of the atomic and molecular constituents (other than carbon and hydrogen) which are present may become entangled either molecularly bound in cages or adsorbed/absorbed in and on the spiral structures. Graphite itself forms intercalation compounds with numerous atoms and molecules as do soot and carbon black. Such materials are likely to show electronic spectra which are characteristic of atoms in matrix environments. The resulting lines will lie at determinable frequencies and also may give rise to interstellar features.

From the moment it was discovered it was clear that  $C_{60}$  was a most promising possible carrier of various old interstellar chestnuts (ref. 17), such as the Diffuse Interstellar Bands, the 2170Å UV band or the Unidentified Infrared Features. These possibilities should prove amenable to unequivocal laboratory verification in due course. Indeed a very weak absorption band of neutral  $C_{60}$  at 3860Å has already been detected (ref. 31). Although this wavelength does not coincide with any of the Diffuse Bands this is a difficult region in which to carry out interstellar spectroscopy. This spectrum was obtained by forming a beam containing complexes of the kind  $C_{60} \cdot X$  where X was weakly attached by Van der Waals forces. By tuning a dye laser across an absorption band of  $C_{60}$  the weakly attached passenger molecule (either  $C_6H_6$  or

$\text{CH}_2\text{Cl}_2$ ) was detached and the event detected by mass spectrometry. This experiment depends on the weakness of the bond between  $\text{C}_{60}$  and X for two reasons; firstly it is important that the electronic spectrum of  $\text{C}_{60}$  is not significantly perturbed and secondly that the weak bond can be broken. In the case of the analogous experiments aimed at testing the conjecture that  $\text{C}_{60}^+$  is the carrier of some of the Diffuse Interstellar Bands, it has not so far been possible to dissociate the complex (ref. 32). It is possible that in this case charge transfer interactions cause the complex to be too strongly bound for the passenger to be readily detached by this technique and also that the various electronic bands that are expected to occur for the ion are strongly shifted and broadened by the interactions. Numerous bands of the cation are expected to lie in more-or-less the correct part of the visible spectrum as can be estimated by applying Koopmans' Theorem to the various calculations on neutral  $\text{C}_{60}$  that have been carried out (ref. 33).

Recently there has been a most interesting radio observation by Rieu, Winnberg and Bujarrabal (ref. 34). They have shown that in the Egg Nebula (CRL2688) the central object is surrounded by a small ammonia cloud which lies more-or-less within the dusty envelope which can be seen optically. Most interesting however is their further observation the dusty region is surrounded by second, large, extended molecular cloud in which significant quantities of the cyanopolyne  $\text{HC}_7\text{N}$  are detected. It is tempting to explain the formation of the chains as starlight photofragmentation products from the outer regions of a large carbonaceous dust cloud and that the presently visible cloud is an inner remnant. It is in just this type of object that our experimental data indicate that  $\text{C}_{60}$  and  $\text{C}_{60}^+$  should remain, as all other material is destroyed.

## SUMMARY

These observations can be summarised as follows: Carbon chains and grains are indeed intimately related and it appears that the chains may be intermediates in the formation of carbon particles. They also appear to be produced by photofragmentation of carbon particles as well. The recent laboratory studies suggest very strongly that any dust which is associated with carbon chain molecules should be very similar in constitution to the particles formed in terrestrial carbon nucleation processes, i.e. quasi-icosahedral spiral graphitic shells.

Most interesting conclusions relate to  $\text{C}_{60}$  itself. In the laboratory we find that whenever chains and carbon particles form so also does  $\text{C}_{60}$  and, what is more, this molecule is exceptionally resistant to chemical attack and to photofragmentation. Thus in regions such as the outer reaches of the Egg Nebula our experiments point unequivocally to presence of  $\text{C}_{60}$  and  $\text{C}_{60}^+$ . The contention that  $\text{C}_{60}$  may be a ubiquitous character in any carbon nucleation scenario has recently been given further credibility by the observation (ref. 27) that  $\text{C}_{60}^+$  is a dominant ion in a sooting flame. It is most satisfying that the proposed carbon nucleation scheme (refs 19,25) predicted that  $\text{C}_{60}$  should be a by-product of the soot formation process prior to this discovery. The observation lends further support to the contention that the scheme has widespread applicability in that carbon cages can

also occur in the presence of hydrogen if the physicochemical conditions are right.  $C_{60}$  is unique in that it should also be the LONE MOLECULAR SURVIVOR of the chaotic processes involved in interstellar particle formation and destruction and thus should have a ubiquitous presence in some of the most hostile regions of space.  $C_{60}$  and its relatives are most interesting possible carrier for some of the various interstellar spectroscopic features. As the ionisation potential lies between 6.4 and 7.9 eV (ref. 17), in unshielded regions it is most probably ionised as  $C_{60}^+$  (ref. 14). Thus for the first time an experimentally based scenario can be presented which gives rise to a solitary possible molecule in space. All previous proposals have been unable to account for the single most important fact about the Diffuse bands; the modest number of bands, their relatively constant wavelengths and their correlation properties point to only one relatively large chemically bound carrier, or at most a very small number of such species. On the basis of molecular orbital calculations on the neutral it is clear that it should have only one strong electronic transition in the visible and near uv whereas the ion should possess a modest number, of the order of a few tens.

It certainly seems almost certain that partially hydrogenated analogues of the spiral shell particles considered here will have infra red emission features very similar to polyaromatic hydrocarbons and thus also the Unidentified IR Bands.

It is satisfying to note that some fairly simple concepts now allow many aspects of interstellar and circumstellar carbon chemistry to fall neatly into place.

I am very happy to acknowledge my coworkers in the work described here: David Walton, Anthony Alexander, Colin Kirby, Julie August, Don McNaughton, Ken McKay, Nenad Trinajstić, Lesley Little, Takeshi Oka, Lorne Avery, Norm Broten, John MacLeod, Jim Heath, Sean O'Brien, Bob Curl and Rick Smalley. I also wish to acknowledge valuable discussions with Bill Klemperer, Mike Jura, and Nguyen-Q-Rieu. In addition I thank Sumio Iijima for sending me his photographs of carbon particles.

#### REFERENCES

- 1 Alexander A J, Kroto H W and Walton D R M, J. Mol. Spectrosc., 62, 175-180 (1976).
- 2 Avery L W, Broten N W, MacLeod J M, Oka T and Kroto H W, Ap. J., 205, L173-175 (1976).
- 3 Kirby C, Kroto H W and Walton D R M, J. Mol. Spectrosc., 83, 261-265 (1980)
- 4 Kroto H W, Kirby C, Walton D R M, Avery L W, Broten N W, MacLeod J M and Oka T, Astrophysics J., 219, L133-L137 (1978).
- 5 Broten N W, Oka T, Avery L W, MacLeod J M and Kroto H W, Ap. J., 223, L105-107 (1978).

- 6 Bell M B, Kwok S, Feldman P A and Matthews H E, *Nature*, 295, 389 (1982)
- 7 Kroto H W, McNaughton D M and Osman O I, *J. Chem. Soc. Chem. Comm.*, 993-994 (1984).
- 8 Kroto H W, McNaughton D M, Little L T and Matthews N, *Mon. Not. R. Astr. Soc.*, 213, 753-759 (1985).
- 9 August J, Kroto H W and Trinajstić N, *Astrophys. Space Sci.* 128, 411-419 (1986)
- 10 Kroto H W, *Int. Revs Phys. Chem.*, 1, 309-376 (1981).
- 11 Kroto H W in *Submillimetre Wave Spectroscopy*, J E Beckman and J P Phillips (eds.), Cambridge University Press, 203-217 (1982).
- 12 Kroto H W, *Chem. Soc. Revs.*, 11, 435-491 (1982).
- 13 Kroto H W, *Proc. Roy. Inst.*, 58 45-72 (1986)
- 14 Kroto H W, *Polycyclic Aromatic Hydrocarbons and Astrophysics*, ed. A Leger et al. pp 197-206 Reidel(pub) (1987)
- 15 Heath J R, Zhang Q, O'Brien S C, Curl R F, Kroto H W and Smalley R E, *J. Am. Chem. Soc.*, 109 359-363 (1987)
- 16 Kroto H W, Heath J R, O'Brien S C, Curl R F and Smalley R E, *Ap. J.*, 314 352-355 (1987)
- 17 Kroto H W, Heath J R, O'Brien S C, Curl R F and Smalley R E, *Nature*, 318, 162-163, (1985).
- 18 Heath J R, O'Brien S C, Zhang Q, Liu Y, Curl R F, Kroto H W, Tittel F K and Smalley R E, *J. Am. Chem. Soc.*, 107, 7779-7780 (1985).
- 19 Zhang Q, O'Brien S C, Heath J R, Liu Y, Curl R F, Kroto H W and Smalley R E, *J. Phys. Chem.*, 90, 525-528 (1986).
- 20 Liu Y, O'Brien S C, Zhang Q, Heath J R, Tittel F K, Curl R F, Kroto H W and Smalley R E, *Chem. Phys. Letts*, 126, 215-217 (1986).
- 21 O'Brien S C, Heath J R, Kroto H W, Curl R F and R E Smalley, *Chem. Phys. Letts.*, 132, 99-102, (1986)
- 22 Heath J R, O'Brien S C, Curl R F, Kroto H W and Smalley R E, *Comm. Cond. Matter Phys.* 13, 119-141 (1987)
- 23 Heath J R, O'Brien S C, Curl R F, Kroto H W and Smalley R E, *Acc. Chem. Res.*, in press

- 24 Kroto H W, Nature, 329, 529-531 (1987)
- 25 Kroto H W and McKay K G, Nature, (1988) in press.
- 26 Iijima S, J Crystal Growth 5, 675-683 (1980)
- 27 Gerhardt Ph, Loffler S and Homann K H, Chem Phys Letts 137, 306-309 (1987)
- 28 Duley W W and Williams D A, Mon. Not. Roy. Astron. Soc. 196 269 (1981)
- 29 Leger A and Puget J L, Astr. Ap. 137, L5 (1984)
- 30 Allamandola L J, Yielens A G G M, and Barker J R, Ap. J. 290, 25-28 (1985)
- 31 Heath J R, Curl R F and Smalley R E, J. Chem. Phys. 87, 4236-4238 (1987)
- 32 Heath J R, Curl R F, Kroto H W and Smalley R E (unpublished results).
- 33 Negri F, Orlandi G and Zerbetto P, (and papers referenced, to be published)
- 34 Nguyen-Q-Rieu, Winnberg A and Bujarrabal V Astron. Astrophys. 165, 204-210 (1987)

**STUDIES OF CARBON FROM SPACE**

# SPACE INFRARED TELESCOPE FACILITY



Fig. 1. SIRTf -- The Space Infrared Telescope Facility

## SIRTF: PROBING THE DARK CORNERS OF THE GALAXY

Michael W. Werner  
NASA Ames Research Center  
and  
Dora S. Willoughby  
Information Management International

### ABSTRACT

SIRTF - the Space Infrared Telescope Facility - is planned for launch by NASA in the mid-1990's. It will be a cryogenically-cooled observatory for infrared astronomy and will carry several focal plane instruments which will provide a wide range of imaging, photometric, and spectroscopic capabilities. SIRTF will build on the scientific and technical progress of the successful IRAS mission and take the next step in the exploration of the Universe at infrared wavelengths.

Most of the observing time during the five-to-ten year SIRTF mission will be available to General Investigators, so there will be ample opportunities for the pursuit of problems originating from within the Space Life Sciences community. This paper will review the capabilities of SIRTF for this style of investigation, using the study of carbon in the Galaxy as a specific example. The very high sensitivity of SIRTF's spectrometers to diffuse emission will allow studies of carbon in both the gaseous and solid phase in the interstellar medium and should be of particular importance for the identification of the carbon-bearing macromolecules believed to be responsible for the emission features identified in the near infrared. SIRTF will also carry out studies of a wide variety of evolved stars which are returning gas and solid phase carbon to the interstellar medium and contribute to our understanding of the carbon "budget" in the Galaxy. These studies in the area of galactic astronomy will be complemented by detailed investigations of carbon-bearing compounds in solar system objects, including the surfaces of distant asteroids and cometary nuclei which are too faint to be studied in any other way.

### INTRODUCTION

This paper will look into the future to discuss the use of SIRTF, the Space Infrared Telescope Facility, for the study of problems discussed at this conference and similar problems in Space Life Sciences. SIRTF should permit a specific style of investigation in this area, described in greater detail below, which I refer to as "probing the dark corners of the Galaxy." The paper includes a general description of SIRTF and examples of specific problems where SIRTF should have a major impact. The opportunities for general participation in the SIRTF program will also be described.

### SIRTF, THE OBSERVATORY

SIRTF, the Space Infrared Telescope Facility, is a cryogenically cooled telescope for infrared astronomy to be launched in the mid 1990's, perhaps 1996 or 1997 on the present schedule. SIRTF will have a long lifetime, of the order of five years, which will be achieved by on-orbit replenishment of its liquid helium cryogen at two-to-three year intervals. There will be an extensive guest investigator program -- SIRTF is envisioned as an observatory for the entire scientific community, and is being developed as such at NASA Ames Research Center.

The unique capabilities of a cryogenic telescope for infrared astronomy from space give SIRTf tremendous power for the types of scientific problems which are being discussed at this conference. Figure 2 illustrates this in two ways. The upper curve shows the atmospheric transmission at infrared wavelengths from 2 to 1000 microns as it would be on a good mountain top site. Even on a good mountain like Mauna Kea the entire wavelength band from 30 to 300 microns, which includes many transitions of carbon-bearing molecules as well as the critical fine structure line of the  $C^+$  ion, is totally unobservable from the ground. Radiation in several other infrared bands, including the 5-8 micron window where solid state and gaseous absorption features can be studied, also doesn't get through to the ground, nor does radiation in the region around 3 microns. One can get above some of this absorption by using an airplane such as the Kuiper Airborne Observatory, but not above all of it; so there is a great advantage in going into space just to get above the atmospheric absorption.

The other major advantage of going into space is shown in the lower set of curves in Figure 2, which show the brightness of the sky -- that is to say, the brightness of the background against which one is trying to detect infrared sources -- as a function of wavelength for several situations. From the ground, or from an airplane using an ambient temperature telescope, the background is quite bright, basically that of a 250-300 K black body with emissivity  $\sim 0.1$ . The background is contributed both by the atmosphere and by the telescope itself. However, if one goes into space, the natural

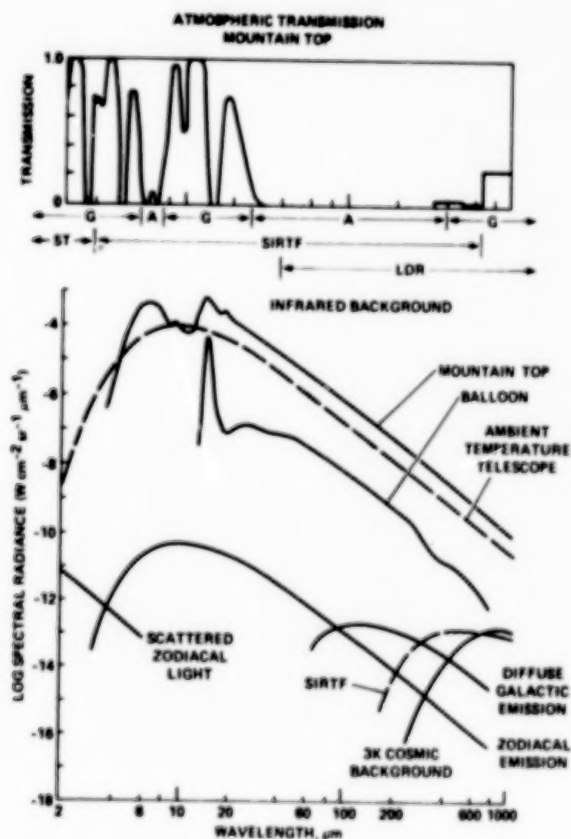


Fig. 2. Atmospheric transmission of infrared radiation at mountain top altitude (upper curve), and background radiation due to the atmosphere and ambient temperature telescope at mountain top and balloon altitudes, compared with the much lower astrophysical and instrumental backgrounds which characterize the SIRTf operating environment.

background -- primarily due to scattered sunlight or emitted radiation from the tenuous zodiacal dust cloud -- is about six or seven orders of magnitude lower. Very faint infrared sources stand out much more prominently against this background, and the limiting noise, which is due to the fluctuations in the rate of photon arrival, is reduced by three to four orders of magnitude as compared to an ambient temperature telescope. If the telescope is cooled so that it doesn't produce appreciable infrared emission, as will be done with SIRTf, very low backgrounds and exceedingly high sensitivity can be achieved. So a cryogenic telescope like SIRTf promises a three or four orders of magnitude increase in sensitivity over current capabilities over much of the infrared spectrum. The tremendous potential of SIRTf has been tantalizingly foretold by the Infrared Astronomical Satellite (IRAS) survey mission, which has demonstrated the power of a cooled telescope in space. IRAS worked primarily in just four broad spectral bands at 12, 25, 60, and 100  $\mu\text{m}$ , while SIRTf will provide both photometric and spectroscopic capabilities across the entire infrared.

The characteristics of the SIRTf mission and telescope are shown in Table A. The telescope aperture will be 85 cm, making it a one meter class telescope. The wavelength range will be from 2-700 microns with 1 arcsec images in the near infrared. The pointing accuracy and stability will be  $\sim 0.15$  arcsec, consistent with the short wavelength images. Mission duration will be in excess of five years. In addition, there will be planetary tracking capability so one can study solar system phenomena. Further details concerning the SIRTf facility and instruments are given in a paper by Werner and Eisenhardt (1988)<sup>1</sup>, and the broad scope of SIRTf science is discussed by Reike et al. (1986)<sup>2</sup>.

Three instruments, an infrared array camera, a spectrometer, and a multiband imaging photometer, are under development for SIRTf by different university teams. These are described in Table B. SIRTf's instruments will exploit the rapid progress now occurring in the development of monolithic arrays for infrared astronomy (Wynn-Williams and Becklin, 1987)<sup>3</sup>.

SIRTf will be capable of mapping and photometry throughout the 2-700 micron band. Its imaging capabilities will be particularly impressive at the shorter wavelengths where large arrays will provide images  $\sim 5$  arcminutes in extent with arcsec resolution. A variety of filters will be available for use with the imaging arrays, including filters which might be tuned to some of the features of interest in studying carbon compounds. SIRTf will have capability for polarimetry and an emphasis on obtaining the highest possible spatial resolution.

In addition, SIRTf will have spectroscopic capability in two modes, a low resolution mode at resolving power of about 100 from 2-120 microns, and a higher mode with resolving power of about 2000 from 4 to about 200 microns. Again, detector arrays will be used for spectroscopy, obtaining spectra at several points along the slit as well as dispersing the spectrum perpendicular to the slit.

Figure 3 shows a comparison of the sensitivity which SIRTf will achieve in low, medium and high resolution modes compared with the sensitivity which IRAS was able to achieve, with the current capabilities of ground based and airborne facilities and with the signals from some astronomical objects of potential interest. In broad spectral bands, SIRTf will be one to ten thousand times more sensitive than IRAS. Of particular importance for the problems discussed at this conference is SIRTf's spectroscopic capability. SIRTf will be able to obtain quite quickly detailed spectra of any IRAS source. For example, SIRTf spectra of the 700 carbon stars discovered by IRAS would permit determination of the molecular content of their atmospheres.

TABLE A

**SIRTF — SPACE INFRARED  
TELESCOPE FACILITY**

**SYSTEM CHARACTERISTICS**

APERTURE: 85 CM  
 WAVELENGTH RANGE: 2-700  $\mu\text{m}$   
 DIFFRACTION-LIMIT:  $<4 \mu\text{m}$   
 FIELD OF VIEW: 7 ARCMINUTES  
 ANGULAR RESOLUTION: 1 ARCSEC @  $4 \mu\text{m}$   
 POINTING ACCURACY/STABILITY [ARCSEC]: 0.15/0.15  
 MISSION DURATION:  $>5$  YEARS  
 PLANETARY TRACKING CAPABILITY

TABLE B

SIRTF INSTRUMENTATION

<u>INSTRUMENT</u>	<u>PI</u>	<u>CHARACTERISTICS</u>
INFRARED ARRAY CAMERA (IRAC)	G. FAZIO, SAO	Wide field and diffraction-limited imaging, 2-30 $\mu\text{m}$ , using arrays with up to 128 x 128 pixels. Simultaneous viewing in 3 wavelength bands, selectable filters. Polarimetric capability.
INFRARED SPECTROMETER (IRS)	J. HOUCK, CORNELL	Grating spectrometers, ~ 2-200 $\mu\text{m}$ , using two-dimensional (~ 10x50) detector arrays. Resolving power from 50 to $> 1000$ . Low and high resolution options at most wavelengths.
MULTIBAND IMAGING PHOTOMETER (MIPS)	G. RIEKE, ARIZONA	Photometry, 3-200 $\mu\text{m}$ , using small arrays with pixels sized for complete sampling of Airy disk. Wide field, high resolution imaging, 60-120 $\mu\text{m}$ . Broad band photometry and mapping, 200-700 $\mu\text{m}$ . Polarimetric capability.

# THE DARK CORNERS OF THE GALAXY

From the astrophysical point of view SIRTf is often thought of as a discovery instrument. Its great sensitivity will allow new phenomena to be discovered by the imaging instruments and followed up with the spectrograph. A number of SIRTf's most important science goals have this character. But thinking about the use of SIRTf to study the problems discussed at this conference reminds me of the story about the drunk who was searching for a lost dollar bill under a light post. Some guy came along and said "Where'd you lose it?" He said "I lost it over there, but the light's

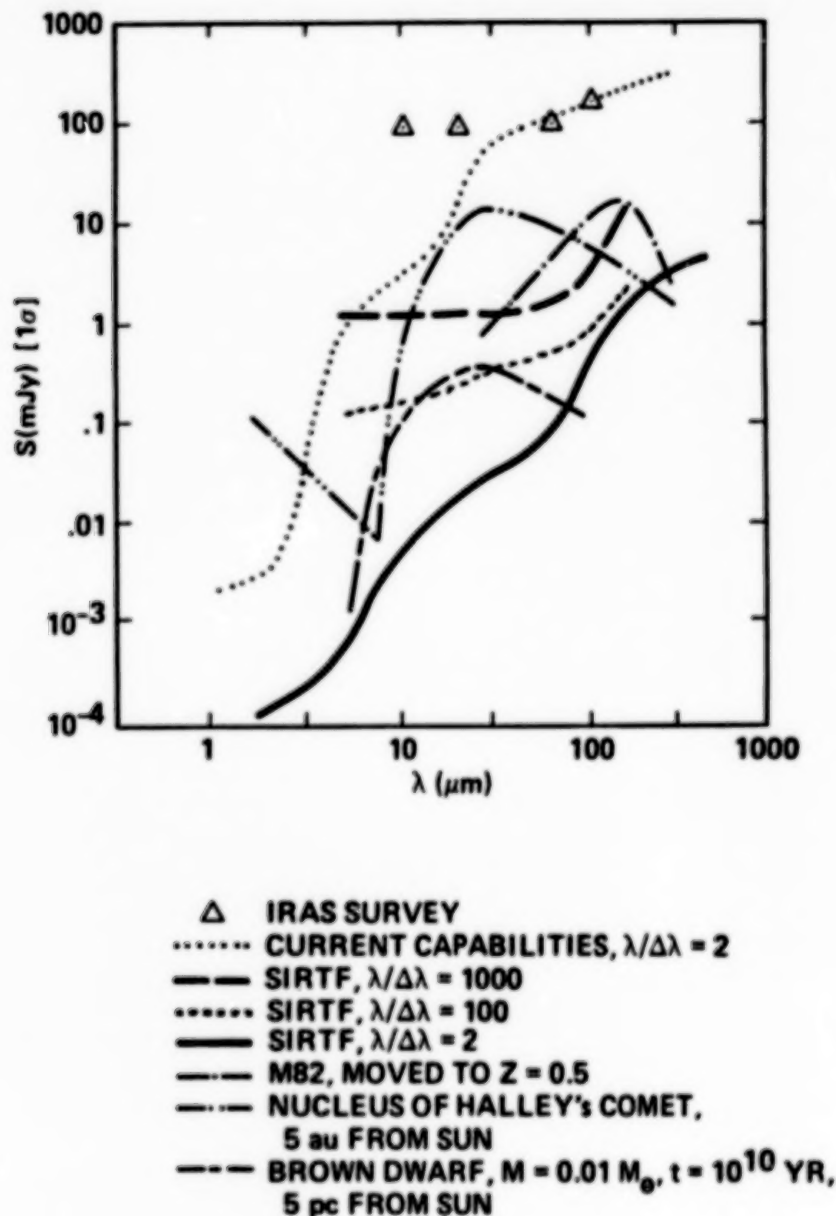


Fig. 3. The sensitivity of SIRTf in photometric and spectroscopic modes compared with the sensitivities of current telescopes and IRAS. Also shown are computed signals expected from a galaxy similar to M82 at a distance of  $z=0.5$ , Halley's comet at 5 AU from the sun, and a brown dwarf 15 light years away, typical of objects which SIRTf might study.

a lot better here." With SIRTf, however, we can look for the dollar at the place where it was lost. In other words, SIRTf will allow us to look into the dark corners of the Galaxy to see where most of the matter and most of the carbon reside, and to see the fainter and less dramatic manifestations of phenomena for which we can see only one or two unusual cases with our current capabilities. SIRTf will vastly increase the dynamic range over which these interesting phenomena can be studied.

#### A. Absorption by Grain Mantles

Figure 4 shows the extremely nice spectrum of the infrared absorption by icy grain mantles along the line of sight to W33A (Tielens and Allamandola, 1987).<sup>4</sup> Figure 5 shows a cartoon version of the cloud of dust and gas which surrounds W33A. W33A, an extremely bright object, is presumably having a tremendous perturbing effect upon the local grain mantle composition and chemistry, and its influence is

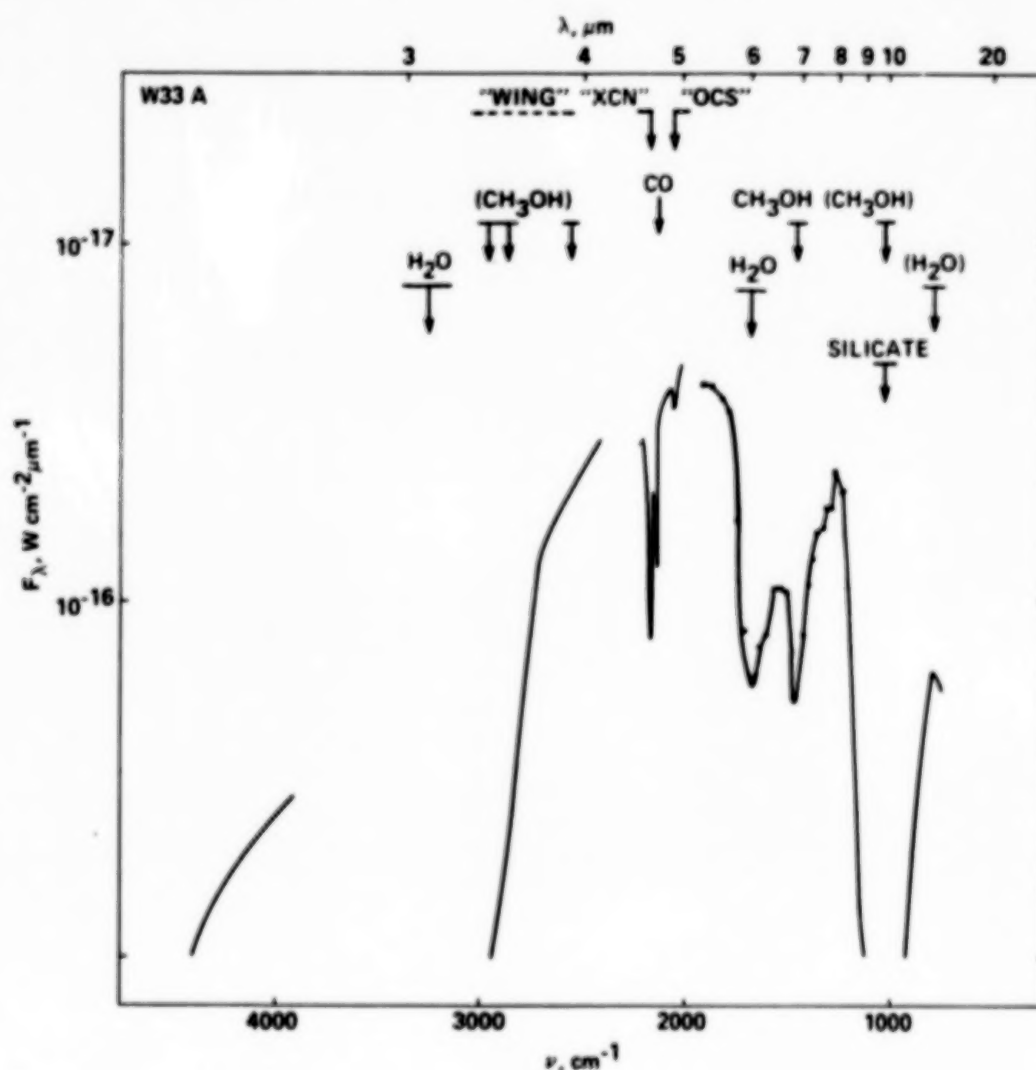


Fig. 4. The 2-13  $\mu\text{m}$  spectrum of the protostar W33A, (from Tielens and Allamandola, 1987), showing absorption features at 3.08, 4.61, 4.67, 4.9, 6.0, 6.85, and 10  $\mu\text{m}$ . The peak frequencies and widths of likely identifications for these features are shown as arrows and bars. Except for the 10  $\mu\text{m}$  silicate, all of the other features are ascribed to molecules in icy grain mantles in the dust cloud surrounding this source.

inextricably folded into the observed spectrum. With current observing capabilities, however, this perturbation is unavoidable. With SIRTf, however, one could look not only at W33A, a very bright source, but also at random background stars behind this dark cloud, which have no effect whatever upon the material within it. One could study the grain composition at various positions across the cloud as a function of density and temperature, and get a much better understanding of how the icy mantles evolve. To show that this is feasible, consider that the SIRTf limit for 1% resolution spectroscopy at five microns is about 10,000 times (10 stellar magnitudes) fainter than W33A, corresponding to 13th or 14th magnitude. The density of stars of that brightness in a random direction in the sky is such that behind a typical dark cloud there should be five to ten stars sufficiently bright to be used as probes to assess the absorption in the cloud and determine the mantle materials. Such background stars could be found very easily using SIRTf's cameras to image the cloud -- objects which can be detected spectroscopically are quite bright to SIRTf in its photometric mode. One could complement these observations by gas phase spectroscopy at higher resolution, and by continuum observations in the far infrared and submillimeter. These would permit determination of the dust and gas content along the

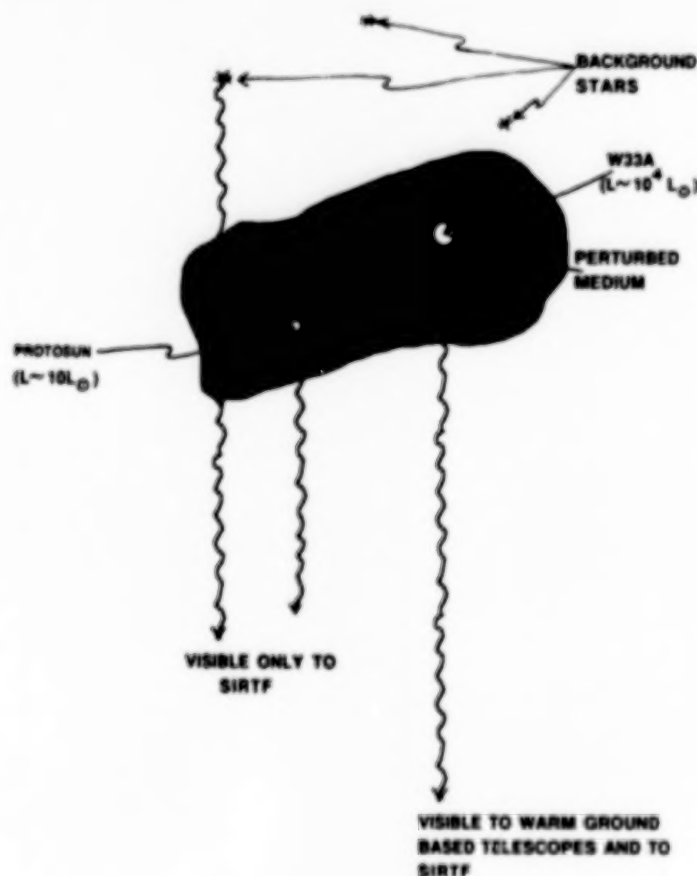


Fig. 5. This cartoon depicts a dense molecular cloud surrounding the highly luminous protostar W33A, which seriously perturbs the cloud material close to it. At present, the only way to study the cloud composition is by its effect on radiation from W33A which has passed through the perturbed region around the protostar. To study the unperturbed cloud material by observing the spectra of stars behind the cloud, or to study less luminous solar-type protostars within the cloud requires telescopes more sensitive than those currently available. SIRTf, however, will be able to do spectroscopic studies of both such objects.

line of sight for which the absorption has been measured. This is one dark corner that SIRTf can look into.

### B. Gas Phase Spectroscopy

It will also be possible to do interesting gas phase spectroscopy of the biogenic elements with SIRTf. A number of lines in the far infrared are of interest for abundance determinations. These include the 63 and 145.5  $\mu\text{m}$  lines of neutral oxygen, the 52 and 88  $\mu\text{m}$  lines of  $\text{O}^{++}$ , the 57  $\mu\text{m}$  line of  $\text{N}^+$ , the 122  $\mu\text{m}$  line of  $\text{N}^{++}$ , the 158  $\mu\text{m}$  line of  $\text{C}^+$ , and the 370 and 609  $\mu\text{m}$  lines of neutral carbon. Many of these have been discussed at this conference. It has already been possible to look at the ratio of oxygen to nitrogen in the brighter ionized regions at various points through the galaxy, to get some idea of how the history of nuclear evolution has varied throughout the galaxy. Some of the data that have been obtained are shown in Figure 6 (taken from Lester et al. 1987),<sup>5</sup> where the abundance ratio of doubly ionized nitrogen to doubly ionized oxygen is plotted as a function of the distance of the ionized region from the center of the galaxy. These data show evidence for an increase in the nitrogen to oxygen ratio as one moves toward the center of the galaxy. This has been interpreted as indicating more star formation and thus more nuclear processing in the inner regions of the galaxy over the past 10 billion years. With SIRTf one will easily be able to extend this type of study to distant galaxies using the same infrared lines, which provide very good abundance determinations. In this way, we can look at the history of star formation and thus at the return of processed matter to the interstellar medium in other galaxies.

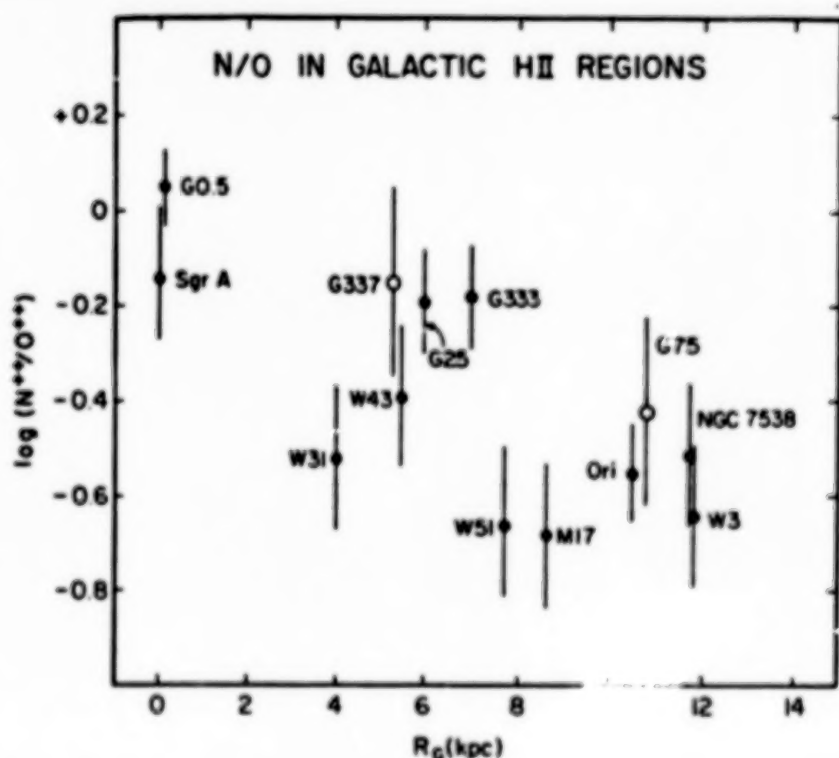


Fig. 6. The N/O ratio in galactic H II regions plotted vs. distance from the galactic center (from Lester, et al., 1987). The higher ratio of nitrogen to oxygen near the galactic center is indicative of more star formation and more nuclear processing in the inner regions of the galaxy.

Also in the area of gas phase spectroscopy is the possibility of looking at the  $C^+$  line in circumstellar shells, discussed earlier as of importance in the chemistry of such regions. Figure 7 shows the spectrum of the  $158\ \mu\text{m}$  line of  $C^+$  in NGC 7027, the brightest planetary nebula in the sky (Ellis and Werner, 1984).<sup>6</sup> A planetary nebula consists of a bright hot star, an ionized shell (seen in the radio continuum and in lines characteristic of ionized material), and an exterior molecular shell which is seen in emission lines of CO and other molecules. Clearly there must be an intermediate atomic region in which the gas is undergoing a transition from being ionized to being molecular. The transition region will be heated and partially ionized by the low energy ultraviolet photons from the central star; such a region should be bright in the  $C^+$  line. That's exactly what one sees in the case of NGC 7027. The masses of material in each of these three regions are, approximately: 0.1 solar mass in the ionized shell, 0.25 solar masses in the atomic region, and 0.5 solar masses in the molecular shell. In this particular case the atomic region, which cannot be easily detected in any other way except through the  $63\ \mu\text{m}$  line of neutral oxygen, is comparable in mass with the molecular and the totally ionized portions of the circumstellar shell. Thus the  $C^+$  line in this case is a diagnostic of the rate of return of matter to the interstellar medium, matter enriched in carbon, nitrogen and oxygen. Its abundance in such shells is also of importance because of its effect on chemical processes and thus on the chemical composition of the returned matter. SIRTf's capability to detect  $C^+$  lines with a flux of  $1.5 \times 10^{-18}$  watts per square meter (0.01 percent of the brightness of the line in NGC 7027) will make it possible to detect as little as  $10^{-5}$  solar masses of ionized carbon in an object at the distance of the galactic center, which is 30,000 light years away. Thus, instead of having to look only at the brightest and nearest planetary nebulae, one could easily study all of the planetary nebulae that are now known.

Since the mass that one can see scales inversely as the square of the distance, in the solar neighborhood at 300 light years from the sun, one could see as little as

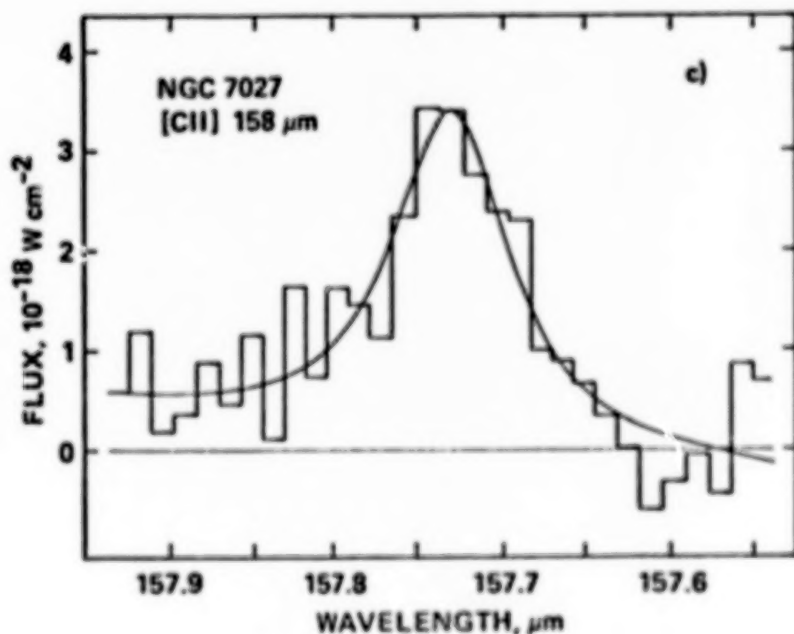


Fig. 7. The spectrum of the  $158\ \mu\text{m}$  line of  $C^+$  in the planetary nebula NGC 7027 (from Ellis and Werner, 1984). The strength of this line in planetary nebulae is a measure of the return of biogenic elements to the interstellar medium.

$10^{-9}$  solar masses of carbon, which is much less than the mass of carbon in the solar system. This assumes that the carbon is ionized and that the upper state of the C<sup>+</sup> line is well populated, which will occur over a substantial range of density and temperatures. With SIRTf's ability to detect  $10^{-9}$  solar masses of C<sup>+</sup>, or even smaller amounts for closer objects, one should think about looking for gas in "Vega shells", clouds of debris around stars, which may be relics of a planetary formation phase. Vega and Beta Pictoris provide the best known examples of this phenomenon, but IRAS discovered such shells around approximately 20% of nearby stars of masses  $\leq 2M_{\odot}$ . Based on statistical extrapolations of the results from IRAS, Backman and Gillett (1987) estimate that most solar type stars are circled by particle clouds which emit in the far infrared. The IRAS number of 20% is set not because that's all there are, but by the dynamic range of our ability to detect them. So here is a whole new area of science which SIRTf can explore. There is material around stars which may well be the debris of the planetary formation phase, and studying its composition in the infrared either through gas phase or solid phase spectroscopy should be extremely interesting. This would be a very potent application of SIRTf because it can resolve the Vega shell, which is some 20 arcsec in diameter, and because it could detect objects of the scale of the Vega shell around stars thousands of light years away, and more modest examples around nearer stars.

### C. Comets

A third exciting area is the study of comets. Some very nice ground-based spectroscopy by Baas et al. (1986)<sup>8</sup> discovered in the spectrum of Halley's comet a complicated feature, shown in Figure 8, at a wavelength of about 3.25  $\mu$ m. They suggest that this is due to UV-pumped fluorescence of organic molecules, either molecules on small grains or free molecules. SIRTf could have detected this particular brightness from Halley's comet at a distance of 3 AU from the sun (out past the asteroid belt) as the comet approached the inner solar system. SIRTf could study the development of this feature, verify the excitation mechanism, and perhaps

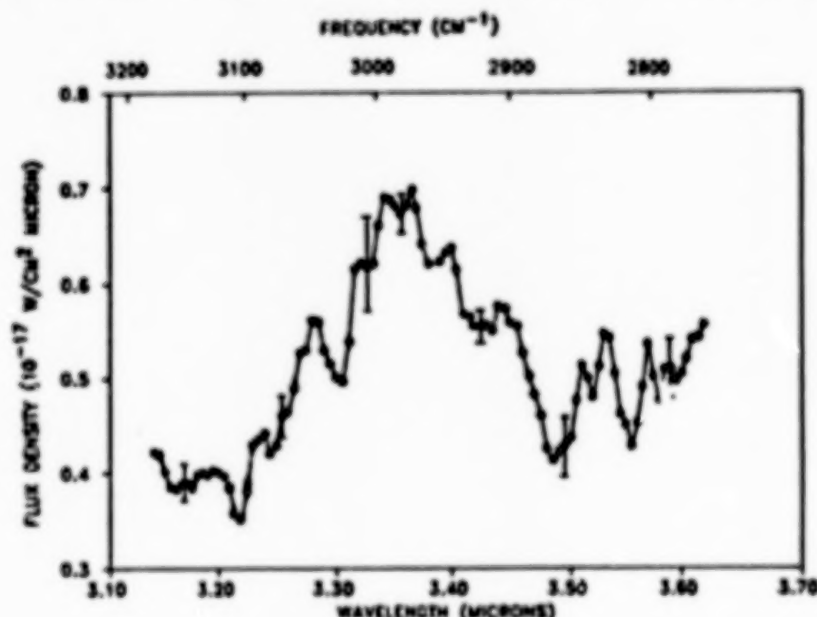


Fig. 8. The spectrum of Halley's comet in the wavelength region around 3.35  $\mu$ m (from Baas et al. 1986). The presence of this peak in the spectrum can be interpreted as evidence for UV-pumped fluorescence of organic molecules, either on small grains or as free molecules.

determine the temperature at which this material, whatever it is, starts to come off the cometary grains. This is the sort of project which could be done with spectral resolving power of about 100, consistent with the SIRTf instrumentation.

#### D. Diffuse Emission from the Interstellar Medium

A cryogenic telescope like SIRTf is particularly sensitive to low surface brightness extended emission, and SIRTf will be intensively used in studies of diffuse infrared emission from the interstellar medium. One of the main phenomena to be explored in this fashion is the non-equilibrium emission seen from 2 to 30  $\mu\text{m}$  in many interstellar regions; it was to explain this non-equilibrium emission that polycyclic aromatic hydrocarbons (PAHs) were postulated as an abundant carbon-bearing constituent of the interstellar medium (Leger and Puget (1984)<sup>9</sup>; Allamandola, Tielens, and Barker (1985)<sup>10</sup>).

This non-equilibrium emission was first discovered in bright reflection nebulae like NCC 7023 (Sellgren et al. 1985).<sup>11</sup> Figure 9 shows the infrared spectrum of the bright inner region of NCC 7023. At wavelengths longward of 30  $\mu\text{m}$  there is an emission peak which is consistent with thermal emission from grains in equilibrium

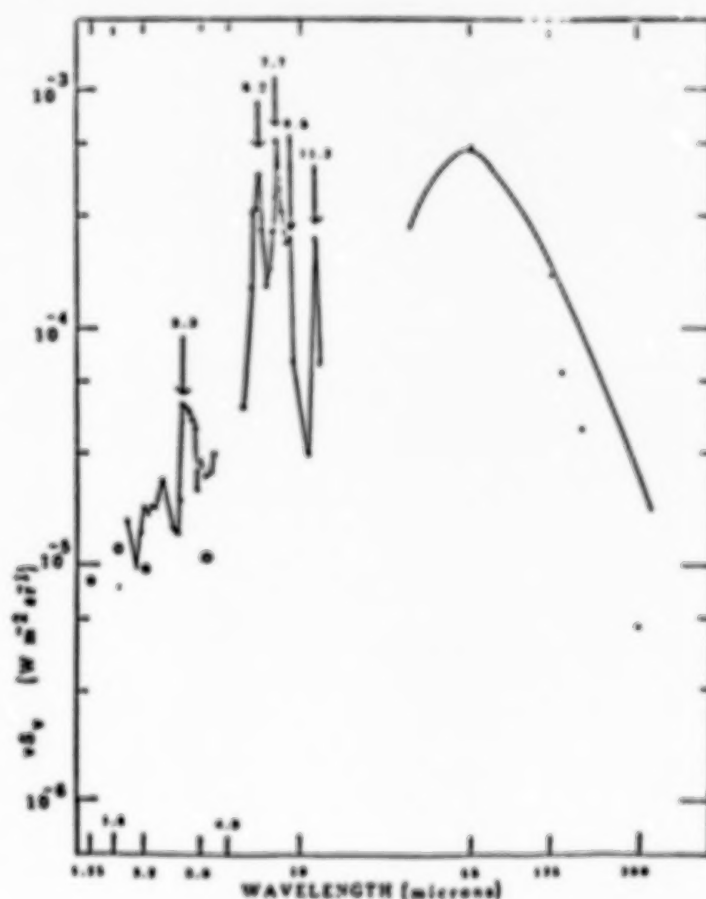


Fig. 9. The infrared spectrum of the reflection nebula NCC 7023 (from Sellgren et al. 1985, and Whitcomb et al. 1981<sup>12</sup>) showing a peak longward of 30  $\mu\text{m}$ , attributed to thermal emission from grains in equilibrium with radiation from the illuminating star, and showing peaks in the range 2-11  $\mu\text{m}$  due to non-equilibrium emission from polycyclic aromatic hydrocarbons (PAHs).

with the radiation from the star which illuminates this nebula. At shorter wavelengths we see the very pronounced emission features which are attributed to the PAHs, and perhaps some continuum as well. If one extrapolates the thermal emission curve to shorter wavelengths, it falls far below these emission features, and since there is nothing exotic going on in the reflection nebula, one is forced by these data to infer that this emission is excited in some kind of non-equilibrium way. What IRAS saw when it looked in a region like this was just the four broad points at 100, 60, 25 and 12 microns; where it averaged over whatever spectral structure there might be. SIRTf will be able to resolve the features in this part of the spectrum and take an inventory of the emission features seen in regions of various types and under differing excitation conditions. In addition, SIRTf can obtain spectra of many such regions, as opposed to the handful now accessible.

An example of the type of region which SIRTf can study in this fashion -- another type of region in which IRAS found infrared emission which may have this non-equilibrium character at the shortest wavelengths -- is Cas A, which is a supernova remnant. In Figure 10, IRAS maps of Cas A at 12, 25, and 60 microns are compared with an X-ray map of the same region (Dwek et al. 1987a).<sup>13</sup> The emission seen in the X-ray clearly comes from a very hot plasma, and the infrared emission comes from dust particles mixed within that plasma. The dust particles are heated not by photons, which is the normal way that dust is heated in our galaxy, but by collisions with energetic particles in the plasma, which has a temperature of about  $10^7$  K. As these particles pass through the dust grains they lose energy by ionization losses which

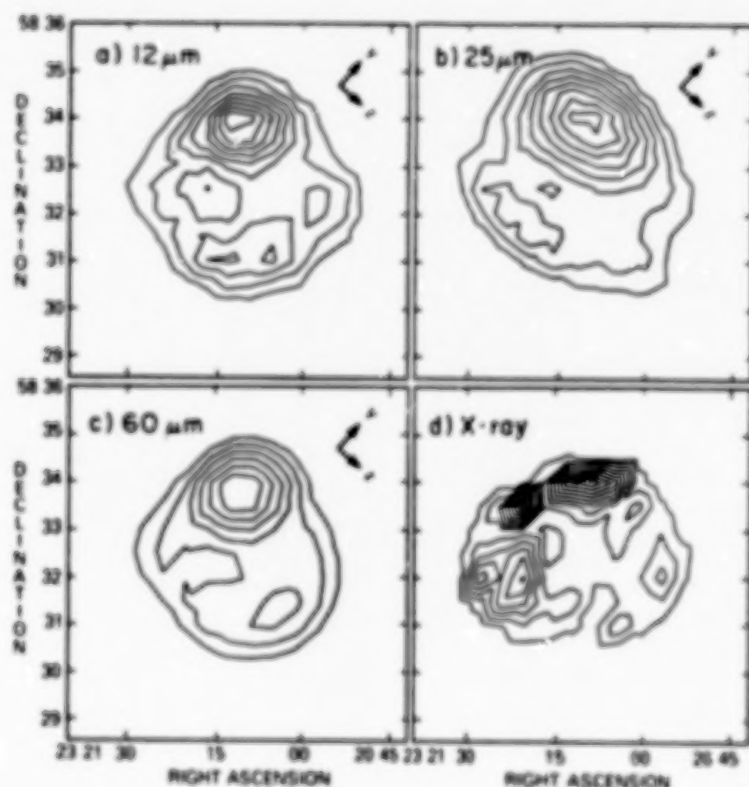


Fig. 10. IRAS-measured contours of Cas A at 12, 25, and 60  $\mu\text{m}$  compared with X-ray contours of the same region (from Dwek, et al. 1987a). The X-ray emission is from hot plasma; the infrared emission is from dust grains embedded in the plasma, and heated by collisions with hot plasma particles.

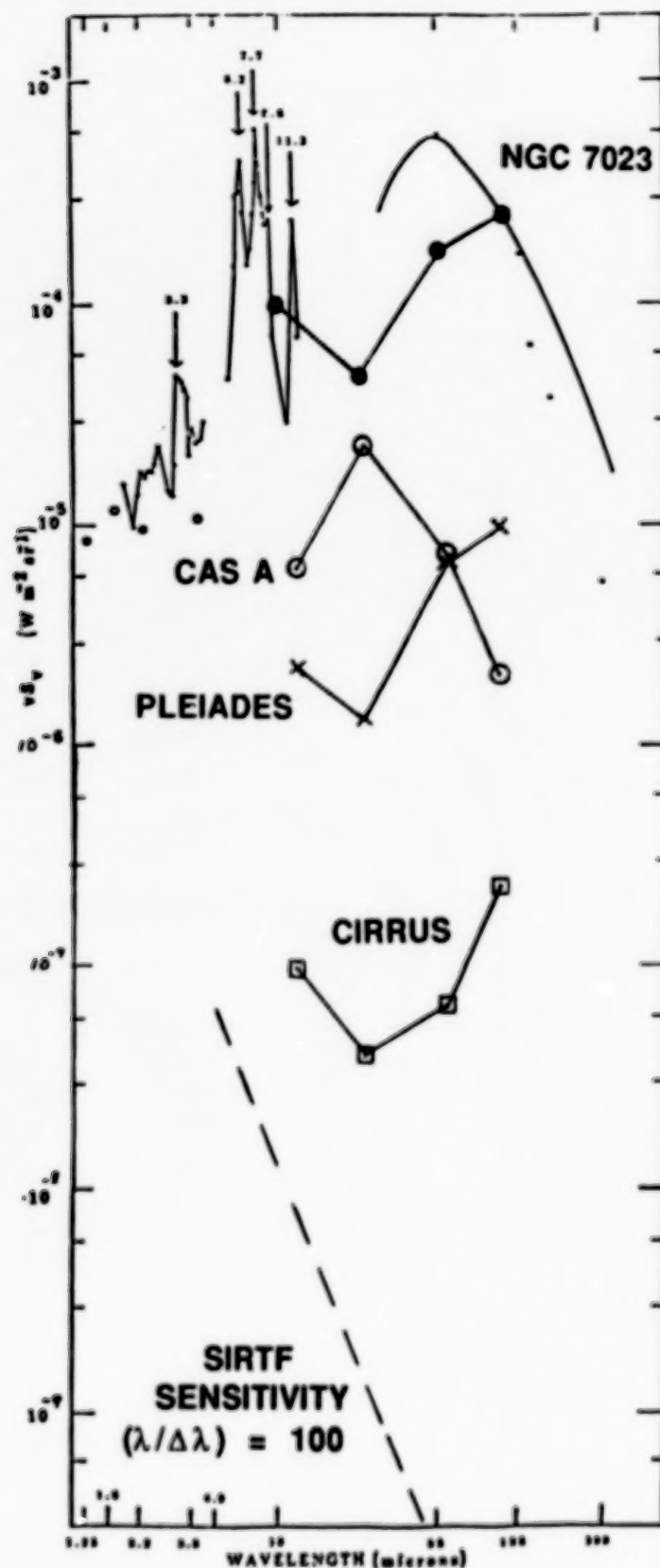


Fig. 11. The spectrum of NGC 7023 (from Sellgren et al. 1985 and Whitcomb et al. 1981) and IRAS observations of NGC 7023, Cas A, reflection nebulae in the Pleiades, and the galactic cirrus, compared with the sensitivity with which SIRTf will be able to make spectroscopic studies of these and similar objects with a resolution of  $\lambda/\Delta\lambda$  of 100.

heats the dust particles and causes the observed radiation. There is a series of very nice papers on this process by Dwek et al. (1987b)<sup>14</sup> on the data from IRAS. Clearly, if one is interested in grain destruction and what happens to grains in supernova shocks, then certainly the spectrum of the emission from these regions must be studied.

Another type of region of interest for SIRTf to study is the infrared cirrus, wisps of radiation seen away from the galactic plane, which have been given the name "cirrus" because they look like the cirrus clouds which astronomers are all too familiar with from ground-based work. The cirrus appears to be emission from fairly random patches of dust in the interstellar medium illuminated by ambient starlight. These patches reside in what must be the most benign environment in which particles can exist in the interstellar medium.

Figure 11 shows a comparison of expected fluxes from these three types of regions with what the capabilities of SIRTf will be. NGC 7023 is shown as the brightest region of this general type; the solid circles show the average (as opposed to peak brightness of NGC 7023 based on IRAS data; the open circles, x's, and squares show the IRAS observations of the emission from Cas A, moderately bright reflection nebulae in the Pleiades (Castelaz, et al. 1987),<sup>15</sup> and the IR cirrus respectively. The cirrus is about as faint a region as IRAS can see, and is far fainter than can be seen from the ground or with warm telescopes. Even the bright reflection nebulae in the Pleiades are inaccessible to currently available instruments. The sensitivity which SIRTf will achieve with a resolving power of 1 $\lambda$  is shown by the dashed curve at the bottom of the figure. Clearly, SIRTf will have the ability to obtain spectra of any of these regions at the 1 $\lambda$  level. One can then look for the presence and the structure of the emission features and see how they vary as one goes from a supernova remnant where there is shock processing to regions like the Pleiades where the radiation density is quite high, and finally -- to the darkest corners of the galaxy -- to regions where the radiation density is low and the material undisturbed.

## CONCLUSIONS

SIRTf will be operated as an observatory-class facility. Beginning four months after launch, 50% or more of the observing time will be used by general investigators selected competitively from the broad community.

SIRTf has great potential for the study of carbon in space, and of other problems in the area of Space Life Sciences. More active involvement of the Space Life Sciences Community in the SIRTf project definition would be most welcome. Specific suggestions or requests for more information concerning SIRTf are solicited, and should be passed on to the author of this article. Ultimately, members of this community should be thinking about proposing observing programs for SIRTf.

This talk has concentrated on SIRTf, but the European Space Agencies are developing a project called ISO, the Infrared Space Observatory, which will be intermediate in capability between IRAS and SIRTf, and come along earlier than SIRTf, perhaps as early as 1993. The Space Telescope, and other major U.S. astrophysical observatories also will have great potential for studying various aspects of these problems.

## References

1. Werner, M. W. and Eisenhardt, P.: SIRTf, The Space Infrared Telescope, *Astrophys. Lett. and Comm.* (in press) 1988.
2. Rieke, G. H., Werner, M. W., Thompson, R. I., Becklin, E. E., Hoffman, W. F., Houck, J. R., Low, F. J., Stein, W. A., Witteborn, F. C.: *Infrared Astronomy after IRAS*, *Science*, 231, 807, 1986.
3. Wynn-Williams, C. G., and Becklin, E. E. eds.: *Infrared Astronomy with Arrays, Proceedings of the Workshop on Ground-Based Astronomical Observations with Infrared Array Detectors, March 24-26, 1987*. Univ. of Hawaii, University of Hawaii Institute for Astronomy, Hilo, 1987.
4. Tielens, A. G. G. M. and Allamandola, L. J.: *Evolution of Interstellar Dust in Physical Processes in Interstellar Clouds*, G.E. Marfill and M. Schoter eds., p. 333, D. Reidel, 1987.
5. Lester, D. F., Dinerstein, H. L., Werner, M. W., Watson, D. M., Genzel, R., and Storey, J. W. V.: *Far-Infrared Measurements of the N/O in HII Regions: Evidence for Enhanced CN Process Nucleosynthesis in the Inner Galaxy*, *Ap. J.* 320, 573, 1987.
6. Ellis, H. B. and Werner, M. W.: *Observations of the Far Infrared Emission Lines of OI and CII in Planetary Nebulae*, *Bulletin of the American Astronomical Society*, 16, 463, 1984.
7. Backman, D. E., Gillett, F. C., and Low, F. J.: *IRAS Observations of Nearby Main Sequence Stars, and Modeling of Excess Infrared Emission*, in *Advances in Space Research*, Vol. 6, p. 43, 1986.
8. Baas, F., Geballe, T. R., and Walther, D. M.: *Spectroscopy of the 3.4 Micron Emission Feature in Comet Halley*, *Ap. J.* 311, L97, 1986.
9. Leger, A. and Puget, J. L.: *Identification of the "Unidentified" IR Emission Features of Interstellar Dust*, *Astron. Astrophys.* 137, L5, 1984.
10. Allamandola, L. J., Tielens, A. G. G. M., and Barker, J. R.: *Polycyclic Aromatic Hydrocarbons and the Unidentified Infrared Emission Bands: Auto Exhaust Along the Milky Way*, *Ap. J.* 290, L25, 1985.
11. Sellgren, K., Allamandola, L. J., Bregman, J. D., Werner, M. W. and Wooden, D. H.: *Emission Features in the 4-13 Micron Spectra of the Reflection Nebulae, NGC 7023 and NGC 2023*, *Ap. J.* 299, 416, 1985.
12. Whitcomb, S. E., Gatley, I., Hildebrand, R. H., Keene, J., Sellgren, K., and Werner, M. W.: *Far-Infrared Properties of Dust in the Reflection Nebula NGC 7023*, *Ap. J.* 246, 416, 1981.
13. Dwek, E., Dinerstein, H. L., Gillett, F. C., Hauser, M. G., and Rice, W. L.: *Physical Processes and Infrared Emission from the Cassiopeia A Supernova Remnant*, *Ap. J.* 315, 571, 1987a.

14. Dwek, E., Petri, R., Szymkowiak, A., and Rice, W. L.: IRAS Observations of Supernova Remnants: A Comparison Between Their Infrared and X-Ray Cooling Rates, Ap. J. 320, L27, 1987b.
15. Castelaz, M. W., Sellgren, K, and Werner, M. W.: IRAS Surface Brightness Maps of Reflection Nebulae in the Pleiades, Ap. J. 313, 853, 1987.

# **Research Opportunities on the Space Station**

Guy Fogleman\*  
Mail Stop 239-12  
NASA Ames Research Center  
Moffett Field, CA 94035

(\*RCA Government Services)

## **1. Introduction**

This paper reviews two interdisciplinary facilities that have been proposed for the Space Station: the Gas-Grain Simulation Facility and the Cosmic Dust Collector Facility. Both of these facilities provide opportunities for scientists interested in carbon related research to perform experiments in earth orbit. Most of this paper is devoted to the Gas-Grain Simulation Facility<sup>1</sup> (GGSF). The Cosmic Dust Collector<sup>2</sup> (CDC) will be discussed briefly at the end of the paper.

## **2. The Gas-Grain Simulation Facility**

Numerous experiments involving clouds and small particles cannot be performed on Earth due to the Earth's gravitational field. In 1g, the large sedimentation rate of micron sized particles and the effects of gravity induced convection prohibit many interesting studies of particle phenomena. Although such studies cover a wide range of disciplines, they all have in common the study of processes involving small particles and weak interactions and would benefit greatly from the microgravity environment of the Space Station. Because of the very low gravitational acceleration experienced by particles in the Space Station, many experiments that are impractical or impossible on Earth become feasible in the Space Station environment. The advantages of the Space Station's microgravity environment are discussed in more detail in Section 3.

The GGSF (see the figure for a functional diagram) is a facility-class payload being developed for the Space Station by the Exobiology Flight Program at Ames Research Center. The purpose of the GGSF is to perform basic research; the GGSF will be used to investigate and simulate fundamental chemical and physical processes such as condensation, growth, formation, nucleation, evaporation, accretion, coagulation, scavenging, collisions and mutual interactions of droplets, crystals, grains and other particles in a microgravity environment. Examples of experiments that have been suggested for the GGSF will be discussed in Section 4. The GGSF is a "lab in space" that will extend ground based experimental programs to new domains as well as allow completely new types of experiments to be performed. Although the facility is simple in concept, it will be able to perform a variety of experiments in a wide range of disciplines: Exobiology, Planetary Science, Astrophysics, Atmospheric Science, as well as basic Physics and Chemistry.

The GGSF, which would occupy a Space Station double rack, consists of a number of subsystems supporting an experimental chamber. The experimental chamber will have a working internal volume of four to ten liters and may be connected to subsystems that provide environmental (e.g., temperature, pressure, gas mixture and humidity) controls, mechanisms for injecting and removing particles and clouds of particles, levitation systems (e.g., electrostatic, acoustic, laser trapping and aerodynamic) to keep particles in fixed positions away from the chamber walls, energy sources (e.g., UV light), and a number of experiment monitoring and measuring devices (e.g., video cameras, optical particle counters,

spectrometers). See reference 3 for a recent determination of the functional requirements of the GGSF.

Because of limitations on crew time, the facility will be designed to operate in a nearly autonomous mode. One possible scenario is as follows: A chamber designed for a sequence of experiments is "plugged in" to the GGSF and subsystems attached in the configuration necessary for the first experiment. A command is then given to begin the execution of preprogrammed instructions to perform the experiment. After the first experiment is completed, the system may be reconfigured for the second experiment. The experiments would be performed in a logical order, perhaps from "clean" to "dirty." When the sequence of experiments associated with the first chamber is completed, the chamber is removed and stored for return to earth and a second chamber is attached for the next sequence of experiments (alternatively, a chamber cleaning subsystem could be activated before a second sequence of experiments is performed in the same chamber). New experiment chambers will be brought to the Space Station periodically, so the GGSF would have a very long useful lifetime.

The GGSF will be designed to have an adaptable configuration; the subsystems may be connected to the experiment chamber in a number of ways. Also, the GGSF will be implemented in an evolutionary fashion. The earliest experiments performed on the GGSF will be those that are the simplest (i.e., require the smallest number of subsystems); the more complicated experiments will be performed later in the facility's development. The above can be achieved by requiring the facility to be modular in design. Modularity will also allow subsystems that become outdated to be replaced by those using more modern technology.

The status of the GGSF program as of November 1987 is as follows: Two workshops have been held - one in 1985 to establish the scientific feasibility of the facility<sup>4</sup> and one in 1987 to create a database of strawman experiments<sup>5</sup>. Recently, Martin Marietta completed a physics feasibility study of the facility<sup>6</sup>, and a preliminary Level 1 Requirements Document was sent to NASA headquarters. Presently, the twenty strawman experiments proposed at the 1987 workshop are being studied in order to determine the science requirements of the facility. A two year GGSF reference design study is scheduled to begin in the middle of 1988. On the completion of the reference design study the Announcement of Opportunity for experiments for the GGSF will be released. The Exobiology Flight Program's goal is to have the GGSF available for launch and ready for use at the time of the Permanent Manned Presence of the Space Station (mid 1990's).

### **3. The Microgravity Environment**

A Space Station laboratory has the advantage of a microgravity environment. Microgravity reduces the effect of many environmental forces. On Earth, one micron particles used in an experiment would fall to the floor of a chamber relatively quickly (a micron-sized particle in one atmosphere would fall a meter in one hour at 1g). On the Space Station, however, the terminal velocity of such a particle falling through a gas would be reduced by as much as five or six orders of magnitude (since the terminal velocity of a particle is proportional to the acceleration due to gravity). This effect allows long duration particle experiments to be performed.

Although the sedimentation rate is reduced, it is not eliminated. Tidal effects and the mass of the Space Station itself create gravitational accelerations of  $10^{-4}$  to  $10^{-6}$  g inside the GGSF. Levitation is required in long duration experiments to counteract the resulting sedimentation. The levitation force required, however, is four to five orders of magnitude weaker than that required to keep particles suspended at 1g. This is a major advantage for experiments that study phenomena involving weak interaction forces. A number of possible techniques to levitate particles, in gas as well as in vacuum, were studied in detail in

reference 6. This study found that all levitation methods either induce coagulation or otherwise render unrealistic the simulation of multiparticle interactions. This issue is not important in single particle experiments, but is critical in cloud or multiparticle experiments. Cloud experiments can be done without levitation, however, as long as wall effects are not important to the experiment.

The large sedimentation rate problem is not the only problem associated with particle experiments in 1g that is resolved by use of microgravity. The reduction of the gravitational convection due to buoyant forces is another major advantage of the microgravity environment. Also, in some experiments, such as the study of fractal particles, the forces studied are so weak that they would be overwhelmed by gravitational forces in 1g.

See references 1 and 4 - 6 for a more detailed discussion of the advantages and problems associated with the microgravity environment of the Space Station.

#### **4. Example GGSF Experiments**

Twenty experiments were suggested for the GGSF at the 1987 workshop<sup>5</sup>. Four example experiments from the 1987 workshop are described in this section. These four were chosen on the basis that they were related to studies of carbon in the galaxy and/or provided instructive examples of types of experiments that could be performed on the GGSF.

(a.) Emission Properties of Particles and Clusters<sup>7</sup>. The objective of this experiment is to measure the radiative properties of clusters of molecules and microparticles in order to understand how radiative energy is converted from UV to infrared. This process, which is not well understood, is important in environments such as circumstellar shells, planetary nebulae, protostellar disks, reflection nebulae and H I/H II interfaces. Clusters of polycyclic aromatic hydrocarbons, carbon grains, or silicates are generated and positioned in the chamber. The baseline emission is measured. The particles are then warmed up or excited by UV radiation and the emission spectrum is measured with spectrometers/monochrometers at different excitation levels. Microgravity is necessary in this experiment because suspension times in 1g are not long enough to accumulate enough signal to measure the emission spectra of free species.

(b.) Dipolar Grain Coagulation and Orientation<sup>8</sup>. The objective of this experiment is to investigate the process of grain agglomeration in dust clouds of grains with an electric dipole moment and to study the polarization of light passing through filamentary agglomerations that are oriented in an external electric field. This experiment investigates this phenomena as a possible mechanism for the formation of elongated grain agglomerates and grain alignment in interstellar clouds resulting in the polarization of light. Dust is produced *in situ* or brought from earth and injected into the chamber. Grain agglomeration and alignment are followed in time using light scattering techniques and polarization measurements. The process is repeated using different values of an external electric field. Microgravity is necessary in this experiment because the dipole-dipole interaction between grains is weak and would be overwhelmed by gravitational forces at 1g. Also, suspension time at 1g would not be long enough for large aggregates to form.

(c.) Surface Condensation and Annealing of Chondritic Dust<sup>9</sup>. The objective of this experiment is to simulate the putative gas-dust reaction textures in extraterrestrial materials, especially carbonaceous chondrite meteorites and interplanetary or cosmic dust, to study surface energy related effects that occur, and to obtain information on chemical composition and complexity of solar system condensates. Oxide cores are injected into the chamber. Metal-bearing gases are then injected sequentially as a function of decreasing condensation temperature. The experimental products are then collected and analyzed on the Space Station or returned to Earth for analysis. Microgravity is necessary because this experiment must be performed without allowing the particles to interact with the chamber walls and

because suspension times of the particles would not be sufficiently long in 1g. Also, the absence of turbulence is required during the first stages of the experiment.

(d) **Studies of Fractal Particles<sup>10</sup>.** The objective of this experiment is to measure the coagulation coefficients of a variety of bare silicates, ice-coated silicates, organic-refractory coated silicates and organic-refractory grains, to grow fractal aggregates of these materials, measure their cohesive strength, and measure their light scattering and extinction properties as a function of wavelength. Refractory silicate nucleation sites are nucleated from vapor and allowed to coagulate. The particles' optical properties are monitored using light scattering techniques. Once grains have grown to a desirable size, they are broken apart with acoustic shock waves to measure their cohesive strength. Particles are allowed to re-coagulate and more measurements are made. Finally, particles are coated with ice or irradiated to obtain organic-refractory coatings on silicates and the measurements are repeated. Microgravity is necessary because of the long suspension times required and because macroscopic fractal particles would be gravitationally unstable at 1g and would collapse under their own weight.

The above examples are representative of the variety of experiments that have been suggested for the GGSF. Other experiments that have been suggested for the GGSF involve low-velocity collisions (important for the understanding of the formation of planetary rings), properties of aerosols, particulate aggregation (important in atmospheric processes such as dust storms), other atmospheric processes, ice growth, and a simulation of the organic haze in Titan's atmosphere.

## **5. The Cosmic Dust Collector Facility**

The Space Station also affords an opportunity to collect cosmic dust. The Cosmic Dust Collector (CDC)<sup>2,11</sup> will be discussed only briefly here. The CDC is a facility class payload being developed for the Space Station by Johnson Space Center. The CDC is an externally attached payload proposed for the Initial Operating Configuration of the Space Station. The facility will be designed to capture individual particles and to measure their trajectories with enough precision to determine their astrophysical source.

Two capture techniques have been suggested: atomized capture and intact capture. Atomized capture in "capture cells" preserve (at most) elemental and isotopic composition. Intact capture, however, would also preserve molecular composition and structural information. Intact capture (in underdense media) would probably be the preferred method for most carbon studies. The Exobiology Flight Program at Ames Research Center is sponsoring a study at the Jet Propulsion Laboratory on intact capture techniques and technology for potential CDC experiment development.

## **6. Conclusion**

A wide range of fundamental scientific problems associated with studies of carbon in the galaxy can be addressed by conducting microgravity particle experiments or by collecting cosmic dust on the Space Station. The Gas-Grain Simulation Facility and the Cosmic Dust Collector are experimental facilities proposed for the Space Station that could open new frontiers in carbon research. Persons wishing to suggest or discuss experiments for either of these facilities should contact the author at the above address.

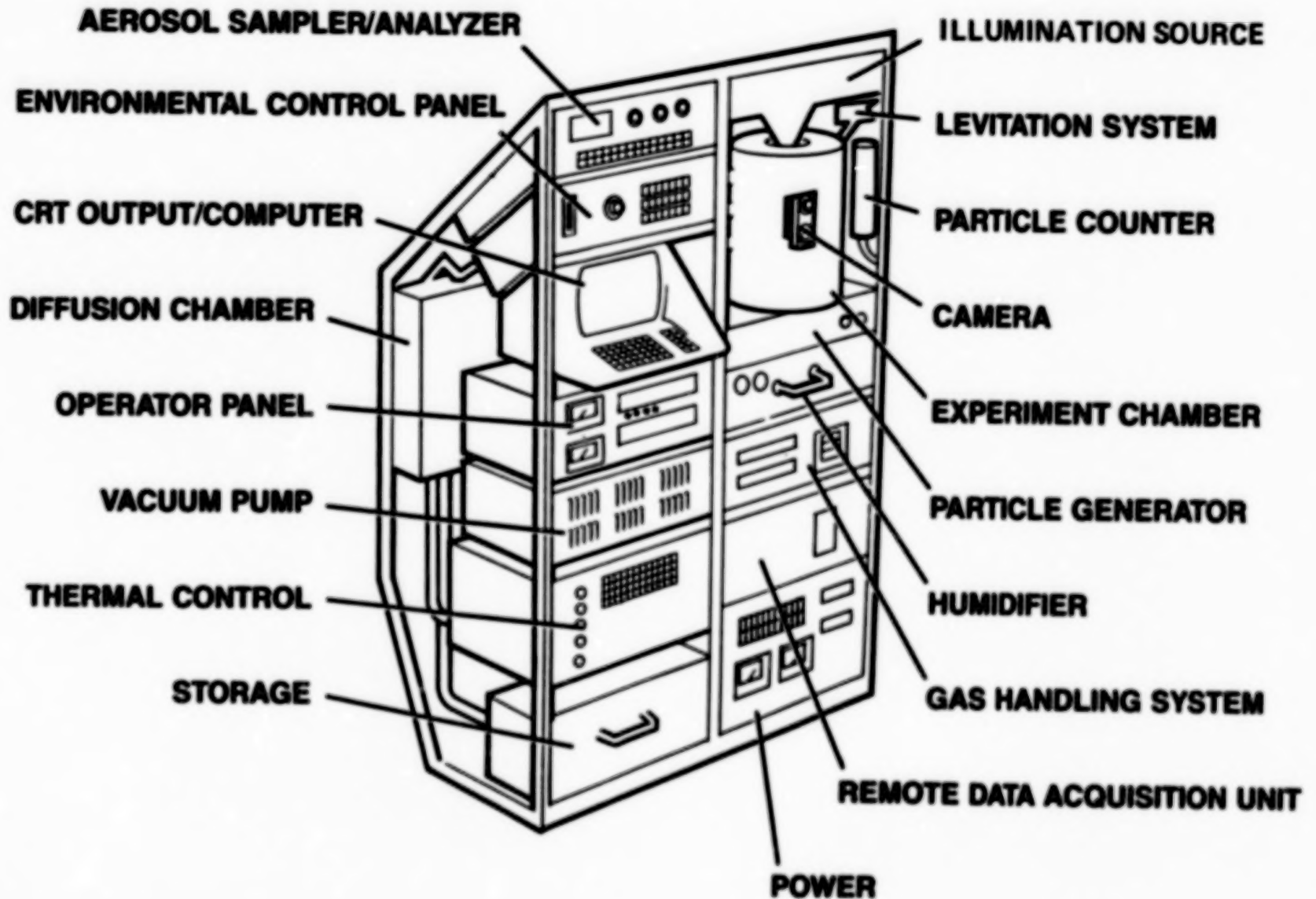
## **Acknowledgement**

The functional diagram of the GGSF is from a sketch by D. Schwartz.

## References

1. C. P. McKay, C. R. Stoker, J. Morris, G. Conley, and D. Schwartz, "Space Station Gas-Grain Simulation Facility: Application to Exobiology," *Adv. Space Res.* **6**,195(1986). See also references 3,4,5 and 6.
2. LPI Technical Report 86-05, "Trajectory Determinations and the Collection of Micrometeoroids on the Space Station," (Report of a workshop held at the Lunar and Planetary Institute,16-18 December 1985).
3. NASA Technical Memorandum 89606. "Life Science Space Station Planning Document: A Reference Payload for the Exobiology Research Facilities."
4. S. W. Squyres, C. P. McKay, and D. E. Schwartz (editors), "Microgravity Particle Research on the Space Station," (Report of a workshop held at NASA Ames Research Center, 22-24 August 1985). NASA CP 2496 (in press).
5. G. Fogleman, M. Fonda, and D. Schwartz (editors), Proceedings of the Space Station Microgravity Gas-Grain Simulation Facility Experiments Workshop held in Sunnyvale, CA, August 31-September 1, 1987 (in preparation). To be published as a NASA Conference Publication.
6. J. B. Miller and B. C. Clark, "Feasibility Study for Gas-Grain Simulation Facility," NASA Contractor Report 177468 (September, 1987).
7. Experiment suggested by L. Allamandola and J. Goebel in reference 5.
8. Experiment suggested by F. Freund in reference 5.
9. Experiment suggested by I. MacKinnon and F. Rietmeijer in reference 5.
10. Experiment suggested by J. Nuth and J. Stephens in reference 5.
11. Proceedings of the Cosmic Dust Collector Workshop, sponsored by the Lunar and Planetary Institute. Held in Carmel, CA, June 29-July 2, 1987 (unpublished).

## GAS-GRAIN SIMULATION FACILITY



**SUMMARY AND CONCLUDING REMARKS**

## WHAT HAVE WE LEARNED; WHERE DO WE GO FROM HERE?

J. Mayo Greenberg

University of Leiden

The key question one must ask at a meeting of this sort is "Why are we interested in the subject." The answer is that we think that, somehow, what happens to carbon in the galaxy must ultimately bear on the origin of life and why we are here to talk about it.

Except for the after dinner talk none of the speakers directly addressed the origin of life question. What they did was to approach the subject of carbon in the galaxy from such a variety of points of view - from observational astronomy to stellar and solar system astrophysics, to laboratory methods and basic chemistry - that we were certainly given enough of a perspective to see where the problems exist and, hopefully, to lay the foundation for future lines of investigation. I have certainly learned about many new and interesting problems from the excellent reports presented here.

All conceivable sources and kinds of carbon that one could imagine were mentioned and, since clearly the form in which carbon is found in such primitive solar system objects as meteorites and comets is of most direct interest, these were discussed first at the meeting. However, although we started from this point I find it easier to summarize in reverse order; that is, to consider where the carbon comes from and then see if we can understand why and how it is found in the forms we are analyzing "close at hand".

We had a number of papers on the stellar sources of carbon. Mass loss from cool evolved (AGB) stars is believed to be the major source of carbon in the interstellar medium. Some observational and theoretical aspects of this were developed by Michael Jura and John Bieging to show how and why either solid or molecular forms of carbon are injected into space. What happens to this carbon henceforth is a complex and tangled sequence of events some of which can be studied by following the evolution of simple molecules such as the very abundant CO. But other much less abundant species such as CH, CN, C<sub>2</sub> may also provide clues on the chemical evolution in space. As was pointed out by Jocelyn Keene, in the cold interstellar medium CI and CII along with CO are the main gas phase tracers of the chemistry and that, in the gas phase carbon story, the major emphasis is to be placed on the photoinduced effects from the interstellar ultraviolet radiation field.

In the circumstellar envelopes cosmic ray penetration provides a source of photochemical processing similar to that directly produced by the interstellar ultraviolet in molecular clouds. How the carbon exchange between solid and gaseous forms was questioned. However, it is now becoming increasingly apparent

that the solid grains in space must be brought into the picture if we are ever to realize the sources of the most interesting complex carbon molecules - certainly from the point of view of prebiotic chemistry. Why and to what extent the pure gas phase processes "fail spectacularly" to provide the abundances of the larger molecules in dense molecular clouds was noted by Geoffrey Blake. As he pointed out this problem must be honestly appraised not only by improving our techniques of observation but also by reexamining the theoretical models of interstellar chemistry. It is my impression that one of the key questions to be raised in many of the ion-molecule schemes is the use of unrealistic C/O ratios in the gas.

A fair evaluation of purely gas phase chemistry providing abundant complex molecules in molecular clouds can not be made if one is allowed to use C/O ratios which are even higher than that given by cosmic abundances. In fact, the presence of solid dust automatically creates a deficit of carbon relative to oxygen. Jumping ahead of the story a bit, the situation in dense molecular clouds is, to at least a large extent, reflected by the chemical components of comets and in these there is a well known problem of the "missing carbon mystery" in the volatile molecules of the coma. By implication, and now by observation, this missing carbon is to be found in the comet dust in the form of a refractory form of carbon.

Where does this refractory carbon in space come from? Notice that I did not say "solid" carbon. The reason is that there appear to be many varieties of carbon that, in a way, may be thought of as surviving better than simple molecules but are not necessarily solid in a simple sense. By refractory, therefore, must be included such things as the polycyclic aromatic hydrocarbons (PAH's) and the stable carbon species  $C_{60}$ , more familiarly known as "bucky balls". A substantial part of the meeting - particularly the talks by Smalley and Kroto - were devoted to this new and at first glance exotic form of carbon resembling (hollow) soccer balls. Both from theoretical and experimental points of view this molecule presents some extremely interesting possibilities but it appears that although the theoretical implications of, e.g., Smalley's studies, are interesting, a great deal more must be done before its role as a possible or significant candidate for the astrophysical evolution of carbon is clearly established. The PAH's, while having problems of their own in terms of universal acceptance, have much stronger support from the observational point of view. These large molecules, which in some ways may act like very small particles bearing a resemblance to graphite flakes, appear to provide some of the most important infrared emissions in our galaxy - as well as in others. Exactly how they are formed is not yet clear and, although circumstellar dust shells have most generally been suggested as the major source, their subsequent survival without modification in interstellar space seems to be difficult to understand in view of the many destructive processes, not only harsh ultraviolet but also shocks, in the less dense regions of space. The fact that the PAH's resemble graphite may be a hindrance rather than a support to their acceptance (which otherwise is quite reasonable) now that graphite itself has lost much of its basis for acceptance as an important component in interstellar space or in primitive solar system bodies.

Several pathways for manufacturing solid or at least large molecules by pure gas phase processes were suggested by Frenklach. A circumstellar wind model was

calculated with the result that it produced 1-2% of C in the form of PAH's. This would not be enough in the light of subsequent destructive processes but it is suggestive - a factor of 10 more would be helpful.

In addition to the theories of the formation of complex carbon and hydrocarbon clusters there were a number of discussions of the use of laboratory techniques for the investigation of carbon production, four in fact, by Smalley, Ulrich, Kroto and Saykally. Although a number of intriguing suggestions were made, the connection with the astronomical evolution of carbon and observational evidence remains to be further explored. The sophistication of the laboratory methods was, in some cases, remarkable.

The observational, theoretical and laboratory results on the photochemical evolution of interstellar dust were well summarized by Tielens and Allamandola. One of the major advances in the past 10 years has been that the physical and chemical evolution of the dust can not only be traced by infrared spectroscopy in a variety of space conditions - from diffuse clouds to molecular clouds to protostellar objects - but there are laboratory methods for following these processes for direct comparison. Photochemical and physical (heating/cooling) processing of simple mixtures of ices -  $H_2O$ ,  $CO$ ,  $NH_3$ ,  $CH_4$  - leads to the production of new molecules in various configurations whose infrared spectra mimic those of interstellar dust. The ultimate product of ultraviolet processing and heating of interstellar dust is a complex organic mixture which, at least in part, may resemble hydrogenated amorphous carbon. But, it also must contain molecules of direct prebiotic significance. Although it was not specifically mentioned at the meeting, the discovery of the cyanate ion  $OCN^-$  in the dust around a protostellar object leads to the suggestion that one of the basic building blocks of life could have been formed by the combination of the cyanate ion with cyanoacetylene (accreted from the gas) to form cytosine. And, since cytosine hydrolyzes quite readily to uracil, these reactions constitute a prebiotic synthesis of the pyrimidines.

Not only were the laboratory organic refractory spectra compared with interstellar infrared spectra but also various intermediate states which, by presumption, appear to provide a logical sequence of interstellar evolutionary steps leading from simple ices to complex organic compounds.

That there are many avenues by which complex and solid carbon, whether prebiotic or not, may be produced or evolve in space was a well covered topic. The problem of its survival is equally complex. At least one of the consequences to be drawn from the discussion by Seab of the estimated rate of destruction of solid carbon by shocks from the expansion of supernova blast waves is that the only likely form of carbon which can be replenished at an equal rate to its destruction is the organic refractory material formed in interstellar clouds.

A concomitant and exciting suggestion which Tielens made was that the same shocks which destroy particles may also partly convert graphite - if it exists in the first place - into diamond. Diamonds are hardly an organic form of carbon (even if they are a girl's best friend). But if they really can be produced in

sufficient abundance, there are some provocative and exotic aspects which, as small particles, their ultraviolet and infrared properties introduce into the interstellar dust extinction, scattering and absorption.

Finally, how do we see carbon playing a role in solar system chemistry? Carbon in comet Halley is now known to provide the major fraction of its dust. There is a vast variety of atomic and molecular compositions of the dust analyzed by the Particle Impact Analyzer (PIA) as summarized by Clark: pure organic (CHON) to mixed organic plus anorganic (rocky) Mg, Si, S, Fe with significantly different ratios of one element with respect to the other from particle to particle. There is no complete consensus of where and how these materials aggregated to form comets but there is no question that they must be at least similar to those of interstellar space. The chemical resemblance to interstellar dust and the fact that the comet dust particles for which mass spectra have been taken are individual micron and submicron sizes further suggests the interstellar dust connection. This is certainly a good working hypothesis. And, while the full data analysis is in progress, this must remain a topic for further detailed scientific investigation.

From the other end a comparison between Comet Halley dust and the meteorite materials, including the interplanetary dust particles (IDP's) collected in the upper atmosphere has provided additional connections. There appears to be a sequence from high to low carbon content going from Halley dust to IDP's to meteorites: from ~25% to ~5% to ~2%. This should tell us something about how these particles were born, how they have evolved, and where they come from. If we had included interstellar dust in the list their carbon content (in the refractory component) is the same as comet dust.

The porous IDP's are most representative of particles which appear to be of cometary origin. On the other hand Halley dust appears to be very different from carbonaceous chondrites.

Now we get to the first paper at the meeting on meteorites. Although, we believe that comets are the most primitive objects in the solar system, with IDP's perhaps next, meteorites provide the most abundant materials for detailed laboratory study of their chemical, isotopic and physical properties. In all cases we should, quoting Kerridge, "Note that, even in so-called primitive meteorites, there is no guarantee that primary material has not been altered by secondary processing." I think the same qualification may be borne in mind for all "primitive" material including comets, although the latter are indeed the most likely to be self preserving. As Kerridge pointed out, the carbon in meteorites is only a fraction of what was there originally. This makes it much more difficult to establish the sequence from pre-solar to meteoritic composition. Indirect approaches, studying mineralogy and isotopic composition, have been used to provide the evolutionary sequences.

The most abundant carbon in meteorites is organic. This seems very important. Are we seeing molecular forms which preserve or at least reflect their origins? This question can not easily be answered directly. The use of

isotopic abundances may provide the best tool. The D:H ratio is certainly important in the carbon. How and when did the hydrogen combine with the carbon? Are we seeing interstellar carbon? The isotopic ratios of the heavy noble gases Ar, Kr, Xe, found in meteorites also show that they have had a presolar origin. These gases appear to be concentrated in the carbonaceous fraction, a connection which suggests that they were first trapped in the organic refractory interstellar grain mantles in the pre solar (interstellar) molecular cloud and have been preserved in their original abundance by virtue of not having been too heavily metamorphosed by; for example, high temperatures. If this is true then the parent bodies of meteorites are cousins of comets with two of the basic differences in their compositions being due to the fact that the former ended up much more dense - perhaps because of self gravitation and certainly underwent more internal heating.

What we find out in the future about carbon in the galaxy will, as in the past, be based on observational, laboratory and theoretical investigations. Both the observational and laboratory approaches may be substantially improved by being extended into space as well as by making use of advanced technological applications to ground based astronomy. In space, removing the atmosphere curtain opens up a vast window to observe spectral features of complex gas and solid carbon species with spatial and spectral resolution heretofore unattainable. The Space Infrared Telescope Facility (SIRTF) is one of the major space observational instruments which will serve this purpose. For example, the infrared spectrum between 5  $\mu$  and 9  $\mu$ m encompasses some of the most important diagnostic features of complex organic molecules particularly those of prebiotic significance.

Space station opens up new experimental capabilities for the study of small particles - how they aggregate in vacuum; accretion and chemical photoprocessing of ice mantles. Nucleation experiments with possible relevance to particle growth should be of great interest. A true microgravity chamber will provide these possibilities as illustrated in Fogelman's summary.

In addition to the space observational facilities we should bear in mind the fact that future ground based millimeter and submillimeter opportunities to study molecules and dust with exceedingly high spatial resolution will provide information on chemical processes very close to the centers of star formation which must be important for our understanding of the formation of solar systems. After all, without planets there would be no life.

As we have seen already at this meeting, the capabilities of doing laboratory analog studies of relevance to the formation of carbon "stuff" in space has, in a sense, just begun to show its power. Whether or not all such approaches end up as being astrophysically important, the development of more and more techniques to study and understand carbon can not help but lead to useful results. It is clear that organic chemistry is of great relevance not only on the earth but in space as the interstellar dust, comet Halley and meteorites bear witness. Some of the connections are still tenuous but, with future space missions to comets and asteroids as well as to planets we may be sure that we will answer some of the questions of today.

I would like to conclude by saying that when a piece of comet is returned for detailed chemical, isotopic and morphological analysis all of the remarkable techniques which are now being developed for the study of IDP's and meteorites will be put to their ultimate test. Will we be capable of determining the original interstellar matter from which the solar system was created? On a microscale we may even be able to probe backwards an additional 4-5 billion years of the milky way evolution. And, finally, will we find or be capable of seeing the basic building blocks from which life on earth orginated?

**ABSTRACTS FROM CONTRIBUTED POSTER PAPERS**

The Possible Presence of Interstellar PAHs in Meteorites and  
Interplanetary Dust Particles

L.J. Allamandola<sup>1</sup>, S.A. Sandford<sup>1</sup>, and B. Wopenka<sup>2</sup>

<sup>1</sup>NASA-Ames Research Center, MS:245-6, Moffett Field, CA

<sup>2</sup>McDonnell Center for the Space Sciences and Dept. of Earth and  
Planetary Sciences, Washington University, St. Louis, MO

The Raman spectra of interplanetary dust particles (IDPs) collected in the stratosphere show two bands at about 1350 and 1600  $\text{Åcm}^{-1}$  and a broader feature between 2200 and 3300  $\text{Åcm}^{-1}$  that are characteristic of aromatic molecular units with ordered domains smaller than 25 Å in diameter (see Figure 1 and reference (1)). This suggests that the carbonaceous material in IDPs may be similar to the polymeric component seen in meteorites, where this material is thought to consist of aromatic molecular units that are randomly inter-linked by short aliphatic bridges (cf. reference (2)).

The features in the Raman spectra of IDPs are similar in position and relative strength to interstellar infrared emission features that have been attributed to vibrational transitions in free molecular polycyclic aromatic hydrocarbons (PAHs) (see Figure 2). The Raman spectra of some IDPs also showed photoluminescence (see Figure 1) that is similar to the excess red emission from some astronomical objects and that has also been attributed to PAHs and PAH-related materials. Moreover, a part of the carbonaceous phase in IDPs contains deuterium to hydrogen ratios that are far greater than those found in terrestrial samples (3). Deuterium enrichment is expected in small free PAHs that are exposed to ultraviolet radiation in the interstellar medium (1,4).

Taken together, these observations suggest that some fraction of the carbonaceous material in IDPs may have been produced in circumstellar dust shells and only slightly modified in interstellar space. Since many, if not most, IDPs come from comets, this supports the view that cometary material contains "primitive" components which can provide clues about early solar system (and perhaps even interstellar and circumstellar) processes.

References:

- (1) L.J. Allamandola, S.A. Sandford, and B. Wopenka (1987), *Science* **237**, 56-59.
- (2) R. Hayatsu and E. Anders (1981). *Top. Curr. Chem.* **99**, 1-37.
- (3) K.D. McKeegan, R.M. Walker, and E. Zinner (1985). *Geochim. Cosmochim. Acta.* **49**, 1971-1987.
- (4) L.J. Allamandola, A.G.G.M. Tielens, and J.R. Barker (1987). *Astrophys. J.*, submitted.
- (5) J. Bregman, L.J. Allamandola, J. Simpson, A. Tielens, and F. Witteborn (1984). *NASA/ASP Symposium on Airborne Astronomy*, NASA Conf. Pub. 2353.

Figure 1 - Examples of the Raman spectra of IDPs. Many spectra are dominated by the Raman bands of disordered carbonaceous material (see the top two spectra), while others are dominated by red luminescence (see the bottom two spectra). The relative contribution from these two effects varies from particle to particle. The designations F, S, and Lum in the figure label the first- and second-order Raman bands and red luminescence, respectively. The large increase in counts near 0  $\text{cm}^{-1}$  is from Rayleigh-scattered incident laser light. All the spectra shown were taken at a resolution of  $5 \text{ cm}^{-1}$  and the sample was excited by the  $5145\text{\AA}$  laser line of  $\text{Ar}^+$ . The upper axis indicates the absolute wavelength of the observed emission; the lower axis indicates the Raman shift (Stokes lines) with respect to the exciting-laser frequency. Figure adapted from reference (1).

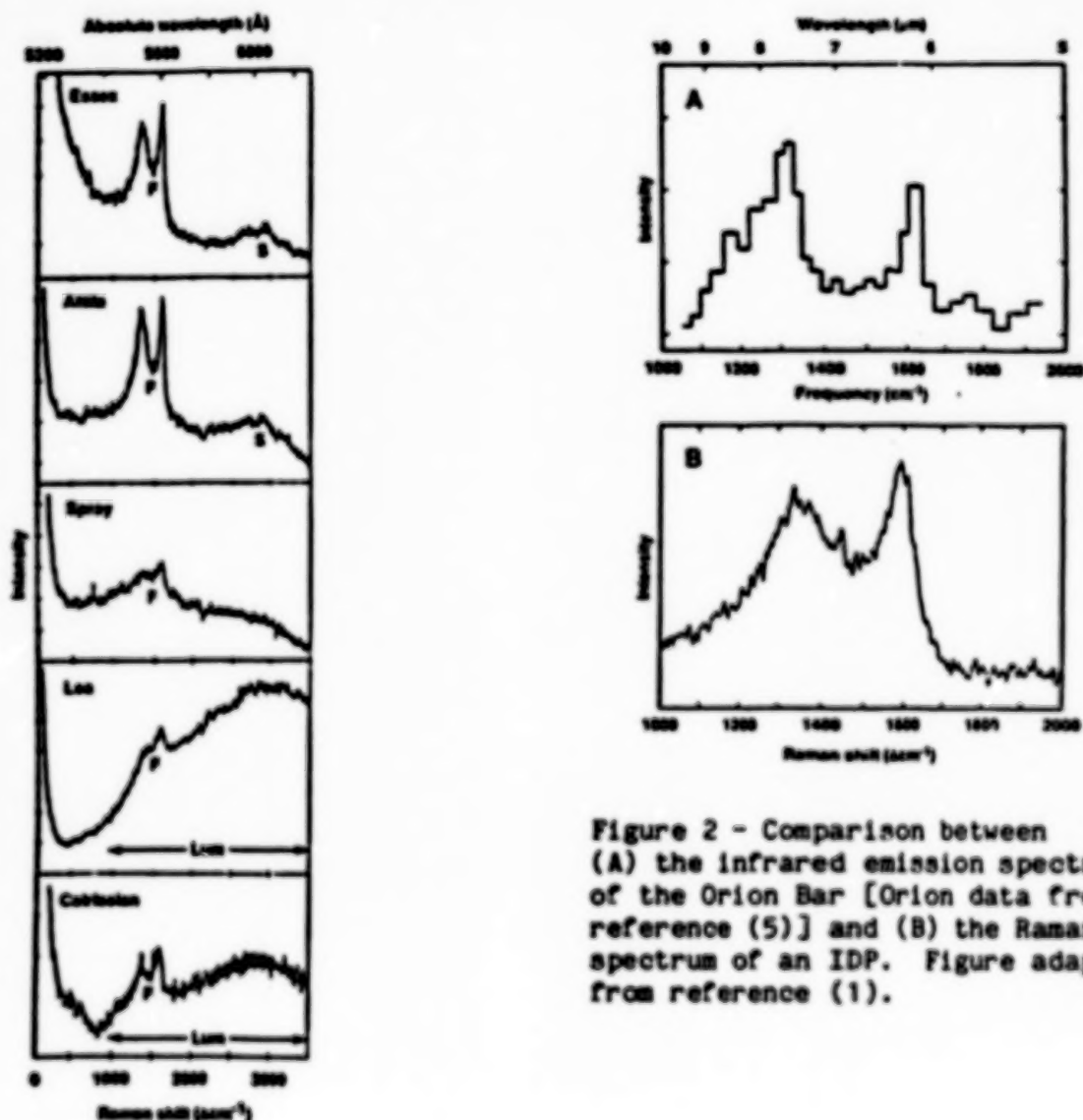


Figure 2 - Comparison between (A) the infrared emission spectrum of the Orion Bar [Orion data from reference (5)] and (B) the Raman spectrum of an IDP. Figure adapted from reference (1).

Laboratory Simulation of Interstellar Grain Chemistry and the  
Production of Complex Organic Molecules

L.J. Allamandola, S.A. Sandford, and G.J. Valero  
NASA-Ames Research Center, MS:245-6, Moffett Field, CA 94035

During the past 15 years considerable progress in observational techniques has been achieved in the middle infrared ( $5000\text{--}500\text{ cm}^{-1}$ ,  $2\text{--}20\text{ }\mu\text{m}$ ), the spectral region most diagnostic of molecular vibrations. Spectra of many different astronomical infrared sources, some deeply embedded in dark molecular clouds, are now available. These spectra provide a powerful probe, not only for the identification of interstellar molecules in both the gas solid phases, but also of the physical and chemical conditions which prevail in these two very different domains.

By comparing these astronomical spectra with the spectra of laboratory ices one can determine the composition and abundance of the icy materials frozen on the cold ( $10\text{K}$ ) dust grains present in the interior of molecular clouds (Allamandola, 1984; Tielens et al., 1984; Tielens and Allamandola, 1987). These grains and their ice mantles may well be the building blocks from which comets are made.

As an illustration of the processes which can take place as an ice is irradiated and subsequently warmed, we present the infrared spectra of the mixture  $\text{H}_2\text{O}:\text{CH}_3\text{OH}:\text{CO}:\text{NH}_3:\text{C}_6\text{H}_{14}$  (100:50:10:10:10). Apart from the last species, the ratio of these compounds is representative of the simplest ices found in interstellar clouds. The last component was incorporated into this particular experiment as a tracer of the behavior of a non-aromatic hydrocarbon. Figure 1 shows the change in the composition that results from ultraviolet photolysis of this ice mixture using a UV lamp to simulate the interstellar radiation field. Photolysis produces  $\text{CO}$ ,  $\text{CO}_2$ ,  $\text{CH}_4$ ,  $\text{HCO}$ ,  $\text{H}_2\text{CO}$ , as well as a family of moderately volatile hydrocarbons. As can be seen in Figures 2 and 3, less volatile carbonaceous materials are also produced.

Figure 2 shows the evolution of the infrared spectrum of the ice as the sample is warmed up to room temperature. We believe that the changes are similar to those which occur as ice is ejected from a comet and warmed up by solar radiation. The warm-up sequence shows that the nitrile or iso-nitrile ( $-\text{C}\equiv\text{N}$  or  $\text{C}\equiv\text{N}-$ ) bearing compound produced during photolysis evaporates between  $200$  and  $250\text{K}$ , suggesting that it is carried by a small molecular species. These molecules could be similar to the source material in Comet Halley that is ejected in grains into the coma, freed by sublimation, and photolyzed by solar radiation to produce the observed  $\text{C}\equiv\text{N}$  jets. The presence of several different types of  $-\text{CH}_3$  and  $-\text{CH}_2-$  bearing molecules in the residues is indicated by the spectral structure in the  $3000\text{--}2700\text{ cm}^{-1}$  ( $3.3\text{--}3.6\text{ }\mu\text{m}$ ) region (Figure 3). The profile and position of the " $3.4\text{ }\mu\text{m}$ " emission feature in Comet Halley shows that the carrier of the cometary band is dominated by  $-\text{CH}_3$  groups, while the band observed towards the galactic center and in this laboratory experiment implies the presence of  $-\text{CH}_2-$  dominated hydrocarbons.

PHOTOCHEMICAL EVOLUTION OF  
 $\text{H}_2\text{O} : \text{CH}_3\text{OH} : \text{NH}_3 : \text{CO} : \text{C}_6\text{H}_6$   
 100 : 50 : 10 : 10 : 10

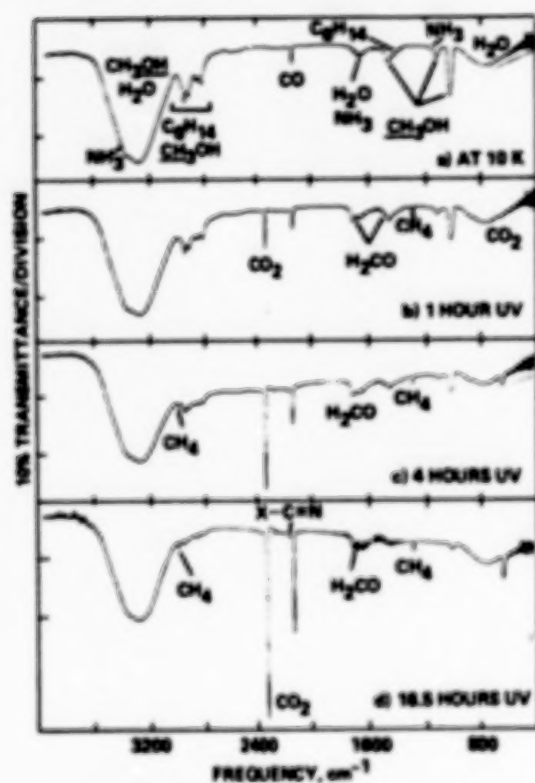


FIGURE 1

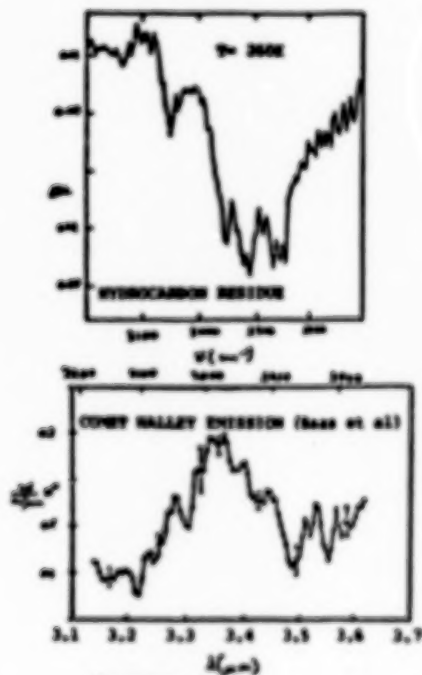


FIGURE 3

WARM-UP BEHAVIOR OF LOW VOLATILITY  
 RESIDUE PRODUCED BY 16 HOURS  
 PHOTOLYSIS OF  $\text{H}_2\text{O} : \text{CH}_3\text{OH} : \text{CO} : \text{NH}_3 : \text{C}_6\text{H}_6$   
 100 : 50 : 10 : 10 : 10

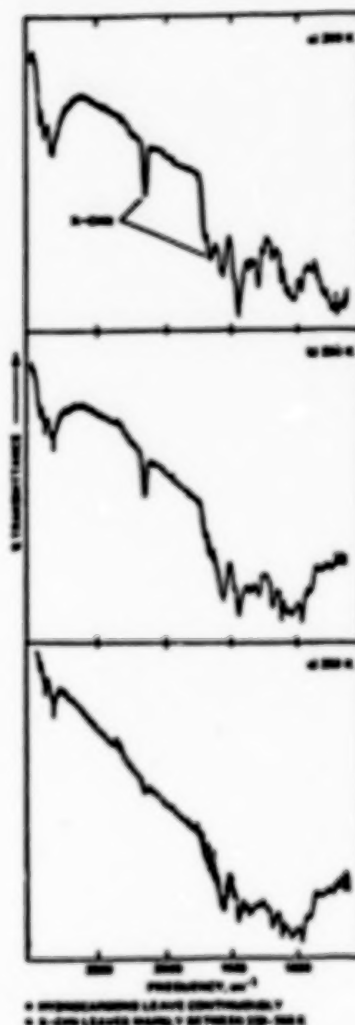


FIGURE 2

References:

- Allamandola, L.J. (1984), in *Galactic and Extra-galactic Infrared Spectroscopy*, ed. F. Kessler and J.P. Phillips (D. Reidel, Dordrecht), 5.
- Allen, D.A., and Wickramasinghe, D.T. 1971, *Nature* **234**, 239.
- Baas, F., Geballe, T.R., and Walther, D.M. 1986, *Astrophys. J.* **311**, 197.
- Jones, T.J., Hyland, A.L., and Allen, D.A. 1983, *Mon. Not. Roy. Astr. Soc.* **202**, 187.
- Tielens, A.G.G.M., and Allamandola, L.J. 1987, in *Physical Processes in Interstellar Clouds*, eds. G. Morfill and M. Scholer, (D. Reidel/Dordrecht), in press.
- Tielens, A.G.G.M., Allamandola, L.J., Bregman, J., Goebel, J., d'Hendecourt, L.B., and Witteborn, F.C. (1984), *Astrophys. J.* **287**, 697.

## NATURE AND ORIGIN OF INTERSTELLAR DIAMOND FROM THE ALLENDE CV3 METEORITE

David Blake\*, Friedemann Freund\*, Ted Bunch\*, Kannan Krishnan\*\*,  
Alexander Tielens\*, Mitch Stampfer\*\* and Sherwood Chang\*

\*NASA Ames Research Center, Moffett Field, CA 94035 USA

\*\*National Center for Electron Microscopy, Lawrence Berkeley Laboratory,  
Berkeley, CA 94720 USA

Recently, microscopic diamond was discovered in oxidized acid residues (the "C<sub>5</sub>" fraction) from several carbonaceous chondrite meteorites (Lewis et al., 1987). The presence in these residues of nitrogen, krypton and xenon ("CCFXe" or "XeHL") with anomalous isotopic compositions has been interpreted to mean that the diamond is interstellar in origin (Ott et al., 1981; Lewis et al., 1983). According to Lewis et al. (1987) the C<sub>5</sub> phase diamond may have formed under disequilibrium conditions by processes similar to those used in recent low-pressure laboratory diamond syntheses. In this abstract we present data and cite experimental evidence which support the contention that the C<sub>5</sub> diamonds may result from grain-grain collisions in supernova shocks in the interstellar medium.

Fragments of the Allende CV3 chondrite were acid-treated (HF/HCl/HClO<sub>4</sub>). A whitish powder was obtained. For the Analytical Electron Microscopy (AEM) a small drop of ethanol suspension was transferred onto holey carbon support films on 3 mm EM grids. The AEM was performed on transmission-thin fragments of the material which overlay holes in the film, to eliminate interference from the substrate. Electron Spectroscopy for Chemical Analysis (ESCA) was performed on a large aliquot of C<sub>5</sub>.

Diamond was identified by selected area electron diffraction. The *a* parameter calculated from the 7 most intense lines of diamond is 0.365 nm, about 2% larger than the ASTM value. Low magnification Transmission Electron Microscope (TEM) micrographs show that the diamond material commonly occurs as 10-300 nm aggregates of crystals. Bright and dark field imaging reveals 0.5-10.0 nm crystallites with an irregular morphology. Micro-micro diffraction using a 20 nm stationary probe yields a Debye-Scherrer powder pattern with superimposed single crystal spots which can be indexed as diamond. This result confirms the exceptionally small grain size of most crystals and the presence of a few larger individuals. High resolution TEM images of (111) planes of the C<sub>5</sub> phase diamond show a mosaic structure in which individual 2-4 nm crystallites are separated from one another by disordered interfacial regions.

Scanning Transmission Electron Microscope / Energy Dispersive X-ray (STEM-EDS) microanalyses of the C<sub>5</sub> diamond, using a light-element detector, show that oxygen and possibly nitrogen are the only impurities consistently present. ESCA spectra from bulk C<sub>5</sub> material confirm the presence of N at a level of 0.35 % or less. Under UV irradiation a yellow-red fluorescence is observed, consistent with that of natural diamonds

containing substitutional N. Electron Energy Loss Spectra (EELS) were recorded at 2 eV resolution from the C<sub>5</sub> diamond, high pressure synthetic diamond, a diamond film produced in a low pressure plasma by chemical vapor deposition (CVD) on a heated silicon substrate (Roy, 1987), graphite, and amorphous arc sputtered carbon. Comparison of the carbon K edge shape and fine structure shows the Allende C<sub>5</sub> phase to be largely diamond, but with a significant pre-edge absorption feature indicative of transitions of C 1s electrons into  $\pi^*$  orbitals which are absent in the purely  $sp^3$ -bonded diamond but present in graphite and amorphous carbon.

A comparison was made of ESCA spectra recorded from gem quality diamond, C<sub>5</sub> phase, graphite, and CVD diamond film. Both the CVD diamond film and the Allende C<sub>5</sub> spectra exhibit shake-up satellite peaks which arise from electron transitions into  $\pi^*$  energy levels which are not present in purely  $sp^3$ -bonded diamond. In addition, the C 1s peak of C<sub>5</sub> is significantly broader than that of either the CVD or gem quality diamond. The broadening of the C 1s peak for the C<sub>5</sub> is due to contributions from C atoms in slightly different environments such as in bulk diamond crystallites and in interfacial regions. The EELS pre-edge feature and the ESCA  $\pi \rightarrow \pi^*$  shake-up peaks are thought to originate from  $sp^2$  dangling bond type defects present in the synthetic CVD diamond films and associated with the interfacial regions of the C<sub>5</sub> phase diamond. This interpretation is supported by the calculated energy differences between bulk and free surface C atoms in diamond and the observed difference in the ESCA binding energies of the diamond surface (Vanderbilt and Louie, 1984; Morar et al., 1986).

According to Tielens et al. (1987) interstellar carbon grains, typically 10-300 nm in size, can be accelerated to velocities of the order of 10-100 km/sec behind shock waves from supernova explosions. Grain-grain collisions at these velocities will produce shock melting. Unloading of the melt droplets in the diamond stability field leads to rapid crystallization of 0.5-10 nm sized diamonds. R. Greiner (this Conference) has recently obtained diamonds of 3-7 nm in size in 10 km/sec explosive shock waves.

It remains to find diamond *in situ* in carbonaceous chondrite meteorites so that detailed petrographic investigations can be conducted. This research was sponsored in part by NASA, NRC, and DOE.

Lewis, R.S., et al.: 1983, *Nature* **305**, 767-771.

Lewis, R.S., et al.: 1987, *Nature* **326**, 160-162.

Morar, J.F., et al.: 1986, *Phys. Rev. B* **33**(2), 1346-1350.

Ott, U., et al.: 1981, *Geochim. Cosmochim. Acta* **45**, 1751-1788.

Roy, R.: 1987, *Nature* **325**, 17-18.

Tielens, et al.: 1987, *Ap. J. Lett.* **319**, 2103.

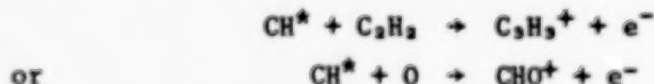
Vanderbilt, D. and Louie, S.G.: 1984, *Phys. Rev. B* **30**(10), 6118-6130.

# AN IONIC MECHANISM OF CARBON FORMATION IN FLAMES

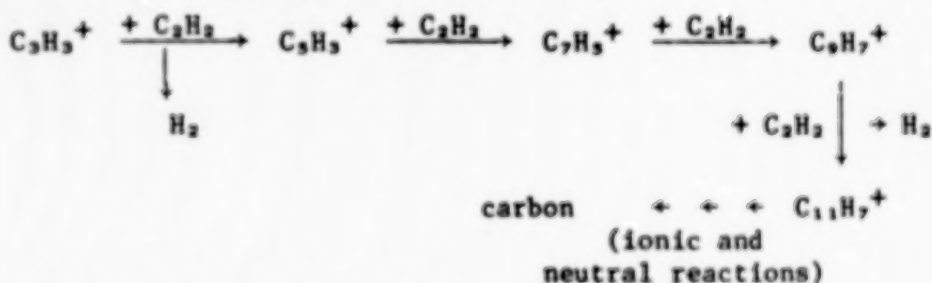
H.F. Calcote

AeroChem Research Laboratories, Inc., P.O. Box 12,  
Princeton, New Jersey 08542

The formation of incipient carbon in flames can be described by a series of elementary reactions in which the precursor of soot is the ion  $C_3H_3^+$ , and the major building block is acetylene, polyacetylenes, or other hydrocarbon fragments which are present in large concentrations. The precursor ion is produced by nonequilibrium chemi-ionization reactions, e.g.



The  $CHO^+$  rapidly becomes  $C_3H_3^+$  through a series of ion-molecule reactions. The chemi-ion then adds acetylene in a series of very rapid ion-molecule reactions producing larger and larger ions:



Ions isomerize very rapidly to produce aromatic structures overcoming one of the major problems with neutral species mechanisms: how to form the first carbon ring. As the ions grow, their recombination rate coefficients with electrons increase so that the larger ions are removed by dissociative recombination:



These neutral species now continue to grow by the addition of more acetylene producing even larger neutral species. With increasing size, the rate coefficient of electron attachment also increases causing the reaction



to become important, depending upon the temperature. Appreciable concentrations of negative ions shift the ion removal process to dissociative ion-ion recombination:



which is orders of magnitude slower than ion-electron recombination. As the neutral species continue to grow by the addition of acetylene, they gradually take on the aspect of particles, i.e., the bulk properties of the substance  $C_{x,y}H$  dominate over the chemical properties. This change is gradual and there is no distinct size at which a large molecule becomes a particle.

Evidence will be presented supporting the above mechanism. All of the ions proposed in the mechanism have been observed by mass spectrometric analysis, their concentrations measured, and their rates of reaction in the flame environment determined to be adequate to account for the observed rate of formation of carbon.

## ON PLANETARY NEBULAE AS SOURCES OF CARBON DUST: INFRARED EMISSION FROM PLANETARY NEBULAE OF THE GALACTIC HALO

Harriet L. Dinerstein and Daniel F. Lester  
Astronomy Department and McDonald Observatory,  
University of Texas, Austin, Texas 78712-1083 USA

Planetary nebulae of the galactic disk are generally seen to emit a thermal continuum due to dust grains heated by stellar and nebular photons. This continuum typically peaks between 25 and 60  $\mu\text{m}$ , so that the total power emitted by the dust is sampled well by the broad-band measurements made by IRAS. We examine here the characteristics of the infrared emission from the four planetary nebulae which are believed on the basis of their low overall metallicities to belong to the halo population. These nebulae are of particular interest because they are the most metal-poor ionized nebulae known in our Galaxy, and offer the opportunity to probe possible dependences of the dust properties on nebular composition. We present fluxes extracted from co-addition of the IRAS data\*, as well as ground-based near infrared measurements. Each of the four halo objects, including the planetary nebula in the globular cluster M15, is detected in at least one infrared band. We compare the estimated infrared excesses of these nebulae (IRE, the ratio of measured infrared power to the power available in the form of resonantly-trapped Lyman alpha photons) to those of disk planetary nebulae with similar densities but more normal abundances. Three of the halo planetaries have IRE values similar to those of the disk nebulae, despite the fact that their Fe- and Si-peak gas phase abundances are factors of 10-100 lower. However, these halo nebulae have normal or elevated C/H ratios, due to nuclear processing and mixing in their red giant progenitors. Unlike the other halo planetaries, DDDM1 is deficient in carbon as well as in the other light metals. This nebula has a substantially lower IRE than the other halo planetaries, and may be truly dust deficient. We suggest that the deficiency is due to a lack of the raw material for producing carbon-based grains, and that the main bulk constituent of the dust in these planetary nebulae is carbon.

\*The co-additions were carried out at the Infrared Processing and Analysis Center (IPAC), funded by NASA as part of the IRAS Extended Mission program. This research was supported in part by NASA Contract 957285, through the Jet Propulsion Laboratory.

## IMPACT FRACTURE EXPERIMENTS SIMULATING INTERSTELLAR GRAIN-GRAIN COLLISIONS

Friedemann Freund, Sherwood Chang and J. Thomas Dickinson\*

NASA Ames Research Center, MS 239-4, Moffett Field, CA 94035 USA

\* Dept. of Physics, Washington State University, Pullman, WA 99164 USA

Oxide and silicate grains condensing during the early phases of the formation of the solar system<sup>1</sup> or in the outflow of stars are exposed to high partial pressures of the low-z elements H, C, N and O and their simple gaseous compounds. Though refractory minerals are nominally anhydrous and non-carbonate, if they crystallize in the presence of H<sub>2</sub>O, N<sub>2</sub> and CO or CO<sub>2</sub> gases, they dissolve traces of the gaseous components<sup>2-5</sup>.

The question arises: How does the presence of dissolved gases or gas components manifest itself when grain-grain collisions occur? What are the gases emitted when grains are shattered during a collision event?

We report on fracture experiments in ultrahigh vacuum (UHV,  $\leq 10^{-8}$  mbar) designed to measure (by means of a quadrupole mass spectrometer, QMS, with  $\mu$ s to ms time resolution) the emission of gases and vapors during and after impact (up to 1.5 sec)<sup>6</sup>. Two terrestrial materials were chosen which represent structural and compositional extremes: olivine (San Carlos, AZ), a densely packed Mg-Fe<sup>2+</sup> silicate from the upper mantle, available as 6-12 mm single crystals, and obsidian (Oregon), a structurally open, alkaline-SiO<sub>2</sub>-rich volcanic glass. In the olivine crystals OH<sup>-</sup> groups have been identified spectroscopically<sup>7</sup>, also H<sub>2</sub> molecules<sup>8</sup>. Obsidian is a "water"-rich glass containing OH<sup>-</sup> besides H<sub>2</sub>O molecules. Olivine from the mantle often contains CO<sub>2</sub>, either as CO<sub>2</sub>-rich fluid in fluid inclusions<sup>9,10</sup> or structurally dissolved<sup>5</sup> or both. By analogy to synthetic glasses CO<sub>2</sub> in the obsidian may be present in form of CO<sub>2</sub> molecules in voids of molecular dimensions, or as carbonate anions, CO<sub>3</sub><sup>2-</sup>. No organic molecules have been detected spectroscopically in either material.

Fig. 1 shows six QMS scans, each 80 ms, of the gas emission from an olivine crystal upon impact fracture. The top scan represents the residual gas spectrum in the UHV system composed mainly of H<sub>2</sub>, H<sub>2</sub>O, N<sub>2</sub>/CO and CO<sub>2</sub>. Fracture occurred during the second scan near mass 60 m/e (*t*=0) and is followed by a strong emission of organic fragments at 65, 77, 91 and 105 e/m, the latter probably due to benzaldehyde. The next scan (40-110 ms after fracture) shows a slightly elevated H<sub>2</sub>, a strong H<sub>2</sub>O, a moderate N<sub>2</sub>/CO emission, but little CO<sub>2</sub>, while the organic fragments still have high intensities and remain measureable even 1150-1230 ms after fracture. Olivine fracture often also led to a long lasting ( $\leq 300$  ms) emission of Mg (possibly Fe) vapor similar to MgO fracture<sup>6</sup>. In the case of obsidian we observed simultaneous emission of reduced gases such as H<sub>2</sub>, CH<sub>4</sub>, CO plus Na and K vapor besides H<sub>2</sub>O, O<sub>2</sub>, (possibly O) and CO<sub>2</sub>.

These results indicate that refractory oxide/silicates which contain dissolved traces of the H<sub>2</sub>O and CO/CO<sub>2</sub> components but no spectroscopically detectable traces of organics may release complex H-C-O (possibly H-C-N-O) molecules upon fracture, plus metal vapor.

This points (1) at complex reaction mechanisms between dissolved H<sub>2</sub>O, CO/CO<sub>2</sub> (and N<sub>2</sub>) components within the mineral structure or during fracture and (2) at the possibility that similar emission processes occur following grain-grain collisions in interstellar dust clouds.

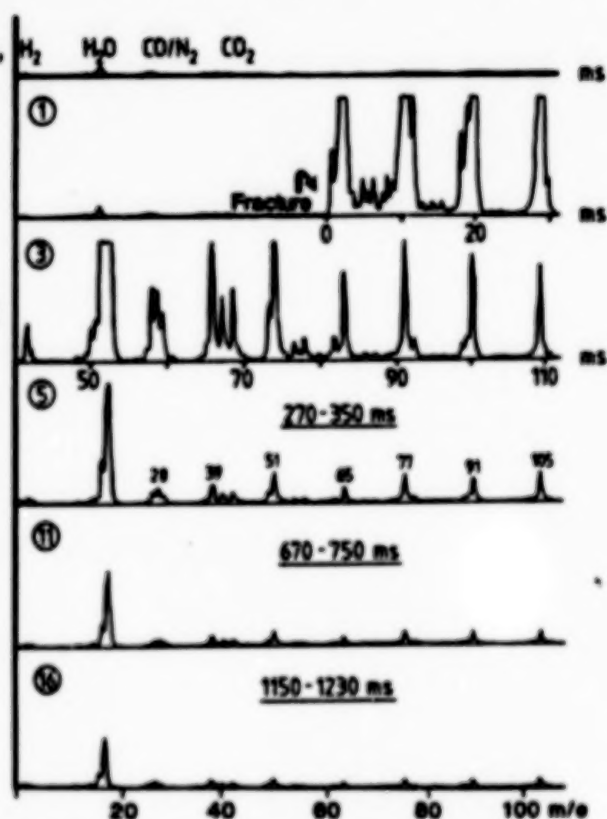


Fig. 1: Impact fracture gas emission in from a San Carlos olivine single crystal

- (1) Grossman, L. 1977, in: NASA Spec. Publ. 370, 587; (2) Martin, R.F. and Donney, G. 1972, *Amer. Mineral.* 57, 554; (3) Wilkins, R.W.T. and Sabine, W. 1973, *Amer. Mineral.* 58, 508; (4) Stolper E. 1982, *Geochim. Cosmochim. Acta* 46, 2609; (5) Freund, F. 1987, *Phys. Chem. Minerals* in press; (6) Dickinson, J.T., Jensen, L.C., McKay, M.R. and Freund, F. 1986, *J. Vac. Sci. Technol.* A4, 1648; (7) Beran, A. and Putnis, A. 1983, *Phys. Chem. Minerals* 9, 57; (8) Freund, F. and Oberheuser, G. 1986, *J. Geophys. Res.* 91, 745; (9) Roedder, E. 1984, *Rev. Mineral.* 12, 503; (10) Bergman, S.C. and Dubessy, J. 1984, *Contrib. Mineral. Petrol.* 85, 1.

## DIAMONDS IN DETONATION SOOT

N. Roy Greiner,\* Dave Phillips,\* J. D. Johnson,\* and Fred Volk\*\*

\*Los Alamos National Laboratory, Los Alamos, NM 87545

\*\*Fraunhofer-Institut für Treib- und Explosivstoffe, D-7507  
Pfinztal/Berghausen, West Germany

Diamonds 4-7 nm in diameter have been identified and partially isolated from soot formed in detonations of carbon-forming composite explosives. The morphology of the soot has been examined by transmission electron microscopy (TEM), and the identity of the diamond has been established by the electron diffraction pattern of the TEM samples and by the X-ray diffraction (XRD) pattern of the isolated solid. Graphite is also present in the form of ribbons of turbostratic structure with a thickness of 2-4 nm. A fraction, about 25% of the soot by weight, was recovered from the crude soot after oxidation of the graphite with fuming perchloric acid. This fraction showed a distinct XRD pattern of diamond and the diffuse band of amorphous carbon. The IR spectrum of these diamonds closely matches that of diamonds recovered from meteorites (Lewis et al., 1987), perhaps indicating similar surface properties after the oxidation. If these diamonds are produced in the detonation itself or during the initial expansion, they exhibit a phenomenal crystal growth rate ( $5 \text{ nm}/0.00001 \text{ s} = 1.8 \text{ m/hr}$ ) in a medium with a very low hydrogen/carbon ratio. Because the diamonds will be carried along with the expanding gases, they will be accelerated to velocities approaching 8 km/s.

R. S. Lewis, T. Ming, J. F. Wacker, E. Anders, and E. Steel: 1987, *Nature* **326**, 160-162.

## Probing the Possibility of a $^{12}\text{C}/^{13}\text{C}$ Galactic Abundance Gradient

*Isabel Hawkins, IGPP*

*Lawrence Livermore National Laboratory*

I have performed high  $S/N$  ( $\geq 500$ ) observations of interstellar  $\text{CH}^+$  with the 3.0 m telescope at Lick Observatory, and the 4.0 m telescope at CTIO, of the reddened, early-type stars *HD 183143*, *HD 24432*, and *HD 157038* in an effort to probe the existence of a  $^{12}\text{C}/^{13}\text{C}$  abundance gradient in our Galaxy. Previous very high quality optical observations of interstellar  $\text{CH}^+$  toward five stars within 1 kpc of the Sun have yielded a precise weighted mean  $^{12}\text{C}/^{13}\text{C}$  isotope ratio of  $43 \pm 4$  ( $1\sigma$ ) (Hawkins, Jura, and Meyer 1985; Hawkins and Jura 1987). The isotope ratios derived toward four lines of sight in the local ISM are uniform within 12%. The similarity among these carbon isotope ratios determined in diffuse clouds possessing different physical conditions precludes the possibility that the  $\text{CH}^+$  molecule is suffering from isotope selective effects in these regions. The precise  $^{12}\text{C}/^{13}\text{C}$  derivable from high quality observations of  $^{12}\text{CH}^+$  and  $^{13}\text{CH}^+$  provide the unique opportunity to probe the homogeneity of the ISM in a large scale and the history of nucleosynthesis in our Galaxy. Since  $\text{CH}^+$  seems to be the most sensitive probe of  $^{12}\text{C}/^{13}\text{C}$  in the diffuse ISM, observations toward more distant stars located up to 2.5 kpc from the Sun are the best way to study the possibility of a Galactic  $^{12}\text{C}/^{13}\text{C}$  abundance gradient. I obtained 4232 Å data toward all three of the stars mentioned above, 3957 Å data toward *HD 183143* and *HD 157038*, and 3745 Å data toward *HD 157038*. Because of the poorer quality of the *HD 24432* spectrum, and its weaker  $\text{CH}^+$  absorption lines, the satellite  $^{13}\text{CH}^+$  line was not detected, and thus only a lower limit on the  $^{12}\text{C}/^{13}\text{C}$  ratio toward this star was obtained. However, the data toward the other two stars have yielded clean detections of this weak isotopic species. Observations of at least the (0,0) and (1,0)  $\text{CH}^+$  bands, and preferably also of the (2,0) band, are required to ascertain the amount of  $\text{CH}^+$  saturation and to perform a reliable curve-of-growth analysis. The results obtained from careful reduction and analysis of the data toward these stars in the Northern and Southern Hemispheres are presented.

### References

- Hawkins, I., Jura, M. and Meyer, D. M.: 1985, *Ap. J. (Letters)*, **294**, L131.  
Hawkins, I. and Jura, M.: 1987, *Ap. J.*, **317**, 926.

## NEW OBSERVATIONS OF INTERSTELLAR ORGANIC MOLECULES

W.M. Irvine,\* P. Friberg,\*\* H.E. Matthews,\*\*\* Y.C. Minh\* and L.M. Ziurys\*

\*Five College Radio Astronomy Observatory, University of Massachusetts, Amherst, MA 01003 USA

\*\*Onsala Space Observatory, Onsala, Sweden S-43900

\*\*\*Herzberg Institute of Astrophysics, NRC, Ottawa, Canada K1A 0R6

We report new observations of 3 carbon-containing interstellar molecules which play an important role in the chemistry of dense molecular clouds: protonated carbon dioxide, formic acid, and propynal.

In 1984 a new oxide of carbon,  $C_2O$ , was discovered in the interstellar medium (Matthews et al. 1984; Brown et al. 1985). Theoretical models suggest that  $C_2O$  is produced by dissociative electron recombination with the ion  $H_2C_2O^+$ . Although no laboratory data for the branching ratios of such a recombination exist, it seemed to us likely that additional products would include  $H_2C_2O$ . This molecule has more than one isomeric form, but one stable species is propynal ( $HC_3CHO$ ), which had been suggested as a possible interstellar molecule by Winnewisser (1973). In observations at the National Radio Astronomy Observatory 43 m telescope in Green Bank earlier this year, we detected a line in the cold cloud TMC-1 which we assign to the  $2(0,2)-1(0,1)$  transition of propynal. The observed line agrees with the laboratory frequency to well within the experimental uncertainty, a few parts in  $10^7$ . We sought and failed to detect the corresponding  $2(1,1)-1(1,0)$  line, which is understandable given the presence of both a and b components of the electric dipole moment in propynal. The b type transitions will drain population from energy levels with  $K_p \neq 0$  into the  $K_p = 0$  stack. If our assignment is correct, this is the first interstellar detection of propynal. Assuming typical rotational temperatures for TMC-1 and that the line is optically thin, the column density determined is about  $5 \times 10^{12} \text{ cm}^{-2}$ , or about three times that for  $C_2O$ .

Formic acid ( $HCOOH$ ) was the first organic acid to be observed in the interstellar medium, in the Galactic center source Sgr B2. The only other interstellar detection has been recently made in the giant molecular cloud in Orion. As part of the same project that led to the detection of propynal, we sought formic acid in the nearby, cold dark clouds TMC-1 and L134N. It is seen only in L134N. This difference

between the two clouds appears to be consistent with a model in which the oxygen/carbon ratio is higher in L134N. This would be consistent with the higher abundances for SO and SO<sub>2</sub> observed in that cloud, and the higher abundances of many carbon-rich species in TMC-1 (Irvine et al. 1985).

Considerable uncertainties remain as to the principal repositories of carbon in dense molecular clouds. Carbon monoxide is the most abundant detected molecule in the gas phase, but typically seems to account for only about 10% of the cosmic complement of carbon. There is little observational evidence concerning the fraction of carbon in hydrocarbons, although Knacke et al. (1985) have shown that CH<sub>4</sub>/CO < 10<sup>-2</sup> toward two infrared sources embedded in dense molecular clouds. It is difficult to directly assess the importance of carbon dioxide as a carbon reservoir, because this molecule lacks a permanent electric dipole moment and hence pure rotational transitions. The CO<sub>2</sub> abundance may be estimated, however, from that of its protonated ion, HCO<sub>2</sub><sup>+</sup>. Heretofore HCO<sub>2</sub><sup>+</sup> has been detected only toward the Galactic Center (Thaddeus, Guélin and Linke 1981). To assess the situation in other molecular clouds, we have conducted a search for HCO<sub>2</sub><sup>+</sup> in a number of both giant molecular clouds and cold dark clouds. We have failed to detect protonated carbon dioxide in any source outside of the Galactic Center, where, curiously enough, it is quite extended over a region about 10x10 arcmin. Even in Sgr B2, however, we estimate that CO is about an order of magnitude more abundant than CO<sub>2</sub>. In other regions, the difference appears to be even larger. Thus, CO<sub>2</sub> does not appear to be a significant carbon reservoir in the gas phase in interstellar molecular clouds.

This research was supported in part by NASA grant NAGW-436.

#### REFERENCES:

- Brown, R. D., Godfrey, P. D., Cragg, D. M., Rice, E. H. N., Irvine, W. M., Friberg, P., Suzuki, H., Ohishi, M., Kaifu, W., and Morimoto, M.: 1985, Ap. J., **297**, 302.
- Irvine, W. M., Schloerb, F. P., Hjalmarsen, A., and Herbst, E.: 1985, in Protostars and Planets II, ed. D. C. Black and M. S. Matthews (U. Arizona, Tucson) pp. 579-620.
- Knacke, R. F., Geballe, T. R., Noll, K. S., and Tokunaga, A. T.: 1985, Ap. J. (Lett.), **298**, L67.
- Matthews, H. E., Irvine, W. M., Friberg, P., Brown, R. D., and Godfrey, P. D.: 1984, Nature, **310**, 125.
- Thaddeus, P., Guélin, M., and Linke, R. A.: 1981, Ap. J. (Lett.), **246**, L41.
- Winnewisser, G.: 1973, J. Mol. Spec., **46**, 16.

## SEARCH FOR INTERSTELLAR METHANE

R. F. Knacke,\* Y. H. Kim,\* K. S. Noll<sup>†</sup> and T. R. Geballe\*\*

\*SUNY, Stony Brook

\*\*UKIRT

We have searched for interstellar methane in the spectra of infrared sources embedded in molecular clouds. New observations of several lines of the P and R branches of the  $\nu_3$  band of  $\text{CH}_4$  near 3.3 microns give column densities in the range  $N < 1^{-2} \times 10^{-16} \text{ cm}^{-2}$ . Resulting abundance ratios are  $(\text{CH}_4)/(\text{CO}) < 3.3 \times 10^{-2}$  toward GL961 in NGC 2244 and  $< 2.4 \times 10^{-3}$  toward GL989 in the NGC 2264 molecular cloud. The limits, and those determined in earlier observations of BN in Orion and GL490, suggest that there is little methane in molecular clouds. The result agrees with predictions of chemical models. Exceptions could occur in clouds where oxygen may be depleted, for example by  $\text{H}_2\text{O}$  freezing on grains. The present observations probably did not sample such regions.

## RAMAN SPECTROSCOPIC STUDIES OF CARBON IN EXTRA-TERRESTRIAL MATERIALS

John Macklin,\* Donald Brownlee,\* Sherwood Chang\*\*  
and Ted Bunch\*\*

\*Departments of Chemistry and Astronomy, respectively  
University of Washington, Seattle, WA 98195 USA

\*\*NASA Ames Research Center, Moffett Field, 94035 USA

The measurements obtained in this work indicate ways in which micro-Raman spectroscopy can be used to elucidate structural characteristics and distribution of carbon in meteorites and interplanetary dust particles (IDPs). Existing information about structurally significant aspects of Raman measurements of graphite (Lespade, *et al.*, 1984 and Vidano and Fishbach, 1978) is combined with structurally relevant findings from the present micro-Raman studies of carbons prepared by carbonization of polyvinylidene chloride (PVDC) at various temperatures (Ban, *et al.*, 1975) and natural material, as well as several acid residues, from the Allende and Murchison meteorites in order to establish new spectra-structure relationships. Structural features of many of the materials in this study have been measured by X-ray analysis and electron microscopy; thus, their structural differences can be directly correlated with differences in the Raman spectra. The spectral parameters consequently affirmed as indicators of structure are used as a measure of structure in materials that have unknown carbon structure, especially IDPs.

The unique applicability of micro-Raman spectroscopy is realized not only in the ability to conveniently measure spectra of micron-sized IDPs, but also micron-sized parts of an inhomogeneous material. For example, Raman measurements at visibly distinct features across a microtomed section of an Allende meteorite sample give similar carbon spectra and various bands attributable to mineral suggesting that the structure of carbon in the sample is uniform and independent of its environment. Another example is given by measurements of bright appearing microcrystalline regions of a Murchison acid residue. An unusual sharp band is sometimes observed between 1300 and 1350  $\text{cm}^{-1}$  in these spectra that can be assigned as due to diamond. This feature could not be observed in bulk measurement. Moreover, micro-Raman spectra can be correlated with other micro-measurements at the same position on the sample.

Microcrystalline graphite is known to give Raman spectra that differ dependent on crystallite size (see e.g., Lespade, *et al.*, 1984, or Nemanich and Solin, 1979). The spectral changes that accompany decreasing particle size include increase in the ratio (R) of the intensity of the band near 1350  $\text{cm}^{-1}$  (D band) to that of the band near 1600  $\text{cm}^{-1}$  (G band) increase in the half width of the D band (wD) increase in the frequency maximum of the G band and increase in the half-width (wG) of the 2nd order band near 2700  $\text{cm}^{-1}$  (G') band.

## CAN THE CHIRALITY OF THE ISM BE MEASURED?

Y. Pendleton, S. Sandford, M. Werner, J. Lauer, and S. Chang  
NASA Ames Research Center, Moffett Field, California 94035 USA

Many moderately complex carbon-based molecules of the type associated with biological systems can exist in one of two mirror-image forms (left-handed and right-handed), which can be distinguished on the basis of their influence on the state of polarization of a light beam. Both forms are possible in nature; yet in living organisms it is invariably the rule that one of the two species predominates. This gives rise to a net "chirality". One possible explanation for the net chirality is that the early earth was somehow "seeded" from the ISM with an excess of chiral organic compounds which led to the development of life forms which are based on left-handed amino acids and right-handed sugars.

Molecular spectroscopy of the interstellar medium (ISM) has revealed a complex variety of molecular species similar to those thought to have been available in the oceans and atmospheres of the earth at the time life formed. The detection of such molecules demonstrates the generality of the chemical processes occurring in both environments. If this generality extends to the processes which produce chirality, it may be possible to detect a net chirality in the ISM. This is of particular interest because determining whether or not net chirality exists elsewhere in the universe is an essential aspect of understanding how life developed on earth and how widely distributed it might be. We report preliminary results of a feasibility study to determine whether or not a net chirality in the ISM can be measured.

A net excess of chiral molecules, i.e., a solution of one of the two enantiomeric forms, can affect the transmittance of polarized light in the following ways. The complex index of refraction,  $m=n+ik$ , of the material through which the light passes will cause differing effects for the left and right handed components of circularly polarized light (CPL). In the infrared, the absorption, which is governed by the imaginary component,  $k$ , can be greater for either the left or right hand component of CPL if there is a net chirality. Differences in the relative absorption of the right and left hand CPL components by enantiomerically pure solutions has been demonstrated in the laboratory at infrared wavelengths and is referred to as vibrational circular dichroism (VCD). This effect has been successfully detected by Freedman and Naife (1986) in the study of relatively simple molecules similar to the types of molecules likely to exist in the interstellar medium. However, the effect is a small one for the molecules which have been tested to date and further work is required to estimate the magnitude of such an effect for molecules which would be of astrophysical interest.

A related effect of chiral molecules on polarized light is governed by the real compo-

ment of the complex index of refraction,  $n$ . As the two components of CPL propagate through a medium consisting primarily of either right or left handed molecules, the configuration of the molecule presented to the right hand component of CPL will differ from that presented to the left hand component of CPL. This condition translates to a situation where one component of the light is able to traverse the medium faster than the other resulting in an overall phase shift between the two components. In the case of linearly polarized light, which can be thought of as a superposition of equal amounts of right and left hand circularly polarized light with a fixed phase relation, such a phase shift would cause a rotation in the plane of polarization. This effect would be detectable as a change in the plane of polarization, relative to that at adjacent wavelengths, in the appropriate spectral bands of chiral molecules.

Laboratory studies of both the VCD effect and the rotation of the polarization plane of linearly polarized light have not been carried out for molecules of astrophysical interest. However, it is encouraging to note that at the present time several groups are studying VCD in order to better understand molecular structure. Ideally one would hope to find a noticeable effect among simple molecular structures since it is those types of molecules that are likely to be present in the ISM. Freedman *et al.* (1987) report the detection of VCD effects in deuterated  $C_2OH_4$ , a simple molecule that may help to predict the magnitude of the effect of VCD that could be expected for molecules likely to exist in space. In addition to analyzing the VCD effect of such molecules, we plan to investigate the effective rotation of linearly polarized light through enantiomerically pure solutions of simple molecules. If the effect is significant, one could look for the effect in astrophysically interesting molecules along lines of sight where strong background sources of linearly polarized infrared light can be seen through molecular clouds. The infrared portion of the spectrum is more suitable than the visible region for such a study since the longer wavelength infrared light from young stellar objects can penetrate the high molecular density of the material surrounding them. Nature has provided linearly polarized background sources known as infrared reflection nebulae (Werner *et al.* 1983; Pendleton *et al.* 1986). Infrared reflection nebulae are regions of high linear polarization caused by the scattering of light from a nearby, dust embedded pre-stellar object. These regions are seen through large column densities of dust and gas which could contain molecules of interest to this study. If laboratory results identify candidate chiral molecules that might exist in the ISM, the next step in this feasibility study will be to estimate the detectability of the chiral signature in astrophysical environments.

Freedman, T., Paterlini, M., Lee, N., and Naife, L.: 1987, *J. Am. Chem. Soc.* **109**, 4727.

Freedman, T. and Naife, L.: 1987, *Topics in Stereochem.* **17**, 113.

Pendleton, Y., Werner, M., Capps, R., and Lester, D.: 1986, *Ap. J.* **311**, 360.

Werner, M., Dinerstein, H., and Capps, R.: *Ap.J. (Letters)*, **265**, L13.

## ON DIAMOND, GRAPHITIC AND AMORPHOUS CARBONS IN PRIMITIVE EXTRATERRESTRIAL SOLAR SYSTEM MATERIALS.

Frans J. M. Rietmeijer, Department of Geology, University of New Mexico, Albuquerque, NM 87131, U.S.A.

Carbon is among the most abundant elements in the universe and carbon chemistry in meteorites<sup>1</sup> and comets<sup>2</sup> is an important key to understanding many Solar System and interstellar processes<sup>3</sup>. Yet, the mineralogical properties and interrelations between various structural forms of elemental carbon remain ambiguous. Crystalline elemental carbons include rhombohedral graphite, hexagonal graphite, cubic diamond, hexagonal diamond (i.e. lonsdaleite or carbon-2H) and chaoite. Elemental carbon also occurs as amorphous carbon and poorly graphitised (or turbostratic) carbon but of all the forms of elemental carbon only graphite is stable under physical conditions that prevail in small Solar System bodies and in the interstellar medium.

The recent discovery of cubic diamond in carbonaceous chondrites<sup>4,5</sup> and hexagonal diamond in chondritic interplanetary dust particles (IDPs)<sup>6</sup> have created a renewed interest in the crystalline elemental carbons that were not formed by shock processes on a parent body. For example, cubic diamond in carbonaceous chondrites may have an interstellar origin<sup>4</sup> and hexagonal diamond in chondritic IDPs could result from low-temperature aqueous alteration processes<sup>6</sup>. In addition, amorphous and poorly graphitised carbons (PGCs) are common constituents of primitive Solar System materials<sup>7-10</sup>. These elemental carbons have been identified by conventional transmission electron microscope (TEM) imaging and selected area electron diffraction (SAED).

Another technique, Raman spectroscopy, confirms a widespread occurrence of "disordered graphite" in the Allende carbonaceous chondrite<sup>11</sup> and in chondritic IDPs<sup>3</sup>. Elemental carbons have also been identified by their characteristic K-edge features in electron energy loss spectra (EELS)<sup>5</sup>. However, the spectroscopic data do not necessarily coincide with those obtained by SAED. This has led to propositions for disequilibrium formation of elemental carbons in meteorites<sup>5</sup>. For example, the shape and structure of the carbon K-edge in EELS spectra from carbon in an acid residue from the Allende chondrite show signatures of both diamond ( $sp^3$  bonds) and amorphous carbon<sup>5</sup>.

In order to interpret these data in terms of rational crystalline structures, it may be useful to consider the principles underlying electron diffraction and spectroscopic analyses. Electron diffraction depends on electron scattering, on the type of atom and the distance between atoms in a crystal lattice. Spectroscopic data are a function of the type of atom and the energy of bonds between atoms. Also, SAED is a bulk sampling technique when compared to techniques such as Raman spectroscopy or EELS. Thus, it appears that combined analyses provide contradictory results and that amorphous, or short-range ordered, carbon identified by conventional TEM imaging and SAED may show evidence for  $sp^3$  bonds in EELS spectra.

Nanometer-scale structural heterogeneity could influence the carbon signature acquired by SAED, Raman or EELS analyses. The possibility of structural heterogeneity in elemental carbons can be understood if the very small differences in Gibbs free energy and entropy of crystalline elemental carbons are considered. Unfortunately, data are only available for graphite and diamond (Gibbs free energy 0.00 and 2.90 kJ/mol; entropy 5.74 and 2.38 J/mole.K, respectively)<sup>12</sup>. The free enthalpies of amorphous and poorly graphitised carbons are only known qualitatively with respect to the free enthalpy of graphite<sup>13</sup>. Based on these data, it is probable that small differences in Gibbs free energy and entropy exist for all elemental carbons. If this is the case, the structural forms of elemental carbon could display a complex mineralogical behaviour which may be analogous to that of the  $Al_2SiO_5$  polymorphs<sup>14</sup>. Phase Equilibrium experiments for

these polymorphs show that the stability fields are strongly influenced by structural defects, chemical impurities and kinetic factors<sup>14</sup>. As a result, a polymorph may form metastably near the transformation temperature and persist in a P-T field where another polymorph is stable. Similar kinetic factors may be important for elemental carbons in extraterrestrial environments. Considering the analytical techniques and thermodynamic properties of elemental carbons, high-resolution TEM (HRTEM) imaging in conjunction with spectroscopic analyses should be a prerequisite in any study of elemental carbons.

For example, HRTEM of vacuum deposited amorphous carbon showed small (<10nm in diameter) circular and polygonal rings of graphite-like structures<sup>15</sup>. The rings consist of concentrically arranged single layers of carbon forming hollow polyhedra<sup>15</sup>. In order to accommodate a closed polyhedral shell structure, single carbon layers are bent to angles varying between  $120 \pm 20$  degrees. Iijima<sup>15</sup> recognised two types of bending: (i) gradual and (ii) sharp bending. The gradual bending gives rise to strained trigonal bonds between carbon atoms. As a result, the trigonal  $sp^2$  bond of perfect single crystal graphite is altered and local formation of tetrahedral  $sp^3$  carbon bonds occur<sup>15</sup>.

HRTEM of carbon-rich acid residues of the Allende carbonaceous chondrite also showed concentric circular and polygonal, disc-shaped structures about 10-50nm in diameter. These structures showed a lattice fringe spacing of 0.34nm<sup>8</sup>. This lattice fringe spacing corresponds to randomly stacked graphitic carbon layers as the basal spacing of perfectly stacked graphite is 0.335nm<sup>16</sup>. The similarity of spherical graphite-like structures in both types of carbon<sup>8,15</sup> suggests that strained  $sp^2$  bonds in the Allende acid residue may cause a diamond-like carbon K-edge in EELS spectra<sup>4</sup> of Allende carbon.

These concentric circular and polygonal rings are simpler than single graphite ribbons and the tangled ribbon structures typical of PGC in carbonaceous chondrites<sup>7-10</sup>. The typical tangled structure of PGCs forms in response to thermal annealing of an amorphous precursor<sup>17</sup>. I agree with Smith and Buseck<sup>8</sup> that the tangled ribbon-type structure may be inherent to the Allende acid residue sample and may not result from the HF-HCl acid treatment of the meteorite sample. However, primitive ring structures could have been produced during HNO<sub>3</sub>-etching of the residues<sup>4</sup>. Iijima<sup>15</sup> suggested that the graphite-like rings probably formed during vapour deposition of the amorphous carbon. Assuming that formation of the primitive graphite-like rings is a surface phenomenon, subtle changes in the energy budget may cause graphite nucleation. The driving force is to lower the Gibbs free energy of amorphous carbon via nucleation of graphite, or graphitic carbon.

I suggest that complex, nanometer-scale, mineralogical interrelations are common to all elemental carbons irrespective of their origin. The subsequent thermal history, or energy balance, will determine the ultimate microstructure. The resulting structural heterogeneity will be represented in a different manner by SAED, Raman or EELS analyses and will give rise to conflicting interpretations if all types of data are not considered.

**REFERENCES:** (1) Hayatsu R & Anders E (1981) in *Topics in Current Chemistry* (FL Boeschke, ed) 1-37 (Springer-Verlag, New York); (2) Kiesel J & Krueger FR (1987) *Nature* 326, 755-760; (3) Allamandola LJ et al. (1987) *Science* 237, 56-59; (4) Lewis RS et al. (1987) *Nature* 326, 160-162; (5) Blake DF et al. (1987) *Meteoritics* 22, in press; (6) Rietmeijer FJM & Mackinnon IDR (1987) *Nature* 326, 162-165; (7) Lumpkin GR (1981) *Lunar Planet. Sci. XVII*, 502-503; (8) Smith PPK & Buseck PR (1981) *Science* 213, 322-324; (9) Rietmeijer FJM & Mackinnon IDR (1985) *Nature* 316, 733-736; (10) Mackinnon IDR & Rietmeijer FJM (1987) *Rev. Geophys.*, in press; (11) Fraundorf P et al. (1982) *Lunar Planet. Sci. XIII*, 229-230; (12) Robie RA et al. (1978) *U.S. Geol. Survey Bull.* 1452 (US Government Printing Office, Washington) 456pp; (13) Fitzer E & Kegel B (1968) *Carbon* 6, 433-442; (14) Zen E-an (1969) *Am. J. Science* 267, 297-309; (15) Iijima S (1980) *J. Crystal Growth* 50, 675-683; (16) Jenkins GM & Kawamura K (1976) *Polymeric Carbons - Carbon Fibre, Glass and Char* (Cambridge Univ. Press) 178pp; (17) Ban LL et al. (1975) *J. Appl. Cryst.* 8, 415-420.

## FT-IR SPECTROSCOPIC STUDIES OF POLYCYCLIC AROMATIC HYDROCARBONS

D. W. Salisbury<sup>1,2</sup>, J. E. Allen, Jr.<sup>2</sup>, B. Donn<sup>2</sup>,  
W. J. Moore<sup>1</sup>, R. K. Khanna<sup>1</sup>

1. Chemistry Dept., U. of MD, College Park, MD 20742

2. Code 691, NASA/GSFC, Greenbelt, MD 20771

3. Naval Research Laboratory, Washington, D.C. 20375

Proper assessment of the hypothesis which correlates polycyclic aromatic hydrocarbons with the unidentified infrared emission bands requires additional experimental laboratory data. In order to address this need, thermal infrared emission studies have been performed on a subset of PAHs suggested to be of astrophysical importance. It has been proposed that infrared emission from interstellar PAHs occurs following absorption of an ultraviolet photon. Since energy transfer to the ground electronic state can be rapid for a species in which intersystem crossing is negligible, the emission spectrum may be viewed as resulting from an equilibrium vibrational temperature (Léger and d'Hendecourt, 1987). This has been the basis for using infrared absorption spectra to calculate the corresponding emission spectra at various temperatures. These calculations have been made using room temperature infrared absorption coefficients instead of those at the temperature of interest because of the latter's unavailability.

The present studies are designed to address the differences between the calculated and experimental thermal emission spectra and to provide information which will be useful in future ultraviolet induced infrared fluorescence studies. The emission spectra have been obtained for temperatures up to 825K using an emission cell designed to mount against an external port of an FT-IR spectrometer. These spectra provide information concerning relative band intensities and peak positions which is unavailable from previous calculations.

Léger, A. and d'Hendecourt, L.: 1987, Polycyclic Aromatic Hydrocarbons and Astrophysics, p. 232. NATO ASI Series, Series C: Vol. 191.

## CARBON IN THE OUTER SOLAR SYSTEM

D.P. Simonelli, J.B. Pollack, and C.P. McKay  
NASA Ames Research Center, Moffett Field, California 94035

The satellites of Uranus, with densities between  $1.3$  and  $1.7 \text{ g cm}^{-3}$  (from Voyager 2 observations), and the Pluto-Charon system, with a mean density of just above  $1.8 \text{ g cm}^{-3}$  (from terrestrial observations of mutual eclipse events), are too dense to have a significant amount of methane ice in their interiors. However, the observed densities do not preclude contributions from such organic materials as the acid-insoluble residue in carbonaceous chondrites and laboratory-produced tholins, which have densities on the order of  $\approx 1.5 \text{ g cm}^{-3}$ . These and other considerations have led us to investigate the carbon mass budget in the outer solar system, with an emphasis on understanding the contribution of organic materials.

Modeling of the interiors of Pluto and Charon (being carried out by R. Reynolds and A. Summers of NASA/Ames), assuming rock and water ice as the only constituents, suggests a silicate mass fraction for this system on the order of  $0.65$ - $0.70$ . Such a composition has two implications: (1) The silicate fraction for Pluto/Charon is larger than the typical silicate fraction of  $\approx 0.55$  found for satellites of the giant planets (Johnson et al., 1987). This compositional difference may be a result of different formation mechanisms: while Pluto and Charon formed directly from the solar nebula, and retain its rock and ice fractions, the satellites may have formed from the outer portions of the envelopes of the forming giant planets—in which case the satellites would have a lower silicate fraction than the nebula because as planetesimals bombard the forming planet, icy planetesimals dissolve in the envelope more readily than rocky planetesimals (Pollack et al., 1986). (2) The silicate fraction of objects formed directly from the solar nebula depends strongly on the fraction of nebular carbon that is in the form of CO: a greater CO abundance means that there is less oxygen available to form water ice, and implies that condensed material in the nebula will have a greater rock/ice ratio (Pollack and Bodenheimer, 1987). Simple calculations based on solar abundances suggest that in order for the Pluto-Charon system to have a silicate fraction as high as  $0.65$ - $0.70$ , the majority of the carbon in the outer solar nebula—on the order of  $70$ - $85\%$ —must

have been in the form of carbon monoxide gas.

After constraining the amount of carbon in gaseous CO, we next put limits on the fraction of the remaining carbon that is in condensed materials by modeling the enhancement in C/H (over and above the solar C/H ratio) that is observed in the atmospheres of the giant planets. We use an approach first developed by Pollack et al. (1986) that emphasizes planetesimal dissolution in the envelopes of the forming giant planets; this approach assumes that the C/H enhancement depends on both the fraction of nebular C in condensed material and the fraction of carbon-bearing planetesimals bombarding a planet that dissolve in the envelope—and assumes that if all such planetesimals do dissolve, the C/H enhancement in the atmosphere would mimic the observed enhancement in the high  $z$ /low  $z$  mass ratio of the planet as a whole (where "high  $z$ " means condensed materials, "low  $z$ " refers to  $H_2$  and He gas, and enhancement is relative to predictions from solar abundances). The present work includes the most recent estimates of the C/H enhancements and high  $z$ /low  $z$  ratios of the giant planets (Pollack and Bodenheimer, 1987), and involves a more careful estimation of the high  $z$ /low  $z$  mass ratio expected from solar abundances than was used in Pollack et al. (1986), including the influence of the fraction of C in CO on the amount of condensed water ice. These calculations indicate that for a particular fraction of C in CO and a given fraction of C-bearing planetesimals that dissolve in the envelope (most likely in the range 0.50-0.75), (1) Jupiter and Saturn require a larger fraction of C in condensed materials than Uranus and Neptune, but (2) the Jupiter and Saturn results are much less strongly constrained by the error bars on the observed C/H enhancements and high  $z$ /low  $z$  ratios than is the case for Uranus and Neptune. The clearest result is that in the region of the solar nebula near Uranus and Neptune, the minority of carbon that is not in gaseous CO (1) must include a nonzero amount of condensed material, but (2) is most likely not condensed material alone, i.e. there must be a third carbon-bearing component besides condensed material and gaseous CO. Given the implied dearth of methane ice, the condensed carbon is likely dominated by organic material, and the third component present in addition to CO and organics is assumed to be  $CH_4$  gas.

#### References

- Johnson, T. V., Brown, R. H., and Pollack, J. B.: 1987, submitted to J. Geophys. Res.
- Pollack, J. B., and Bodenheimer, P.: 1987, review chapter in upcoming book "Origin and Evolution of Planetary and Satellite Atmospheres".
- Pollack, J. B., Podolak, M., Bodenheimer, P., and Christofferson, B.: 1986, Icarus 67, 409.



## Report Documentation Page

1. Report No. NASA CP-3061		2. Government Accession No.		3. Recipient's Catalog No.	
4. Title and Subtitle Carbon in the Galaxy: Studies From Earth and Space				5. Report Date April 1990	
				6. Performing Organization Code	
7. Author(s) Editors Jill C. Tarter,* Sherwood Chang, and Doug J. DeFrees **				8. Performing Organization Report No. A-90031	
				10. Work Unit No. 199-52-12	
9. Performing Organization Name and Address Ames Research Center Moffett Field, CA 94035-1000				11. Contract or Grant No.	
				13. Type of Report and Period Covered Conference Publication	
12. Sponsoring Agency Name and Address National Aeronautics and Space Administration Washington, DC 20546-0001				14. Sponsoring Agency Code	
15. Supplementary Notes Point of Contact: Sherwood Chang, Ames Research Center, MS 239-4, Moffett Field, CA 94035-1000 (415) 604-5733 or FTS 464-5733 *SETI Institute, Mountain View, CA **Molecular Research Institute, Palo Alto, CA					
16. Abstract <p>This report contains the text of the invited papers presented during a meeting entitled "Carbon in the Galaxy: Studies from Earth and Space" that was held at NASA Ames Research Center on November 5 and 6, 1987. For completeness, abstracts from all of the poster papers and the text of a paper summarizing what was learned during the course of the meeting are also included. The underlying premise for the meeting was that there is much to be gained by bringing together scientists from very different disciplines, all of whom study carbon in different ways for different reasons. The interchanges that took place during the meeting and the contents of the enclosed papers validate that premise.</p>					
17. Key Words (Suggested by Author(s)) Carbon Organic matter Exobiology			18. Distribution Statement Unclassified-Unlimited  Subject Category - 88		
19. Security Classif. (of this report) Unclassified	20. Security Classif. (of this page) Unclassified		21. No. of Pages 360	22. Price A16	

344